

DESIGN AND SYNTHESIS OF ENANTIOPURE ORGANOMETALLIC KINASE INHIBITORS AS POTENTIAL CHEMOTHERAPEUTICS

Thesis submitted in partial fulfilment of the requirements of
the degree Doctor of Science (Dr. rer. nat.) of the
Faculty of Chemistry,
the PHILIPPS-UNIVERSITÄT MARBURG,
Marburg an der Lahn, Germany

by

Rajathees Rajaratnam, Dipl.-Ing. (FH)
Araly, Sri Lanka

Marburg an der Lahn, 2016

The experimental work leading to the results presented in this dissertation have been performed from January 2012 to March 2015 at the Faculty of Chemistry of the PHILIPPS-UNIVERSITÄT MARBURG.

The present dissertation was accepted by the Faculty of Chemistry of the PHILIPPS-UNIVERSITÄT MARBURG (University ID: 1180) on 28.09.2016.

Supervisor: Prof. Dr. Eric Meggers

Second Reviser: Prof. Dr. Gerhard Klebe

Date of the oral exam:

10.11.2016.

for my family

*“Most people say that it is the intellect which makes a great scientist.
They are wrong: it is character.”*

Albert Einstein

Acknowledgment

I thank Prof Dr. Eric Meggers for the opportunity to contribute to the exciting and challenging development of metal based kinase inhibitors. The aim to design and synthesise highly sophisticated, unique, and effective metal based inhibitors in ideally enantiopure fashion offered me the chance to apply and increase my knowledge in nearly all fields of chemistry. These firm capabilities were initialised during the master study program of medicinal chemistry and continuously supported during three years of my PhD study by valuable ideas and impulses to implement new methods and techniques. Moreover, during this time Prof. Dr. Meggers not only supported my work on a professional basis but also encouraged my endurance and confidence during viewless project phases with valuable advices, which significantly contributed to my development becoming a complete scientist.

I thank Prof. Dr. Gerhard Klebe for the revision of my dissertation. Moreover, I would like to thank Prof. Dr. Gerhard Klebe for the various opportunities to gather valuable insights in pharmaceutical chemistry and drug design in lectures and research projects during my master study.

I thank Prof. Dr. Paultheo von Zezschwitz for his participation in the examination board. Moreover, I would like to thank Prof. Dr. Paultheo von Zezschwitz for the excellent teaching of organic chemistry in lectures and his supervision in practical courses during my master study.

Furthermore, I thank Prof. Dr. Peter Kolb for his valuable ideas and contributions as well as the offer to employ resources of his group to promote the progress on the PI3K project during my PhD study. In this context, although the obtained data of our collaboration are not shown in the present dissertation, a special gratitude goes to the PhD student Florent Chevillard, who promoted the progress on the PI3K topic with his expertise in computer aided drug design and his supervision of my master student Georg Rennar. Moreover, Georg Rennar, Khang Ngo, and Oliver Born participated in ligand and complex synthesis on the PI3K topic. Without these valuable contributions the whole realisation of this project would have been impossible.

Prof. Ronen Marmorstein and Prof. Weiwei Dang and their groups earned a special thank for their contribution to several projects. In this context, a special thank goes to Jie Qin, Jemilat Salami, Julie S. Barber-Rotenberg, John Domsic, Patricia Reyes-Urbe, Haiying Liu, Shelley L. Berger, and Jessie Villanueva for their effort solving the crystal structure of compound **87** bound to S6K1 and the biochemical characterisations. Without these valuable contributions, the entire interpretation and evaluation of the ligand scaffold would have been impossible. The same is true for the contribution of Jasna Maksimoska in case of the data collection for the determination of IC₅₀ values of the synthesised compounds of the PI3K project.

Moreover, I thank all members of the analytical department of the Faculty of Chemistry of the PHILIPPS-UNIVERSITÄT MARBURG for their technical support during the data collection of the compounds and the evaluation: Dr. Uwe Linne, Tina Krieg, and Jan Bamberger for their assistance recording mass spectra; Dr. Klaus Harms, Michael Marsch, and Radostan Riedel for their assistance recording and processing crystallographic data of

the complexes obtained during this work; Cornelia Mischke for her friendly patience and will to record NMR spectra of the obtained compounds at any time; Dr. Istemi Kuzu for his introduction into the IR spectrometer and the opportunity to use the equipment and measure any time by myself.

Furthermore, I cordially thank the present and former Meggers group, Höbenreich group, and Vasquez group members not only for their professional contribution but also for their heartwarming support as colleagues in the daily lab work and as friends in everyday life. Especially, Markus Dörr as my box mate for the exchange of ideas and intermediates for synthesis, his patience tolerating my frustration about failed experiments and for finding the right words at the right time in combination with the right amount of beer; Thomas Cruchter, for his incredible readiness to support experiments and to meet reaction times by regulating the equipment at inhuman time points, regardless of basic needs like sleep or nutrition; Elisabeth Martin for her enormous support in various projects and the exchange of ideas and intermediates as well as her friendly company and scientific contributions on conferences; Jens Henker, Melanie Helms, and Cornelia Ritter not only for interesting conversations about various scientific topics, but also for discussing daily challenges and the unconditional hosting in their apartments; Nathalie Nett, Thomas Mietke, Timo Völker, Henrik Löw, Wei Zuo, Haohua Huo, Jiajia Ma, Chuanyong Wang, and Yu Zheng for their reliable support in running the lab and maintaining the equipment; and closing, Ina Pinnschmidt and Andrea Tschirch for their support on any administrative issues.

Moreover, for their support in computational chemistry during my master and PhD study the Klebe group members Tobias Craan, Felix Gut, Alexander Metz, Gerd Neudert, Andreas Spitzmüller, Michael Betz, and Sven Siebler earned special thanks.

Furthermore, a plenty of bachelor and master students participated on my research aim with different subprojects and thus contributed significantly with their effort and ideas to the success of the present work. Therefore, I thank my students Oliver Born, Sophie Franz, Hauke Löcken, Khang Ngo, Georg Rennar, Andreas Schmidt, Sören Seidler, and Benjamin Wenzel.

As everything comes to an end, the written completion of my PhD study is the present dissertation and a lot of group members and friends helped by proofreading the manuscript. In this context, I thank Markus Dörr, Elisabeth Martin, Cornelia Ritter, Nathalie Nett, Jens Henker, Florent Chevillard, Melanie Helms, and Sivakkumaran Sukumaran.

Last but not least, I thank my entire family for their support and for encouraging me unconditionally during all phases of my life. Especially, Jegatheeswary Rajaratnam and Rajaratnam Sivasambo, who continuously emphasised me with the value of education and who made all this possible with their heartwarming way and will to resign their own needs for our best. I thank my brothers, Rajatutheeskumaran Rajaratnam and Piratheeskumaran Rajaratnam, for honoring my achievements, listening to my problems, and giving me advices through all situations as well as for respecting me as elder brother. I thank my wife, Christina Rajaratnam, for being the anchor in my life, for being the save haven to calm down, and for giving me the greatest happiness in my life of becoming father of our cute daughter Marie Mayuri Rajaratnam. There are so many more family members and friends who I have not named here personally but have contributed to my work by offering me a happy and cheerful life beside the lab and therefore they also have earned my honest gratitude.

List of Publications

Parts of the results presented in this dissertation have been published:

Scientific Publications

“Correlation between the Stereochemistry and Bioactivity in Octahedral Rhodium Prolinato Complexes”

R. Rajaratnam, E. K. Martin, M. Dörr, K. Harms, A. Casini, E. Meggers, *Inorg. Chem.* **2015**, *54*, 8111-8120.

“Development of Organometallic S6K1 Inhibitors”

J. Qin, R. Rajaratnam, L. Feng, J. Salami, J. S. Barber-Rotenberg, J. Domsic, P. Reyes-Urbe, H. Liu, W. Dang, S. L. Berger, J. Villanueva, E. Meggers, R. Marmorstein, *J. Med. Chem.* **2015**, *58*, 305-314.

“Continuous Synthesis of Pyridocarbazoles and Initial Photophysical and Bioprobe Characterization”

D. T. McQuade, A. G. O'Brien, M. Dörr, R. Rajaratnam, U. Eisold, B. Monnanda, T. Nobuta, H.-G. Löhmansröben, E. Meggers, P. H. Seeberger, *Chem. Sci.* **2013**, *4*, 4067-4070.

Scientific Poster Presentations

R. Rajaratnam, K. Harms, E. Meggers, *Protein Kinases in Drug Discovery Conference*, 8th – 9th May **2014**, Berlin.

R. Rajaratnam, O. Born, K. Harms, E. Meggers, *International Symposium on Functional Metal Complexes that Bind to Biomolecules*, 9th - 10th September **2013**, Barcelona.

Index

1	Abstract / Zusammenfassung	17
2	Introduction	21
2.1	Kinases	21
2.1.1	Classification and Role in Cellular Signal Transduction	21
2.1.2	Structural Properties	22
2.1.3	The Catalytic Mechanism of Phosphate Group Transfer	26
2.1.4	Kinases Related Disorders	28
2.1.5	Mechanisms of Kinase Inhibition	30
2.2	Metal Complexes as Kinase Inhibitors	36
2.3	Octahedral Complexes – Taming the Structural Scope	38
3	Results and Discussion	43
3.1	The Pyridocarbazole Pharmacophore Ligand	43
3.2	Development of S6K1 Inhibitors	47
3.2.1	Target Synopsis and Aim	47
3.2.2	Synthesis and Structural Investigations of Organoruthenium(II) Complexes	48
3.2.3	Biological Investigations	51
3.2.4	Interpretation	59
3.3	Enantiopure Organorhodium(III) Complexes	64
3.3.1	Target Synopsis and Aim	64
3.3.2	Synthesis and Structural Investigations	68
3.3.3	Kinome Profiling and Biological Investigations	77
3.3.4	Interpretation	79
3.3.5	Scanning the Binding Pocket - Further Development of Tridentate Chiral Ligands	81
3.3.6	Synthesis and Structural Investigations	82
3.3.7	Biological Investigations	84
3.3.8	Interpretation	85
3.3.9	Scanning the Binding Pocket – Modifications of the Pyridocarbazole Pharmacophore	87
3.3.10	Biological Investigations	88
3.3.11	Interpretation	88
3.4	Design of Phosphatidylinositol-3-Kinases (PI3K) Inhibitors	89
3.4.1	Target Synopsis and Aim (III)	89
3.4.2	Organometallic Inhibitor Design	91
3.4.3	Hot Spot Analysis – a First Clue to Address the Right Sites	92
3.4.4	Elaborating the Ligand Scaffold	99
3.4.5	The Selection of Amino Acids for the Ligand Design	101
3.5	Proof of Concept	105
3.5.1	Subsequent Synthesis of Selected Amino Acid	105
3.5.2	Complex Synthesis	108
3.5.3	Biological Investigations and Target Selectivity	112
3.5.4	Interpretation	112

4	Conclusion and Outlook.....	119
5	Experimental	121
5.1	General Information	121
5.2	Synthetic Procedures.....	122
5.2.1	Synthesis of pyridocarbazoles and related intermediates	122
5.2.2	Synthesis of ligands and related intermediates.....	138
5.2.3	Synthesis of complexes and related intermediates	165
5.3	Biological Experiments.....	187
5.3.1	PI3K Kinase-Glo Assay	187
5.3.2	Cloning, Expression, and Purification of S6K1 Constructs	187
5.3.3	Cloning, Expression, and Purification of S6K2 Construct	188
5.3.4	Radioactive Kinase Assay targeting S6K1 and S6K2 constructs.....	188
5.3.5	Cell Culture and Western Blotting	188
5.3.6	Yeast Cell Culture and Lysis	189
5.3.7	Radioactive Kinase Assay targeting PIM-1, Aurora A, and FLT 3	189
5.4	Kinase Profiling	190
5.4.1	Kinase Profiling of Complexes 85 , and 86	190
5.4.2	Kinase Profiling of Complexes 87 , Δ -(<i>R</i>)- 106 , Δ -(<i>S</i>)- 106 , Δ -(<i>R</i>)- 107 , and Δ -(<i>S</i>)- 107	194
5.5	Computational Procedures.....	208
5.5.1	The Hot Spot Analysis	208
5.6	Crystallographic Data	209
5.6.1	Crystallographic Data of 96	209
5.6.2	Crystallographic Data of Δ -(<i>R</i>)- 106 and Δ -(<i>S</i>)- 106	210
5.6.3	Crystallographic Data of Δ -(<i>S,R</i>)- 125	213
5.6.4	Crystallographic Data of Δ -(<i>R</i>)- 127	215
5.6.5	Crystallographic Data of Δ -(<i>S</i>)- 191	217
5.6.6	Crystallographic Data of Δ -(<i>S</i>)- 195	219
5.6.7	Crystallisation and Structure Determination of S6K1	221
6	Appendix.....	223
6.1	Kinase Classification	223
6.1.1	AGC Kinases	223
6.1.2	CMGC Kinases.....	223
6.1.3	CK1 group.....	223
6.1.4	STE group.....	223
6.1.5	CAM Kinases	223
6.1.6	TK group	224
6.1.7	TKL group	224
6.1.8	RGC group.....	224
6.1.9	PKL group.....	224
6.1.10	Pseudokinases	225
6.2	Structural Overview of Synthesised Compounds	226
6.2.1	Compounds of Chapter 3.1	226
6.2.2	Compounds of Chapter 3.2	227

6.2.3	Compounds of Chapter 3.3	227
6.2.4	Compounds of Chapter 3.4	229
6.3	List of abbreviations	231
7	Literature	235
8	Declaration of Authorship.....	253
9	Scientific Career.....	255

1 Abstract / Zusammenfassung

The exploration of the structural scope of the octahedral coordination mode and investigations of defined structural isomers regarding their physico-chemical properties are of valuable interest for applications in the field of catalysis, materials sciences, and life sciences. The MEGGERS group established a variety of different transition metals as structural templates to gain access to highly potent and selective kinase inhibitors. During this effort, the effectiveness of metal complexes as kinase inhibitors with potential anticancer properties has repeatedly been proven *in vitro* as well as *in vivo*. The ambition to establish metals as structural templates led from initial half sandwich complexes to highly sophisticated octahedral complexes.

In the current thesis, the challenge to selectively synthesise a desired enantiomer is presented highlighting the application of symmetric polydentate ligands and chiral polydentate ligands.

As a first example, regarding the chemical and biological properties, an *N*-methyl-1,4,7-trithiacyclodecan-9-amine based ruthenium(II) complex, in context of S6 kinase 1 (S6K1) inhibition, is presented. Aberrant activation of S6K1 is found in many diseases, including diabetes, aging, and cancer. The presented ATP competitive organometallic kinase inhibitors were inspired by the pan-kinase inhibitor staurosporine, and specifically inhibit S6K1, and verify the strategy successfully applied previously to target other kinases. Furthermore, the obtained biochemical data demonstrate that the compounds inhibit S6K1 with an IC_{50} value in the low nanomolar range at 100 μ M ATP. Moreover, the crystal structures of S6K1 bound to staurosporine, and two ruthenium(II) based inhibitors reveal that the compounds bind in the ATP binding site and exhibit S6K1-specific contacts, resulting in

changes to the p-loop, α C helix, and α D helix compared to the staurosporine bound structure. *In vitro* assays reveal inhibited S6K phosphorylation in yeast cells. These cumulated biological studies demonstrate that potent, selective, and cell permeable metal based inhibitors can provide a scaffold for the future development of compounds with possible therapeutic applications.

However, the so far presented complexes are racemic mixtures. Thus, to apply these compounds for the therapeutic use the pharmacologic and toxicological characterisation of each present structural isomer is obligatory. Therefore, the asymmetric synthesis of desired structural isomers of the metal based kinase inhibitors is highly favourable.

Thus, controlling the metal centered relative stereochemistry represents the key to achieve this task. The application of a proline based chiral tridentate ligand to decisively influence the coordination sphere of an octahedral rhodium(III) complex is described as possible solution to face this issue. The mirror-like relationship of synthesised enantiomers and differences between diastereomers were investigated. Furthermore, the application of the established pyridocarbazole pharmacophore* ligand as part

* The term „pharmacophore“ in this thesis is used as a structural unit coordinated to the metal core and mainly mediating the interactions to the biological target.

The IUPAC definition (1998) of “pharmacophore” is given as:

- A pharmacophore is the ensemble of steric and electronic features that is necessary to ensure the optimal supramolecular interactions with a specific biological target structure and to trigger (or to block) its biological response.
- A pharmacophore does not represent a real molecule or a real association of functional groups, but a purely abstract concept that accounts for the common molecular interaction capacities of a group of compounds towards their target structure.
- A pharmacophore can be considered as the largest common denominator shared by a set of active molecules. This definition discards a misuse often found in the medicinal chemistry literature which consists of naming as pharmacophores simple chemical function-

of the organometallic complexes to obtain kinase inhibitors is demonstrated. Moreover, the importance of the relative stereochemistry at metal in chiral environments like biomolecules is highlighted by both, protein kinase profiling and competitive inhibition studies. The cumulated results confirm that the proline based enantiopure rhodium (III) complexes differ entirely in their selectivity and specificity despite their unmistakably mutual origin.

The successful work using proline as a chiral building block inspired to implement other chiral amino acids into the ligand design. For this aim, a versatile set of amino acids were elaborated as starting points for the ligand synthesis. As highly functionalised building blocks, they offer the possibility to orient a particular functional group into a defined site of the enzyme pocket, overall predefined by the chirality-at-metal. However, the ambitious attempts were limited by the synthetic issues accompanying the implementation of primary amino acids into the ligand design due to steric effects influencing the yields. Nevertheless, the biological data evaluating the obtained complexes offered valuable hints for the future ligand scaffolds.

alities such as guanidines, sulfonamides or dihydroimidazoles (formerly imidazolines), or typical structural skeletons such as flavones, phenothiazines, prostaglandins or steroids.

- A pharmacophore is defined by pharmacophoric descriptors, including H-bonding, hydrophobic and electrostatic interaction sites, defined by atoms, ring centers and virtual points

Die Erkundung des dreidimensionalen Raumes anhand der Strukturen, welche durch die oktaedrische Koordinationssphäre ermöglicht werden, führt zu Isomeren, deren physiko-chemische Eigenschaften für die Forschungsfelder der Katalyse, Materialwissenschaften und Lebenswissenschaften von besonderem Interesse sind. Der Arbeitskreis MEGGERS hat hierzu eine Vielzahl von unterschiedlichen Übergangsmetallen als Strukturtemplate etabliert, um Zugang zu hochpotenten, selektiven sowie strukturell hochdiversifizierten Kinaseinhibitoren zu erhalten. Im Zuge dieser Anstrengungen, wurden Kinaseinhibitoren entwickelt, deren antitumorogene Wirkung mehrfach, sowohl *in vitro* als auch *in vivo*, belegt werden konnten. Hierbei führten die Ambitionen, Metalle als Strukturtemplate zu verwenden, über anfängliche Halbsandwich-Komplexe zu hochdiversifizierten oktaedrischen Komplexen.

In der vorliegenden Arbeit sollen insbesondere die Herausforderungen und die Umsetzung der selektiven Synthese von angestrebten Enantiomeren anhand von mehrzähligen symmetrischen Liganden sowie anhand von mehrzähligen chiralen Liganden verdeutlicht werden.

Als erstes Beispiel dient hierzu die Betrachtung der chemischen und biologischen Eigenschaften eines auf *N*-methyl-1,4,7-trithiacyclodecan-9-amin basierenden Ruthenium(II) Komplexes, im Kontext der S6 Kinase 1 (S6K1) Inhibierung. Eine gestörte Aktivierung von S6K1 wird mit zahlreichen Erkrankungen wie z.B.: Diabetes, Krebs und Alterungsprozessen in Verbindung gebracht. Die vorgestellten ATP kompetitiven metallbasierten Inhibitoren sind von dem Pan-Kinaseinhibitor Staurosporin abgeleitet, doch inhibieren spezifisch S6K1. Darüber hinaus verifizieren sie das Konzept, welches bereits erfolgreich bei der Inhibierung anderer Kinasen Anwendung gefunden hat. Die erhaltenen biochemischen Daten zeigen, dass die Ruthenium(II) basierten Verbindungen S6K1 mit einem IC₅₀ Wert im

nanomolaren Bereich inhibieren bei einer ATP Konzentration von 100 μM ATP. Zusätzlich konnte anhand der Kristallstrukturen von Staurosporin in S6K1 und von zwei Metallkomplexen in S6K1, die Bildung von S6K1 spezifischen Kontakten, welche im Falle der metallbasierten Inhibitoren im Vergleich zu Staurosporine zu Änderungen in der p-Schleife, der αC Helix und der αD Helix führen, gezeigt werden. *In vitro* Untersuchungen zeigten eine inhibierte S6K Phosphorylierung in Hefe Zellen. Die Gesamtheit der biologischen Studien zeigen, dass potente, selektive sowie zellpermeable metallbasierte Inhibitoren eine Grundstruktur für die Entwicklung von potentiellen Chemotherapeutika bereit halten.

Zu beachten ist, dass die hierbei gezeigten Komplexe in racemischer Form vorliegen. Um diese Verbindungen in der Therapie einsetzen zu können, müssen somit auch die pharmakologischen und die toxikologischen Eigenschaften beider Isomere charakterisiert und miteinander verglichen werden. In diesem Zusammenhang ist die asymmetrische Darstellung eines gewünschten Isomers eines metallbasierten Inhibitors sehr erstrebenswert.

Daher stellt die Kontrolle der relativen und absoluten metallzentrierten Stereochemie eine Schlüsselaufgabe zur Realisierung dieses Zieles dar. Die Anwendung von prolinbasierten dreizähligen Liganden zur entschiedenen Beeinflussung der Koordinationsphäre von Rhodium(III) Komplexen wird daraufhin als mögliche Lösung dieser Herausforderung diskutiert. Die spiegelbildliche Beziehung der synthetisierten Enantiomere und die Unterschiede zu den entsprechenden Diastereomeren werden durchleuchtet. Zudem wird die Anwendung des etablierten Pyridocarbazole Pharmakophorliganden* als

Teil des metallbasierten Komplexes zur Darstellung von Kinaseinhibitoren demonstriert. Darüber hinaus, wird die enorme Bedeutung der relativen Stereochemie am Metallzentrum bei der Wechselwirkung mit chiralen Umgebungen wie Biomoleküle durch Kinase Profiling Untersuchungen und kompetitiven Inhibitionsstudien verdeutlicht. Die gesammelten Daten bestätigen, dass die unterschiedlichen Rhodium(III) Isomere sich gänzlich in Ihrer Selektivität und Spezifität unterscheiden, trotz eines eindeutig gemeinsamen Ursprungs.

Die erfolgreichen Arbeiten mit der Verwendung von Prolin als Gerüstbaustein inspirierte folgerichtig zu dem Einsatz weiterer Aminosäuren im Ligandendesign. Hierzu wurde eine vielseitige Auswahl an Aminosäuren als Ausgangspunkt für die Ligandensynthese erarbeitet. Die Arbeiten mit primären Aminosäuren zeigten deren Potential zur Eröffnung von hochdiversifizierten oktaedrischen Komplexen. Als hochfunktionalisierte Gerüstbausteine ermöglichen sie die Positionierung von funktionellen Gruppen in bestimmte Raumrichtungen einer Enzymtasche, welche durch die Chiralität-am-Metall vorgegeben wird. Jedoch wird dieses ambitionierte Ziel durch synthetische Schwierigkeiten bei der Koordination von aminosäurenbasierten Liganden, begründet in sterischen Effekten und den reduzierten Ausbeuten, limitiert. Nichtsdestotrotz, eröffnen die erhaltenen biologischen Daten wichtige Erkenntnisse für das zukünftige Ligandendesign.

* Der Begriff "Pharmakophor" wird im Rahmen dieser Dissertation für eine Struktureinheit verwendet, welches als metal-koordinierter Ligand hauptsächlich für die Wechselwirkungen mit dem biologischen Zielmolekül verantwortlich ist.

2 Introduction

2.1 Kinases

More than 518 different protein kinases have been identified in the human proteome and represent approximately 1.7% of the human genome.^[1–3] Among these 518 kinases, 478 are classified as typical kinases, and 40 as atypical, based on the fact that the latter still have biochemical kinase activity but lack sequence similarity to the typical kinases.^[1,4,5] The typical kinases are further subdivided into two categories depending on the phosphorylated amino acid residue: either serine/threonine (388 kinases) or tyrosine (90 kinases).^[6,7]

2.1.1 Classification and Role in Cellular Signal Transduction

The eukaryotic protein kinases have evolved in a divergent manner than prokaryotic protein kinases, that are indeed abundant, but poorly understood.^[8,9] However, in eukaryotic cells kinases play an inevitable role in the majority of cellular signaling pathways by regulating the flow of information via protein phosphorylation.^[10,11] The phosphorylation of protein substrates results in versatile effects, covering increased or decreased enzyme activity of the effector proteins, the creation of recognition sites for protein assembly or conformational changes inducing structure related effects, like contraction and relaxation on macro-molecular level.^[12]

An overview of the kinase classification is provided in Chapter 6.1. Moreover, a detailed discussion of kinase classification, structural difference, and role in physiological processes is out of the scope of this thesis. Therefore, further publications are recommended giving detailed insights in each kinase family, see Chapter 6.1.

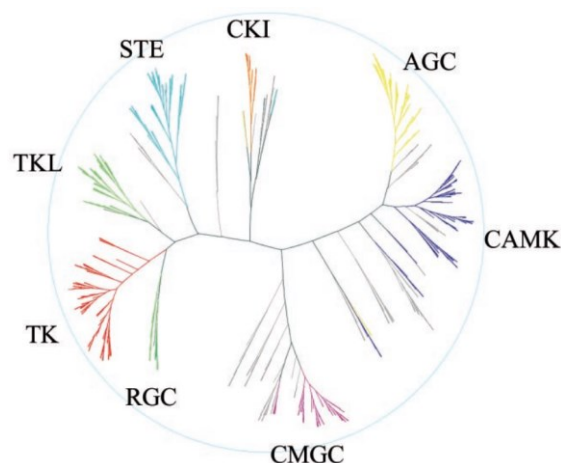


Figure 1: Dendrogram of the human kinome. AGC: named after protein kinase A, G, and C. CAMK: acronym for Ca^{2+} /Calmodulin-dependent protein kinases. CMGC: acronym based on initials of key members CDK, MAPK, GSK, and CDK. RGC: receptor guanylate cyclase group. TK: tyrosine kinases. TKL: tyrosine kinases like group. STE: homologues of yeast Sterile 7, Sterile 11, and Sterile 20 kinases group. CK1: casein kinase 1 group.^[1]

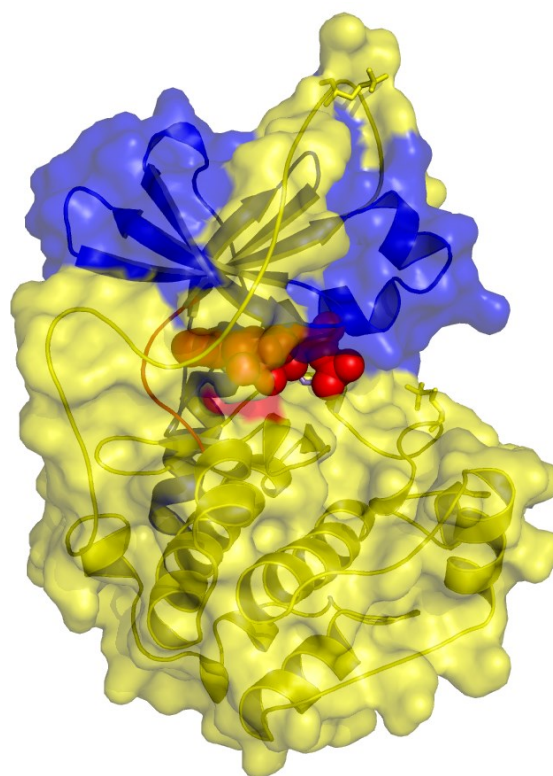


Figure 2: Crystal structure of ATP bound to PKA (pdb: 1ATP). The N-lobe is coloured in blue and the C-lobe in yellow. The ATP molecule is showed as red spheres and the hinge region is coloured in magenta. The manganese ions and the peptide inhibitor IP20 were omitted for clarity.^[13]

2.1.2 Structural Properties

Protein kinases themselves are regulated by phosphorylation,^[14] among other mechanisms, leading either to the active conformation or the inactive conformation.^[12,15] The active conformation was first investigated on the protein kinase A (PKA) crystal structure,^[16] whereas, the inactive conformation was first investigated on the crystal structure of cyclin-dependent protein kinase 2 (CDK2).^[17] Moreover, PKA as one of the first reported kinases ever in 1968 by WALSH *et al.*,^[18] beside the phosphorylase kinase by KREBS and FISCHER in the late 1950's,^[19] is one of the most characterised ones in literature.^[16,20–22] Thus, numerous structural investigations discussing PKA, an AGC kinase,^[23] have been performed showing that this is an ideal representative for the elucidation of the structural properties of protein kinases and their catalytic mechanism. The first crystal structure of PKA was obtained with manganese ions instead of magnesium and the peptide inhibitor IP20.^[13] Although, PKA serves as the model system, the crucial residues are highly conserved throughout the kinome.^[24,25]

2.1.2.1 The N-Lobe

Two structurally and functionally distinct lobes contribute in a unique way to the catalytic function and the regulation of a kinase, see Figure 2.^[23,26] The smaller one, the *N*-lobe, is dominated by five β -sheets, incorporating two α -helical subdomain, α B-helix and the α C-helix, see Figure 3. The β 5-sheet is structurally connected via the hinge region to the C-lobe. In contrast, the α C-helix forms functional contacts to the C-lobe. Thus, the β 5-sheet and the α C-helix, are the only two structural elements, which interact between the two main segments.^[27,28] The β 1, β 2, and β 3 strands possess two highly conserved sequence

motifs. The first motif (GxGxxG) is called the glycine rich loop (Gly-loop), between β 1 and β 2 and the second is the AxK motif in the β 3 strand.

The Gly-loop is the most flexible part of the *N*-lobe. Its main function is to fold over and enclose the nucleotide for the proper positioning the γ -phosphate of adenosine triphosphate (ATP) for catalysis.^[29] Further, it is noteworthy to distinct Gly-loop from the P-loop (Walker-A motif, (GxxxxGKT/S)).^[30] Although, both loops anchor the phosphonucleotides, their interaction mechanism is different. Whereas, the P-loop does not form any contacts to the purine moiety, the Gly-rich loop connects the β 1 and β 2-strands enclosing the adenine ring, see Figure 3. Highly conserved residues of the P-loop and the Gly-loop are a Ser/Thr binding γ -phosphate and a Val residue (Val57 in PKA) forming hydrophobic contacts to the purine base, respectively.

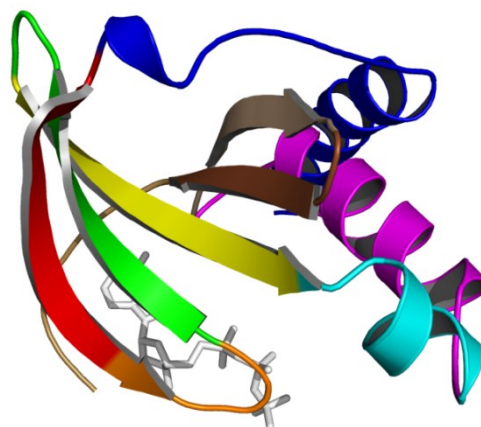


Figure 3: Crystal structure of ATP bound to PKA (pdb: 1ATP). The β -sheet core and the α -helical domains of the *N*-lobe are highlighted. The distal *N*-terminal α A-helix is shown in blue, further turning into the β 1 sheet (red). The β 2-sheet is shown in green followed by the β 3 sheet in yellow. The Gly-loop is depicted in orange. The α B-helix is coloured in cyan directly driving into the α C-helix (magenta). The β 4-sheet is coloured in sienna and the β 5 in brown followed by the hinge region in wheat. The ATP molecule is coloured in white and is covered by the β 1, β 2 sheet and the Gly-loop. The C-lobe, manganese ions, and the peptide inhibitor IP20 were omitted for clarity.^[13]

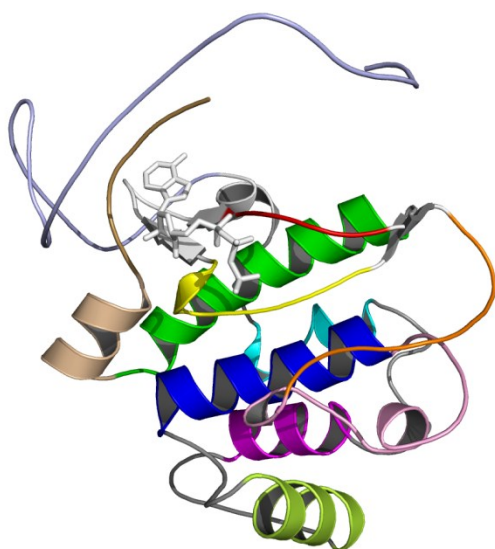


Figure 4: Crystal structure of ATP bound to PKA (pdb: 1ATP). The hinge region connecting the *N*-lobe and the *C*-lobe is coloured in wheat. The α D (ivory), α E (green), α F (blue), α G (olive), α H (magenta) and α I (cyan) form the helical core of the *C*-lobe. The catalytic loop is shown yellow; the phosphate binding site containing the DFG-motif is highlighted in red. Moreover, the activation segment is presented in orange, and the β 6- β 9 sheets in white. The ATP molecule is shown as white sticks. The *C*-terminal end is shown in light blue. The *N*-lobe, manganese ions, and the peptide inhibitor were omitted for clarity.^[13]

The second important AxK motif, located in the β 3 strand, fixes the phosphates of ATP towards the *C*-helix (Lys72 in PKA). Moreover, the β 3 strand further descends into the α B-helix and then into the α C-helix. The latter is very dynamic as well as flexible and acts as a crucial regulatory element in the protein kinase. Although, belonging to the *N*-lobe due to the primary sequence, it occupies an important structural position functionally connecting many different parts of the kinase. Thus, the α C-helix serves as a “signal integration motif”.^[22] Whereas, its *C*-terminus is connected via β 4 to β 5 and subsequently to the *C*-lobe, its *N*-terminus points towards the activation loop for efficient catalysis. The right positioning of the α C-helix is one of the crucial steps for the kinase catalysis defining the open and closed conformations.^[31] The α C-helix contains a highly conserved glutamate residue, Glu91 in PKA, which functionally interacts with Lys72 in the β 3-strand forming a salt bridge. The formation of this interaction is an

indispensable characteristic of the activated state of a kinase. Furthermore, this interaction, when the α C-helix is bound to the β -sheet core, induces a conformational change moving the entire rigid *N*-lobe and subsequently the Gly-loop, which forms interactions to the triphosphate of ATP.^[20]

2.1.2.2 The *C*-lobe

The large *C*-lobe consists mainly of α -helices, see Figure 4. The *C*-lobe helical subdomains are very stable and harbour the substrate binding site. Most of the α -helices (D, E, F, and H) backbone amides are oriented away from solvent,^[32,33] despite the α G-helix, which is solvent exposed. Four short β -strands, β 6 to β 9, contain most of the amino acid residues responsible for the catalytic transfer of the γ -phosphate from ATP to the protein substrate. Moreover, the anchoring of these loops to the helical core is mainly mediated by hydrophobic interactions. The catalytic loop is located between β 6 and β 7, whereas β 8 and β 9 flank conserved Asp-Phe-Gly (DFG) motif. The aspartate of the DFG motif, Asp184 in PKA, offers the chelating carboxyl group, which is urgently needed for magnesium ion complexation and subsequent ATP recognition, see Figure 8. The activation segment is followed by the F-helix, which is the most variable part in sequence and length throughout the kinome, offering the possibility to selectively turning a certain kinase off and on beside others.^[34–36] Moreover, it anchors firmly other motifs in the *C*-lobe including the catalytic loop, the P+1 loop, the activation segment, and the α H- α I loops via hydrophobic interactions. The remaining α G, α H and, α I helices, often termed as the GHI-domain, play an additional role as allosteric binding sites for substrate proteins and regulatory proteins.^[37]

2.1.2.3 The ATP Binding Site

The ATP binding site is highly conserved through the human kinome assuring its common recognition. In general, the active conformation is defined by several regions contributing to the γ -phosphate transfer. A flexible loop, the hinge region, connects the β 5-sheet of the *N*-lobe with the α D-helix of the *C*-lobe. Further, the *C*-lobe includes the activation segment, which is a region of a 20 to 35 amino acids covering sequences located between a conserved Asp-Phe-Gly motif (the DFG motif) and a less conserved Ala-Pro-Glu motif (APE motif).^[26,40] The main characteristic of the active conformation is the α C helix arranged towards the *N*-terminal lobe, and the aspartate of the DFG chelating an Mg^{2+} ion to preorganise the ATP substrate, “DFG-in”, see Figure 8.^[41] In opposite, in the inactive conformation the phenylalanine residue is turned into the ATP binding site, “DFG-out”, excluding a Mg^{2+} coordination.

The adenine ring forms specific hydrogen bonds between N1 and N6 to the main chain of the hinge region along with nonpolar aliphatic groups providing VAN-DER-WAALS contacts to the purine moiety, see Figure 6. Val57 in β 2 and Ala70 from the AxK-motif in β 3 form VAN-DER-WAALS contacts to the adenine ring of ATP in the same way as Leu173, which is located in the middle of β 7 and is always flanked by two hydrophobic residues, Leu172 and Leu174 in PKA.^[42] These two residues contact a hydrophobic residue from the α D-helix, Met128, which in turn is in touch with residues of the α F-helix (Leu227 and Met231). The hydroxyl groups of the ribose ring form hydrogen bonds to the side chain of Glu127 and the main chain carbonyl oxygen of Glu170, respectively. The triphosphate group is directed offside the adenosine pocket for optimal accessibility and transfer of the γ -phosphate to the peptide substrate. For the optimised orientation of the α - and β -phosphate groups the Glu91 residue, within the α C helix, and Lys72 as-

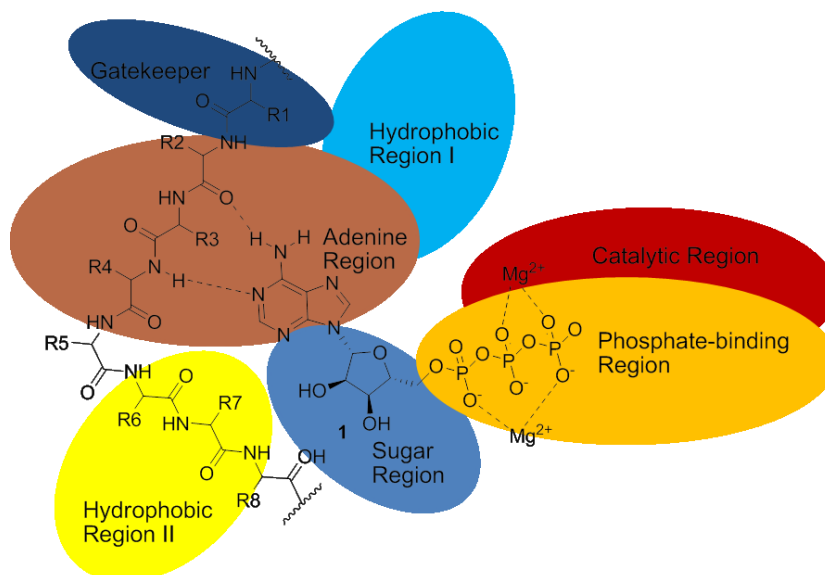


Figure 5: A schematic version of the interacting regions involved in adenosine triphosphate (1) binding to the catalytic site of PKA. The gatekeeper residue R1 is Met120 (dark blue) in PKA excludes large residues via sterical hindrances. The purine moiety of ATP forms two hydrogen bonds to the peptide backbone of R2 and R4 of the hinge region (sienna); in PKA residues Glu121 and Val123. The highly negatively charged triphosphate group is oriented towards the catalytic DFG motif (maroon) and is further enclosed by the glycine rich loop (dark orange). Moreover Mg^{2+} ions assist the preorganization of the triphosphate group. The ribose moiety forms polar interactions with the sugar binding region (blue). Two hydrophobic regions, the hydrophobic region I (cyan) and the hydrophobic region II (yellow) are poorly addressed by ATP.^[38,39]

sist the coordination. Furthermore, a network of interactions mediated by a magnesium ion, fixed by Asp184 of the DFG motif and Asn171, ensure correct positioning required for ATP binding and catalysis. A second magnesium ion chelated by Asp184 coordinates to the β - and γ -phosphate for further stability. Moreover, the compensation of the negative charges of the triphosphate group by the magnesium ions decreases electrostatic repulsion and facilitates the convergence of a nucleophilic reaction partner.^[43] The glycine rich loop further contributes to the stabilizing effect mediated by the interactions formed with the β - and γ -phosphate, see Figure 6.

Moreover, the HRD-motif is of special interest for the catalytic mechanism. In PKA the histidine of the HRD-motif is substituted by a tyrosine leading to the residues Tyr164, Arg165, and Asp166. Whereas the hydrophobic Tyr164 is part of the regulatory spine, Arg165 residue forms ionic interactions to the phosphorylated Thr197 mediating the conformational change of the activation loop to the rest of the enzyme.^[36] Furthermore, Asp166 is positioned to act as a weak catalytic base deprotonating the peptide substrate for eased nucleophilic attack.^[43,44]

An additional important role in protein kinase activation is occupied by the “gatekeeper” residue, Met120 in PKA, positioned at the *N*-terminal side of the hinge region, see Figure 6.^[45] An investigation of the human kinome reveals that 77% of the human kinases possess relatively large residues (Leu, Met, Phe) in opposite to 21%, mainly tyrosine kinases, bearing smaller gatekeeper residues (Thr, Val).^[46] The gatekeeper residue not directly inflicts the ATP binding, but mutagenesis of large gatekeepers to smaller residues allows the binding of bulky synthetic analogues of ATP, and consequently influences substrate selectivity.^[45]

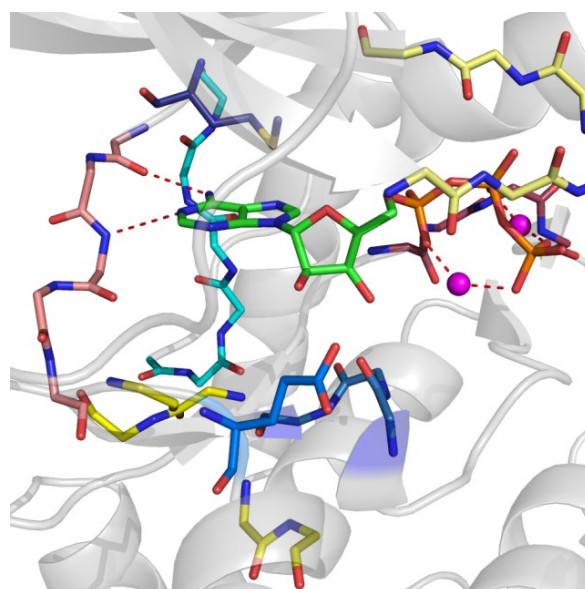


Figure 6: Crystal structure of adenosine triphosphate (1) bound to the catalytic site of PKA (pdb: 1ATP); three dimensional representation of Figure 5. ATP forms two hydrogen bonds to the hinge region (red dashes). The triphosphate group is coordinated by two Mg^{2+} ions (red dashes). Carbon atoms of ATP are colored in green. Carbon atoms of the gatekeeper residue are colored in dark blue. Carbon atoms of the hinge region are colored in sienna. Carbon atoms of the hydrophobic region I are colored in cyan. Carbon atoms of the hydrophobic region II are colored in yellow. Carbon atoms of the sugar region are colored in blue. Carbon atoms of the catalytic DFG residues are colored in maroon. Carbon atoms of the glycine rich loop are colored in dark orange. Magnesium ions are shown as magenta spheres. Oxygen atoms are colored in red, nitrogen in blue, phosphorus in orange and sulfur in yellow. The residual structure of PKA is represented as cartoon in grey. The side chains of the highlighted regions, except of the gatekeeper residue, were omitted for clarity.^[13]

2.1.2.4 The Substrate Binding Site

The substrate-binding is mainly mediated by the activation segment. Whereas, the activation segment of the inactive kinase conformation is often partially disordered, the catalytically competent active conformation, forming the peptide binding site, is triggered in many kinases by phosphorylation.^[12,14,15] For instance, Thr197 of PKA in its phosphorylated phosphothreonine state, acts as an organizing centre forming hydrogen bonds to the side chains of His87, Arg165, and Lys189.^[16] The resulting conformational changes promote closure of the

N- and *C*-lobe inducing the correct conformational arrangement of the activation segment for substrate binding. Although, the phosphorylation of a regulatory residue offers a control mechanism for kinase activation and many kinases are capable of adopting the correct activation segment conformation without a preceding phosphorylation, i.e.: phosphorylase kinase (PhK),^[47] epidermal growth factor receptor (EGFR),^[48,49] cyclin-dependent kinase 5 (CDK5).^[50] In some kinases, additional secondary structures in the activation segment further increase the substrate selectivity.^[51,52]

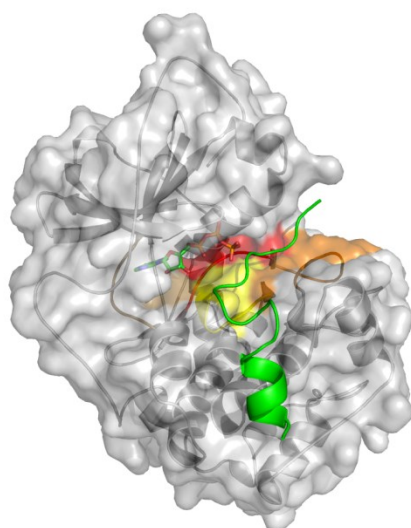


Figure 7: Crystal structure of ATP and peptide inhibitor IP20 bound to PKA (pdb: 1ATP). PKA is presented in grey with surface. The peptide inhibitor IP20 (green) occupies the substrate binding site. Beside the helical core of the *C*-lobe, the activation segment and the P+1 loop (orange) is mainly responsible for the peptide substrate binding. The residue of the peptide substrate for phosphorylation is oriented towards the catalytic region (yellow) and the DFG motif (red) for optimal phosphoryl group transfer.^[13]

Besides the highly conserved ATP binding site, all kinases share in common the orientation of the substrate, whereas the hydroxyl group is directed for functionalization directly towards the catalytic aspartate, Asp166 in case of PKA. In serine/threonine kinases, a lysine residue two residues next to the catalytic aspartate contacts the γ -phosphate and is assumed to stabilise the

developing negative charge during catalysis.^[43] In tyrosine kinases, the stabilizing amino acid is four residues away and is an arginine instead of a lysine offering more space for the larger tyrosine residue.^[53] Moreover, two additional chains of conserved hydrophobic residues, termed the catalytic and regulatory spines, which assemble as a response to changes within the catalytic site due to kinase activation and conduct those changes to the rest of the domain.^[34,35,54] The regulatory spine describes an assembly of interactions of residues located in the *N*- and *C*-terminal lobes and promoted by the conformational changes of the activation segment.^[40] Thus in turn, is responsive to peptide binding. Whereas, active kinases share a common catalytically competent conformation, the inactive kinases are structurally diverse especially in the conformation of the hydrophobic regulatory spine.^[55] This diversity is based on the abundance of catalytic requirements and constrains missing in the inactive state, allowing the different conformations.^[15,26,39,54] Although common structural themes across the kinome for the inactive form are existing, the possible conformations differ more extensively than the conformations of the active form. Therefore, addressing the inactive form offers possibilities to selectively address single kinases among others, see Chapter 2.1.5.

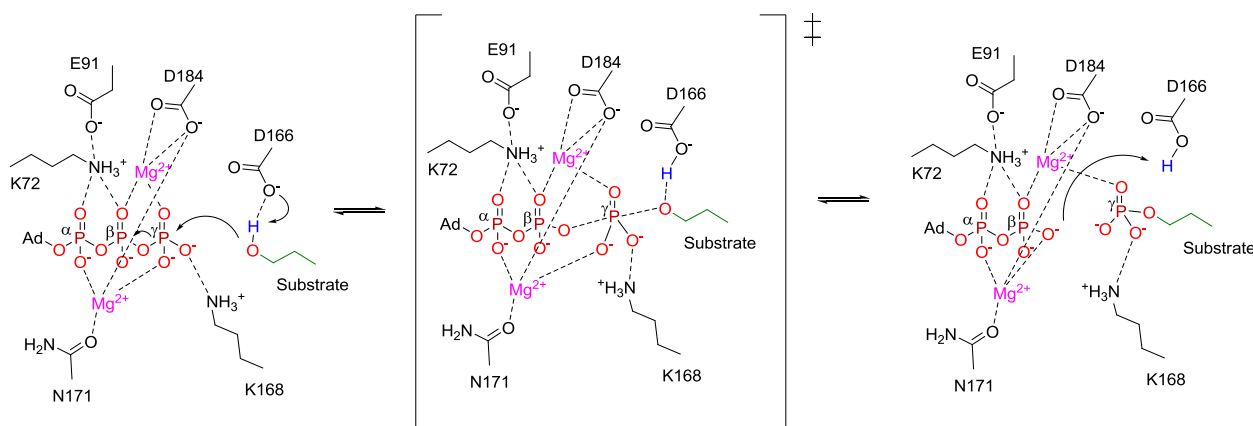
2.1.3 The Catalytic Mechanism of Phosphate Group Transfer

Protein kinases catalyse the transfer of the γ -phosphate from ATP to the hydroxyl group of serine, threonine, or tyrosine residues in protein substrates and recognise local regions around the site of phosphorylation. They usually phosphorylate sites of less ordered parts of the protein substrate exposed on the surface.^[56] This preference allows the kinase to induce an extended conformational change to the substrate protein fitting the catalytic site and allowing the

localization of specificity determining residues.^[57] Moreover in numerous kinases, remote docking sites located either offside the catalytic domain, i.e.: the mitogen-activated protein kinases (MAPKs),^[58] or on separate domains or subunits, i.e.: the Cdk2/cyclin complexes,^[59] contribute to an additional mechanism of target recognition and selectivity.

The chemical principle of the phosphorylate transfer step is simple and depends on the correct orientation of the two substrates. The γ -phosphate of ATP and the hydroxyl group of the serine, threonine, or tyrosine residue to be phosphorylated must be orientated in the right fashion based on the structural properties of the kinase, see Chapter 2.1. Kinetic studies using

a)



b)

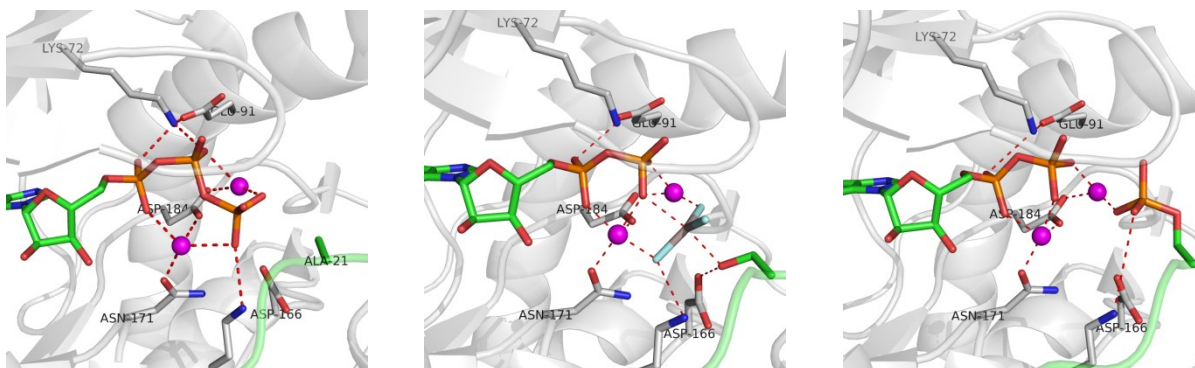


Figure 8: a) Mechanistic details of the γ -phosphate group transfer in the PKA binding site.^[7,43] Left: The triphosphate is preorganised for the catalytic reaction by a network of interactions. One magnesium ion (magenta) coordinates the α - and γ -phosphate, and is itself anchored by Asn171 and Asp184, whereas the second ion coordinates to the β - and γ -phosphate anchored by Asp184. Further, the Lys72 and Lys168 side chains form hydrogen bonds to the α - and β -phosphate, and to the γ -phosphate, respectively. Asp166 assists the deprotonation of the substrate hydroxyl group for phosphorylate group transfer. Middle: γ -phosphate in a trigonal-bipyramidal transition state. Right: γ -phosphate transferred to the substrate hydroxyl function. Oxygen atoms of the triphosphate group and the substrate are highlighted in red; magnesium ions in magenta, phosphor atoms in orange, the substrate carbons in green, and the substrate hydrogen in blue. Ad = Adenosine. **b)** Crystal structures of the phosphorylate group transfer from ATP to a substrate inhibitor molecule, reflecting the principles of a) in the PKA binding site. Left: The triphosphate group is preorganised as described above. Note that the peptide inhibitor IP20 has no serine residue being capable of accepting the γ -phosphate, thus bearing an alanine instead at this position for the crystallisation of ATP in the binding site, (pdb: 4DH3).^[60] Middle: AIF₃ is crystallised as a transition state mimic of the trigonal-bipyramidal form of the γ -phosphate during catalytic transfer together with ADP and magnesium ions in the ATP binding site of PKA, (pdb: 1L3R).^[29] In this, and the third case, the peptide inhibitor molecule offers a serine residue at the proper position. Right: The γ -phosphate group has been transferred to the substrate molecule SP20, (pdb: 4IAD).^[61] Carbon atoms of ATP and ADP are represented in green, phosphor atoms in orange, oxygen in red, nitrogen in blue. The peptide inhibitor IP20 and SP20 are shown as cartoon in green. PKA is shown as cartoon in grey as well as the carbon atoms of the highlighted residues.

$[\gamma\text{-}^{32}\text{P}]\text{-ATP}$ or radiolabelled peptide substrate with PKA indicate that both substrates have unrestricted access to the catalytic site.^[62] Moreover, the binding of one substrate does not exclude the other, although at high ATP concentrations, which are typical in the cellular media, there is a preference for sequenced binding with ATP first.^[62]

Thereafter, the phosphorylate group transfer reaction proceeds attacking the hydroxyl group of the substrate in a trajectory opposite and in line to the leaving β -phosphate group, leading to the Walden-inversion at the phosphorus atom of the γ -phosphate, indicating the absence of a phosphorylated kinase intermediate. This postulated geometry was supported by structural studies of PKA co-crystallised with the transition state analogue aluminium trifluoride, see Figure 8.^[29] Furthermore, the reaction mechanism highlights the importance of the coordinated magnesium ions stabilising the significant amount of negative charges and aiding the controlled release of ADP.^[43]

The transition state intermediate is discussed to be either dissociative, where the bond to the leaving group is broken before the new bond is formed, or associative, where the reaction proceeds through a pentavalent phosphorane intermediate with bond formation first by the attacking group or at least at the same time as bond breaking by the leaving group.^[63] Beside the phosphorylate group transfer mechanism, a base catalysis from the catalytic aspartate deprotonating the attacking hydroxyl group followed by a subsequent transfer of the proton to the reaction product facilitates the entire reaction cascade, see Figure 8 a).^[64] Nevertheless, deprotonation of the nucleophilic hydroxyl group in the early stages of the reaction is not a rate-limiting step.^[65] Once the substrates have been correctly oriented, the rate-limiting step is the release of products.^[62,64,66,67]

2.1.4 Kinases Related Disorders

The regulating mechanisms of protein kinases is based on the inhibition or activation of assembling protein partners,^[68] their phosphorylation,^[14,26,69,70] their cellular expression and localization,^[71] the limitation of substrates and activating cofactors, and their degradation.^[72–74] The dysregulation of protein kinase activity mediated by mutations leading to constitutively active forms, the loss of down-regulating mechanisms, or chromosomal rearrangements are associated with numerous disorders including cancer,^[75,76] neurodegenerative,^[77,78] neurologic,^[79] or cardiovascular disorders.^[80] Moreover, a detailed physiological and pathophysiological role of the investigated kinases during this work will be discussed in the results section in detail. Nonetheless, since the first description of protein kinases, they achieved special interest as drug targets, confirmed today by the numerous FDA approved small molecule compounds successfully applied in therapy.^[81] The increasing insights of the structural properties of the protein kinases had a significant impact on the development of selective and specific inhibitors.

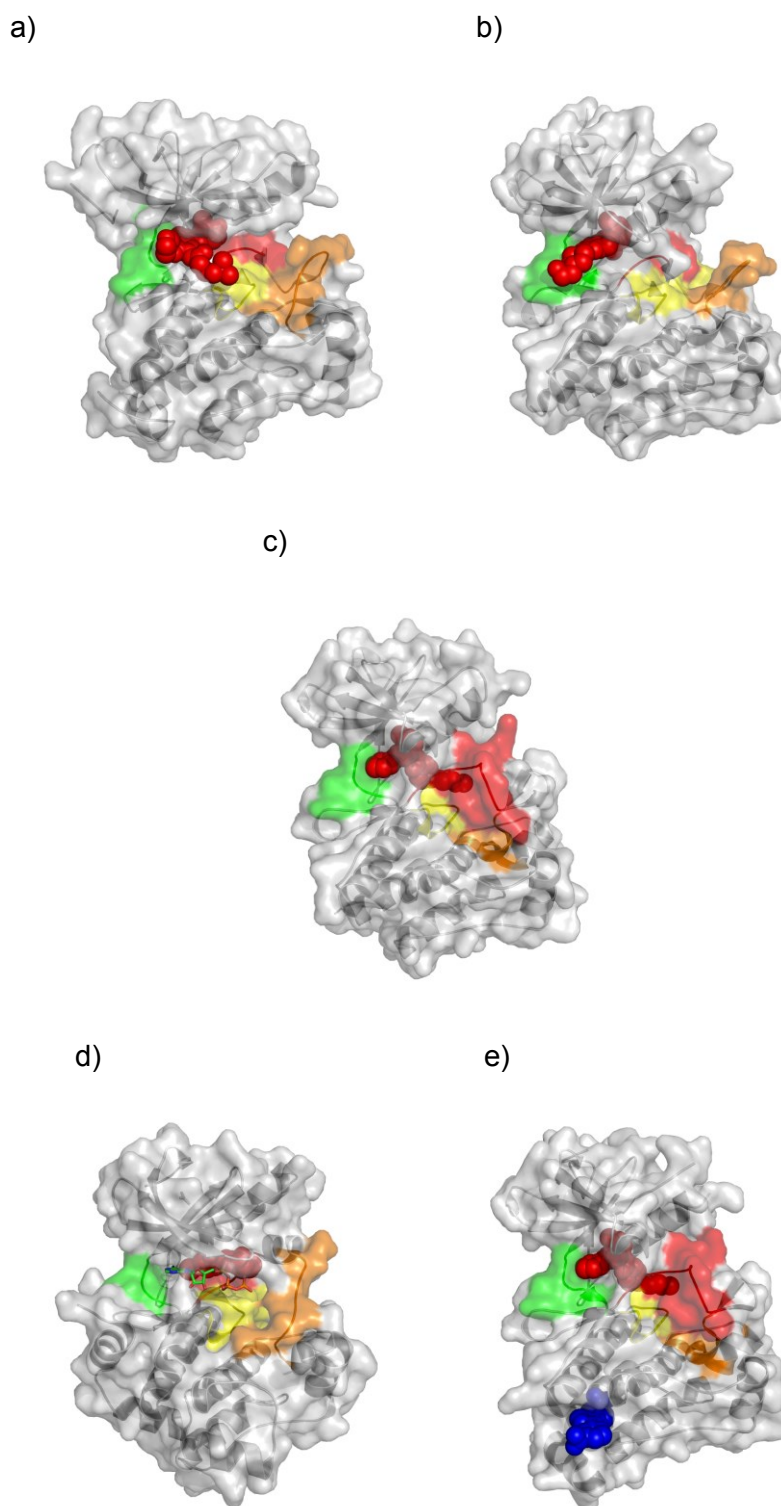


Figure 9: Comparison of different types of kinase inhibition mediated by small molecules. **a)** The irreversible inhibitor afatinib (**2a**) binds to a similar active conformation of EGFR (pdb: 4G5P) as observed for type I inhibitors.^[82] **b)** Type I inhibitors like dasatinib (**3**) bind to the active conformation of the target kinase, here BCR-ABL (pdb: 2GQG),^[83] with the DFG in motif. **c)** Type II inhibitors like imatinib (**4**) bind to the inactive DFG out conformation of the target kinase BCR-ABL (pdb: 1IEP).^[84] Moreover, the P+1 loop contributing to peptide substrate recognition is disordered. **d)** Type III inhibitors like TAK-733 (**6**) bind to an adjacent allosteric pocket next to the ATP binding site and still allow the binding of ATP (**1**) to target kinase, here MEK1 (pdb: 3PP1).^[85] **e)** Finally, type IV inhibitors like GNF-2 (**7**) (blue spheres) bind to an allosteric site remote the ATP binding site of BCR-ABL (pdb: 3K5V) occupied by imatinib (**4**) in the inactive conformation.^[86] All inhibitors binding to or next to the ATP binding site are presented as red spheres; ATP is presented as sticks with the carbon atoms in green. The hinge region is coloured green, the catalytic loop in yellow, the activation loop with the DFG motif in red, and the P+1 loop in orange. All kinases are represented as cartoon in grey with the surface in grey.

2.1.5 Mechanisms of Kinase Inhibition

Small-molecule kinase inhibitors represent useful tools to investigate and evaluate kinase functions in numerous cellular activities. Nevertheless, due to the highly conserved domains targeting selectively single kinases among others was assumed to be an unconvertible challenge, unless the first selective kinase inhibitors against the epidermal growth factor receptor (EGFR) were reported in the late 1980s.^[87,88] This incidence as a starting point, led to a large number of kinase inhibitors with various structural scaffolds and selectivity profiles aiding to elucidate the molecular recognition of kinase/inhibitor interactions.^[89,90]

The majority of kinase inhibitors target the ATP binding site, which is formed between the *N*- and *C*-lobe, to perturb the ATP fixation; see also Chapter 2.1.2.3. The flexible activation loop containing the DFG motif controls the access to the active site, see Figure 4.^[91] In principle the developed kinase inhibitors can be divided into two classes covering the irreversible and reversible ones. The former ones bind covalently with a reactive nucleophilic cysteine residue adjacent to the ATP binding site resulting in a permanent irreversible extrusion of ATP. In opposite, reversible inhibitors compete with ATP and do not form permanent covalent modifications with the target kinase. Moreover, they are subdivided into four main types based on the conformation of the kinase occupied during binding, see Figure 9.^[92,93] Nevertheless, a strict discrimination into the classes are not always appropriate since some kinase inhibitors, i.e.: bi-substrates and bivalent inhibitors (type V),^[94] exhibit more than one of the mentioned binding modes.

Most of the clinically approved kinase inhibitors are tyrosine kinase inhibitors,^[95] a few are serine/threonine kinase inhibitors, and only one is a lipid kinase inhibitor.^[96] Mechanistically, 26 are

reversible inhibitors and only two are irreversible inhibitors. Moreover, only one type III inhibitor is approved so far, although several promising allosteric kinase inhibitors are being currently in clinical trials at different stages.^[81] Detailed review discussing FDA approved small molecule kinase inhibitors are provided in literature.^[81]

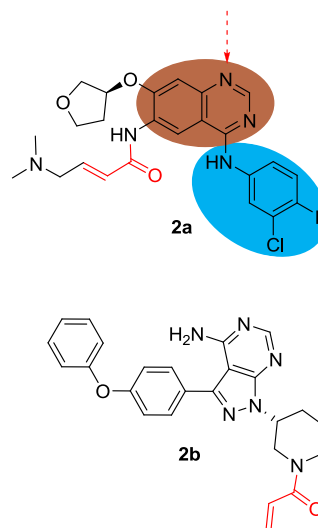


Figure 10: Chemical structure of afatinib (**2a**) and ibrutinib (**2b**). In both inhibitors a MICHAEL acceptor moiety highlighted in red covalently connects the compounds to their corresponding target kinases. In case of afatinib, the residues interacting with specific regions of the ATP binding site are coloured according to Figure 5. The quinazoline core occupies the adenine region, whereas the 3-chloro-4-fluoro-aniline residue is steered to the hydrophobic region I. The quinazoline ring forms a hydrogen bond to the hinge region (red dashed arrow). The *N,N*-(dimethylamino)-but-2-enamide residue contains the MICHAEL acceptor moiety forming the covalent bond to the Cys797 side chain of EGFR.

2.1.5.1 Irreversible Kinase Inhibitors

Currently, two irreversible kinase inhibitors are approved by the FDA, first the EGFR inhibitor afatinib (**2a**), followed shortly by the Bruton's tyrosine kinase (BTK) inhibitor ibrutinib (**2b**).^[97,98] Both of them incorporate a MICHAEL acceptor moiety in their scaffold forming a covalent bond with a reactive cysteine residue in the active site of the appropriate target kinase. Despite the achieved specificity and potency, concerns regarding potential toxicities have to be

considered during the design of irreversible inhibitors to avoid unspecific covalent modification of off-targets.^[99] Nevertheless, the success of these two examples of kinase inhibitors, i.e.: ibrutinib is expected to reach US\$ 9 billion in 2020,^[100] should emphasise further drug design endeavours to consider irreversible inhibitors as a true alternative to develop inhibitors with increased selectivity and potency profile.

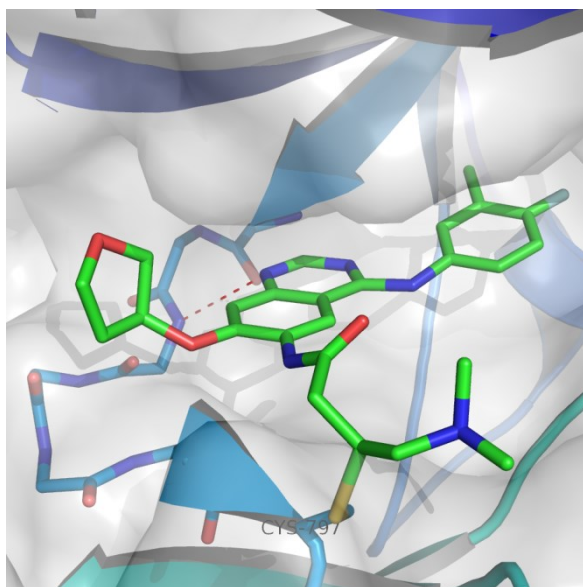


Figure 11: Crystal structure of afatinib (**2a**) bound to the active site of EGFR (pdb: 4G5P). The quinazoline moiety forms a hydrogen bond with the main chain of the hinge region residue Met793 (red dashes). The reactive cysteine residue of Cys797 forms a covalent C–S bond with the MICHAEL acceptor enone group at the edge of the active site in the C-lobe. The carbon atoms of afatinib are presented in green. Nitrogen atoms are shown in blue, oxygen atoms in red, chlorine in green, fluorine in light cyan, and sulfur in yellow. EGFR is presented as cartoon with the surface in grey and the hinge region as sticks.^[82]

However, the detailed mechanism of irreversible inhibitor interaction is best highlighted on the example of afatinib (**2a**). The crystal structure of afatinib bound covalently to the wild type EGFR is shown, see Figure 11. It is noteworthy, that afatinib shows apparently a type I binding, very similar to other approved reversible EGFR inhibitors due to the same common anilinoquinazoline core. For instance, a conserved hydrogen bond is formed between hinge residue Met793 and the quinazoline moiety of the aromatic ring system. The reactive cysteine

residue Cys797 forms the covalent C–S bond with the MICHAEL acceptor enone group at the edge of the active site in the C-lobe.^[82]

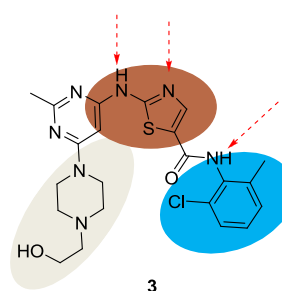


Figure 12: Chemical structure of dasatinib (**3**). The residues interacting with specific regions of the ATP binding site are coloured according to Figure 5. The thiazole core occupies the adenine region, whereas the 2-chloro-6-methylaniline residue is steered to the hydrophobic region I. The piperazine moiety with the attached hydroxyethylene residue is solvent exposed. The thiazole core forms two hydrogen bonds hinge region region, and the aniline residue forms one additional hydrogen bond to the gatekeeper residue Thr315 (red dashed arrows).

2.1.5.2 Type I Kinase Inhibitors

Type I inhibitors are ATP competitive inhibitors binding to the active conformation of the target kinase with the aspartate residue of the DFG motif oriented into the active site. For instance, dasatinib (**3**), as a type I inhibitor, binds to BCR-ABL with the fully extended activation loop ready for substrate binding. In case of dasatinib, see Figure 13, the nitrogen of the heteroaromatic thiazole core and the adjacent bridging amino group form hydrogen bonds with the amid backbone of the hinge residue Met318. The aliphatic hydroxyethylpiperazinyl residue is solvent exposed, whereas the terminal 2-chloro-6-methyl aniline group is oriented towards the hydrophobic pocket I. The latter further interacts via the bridging amide with the gatekeeper by hydrogen bond formation. All compounds addressing the hydrophobic region I are affected by mutation-related drug resistance often mediated by a T315I mutation leading to steric shielding of this important grove, see Chapter 2.1.5.3.^[101]

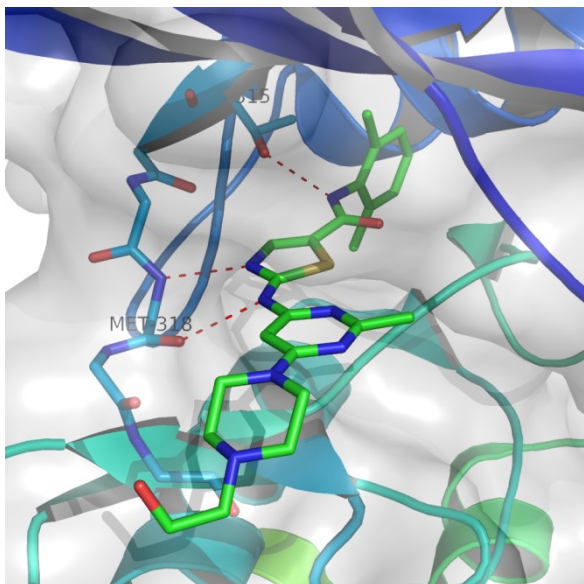


Figure 13: Crystal structure of dasatinib (**3**) bound to the active site BCR-ABL (pdb: 2GQG). The thiazole core forms two hydrogen bond with the main chain of the hinge region residue Met318; an additional hydrogen bond is formed between the aniline residues and Thr318 (red dashes). The carbon atoms of dasatinib are presented in green. Nitrogen atoms are shown in blue, oxygen atoms in red, chlorine in green, and sulfur in yellow. BCR-ABL is presented as cartoon with the surface in grey and the hinge region as sticks.^[83]

2.1.5.3 Type II Kinase Inhibitors

In contrast to the type I inhibitors, the type II inhibitors bind to the inactive forms of the target kinase where the aspartate residue of the DFG motif is oriented outwards of the ATP binding. Moreover, kinases differ in their inactive conformations more extensively than in their active conformation and subsequently offering more differentiable interaction sites, see Chapter 2.1.2.3. Thus, the type II inhibitors exploiting these specific pockets adjacent to the ATP-binding site offer the potential for increased selectivity.

However, BCR-ABL was the first kinase, which was addressed by the first successfully approved small-molecule inhibitor imatinib (**4**).^[102] Beside the revolutionary success for the treatment of patients suffering on chronic myeloid leukemia (CML),^[103] imatinib induced a “gold fever” in the inhibitor development of kinases as druggable therapy targets. Numerous SAR studies

using imatinib led to the design of whole classes of second generation inhibitors and provided a deeper understanding of the inhibition mechanism.^[104,105] Thus, the acting mechanism of type II inhibitors is best highlighted using imatinib as a model.

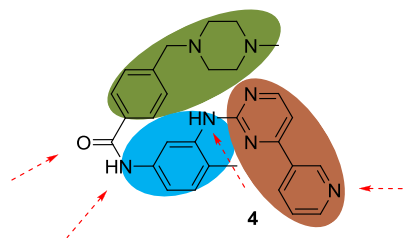


Figure 14: Chemical structure of imatinib (**4**). The residues interacting with specific regions of the ATP binding site are coloured according to Figure 5. The pyridinylprimidine residue occupies the adenine region, whereas the 4-methylbenzene-1,3-diamine core is steered to the hydrophobic region I. The piperazine moiety binds to an allosteric pocket formed by the DFG out motif (olive). Hydrogen bonds were formed mainly by the 4-methylbenzene-1,3-diamine and the pyridine residue (red dashed arrows).

Imatinib binds to the inactive BCR-ABL with the DFG motif occupying the ‘out’ conformation by addressing three different binding pockets, see Figure 14. The 4-(pyridin-3-yl)pyrimidine moiety of imatinib forms a conserved hydrogen bond to the backbone of the hinge residue Met318. The bridging 4-methylbenzene-1,3-diaminyl core occupies the hydrophobic pocket I, whereas the adjacent amine, connecting the 4-(pyridin-3-yl)pyrimidine moiety group, forms a hydrogen bond with the side chain of the gatekeeper residue Thr315. Moreover, the terminal 4-((4-methylpiperazin-1-yl)methyl)benzoic acid, connected via an amide group to the 4-methylbenzene-1,3-diaminyl core, binds to an allosteric pocket, which is formed by DFG out conformation. Furthermore, bidentate ionic interactions with His361 and Ile360 are formed by the methyl piperazinyl group. Closing, the set of molecular interactions is completed by hydrogen bonds formed by the amide group and both the Glu286 and Asp381, see Figure 15.^[84]

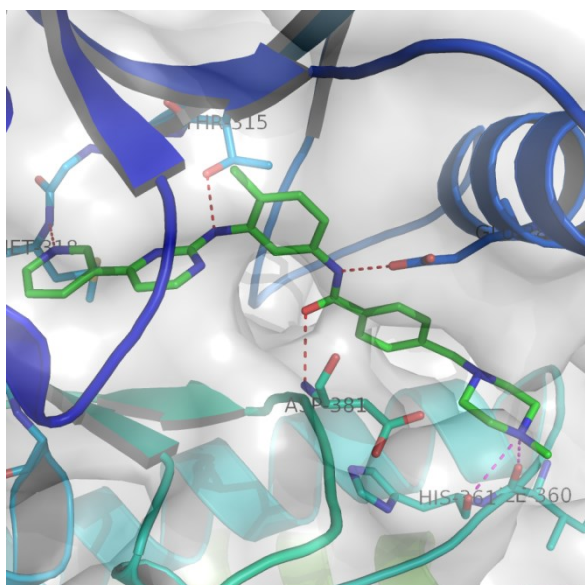


Figure 15: Crystal structure of imatinib (**4**) bound to the active site BCR-ABL (pdb: 1IEP). The pyridinyl-pyrimidine moiety forms a hydrogen bond to the main chain of Met318 (red dashes). The 4-methylbenzene-1,3-diamine core forms two hydrogen bond with the side chain residues of Thr315 and Glu286, whereas the carbonyl oxygen of the amide group forms a hydrogen bond to the main chain of Asp381. The 4-((4-methylpiperazin-1-yl)methyl) benzoic acid residue of imatinib occupies an allosteric binding region only accessible due to the DFG out conformation of BCR-ABL. Beside the hydrophobic interactions, ionic interactions (magenta dashes) between the terminal tertiary nitrogen of the piperazine with His361 and Ile360 complete the set of attracting interactions. The carbon atoms of imatinib are presented in green. Nitrogen atoms are shown in blue, oxygen atoms in red, and sulfur in yellow. BCR-ABL is presented as cartoon with the surface in grey and the hinge region as sticks.^[84]

Despite high efficacy and limited toxicity compared to traditional chemotherapeutic drugs, point mutations, in the kinase domain of BCR-ABL, especially of the gatekeeper residue, led to the development of drug resistance against imatinib.^[106–108] Several potential explanations of this resistance have been discussed; however, a mutation towards larger gatekeeper residues stabilises the R-spine more efficiently than threonine, subsequently shifting the equilibrium to the active conformation instead of the imatinib recognised inactive conformation.^[109] Such a stabilization, in combination with simple steric blocking of the binding site,^[110] prevents the binding of imatinib, and inevitably creates a constitutively active oncogenic kinase. To overcome these resistance mechanisms a proceeding

development of next generation compounds is necessary to ensure a fast substitutional therapy.^[111] Indeed, next-generation drugs like nilotinib,^[112] dasatinib,^[113] or ponatinib^[114] were developed overcoming drug resistance towards imatinib, and the latter even tolerates the gatekeeper mutation.^[115]

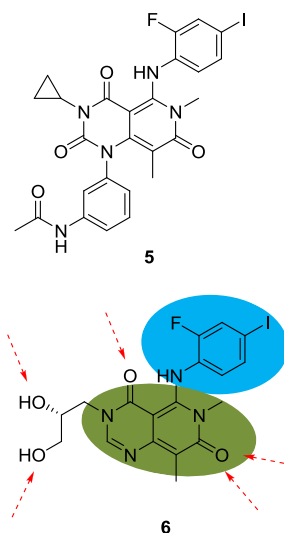


Figure 16: Chemical structure of trametinib (**5**) and TAK-733 (**6**). Specific regions of the ATP binding site are coloured according to Figure 5. TAK-733 as a trametinib derivative crystallised in MEK1 acts as a surrogate to elucidate the molecular interactions of type III kinase inhibitors. The pyridopyrimidine core of TAK-733 interacts with an allosteric pocket (olive) adjacent to the ATP binding site, whereas the halogenated phenylaminy substituent occupies a MEK selective hydrophobic pocket I (cyan). Moreover, hydrogen bonds are formed between the dihydroxypropyl group and the ATP phosphate as well as Lys97, between the carbonyl group of the pyrimidine moiety and Lys97, and between the oxygen in the pyridine moiety to Val211 and Ser212 (red dashed arrows).

2.1.5.4 Type III Kinase Inhibitors

The type III inhibitors bind exclusively in an allosteric pocket adjacent to the ATP binding site. The only FDA approved type III kinase inhibitor so far is trametinib targeting MEK1 and MEK2. It was developed based on a high-throughput screening (HTS) hit and subsequent SAR studies, driven by growth inhibitory activity against cancer cell lines,^[116] guided by the structural features of established MEK inhibitors.^[117]

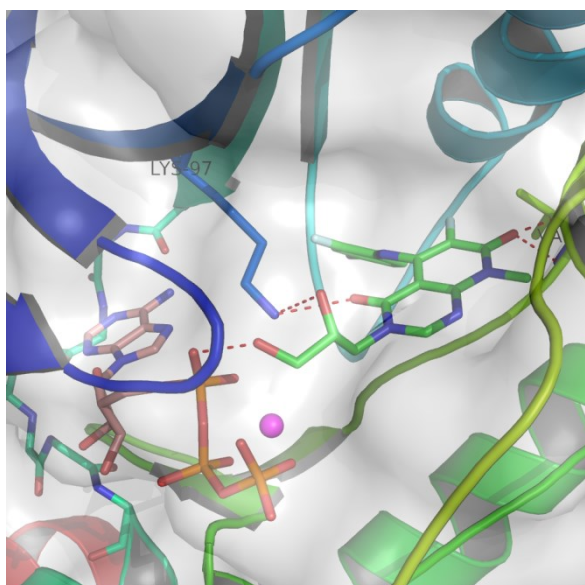


Figure 17: Crystal structure of TAK-733 (**6**) and ATP (**1**) bound to the allosteric and the MEK specific hydrophobic pocket I (pdb: 3PP1). The pyridopyrimidine core of TAK-733 interacts with the allosteric pocket adjacent to the ATP binding site, whereas the halogenated phenylaminy substituent is steered to the MEK selective hydrophobic pocket I. The dihydroxypropyl group and the ATP phosphate as well as Lys97, the carbonyl group of the pyrimidine moiety and Lys97, as well as the oxygen in the pyridine moiety and Val211 and Ser212 form hydrogen bonds (red dashes). The carbon atoms of TAK-733 are presented in green. The carbon atoms of ATP are presented in wheat. Nitrogen atoms are shown in blue, oxygen atoms in red, sulfur in yellow, and the magnesium ion as magenta sphere. MEK1 is presented as cartoon with the surface in grey and the hinge region as sticks.^[85]

Although the co-crystal structure of MEK1 or MEK2 with trametinib could not be achieved by now, an analogue of trametinib, TAK-733, was crystallised successfully in complex with MEK1, see Figure 17, which also showed a type III binding mode and is therefore discussed as a surrogate. The pyridopyrimidinedione core occupies an allosteric pocket in direct proximity to the ATP binding site with hydrogen bond formations of both the oxygen on the pyridine moiety to Val211 and Ser212, as well as the oxygen of the pyrimidine moiety to Lys97. The attached 2-fluoro-4-iodoaniline moiety acts as a MEK-selective recognition motif for the hydrophobic pocket I. The terminal dihydroxypropyl chain forms hydrogen bonds with both hydroxyl functions to the ATP α -phosphate and Lys97 respectively.^[85] Type III inhibitors, like trametinib, are valua-

ble tools to modify kinase activity distinct to type I or type II inhibitors, and as in case for the combination strategy along with the B-Raf inhibitor dabrafenib, they offer diverse possibilities to overcome resistance mechanism.^[118,119]

2.1.5.5 Type IV Kinase Inhibitors

The type IV inhibitors bind to an allosteric site completely offside the ATP binding pocket.^[120] Currently, they are no FDA approved type IV kinase inhibitors in use; although several candidates are in different clinical stages.^[121–124] For instance, GNF-2 is a highly selective non-ATP competitive inhibitor of BCR-ABL ($IC_{50} = 0.14$ mM).^[125] The allosteric myristoyl pocket located near the carboxyl terminus of the ABL kinase domain was discovered as the precise binding site of GNF-2 to the BCR-ABL fusion protein by both NMR and X-ray experiments.^[126–128] GNF-2 replaces the myristoylated peptide occupying an extended conformation with the trifluoromethyl group buried at the same cleft as originally occupied by the final two carbons of the myristate ligand, see Figure 19. Moreover, a favourable, but probably weak, polar interaction between one fluorine atom and the main chain of Leu340 can be described, along with water-mediated hydrogen bonds. No direct hydrogen bonds with the protein can be observed, thus confirms the binding mediated mainly by hydrophobic interactions.

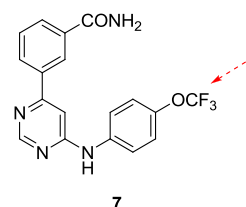


Figure 18: Chemical structure of GNF-2 (**7**). GNF-2 binds to the myristate binding site of BCR-ABL remote the ATP binding site and the catalytic cleft. The molecular interactions are mainly driven by hydrophobic interactions, although a weak polar interaction between one fluorine atom and Leu340 can be assumed (red dashed arrow).

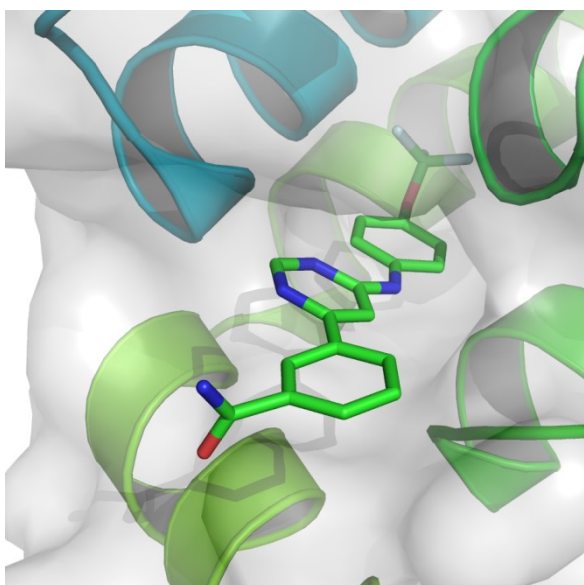


Figure 19: Crystal structure of GNF-2 (**7**) bound to the myristate binding site of BCR-ABL remote the ATP binding site (pdb: 3K5V). The 4-trifluoromethoxy-phenylaminy residue is steered deep into the C-terminal α -helices, whereas the benzamide moiety is solvent exposed. The carbon atoms of GNF-2 are presented in green. Nitrogen atoms are shown in blue, oxygen atoms in red, and fluorine in light cyan. BCR-ABL is presented as cartoon with the surface in grey.^[86]

Nevertheless, allosteric inhibitors are likewise affected by resistance mechanisms.^[86] For instance, mutation of three residues near the entrance of the myristate-binding site (C464Y, P465S and V506L) is found to evoke GNF-2 resistance, presumably caused by steric reasons. However, as described for type III inhibitors, a combination of inhibitors, acting according to different mechanisms, lead to increased selection pressure on oncogenic kinases. Therefore, the likeliness of a kinase successfully handling two distinct binding sites to overcome inhibition by alterations via mutagenesis is significantly decreased. For instance, the simultaneous binding of a myristoyl mimic and an ATP-competitive inhibitor results in the inhibition of both the wild-type and the T315I BCR-ABL kinase activity and cell growth.^[86]

2.2 Metal Complexes as Kinase Inhibitors

The MEGGERS group established a variety of different transition metals as structural templates to gain access to highly sophisticated organometallic complexes serving as catalysts for asymmetric reactions,^[129–132] as DNA intercalators and binders,^[133–135] biorthogonal catalysts,^[136,137] photosensitiser,^[138,139] or as highly potent and selective kinase inhibitors.^[140–142]

Remarkably, the MEGGERS group established the pyridocarbazole pharmacophore ligand, derived from staurosporine, as a bidentate ligand for metal complexation, which proved to be part of highly selective and specific kinase inhibitors with potential anticancer effects, see Figure 21.^[143–145] However, the initial ruthenium based kinase inhibitors elaborated in the MEGGERS group were half-sandwich complexes coordinated to a cyclopentadienyl ligand beside the mentioned pyridocarbazole pharmacophore and a monodentate ligand completing the coordination sphere.^[146]

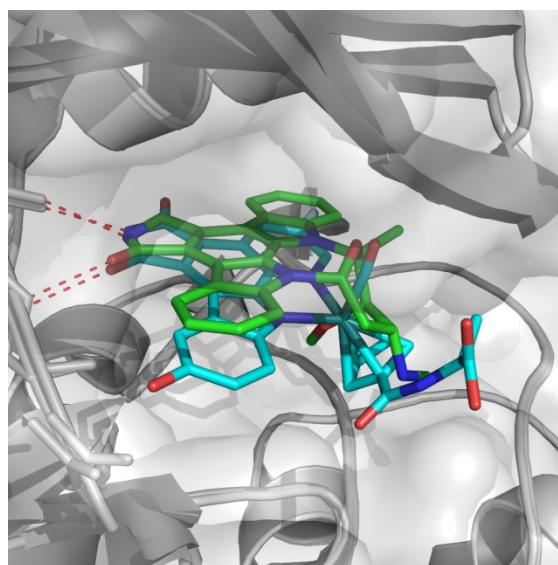


Figure 20: Superimposed crystal structures of staurosporine (**8**) bound GSK-3 β (pdb: 1Q3D) and organometallic inhibitor (*R*)-**10** bound GSK-3 β (pdb: 2JLD). An almost identical position of the indolocarbazole moiety of staurosporine and the pyridocarbazole ligand of (*R*)-**10** in the ATP binding site can be observed forming identical hydrogen bonds to the main chain of Tyr134. The carbon atoms of staurosporine are presented in green and the carbon atoms of (*R*)-**10** are presented in cyan. Nitrogen atoms are shown in blue, oxygen atoms in red, fluorine in light cyan, and the ruthenium core in teal. GSK-3 β is presented as cartoon and the hinge region as sticks with the surface in grey.^[146]

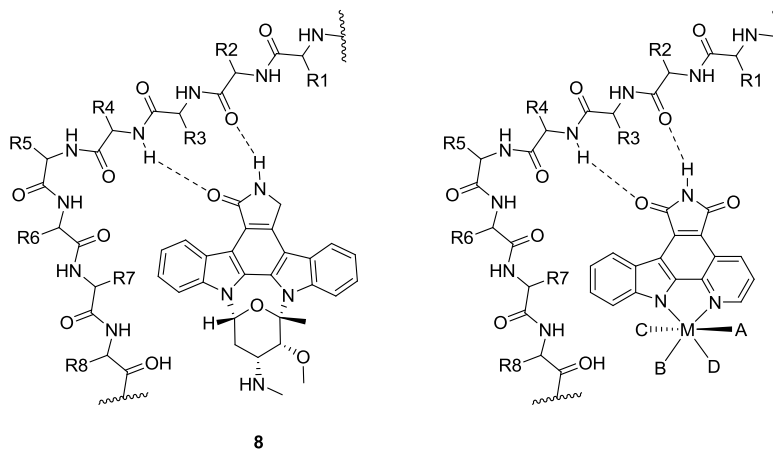


Figure 21: Staurosporine (**8**) serves as a lead structure for metal based kinase inhibitors. The bidentate pyridocarbazole pharmacophore ligand mimics the indolocarbazole moiety of staurosporine and mediates hydrogen bonds to the hinge region as it is true for staurosporine.

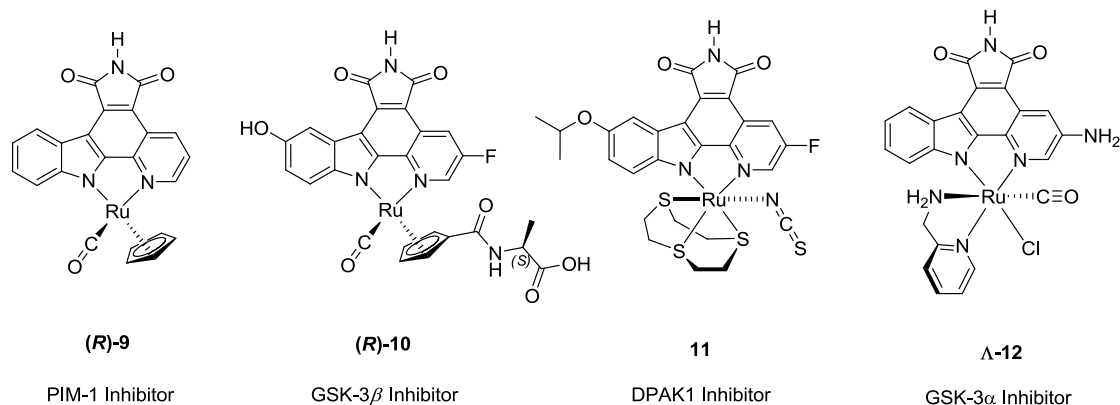


Figure 22: The development of metal based kinase inhibitors led from initial half-sandwich complexes to highly sophisticated octahedral complexes with increasing structural diversity. The shown isomers of (R)-9, (R)-10 and Λ-12, are the more potent ones, whereas 11 is as racemic mixture of two enantiomers both existing as thiocyanate and isothiocyanate.^[147–149]

Subsequent developments led to modifications of the cyclopentadienyl ligand, of the pyridocarbazole ligand, and of the monodentate ligand, see Figure 22.^[147–149] Moreover, the metal core of the kinase inhibitors itself was substituted by a variety of transition metals covering platinum, rhodium, rhenium, osmium, or iridium.^[138,150–153] However, the ambition to establish metals as structural templates lead from initial half sandwich complexes to highly sophisticated octahedral complexes by establishing a variety of ligand scaffolds as part of metal based kinase inhibitors.^[140,143–145,152,154]

Indeed, it is an obvious fact that a tetravalent carbon with its possible two enantiomers is no comparison in its complexity to a hexavalent metal ion with 30 possible structural isomers in case of six distinguishable monodentate ligands, see Figure 23.^[155] But on the other hand, this enormous number of possible stereoisomers has a high demand of well elaborated methods to selectively synthesise the desired structures over the undesired ones. This bidentate pyridocarbazole pharmacophore ligand as a prerequisite for the mentioned purpose of the organometallic compounds, influences the number of possible structural isomers. Whereas, half-sandwich complexes, containing at least one bidentate ligand, form only two enantiomers, octahedral complexes can reach up to 24 different structural iso-

mers using four distinguishable monodentate ligands.^[147,156] Moreover, introducing multidentate ligands into the organometallic complex scaffold further alter the possible number of structural isomers. Since, initially octahedral complexes were designed containing C₂-symmetric ligands, like 1,4,7-trithiacyclononane in complex 11, simplifying the mentioned challenge, more and more sophisticated modified ligands were developed addressing unexplored chemical space, like Λ-12.^[157]

The specificity and selectivity of organometallic compounds against their target kinases of the human kinome are highly dependent on the globular shape and the ligand sphere which is built by the coordinated ligands.^[140,158] Therefore, the consequent development of these organometallic compounds as kinase inhibitors from half-sandwich complexes to octahedral ones is accompanied by the increase of the chances as well as the challenges of the feasibility of particular structural isomers.^[159,160] As the target interaction structures are biomolecules consisting of chiral building blocks, they create a chiral environment which recognises sensitively complementary structures and excludes mismatching ones.^[161] Therefore, methods for the asymmetric synthesis of octahedral organometallic complexes to obtain certain desired structural scaffolds, ideally designed to a correspond-

ing binding site of a target biomolecule, are highly appreciated,^[140,152,159,161] and many articles report about the structural potential disclosed by multivalent organometallic complexes and the associated challenges.^[155,162–167]

2.3 Octahedral Complexes – Taming the Structural Scope

Many ways to control the metal centered relative and absolute stereochemistry have been published with different advantages and disadvantages. In principle, the approaches can be clustered in several groups controlling the relative and absolute stereochemistry via chiral ligands, chiral anions, chiral auxiliaries, or even via catalytic asymmetric synthesis.^[132,162,168–177] However, the approach of these methods must be correlated to the requirements of an organometallic compound being capable of acting as a kinase inhibitor simultaneously.

Structural restrictions of the ligands inevitably lead to the discrimination of certain structures over others. These structural restrictions are mostly represented by chirality introduced into the ligand system; either in the scaffold in direct proximity of the coordinating atoms of a multidentate ligand or via sophisticated linkers which preorganise the ligand for complexation.^[171,172,178–181] For instance, the binaphthyl core of the (S)-2,2'-(1,1'-binaphthyl-2,2'-diyl)bis(7-*tert*-butylquinolin-8-ol) ligand (S)-**13** incorporates an axial chirality into the tetradentate ligand subsequently leading to chirality transfer to the metal core favouring the shown conformation of *cis*- β - Λ -(S)-**14**, Scheme 1. In opposite, the (S, S)-[4,5]-chiragen-[6] ligand **15** projects its chiral information to the metal centre via the aliphatic linker. Both dimethylbicyclo[3.1.1] heptane moieties of **15** act as conformational anchors restricting the possible coordination patterns of the peripheral bipyridinyl residues mediated by the linker. Although, the coordination leads to significant loss of the number of degrees of freedom for the spacious ligand **15** resulting in

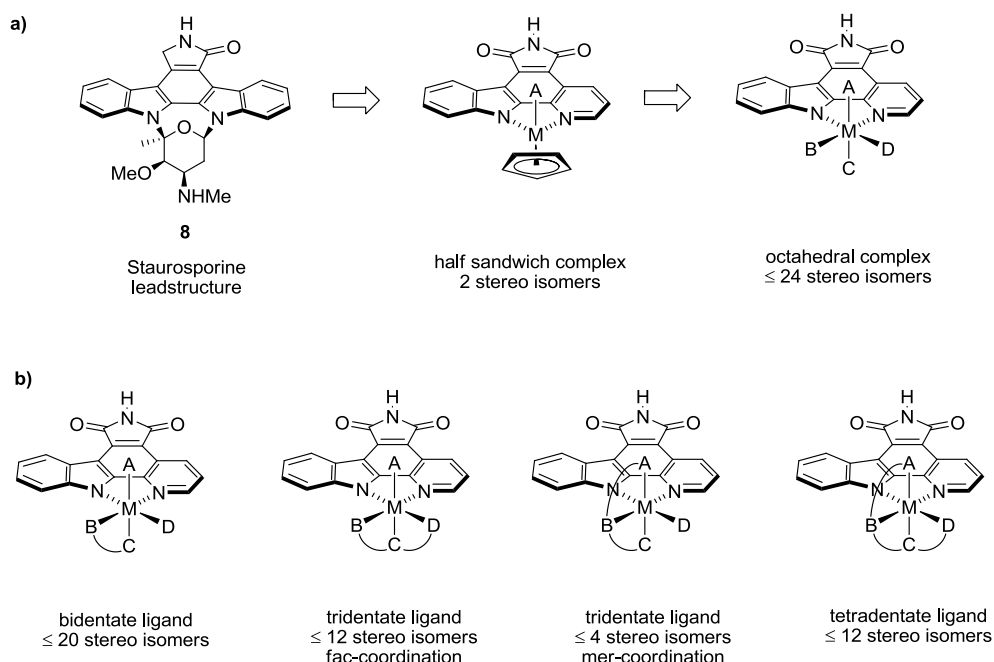
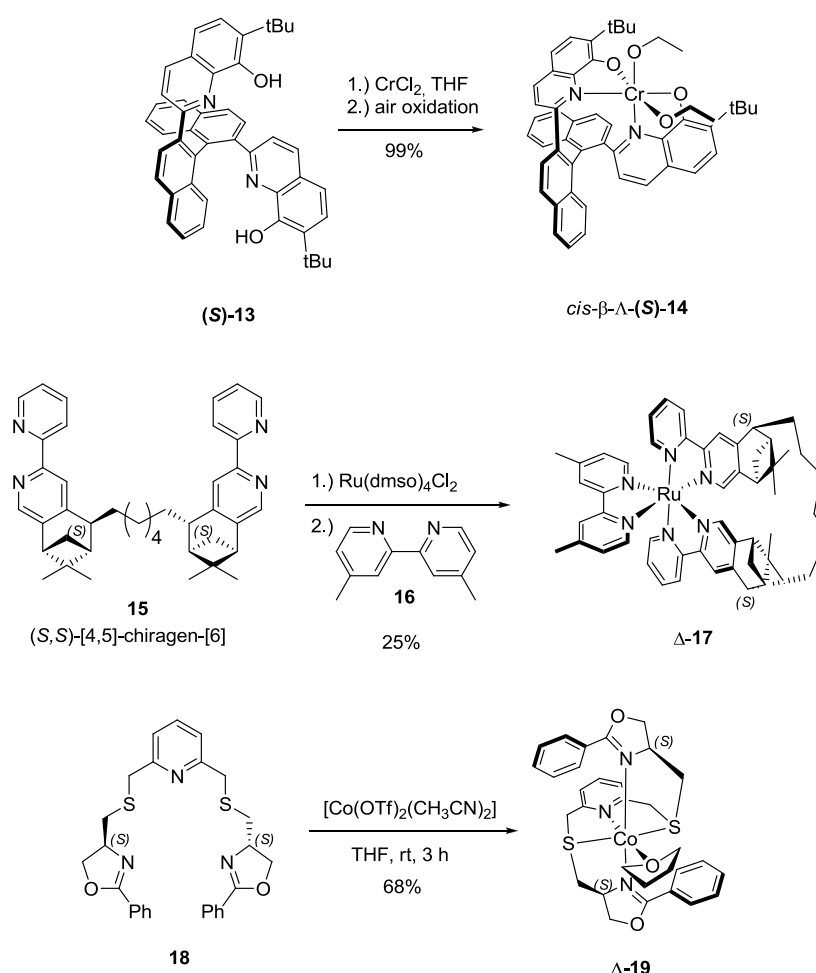


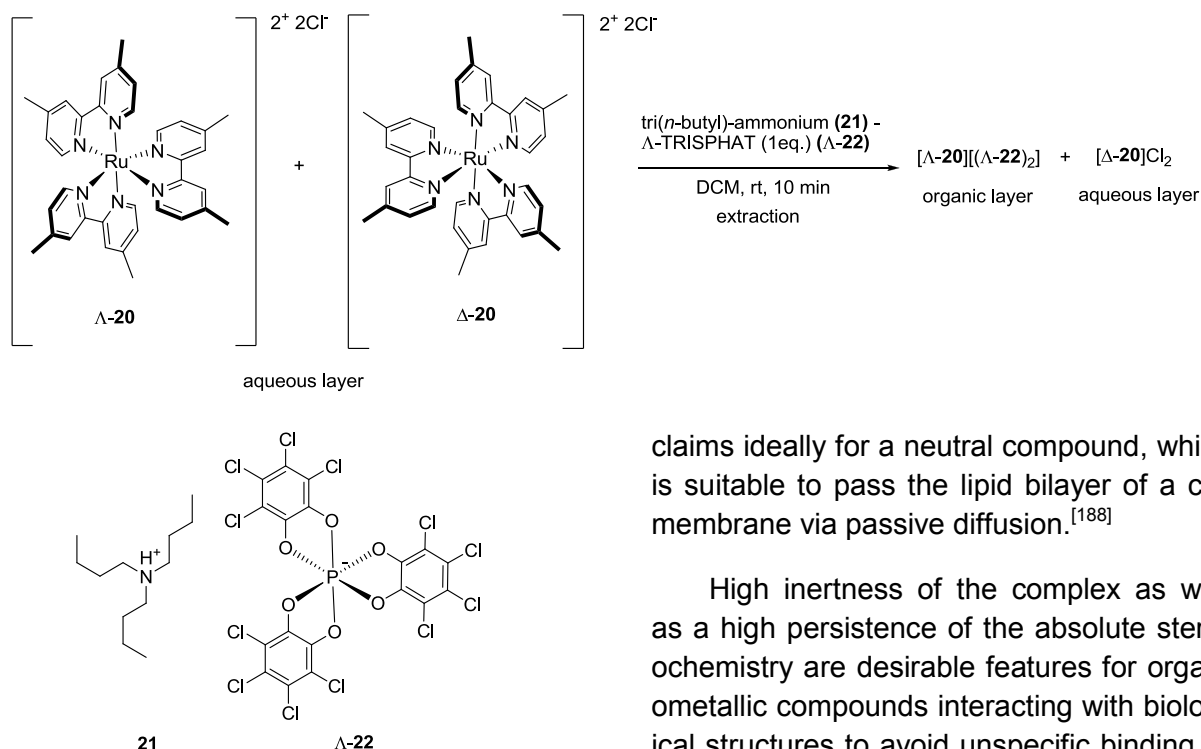
Figure 23: a) Staurosporine (**8**) serves as a lead structure for metal based kinase inhibitors. Depending on the design and connectivity of the residual ligands a diversity of different stereoisomers can be achieved. From two stereoisomers regarding half sandwich complexes to up to 24 regarding octahedral complexes in case of $A \neq B \neq C \neq D$. M: a diversity of transition metals. b) The number of possible stereoisomers can be reduced by connecting monodentate ligands to polydentate ligands.

the low yields observed for the formation of Δ -**17**, Scheme 1.^[182] In contrast, 2,6-bis((((S)-2-phenyl-4,5-dihydrooxazol-4-yl)methylthio)methyl) pyridine ligand **18**, which is C_2 -symmetric, results in the shown conformation of Δ -**19** based on both, the incorporated chirality of the oxazoline moieties and the ligand design itself. The corresponding Δ -**19** complex would be less favoured, because the peripheral phenyl groups of the oxazolines would be placed above and below the ligand backbone leading to steric repulsions, Scheme 1.^[183]

Due to the restricted space offered by the active site of a kinase, the strategy using large linking systems is not suitable to transfer the ligand chirality onto the metal for octahedral organometallic compounds with the purpose of kinase inhibition.^[182,184] The same is true for ligands based on axial chirality which often leads to bulky coordination spheres.^[185] And as the pyridocarbazole is a mandatory prerequisite, the density of possible ligands to form an octahedral scaffold cannot exceed the number of four making many successful approaches with multidentate ligands inapplicable for this case.



Scheme 1: The axial chirality of (**S**)-**13** results into chirality transfer to the metal core leading to *cis*- β - Λ -(**S**)-**14**. The chiral information of **15** is mainly projected via the aliphatic linker. In contrast, the C_2 -symmetric ligand **18** mediates chirality to the metal centre based on the oxazoline moieties and the ligand design itself.

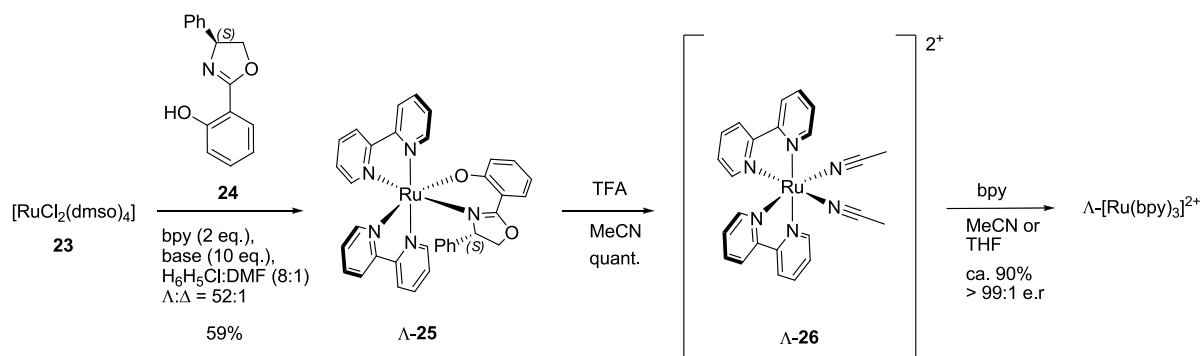


Scheme 2: The TRISPHAT ligand Λ -22 can be applied as auxiliary for the synthesis and separation of enantiomers via extraction forming an ion pair.^[169]

Moreover, the approach of using chiral anions to form certain octahedral scaffolds presupposes a matching charge in the desired organometallic complex.^[169,176,177] For example, the chiral tris(tetrachlorobenzene-diolato)phosphate(V) anion can be obtained either as Δ or Λ form.^[169] Moreover, this compound can be used as an auxiliary in the asymmetric synthesis of organometallic complexes and for the selective extraction of a particular enantiomer via ion pair formation, see Scheme 2.^[176,187] However, the design of a kinase inhibitor in contrast

claims ideally for a neutral compound, which is suitable to pass the lipid bilayer of a cell membrane via passive diffusion.^[188]

High inertness of the complex as well as a high persistence of the absolute stereochemistry are desirable features for organometallic compounds interacting with biological structures to avoid unspecific binding or unintended release of the metal core.^[152,189,190] Coordination compounds of the d_6 metals like RuII, OsII, RhIII, and IrIII fulfill these criteria.^[167] But at the same time this characteristic poses significant challenges for the asymmetric synthesis using auxiliaries coordinating to the metal centre compared to anion mediated asymmetric synthesis. The harsh conditions to coordinate and to substitute the chirality inducing auxiliary by the final ligand limit available methods via this strategy.^[167] After intensive research and experience on this area, the MEGGERS group reported innovative strategies to overcome this issue like using switchable auxiliaries, which can possess different coordination preferences by trigger-



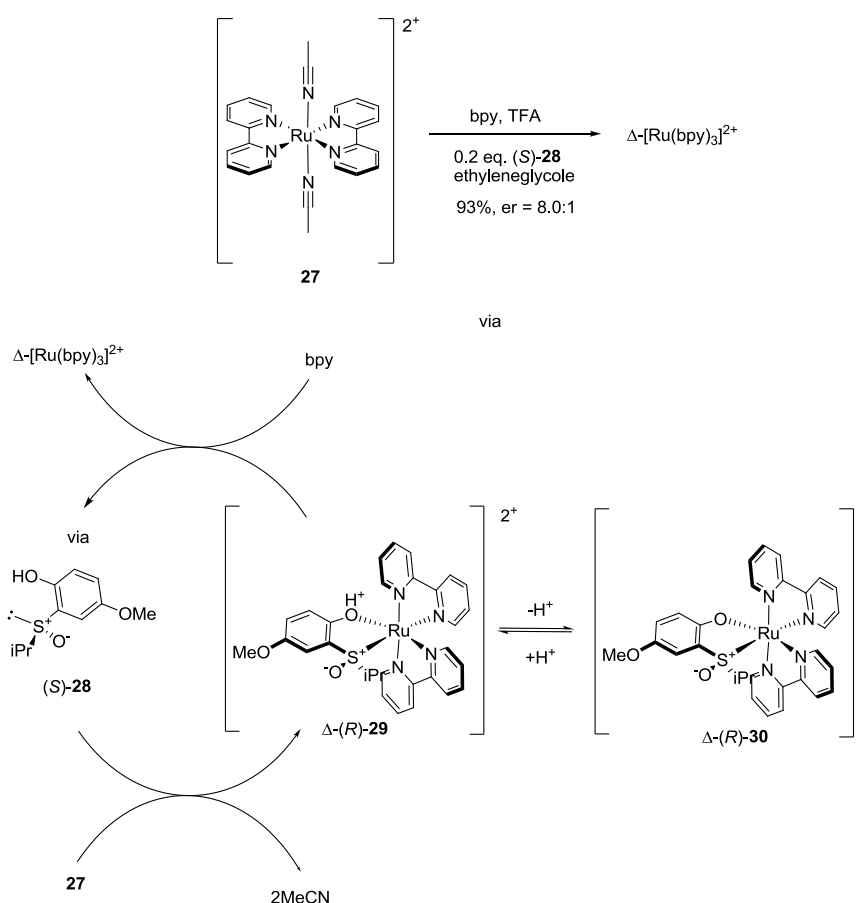
Scheme 3: The (S)-Salox ligand **24**, an auxiliary in asymmetric synthesis, can be labilised by protonation followed by the substitution of other ligands under sustained stereoconfiguration.^[186]

ing a recognition group e.g. via protonation or reduction.^[131,132,191–194] For instance, the (S)-Salox ligand **24**, utilised as auxiliary in asymmetric synthesis, can be labilised by protonation followed by the substitution of other coordinating ligands under sustained stereoconfiguration, Scheme 3.^[186] It is noteworthy, that the proper choice of the appropriate solvent is crucial for stereochemical outcome of the reaction: only coordinating solvents, like acetonitrile or tetrahydrofuran (THF) are capable of suppressing racemization at the applied reaction temperature.^[195]

The smart optimization of reaction conditions can further develop a former auxiliary into a true catalyst. The reaction of **27** 300 mM in ethylene glycol using 0.2 eq. of (S)-**28** in the presence of TFA and bipyridine result in Δ -[Ru(bpy)₃]²⁺ with a yield of 93 % and an er of 8.0:1.0, whereas the chiral compounds **27** acts as true catalyst with

turnover numbers of more than three, Scheme 4.^[132] Although, the feasibility of catalytic asymmetric coordination chemistry has been demonstrated, the broad application must be established in future.

Considering all restrictions, being inevitable for a metal based kinase inhibitor, ends up to following characteristics ideally united in one single compound: enantiopure, neutral, low molecular weight, inert complex, and persistent stereoconfiguration. In this work, ways to fulfill these requirements in a metal compound were elaborated and compared to established ligand systems. Moreover, the chemical modification of the presented ligand systems to improve selectivity and specificity as well as pharmacological properties will be discussed. Closing, structural inspirations guided by computer aided design will be introduced as a potential useful tool.



Scheme 4: A former auxiliary (S)-**28** acts as a true catalyst under specialised conditions. The achiral starting material **27** is converted to enantiomerically pure Δ -[Ru(bpy)₃]²⁺ in an asymmetric catalysis.^[132]

3 Results and Discussion

3.1 The Pyridocarbazole Pharmacophore Ligand

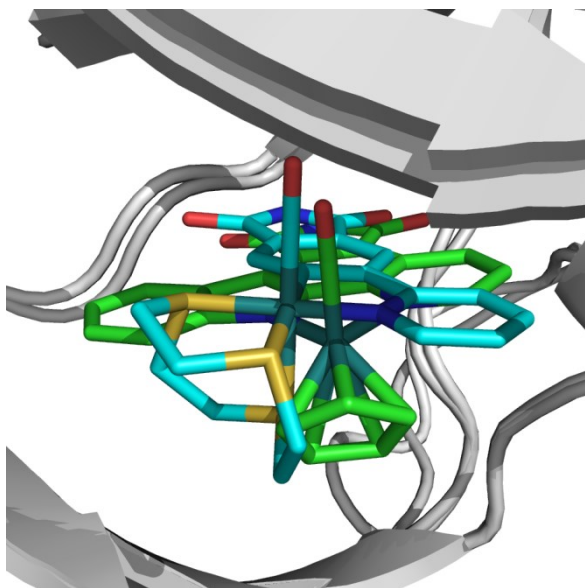


Figure 24: Superimposed crystal structures of pyridocarbazole-based complex (*R*)-**9** (pdb: 2BZH)^[196] and an organoruthenium complex based on the pharmacophore ligand **34** (pdb: 4AS0)^[154] both bound to PIM-1. Both pharmacophore ligands mediate the complex binding into the ATP binding site of the target kinase. However, the residual ligand sphere is significantly shifted in relation to each other, resulting in different selectivity and specificity. The carbon atoms of (*R*)-**9** are presented in green and the carbon atoms of the **34** based organoruthenium complex are presented in cyan. Nitrogen atoms are shown in blue, oxygen atoms in red, sulfur in yellow and the ruthenium cores in teal. PIM-1 is presented as cartoon in grey.

The pyridocarbazole pharmacophore ligand was established in the MEGGERS group as a bidentate ligand for metal complexation mimicking the indolocarbazole moiety of staurosporine (**8**).^[149] As depicted

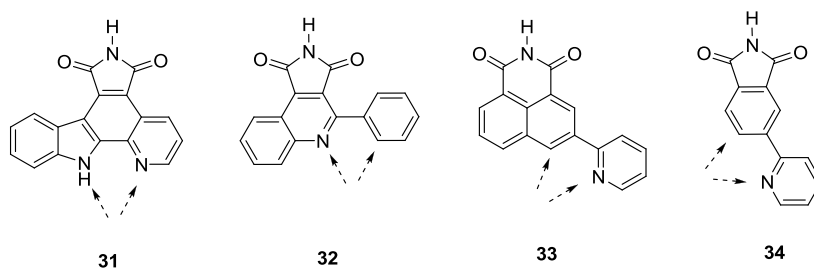
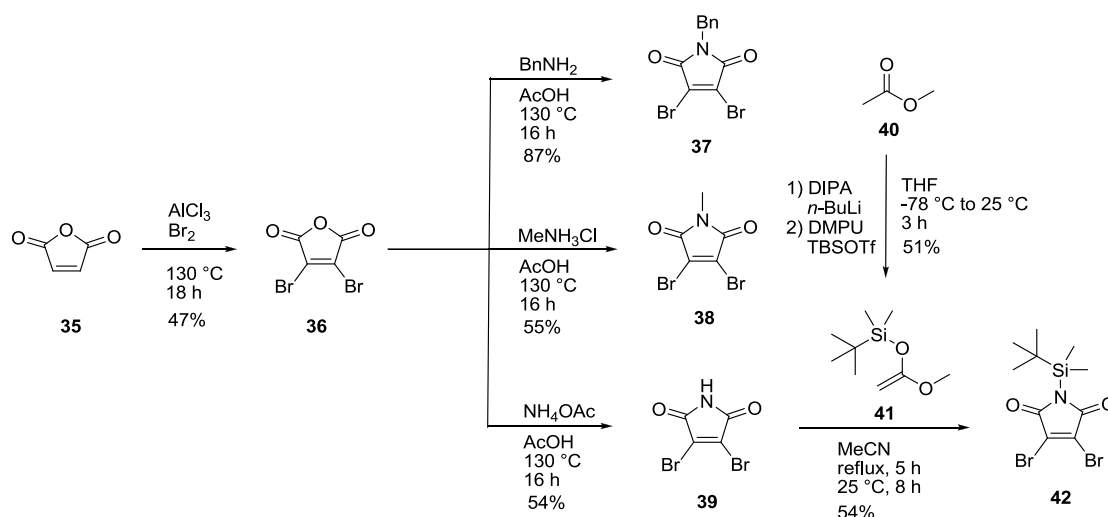


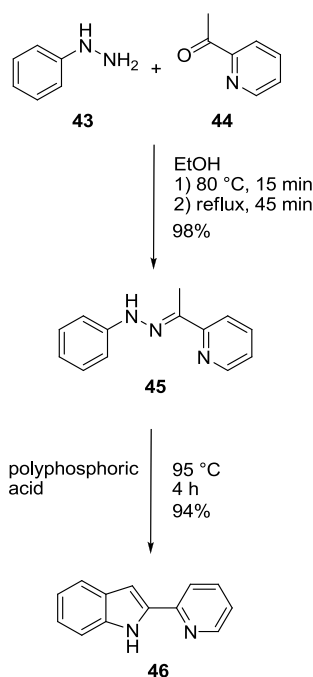
Figure 25: The pyridocarbazole **31** as the first pharmacophore ligand derived from the indolocarbazole moiety of staurosporine served as lead structure for several new pharmacophore ligand scaffolds like **32**, **33**, **34** shifting the position of the coordination sphere and subsequently leading to organometallic kinase inhibitors with diverse affinity and selectivity profiles.^[190,197] The coordinating atoms have been indicated by dashed arrows.

in Figure 21 the pyridocarbazole pharmacophore ligand steers the entire coordination sphere into the kinase hinge region and is therefore the major mediator of target recognition. Nevertheless, additional pharmacophore ligands with modified scaffolds have been successfully designed in the MEGGERS group to enlarge the set of organometallic compounds with new structures addressing the kinome with diverse affinity and selectivity profiles.^[190,197]

However, the pyridocarbazole ligand (**31**) serves as the standard pharmacophore ligand for the complexation reactions in this work. The convergent synthetic route starts with 1*H*-pyrrole-2,5-dione (**35**) which is reacted with bromine in an electrophilic addition for 18 h under reflux conditions and catalysed by aluminium trichloride, see Scheme 5. The resulting 3,4-dibromofuran-2,5-dione (**36**) in a yield of 47% serves as starting point for different maleimides. **36** can be processed using either benzyl amine or methyl ammonium chloride to obtain 1-benzyl-3,4-dibromo-1*H*-pyrrole-2,5-dione (**37**) (87%) or 3,4-dibromo-1-methyl-1*H*-pyrrole-2,5-dione (**38**) (55%), respectively. Both reactions were performed in acetic acid at 130 °C for 16 h. These two modified maleimides can be used directly for the photocyclisation reaction resulting in modified pyridocarbazoles. A sufficient protection group must be applied to obtain an unsubstituted maleimide moiety in the final pyridocarbazole pharmacophore ligand.



Scheme 5: The synthesis of maleimide derivatives **37**, **38**, and **42**.



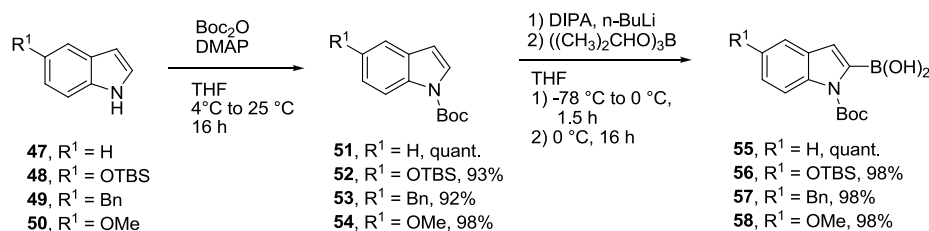
Scheme 6: FISCHER indole synthesis of 2-(pyridin-2-yl)-1H-indole (**46**).

Therefore, 3,4-dibromo-1*H*-pyrrole-2,5-dione (**39**) obtained under the same reaction conditions as **37** and **38** in 54% yield must be protected with the *tert*-butyldimethylsilyl protection group using *tert*-butyl(1-methoxyvinyl)oxydimethylsilane (**41**) (54%) in acetonitrile under reflux conditions for 5 h followed by stirring for 8 h at ambient temperature. Methyl acetate (**40**) was reacted with lithium diisopropylamine, which was generated first *in situ*, 1,3-dimethyl-tetra-

hydropyrimidin-2(1*H*)-one (DMPU), and *tert*-butyldimethylsilyl triflate in THF over 3 h from -78 °C to ambient temperature to obtain **41** in 51% yield. 3,4-dibromo-1-(*tert*-butyldimethylsilyl)-1*H*-pyrrole-2,5-dione (**42**) as the resulting intermediate can then be applied for the photocyclisation in analogue to **37** and **38**.

The second component for the photocyclisation reaction is 2-(pyridin-2-yl)-1*H*-indole (**46**) or its modified derivatives. The unsubstituted **46** can be obtained in a FISCHER indole synthesis by reacting phenylhydrazine (**43**) and 2-methylpyridyl ketone (**44**) in ethanol under slow heating to 80 °C over a period of 15 min and reflux conditions for 45 min, see Scheme 6. The resulting 2-(1-(2-phenylhydrazono)ethyl)pyridine (**45**) (98%) is then further reacted to **46** (94%) by the sequential addition of small portions into polyphosphoric acid and heating at 95 °C under firm stirring for 4 h.

In contrast to the general reaction conditions applicable for maleimide derivatives described above, the FISCHER indole synthesis cannot be applied universally to obtain modified pyridylindoles due to the harsh conditions of the reaction and the reaction mechanisms itself, which bears the potential leading to rearrangements or the loss of attached groups.^[198]



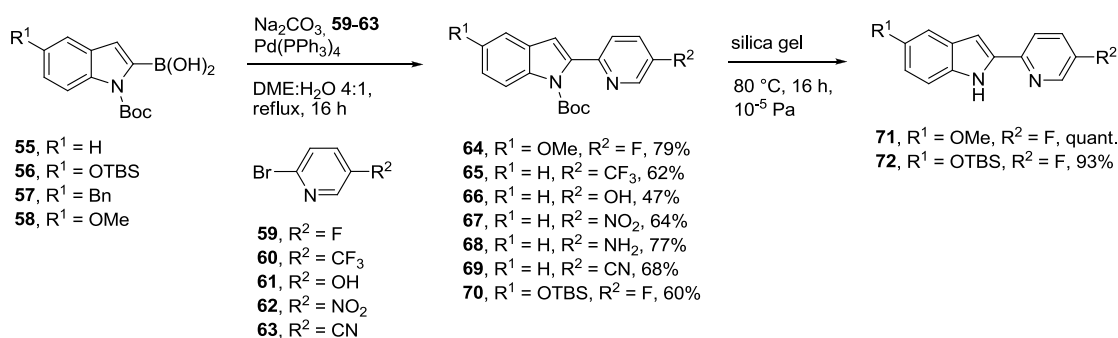
Scheme 7: The synthesis of the boronic acids **55** to **58** as coupling partners for the SUZUKI reaction.

Therefore, to synthesise modified pyridylindoles a synthetic route applying the Suzuki coupling was established, see Scheme 7.^[149] First, the indole has to be protected with the *tert*-butyl carboxylate group using di-*tert*-butyl dicarbonate. The protection group masks the indole nitrogen and hinders potential interferences during the synthetic route. Moreover, it supports the deprotonation of the indole at the 2 position for the formation of the boronic acid. Therefore, indole (**47**) was reacted with di-*tert*-butyl-dicarbonate and dimethylamino-pyridine in THF at 4 °C for 16 h to afford *tert*-butyl 1*H*-indole-1-carboxylate (**51**) in quantitative yield. The same reaction conditions were applied to obtain *tert*-butyl-5-(*tert*-butyldimethylsilyl)-1*H*-indole-1-carboxylate (**52**) (93%), *tert*-butyl-5-benzyl-1*H*-indole-1-carboxylate (**53**) (92%), and *tert*-butyl-5-methoxy-1*H*-indole-1-carboxylate (**54**) (98%).

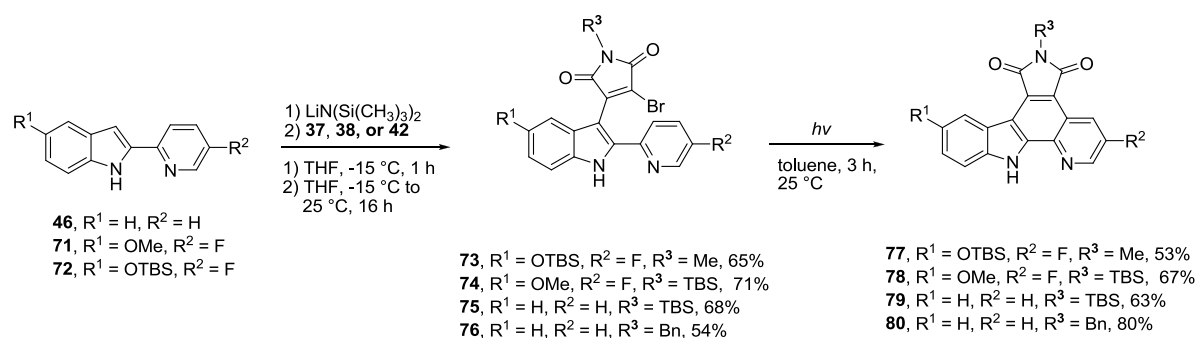
All protected indole derivatives were then transformed into the appropriate boronic acids for the SUZUKI coupling using *in situ* generated lithium diisopropylamide and triisopropyl borate in THF in almost quantitative yields. Nevertheless, the resulting boronic acids must be processed promptly due

to the limited stability of the intermediates, see Scheme 8. As coupling partner, a selection of modified pyridines, **59** to **63**, were used and combined with the synthesised boronic acids **55** to **58**. The reaction was performed using tetrakis(triphenylphosphine) palladium(0) and sodium carbonate in a dimethoxyethane : water (4:1) mixture under reflux conditions for 16 h. The yields of the synthesised pyridylindoles **64** to **70** varied from 47% to 79%.

However, due to investigational findings achieved during this work, only three different pyridylindoles **46**, **71**, and **72** were processed to the appropriate pyridocarbazoles. Prior to the use of the pyridylindoles for the monobromide synthesis and the following photocyclisation step, the deprotection of the *tert*-butyl-carboxylate group must be performed. Soaking the compounds **64** and **70** on silica gel under heating at 80 °C *in vacuo* for 16 h afforded the unprotected pyridylindoles **71** and **72** in quantitative and 93% yield, respectively.



Scheme 8: The SUZUKI coupling using different boronic acids in combination with different pyridine derivatives led to the formation of a set of protected pyridylindoles **64** to **70**. Two derivatives were further proceeded and deprotected.



Scheme 9: The monobromide synthesis and the following photocyclisation reaction affording the pyridocarbazole pharmacophore ligand.

The pyridylindoles **46**, **71**, and **72** were reacted with the maleimides **37**, **38**, or **42** in a MICHAEL reaction using lithium bis(trimethylsilyl)amide as base in THF to obtain the monobromides **73** to **76** in varying yields from 54% to 71%, see Scheme 9. These intermediates had to be converted immediately into the corresponding pyridocarbazoles due to their instability. The photocyclisation itself was performed in toluene under continuous water cooling. For this purpose, the compounds were irradiated with an iron iodide endowed mercury UV lamp of 700 W power and a wavelength of $\lambda_{\text{max}} = 350$ nm. The finished pyridocarbazoles **77** to **80** were obtained in yields varying from 53% to 80%. The pyridocarbazoles **77** to **80** were then used for the complexation reactions discussed in this work. Moreover, the pyridocarbazole derivatives **81** to **84** from the internal compound library of the MEGGERS group have been used to synthesise novel complexes with diverse inhibition profiles, see Figure 26.

The established pyridocarbazole synthesis, offers many possibilities to introduce additional functional groups. Especially, the convergent synthetic route increases the general flexibility and the quick access to a plethora of different structures. Nevertheless, the multistep synthesis is a disadvantage. One of the major tasks of the alternatively established compounds **32**, **33**, and **34**, beside the development of new scaffolds, was to decrease the number of synthetic steps.^[190,197] However, the pyrido-

carbazole ligand itself serves as reference pharma-cophore ligand to investigate the complementarily coordinating ligands presented in this work.

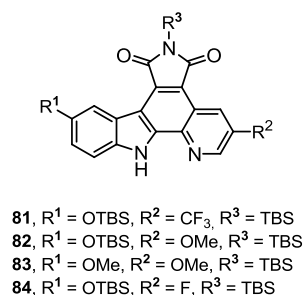


Figure 26: Pyridocarbazole derivatives retrieved from the MEGGERS group internal compound library.

3.2 Development of S6K1 Inhibitors

3.2.1 Target Synopsis and Aim

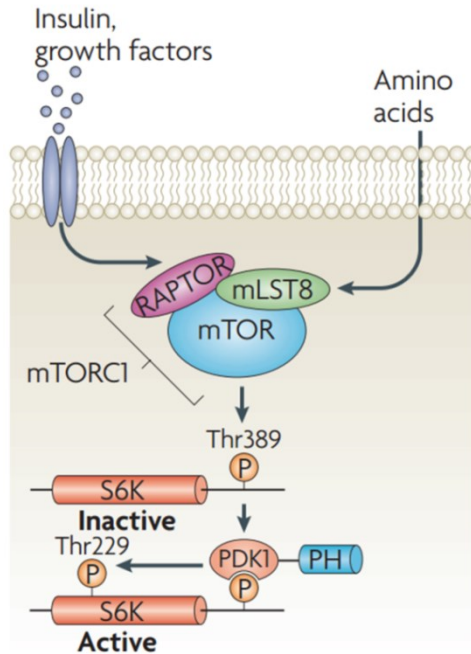


Figure 27: Growth factors, hormones, and amino acids, as proliferation and anabolism mediators, activate the downstream located mTORC1. This complex consecutively phosphorylates Thr389 in the hydrophobic motif of S6K, providing a docking site for PDK1, which then phosphorylates Thr229 in the activation segment, converting S6K into its active form.^[23]

S6 kinases (S6K) are members of the AGC serine/threonine kinases which belong to the RSK family. The catalytic domain is highly conserved and the phosphorylation of Thr-389 within the activation loop triggers the kinase induced by the phosphoinositide-dependent kinase-1 (PDK1), see Figure 27.^[199,200] The S6 kinases act downstream of the phosphatidylinositol-3-kinase (PI3K) pathway. Beside PDK1, mTOR is also involved in the activation of S6K1.^[199–201] Whereas yeast contains one S6K kinase, called *sch9Δ*, the human kinome covers two isoforms called S6K1 and S6K2. S6 kinases are associated with many cellular processes, including protein

synthesis, mRNA processing, cell growth, and cell survival mainly based on the phosphorylation of glycogen synthase kinase 3 (GSK3) and the ribosomal S6 protein.^[202,203] Both isoforms of S6K phosphorylate and activate the 40S ribosomal protein S6, which promotes protein synthesis through an increased rate of mRNA transcription.^[204] S6K1 also regulates cell proliferation through the cell cycle, in addition to promoting cell survival by inactivating the proapoptotic protein BAD.^[205–207]

Whereas S6 kinases are involved in indispensable cellular processes, a perturbed activation leads to severe diseases. Alterations in S6 kinase activity have been shown to play a critical role in many pathologic incidences, including diabetes, obesity, aging, and cancer.^[208–210] Many melanoma cells exhibit constitutive activation of the PI3K-AKT pathway, which results in AKT phosphorylation and leads to an amplification of the downstream targets mTOR and S6K1.^[211] This increase in phosphorylation of ribosomal S6 by S6K1 results in increased protein translation and cell growth. This effect can be abolished by the treatment with rapamycin, an allosteric mTOR inhibitor, causing a significant dephosphorylation of S6K1 and consequently to a decreased cell growth.^[212] However, the treatment with rapamycin is accompanied by drawbacks, mainly reasoned in the abrogation of feedback inhibitions of other pathways.^[213] This cross-talk perturbation leads to side effects such as hyperglycaemia, hypercholesterolemia, and hyperlipidaemia.^[214] Therefore, inhibition of S6K1 represents an alternative therapeutic strategy that may bypass the disadvantages of mTOR inhibition. Recent studies reveal S6K as being a critical node linking HER-family and PI3K pathway signaling, making it an effective target for single-agent therapy.^[215]

3.2.2 Synthesis and Structural Investigations of Organoruthenium(II) Complexes

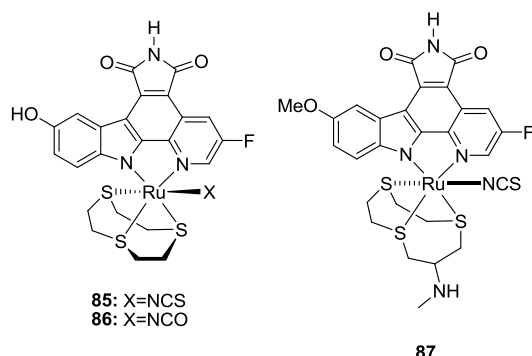
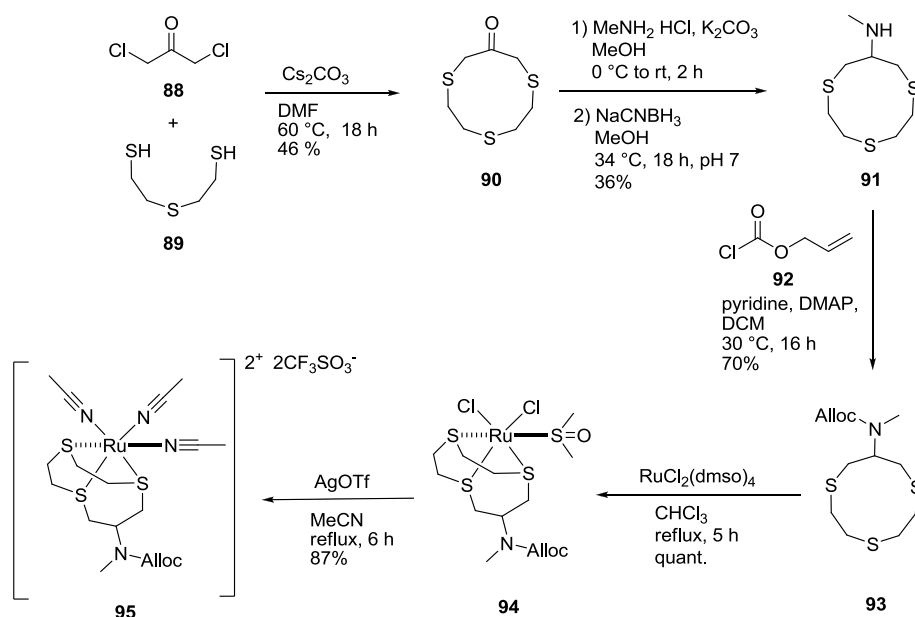


Figure 28: Octahedral organoruthenium complexes inhibiting S6K1.

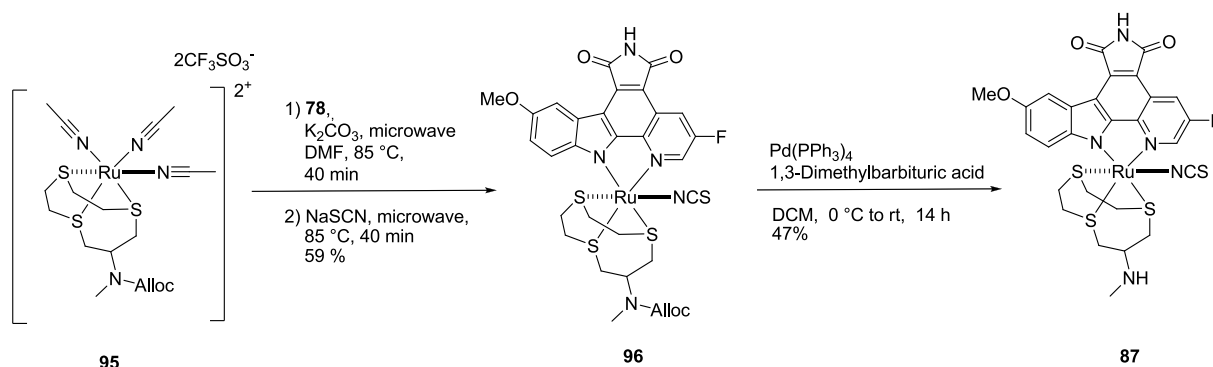
Highly sophisticated octahedral complexes were realised by an extensive screening of potential ligands suiting the requirements of a hexavalent metal centre.^[143–145,152] The tridentate 1,4,7-trithia-cyclononane ligand is capable of both, being a synthetically quickly accessible compound, and fitting in numerous binding sites as a part of organometallic inhibitors.^[140,151,152,154] **85** and **86**, which were synthesised during former studies in the

MEGGERS group, also contain this motif and turned to be selective and potent S6K1 inhibitors, beside **87**, see Figure 28.^[216] But, the ligand is only capable of forming hydrophobic VAN-DER-WAALS contacts and offers no additional functional groups to either form hydrogen bonds or to enhance physico-chemical properties, e.g.: solubility. Therefore, ligands offering modification sites to improve biomolecular recognition as well as physico-chemical parameters for the consequent development of octahedral organometallic complexes are highly desirable.

Keeping the sulfur atoms for complexation sustained, we introduced a methylene group into the cyclic ring system to include a secondary amine function. This additional group is known to act as both, a hydrogen bond acceptor and hydrogen bond donor.^[217–219] Moreover, a secondary amine influences the protonation state of the complex at different pH levels and subsequently the potential membrane permeability.^[220–222]



Scheme 10: Synthesis of complex precursor **95**. The key steps are the formation of the medium-sized ring **90** by a nucleophilic substitution, the functional group interconversion by a reductive amination to **91**. Prior to the complexation a potential cross-coordination has to be avoided by protecting the secondary amine group by allyl chloroformate. To obtain the reactive precursor **95**, a substitution of all monodentate ligands towards acetonitrile as better leaving group for the pyridocarbazole introduction is necessary.



Scheme 11: Synthesis of ruthenium(II) complex **87**. The acetonitrile ligands of the reactive precursor **95** were sequentially substituted by the pyridocarbazole ligand **78** and sodium thiocyanate. The deprotection step of the allyloxycarbonyl using tetrakis(triphenylphosphine) palladium(0) results in the final complex **87**.

The synthesis of the modified ligand is similar to the published one of 1,4,7-trithiacyclononane, according to Blower *et al.*,^[223] with slight modifications, see Scheme 10. First, the ten-membered ring has to be formed. For this reason, caesium carbonate was suspended in dimethylformamide (DMF) and heated to 60 °C. Caesium carbonate acts as a base, deprotonating the thiol groups of the 2,2'-thiodiethanethiol (**89**) and increasing their nucleophilic character. The use of caesium carbonate at this step is substantial, due to the size of the caesium ion preorganizing **89** for the nucleophilic substitution reaction.^[223,224] Furthermore, this preorganisation reduces the competing polymerisation reaction beside the intended cyclisation. 1,3-dichloroacetone **88** was pre-diluted in DMF and added drop wise to the reaction mixture. The drop wise addition of the reactants was performed over a time period of 9 h followed by an additional 9 h of stirring at 60 °C. The low concentration (38 mmol/L) of both reaction partners is crucial to avoid the mentioned polymerisation. This fact limits the amount of reactants applicable in a single reaction batch. The yield of 46% is low but not unusual for medium-sized ring synthesis.^[225]

The resulting 1,4,7-trithiacyclodecan-9-one (**90**) was then processed in a reductive amination using potassium carbonate and methyl ammonium chloride to form the imine intermediate *in situ*. The reaction was performed in methanol at 34 °C for 2 hours. Sodium cyanoborohydride was used as a reducing agent and the reaction mixture was stirred over night at 34 °C. The *N*-methyl-1,4,7-trithiacyclodecan-9-amine (**91**) ligand was obtained at 36% yield. It is noteworthy that the sp^2 -carbon centre of **90** turned into a prochiral sp^3 -carbon during this reaction procedure. Due to the symmetric character of the ligand, this fact has no further influence on the synthesis, unless it is coordinated to the metal centre, see Chapter 3.2.4.

Prior to complexation, the secondary amine of **91** had to be protected to avoid competing cross-coordination towards a second metal ion. The most suitable protection group for this purpose is the allyloxycarbonyl group, which can be cleaved under mild orthogonal conditions after complexation. Therefore, **91** in methylene chloride was reacted with allyl chloroformate (**92**), pyridine, and 4-dimethylaminopyridine at 0 °C according to standard protection procedure.^[226] The allyl methyl (1,4,7-trithiacyclodecan-9-yl) carbamate ligand (**93**) was obtained in a yield of 70% and was further processed in the complexation reaction.

Dichlorotetrakis(dimethylsulfoxide) ruthenium(II) as a standard precursor was used to coordinate (**93**). The reaction was performed in chloroform under reflux conditions for 5 h. The preliminary resulting complex **94** was directly processed to ligand exchange by precipitating the chlorido ligands using silver trifluoromethanesulfonate in acetonitrile under reflux conditions for 6 h. **95** could be obtained in 87%. It is noteworthy that the prochiral carbon centre of **91** turns into a stereogenic centre during the complexation reaction. Due to the high moisture sensibility of this compound, a direct continuance into the complex synthesis is necessary.

Therefore, the pharmacophore ligand **78** was reacted with the ruthenium precursor **95** using potassium carbonate as a base, in DMF at 85 °C under microwave irradiation for 40 min, followed by addition of sodium thiocyanate as the residual monodentate ligand, see Scheme 11. After an additional 40 min at 85 °C and column chromatography, the organometallic complex **96** was obtained as a racemic mixture in 59% yield. The crystal structure of **96** reveals the coordination pattern of the ligands towards the ruthenium metal centre, see Figure 29. The tridentate ligand forms two five-membered and one six-membered metallacycles. The six-membered metalla-

cycle aligns in a chair conformation as observed for aliphatic rings. It must be highlighted, that the secondary amine function is oriented in equatorial position minimising the steric hindrance of the bulky allyloxycarbonyl protection group with the residual coordination sphere. The isothiocyanate ligand is observed to be coordinated in the *N*-bound form.

To obtain the final complex **87**, the allyloxycarbonyl protection group was cleaved using tetrakis(triphenylphosphine) palladium(0) in methylene chloride for 14 h and allowing the reaction mixture to warm from 0 °C to ambient temperature. The reaction was quenched using sodium hydrogen carbonate, and after column chromatography, the metal complex **87** was obtained in 47% yield.

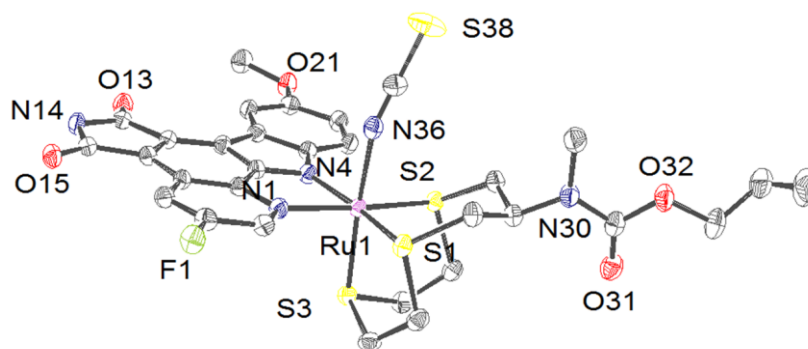


Figure 29: Crystal structure of **96**. Solvent Molecules were omitted for clarity. ORTEP drawing with 50% probability of thermal ellipsoids. Selected bond lengths [Å] for **96**: Ru1-N1 = 2.1411(18), Ru1-N4 = 2.124(2), Ru1-N36 = 2.061(2), Ru1-S1 = 2.2862(7), Ru1-S2 = 2.2802(6), Ru1-S3 = 2.3029(6).

3.2.3 Biological Investigations

3.2.3.1 Screening and IC_{50} Determination

A screening set of ten different staurosporine-inspired organometallic ruthenium complexes against a diverse panel of 283 protein kinases by Millipore (Kinase ProfilerTM) led to the identification of **85** as a potential inhibitor of S6K1, with 7% activity at a concentration of 100 nM in the presence of 10 μ M ATP. **86** has an almost identical chemical structure, differing only in the exchange of the substituted isothiocyanate towards an isocyanate, see Figure 28, leading to significantly less, only 54%, activity under the same conditions. In the kinase panel, the inhibitor **85** inhibited only 41 kinases (16%) to less than 10% activity, including S6K1 and the related S6K family members RSK1, RSK2, RSK3, and RSK4.

To characterise the preliminary hits, biological investigations were performed in the MARMORSTEIN group. For this purpose, a radioactive kinase assays were performed to determine the activity of S6K1 protein constructs prepared in baculovirus-infected insect cells, in order to identify a construct that would be suitable for inhibitor testing. The construct preparation and the radioactive kinase assays were performed by JIE QIN and JULIE S. BARBER-ROTENBERG. Initial tests revealed, that the full-length α -I isoform of S6K1, S6K (1-525), and the isolated kinase domain, S6K (84-384), had low kinase activity, although the full-length kinase showed more activity than the kinase domain, see Figure 30. The S6K1 protein constructs had low kinase activity because the full-length kinase contained the C-terminal auto-inhibitory domain. To address this issue and express a more active kinase for further inhibitor studies, a S6K1 (1-421) construct was prepared, including both the Thr-252 and Thr-412 phosphorylation sites, based on previous data from Keshwani *et*

al.^[227] The results indicate that the catalytic domain of the S6K1 α I isoform (residues 1-398) is analogous to S6K1 (1-421) of the α -I isoform. To further enhance the catalytic activity of S6K1 (1-421), the T412E mutant was prepared to mimic phosphorylation at this position and was co-expressed with PDK1 to promote phosphorylation of T252. Preparation of the S6K1 (1-421, T412E, PDK1 activated) protein resulted in a highly active kinase that was suitable for further inhibition studies *in vitro*, Figure 30.

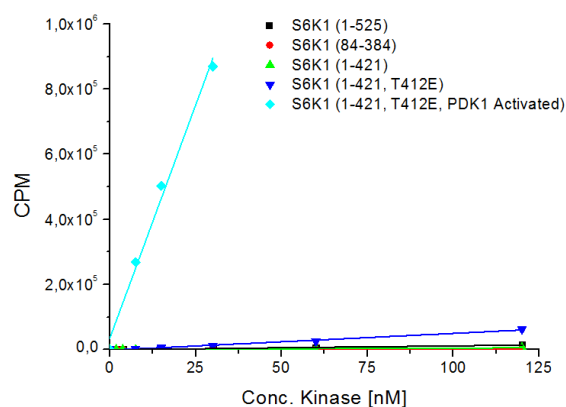


Figure 30: Radioactive kinase assays performed by JIE QIN and JULIE S. BARBER-ROTENBERG were used to determine the activity of five different protein constructs of S6K1. Only the S6K1 (1-421, T412E, PDK1 activated) construct (cyan) resulted in a highly active kinase, which was suitable for further radioactive competition studies *in vitro*.

Both organoruthenium metal complexes were assayed against the construct S6K1 (1-421, T412E, PDK1 activated) in a radioactivity-based kinase assay by JULIE S. BARBER-ROTENBERG to determine the IC_{50} values of 33.9 nM for **85** and 23.5 μ M for **86**, respectively, at an ATP concentration of 100 μ M, see Figure 32. As a control, the IC_{50} value of the unselective kinase inhibitor staurosporine was determined resulting in 64.1 nM under the same conditions. Moreover, the S6K1 inhibitor PF-4708671 (**97**) was tested against S6K1 under the same conditions as a literature known specific S6K1 inhibitor, see Figure 31. An IC_{50} value of 142.8 nM was determined for PF-4708671, consistent with published results.^[228]

Given the apparent specificity and potency of **85**, it became the lead structure for the development of second-generation organometallic S6K1 inhibitors covering charged and neutral octahedral organoruthenium and organorhodium complexes.

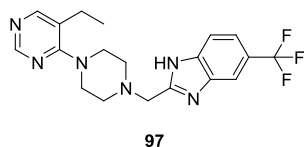


Figure 31: S6K1 inhibitor PF 4708671 (**97**).^[83]

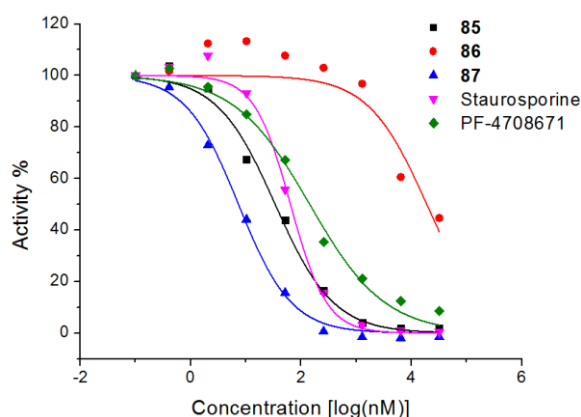


Figure 32: **85** (33.9 nM), **86** (23.5 μ M), **87** (7.3 nM), Staurosporine (64.1 nM), and PF-4708671 (**97**) (142.8 nM) were assayed by JULIE S. BARBER-ROTENBERG against the construct S6K1 (1–421, T412E, PDK1 activated) in a radioactive kinase assay using 100 μ M ATP and 2 nM of enzyme. Data points represent mean values calculated from triplicates.

3.2.3.2 Crystallisation Studies of **85**

To investigate the binding mechanisms the crystallisation and structure determination of **85** bound in the ATP binding pocket of S6K1 were performed. In this context, the crystal growth, preparation, and compound soaking was performed by JIE QIN and the structure was solved by JOHN DOSMIC. These studies revealed an unusual binding conformation. Whereas, initial trials to co-crystallise the S6K1 kinase domain (S6K1KD, residues 84–384) bound to **85**, using several factorial screens, failed, the reproduction of the crystals of the S6K1 kinase domain in complex with staurosporine,

according to SUNAMI *et al.* were successful.^[229] Thereafter, soaking of these crystals with high concentrations of **85**, for the exchange of staurosporine by the organoruthenium inhibitor, led to crystals which diffracted to about 2.5 Å resolution and formed in space group P2₁ with two molecules per asymmetric unit. The structure was refined to R_{work} and R_{free} values of 19.15% and 22.21%, respectively, with excellent geometry, see Table 13. Closing, the inhibitors were modelled after the full refinement of the protein.

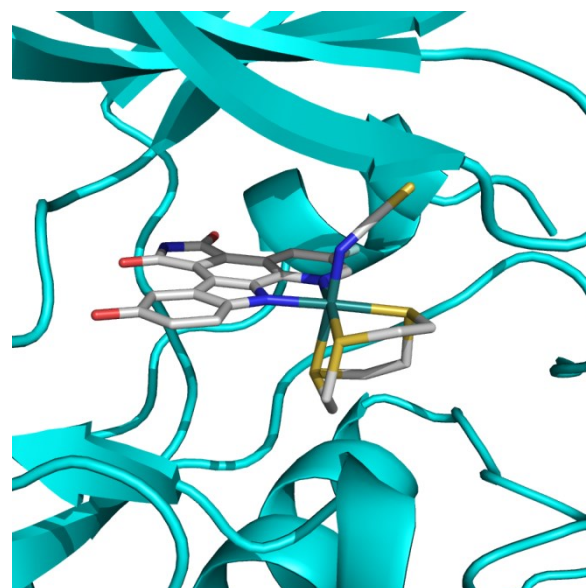


Figure 33: **85** bound to the active site of one of two S6K1 kinase molecules in the asymmetric unit (pdb: 4RLO). The β -sheet rich N-lobe and the α -helix rich C-lobe enclose the ATP-binding site. The protein surface discloses the substrate binding groove perfectly occupied by the organometallic inhibitor. Oxygen atoms are depicted in red, nitrogen in blue, fluorine in light blue, and sulfur in yellow. Carbon atoms of **85** are depicted in grey. S6K1 is represented as cartoon in cyan.

In accordance to the published structures of the S6K1 kinase domain, the kinase domain is bilobal, consisting of an β -sheet rich N-lobe and a α -helix rich C-lobe.^[229,230] The crystal structure revealed that only one staurosporine molecule could be substituted by **85** of the two protein molecules in the asymmetric unit. This is an additional proof that **85** is indeed an ATP-competitive inhibitor, displacing staurosporine from the active site. Both, the staurosporine as well as the

85-bound protein molecules in the asymmetric units are similar to each other with an overall r.m.s.d. of 0.68 Å for the shared atoms.

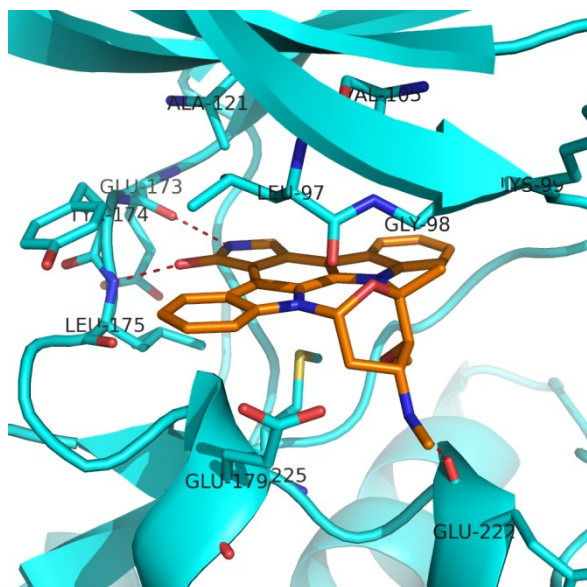


Figure 34: Staurosporine bound to the active site of one of two S6K1 kinase molecules in the asymmetric unit (pdb: 4RLO). The γ -lactam ring of staurosporine forms two hydrogen bonds (red dashes). The backbone nitrogen of Leu-175 interacts with the lactam oxygen and the backbone oxygen of Glu-173 with the lactam nitrogen. The methylamine group of staurosporine forms a third hydrogen bond (red dashes) to the backbone oxygen of Glu-222. Additional amino acid residues involved in VAN-DER-WAALS contacts are highlighted and labelled. Oxygen atoms are depicted in red, nitrogen in blue, and sulfur in yellow. S6K1 is depicted as cartoon with carbon atoms in cyan and carbon atoms of staurosporine are depicted in orange.

Although both molecules bind in the ATP binding pocket, the increased S6K1 potency of the organoruthenium complex is caused by extensive interaction compared to staurosporine. The latter forms hydrogen bonds to S6K1 via the backbone oxygen of Glu-222 of the kinase with the nitrogen of the methylamine residue of the aliphatic ring system of staurosporine. Furthermore, the pyrrolidine ring of the aromatic indolocarbazole moiety of staurosporine forms hydrogen bonds to the backbone nitrogen of Leu-175 and the backbone oxygen of Glu-173 of the kinase hinge region via the oxygen and nitrogen atom, respectively. Beside the hydrogen bonds VAN-DER-WAALS contacts are formed by Leu-97, Lys-99, Gly-98, Val-105,

Ala-121, Tyr-174, Glu-179, and Met-225, see Figure 34.

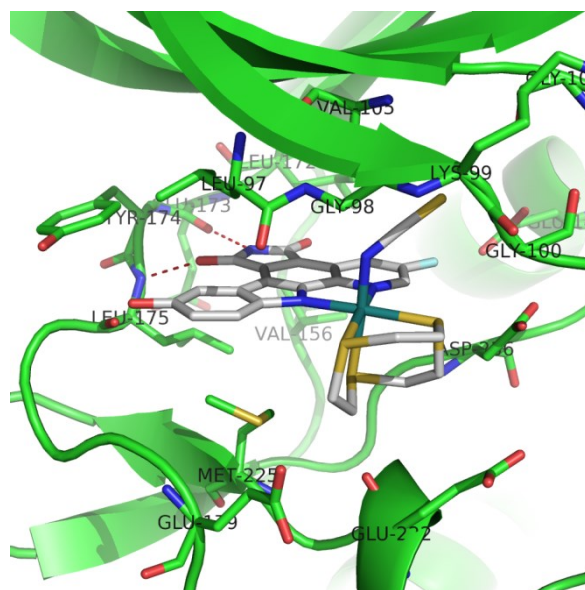


Figure 35: **85** bound to the active site of one of two S6K1 kinase molecules in the asymmetric unit (pdb: 4RLO). The maleimide moiety of the pyridocarbazole ligand forms two hydrogen bonds (red dashes). The backbone nitrogen of Leu-175 interacts with the maleimide oxygen and the backbone oxygen of Glu-173 with the maleimide nitrogen. Additional amino acid residues involved in VAN-DER-WAALS contacts are labelled. Oxygen atoms are depicted in red, nitrogen in blue, fluorine in light blue, and sulfur in yellow. S6K1 is depicted as cartoon with carbon atoms in green and carbon atoms of **85** are depicted in grey.

Compared to staurosporine, **85** retains two hydrogen bonds between the backbone atoms of the hinge residues (Glu-173 and Leu-175) and the maleimide ring of **85**, as well as all of the VAN-DER-WAALS interactions, but forms additional interactions between the ruthenium coordination sphere and the protein, as shown in Figure 35. In particular, the isothiocyanate group of **85** leads to VAN-DER-WAALS interactions with Gly-100 and Val-105 of the kinase p-loop. The 1,4,7-trithiacyclononane ligand forms VAN-DER-WAALS contacts to Gly-100 of the p-loop, Glu-179 and Glu-222 across from the p-loop, where the protein substrate is likely to bind, as well as to Thr-235 and Asp-236 of the activation loop. Comparing the staurosporine bound S6K1 structure to the **85** bound S6K1 structure of the asymmetric unit indicate a dramatic movement of these ami-

no acid residues towards **85**, see Figure 36. The binding of **85** to S6K1 also introduces significant structural changes in the kinase relative to the staurosporine complex. These structural changes appear to be indirectly caused by the 1,4,7-trithiacyclononane ligand of **85**. The α D-helix of the staurosporine complex is about two turns longer at its *N*-terminus than the corresponding helix of the **85** complex, where the corresponding segment takes on a β -strand conformation. This structural difference appears to be driven by the interaction of the tridentate ligand of **85** with Glu-179.

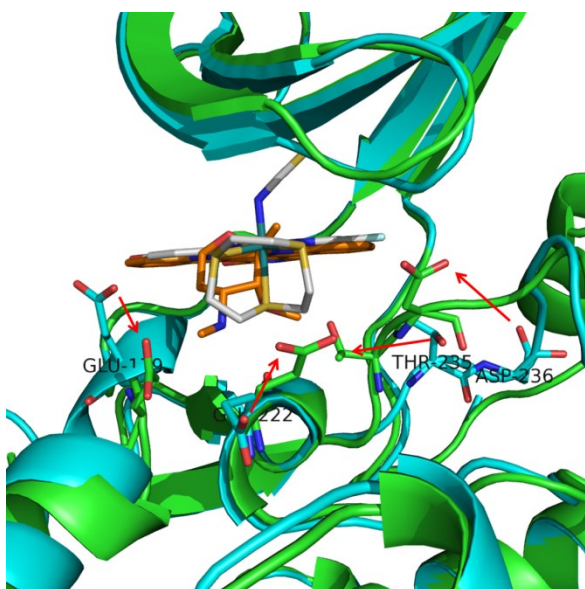


Figure 36: Superimposed structures of S6K1 bound to staurosporine and bound to **85**. Glu-179, Glu-222, Thr-235 and Asp-236 undergo a dramatic movement comparing the staurosporine bound conformation to the **85** bound conformation (red arrows) (pdb: 4RLO). The tridentate 1,4,7-trithiacyclononane ligand of **85** seems to cause these drastic alterations in the secondary structure, whereas the α D-helix of the staurosporine complex is nearly two turns longer at its *N*-terminus than the corresponding helix in the **85** bound form possessing a β -sheet conformation instead. Oxygen atoms are depicted in red, nitrogen in blue, fluorine in light blue, and sulfur in yellow. S6K1 bound to **85** depicted as cartoon with carbon atoms in green and carbon atoms of **85** in grey; S6K1 bound to staurosporine is depicted as cartoon with carbon atoms cyan and carbon atoms of staurosporine in orange.

On the opposite side of the inhibitor, the staurosporine complex has an activation loop folded towards the ATP active site in an inactive conformation without an ordered α C-helix, as previously reported.^[230] Striking-

ly, the **85** complex contains a well-defined α C-helix of about 2 turns. The different alignment of the α C-helix in the two structures appears to be centred around the *N*-terminal region of the activation loop that undergoes about a 6 Å movement towards **85** compared to staurosporine. The movement of the activation segment towards the **85** inhibitor appears to be mediated by the VAN-DEER-WAALS interactions between Thr-235 and Asp-236 with the 1,4,7-trithiacyclononane ligand, see Figure 36. This in turn, provides enough space for the α C-helix to be formed and being stabilised by VAN-DEER-WAALS contacts between Phe-237 of the activation loop and Leu-147 of the α C-helix as well as a hydrogen bond between Lys-123 of the small domain and Glu-143 of the α C-helix, see Figure 37. Interestingly, these interactions are characteristics of the active conformations of kinases, even though the activation segment is in an inactive conformation.

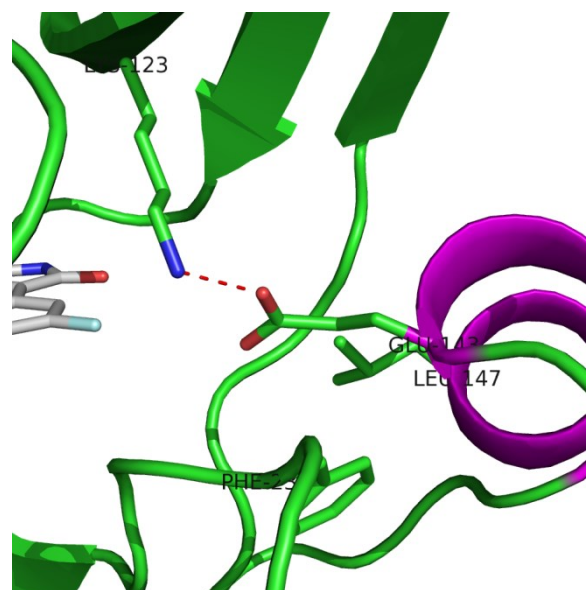


Figure 37: The α C-helix (magenta) is more ordered in the **85**-bound S6K1 structure. This conformation is based on hydrophobic interactions between Phe-237 and Leu-147, and a hydrogen bond between Lys-123 and Glu-143 (pdb: 4RLO). Oxygen atoms are depicted in red, nitrogen in blue, fluorine in light blue. S6K1 bound to **85** is depicted as cartoon with carbon atoms in green and carbon atoms of **85** are depicted in grey.

In contrast, the activation loop is turned outwards in case of the staurosporine bound S6K1 placing Phe-237 and Asp-236

in sterically hindered positions to form the α C-helix, see Figure 36. Concluding, whereas staurosporine bound to S6K1 induces the inactive conformation, the S6K1/**85** complex has characteristics of both, the inactive and active kinase, conformations.

3.2.3.3 Development of Second Generation Organometallic Ruthenium Inhibitors

85 offered an IC_{50} value in the mid-nanomolar range and the co-crystal structure confirmed that it is a competitive inhibitor binding in the ATP-pocket of the S6K1. Therefore, **85** was a promising lead structure for the design of second generation S6K1 inhibitors. The organometallic compounds offer plenty of possible positions for modifications regarding e.g.: the pyridocarbazole moiety or the different coordinated ligands. As previous work proved, modifications in the coordination sphere can have significant effects on binding affinities and kinase selectivity.^[140,149,231] Moreover, the crystal structure of **85** bound to S6K1 indicated several positions suitable for chemical elaboration to improve specificity for the kinase. A series of 64 derivatives of **85** were synthesised by the MEGGERS group with modifications at the pyridocarbazole and the remaining ligand sphere. Then, they were tested for inhibition of S6K1 activity using both a radioactive kinase assay and an ADP-Glo assay with 1 μ M of compound, by the MARMORSTEIN group.^[232] Twenty-five of these inhibitors were further screened using 250 nM of compound. The eight compounds that inhibited S6K1 to less than 25% activity, were assayed to determine their IC_{50} values (at 100 μ M ATP). This analysis produced several compounds that inhibited S6K1 similarly or more potently than **85** with compound **87** (Figure 28) as the most potent one with an IC_{50} of 7.3 nM, using 100 μ M of ATP and 2 nM of enzyme, see Figure 32.

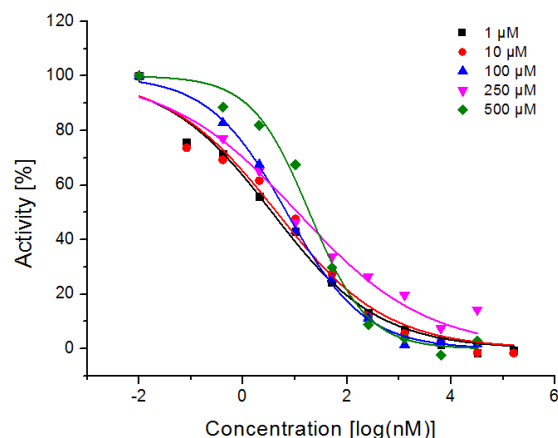


Figure 38: **87** was analysed by JULIE S. BARBER-ROTENBERG against the construct S6K1 (1–421, T412E, PDK1 activated) in a radioactive kinase assay using varying concentrations of ATP and 2 nM of enzyme. The determined IC_{50} values are: 3.61 nM (1 μ M ATP), 4.46 nM (10 μ M ATP), 6.90 nM (100 μ M ATP), 11.23 nM (250 μ M ATP), and 18.86 nM (500 μ M ATP). Data points represent mean values calculated from triplicates.

3.2.3.4 Characterisation of **87**

The radioactive kinase assays, using either S6K1 or S6K2 as target molecule, resulting to the following IC_{50} values were performed by JULIE S. BARBER-ROTENBERG. Testing the inhibitor **87** at a range of concentrations from 1 μ M ATP to 500 μ M ATP resulted in an expected increase of the IC_{50} value concurrent with the increasing ATP concentrations from 3.61 nM at 1 μ M ATP to 18.86 nM at 500 μ M ATP, confirming that **87** is an ATP competitive inhibitor, see Figure 38. The increase in IC_{50} values between 1 μ M and 500 μ M ATP is quite modest compared to the range published before, indicating that the inhibitor binds very tightly within the ATP binding site.^[232]

To further prove the specificity of **87** for the S6K1 isoform, the compound was also analysed against recombinant S6K2, which resulted in an IC_{50} value of 11.2 nM, which is in the same range as the IC_{50} value for S6K1, see Figure 39. Thus, leads to no significant prevalence of **87** for any S6K isoform. Indeed, S6K1 and S6K2 share 83% sequence identity in the catalytic domain.^[233]

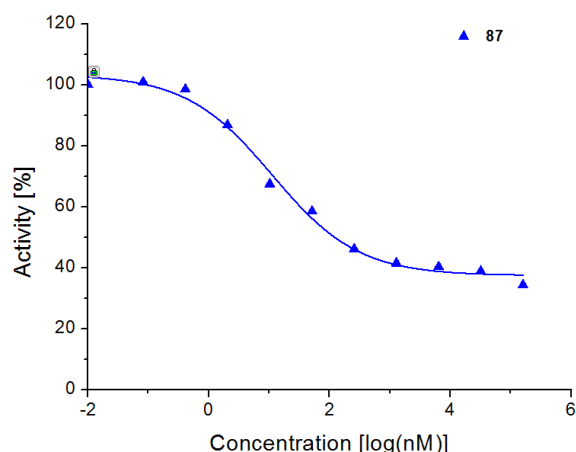


Figure 39: Radioactive kinase assay of **87** (11.2 nM) against S6K2 using 100 μ M of ATP and 2 nM of enzyme; performed by JULIE S. BARBER-ROTENBERG.

To establish the kinase selectivity profile of **87**, the compound was submitted at a concentration of 100 nM to the DiscoverX KINOMEScanTM performed by LeadHunter Discovery Services. **87** was tested against 456 kinases. The results for primary screen binding interactions are reported as percent of control ('% Ctrl', (POC)), where lower numbers indicate stronger hits and larger red circles in the dendrogram, see Figure 40. Empiric investigations proved that binding constants (K_d) are correlated with primary screening results, whereas lower POC values correlate with low K_d values (higher affinity interactions). Moreover, the selectivity score (SS) is a quantitative measure of compound selectivity. It is calculated by based on the number of kinases bound by the compound divided by the total number of distinct kinases tested, excluding variants. Furthermore, this score value can be calculated for different selectivity levels using POC as a potency threshold, e.g. below 35% or 10%. These SS clustered in different selectivity score types (SST) provide a quantitative method of describing compound selectivity and allow a facilitated comparison of different compounds among each other.

87 demonstrated a high degree of kinase selectivity. Only 10 kinases (2.2%) showed less than 10% activity (SST(10)) and only 26 kinases (5.7%) showed less

than 35% (SST(35)). In analogue to **85**, **87** showed characteristic inhibition of the CAM, DAP, FLT, PIM, and RSK family member kinases. Unexpectedly, S6K1 itself had a residual activity of 71% in the DiscoverX KINOMEScanTM with 70 kinases (15.3%) showing a higher degree of inhibition than S6K1. The potency of **87** seems to be greater against the S6K1 prepared by our protocol than the preparation performed by Lead Hunter Discovery Services. The different S6K1 kinase preparation and/or phosphorylation state, used by Lead Hunter Discovery Services, may have led to the different **87** potencies measured for S6K1. Nevertheless, taking together the analysis of **87** against S6K1 and the kinase profiling results led to the conclusion, that **87** exhibits a high degree of kinase selectivity.

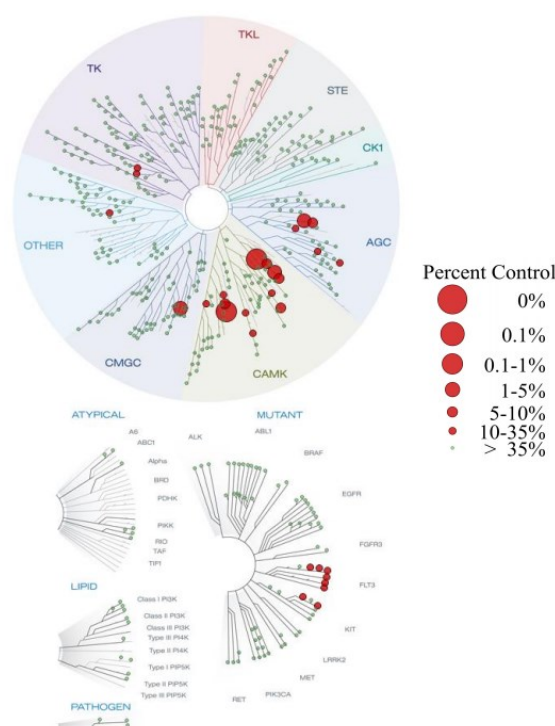


Figure 40: Kinase profiling of **87**. The complex was tested against 456 human kinases at 100 nM by an active-site-directed affinity screening (KINOMEScanTM, DiscoverX, LeadHunter Discovery Services). The dendrograms show the remaining POC levels of the kinases in percent to the control depicted as red circles. The selectivity score type (SST), the number of hits (NH) as well as the selectivity score (SS) of **87** are: SST(35) NH(20) SS(0.051); SST(10) NH(10) SS(0.025); SST(1) NH(2) SS(0.005).

3.2.3.5 Crystallisation Studies with **87**

To investigate the molecular mechanisms for the increased potency of **87** over **85**, the X-ray crystal structure of **87** in complex with S6K1 to 2.7 Å resolution was determined, see Table 13. In this context, the crystal preparation and growth was performed by JIE QIN, the compound soaking was performed by JEMILAT SALAMI, and the structure was solved by JOHN DOSMIC. The overall structure for the **87**-bound S6K1 (pdb: 4RLP) is very similar to the **85**-bound structure (pdb: 4RLO), with an r.m.s.d. of 0.54 Å for all atoms. Especially the p- and activation-loops, the α D, and the α C-helices take an almost identical conformations, although the α C-helix is about one turn shorter at its N-terminal end, see Figure 41.

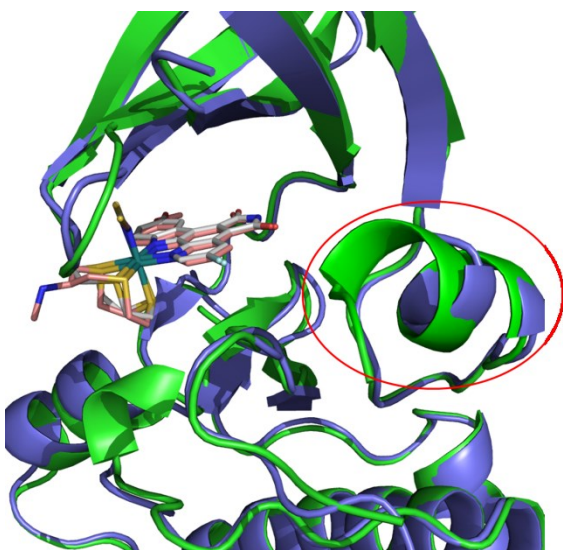


Figure 41: Superimposed structures of S6K1 bound to **85** (green) (pdb: 4RLO) and bound to **87** (blue) (pdb: 4RLP). The α C-helix of S6K1 (red circle) is one turn shorter at its N-terminal end of the **87**-bound structure compared to the **85**-bound structure. Oxygen atoms are depicted in red, nitrogen in blue, fluorine in light blue. S6K1 bound to **85** is depicted as cartoon with carbon atoms in green and carbon atoms of **85** in grey. S6K1 bound to **87** is depicted as cartoon with carbon atoms in navy and carbon atoms of **87** in apricot.

87 retains all interactions made by **85**, covering some additional interactions including a hydrogen bond between the backbone carbonyl of Lys-99 of the kinase p-loop with the amine ligand of the

N-methyl-1,4,7-trithiacyclodecan-9-amine ligand. The methoxy group of the pyridocarbazole moiety forms VAN-DER-WAALS interactions with Tyr-174 of the kinase hinge region, see Figure 42. These additional interactions of **87** likely contribute to the increased potency of **87** over **85**. The protrusion of the amine ligand into the region where protein substrate binds for phosphorylation probably also contributes to the increased inhibitor potency.

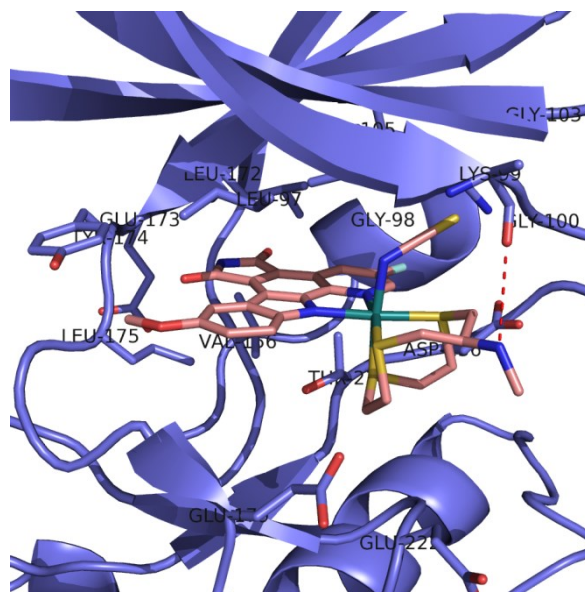


Figure 42: **87** forms more interactions with the ATP binding site of S6K1 compared to **85** (pdb: 4RLP). An additional hydrogen bond between the methylamine group and Lys-99 can be observed. The methoxy group of the pyridocarbazole pharmacophore ligand increases VAN-DER-WAALS contacts especially to Tyr-174. Oxygen atoms are depicted in red, nitrogen in blue, fluorine in light blue. S6K1 bound to **87** is depicted as cartoon with carbon atoms in navy and carbon atoms of **87** in apricot.

3.2.3.6 Cellular Properties of **87**

After establishing that **87** functions as a potent ATP competitive S6K1 inhibitor *in vitro*, studies to characterise the cellular activity have been performed by PATRICIA REYES-URIBE. **87** was first tested for overall cell cytotoxicity and downregulation of phosphorylation of S6 in the 451Lu (BRAFFV600E mutant) and 451Lu-MR (BRAFF/MEK-inhibitor resistant) melanoma cell lines. Cells were treated with inhibitor

ranging from 0.001 μM to 10 μM for 22 h, see Figure 43. Neither the 451Lu or 451Lu-MR cell lines showed a significant decrease in S6 phosphorylation, nor a decrease in cell viability as indicated by the absence of cleaved PARP. There was also no change in total S6 or peEF2K levels, indicating that mTOR was not targeted by **87**.

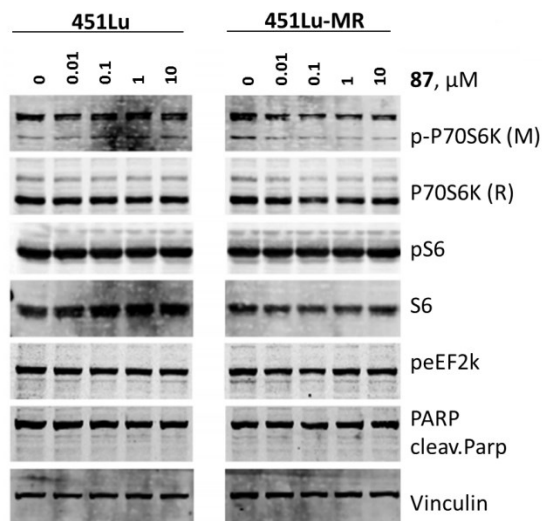


Figure 43: Western Blot of human cells treated with **87**. 451Lu (BRAFV600E mutant) and 451Lu-MR (BRAF/MEK-inhibitor resistant) melanoma cells were treated with increasing concentrations of **87** for 22 h. Cells were lysed and blotted for pS6 and other downstream effectors of S6K1. Neither the 451Lu or 451Lu-MR cell lines showed a significant decrease in S6 phosphorylation. The absence of cleaved PARP indicates unaffected cell viability. No change in total S6 or peEF2K levels indicate that mTOR was not affected by **87**. The experiment was performed by PATRICIA REYES-URIBE.

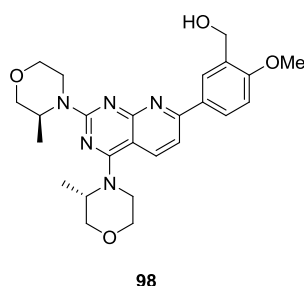


Figure 44: AZD8055, an ATP-competitive dual mTORC1 and mTORC2 inhibitor.^[234,235]

Furthermore, the effect of **87** in 293T cells, at both 3 h and 16 h of treatment, was investigated, see Figure 46. As controls, AZD8055 (**98**), PF-4708671 (**97**), and **99** were measured in parallel. AZD8055 is an

ATP-competitive dual mTORC1 and mTORC2 inhibitor that inhibits their phosphorylation and consequently the phosphorylation of the substrates S6K1 and 4EBP1 as mTORC1 substrates, as well as the phosphorylation of AKT, which is the downstream target of mTORC2.^[234,235] PF-4708671 is a reported S6K1 inhibitor that does not affect the phosphorylation of AKT. **99** is an **87** analogue with an IC_{50} of 11 nM towards S6K1. In **99** the fluorine of **85** is substituted by a hydroxymethyl group and the thiocyanate ligand by selenocyanate.

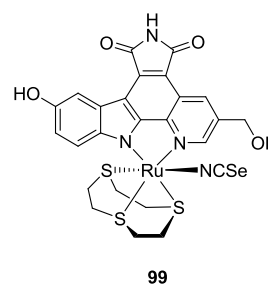


Figure 45: Second generation S6K1 inhibitor **99**.

Previous studies using **97** demonstrated a significant reduction in S6 phosphorylation in 293T cells within 30 minutes.^[228] Therefore, both a short time point of 3 h and long-time point of 16 h for treatment were evaluated. As expected, the **98** mTOR inhibitor showed a significant decrease in downstream target levels of pS6 at both the S235 and S240 sites, along with a decrease in pAKT at T308 and S473. The **97** compound showed a modest decrease in phosphorylation of S6 at the 3 h time point, but this phosphorylation returned to near basal levels by the 16 h time point. No effect on the phosphorylation of AKT was observed. Notably, neither **87** nor **99** inhibited phosphorylation of S6 or AKT. Therefore, **87** either has poor cell membrane permeability or the inhibition of S6K1 in cells does not significantly reduce S6 phosphorylation. The latter possibility is consistent with the fact that the structurally unrelated compound **97** also shows poor inhibition of S6 phosphorylation in cells.

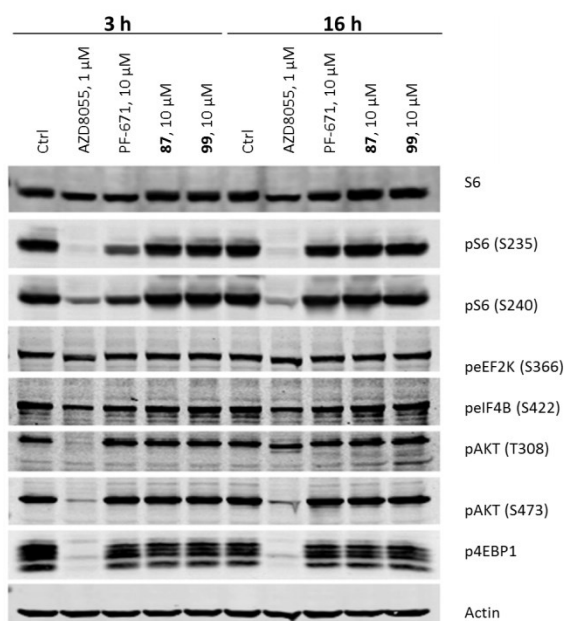


Figure 46: Western Blot of 293T cells treated with AZD8055 (**98**) (dual mTORC1 and mTORC2 inhibitor), PF-671 (4708671) (**97**), **87**, or **99** for 3 or 16 h. AZD8055 shows a significant decrease of pS6 at the S235 and S240 sites and a decrease of pAKT at T308 and S473. PF-4708671 shows a modest decrease in phosphorylation of S6 after 3 h, but almost basal levels after 16 h, and no effect on the phosphorylation of AKT. Neither **87** nor **99** inhibit phosphorylation of S6 or AKT. The experiment was performed by PATRICIA REYES-URIBE.

Moreover, S6K2 is also capable of S6 phosphorylation and could circumvent an S6K1 inhibition in a cellular system.^[236] To verify if **87** is able to inhibit S6 phosphorylation in a setting excluding S6K2, its inhibition potency of S6 phosphorylation in budding yeast was investigated by HAIYING LIU, where only a single kinase, *sch9Δ*, is orthologous to human S6K1. In this system, the treatment of wild-type budding yeast cells (BY4742) with **87** significantly decreased the level of phosphorylated S6 in a dose dependent manner, see Figure 47. At the highest dosage, S6 phosphorylation was reduced to a level similar to the *sch9Δ* knockout strain. This control experiment suggests that **87** functions as an inhibitor of S6 kinases *in vivo* in a yeast cellular system.

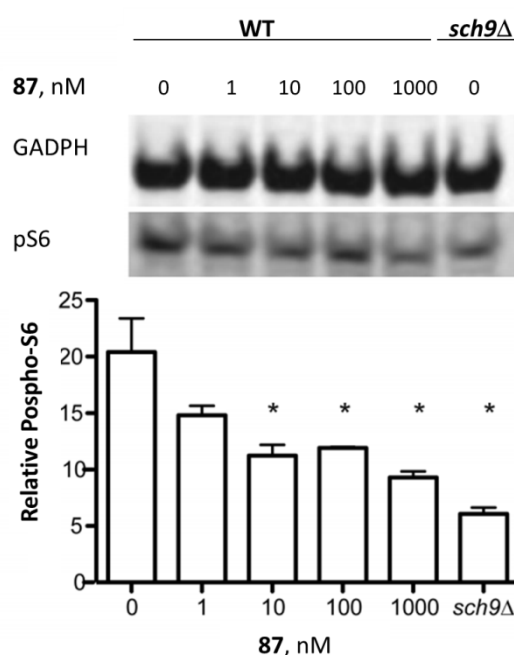


Figure 47: Western Blot of BY4742 budding yeast cells treated with **87** for 4 h. They were then lysed and blotted for pS6. **87** significantly decreased the level of phosphorylated S6 in a dose-dependent manner. At 1 μ M dosage, S6 phosphorylation level is similar to the *sch9Δ* knockout strain. Quantitative Western blot signals were detected by Li-Cor, and the relative pS6 levels were calculated by normalizing raw pS6 measurements to GAPDH signals. (*) $p < 0.05$ (two-tailed student-t test, $n = 3$). The experiment was performed by HAIYING LIU.

3.2.4 Interpretation

The Millipore Kinase Profiler and radioactivity-based kinase assays proved **85** as a selective and potent S6K1 inhibitor with an IC_{50} of 100 nM and inhibiting 93% of S6K1 activity and only 16% of 283 kinases by less than 90%. Furthermore, it served as a lead compound for a second generation of potent and selective S6K1 inhibitors. **86**, an analogue in which an isocyanate group replaces the monodentate isothiocyanate is about 1000-fold less potent, implying that potency and specificity could be further optimised. The crystal structure of **85** bound to S6K1 provided important molecular insights for the development of **87**, a compound containing a novel ligand scaffold and an IC_{50} in the single digit nanomolar range for S6K1.

Moreover, the crystal structure of **87** bound to S6K1 revealed the molecular basis for the compound's potency and selectivity to S6K1.

To investigate the efficacy of **87** in living cells, the inhibitor was evaluated in both human 293T and BRAFV600E mutant melanoma cells and in budding yeast. **87** was only able to inhibit S6 phosphorylation in yeast cells. This results may be evoked by the following suggested incidences: either the compound is unable to enter human cells, a significant shift in the IC_{50} of the compound occurs in the presence of physiological levels of ATP, or the uninhibited S6K2 isoform in human cells, is still capable of maintaining S6 phosphorylation. Regarding that **87** had previously been used to successfully target MST1, PAK1, and PI3K in cells, the second possibility seems to be plausible.^[159,188,231]

The setting of the radioactive kinase assay prohibits measurements at physiological levels of ATP. Nevertheless, the activity of **87** against S6K1 using an ATP range from 10 μ M to 500 μ M and the subsequent increase of IC_{50} values with increasing ATP concentrations, is consistent with **87** binding competitively to ATP in the ATP binding site. Moreover, this conclusion is further confirmed by the crystal structure of the S6K1/**87** complex. Interestingly, the IC_{50} ranged from 3.91 nM at 10 μ M ATP to only 25.79 nM at 500 μ M ATP (a 6-fold increase), suggesting that S6K1 binds ATP relatively loosely. Therefore, it is likely that **87** is able to displace ATP even at the higher physiological concentration. Based on this accumulated data, **87** is supposed of being unable to inhibit S6 phosphorylation in human cells because S6 is still phosphorylated by the uninhibited S6K2.

S6K1 and S6K2 share 83% sequence identity in the catalytic domain.^[233] A study involving S6K1/2 knockdown in mice suggests that both S6K1 and S6K2 are required for full phosphorylation of S6, but

S6K2 may be the more important one for the phosphorylation of S6.^[236] The MEK inhibitor AZD6244 (**100**) showed additive effects on decreasing the phosphorylation of S6 *in vitro*, when treated in combination with siRNA inhibition of both S6K1 and S6K2, indicating the importance of S6K2 in the phosphorylation of S6.^[237] Furthermore, while pathologically inconspicuous tissues often express low levels of S6K2, overexpression of S6K2 in cancer cells is observed more commonly than an overexpression of S6K1.^[238–241] Concluding, targeting S6K2 either alone or in combination with S6K1 may be a more promising option for direct S6 inhibition in melanoma cells and potentially other cancer forms.

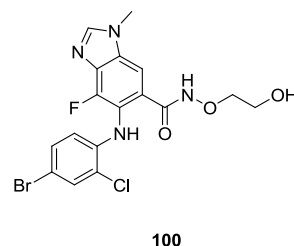


Figure 48: Structure of the MEK inhibitor Selumetinib (AZD6244) (**100**).^[242]

Despite the similarities in the catalytic domain, homology modelling between S6K1 and S6K2 indicates an important difference in residue Tyr-174 which is crucial for binding of **87** and is exchanged for a cysteine in S6K2.^[243] This residue is located in the hinge region of S6K1 and forms an important VAN-DER-WAALS contact with the methyl group of the secondary amine, which cannot be formed with a cysteine residue. This circumstance suggests that **87** may not be a potent inhibitor for S6K2. However, the cumulated data show no significant prevalence of **87** towards S6K2. The perinatal lethality of S6K1-/-/S6K2-/- knockout mice implies that S6K2 targeting may need to be selective for therapeutic value.^[236] Up to now, no commercially available S6K2-selective inhibitors are reported, indicating a potential target for the next series of organometallic inhibitors.

Taken together, **87** is a potent and selective S6K1 inhibitor that should be useful to probe S6K1 function and could act as a starting point for the development of efficacious S6K inhibitors for therapeutic use. Although, to realise the selective targeting of S6K2, especially the structural challenges of the metal based inhibitor had to be solved. In particular, **87** is based on the **85** lead structure, but it differs by a methoxy group instead of the hydroxyl group at the pyridocarbazole moiety and the ten-membered thioether-containing tridentate ligand instead of the nine-membered ring. Especially the substitution of the nine-membered ring from the symmetrical 1,4,7-trithiacyclononane ligand to a prochiral 1,4,7-trithiacyclodecane bearing a basic *N*-methylamine group at the 9-position significantly increased the structural complexity of the inhibitor, which is exemplified by the number of possible stereoisomers. This prochiral stereogenic centre becomes a true stereocentre after the complexation reaction compared to the tridentate ligand in the uncoordinated state.

Therefore, the coordination must be controlled to obtain the desired complex which directs the hydrogen bond accepting as well as donating *N*-methylamine group in the ATP binding site of S6K1 in optimised fashion. The orientation of the *N*-methylamine functionality coordinated to the metal centre underlies several synthetic principles, which can be utilised by a smart reaction procedure. Therefore, a detailed analysis of the stereogenic effects during complexation must be considered to transfer and improve the concepts to design future complexes with desired structure.

During this synthetic route, the allyloxycarbonyl group was chosen to protect the *N*-methylamine functionality combining several favourable advantages at once. The most important reason is to avoid the formation of possible side products during the complexation reaction itself due to the cross-coordination of the *N*-methylamine group to a second metal ion. Further, the

synthetically orthogonal deprotection of the allyloxycarbonyl group can be performed under mild conditions using tetrakis(triphenylphosphine)palladium. Nevertheless, due to its bulkiness, the allyloxycarbonyl group is an ideal modification to implement a large residue to the *N*-methyl-1,4,7-trithiacyclodecan-9-amine ligand leading to a substrate based stereocontrol during the complexation reaction. The ruthenium precursor has two different possibilities to coordinate to the tridentate ligand resulting in different orientations of the allyloxycarbonyl protected *N*-methylamine functionality, see Figure 49. Both, the coordination from the front side and from the back side, lead to a six membered ring with the metal ion at one end, highlighted in red. This cyclic six membered metallacycle can be assumed to act similarly to cyclohexane with the corresponding sterical and conformational principles. Therefore, the coordination of the metal ion from the front side leading to a six membered metallacycle in a stable chair conformation as well as setting the allyloxycarbonyl protected *N*-methylamine group into an equatorial position is highly favoured in contrast to all other possible structural isomers.

The final exchange of the three monodentate ligands by the pyridocarbazole and the isothiocyanate also underlies mainly steric effects forced by the coordinated allyl-*N*-methyl-(1,4,7-trithiacyclodecan-9-yl) carbamate. The bulky pyridocarbazole ligand coordinates as far as possible from the tridentate ligand and coordinates therefore at the opposite positions to the sulfur atoms of the six-membered metallacycle, leaving only one residual position for the isothiocyanate. Furthermore, the described principles could be assured by the obtained crystal structure of the allyloxycarbonyl protected precursor of **87**, see Figure 29. Since the coordination positions for the two nitrogen atoms of the pyridocarbazole ligand towards the metal centre are both equal but the pyridocarbazole itself is asymmetric, a 180° flip

of the pharmacophore ligand leads exactly to the enantiomer, which is the bioactive one, see Figure 42.

The stereocontrol of the coordination sphere induced by the bulky allyloxycarbonyl-group is comparable to the concept introduced in Chapter 2.3. Even though the influence of the protection group during synthesis is valuable, its presence in the final inhibitor would be a disadvantage due to steric hindrances in the binding site of target kinases. For the purpose of inhibitor design with predefined structural scaffold, large persisting groups controlling the coordination sphere via steric effects cannot be applied for future development. Moreover, cleavable groups claim for additional synthetic steps, dramatically increasing the effort of the entire workflow. Nevertheless, the chirality-at-metal itself was not affected by the *N*-methyl 1,4,7-trithiacyclodecan-9-amine ligand due to its intrinsic symmetry. Therefore, the investigated complex **87** was obtained as a racemic mixture. However, the investigation of single enantiomers is standard for chiral organic compounds in biological context. To make organometallic compounds more and more adequate to the requirements of drug-like molecules, methods have to be developed to obtain a particular isomer in an enantiopure fashion.

Several concepts could be pursued to achieve this goal based on different approaches. To avoid a racemic mixture the synthesis of organometallic kinase inhibitors must avoid the formation of enantiomers, e.g.: by forming separable diastereomers during the complexation, or forming only one possible coordination product in analogue to organic *meso*-compounds. Whereas the first approach could be achieved using chiral ligands transmitting the chiral information into the metal complex, the latter one could be achieved via highly symmetric ligands. Both concepts were investigated and the advantages and disadvantages will be discussed in the following Chapters.

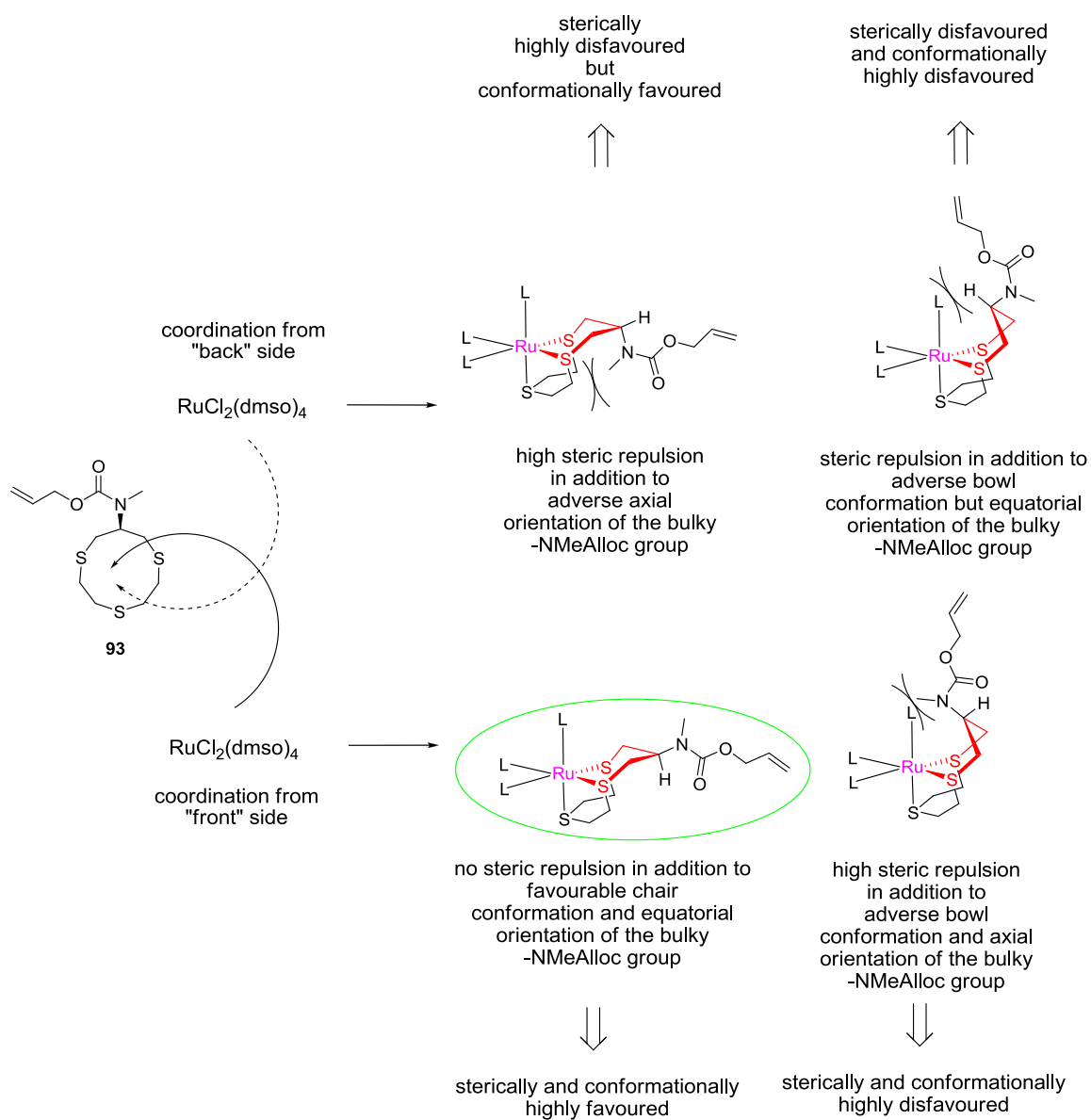


Figure 49: Interpretation of steric effects leading to the observed conformation and configuration of **94**.

3.3 Enantiopure Organorhodium(III) Complexes

3.3.1 Target Synopsis and Aim

3.3.1.1 PIM Kinases

The proviral insertion in murine (PIM) lymphoma protein genes were first identified as oncogenes in mouse models in the 1980s.^[244] They are constitutively active and the regulation of activity is mainly regulated at the transcriptional and translational level induced by diverse signals depending on the cell type.^[245,246] PIM kinases are expressed in haematopoietic,^[247–249] neuronal,^[250,251] vascular smooth muscle,^[252] cardiomyocyte,^[253] endothelial,^[254] and epithelial cell lineages.^[255,256] Moreover, they are already expressed in early progenitors of some of these cells types,^[257,258] and in embryonic stem cells.^[248,254,259]

PIM kinases, covering PIM-1, PIM-2, and PIM-3, play important physiological roles evidenced by knock-out mice experiments. For instance, PIM-1 deficient mice had a specific defect in IL-7 driven growth of pre-B cells, as well as IL-3 dependent growth of bone marrow-derived mast cells.^[248,257] PIM-2 deficient mice had reduced T cell activation and expansion in the presence of the serine/threonine protein kinase mTOR inhibitor rapamycin.^[260] PIM-3 deficient mice had an increased glucose tolerance.^[261]

However, the physiological activities of the PIM kinase family is mediated through the phosphorylation of a broad range of cellular effectors subdivided in different classes, i.e.: transcriptional regulators such as Myc,^[262] Myb,^[263] RUNX1 and RUNX3,^[264] cell cycle regulators such as p21,^[256,265] CDKN1B,^[266] Cdc25A,^[267] Cdc25C,^[268] signalling intermediates such as Socs-1,^[269] Socs-3,^[270] and MAP3K5,^[271] protein transla-

tion regulators such as eIF4B,^[272] eIF4EBP1,^[245] and apoptosis regulators such as BAD.^[245,273–275]

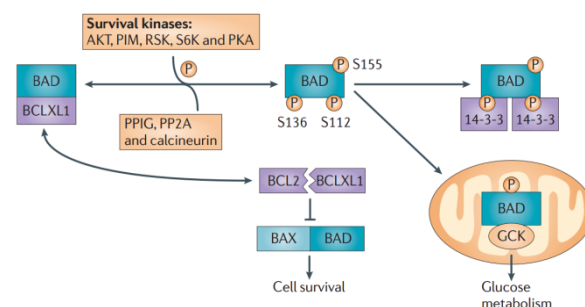


Figure 50: BAD has strong pro-apoptotic activity by binding to and neutralizing anti-apoptotic Bcl-2 partners.^[276] Moreover, BAD regulates glucose-dependent mitochondrial respiration in hepatocytes and pancreatic β -cells by activating glucokinase (GCK) via dimerization.^[276] The regulatory phosphorylation sites of BAD are Ser112, Ser135 and Ser155,^[276] phosphorylation of Ser112 and Ser135 lead to the binding of 14-3-3^[274,276,277] required for phosphorylation on Ser155. The Ser155 phosphorylation is the rate-limiting step for the dissociation from BCL-2 and BCL2L1.^[276] Several survival kinases like AKT, PIM, S6K1, PKA, RSK1 have been found to phosphorylate BAD, leading consequently to increased cell survival.^[274,276,278]

Due to the manifold interaction partners and substrates, and their role in cell signaling, PIM kinases are potent oncogenes overexpressed in a range of hematopoietic malignancies and solid cancers. PIM kinases are often overexpressed in the context of increased Myc levels,^[279] where the overexpression of PIM-1 has been observed to counteract Myc-induced apoptosis.^[280] In addition, PIM kinases prevent cells from apoptosis by the phosphorylation of the proapoptotic BCL-2-associated agonist of cell death (BAD), which abolishes the binding with the anti-apoptotic protein BCL-2, leading consequently to increased cell survival, see Figure 50.^[274] Moreover, they are involved in the cell proliferation through the phosphorylation of the cyclin-dependent kinase inhibitors p21.^[266] Due to their digressive expression in several human tumors, they could be important contributors in the pathogenesis of neoplasias including lymphomas, gastric, colorectal and prostate cancers.^[281–283] PIM kinase expression is correlated with poor prognosis in most hem-

atopoietic malignancies.^[284–287] A similar association was observed in pancreatic ductal carcinoma,^[288] non-small-cell lung cancer,^[289] in gastric cancer,^[290] and squamous cell carcinoma of the head and neck.^[291] The cumulated findings make PIM kinases to appealing targets for specific treatment of cancer and autoimmune diseases.^[278,292,293]

3.3.1.2 FLT-3

The FMS-like tyrosine kinase 3 (FLT-3) is a 993 amino acid long membrane bound receptor tyrosine kinase (RTK) of the subclass III family. It is composed of five immunoglobulin-like extracellular domains, a transmembrane domain, a juxtamembrane domain and two intracellular tyrosine kinase domains linked by a kinase-insert domain.^[294] Two forms of human FLT-3 have been described: a 158–160-kDa membrane bound protein glycosylated at the extracellular *N*-terminus and an unglycosylated cytosolic 130–143-kDa protein.^[295,296] In the inactive state, the conformation of the receptor might result in steric inhibition of dimerization and to the exposure of phosphorylate acceptor sites in the tyrosine kinase domain by the juxtamembrane domain. This occurs to be a general inhibition mechanism also found in other families of tyrosine kinases.^[297] Thus, after ligand binding, the membrane-bound FLT-3 changes its conformation, forming a homodimer and exposing phosphorylate acceptor sites in the tyrosine kinase domain.^[298] The dimerization leads to a stabilizing conformational change, further increasing the activation of the receptor.^[299] In contrast, the receptor inactivation is mainly driven by receptor internalization and degradation.^[298]

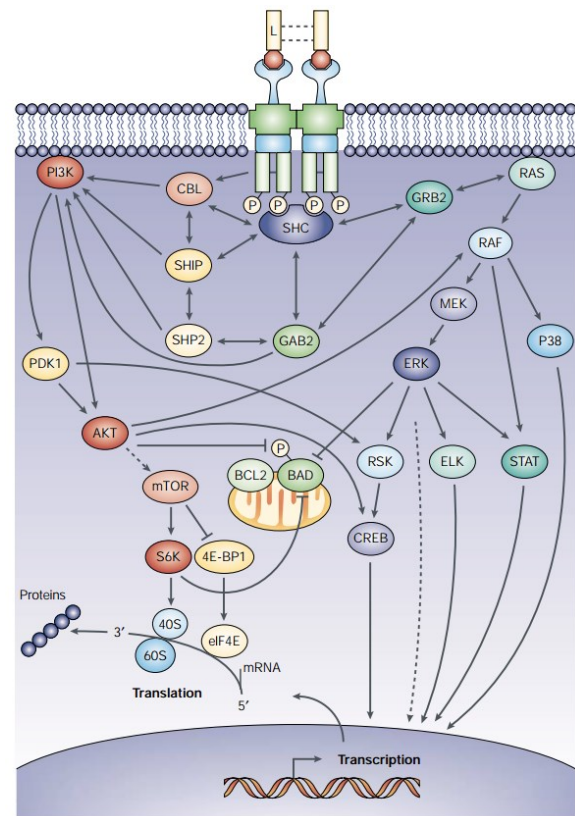


Figure 51: FLT-3 signalling cascade has not been entirely characterised. However, the binding of FLT-3 ligand (L) to FLT-3 activates the Akt/mTOR and Ras-Raf pathways resulting in increased cell proliferation and the inhibition of apoptosis.^[300–302]

FLT-3, triggers both the Ras-Raf-MEK signaling pathway via the activation of the growth factor receptor-bound protein 2 (Grb2)^[303,304] and the Akt/mTOR signaling pathway mediated by Gab, Ship, Cbl, which subsequently activate the phosphatidylinositol-3-kinase (PI3K),^[303,305,306] see Figure 51.^[301,302] These interactions lead to the phosphorylation of associated proteins and the activation of downstream effectors involved in haematopoiesis.^[301,302] Moreover, the FLT-3 receptor was found to be associated with SH2-domain-containing inositol phosphatase (Ship) activity.^[307] Beside the primary role of Ship in phospholipid metabolism, it also acts as a negative regulator of cell proliferation mediated by the competitive binding of phosphorylated SHC proteins, which would otherwise activate the Ras-Raf-Mek-Erk pathway.^[303] However, FLT-3 pathways seem to be highly species and tissue specific;^[301,303,306] whereas, in healthy state, FLT-3 is expressed mainly in early

myeloid and lymphoid progenitors,^[308] but not in erythroid cells,^[309] megakaryocytes,^[310] or mast cells.^[311]

As all members of the RTK class III, FLT-3 plays an important role in the early hematopoiesis, being involved in proliferation, differentiation and apoptosis.^[300,312] Moreover, its increased expression was reported in 70-90% cases of acute myeloid leukemia and acute lymphoblastic leukemia,^[296,308,313–315] but not in chronic myeloid leukemia (CML) and chronic lymphocytic leukemia (CLL) above all possessing a common progenitor stem cell.^[316] Despite the widespread expression of FLT-3 and its role in signaling pathways, it is surprising that *flt-3*-knockout mice had relatively inconspicuous haematopoiesis without severe morphological changes in the bone marrow.^[317] However, mice with both, *kit* and *flt-3* knockouts, developed lethal haematopoietic deficiencies indicating a conjunction of FLT-3 with other growth factor receptors to promote the proliferation and differentiation of myeloid and lymphoid cells.^[317]

These findings suggest a significant but not absolute role of FLT-3 in healthy haematopoiesis and thus indicate selective FLT-3 inhibition as a treatment option to block inappropriate FLT-3 activation in leukaemia cells avoiding severe haematopoietic side-effects. Moreover, considering the high frequency of activating FLT-3 mutations in patients with AML, FLT-3 and its downstream pathway members are attractive targets for directed inhibition.^[300,318]

3.3.1.3 Aurora Kinases

The serine/threonine Aurora kinases, play important roles in the control of the centrosome and nuclear cycles, and have essential functions in mitotic processes covering the chromosome condensation, spindle dynamics, kinetochore-microtubule interactions, chromosome orientation and establishment of the metaphase plate.^[319–325] Moreover, they are also involved in cytokinesis. Due to the first description of Aurora A in the spindle pole regions, it was named after the polar lights.^[322] However the family consist of Aurora A, B, and C whereas human Aurora A and B share 71% identity.^[326,327] Nevertheless, the main differences are located in the amino-terminal domain.^[328,329] Especially Aurora A and B are of high interest in research, whereas little is known about Aurora C.^[326,327]

Aurora A associates with the separating centrosomes during late S/early G2, which is directed independently by the amino-terminal region as well as the carboxy-terminal catalytic domain.^[330] But the catalytic kinase activity is not necessarily required for the association. Thereafter TPX2 has been found to mediate Aurora-A activation and localization to the spindle microtubules, but not to the spindle poles.^[331] During cell maturation the absence of Aurora A, has significant adverse effects on the recruitment of several components of the pericentriolar material, like γ -tubulin, to the centrosome and downstream effectors leading to a decreased microtubule mass of spindles by about 60%.^[332–334] Moreover, Aurora A was identified as a component of the progesterone signalling pathway.^[335] Its activation is an early event after progesterone induced signal transduction resulting in the activation of the ERK/MAPK pathway.

The regulation of Aurora A is complex and involves phosphorylation and dephosphorylation as well as protein degradation.^[336] Aurora A has three phosphorylation sites, Ser53, Thr288, Ser349, whereas the first two sites are important for kinase regulation, the third is not essential for catalytic activity but structural stability.^[336] The degradation of Aurora A occurs in the late mitosis/early G1 by the APC/C.^[73,74]

Human Aurora B is a chromosomal passenger protein with full expression peak at the G2–M transition state, and maximal kinase activity during mitosis.^[328,337] Whereas the protein exchanges continuously with the surrounding cytoplasmic pool, the kinase association with central spindle microtubules during anaphase is highly reduced.^[338] Aurora B also seems to have an important role in the regulation of kinetochore–microtubule interactions in higher eukaryotes, whereas perturbation of its activity causes defects in chromosome congression.^[339–342] Moreover, Aurora-B kinases are important for the phosphorylation of histone H3.^[343]

To date, most interest has focused on Aurora A, due to its high potential as oncogene and its amplified expression in a number of cancer cell lines and primary tumours.^[328,344,345] Moreover, malfunction of Aurora A, as well as the overexpression of Aurora B or Plk1, cause cytokinesis failure and perturbed centrosome duplication.^[346,347] Remarkably, even catalytically inactive kinase forms induce cytokinesis failure and centrosome amplification.^[347] Aurora induced mitotic abnormalities are exacerbated in cells that lack p53 due to its inactivating influence on the kinase function.^[347,348] Nevertheless, Aurora B has also been implicated in cancer reasoned in the elevated levels of phosphorylated histone H3 and defects in chromosome segregation and cytokinesis.^[349] The resulting cells are aneuploid and can produce aggressive tumours as observed in human colorectal tumour cell lines.^[349] Taking all together, the important role of Aurora kinases in cell cycle progres-

sion and their role as oncogene in several tumor types revealed them as potential new target for cancer treatment, i.e.: of the treatment of prostate cancer.^[350–352] Further information is provided in literature.^[320,353–355]

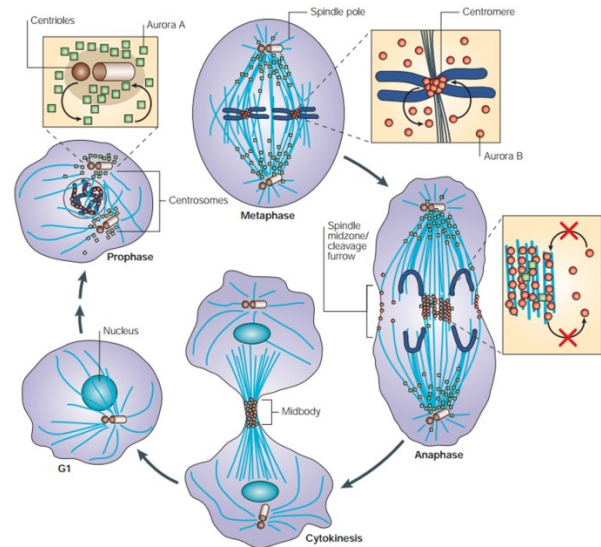


Figure 52: Starting from G1 phase, the expression of Aurora kinase A (green boxes) and Aurora B (red circles) increases turning into the prophase. Aurora A is mainly concentrated around the centrosomes. In opposite, Aurora B associated nuclear. During metaphase, Aurora A is attached to the microtubules adjacent to the spindle poles, whereas Aurora B is fixed to the inner centromere. In the next cell cycle phase, the anaphase, Aurora A is mainly located on the polar microtubules, although some might also be located in the spindle midzone. In contrast, Aurora B is exclusively concentrated in the area of spindle midzone and at the appropriate cell cortex at the site of cleavage-furrow ingression. In cytokinesis, both kinases are concentrated in the midbody.^[320]

3.3.2 Synthesis and Structural Investigations

One strategy to control relative and absolute configuration of a metal centre is the use of chiral multidentate ligands, see Chapter 2.3. Along these lines, during previous work of the MEGGERS group, a chiral tridentate proline-containing ligand as being part of a cyclometalated rhodium(III) complex with the pharmacophore ligand **32** led to enantiopure metal complexes.^[197] This promising initial work inspired us to investigate this chiral ligand in the context of the established metallo-pyridocarbazole kinase inhibitors.

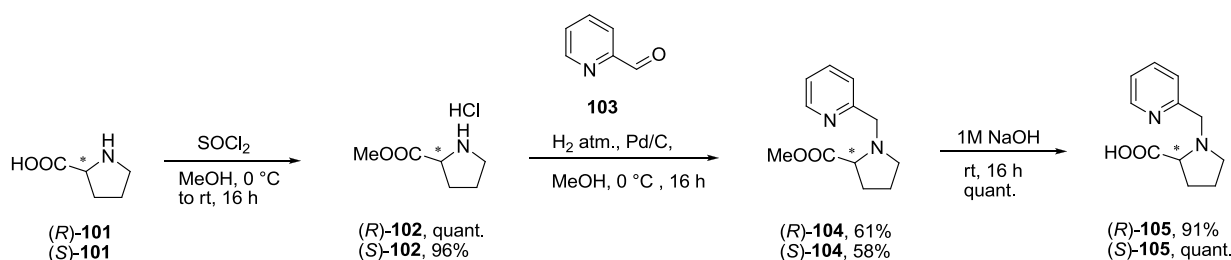
3.3.2.1 Synthesis of Enantiopure Prolinato Organorhodium(III) Complexes

Starting with either enantiopure (*R*) or (*S*)-pyrrolidine-2-carboxylic acid ((*R*)-**101** and (*S*)-**101**) first the protection of the carboxyl group to methyl ester was performed by suspending the starting material in methanol and adding thionylchloride drop wise at 0 °C, followed by a slow warm up to ambient temperature over 16 h, see Scheme 12. The methyl pyrrolidine-2-carboxylate hydrochloride product was obtained in quantitative yield for (*R*)-**102** and 96% for (*S*)-**102**.

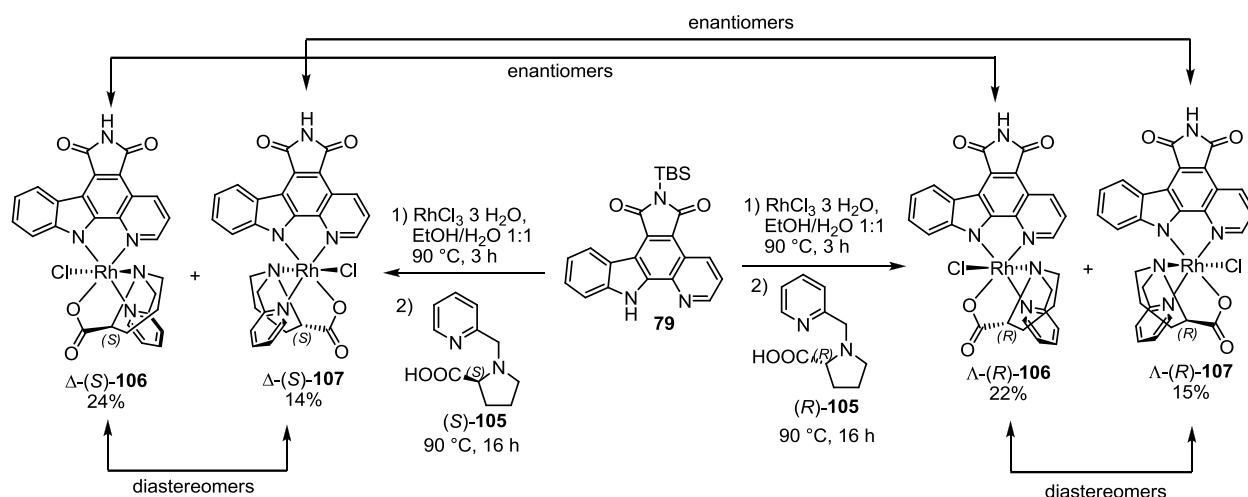
After the protection of the carboxyl group, a reductive amination using picolinaldehyde (**103**) was performed to attach a pyridine ring to (*R*)-**102** and (*S*)-**102**, respectively. Hence, palladium on carbon (10 wt. %) was suspended in methanol, pic-

olinaldehyde, and sodium acetate were added at 0 °C. After addition of (*R*)-**102** or (*S*)-**102**, the reaction mixture was stirred for 1 h and the nitrogen atmosphere was completely substituted by hydrogen in three turns. The reaction was continued for 16 h allowing the mixture to warm up to ambient temperature. After chromatographic purification, 61% of (*R*)-**104** and 58% of (*S*)-**104** were obtained. Prior to the complexation reaction the methyl ester must be cleaved to reveal the carboxyl group. Therefore, both compounds were dissolved in sodium hydroxide (1 M, aq.) and reacted for 16 h at ambient temperature. (*R*)-**105** was obtained in 91% and (*S*)-**105** in quantitative yields.

The rhodium(III) complexes were synthesised in a one-pot reaction under nitrogen atmosphere in sealed vessels, see Scheme 13. Accordingly, the pyridocarbazole ligand **79** was reacted first in a sequential addition to a suspension of RhCl₃·3H₂O in an ethanol/water mixture at 90 °C for 3 h followed by addition of the chiral tridentate ligand (*R*)-**105** or (*S*)-**105**. Reacting the mixtures at 90 °C for 16 h led to the formation of the two diastereomers Λ -(*R*)-**106** (22%) plus Λ -(*R*)-**107** (15%) starting from (*R*)-**105**, and Δ -(*S*)-**106** (24%) plus Δ -(*S*)-**107** (14%) starting from (*S*)-**105**. Note that the absolute configuration of the chiral ligand controls the absolute metal centred configuration with *R*-ligand leading to Λ -metal and *S*-ligand to Δ -metal so that in the course of each reaction only two diastereomers are generated. These two diastereomers could be separated by silica gel chromatography with methylene chloride/methanol 20:1 to 10:1 followed by a preparative TLC for each single



Scheme 12: Synthesis of enantiopure chiral tridentate ligand (*R*)-**105** and (*S*)-**105**.



Scheme 13: Asymmetric synthesis of organorhodium complexes Δ -(R)-106, Δ -(R)-107, Δ -(S)-106 and Δ -(S)-107.

compound using methylene chloride/methanol 15:1. The *tert*-butyl-dimethyl silyl protection group of ligand **79** was cleaved under the reaction conditions. Additional isomers were not detected which can be rationalised with the restricted possible conformations of the proline-based ligand. The low yields of this reaction may arise from the usage of $\text{RhCl}_3 \cdot 3\text{H}_2\text{O}$ as starting material. Indeed, rhodium(III) complexes typically react very slowly.^[356] Moreover, the labilizing *trans* effect of chloride is greater than that of the aqua ligand leading among others to a *fac*- $[\text{RhCl}_3(\text{H}_2\text{O})_3]$ configuration possessing all aqua ligands in opposite positions to the chloride ligands.^[356] This *fac*- $[\text{RhCl}_3(\text{H}_2\text{O})_3]$ configuration is inert to further aquation and thus may also be adverse for the ligand exchange by i.e. ligand **79**, (R)-**105**, or (S)-**105** respectively. The formation of *fac*- $[\text{RhCl}_3(\text{H}_2\text{O})_3]$ is promoted by free chloride ions which are inevitably released during the coordination of **79** to the metal centre of already reacted $\text{RhCl}_3 \cdot 3\text{H}_2\text{O}$. Therefore, scavenging free chloride ions in solution or pre-activating $\text{RhCl}_3 \cdot 3\text{H}_2\text{O}$ into precursors with labilised ligands like $[\text{Rh}(\text{C}_4\text{H}_8\text{S})_3\text{Cl}_3]$ may improve the product yield.^[151]

3.3.2.2 Assignment of The Relative Stereoconfiguration

The assignment of the stereoconfiguration in case of the presented complexes Δ -(R)-106, Δ -(R)-107, Δ -(S)-106 and Δ -(S)-107 is not trivial. Thus, a short abstract of the operations leading the nomenclature is mandatory. To describe the absolute configuration, and to distinguish the enantiomers of coordination compounds, two major, but fundamentally different, systems have been elaborated and documented by the IUPAC in the *Red Book*.^[357] Although, a short overview is indispensable:

The first is based on the chemical constitution of the compound and is related to the R/S convention established by Cahn-Ingold-Prelog (CIP) and is applied to describe tetrahedral centres. In contrast, the closely related C/A (C = clockwise, A = anti-clockwise) convention was established for other polyhedral coordination spheres. The R/S and C/A conventions use the priority sequencing according to Cahn-Ingold-Prelog, where the atomic number and the substituents of the coordinating atoms have to be respected to assign a priority, see Figure 53 a) and b).^[358,359] This system is often also applied to describe the configuration of

coordinated ligands beside the tetrahedral metal centres. Moreover, in case of pseudo-tetrahedral organometallic complexes, i.e.: a cyclopentadienyl ligand, the π -ligands were treated as monodentate ligands of highest priority, as it is true for (*R*)-**9**, see Figure 53 a). To assign the correct chirality symbol to an octahedral complex according to the C/A nomenclature the reference axis has to be identified: the coordinating atom of the highest CIP priority and the *trans* coordinated atom of lowest possible CIP priority form the reference axis. The reference axis is then oriented pointing the highest CIP priority ligand upwards and the residual coordination plane aligned perpendicular to the reference axis. Thereafter, the orientation of the ligands and their sequence of CIP priority numbers are compared, see Figure 53 b). Closing, a sequence readable in clockwise orientation is assigned by the symbol C, and a sequence readable in anticlockwise orientation is assigned by the symbol A.

The second nomenclature principle is based on the geometry of the molecule and is based on the skew-lines convention.^[357] This principle is mainly established to describe octahedral complexes and the two enantiomers are identified by the symbols Δ and Λ , Figure 53 c). A chiral enantiomeric pair of octahedral complexes in three-dimensional space corresponds unambiguously to a screw (or often referred as a helix) and is either right-handed leading to the Δ isomer or left-handed leading to the Λ isomer.

To describe the absolute configurations of octahedral complexes, both, the Δ/Λ system or the C/A system can be applied, but the first is used more commonly. Nevertheless, the C/A system is more general and probably used for most complexes. Moreover, the Δ/Λ system is only applicable to tris(bidentate), bis(bidentate) and closely related systems.

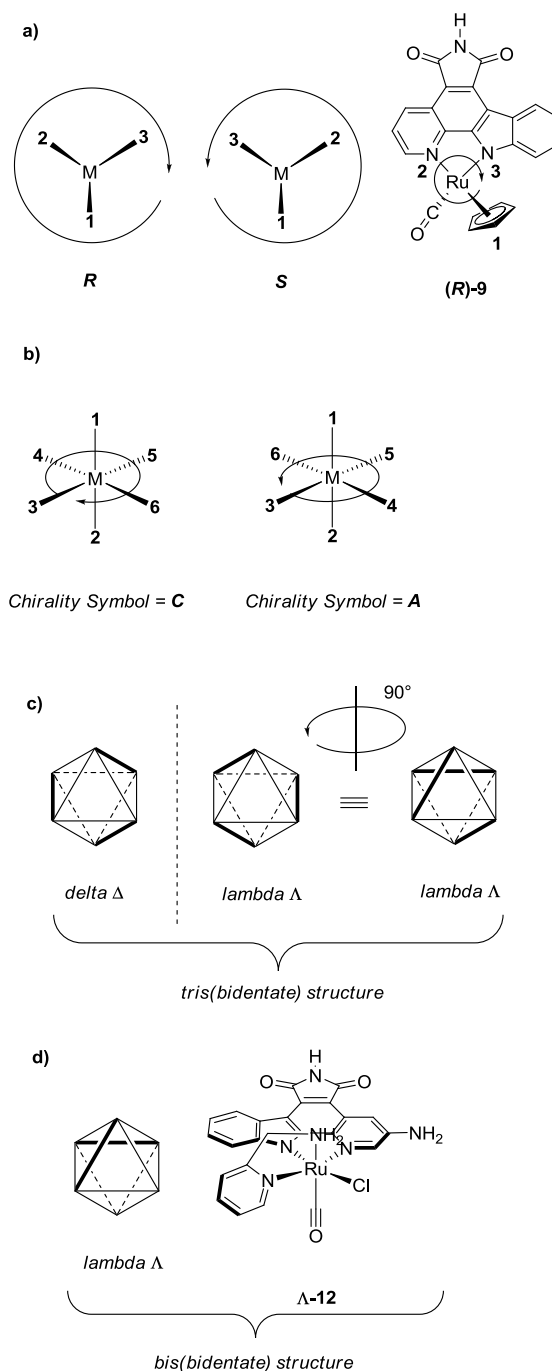


Figure 53: Assigning the relative stereoconfiguration of metal complexes. **a)** Tetrahedral metal centres can be assigned analogously to the Cahn-Ingold-Prelog (CIP) nomenclature established for organic compounds.^[358,359] The same priority rules are valid. However, π -ligands were treated as monodentate ligands of highest priority as in case of (*R*)-**9**. **b)** The coordinating atom of the highest CIP priority defines the reference axis. The highest CIP priority ligand is oriented upwards and the residual coordination plane is oriented perpendicular to the reference axis. The clockwise (C) or anticlockwise (A) oriented sequence of ligands leads to the appropriate chirality symbol. **c)** A chiral enantiomeric pair of octahedral complexes in three-dimensional space forms a screw being right-handed (Δ) or left-handed (Λ) isomer. **d)** The Δ/Λ -nomenclature is also applicable to bis(bidentate) and other related systems as illustrated for Λ -12.

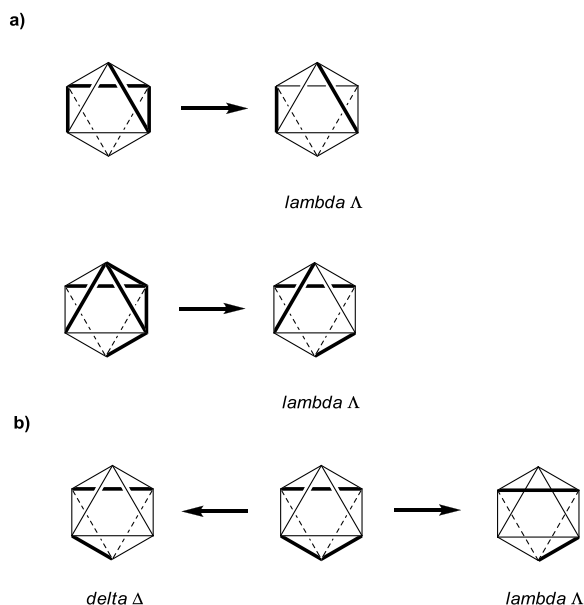


Figure 54: The terminal edge convention (TEC) simplifies polydentate ligands coordinated to octahedral complexes to apply the Δ/Λ -nomenclature. **a)** Only the edges of polydentate ligands were taken to account, whereas the connections inbetween were disregarded.^[360] The simplification via the TEC operation results in model complexes suitable for the Δ/Λ system. **b)** The TEC operation results not in a doubtless assignment of Δ or Λ configuration in case of octahedral complexes containing both a bidentate and a tridentate ligand.

To transfer the Δ/Λ -nomenclature on complexes of higher polydentate ligands additional rules are required and some solutions have been suggested in literature, i.e.: the terminal edges convention (TEC).^[360] However, they were not aimed as general nomenclature proposal, see Figure 54, and consequently the possible solutions to fit polydentate ligands to the Δ/Λ -nomenclature have not been adopted by the IUPAC to a general recommendation by now.^[357]

However, as the aim of this work is the clean comparison of enantiomers of octahedral complexes and their biological activities, the unambiguous definition of the stereoconfiguration according to the Δ/Λ -nomenclature is highly appreciable. Moreover, this would offer a quick correlation of the newly synthesised complexes to former ones based on tris(bidentate) or bis(bidentate) scaffolds as Λ -12. Unfortunately, the mentioned TEC fails considering octahedral complexes containing both bi-

dentate and tridentate ligands as it is true for Λ -(R)-106, Λ -(R)-107, Δ -(S)-106 and Δ -(S)-107; there is simply no terminal edge in a tridentate ligand, see Figure 54 b).

Thus, to assign the stereoconfiguration of the newly synthesized complexes an additional stereodescription step was introduced based on the already established conventions, see Figure 55. First, the priority of all coordinating atoms were determined according to CIP. Then, the ligand with the highest priority was assigned as reference ligand and oriented upwards in the vertical lane according to the established procedure of the C/A nomenclature. At this point, the assignment of chirality symbols according to the C/A nomenclature is possible as recommended by the IUPAC. However, as the aim is to apply the Δ/Λ nomenclature for these octahedral complexes, the stereodescriptive operation “*reference ligand expansion*” (RLE) was introduced. In this operation the reference ligand is virtually connected to the tridentate ligand. The virtual connection has to be performed between the coordinating atom of the tridentate ligand with highest priority and the reference ligand. Furthermore, the coordinating atom of the tridentate ligand has to be in the plane which is oriented perpendicular to the vertical lane of the reference ligand. This operation converts the tridentate ligand into a virtual tetradentate ligand, which is now suitable for the TEC operation, see Figure 55. The additional stereodescriptive RLE operation turns octahedral complexes containing both bidentate and tridentate ligands into models suitable to apply the Δ/Λ -nomenclature. All further complexes with these specifications, presented in this thesis, have been processed analogously.

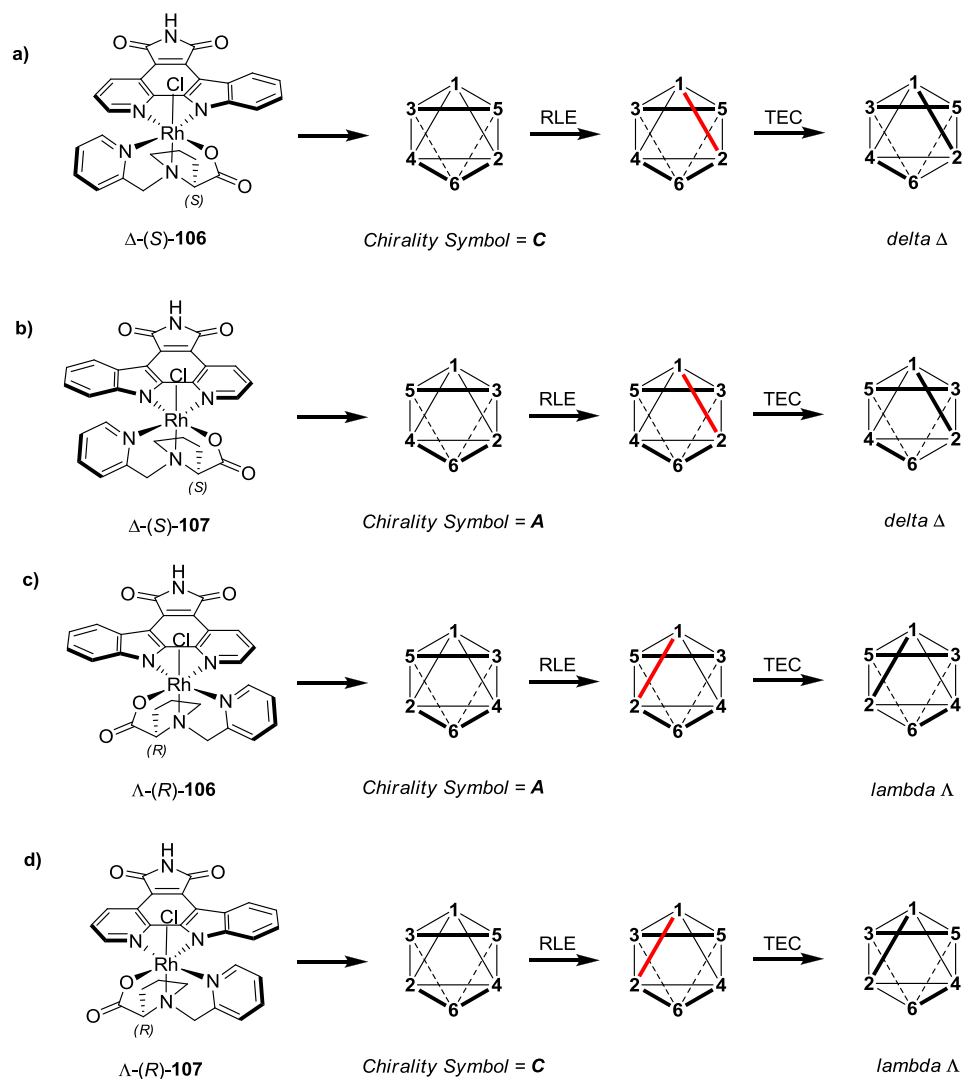


Figure 55: Assignment of stereoconfiguration $\Delta\text{-(S)-106}$ (a), $\Delta\text{-(S)-107}$ (b), $\Lambda\text{-(R)-106}$ (c), and $\Lambda\text{-(R)-107}$ (d) according to the Δ/Λ -nomenclature. In the second column the assignment according to the C/A -nomenclature is demonstrated. The reference ligand expansion (RLE) adds a virtual connection from the ligand of highest priority to the tridentate ligand shown in the third column. The connection is formed to the atom of highest Cahn-Ingold-Prelog (CIP) priority located in the perpendicular plane of the tridentate ligand. After this virtual operation the terminal edges convention can be applied as reported in literature to fit the complex to the Δ/Λ system.^[360]

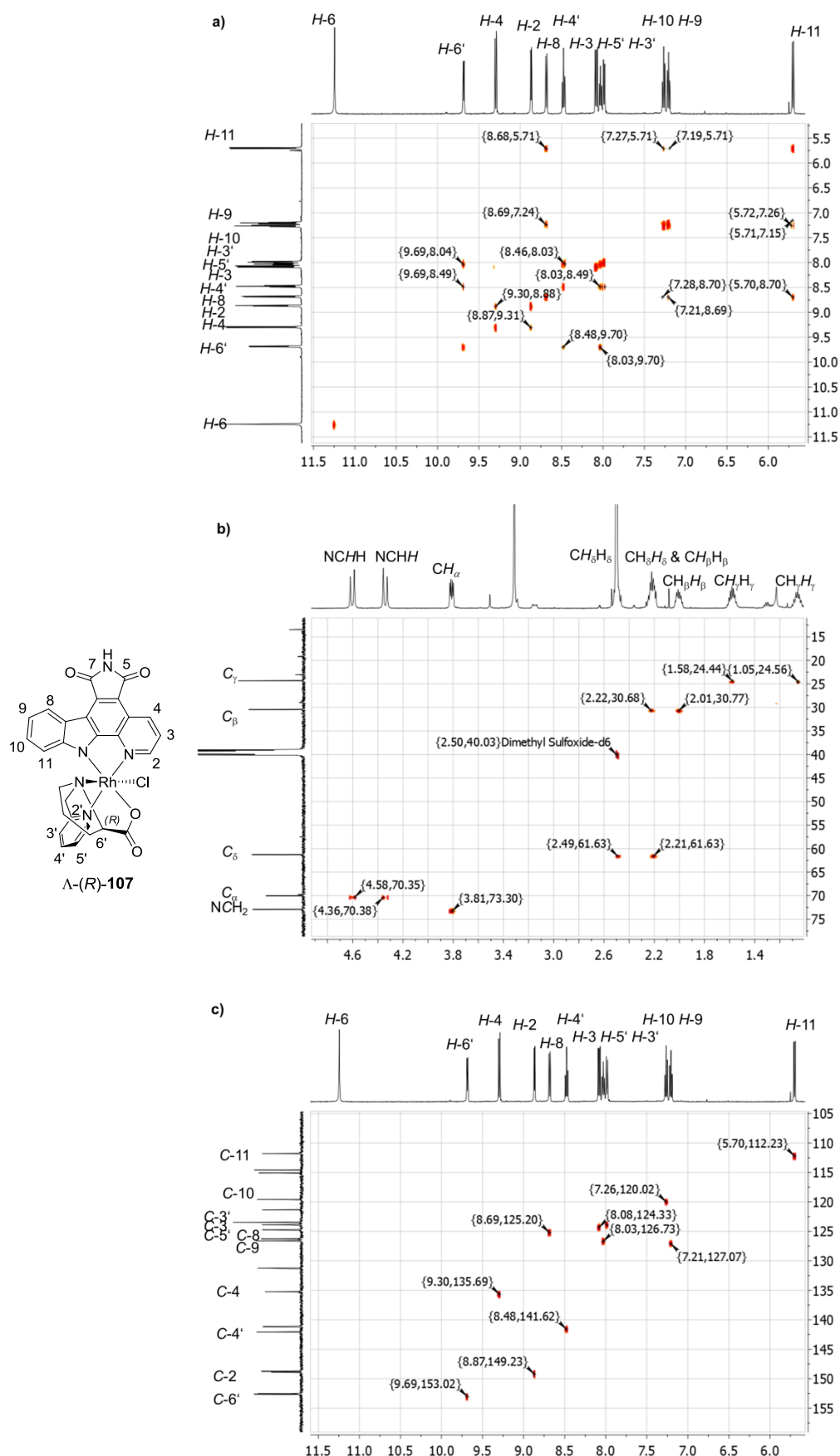


Figure 56: 2D-spectra of Λ -(R)-107 as an example for the determination of the stereoconfiguration (500 MHz, (CD₃)₂SO). (a) H-H-COSY spectrum of Λ -(R)-107 of the aromatic protons. (b) HSQC spectrum of Λ -(R)-107 of the aliphatic protons and carbons. (c) HSQC spectrum of Λ -(R)-107 of the aromatic protons and carbons.

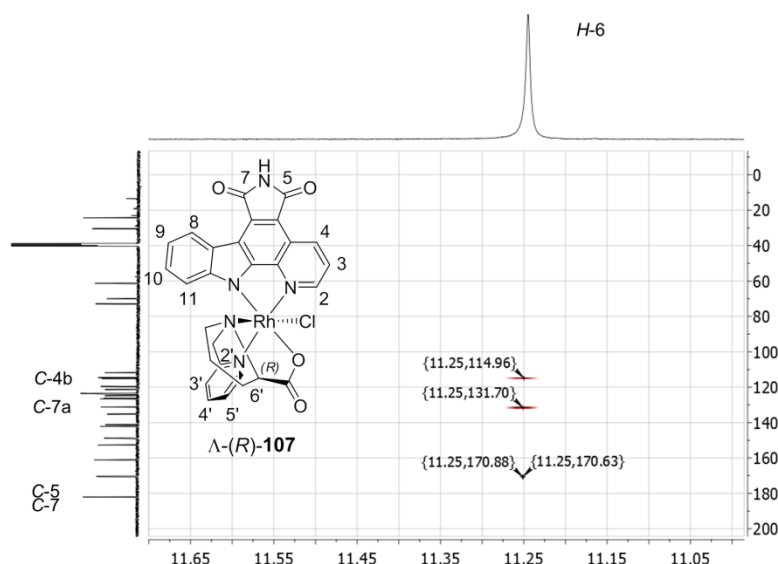


Figure 57: HMBC spectrum of H-6 of Δ -(*R*)-**107** to determine the bridging carbon atoms (500 MHz, $(\text{CD}_3)_2\text{SO}$).

3.3.2.3 Determination of The Relative Stereoconfiguration

To determine the relative stereoconfiguration the unambiguous assignment of the protons and carbons of the obtained complexes was necessary. For this purpose, several 2D-NMR techniques were applied to elucidate the structural properties of the compounds. As a model Δ -(*R*)-**107** is presented in Figure 56, whereas Δ -(*R*)-**106**, Δ -(*S*)-**106**, and Δ -(*S*)-**107** were processed analogously. The assignment of all aromatic protons by a proton-proton correlation spectroscopy experiment (H,H-COSY) revealed a significant upfield shift of the hydrogen atom at position 11 of the pyridocarbazole in Δ -(*R*)-**107** to a chemical shift of $\delta = 5.7$ ppm, see Figure 56 a) and Figure 58 a). Furthermore, the assignment of the carbon atoms bearing the investigated protons via an heteronuclear single quantum coherence experiment (HSQC) revealed that also an upfield shift of the C-11 is observed to a chemical shift of $\delta = 112.23$ ppm, see Figure 56 c). The aliphatic proton signals were identified also via the HSQC experiment, whereas the DMSO- d_6 solvent signal overlays one proton of the prolinato ligand (H_δ),

see Figure 56 b). After the assignment of proton and carbon atoms via H,H-COSY and HSQC experiments, the bridging carbon atoms of the compound were assigned via an heteronuclear multiple bond correlation (HMBC) experiment. Figure 57 illustrates the assignment of C-5, C-7, C-7a and C-4b via the HMBC signals of H-6. This procedure was repeated in case of the protons H-4, H-8, and H-11 to identify the proximal carbon atoms. Closing, the remaining bridging carbon atoms were assigned correlating their observed chemical shifts in the ^{13}C -NMR spectrum to their chemical environment.

As both, the H,H-COSY and HSQC experiments, in case of Δ -(*R*)-**107**, unambiguously correlated the previously described signals $\delta = 5.7$ ppm to H-11 and $\delta = 112.23$ ppm to C-11, structural properties had to be considered leading to the significant upfield shift. Due to the characteristics of the pyridocarbazole and the applied tridentate ligand, certain structural features can be exploited to distinguish the stereoisomers and explaining the observed spectral incidences highlighted by the comparison of the diastereomers Δ -(*R*)-**106** and Δ -(*R*)-**107**. Correlating their ^1H -NMR spectra reveals that the H-11 proton of Δ -(*R*)-**106** possesses a chemical shift

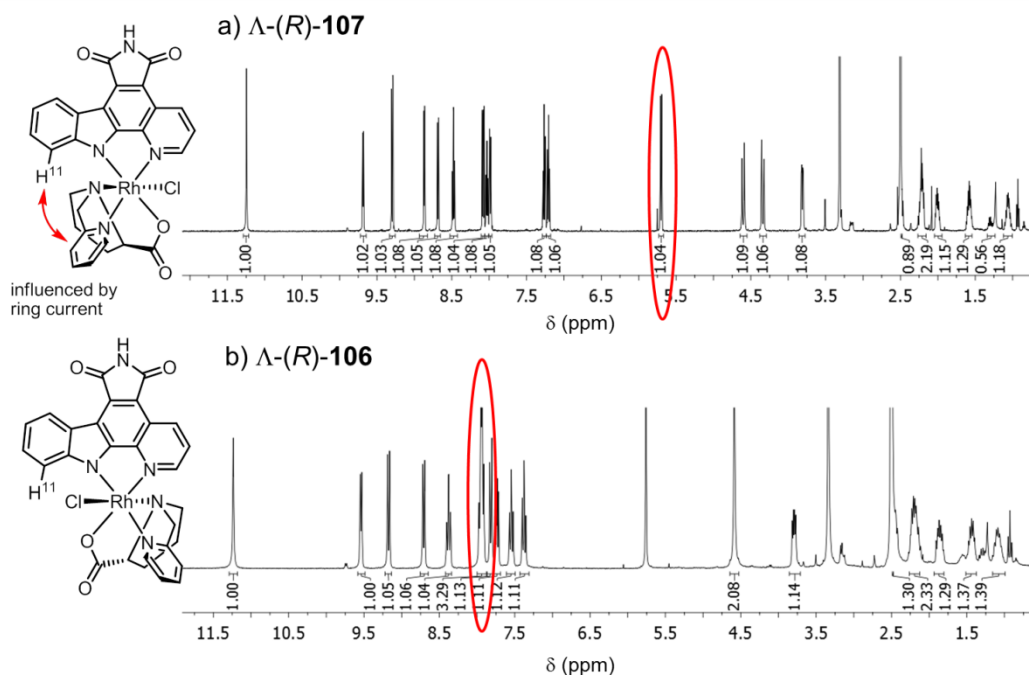


Figure 58: ^1H -NMR spectra of the diastereomers Δ -(*R*)-**107** and Δ -(*R*)-**106** (500 MHz, $(\text{CD}_3)_2\text{SO}$). The proton H-11 (red circle) of Δ -(*R*)-**107** (a) is upfield shifted by 2.1 ppm compared to Δ -(*R*)-**106** (b) and allows to assign its relative configuration. (in b) additional solvent signal of methylene chloride)

of $\delta = 7.8$ ppm which is located 2.1 ppm lowfield than the H-11 signal of Δ -(*R*)-**107**. This is based on the aromatic ring current induced by the *cis*-coordinated pyridine ring, see Figure 58. The H-11 proton positioned inside the aromatic ring of the pyridine ring moiety of the tridentate ligand experiences a shielding effect. This effect can only be observed when the pyridine ring of either (*R*)-**105** or (*S*)-**105** is coordinated *cis* and

almost perpendicular to the indole moiety of the pyridocarbazole ligand as it is the case for Δ -(*R*)-**107** and Δ -(*S*)-**107**. This effect has been described also previously in context of other complexes synthesised in the MEGGERS group with related structures and therefore support the concluded stereo-configuration.^[361]

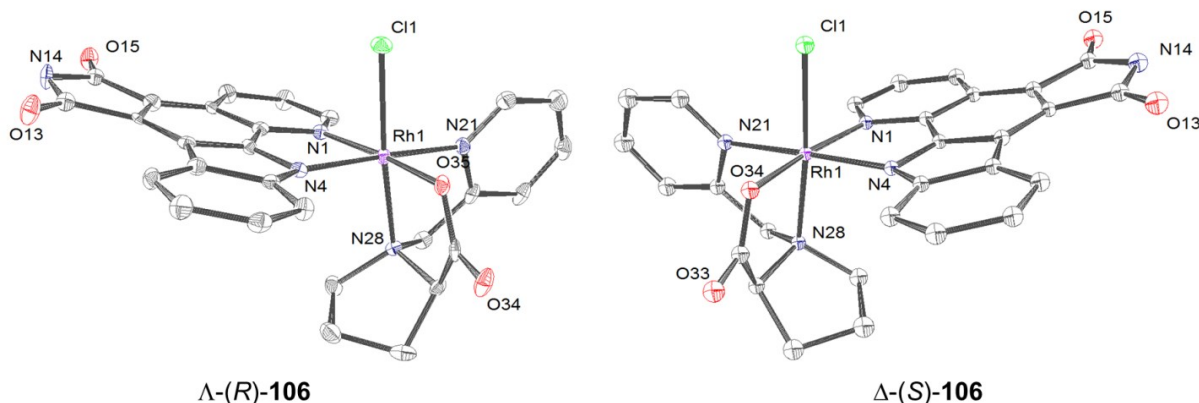


Figure 59: Crystal structures of Δ -(*R*)-**106** and Δ -(*S*)-**106**. Solvent Molecules were omitted for clarity. ORTEP drawing with 50% probability of thermal ellipsoids. Selected bond lengths [Å] for Δ -(*R*)-**106**: Rh1-O35 = 2.004(4), Rh1-N21 = 2.032(4), Rh1-N4 = 2.032(4), Rh1-N28 = 2.057(5), Rh1-N1 = 2.071(5), Rh1-Cl1 = 2.3399(16). Selected bond lengths [Å] for Δ -(*S*)-**106**: N1-Rh1 = 2.076(3), N4-Rh1 = 2.036(3), N21-Rh1 = 2.043(3), N28-Rh1 = 2.058(3), O34-Rh1 = 2.004(3), Cl1-Rh1 = 2.3440(11).

The crystal structures of Λ -(*R*)-**106** and Δ -(*S*)-**106** lead to the determination of their relative stereoconfiguration and supported the conclusions resulted from the NMR experiments, see Figure 59. The comparison of the crystal structures of both isomers demonstrates that they are enantiomers and diastereomeric towards Λ -(*R*)-**107** and Δ -(*S*)-**107**. This relationship between the structural isomers was further investigated via CD-spectroscopy as shown in Figure 61, revealing the enantiomeric character of Λ -(*R*)-**106** compared to Δ -(*S*)-**106**; the same is true for Λ -(*R*)-**107** and Δ -(*S*)-**107**.

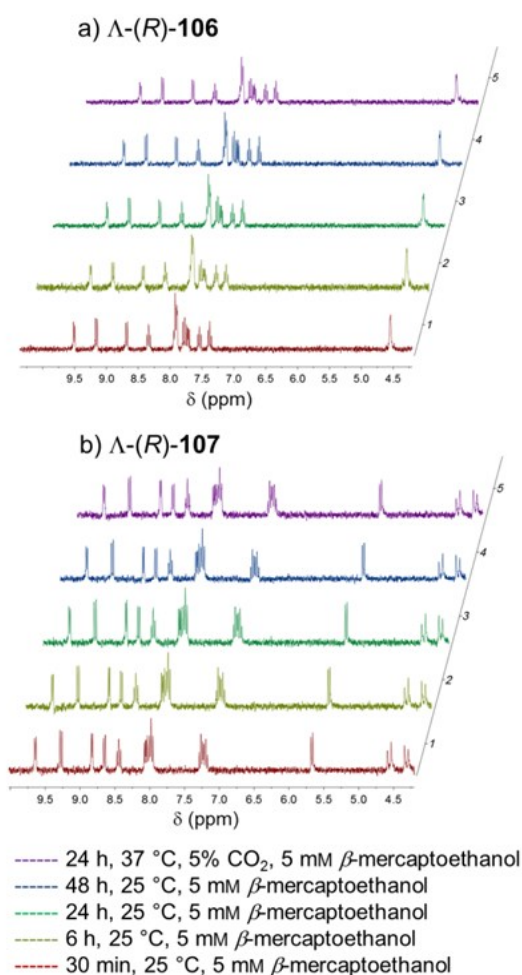


Figure 60: Stability of rhodium complexes in DMSO-*d*₆/D₂O 9:1 (5 mM) in the presence of β -mercaptoethanol (5 mM) determined by ELISABETH MARTIN. Excerpts of the ¹H-NMR spectra of the diastereomers Λ -(*R*)-**106** and Λ -(*R*)-**107** are shown after 30 min (red), 6 h (kaki), 24 h (green), and 48 h (blue) at 25 °C as well as 24 h (purple) at 37 °C.

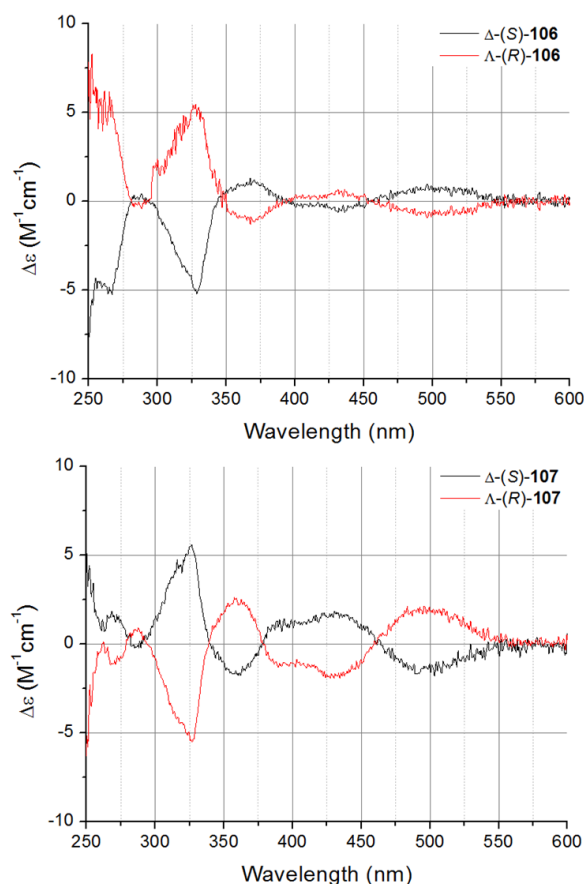


Figure 61: CD-spectra of the rhodium(III) complexes in dimethylsulfoxide (DMSO) at a concentration of 0.25 mM. The direct correlation of Δ -(*S*)-**106** to Λ -(*R*)-**106** as well as Δ -(*S*)-**107** to Λ -(*R*)-**107** reveals a mirror-inverted relationship of CD-light refraction between the corresponding enantiomers.

3.3.2.4 Stability of Enantiopure Prolinato Organorhodium(III) Complexes

The time dependent complex stability was performed by ELISABETH MARTIN. Thus, Λ -(*R*)-**106** and Λ -(*R*)-**107** were dissolved in DMSO-*d*₆/D₂O (9:1) at a final concentration of 5 mM. In addition, to investigate the complex inertness towards free nucleophiles, β -mercaptoethanol at a final concentration of 5 mM was added. Indeed, during the investigated time period covering either up to 48 h at 25 °C or 24 h at 37 °C no alterations in the ¹H-NMR spectra could be observed. This confirms the complex stability in the presence of free thiol groups which are ubiquitous in biological environments, see Figure 60.

3.3.3 Kinome Profiling and Biological Investigations

To investigate the potential kinase inhibition properties of the four stereoisomeric rhodium complexes, they were tested for their protein kinase binding affinity profile against in the DiscoverX KINOMEScanTM by LeadHunter Discovery Services. This was accomplished by an active-site-directed affinity screening against 456 human protein kinases.^[362,363] The compounds were screened at 1 μ M and results for primary screen binding interactions are reported as “percent of control” (POC), where lower numbers indicate stronger interactions, correlating with larger red circles in the dendrogram, see Figure 62. Empiric investigations demonstrated that binding constants (K_d) are correlated with such primary screening results, where lower POC values are associated with low K_d values (higher affinity interactions). Moreover, the selectivity score (SS) is a quantitative measure of compound selectivity. It is calculated by dividing the number of kinases that compounds bind to, by the total number of distinct kinases tested, excluding mutant variants. Further, this score value can be calculated for different selectivity levels using POC as a potency threshold, e.g. below 35% or 10%. These SS clustered in different selectivity score types (SST) provide a quantitative method of describing compound selectivity and allow a facilitated comparison of different compounds among each other.

Depending on using L- or D-proline as the starting point for the ligand synthesis of (S)-**105** or (R)-**105**, the derived complexes differ entirely in their biological properties. Whereas complexes Λ -(R)-**107**, Δ -(S)-**107**, and Δ -(S)-**106** act as kinase inhibitors, complex Λ -(R)-**106** is almost ineffective against the tested kinase panel.

This is evidenced by the different selectivity scores of the individual compounds. Indeed, Λ -(R)-**107** possesses a selectivity score of 0.041 at a SST of 35% and 0.013 at a SST of 10%; Δ -(S)-**107** possesses a selectivity score of 0.025 at a SST of 35% and 0.005 at a SST of 10%; Δ -(S)-**106** possesses a selectivity score of 0.076 at a SST of 35% and 0.025 at a SST of 10%. In opposite, Λ -(R)-**106** didn't hit any kinase at the SST level of 35%, 10%, or even 1% in the tested concentration of 1 μ M. None of the four compounds inhibited a kinase in the tested panel at a POC lower than 1%, see Figure 62. These remarkable differences of the tested compounds, not only regarding the selectivity across the whole kinome but also the preference to distinct kinase subfamilies addressed by them, indicate the importance of the relative configuration around the rhodium metal centre.

To further verify the primary hits of the kinome profiling, all four compounds were tested in competitive studies using [γ -³³P]-ATP. Therefore, one target kinase for each compound with a POC lower than 10% was selected. Three kinases were chosen regarding their commercial availability and role in human pathogenesis: FLT-3 (4.9%) addressed by Δ -(S)-**107**, Aurora A (2.4%) addressed by Δ -(S)-**106**, and PIM-1 (1.8%) addressed by Λ -(R)-**107**. The [γ -³³P]-ATP competitive studies confirmed the primary results of the KINOMEScanTM. As expected, the target kinases were inhibited profoundly by the compound identified in the kinome profiling, see Figure 62 and Figure 63.

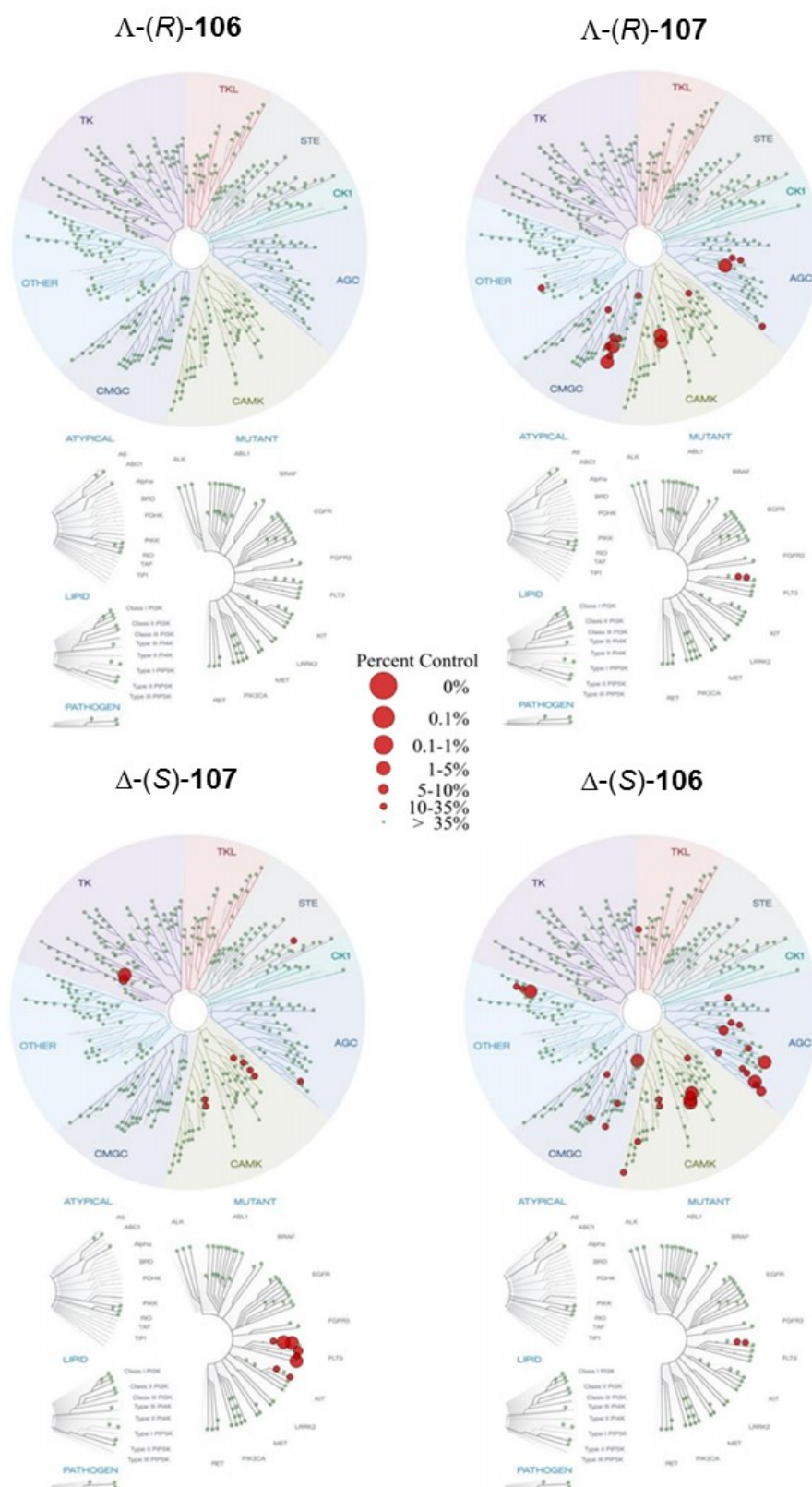


Figure 62: Kinase profiling of Δ -(R)-106, Δ -(R)-107, Δ -(S)-107, and Δ -(S)-106. All complexes were tested against 456 human kinases at a concentration of 1 μ M by an active-site-directed affinity screening (KINOMEScanTM, DiscoverRx, LeadHunter Discovery Services). The dendrograms show the remaining POC levels of the kinases depicted as red circles. The selectivity score type (SST), the number of hits (NH) as well as the selectivity score (SS) of the single enantiomers are: Δ -(R)-107: SST(35) NH(16) SS(0.041); SST(10) NH(5) SS(0.013). Δ -(S)-107: SST(35) NH(10) SS(0.025); SST(10) NH(2) SS(0.005). Δ -(S)-106: SST(35) NH(30) SS(0.076); SST(10) NH(10) SS(0.025).

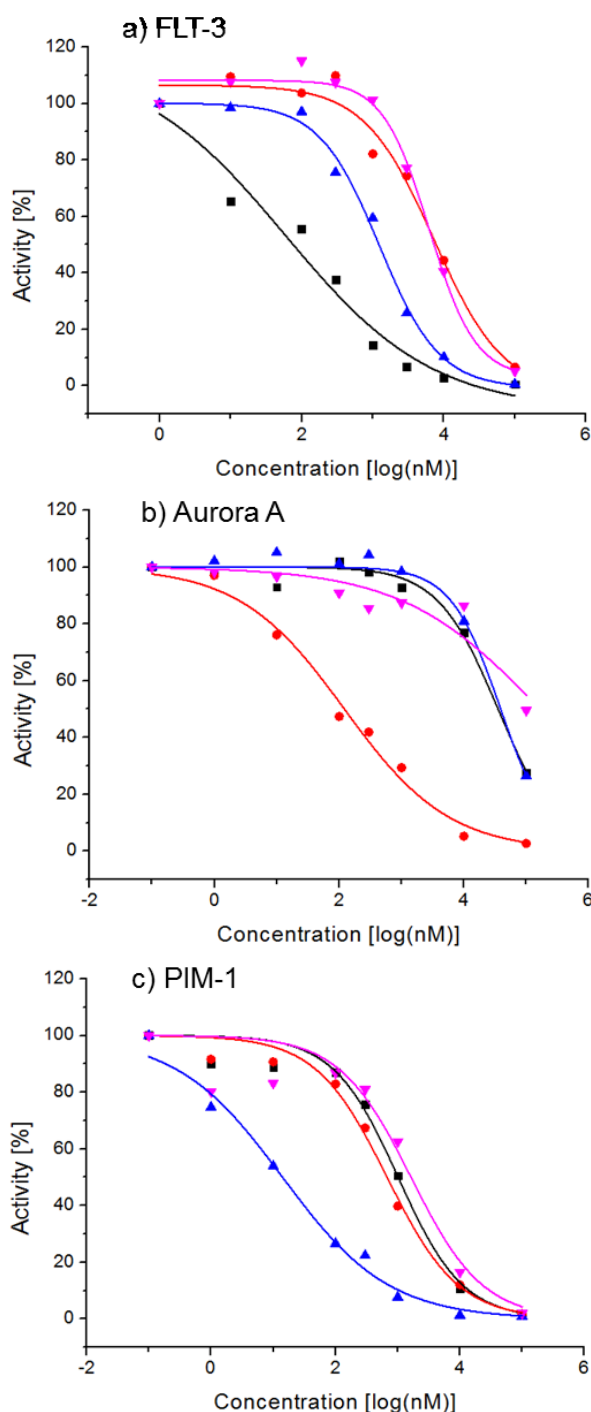


Figure 63: One single target kinase for each compound with a POC lower than 10% was selected for $[\gamma\text{-}^{33}\text{P}]\text{-ATP}$ competitive assays with an ATP concentration of 10 μM (double determination). $\Delta\text{-(R)-106}$ (purple triangle), $\Delta\text{-(R)-107}$ (blue triangle), $\Delta\text{-(S)-107}$ (black squares), and $\Delta\text{-(S)-106}$ (red circle). **a)** FLT-3: $\Delta\text{-(R)-106}$ = 8.47 μM , $\Delta\text{-(R)-107}$ = 1.2 μM , $\Delta\text{-(S)-107}$ = 137 nM, and $\Delta\text{-(S)-106}$ = 8.26 μM . **b)** Aurora A: $\Delta\text{-(R)-106}$ = 164 μM , $\Delta\text{-(R)-107}$ = 39 μM , $\Delta\text{-(S)-107}$ = 35 μM , and $\Delta\text{-(S)-106}$ = 121 nM. **c)** PIM-1: $\Delta\text{-(R)-106}$ = 1.99 μM , $\Delta\text{-(R)-107}$ = 15 nM, $\Delta\text{-(S)-107}$ = 1.03 μM , and $\Delta\text{-(S)-106}$ = 0.88 μM .

Indeed, $\Delta\text{-(R)-107}$ inhibited PIM-1 with an IC_{50} of 15 nM, $\Delta\text{-(S)-107}$ inhibited FLT-3 with an IC_{50} of 137 nM, and $\Delta\text{-(S)-106}$ Aurora A with an IC_{50} of 121 nM. Further, other structural isomers of the rhodium(III) complexes differ significantly in their IC_{50} values towards the non-target kinases. For instance, $\Delta\text{-(R)-106}$ (8.47 μM), $\Delta\text{-(R)-107}$ (1.2 μM), and $\Delta\text{-(S)-106}$ (8.26 μM) are significantly less affine towards FLT-3 than $\Delta\text{-(S)-107}$. The same is true for Aurora A: $\Delta\text{-(R)-106}$ (164 μM), $\Delta\text{-(R)-107}$ (39 μM), and $\Delta\text{-(S)-107}$ (35 μM) in opposite to $\Delta\text{-(S)-106}$; as well as for PIM-1: $\Delta\text{-(R)-106}$ (1.99 μM), $\Delta\text{-(S)-107}$ (1.03 μM), and $\Delta\text{-(S)-106}$ (0.88 μM) in opposite to the original screening hit $\Delta\text{-(R)-107}$. Moreover, it is noteworthy, that $\Delta\text{-(R)-106}$ is the weakest inhibitor towards all tested kinases. All gathered results of the $[\gamma\text{-}^{33}\text{P}]\text{-ATP}$ competitive studies are in very good congruence to the results of the kinome profiling highlighting the importance of the stereochemistry at the metal centre for metal based kinase inhibitors.

3.3.4 Interpretation

The pros and cons comparing classic organic kinase inhibitors to organometallic complexes have been discussed intensively in literature.^[152,159–161,189,190,364–368] The PIM kinase family have been described above to possess oncogenic and survival promoting properties, see Chapter 3.3.1.1.^[266,274,281–283,287,292,369–371] Therefore, targeting members of the PIM kinase family offers potential treatment options, i.e.: various leukemias,^[372] mantle cell lymphoma,^[287] and diffuse large B-cell lymphoma.^[369] An actual example of a phase I clinical trial PIM kinase inhibitor is AZD1208 (**108**) by Astra-Zeneca.^[370] AZD1208 inhibits the kinase activity of all three PIM kinases with an IC_{50} of 0.4 nM (PIM-1), 5.0 nM (PIM-2), and 1.9 nM (PIM-3).^[371] Moreover, the organic inhibitor AZD1208 was evaluated by the KINOMEScanTM (DiscoverRx) using a panel

of 442 kinases, whereas only 16 kinases had an residual activity of less than 50%, including all three PIM kinases.^[371] In comparison, the kinase profiling of Δ -(*R*)-**107** against 456 kinases revealed 23 kinases with an residual activity of less than 50%. Moreover, PIM-2 with an POC of exactly 50% was not adequately addressed by Δ -(*R*)-**107** as PIM-1 or PIM-3, both 1.8%. This example shows that Δ -(*R*)-**107** with its low nanomolar IC_{50} of 15 nM against PIM-1 and its selectivity profile is quite comparable to literature known fully organic kinase inhibitors, although the exact selectivity profile inevitably differ.

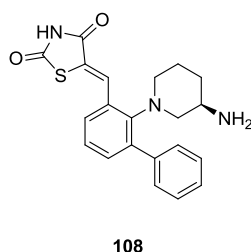


Figure 64: Chemical Structure of AZD1208 (**108**).^[370]

Though, differences in the selectivity profiles comparing classic organic inhibitors with metal based complex inhibitors are likely to expect, similarities like in case of FLT-3 confirm a related mode of action. For instance, FLT-3 inhibitors often affect other members of the type III receptor tyrosine kinases including KIT and PDGFR due to their close structural relationship.^[373] This is true for i.e. SU11248 (**109**) (Sunitinib, Pfizer)^[374] approved for the treatment of renal cell carcinoma (RCC) and imatinib-resistant gastrointestinal stromal tumor (GIST). Beside also affecting other type III receptor tyrosine kinases like KIT and PDGFR in the kinome profiling, the rhodium(III) inhibitor Δ -(*S*)-**107** possesses an determined IC_{50} of 137 nM for FLT-3 which is in the same range as the IC_{50} of SU11248 (250 nM).^[373]

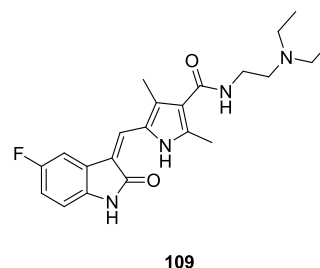


Figure 65: Chemical structure of SU11248 (**109**).^[374]

Closing, many inhibitors targeting the Aurora kinases have been reported before and some are evoking increasing focus in clinical trials.^[353,355,375] For instance, AT9283 developed by Astex Therapeutics is currently in several Phase II studies under the Cancer Research UK.^[376] It is a multi-target tyrosine kinase inhibitor, including Aurora A (IC_{50} = 3 nM) and B (IC_{50} = 3 nM), JAK (IC_{50} = 1.2 nM), and T315I ABL (IC_{50} = 4 nM).^[377] In opposite, Δ -(*S*)-**106** inhibits Aurora A in the medium range of an IC_{50} of 121 nM. Moreover, the kinase profile does not undoubtedly support the mentioned targets of AT9283 as additional targets for Δ -(*S*)-**106**, see Figure 62.

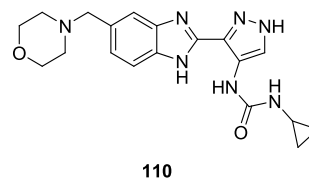
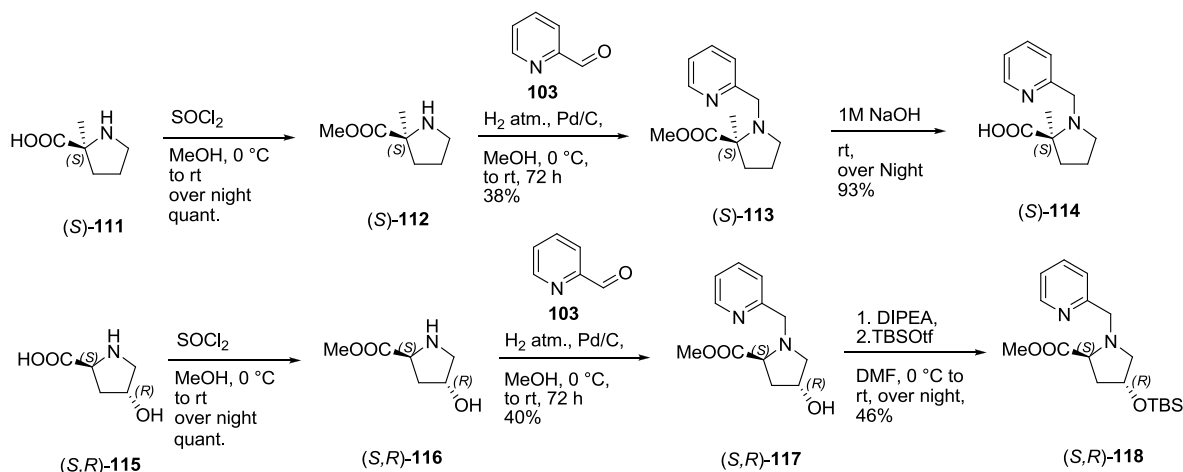


Figure 66: Chemical structure of AT9283 (**110**).^[377]

Despite the short provided framing of the presented rhodium(III) complexes into the context of classic organic kinase inhibitors, it is noteworthy that the obtained results reflect just the beginning of enantiopure metal based kinase inhibitor design. Further improvements of target selectivity and potency are achievable by modifying i.e. the pyridocarbazole pharmacophore ligand **79**^[149] or attaching additional functional groups to the tridentate ligands (*R*)-**105**, or (*S*)-**105**, as described in the following Chapters.

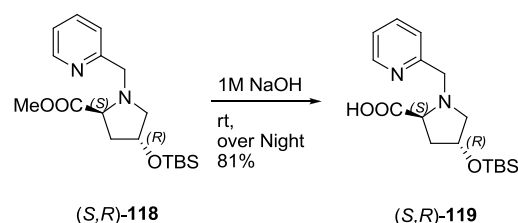


Scheme 14: Synthesis of enantiopure chiral tridentate proline derived ligands (I).

3.3.5 Scanning the Binding Pocket - Further Development of Tridentate Chiral Ligands

The successful synthesis of prolinato organorhodium(III) complexes and the subsequent conclusion of the ligand characteristics leading to the enantiopure kinase inhibitors resulted into new modified ligands. They were able to act both, as tools to asymmetrically synthesise organometallic complexes and being part of highly sophisticated kinase inhibitors.

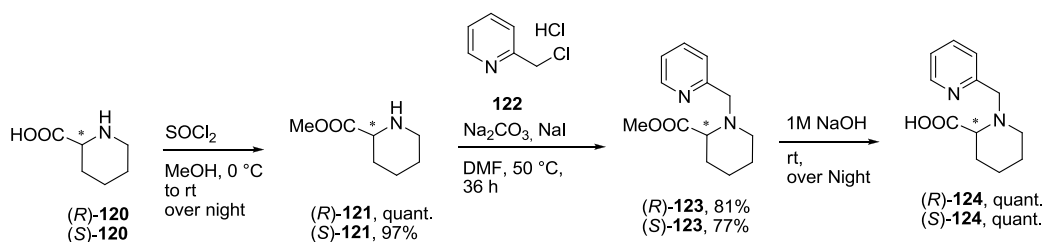
Many synthetically accessible proline derivatives have been reported.^[378–382] Nevertheless, prior to start, a multistep ligand synthesis with different substitution patterns, slight modifications to explore the available chemical space in the ATP binding site of the target kinases must be evaluated first. Moreover, the transferability of the ligand requirements must be verified. Thus, a small set of commercially available proline derivatives like (S)- α -methyl-proline (**(S)-111**), (2S, 4R)-hydroxyproline (**115**), and pipercolinic acid ((S)-**120** and (R)-**120**) were selected, see Scheme 14. In general, the established synthetic route was applied to the single compounds in analogy to (R)-**105** and (S)-**105**.



Scheme 15: Cleavage of the ester function of (S, R)-118.

The methyl esters of the corresponding amino acid building blocks were formed by reacting them with thionylchloride in methanol at 0°C during the drop wise addition, followed by 16 h of stirring the reaction mixture at ambient temperature. The methyl esters were obtained as pure hydrochloride salts after repeated co-evaporation of excessive thionylchloride. The protected amino acid building blocks were obtained in quant. yields in case of (S)-**112**, (S, R)-**116**, and (R)-**121**; in case of (S)-**121** the ester formation led to a yield of 97%.

The methyl esters were then processed to the reductive amination reaction using **103** in methanol. The reaction mixtures were stirred for 72 h at 0°C under hydrogen atmosphere and using palladium on carbon as catalyst. During this period the reaction mixture was allowed to warm up to ambient temperature. After the separation of the heterogeneous catalyst via filtration over CELITE, the intermediates could be purified by flash chromatography using methylene chloride : methanol. Unexpectedly, the re-



Scheme 16: Synthesis of enantiopure chiral tridentate proline derived ligands (II).

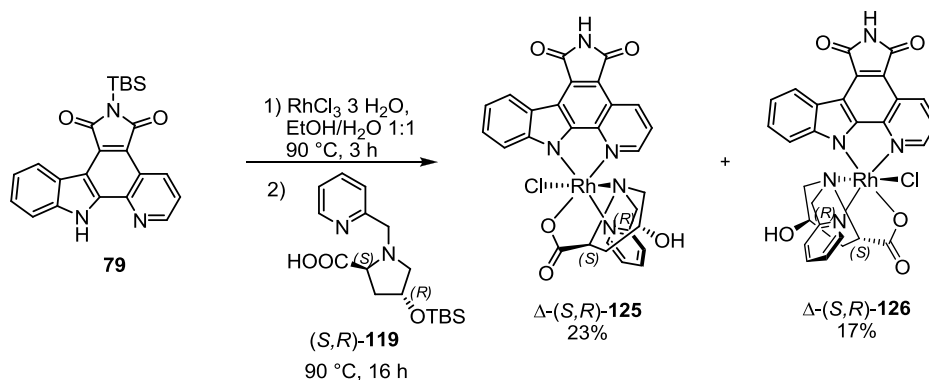
ductive amination reactions were performed with decreased yields as compared to the synthesis of (R) -**105** and (S) -**105**. The yields of 38% in case of (S) -**113** and 40% in case of (S, R) -**117** led to the counteraction of applying a substitutional reaction using 2-(chloromethyl)pyridine hydrochloride (**122**) instead of the established reductive amination. This alternative route was applied in the synthesis of (S) -1-(pyridin-2-ylmethyl)piperidine-2-carboxylic acid ((S) -**124**) and (R) -1-(pyridin-2-ylmethyl)piperidine-2-carboxylic acid ((R) -**124**). Therefore, (R) -methyl piperidine-2-carboxylate ((R) -**121**), or the corresponding (S) enantiomer ((S) -**121**), was reacted with **122** in DMF at 50°C for 36 h using sodium carbonate and sodium iodide. This alternative synthesis with 81% yield outperformed the reductive amination, see Scheme 16.

Finally, after basic ester cleavage, using 1 M sodium hydroxide at ambient temperature for 16 h, the finished tridentate ligands were obtained in 93% ((S) -**114**), 81% (S, R) -**119**, and quant. yields ((R) -**124** and (S) -**124**), respectively. Additional functional groups, like in case of (S, R) -**117**, were protected to avoid a potential cross coordina-

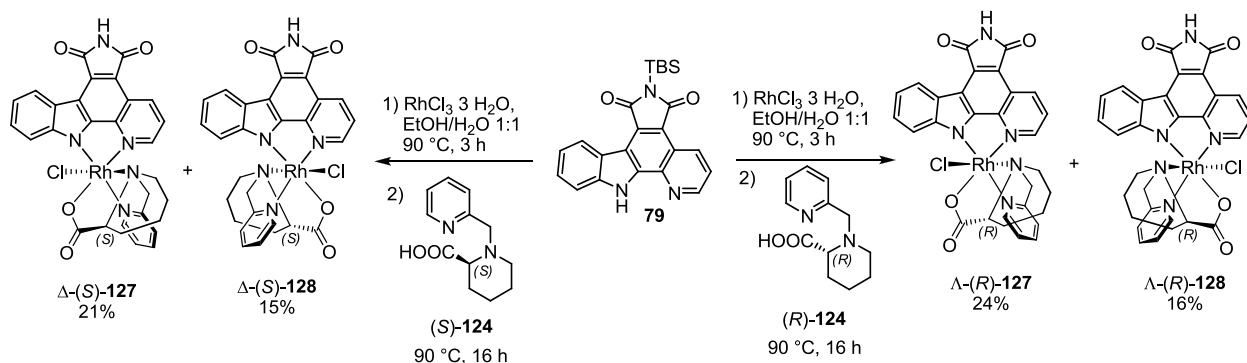
tion with a second metal ion during the complexation reaction, see Scheme 14. The attached *tert*-butyl-dimethylsilyl protection group at the hydroxyl residue fulfills this function, which was attached using diisopropylethylamine (DIPEA) and *tert*-butyldimethylsilyl triflate in DMF.

3.3.6 Synthesis and Structural Investigations

The newly designed ligands for chemical space exploration and asymmetric organorhodium(III) complexation were reacted under the same conditions applied for the synthesis of Λ - (R) -**106**, Δ - (S) -**106**, Λ - (R) -**107** and Δ - (S) -**107**, see Chapter 3.3.2. Thus, makes the reactions comparable, Scheme 17. As observed before the reaction mixtures led to the formation of two diastereomers for each used ligand, like for the ligands (R) -**105** and (S) -**105**.



Scheme 17: Asymmetric synthesis of organorhodium complexes Δ -(S, R)-**125** and Δ -(S, R)-**126**.



Scheme 18: Asymmetric synthesis of organorhodium complexes $\Lambda\text{-(R)-127}$, $\Lambda\text{-(R)-128}$, $\Delta\text{-(S)-127}$ and $\Delta\text{-(S)-128}$.

In analogous way, the diastereomers could be separated by flash column chromatography using methylene chloride : methanol (20:1 \rightarrow 10:1) followed by a preparative TLC for each single compound using methylene chloride : methanol 15:1 for further purification. Like observed before, the *tert*-butyl-dimethylsilyl protection group of ligand **79** was cleaved, see Scheme 17 and Scheme 18. Moreover, the *tert*-butyl-dimethyl silyl protection group of (S, R)-**119** was also cleaved under the reaction conditions, see Scheme 17. All second generation organorhodium(III) complexes were obtained in comparable yields to the proline based progenitors: (S, R)-**119** derived $\Delta\text{-(S, R)-125}$ (23%) and $\Delta\text{-(S, R)-126}$ (17%); (S)-**124** derived $\Delta\text{-(S)-127}$ (21%) and $\Delta\text{-(S)-128}$ (15%); as well as (R)-**124** derived $\Lambda\text{-(R)-127}$ (24%) and $\Lambda\text{-(R)-128}$ (16%).

The relative stereoconfiguration of $\Delta\text{-(S)-125}$ and $\Lambda\text{-(R)-127}$ was determined via X-ray crystallography, see Figure 67 and Figure 68, respectively. Moreover, correlating all physico-chemical properties to the obtained data of $\Lambda\text{-(R)-106}$, $\Lambda\text{-(R)-107}$, $\Delta\text{-(S)-106}$, and $\Delta\text{-(S)-107}$ covering crystal structures and the $^1\text{H-NMR}$ shift of the H-11 proton of the coordinated pyridocarbazole for allowed a doubtless assignment of the relative stereoconfiguration of each second generation organorhodium(III) complex as depicted.

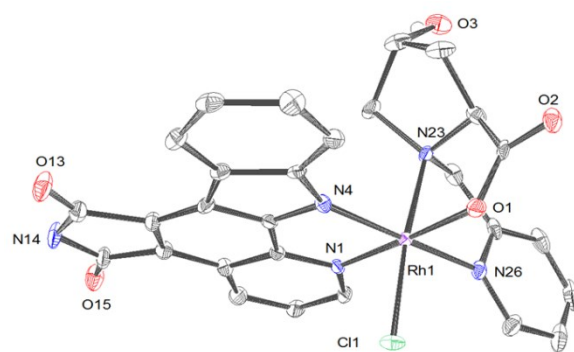


Figure 67: Crystal structure of $\Delta\text{-(S,R)-125}$. Solvent molecules were omitted for clarity. ORTEP drawing with 50% probability of thermal ellipsoids. Selected bond lengths [Å] for $\Delta\text{-(S,R)-125}$: Rh1-N1 = 2.055(3), Rh1-N4 = 2.038(3), Rh1-N23 = 2.073(4), Rh1-N26 = 2.039(4), Rh1-O1 = 2.010(3), Rh1-Cl1 = 2.3256(10).

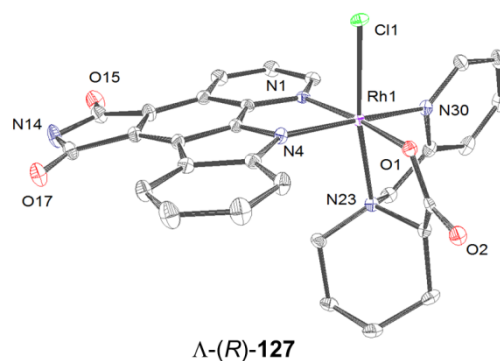
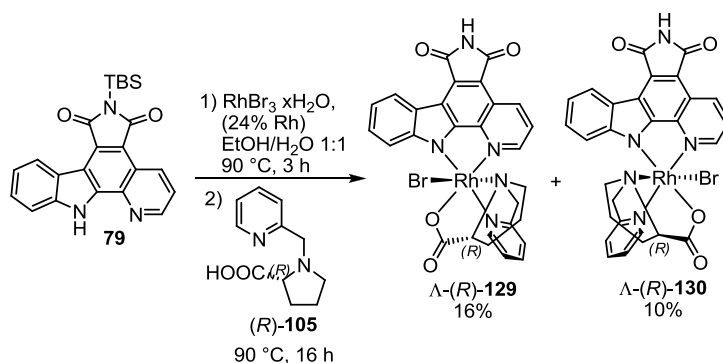


Figure 68: Crystal structure of $\Lambda\text{-(R)-127}$. Solvent molecules were omitted for clarity. ORTEP drawing with 50% probability of thermal ellipsoids. Selected bond lengths [Å] for $\Lambda\text{-(R)-127}$: Rh1-N1 = 2.069(3), Rh1-N4 = 2.043(2), Rh1-N23 = 2.080(2), Rh1-N30 = 2.044(2), Rh1-O1 = 2.009(2), Rh1-Cl1 = 2.3417(7).



Scheme 19: Asymmetric synthesis of organorhodium complexes Δ -(*R*)-129, Δ -(*R*)-130.

Additionally, beside exploring the ligand sphere using modified chiral tridentate ligands, the monodentate chlorine ligand of the enantiopure organorhodium complexes was also substituted by bromine, see Scheme 19. For this purpose, the established synthetic procedure was applied using $\text{RhBr}_3 \cdot x\text{H}_2\text{O}$ (24% Rh) instead of $\text{RhCl}_3 \cdot 3\text{H}_2\text{O}$. **79** was reacted in a sequential addition to a suspension of $\text{RhBr}_3 \cdot x\text{H}_2\text{O}$ in an ethanol/water mixture at 90 °C for 3 h followed by the chiral tridentate ligand (*R*)-**105**. Reacting the mixture at 90 °C for 16 h led to the formation of two diastereomers, which were separated by silica gel chromatography with methylene chloride : methanol 20:1 to 10:1 followed by a preparative TLC for each single compound using methylene chloride : methanol 15:1. The complex Δ -(*R*)-**129** was obtained in 16% yield and Δ -(*R*)-**130** in 10%.

3.3.7 Biological Investigations

To further investigate the biological properties and kinase inhibition potentials of selected second generation organorhodium(III) complexes, they were tested in competitive assays against PIM-1, FLT-3, and Aurora A. Therefore, each investigated structural isomer was correlated to the appropriate prolinato progenitor against its primary target kinase.

FLT-3 was inhibited by Δ -(*S*, *R*)-**126** with an IC_{50} of 780 nM which is 5.7-fold higher than the IC_{50} of 137 nM for Δ -(*S*)-**107** as the appropriate progenitor. A similar relation can be observed for Aurora A. Δ -(*S*)-**106** inhibited Aurora A with an IC_{50} value of 121 nM, whereas the IC_{50} value of 12.5 μM of Δ -(*S*, *R*)-**125** is about 100-fold higher. These two examples demonstrate that the substitution of (*S*)-**105** towards (*S*, *R*)-**119** introducing an additional hydroxyl group significantly impairs the affinity of the resulting inhibitors. The same is true for the enlargement of the aliphatic ring size from a five-membered ring in case of using (*R*)-**105** to a six-membered ring using (*R*)-**124**. The resulting Δ -(*R*)-**128** inhibits PIM-1 with an IC_{50} of 206 nM which is almost 14-fold higher compared to the IC_{50} of 15 nM in case of Δ -(*R*)-**107**. The enlarged ring size and the subsequent conformational changes of the ligand sphere significantly decrease the affinity of the second generation organorhodium(III) complex. In contrast, the substitution of the monodentate ligand to bromine instead of chlorine has only little influence on the affinity as confirmed by the IC_{50} of 32 nM of Δ -(*R*)-**130**, which is quite comparable to the value obtained for Δ -(*R*)-**107**. Moreover, as PIM-1 offers a relatively large ATP-binding site for interactions, the complexes Δ -(*R*)-**129** (735 nM) and Δ -(*R*)-**127** (3.76 μM) were also tested for their affinity. However, the obtained values for them confirmed the primary expectations.

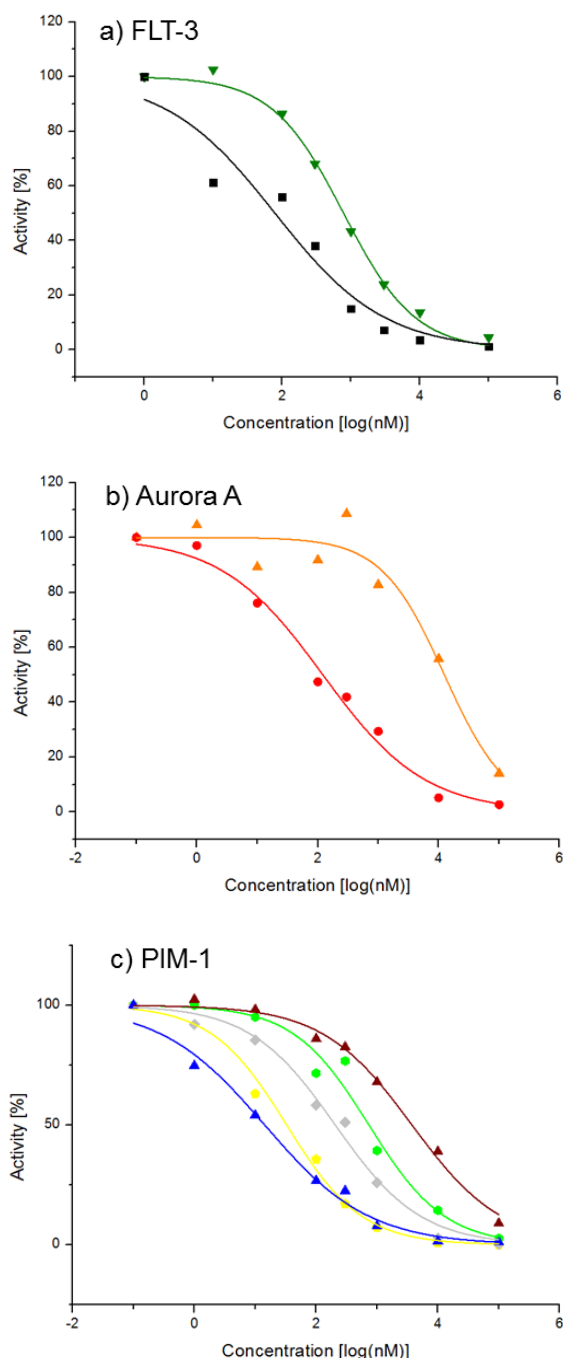


Figure 69: The target kinases of the prolinato organorhodium(III) complexes were tested using the second generation enantiopure organorhodium(III) complexes in $[\gamma\text{-}^{33}\text{P}]\text{-ATP}$ competitive assays with an ATP concentration of $10\text{ }\mu\text{M}$. The data points represent mean values of double determinations and an independent verification assay under same conditions. Additionally, the most potent prolinato organorhodium(III) inhibitor is shown for comparison. **a)** FLT-3: $\Delta\text{-(S)-107}$ (black squares) $\text{IC}_{50} = 137\text{ nM}$, $\Delta\text{-(S, R)-126}$ (green triangle) $\text{IC}_{50} = 780\text{ nM}$. **b)** Aurora A: $\Delta\text{-(S)-106}$ (red circles) $\text{IC}_{50} = 121\text{ nM}$; $\Delta\text{-(S, R)-125}$ (orange triangle) $\text{IC}_{50} = 12.5\text{ }\mu\text{M}$. **c)** PIM-1: $\Delta\text{-(R)-107}$ (blue triangles) $\text{IC}_{50} = 15\text{ nM}$, $\Delta\text{-(R)-130}$ (yellow circles) $\text{IC}_{50} = 32\text{ nM}$, $\Delta\text{-(R)-128}$ (grey rhombi) $\text{IC}_{50} = 206\text{ nM}$, $\Delta\text{-(R)-129}$ (green hexagons) $\text{IC}_{50} = 735\text{ nM}$, $\Delta\text{-(R)-127}$ (brown triangles) $\text{IC}_{50} = 3.76\text{ }\mu\text{M}$.

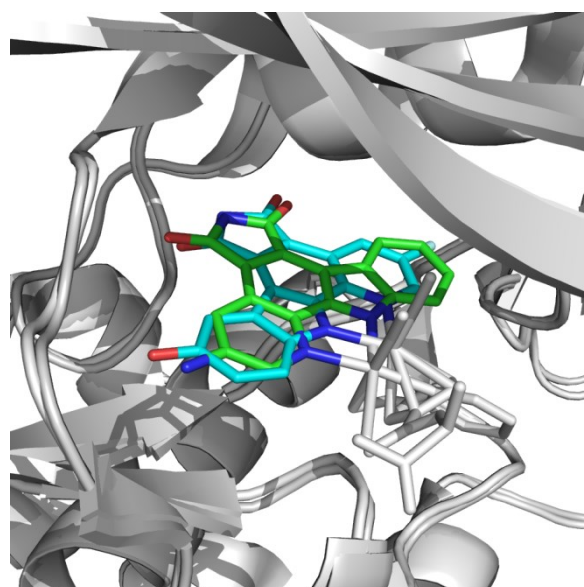


Figure 70: Superimposed crystal structures of organometallic inhibitor (*R*)-**10** (pdb: 2JLD) and Δ -**12** (pdb: 3PUP) bound GSK-3 β . The binding pose of both pyridocarbazole pharmacophore ligands are flipped by 180° in relation to each other. The pyridocarbazole carbon atoms of (*R*)-**10** are presented in cyan and the pyridocarbazole carbon atoms of Δ -**12** in green. Nitrogen atoms are shown in blue, oxygen atoms in red, and fluorine in light cyan. GSK-3 β as well as the residual coordination sphere is presented as cartoon or sticks in white for clarity.^[146]

3.3.8 Interpretation

The initial modifications of the proline core of the chiral tridentate ligands significantly influenced the inhibition profiles of the resulting organorhodium(III) complexes compared to the corresponding structural isomers of the prolinato rhodium(III) complex progenitors. In case of the additional hydroxyl function of (*S, R*)-**119** or enlarging the ring size as in case of (*R*)-**124** led to decreased affinities towards the kinase targets indicating sterical hindrances induced by these groups. Due to the findings of the complexes $\Delta\text{-(S, R)-125}$, $\Delta\text{-(S, R)-126}$, $\Delta\text{-(R)-127}$, and $\Delta\text{-(R)-128}$ the (*S*)-**124** derived complexes $\Delta\text{-(S)-127}$, and $\Delta\text{-(S)-128}$ were not further investigated regarding their inhibitory potential. Moreover, scanning the binding pocket of PIM-1 revealed the toleration of a larger monodentate ligand like bromine instead of chlorine. Indeed, PIM-1 has been reported to possess a relatively

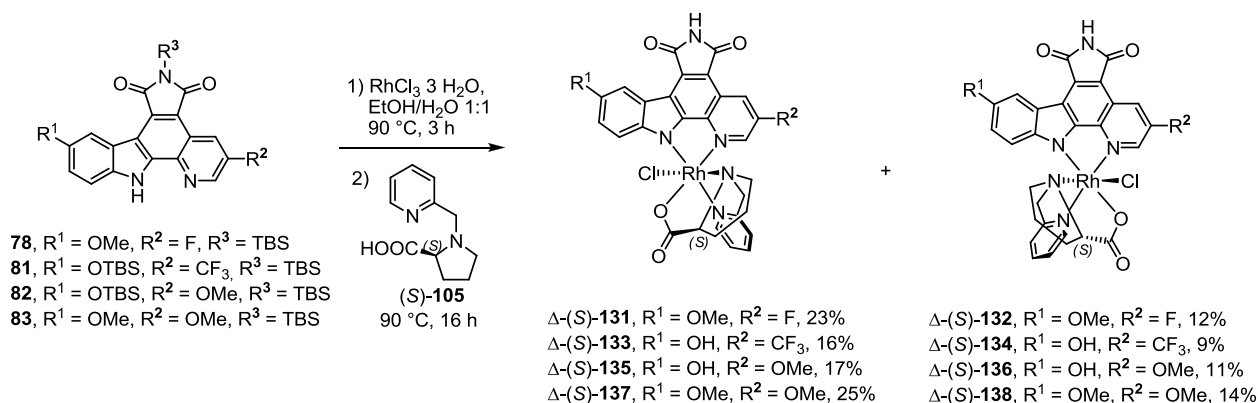
large ATP binding site compared to other kinases.^[140,147,231,292] Thus, PIM-1 is often hit as a target in metal based complex inhibitor investigations examined by the MEGGERS group.^[140,147,231]

Moreover, due to the symmetry of the maleimide moiety of the pyridocarbazole pharmacophore ligand, the residual coordination sphere has an important influence on the binding pose of the entire complex. For instance, superimposing the crystal structures of (*R*)-**10** and Λ -**12** in the binding pocket of GSK-3 β reveals a 180 ° flip of both pyridocarbazole ligands in relation to each other, one occupying the same chemical space with its indole moiety whereas the other with its pyridine moiety and *vice versa*, see Figure 70. The different binding poses of the pyridocarbazole ligands in relation to each other are mainly driven by the monodentate carbonyl ligands, which point towards the glycine rich loop, and the additional substituents at the pyridocarbazoles picking up different molecular interactions.

However, it is noteworthy, that the diastereomers obtained in a single reaction, using the chiral tridentate ligands presented so far, arise from a 180 ° flipped coordination of the pyridocarbazole. Therefore, the ligand sphere of two diastereomers can be superimposed, whereas the pyridocarbazole ligands of each complex is inverted compared to the other. Keeping this fact in mind, modifications in the ligand sphere or introducing additional functional groups at the pyridocarbazole could completely change the preferred binding poses of the resulting isomers.

Therefore, this effect has been investigated in the case of PIM-1 and both, Λ -(*R*)-**127** and Λ -(*R*)-**128**, have been tested in competitive assays. In case of PIM-1, despite offering the mentioned large binding site, the results of the IC₅₀ determinations show the same trends as observed for Λ -(*R*)-**106** and Λ -(*R*)-**107**. Although, the described assumption was not confirmed in

this case, the possibility, that modifications leading to new complexes might also result into distinct binding poses compared to the coresponding progenitor, has to be considered for future investigations to prevent misinterpretations and undisclosed conclusions.



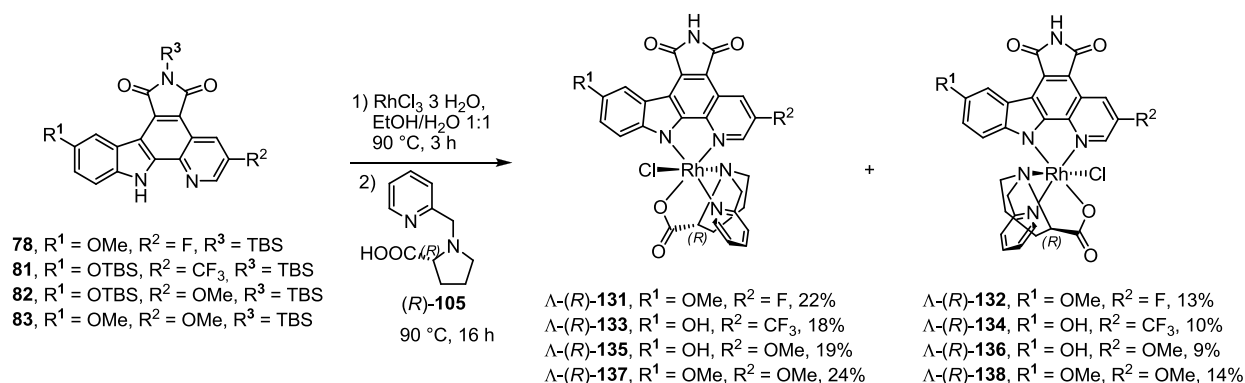
Scheme 20: Asymmetric synthesis of organorhodium complexes with modified pyridocarbazole ligands (I).

3.3.9 Scanning the Binding Pocket – Modifications of the Pyrido-carbazole Pharmacophore

After the results scanning the binding pockets with modified tridentate chiral ligands, additional functional groups to the pyridocarbazole pharmacophore ligand itself were attached to investigate their influences on the inhibition profile. Therefore, different pyridocarbazoles were reacted according to the established synthetic route, see Chapter 3.3.2. Accordingly, the pyridocarbazole ligands **78**, **81**, **82**, and **83** were reacted in a sequential addition to a suspension of RhCl₃·3H₂O in an ethanol/water mixture at 90 °C for 3 h followed by addition of the chiral tridentate ligand (S)-**105** or (R)-**105**, see Scheme 20 and Scheme 21. Reacting the mixtures at 90 °C for 16 h led to the formation of the two diastereomers for each pharmacophore ligand as observed before for **79**. The diastereomers of each single

reaction could be separated by silica gel chromatography followed by a preparative TLC for each single compound resulting in purple complexes. Moreover, the general loss of *tert*-butyl-dimethylsilyl protection groups of the ligands, not only at the maleimide moiety but also at the hydroxyl groups, was observed.

The yields of the obtained complexes are quite comparable to the initial reactions, see Chapter 3.3.2. Although, the disadvantage of protection group cleavage seems to affect the solubility of the ligands and subsequently impairs the yield of the reaction. However, screening of different solvent systems and reaction temperatures failed to form the intended reaction products. Furthermore, the established synthetic route was still applied as a reference procedure to compare the influences of the ligand modifications.



Scheme 21: Asymmetric synthesis of organorhodium complexes with modified pyridocarbazole ligands (II).

3.3.10 Biological Investigations

Closing, the obtained complexes of the pyridocarbazole modifications were tested according to the IC_{50} determination towards the target kinases FLT-3, Aurora A, and PIM-1, as described in Chapter 3.3.3.

FLT-3 was inhibited by Δ -(S)-**132** (474 nM), Δ -(S)-**134** (51 nM), Δ -(S)-**136** (622 nM), but not by Δ -(S)-**138** (5.85 μ M). Moreover, Δ -(S)-**134** outperforms the IC_{50} of 137 nM for Δ -(S)-**107**. Δ -(S)-**106** inhibited Aurora A with an IC_{50} value of 121 nM, whereas Δ -(S)-**131** (6.95 μ M), Δ -(S)-**133** (12.5 μ M), Δ -(S)-**135** (7.71 μ M), and Δ -(S)-**137** (9.46 μ M) are significantly worse inhibitors. PIM-1 was inhibited by Λ -(R)-**107** with an IC_{50} of 15 nM, whereas the inhibitors Λ -(R)-**134** (19 nM), and Λ -(R)-**136** (32 nM) inhibit the kinase at comparable concentrations. Nevertheless, Λ -(R)-**132** (326 nM) and Λ -(R)-**138** (1.29 μ M) possess a decreased affinity to the PIM-1 kinase than the original structural progenitor.

3.3.11 Interpretation

Modifying the chiral tridentate prolinato ligands showed, that the investigated target kinases do not tolerate additional groups on this side of the complex. Moreover, Aurora A excludes simultaneous modifications on the indole as well as on the pyridine moiety of the pyridocarbazole ligand. Nevertheless, in some cases modifications of the pyridocarbazole ligand led to the formation of inhibitors with increased affinity, i.e.: Δ -(S)-**134**. However, these functional groups may offer an additional adjusting point to increase solubility and lipophilic properties to modulate and improve ADME properties.

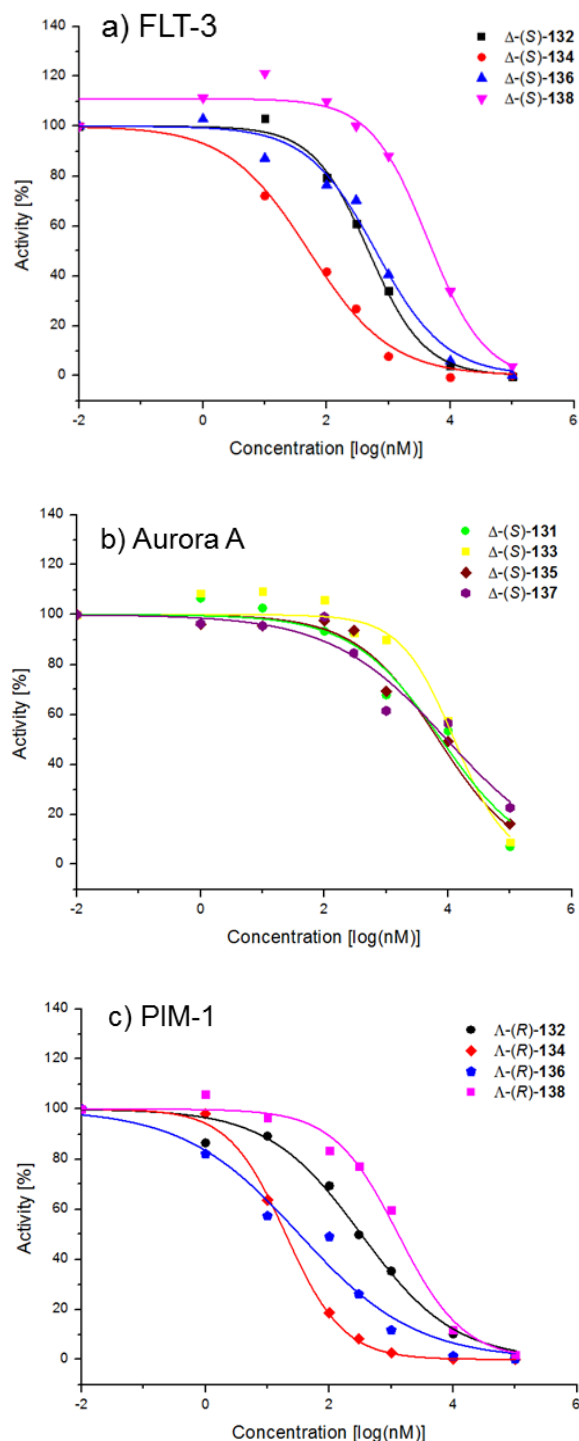


Figure 71: IC_{50} determination by $[\gamma\text{-}^{33}\text{P}]\text{-ATP}$ competitive assays with an ATP concentration of 10 μ M. The data points represent mean values of double determinations and an independent verification assay under same conditions. **a)** FLT-3: Δ -(S)-**132** (474 nM), Δ -(S)-**134** (51 nM), Δ -(S)-**136** (622 nM), and Δ -(S)-**138** (4.31 μ M). **b)** Aurora A: Δ -(S)-**131** (6.95 μ M), Δ -(S)-**133** (12.5 μ M), Δ -(S)-**135** (7.71 μ M), and Δ -(S)-**137** (9.46 μ M). **c)** PIM-1: Λ -(R)-**132** (326 nM), Λ -(R)-**134** (19 nM), Λ -(R)-**136** (32 nM), and Λ -(R)-**138** (1.29 μ M).

3.4 Design of Phosphatidylinositol-3-Kinases (PI3K) Inhibitors

3.4.1 Target Synopsis and Aim (III)

The phosphatidylinositol-3-kinases (PI3K) belong to the family of lipid kinases. In opposite to the regular protein kinases, membrane bound lipids are the phosphorylation targets of PI3Ks acting as subsequent second messenger.^[383] The phosphorylation products play important roles for the regulation of cellular processes like gene expression, carbohydrate metabolism, or apoptosis.^[383,384] Moreover, some members are key players of pathologic processes involved in diseases like diabetes, cancer, cardiovascular diseases and autoimmune deficiencies.^[384,385] Therefore, PI3Ks are interesting targets for the pharmaceutical research.^[386–388]

The PI3Ks consist of a regulatory domain (p85 or p101) and a catalytic domain (p110). Thus, they were clustered into three different classes covering class I, II, and III, due to their structural differences and substrate specificity.^[389,390] The class I is further subdivided into two groups, IA and IB based on their different structure and activator recruitment. Both result into the phosphorylation of phosphatidylinositol-4,5-bisphosphate (PIP₂) to phosphatidylinositol-3,4,5-trisphosphate (PIP₃). In contrast, phosphatase and tensin homologue (PTEN) acts as the cellular counterpart of the PI3Ks class I cleaving the attached phosphorylate group.^[391] PIP₃ as the second messenger activates various effectors via the pleckstrin homology domain (PH), i.e.: PDK1 and mTORC2. Further, it regulates the PIP₃ activated protein kinase B (AKT), which itself regulates a plenty of downstream effectors covering p53, and BAD, see Figure 73.^[389,392]

Class IA PI3Ks are heterodimers consisting of a regulatory p85 binding do-

main isoform (for p110 α , p110 β and p110 δ), a Ras binding domain, a protein kinase C homology domain 2 (C2), a PI3Ka domain, and a catalytic PI3Kc domain.^[389,390] The different binding domains lead to the three isoforms α , β , and δ . The extracellular domain of an attached membrane bound receptor tyrosine kinase activated by growth factors, and insulin among others, phosphorylates the regulatory domain of the PI3Ks. This leads to an activated state of the catalytic domain.^[383] Nevertheless, also synergistic effects of G $\beta\gamma$ and RTKs dependent activation have been reported.^[393–395]

Class IB PI3Ks are also heterodimers. However, in contrast to class IA the regulatory domain (p101) offers an adaptor binding site (AdB).^[383,389] Only one isoform of class IB, PI3K γ , was identified by now.^[389,390] Moreover, the activation is mediated by a G_{i/o}-protein coupled receptor (GPCR).^[384,394,396] It is noteworthy, that in opposite to the usual activation of effectors by the G α subunit, the G $\beta\gamma$ subunit activates PI3K γ , beside other effectors. Thus accelerates the whole signal transduction event faster than the class IA mediated signal cascade.^[388]

Whereas the PI3K α and PI3K β are expressed ubiquitous in all cell types, the isoforms PI3K γ and PI3K δ are mainly expressed in cells of the native and adaptive immune system, the blood pressure regulation, and the blood coagulation.^[385,397] Moreover, PI3K γ is often expressed for a cooperative activation of other receptors and effector proteins, i.e.: PI3K δ .^[388] Chemokines, pro-inflammatory lipids, and bacterial products represent extracellular ligands for PI3K γ activation in immune cells.^[385] The activation subsequently increases the efficiency of neutrophils by accelerated excretion of proteases, reactive oxygen species, and antimicrobial substances.^[398] Moreover, PI3K γ and PI3K δ mediated cellular events leads to the enhanced recruitment of macrophages and monocytes to the inflamma-

tion site.^[398,399] PI3K γ and PI3K β cooperation is responsible for the ADP dependent platelet coagulation.^[388] Moreover, PI3K γ seems to be involved in myocardial muscle cell contraction.^[400] A direct binding to the cAMP-phosphodiesterase and the subsequent reduction of the cAMP level leading to reduced muscle contraction is discussed as the mechanism of action.^[400]

However, the class II PI3Ks lack the p85 domain but offer a C-terminal Phox domain and an additional C2 domain. In contrast, the class III are reduced to the rudimentary structural properties responsible for phosphatidylinositol binding and catalysis, see Figure 72.^[389]

The described important roles of PI3Ks in physiological processes and pathological events turn them to interesting targets for the treatment of hypertonia, autoimmune diseases, and cancer.^[385] Beneficial effects targeting PI3Ks have been observed in mouse models for rheumatoid arthritis and systemic lupus.^[397,401]

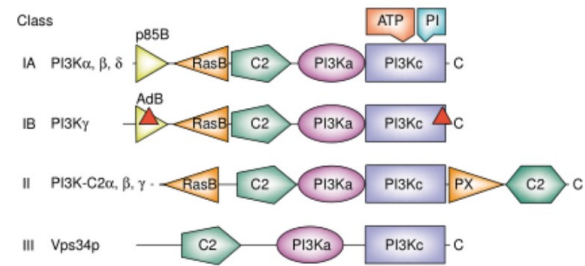


Figure 72: PI3Ks are divided into three classes. All PI3K catalytic subunits consist of a C2 domain, a helical PI3Ka domain and a catalytic PI3Kc domain. Class IA PI3Ks exist in complex with a regulatory p85 subunit isoform. Class II lack the regulatory subunits but have amino- and carboxy-terminal extensions to the PI3K core structure. Class III are structurally reduced to the rudimentary PI3K core.^[389]

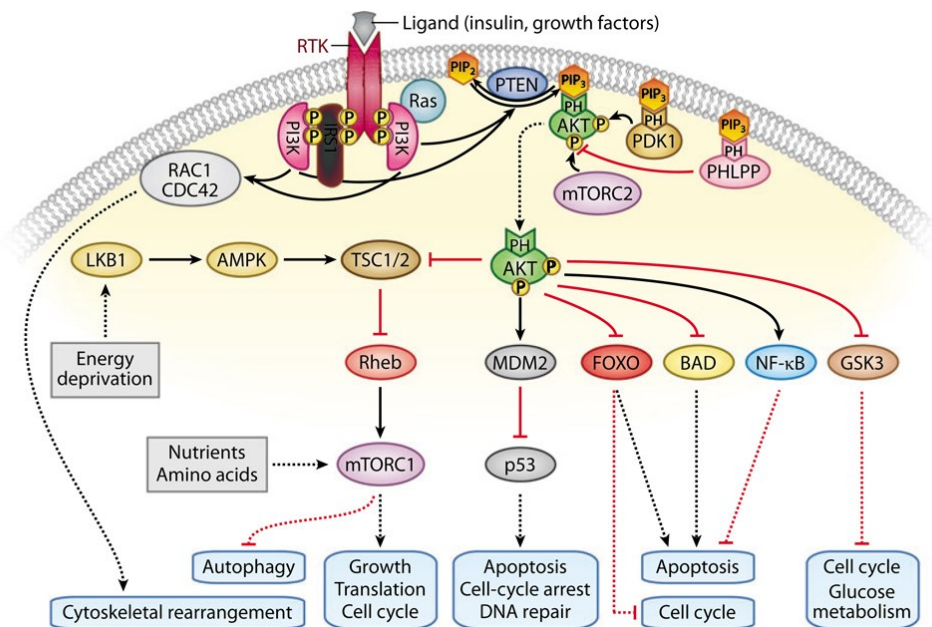


Figure 73: PI3K pathway is initialised by RTKs recruit resulting in increased phosphatidylinositol-3,4,5-trisphosphate (PIP₃) levels. PIP₃ subsequently concentrates many effector proteins to the membrane via their pleckstrin homology (PH) domains including AKT, PDK1, PHLPP. Furthermore, PDK1 and mTORC2 activate AKT, whereas the inactivation is mediated via the dephosphorylation by PHLPP. Activated AKT phosphorylates various substrates, influencing effectors of cellular growth, survival, and proliferation. However, an AKT-independent activation of downstream targets, such as RAC1/CDC42, by PI3K is also possible.^[391]

3.4.2 Organometallic Inhibitor Design

The cumulated results obtained for the investigations described for chiral tridentate ligands claim for a more efficient way to design and anticipate ligand modifications increasing the binding affinity. Scanning a kinase binding pocket by the subsequent introduction of additional functional groups into the ligand scaffold inevitably increases the number of synthetic steps. Moreover, a beneficial effect is not guaranteed turning some elaborated synthetic routes into superfluous efforts. Thus, to avoid the dissipation of time and resources a more sophisticated way to design new organometallic inhibitors has to be elaborated. To face this issue, initial efforts were spent to apply methods established for the molecular modelling of pure organic inhibitors onto the concept of organometallic inhibitors.

The challenge of synthesising enantiopure organometallic complexes has been discussed previously, see Chapter 2.3., and appropriate possible solutions have been presented, see Chapter 3.3.2 and Chapter 3.3.5. Nevertheless, the importance and the need of such systems for the asymmetric synthesis of octahedral complexes is highlighted once again in the context of PI3K γ inhibition. The complex **139** synthesised by STEFAN MOLLIN in the MEGGERS group was only obtained as a racemic mixture consisting of Δ -**139** and Λ -**139**. **139**. The racemic mixture was found to inhibit PI3K γ . Although, a crystal structure of **139** bound to PI3K γ was obtained by JIE QIN in the MARMORSTEIN group, the correct assignment of the enantiomer in congruence to the measured electron density was not unambiguously possible. Moreover, a complicated separation of the enantiomers was not performed during the former investigations, see Figure 75.

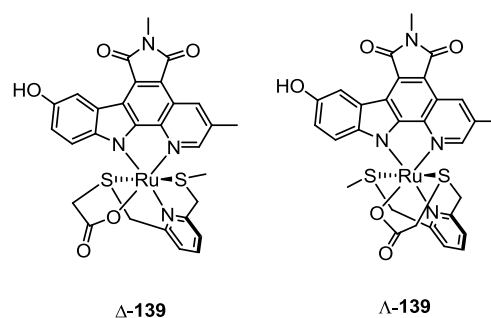


Figure 74: Single enantiomers of Δ/Λ -**139**, which was used as racemic PI3K γ inhibitor.

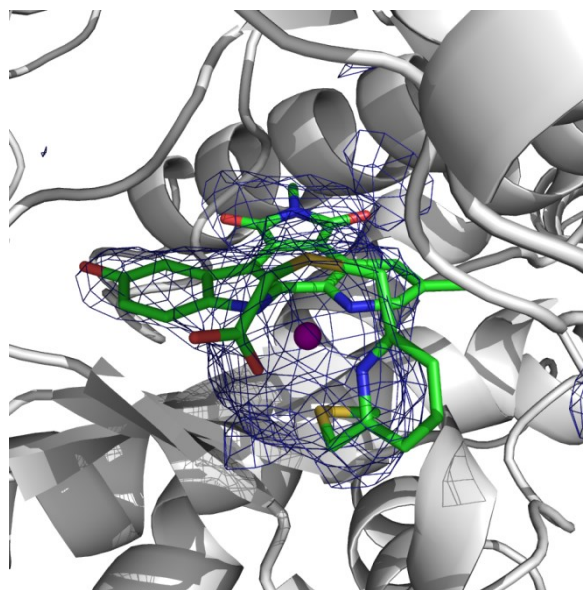


Figure 75: PI3K γ in complex with organoruthenium(II) complex **139** (internal data from MEGGERS group). The map is the *fofc.map* at 2 σ level. The crystals were recorded for 8 h and the resolution was 2.55 Å. The electron density do not allow an accurate assignment of the enantiomer. The chemical structure of Λ -**139** is shown as sticks with the carbon atoms in green. Nitrogen atoms are shown in blue, oxygen atoms in red, sulfur in yellow, and the ruthenium core in purple. PI3K γ is presented as cartoon in white.

To circumvent these problems, the elaborated concepts to synthesise enantiopure metal based inhibitors could be applied to develop a PI3K γ selective inhibitor. Moreover, computer aided design could assist the development of new complexes avoiding superfluous synthetic efforts.

3.4.3 Hot Spot Analysis – a First Clue to Address the Right Sites

The next generation complexes of PI3K γ inhibitors were intended to be designed as octahedral complexes. To assist these attempts a hot spot analysis was applied first to achieve a first clue, if there are favourable interactions present. Thus, two different programs, FCONV and HOTSPOTSX developed by GERD NEUDERT, were applied in collaboration with TOBIAS CRAAN to design the new scaffold.

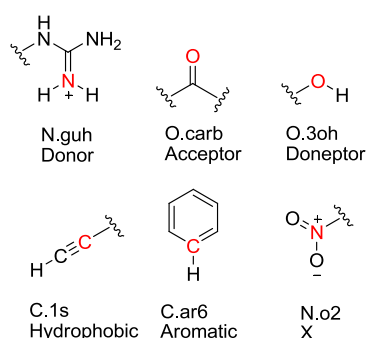


Figure 76: Representative atoms (highlighted in red) assigned according to the internal annotation of FCONV. The annotation includes element symbol, chemical environment, hybridisation state, bonding state and interaction group.

3.4.3.1 FCONV – a program for format conversion, manipulation and feature computation of molecular data

FCONV is applicable for molecule data handling and data parsing problems.^[402] This program assigns internal predefined atom types to the atoms of an input structure. The internal atom type classification considers the element itself, the hybridisation state, and the intermolecular interaction of the appropriate functional group, see Figure 76 for representatives; i.e.: the oxygen of an hydroxyl group is assigned by the descriptors O for oxygen, 3 for sp^3 hybridisation, and oh as the oxygen is bound to an hydrogen atom beside the alkyl residue. On one hand, the hydroxyl group could form hydrogen bonds providing its own hydrogen atom; on the other, it could provide one of its lone pairs for hydrogen bond formation. In the first case the hydroxyl group acts as a donor and in the second as an acceptor. Therefore, the O.3oh atom type belongs to the doneptor group. In opposite, an oxygen of an alkyloxy

Table 1: Overview of the internal atom types of FCONV clustered by their physico-chemical properties. Acceptor (Acc), doneptor (AnD), aromatic (Aro), donor (Don) and hydrophobic (Hyd) properties.

Acceptors		Doneptors	Aromatic	Donor	Hydrophobic
O.carb	O.co2	O.3oh	C.ar6	N.guh	C.1s
N.ar2	O.2po	N.r3	C.ar6x	N.ar6p	C.2r3
N.1	O.2so	N.gu1	C.arp	N.arp	C.3r3
N.oh	O.2p	N.gu2	C.arx	N.ar3h	C.1p
N.aas3	O.2so	N.mi1	C.ar	N.ohac	C.2p
N.aat3	O.3po	N.mi2	N.ar6	N.ims	C.2s
N.2n	O.3so	N.aap	N.ar3	N.amp	C.2t
N.2s	O.o	N.2p	O.ar	N.ams	C.et
N.3t	O.3es	N.3n	S.ar	N.samp	C.ohp
O.r3	O.3eta	N.3p		N.sams	C.ohs
O.n	O.3eta	N.3s		N.mih	C.oht
O.2co2	S.r3	O.h2o		N.4H	C.3p
O.2es	S.thi	O.noh			C.3s
O.2hal	S.2	O.3ac			C.3t
O.am		O.ph			C.3q
					S.sh
					S.s
					S.3
29		15	9	12	18

group assigned by the descriptors O.3eta (O for oxygen, 3 for sp^3 hybridisation, and eta for ether) can not act as a donor and thus belongs solely to the acceptor group.

In total, 157 different atom types were considered and clustered into five different groups considering their main generic physicochemical properties: acceptor (29), doneptor (15), aromatic (9), donor (12), and hydrophobic (18), see Table 1. The atom types that can not be accounted to any of the described groups were defined as X (74). Thus, by correlating and assigning each atom of a molecule by FCONV, enables a description of the local chemical environment, hybridisation, and bonding state.

3.4.3.2 *HotSpotsX – a program to generate contour maps and hot spots*

The second applied program during these investigations was HOTSPOTSX. This program is applicable to predict interaction fields, expressed by contour maps, for the previously defined atom types of an input structure. If the input structure is i.e.: a protein structure, contour maps for the catalytic center, an allosteric binding site, any other binding site, or a protein surface of interest can be predicted. The predictions are knowledge based.^[403,404]

First, atoms of functional groups and structural motifs were assigned and clustered by FCONV as described before. These process was performed not only for the structure of interest, but also for a reference data set like entries from the Cambridge Structural Database (CSD) or the Protein Data Bank (PDB). Then, the experimentally determined distances and angles, deposited in the reference data set, for a predefined atom type and its appropriate interaction partner were correlated by HOTSPOTSX. Here, contour maps for each predefined atom types were calculated expressing the ideal coordinates for the matching interac-

tion partner. The coordinates with high occurrence frequencies in the databases, regarding distance and angle were represented by high propensity and subsequently result into hot spots.

The contour maps can be represented at different map levels, which will be explained by the example of hydrogen bonds below. The length of hydrogen bonds vary between approximately 1.6 Å and 2.0 Å. It depends on different factors like bond strength, temperature, and pressure.^[405,406] Moreover, the bond strength in turn is dependent on temperature, pressure, bond angle, and the individual environment of the interacting molecules.^[405,406] Thus, i.e.: the FCONV atom type N.3p, a primary amine could form an hydrogen bond with a certain partner, i.e.: O.carb (carbonyl oxygen) under a particular distance and a particular angle in one entry of the PDB reference set, see Figure 77 a). However, in a second entry, the hydrogen bond between the same atom types differ slightly due to the environment of the entry in the reference set, see Figure 77 b). Thus, evaluating all N.3p – O.carb pairs of the reference set inevitably leads to a scattering of the ideal coordinates of N.3p around a certain mean value for the distance of interest, see Figure 77 c). The same observation is true for varying distances retaining a particular angle.

Therefore, a single coordinate for the ideal position of N.3p related to O.carb can not be provided. Moreover, plenty of combinations of distances and angles of the hydrogen bonds are possible. However, all converge an ideal distance and angle. Thus, leads to a three dimensional scattering and results subsequently into the mentioned contour maps. Three-dimensional areas with high propensity of N.3p coordinates result into a hot spot for this doneptor group. Moreover, by altering the grade of propensity subsequent contour map levels can be examined.

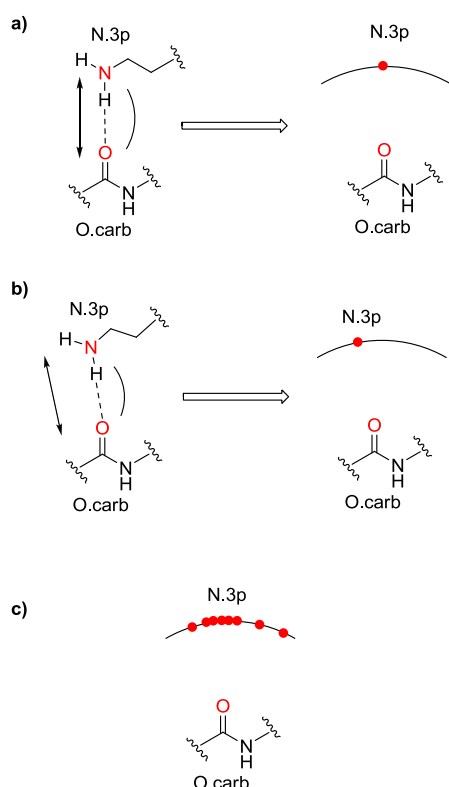


Figure 77: The general principle of contour map calculation by HOTSPOTSX highlighted on an example with altering angles and fixed hydrogen bond distance. **a)** The coordinates of an interaction pair forming hydrogen bonds like N.3p and O.carb were determined. Their coordinates are crucially influenced by the hydrogen bond length and the angle. **b)** In a second N.3p – O.carb interaction pair the individual environment of the molecules force a slight difference in the angle of the hydrogen bond by retaining the hydrogen bond length. This entry of the reference data set leads to slightly altered coordinates for the N.3p atom type related to the O.carb atom type as shown in a). **c)** With increasing number of compared N.3p – O.carb interaction pairs the coordinates for N.3p scatter around a certain mean value. However, plenty of combinations of lengths and angles of the hydrogen bonds are possible. Thus, leads to a three dimensional scattering. This subsequently results into a contour map rather than a single ideal coordinate. Three-dimensional areas with high propensity of N.3p coordinates result into a hot spot for this doneptor group.

The same described procedure was applied for any combination of atom type pairs, which form intermolecular interactions, i.e.: acceptor – donor, acceptor – doneptor, hydrophobic – hydrophobic, aromatic – aromatic, etc. The combined contour maps of all FCONV atom types, which belong to a distinct group of physico-chemical interaction, represent the contour map of the interaction group itself. For instance, the combined contour maps of all 15 single atom types of the doneptor group represent

the contour map of the doneptor group itself, see Table 1. However, some atom types like N.guh, a protonated guanidinium nitrogen, posses less entries in the reference set then other like O.3oh. Thus, the absolute levels for each generic physicochemical interaction group inevitably differ and negative values are favorable values. However, a relative comparison is more appropriate to compare different interaction types than a correlation of the absolute contour map level. Therefore, the percentage above the minimal map level was considered for each physicochemical interaction group for comparison. High percentages are based on high propensities for certain interaction types representing more accurate hot spot.

However, the main focus of the investigations performed during this work was not the evaluation of every single FCONV atom type of PI3K γ to a particular interacting atom type via HOTSPOTSX as described in previous studies.^[407] A general comparison of the different generic physicochemical interaction groups was sufficient to achieve a first clue. These impulses could be implemented in the ligand scaffold. Thus initial hints could significantly inspire the future metal complex design.

3.4.3.3 PI3K γ as investigation target for the hot spot analysis

As a three dimensional structure of the target protein is necessary to perform the hot spot analysis, the crystal structure of **140** in complex with PI3K γ (pdb: 3CST) was selected as template.^[188] The metal based half sandwich inhibitor is composed of a modified pyridocarbazole ligand, a monodentate carbonyl ligand and a modified cyclopentadienyl ligand. Nevertheless, only the structural information of the kinase was accounted for the analysis.

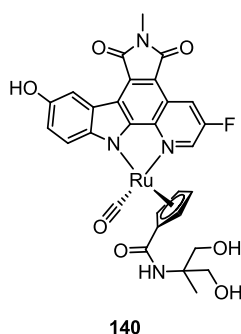


Figure 78: PI3K γ inhibitor **140** (pdb: 3CST).

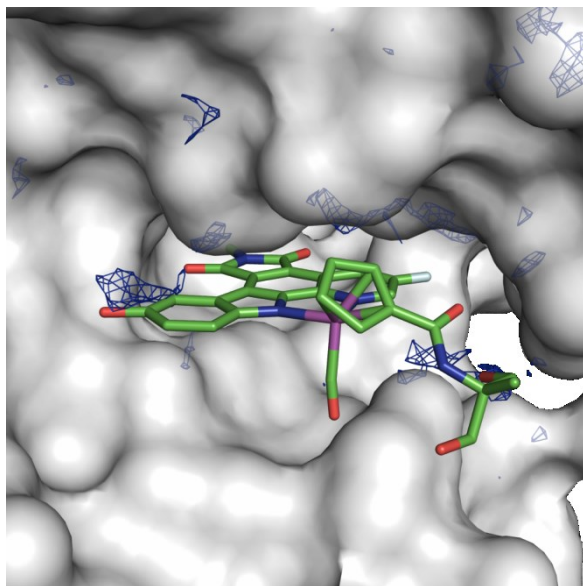


Figure 79: Contour map of the physicochemical interaction type donor (blue) at contour map level of 69% above minimal map level. The carbon atoms of the organometallic complex **140** are depicted in green, the oxygen atoms in red, the nitrogen atoms in blue, the fluorine in light cyan, and ruthenium in purple. The surface of the PI3K γ binding site is shown in white.

The hot spot analysis, applying the introduced programs FCONV and HOTSPOTSX, in case of PI3K γ was performed for each of the five generic physicochemical interaction types: acceptor, donor, doneptor, hydrophobic and aromatic. The donor contour map at a level of 69% is shown in Figure 79 and the acceptor contour map at a level of 46% in Figure 80, both for the PI3K γ binding site.

Figure 79 already reveals a coincidence of the hydroxyl group of the pyridocarbazole ligand of **140** and the donor contour map. Moreover, one of the two hydroxyl groups of the 2-amino-2-methylpropane-1,3-diol residue of **140** is oriented towards but not cov-

ered by the donor contour map. However, the surface of PI3K γ suggests that this binding site area is of limited accessibility.

In Figure 80 the monodentate carbonyl ligand is close to be covered by the acceptor contour map. However, the carbonyl ligand can not be considered as a true hydrogen bond acceptor. Thus, a metal coordinating ligand acting as a true acceptor could improve the affinity. This hypothesis remains to be proven. However, these examples confirm the worthiness of the hot spot analysis for future drug design.

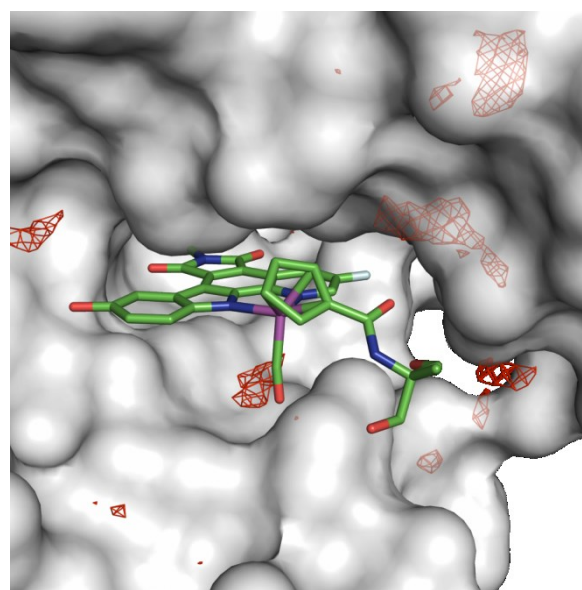


Figure 80: Contour map of the physicochemical interaction type acceptor (red) at contour map level of 46% above the minimal map level. The carbon atoms of the organometallic complex **140** are depicted in green, the oxygen atoms in red, the nitrogen atoms in blue, the fluorine in light cyan, and ruthenium in purple. The surface of the PI3K γ binding site is shown in white.

The separate inspection of already these two contour maps of the PI3K γ binding site suggests, that a simultaneous comparison of all five physicochemical interaction types would rapidly lead into a confusing overall picture for visual evaluation. Therefore, the contour maps of the investigated physicochemical interaction types were converted into discrete spheres by MICHAEL BETZ. These spheres represent a contour map at a certain map level, but allow to selectively hide spheres of disinterest for clari-

ty as shown for the acceptor contour map in Figure 81.

The hot spots are depicted as spheres with ideal positions for hydrogen bond acceptors (red), hydrogen bond donors (blue), doneptors (purple), hydrophobic groups (white) and aromatic groups (yellow). They were selected by visual inspection according to their relevance for prediction, verification, and guidance for synthetic modifications, see Figure 82. The size of the spheres reflect their appropriate contour maps at a certain map level.

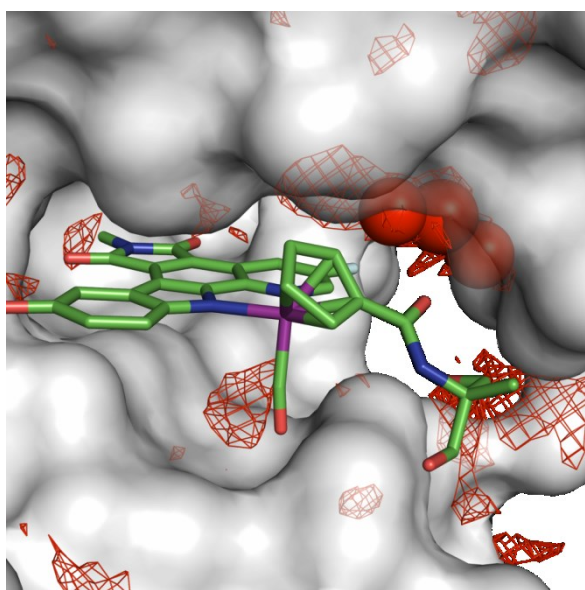


Figure 81: Conversion of the acceptor contour map to corresponding spheres offers the possibility to selectively omit spheres of disinterest for clarity. In this example, three spheres adjacent to the pyridine moiety of the pyridocarbazole ligand of **140** are displayed and others were hidden. The contour map level is 40% above the minimal map level. The carbon atoms of the organometallic complex **140** are depicted in green, the oxygen atoms in red, the nitrogen atoms in blue, the fluorine in light cyan, and ruthenium in purple. The surface of the PI3K γ binding site is shown in white.

Regarding the hot spots in the binding site reveals that the pyridocarbazole ligand of **140** exactly occupies the ideal position for a hydrophobic interaction partner with its maleimide moiety. The hot spot represents the contour map at 82% above minimal map level. This indicates that the hydrophobic interaction might be of major importance for the overall ligand-protein interaction. This observation is in good congruence to the

fact, that the pyridocarbazole ligand faces an aromatic amino acid residue (Tyr-867) in the PI3K γ binding site, see also Figure 83. This residue, along with others in the binding site, indeed favours an hydrophobic interaction partner.

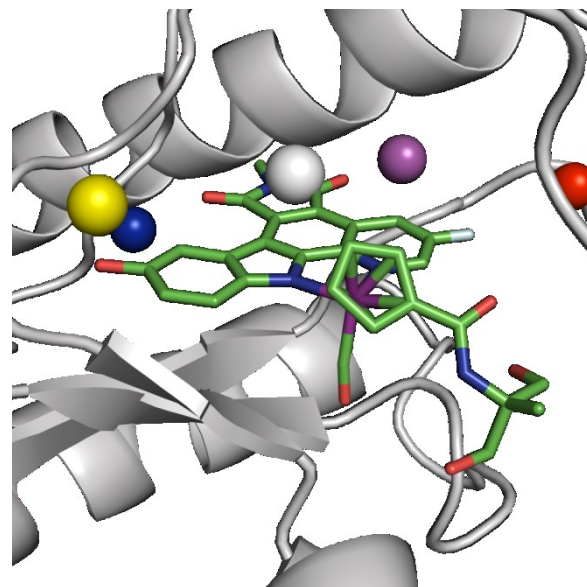


Figure 82: PI3K γ in complex with **140** (pdb: 3CST). The five interaction groups are depicted as spheres: hydrogen bond acceptor (red, 46%), hydrogen bond donor (blue, 69%), doneptors (purple, 52%), hydrophobic (white, 82%) and aromatic (yellow, 80%). **140** is presented as sticks with the carbon atoms in green. Nitrogen atoms are shown in blue, oxygen atoms in red, fluorine in light cyan, and the ruthenium core in purple. PI3K γ is presented as cartoon in white, whereas the only the ATP binding site is shown for clarity.

Moreover, the hydroxyl function of the pyridocarbazole ligand almost occupies the predicted ideal position for a donor interaction type. The hot spot represents the contour map at 72% percent above the minimal map level. Thus, a hydrogen bond donor at this area of the binding site might result into a beneficial contribution to the ligand-protein interaction. A predicted hot spot for a doneptor is in a 2.67 Å distance to the carbonyl group of the maleimide function representing the contour map at 52% above the minimal map level. However, the pyridocarbazole does not meet this potential interaction. A selective modification of the pharmacophore ligand on this moiety is difficult, although synthetically possible and realised in former studies.^[408]

Furthermore, a hot spot for a hydrogen bond acceptor was identified 3.62 Å away of the fluorine atom of the pyridocarbazole reflecting the corresponding contour map at 46% above the minimal map level. However, addressing this potential interaction could be quite challenging due to its location in a cleft of the binding pocket, which is difficult to reach from the inhibitor binding site.

Closing, the hot spot for an aromatic group (82% above minimal map level) and the hot spot for a hydrogen bond donor (80% above the minimal map level) are both located next to the indole moiety of **140**. Although, **140** does not address these interactions, suitable functional groups could be elaborated to address both simultaneously. The hot spot analysis has not resulted in favourable interactions covered by the cyclopentadienyl ligand of **140** at arguable map levels. In addition, potential adjacent favourable donor interactions, as indicated by the contour map, might be difficult to meet, see Figure 81.

However, the hot spots for the acceptor, doneptor, and the donor interaction types are all representing their corresponding contour maps at a map level below 69%. This fact should be evaluated critically, as valuable hot spots for ligand design should aspire map levels of about 90% or even higher.^[407,409,410] However, the hydrophobic and the aromatic interaction types, both above 80% above minimal map level, seem to be the main contributing interactions for the binding of **140**. This observation is of very good congruence to the characteristics of complex **140** as its pyridocarbazole ligand is methylated at the maleimide moiety. This, significantly, turns it into a hydrophobic complex compared to the unmodified ones.

It is noteworthy, that the hot spot analysis was performed only for the binding site itself leading to results only for the ATP binding site. Indeed, different sites of PI3K γ may offer much favourable positions for these interaction types and may reveal po-

tential allosteric binding sites. However, no further favourable functional groups or structural moieties have to be respected for the ligand design using **140** as a starting point. Thus, the ligand design can be entirely focused to face the enantiopure complex synthesis.

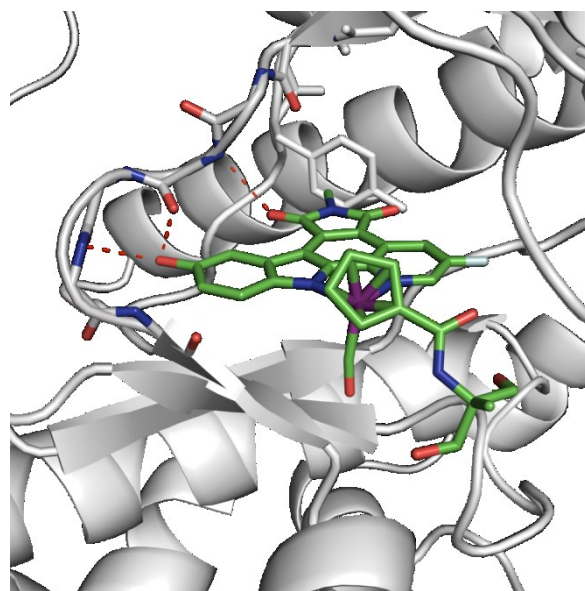
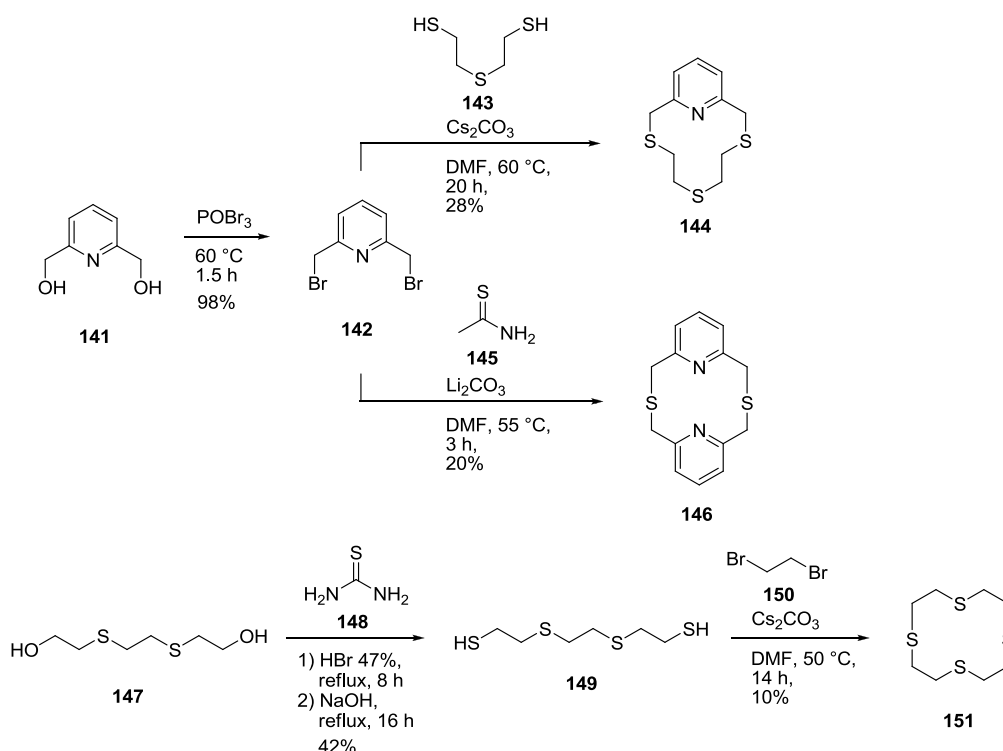


Figure 83: PI3K γ in complex with **140** (pdb: 3CST).^[188] The hydroxyl group forms two hydrogen bonds to Val882 and Asp884 (red dashes). Tyr-867 forms hydrophobic interactions to the pyridocarbazole ligand of **140**. **140** is presented as sticks with the carbon atoms in green. Nitrogen atoms are shown in blue, oxygen atoms in red, fluorine in light cyan, and the ruthenium core in purple. PI3K γ is presented as cartoon in white and the main chain of the hinge region is depicted additionally as sticks.

The results of the hot spot analysis are over all in a very good congruence to the experimentally determined results; especially, comparing them to the crystal structure of **140** in complex with PI3K γ , see Figure 83. First, the hydroxyl group of the pyridocarbazole forms two hydrogen bonds with Val882 and Asp884 and simultaneously occupies the space adjacent to the predicted hot spot for a hydrogen bond donor. Nevertheless, as the hydroxyl group acts as a doneptor, in this case a doneptor hot spot should have been identified at this position. Second, the Tyr-867 determines the corresponding interaction partner and the pyridocarbazole ligand fulfills these requirements ideally occupying the hydrophobic hot spot. This position was assigned as a hydropho-

bic hot spot due to the clustering of the atom types into the different physico-chemical interaction types. However, the atom types assigned to either aromatic or hydrophobic hot spots are related to each other regarding their chemical properties. Therefore, the discrimination is not strict and both interaction types can be addressed by related structures.

However, discrepancies in the positioning should not be overrated. The flexibility of the protein leads to a subsequent shift of the hot spots, which can not be respected in an analysis based on a rigid model. However, further verification experiments for the hot spot analysis could help to improve its accuracy and the effect of preliminary preparation procedures. For instance, the influence of the scope of the input structure, considering binding site versus the use of the entire protein domain could be investigated. Nevertheless, the hot spot analysis on this example indicated its beneficial potential to the future design of PI3K γ inhibitors.



Scheme 22: Synthesis of C2-symmetric tetradentate ligands.

3.4.4 Elaborating the Ligand Scaffold

3.4.4.1 Tetradentate C2-Symmetric Ligands

As the hot spot analysis has not revealed favourable interactions ideally to address by the residual ligands offside the pyridocarbazole, the focus was set on the synthesis of enantiopure metal based PI3K γ inhibitors. Different ways to achieve this goal were pursued. The first approach was the use of C2-symmetric ligands to avoid the formation of diastereomers during a single complexation reaction. Ligands like 2,5,8-trithia-[9](2,6)pyridinophane (**144**), 2,11-dithia[3.3](2,6)pyridinophane (**146**), and 1,4,7,10-tetrathiacyclododecane (**151**) fulfill the requirements of being symmetric and offering coordinating atoms for metal complexation.

The synthesis of the pyridinophane derivatives **144** and **146** starts from the common precursor 2,6-bis(bromomethyl) pyri-

dine **142**, see Scheme 22. **142** can be synthesised in 98% yield starting from 2,6-pyridinedimethanol (**141**) in melted phosphoryl bromide at 60 °C. **142** was extracted and dried *in vacuo* to obtain white needles. Then, different cyclisation conditions result into the related compounds **144** and **146**. Caesium carbonate suspended in DMF at 60 °C for 20 h reacting a homogenous solution of **142** with 2,2-Bis(2-mercaptoethyl)sulfide (**143**) leads to the formation of **144** in 28% yield. It is noteworthy, that a drop wise addition of the reactants via a syringe pump is mandatory to form the medium size ring and to avoid polymerisation to side products. Reacting **142** with thioacetamide (**145**) and lithium carbonate in DMF at 55 °C for 3 h result to the formation of **146**. After extraction and column chromatography the product was obtained as yellow, highly viscous oil.

In opposite 2,2'-(ethane-1,2-diylbis(sulfanedyl))diethanol (**147**) was refluxed with thiourea (**148**) in hydroboric acid (47% aq.) for 8 h followed by the addition of sodium hydroxide and an additional 16 h of reflux condition. After extraction the intermediate

2,2'-(ethane-1,2-diylbis(sulfanediyl))diethanethiol (**149**) was obtained as highly viscous pale oil in 42% yield. The cyclisation was then performed using caesium carbonate suspended in DMF heated to 50 °C and the addition of a homogenous solution of **149** and 1,2-dibromoethane (**150**) drop wise over a period of 12 h via a syringe pump. The reaction was continued for an additional 2 h. The crude material was extracted and the product was recrystallised from chloroform to obtain **151** as white crystals in 10% yield. Ligand **151** and subsequent precursor were synthesised by the research intern SOPHIE FRANZ.

For the synthesis of the medium sized rings, the general problem is the low yields observed for all three examples. Although, the ligands were synthesised successfully, the complexation to the intended complexes were not pursued during this work as these complexes would have been positively charged. This incidence could be adverse for the passive diffusion for targeting PI3K γ , or other kinases, in a cellular model. Therefore, tetradentate C2 symmetric ligands do not offer a suitable solution to synthesise enantiopure metal based kinase inhibitors from the pharmacokinetic point of view. Meanwhile, the success of the chiral prolinato ligand concept in combination with rhodium as the metal centre was applied for PI3K γ inhibitor synthesis leading to promising results. Thus, the tetradentate ligand project was stopped despite the potential of obtaining interesting compounds, due to the lack of time. Nevertheless, the concept itself offers the possibility to achieve access to novel enantiopure octahedral metal complexes. Therefore, they should be considered for future enantiopure complexes with a distinct aim.

3.4.4.2 Amino Acids as Building Blocks for Chiral Multidentate Ligands

The successful work using proline in either L- or D-configuration as a building block for chiral multidentate ligand synthesis inspired to apply the residual proteinogenic amino acids in a similar way to control the stereochemistry of the complexes.

A. STRECKER had synthesised metal based complexes based on amino acids already in 1850, and many successful applications have been reported in literature by now.^[411–415] Crucial for the use of amino acids in metal complexation is the proper handling of the present side chain.^[416] The different functional groups can be either applied as steric effectors, coordinating structural motifs, or interaction partners for other molecules influencing physico-chemical, biological, and toxicological effects.^[416]

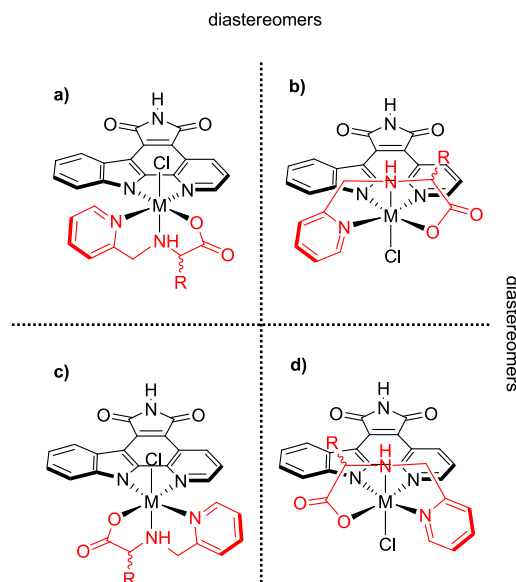


Figure 84: The incorporation of chiral primary amino acids into the design of tridentate ligands lead to the formation of four diastereomers **a)**–**d)** assuming a *fac*-coordination.

Transferred to the principles of octahedral metal complexes observed for prolinato ligands, the incorporation of chiral primary amino acids into the synthetic route should result into several changed characteristics of the expected complexes, see Figure 84:

1. The rigid structure of proline led to the formation of only two diastereomers during the complexation; using primary amino acids should result into four, if the tridentate ligand still occupies a *fac*-coordination and the pyridine ring remains in the same plane as the pyridocarbazole.
2. If enantiopure amino acids are utilised, all resulting four structural isomers of a complexation reaction are diastereomers as the C α chirality centre of the amino acid breaks symmetry.
3. All resulting four diastereomers should differ in their physico-chemical properties and therefore a standard purification should be applicable.

However, as there is a large set of commercially available amino acids, both in (*S*) as well as (*R*) configuration, a rational selection of suitable ones has to be elaborated. The resulting coordination spheres using distinct amino acids result in a different steric demand of the complexes. Moreover, the different functional groups of the amino acid residues may interact with the kinase binding site. In addition, applicability to the synthetic route has to be considered. These aspects have to be weighed wisely to reduce the synthetic effort and the consumption of resources.

3.4.5 The Selection of Amino Acids for the Ligand Design

3.4.5.1 General Strategy

First, the tridentate ligand was retrosynthetically separated into his two main components, see Figure 85. The general ligand design **152** was simplified to two fragments resulting in 2-methylpyridine (**153**) and the amino acid fragment (**154**). **153** remains unmodified in the intended ligands and the focus was set onto the amino acids and their residues. Thus, to solve the introduced issues, see chapter 3.4.4.2, the relevant amino acids were compared regarding their distinct characteristics. Moreover, the pyridocarbazole ligand and the metal core were defined as structural anchors remaining untouched.

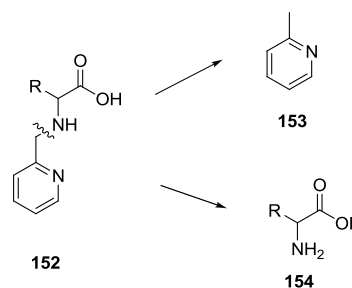


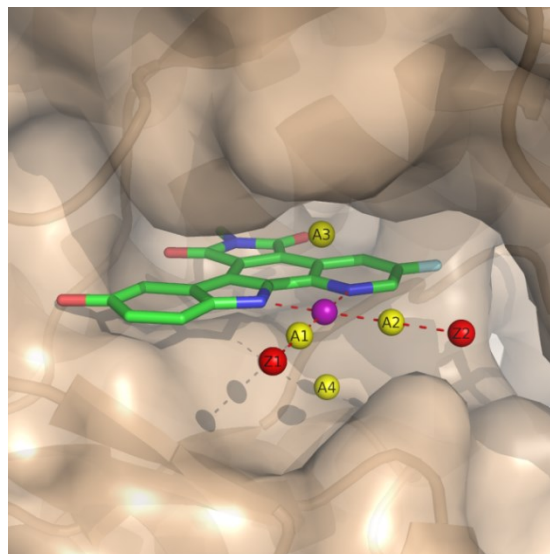
Figure 85: Fragmentation of the tridentate ligand scaffold.

3.4.5.2 Selection Criteria

The estimated accessible space in the binding site of PI3K γ has to be assessed to obtain a first hint for the ligand design. Thus, coordinates for the pyridocarbazole ligand and the metal core were extracted from the PI3K γ (pdb: 3CST) crystal structure and predefined as template structures. All amino acids of the primary sequence of PI3K γ in 4 Å distance to the pyridocarbazole and the metal core were identified and respected as binding site of the pyridocarbazole moiety.

Two different anchor points were defined as A1 and A2. The coordinates of these two anchor points were extrapolated from the crystal structure of Δ -(S)-**106**, see Figure 59, as an octahedral template in opposite to **140**. These anchor points occupy approximately the same positions as the corresponding coordinating atoms of the tridentate proline-based ligand of Δ -(S)-**106**. The distance was set to 2 Å, in congruence to Δ -(S)-**106**, and the anchor points are in the same plane as the pyridocarbazole ligand. Thus, the anchor points A1 and A2 represent the positions, where the coordinating atoms of the intended ligands should be located. Then, the centre Z1 was defined, whereas A1 is located 2 Å away from Z1, which in turn is located 4 Å away from the metal core; all three of them form a line. The same is true for Z2 and A2 related to the metal core, see Figure 86 a). The exact coordinates can be extrapolated by vector calculations based on the coordinates for the coordinating nitrogen atoms of the pyridocarbazole and the ruthenium metal core. The spheres of Z1 and Z2 were defined with 5 Å diameter, see Figure 86 b). These hypothetical spheres represent guidance volumes, which should not be exceeded by the intended amino acids. Indeed, a sphere of 5 Å seems to be a proper limit avoiding steric hindrances.

a)



b)

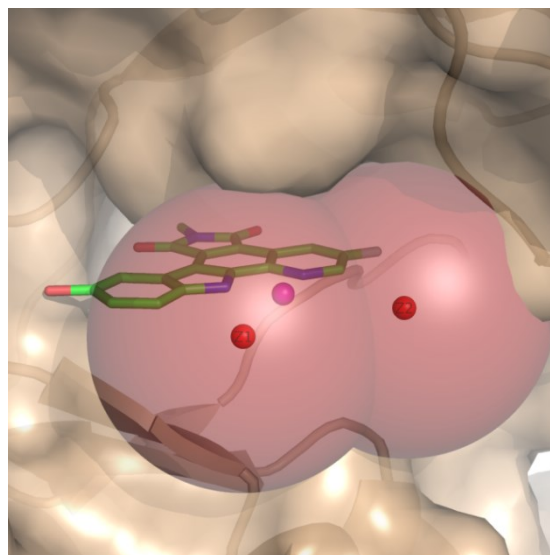


Figure 86: a) Overview of the anchor points A1 to A4 and the two centres Z1 and Z2. A1, Z1, the metal core, as well as the nitrogen atom of the pyridine moiety of the pyridocarbazole are all in line. The distance Z1-metal core is 4 Å, the distance A1-metal core is 2 Å. The same is true for Z2 in correspondence to A2 and the metal centre. A1, A2, Z1 and Z2 as well as the pyridocarbazole and the ruthenium core are all located in the same plane. A3 and A4 mark the residual ideal positions for coordinating atoms. b) The zones around Z1 and Z2 include the space within 5 Å and represent an hypothetic guidance volume. This volume should not be exceeded by the intended amino acids for the tridentate ligand synthesis. The PI3K γ structure as well as the pyridocarbazole structure are derived from the data set pdb: 3CST.^[188] The pyridocarbazole ligand is presented as sticks with the carbon atoms in green. Nitrogen atoms are shown in blue, oxygen atoms in red, fluorine in light cyan, and the ruthenium core in purple. PI3K γ is presented as cartoon in wheat.

For a further definition of the desired complex structure two additional anchor points A3 and A4, see Figure 86 a), were defined, which are derived from the residual coordinating atoms in Δ -(S)-**106**. They describe favourable positions to form an octahedral complex. Therefore, ideal poses of the fragments **153** and **154** should address the anchorpoints A1 and A2, occupying the zones around Z1 and Z2, but not A3 and A4. This is congruent with a presumed *fac*-coordination. Thus, an estimated space of 65.45 Å³ (represented by the spheres around Z1 and Z2 with a diameter of 5 Å) should be accessible and therefore considered as guidance for the amino acid selection.

However, it is also important which sphere, around Z1 or Z2, is occupied either by the amino acid fragment **154** or the 2-methylpyridine moiety **153**, see Figure 86. As the two spheres, in a chiral environment, like the binding site of PI3K γ , are not equal. The different fragments will experience different interactions, when located either in the sphere of Z1 or Z2. For instance, a bulky amino acid residue, like phenylalanine, tyrosine, or tryptophane, could hypothetically lead to steric hindrances, when occupying the sphere of Z2. In opposite, the offered space occupying the sphere of Z1 could be sufficient for the mentioned bulky amino acids.^[417–419] In contrast, a polar charged amino acid, could experience high attraction in Z2 by forming a salt bridge or could experience high repulsion due to adverse hydrophobic interactions or charges of the same polarity.^[418–420]

Further, the chirality at the C α of the amino acid influences significantly the globular shape of the entire complex, see also Figure 84. The C α atom crucially defines the three dimensional space, which is occupied by the corresponding functional group of the amino acid fragment. Thus, whereas a complex based on a (S)-configured amino acid could hypothetically fit into the binding site, the complex based on the corresponding (R)-configured amino acid could experience steric hindrances and a subsequent repulsion.

Moreover, desolvation effects of the amino acid residues have to be considered. Thus, stripping off the hydrate shell of charged or polar groups could significantly decrease the binding affinity towards PI3K γ , if the polar or ionic group is not captured by a sufficient counterpart inside the binding pocket.^[421] Analogous principles are true for hydrophobic side chains and aromatic side chains.^[417–419] In contrast, if they find a sufficient grove to displace water molecules and to meet hydrophobic or aromatic interactions a valuable contribution to the binding affinity could be achieved. However, amino acids with large hydrophobic and aromatic residues result into bulky complexes, which in turn possess decreased water solubility.^[140,156,157,422] They require an increased amount of solvation mediators like dimethylsulfoxid for *in vitro* assays. However, an excessive use of dimethylsulfoxid influences the structural integrity of proteins on secondary, tertiary and quaternary level leading to falsified assay results.^[423]

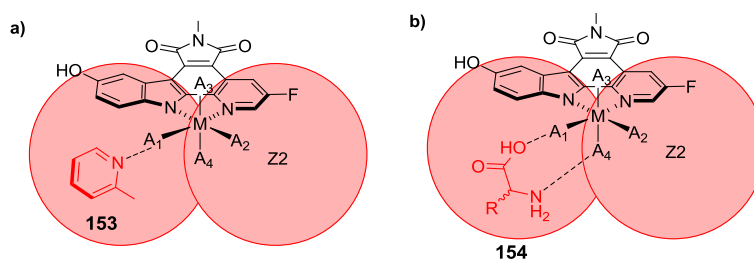


Figure 87: Possible placements of the fragments **153** (a) or **154** (b) into the sphere around Z1. **a)** **153** occupying the sphere of Z1 as a rigid fragment experiences different interactions in a chiral environment like the binding site of PI3K γ as occupying the sphere of Z2. **b)** the same is true for **154**. For both fragments the placement into the sphere of Z1 is shown but the examples are analogously true for the placement into sphere of Z2.

Thus, a simple selection on steric criteria of the amino acids compared to the accessible space of the binding site is acceptable but not entirely sufficient. In addition, functionalised side chains of amino acids require the application of protection group chemistry to avoid interfering coordination during the complexation reaction.^[416,424] These protection groups have to be planed orthogonal to the residual reaction sequence to ensure a cleavage after a certain planned step.

Therefore, a first generation set of amino acids with distinct characteristics to cover the mentioned aspects were selected. Moreover, both positive and negative controls were covered, see also Table 2. These amino acids should ideally act as representatives for related ones, i.e.: phenylalanine as representative for aromatic amino acids. In addition, to minimise protection group chemistry, amino acids with ideally orthogonal protectable functional groups regarding the complex synthesis were preferred.

Thus, the first representative amino acid group consisted of L-alanine ((S)-**155**), D-alanine ((R)-**155**), and L-serine ((S)-**159**) as small sized ones. These amino acids, regarding their VAN-DER-WAALS volume, should hypothetically fit into the binding site. This is only true if the estimated accessible volume of approximately 65.45 Å³ of Z2 complies to the existing conditions of the PI3K γ binding site. Moreover, the influence of the C α stereoconfiguration, during these investigations, should be covered comparing both L-alanine ((S)-**155**) and D-alanine ((R)-**155**).

The second group was represented by L-phenylalanine ((S)-**156**), L-leucine ((S)-**158**), and L-valine ((S)-**160**). These large unpolar amino acids should result into bulky complexes experiencing steric hindrances. Thus, they should subsequently possess a reduced affinity towards the PI3K γ binding site. Due to the rotation around the C α and the C β bond, the bulky

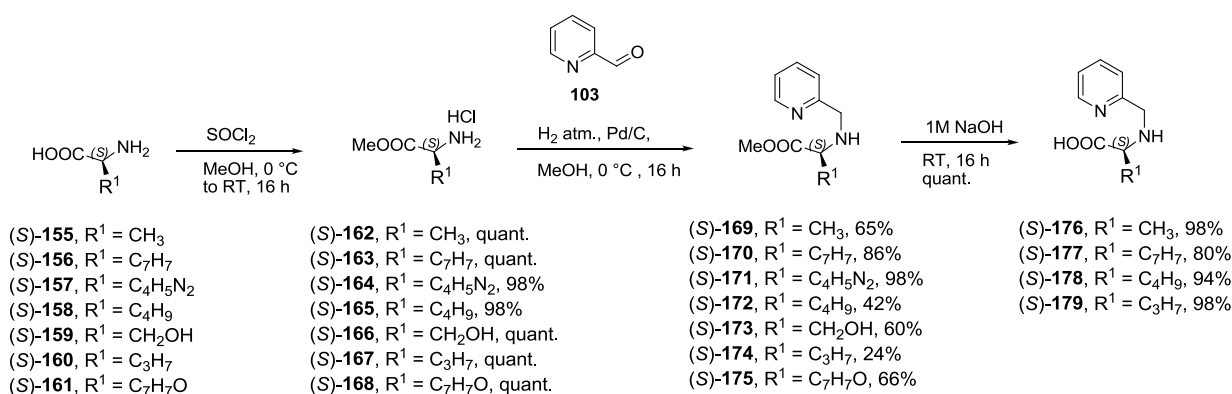
residues of the members of this group could potentially avoid steric clashes. To investigate the elimination of this rotational freedom D-phenylglycine ((R)-**179**) as a non-coded amino acid was added to this group.

As a third group L-histidine ((S)-**157**) and L-tyrosine ((S)-**161**) were selected representing large aromatic but simultaneously polar amino acids. As for the second selection group, the resulting complexes should hypothetically be excluded from the binding site by steric hindrance. Thus, the resulting complexes should also represent negative controls.

As the last group, L-proline ((S)-**101**) as well as D-proline ((R)-**101**) were applied again as established ligand systems due to their successful former application, see Chapter 3.3.2.

Table 2: Amino Acid Characteristics

Amino Acid	Scaffold	Charge	Polarity	vdW Volume [Å ³]	Hydrophobic Index
Alanine	aliphatic	neutral	apolar	67	1.8
Arginine	aliphatic	basic	polar	148	-4.5
Asparagine	aliphatic	neutral	polar	96	-3.5
Aspartate	aliphatic	acidic	polar	91	-3.5
Cysteine	aliphatic	neutral	polar	86	2.5
Glutamate	aliphatic	acidic	polar	109	-3.5
Glutamine	aliphatic	neutral	polar	114	-3.5
Glycine	aliphatic	neutral	apolar	48	-0.4
Histidine	aromatic	basic	polar	118	-3.2
Isoleucine	aliphatic	neutral	apolar	124	4.5
Leucine	aliphatic	neutral	apolar	124	3.8
Lysine	aliphatic	basic	polar	135	-3.9
Methionine	aliphatic	neutral	apolar	124	1.9
Phenylalanine	aromatic	neutral	apolar	135	2.8
Proline	heterocyclic	neutral	apolar	90	-1.6
Serine	aliphatic	neutral	polar	73	-0.8
Threonine	aliphatic	neutral	polar	93	-0.7
Tryptophan	aromatic	neutral	apolar	163	-0.9
Tyrosine	aromatic	neutral	polar	141	-1.3
Valine	aliphatic	neutral	apolar	105	4.2



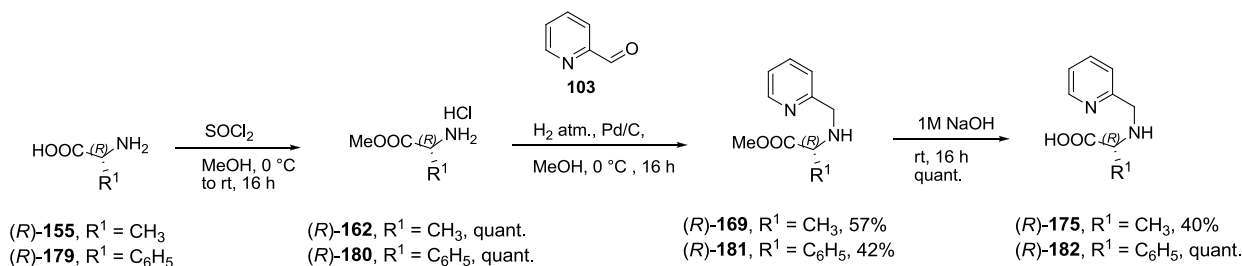
Scheme 23: Synthesis of tridentate chiral ligands based on L-amino acids.

3.5 Proof of Concept

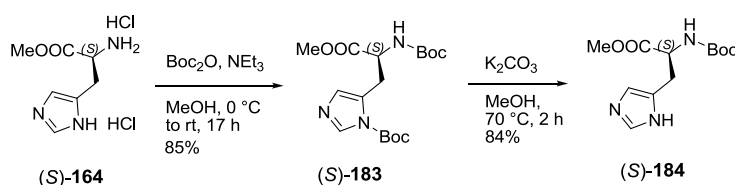
3.5.1 Subsequent Synthesis of Selected Amino Acid

The synthetic route described for the synthesis of (*R*)-**105** and (*S*)-**105** was applied analogously to synthesise the amino acid derived tridentate ligands, see Chapter 3.3.2. The amino acids (1 eq.) were suspended in methanol and thionylchloride (1.1 eq.) was added drop wise at 0 °C. The reaction mixture was refluxed for 16 h. Thereafter, the solvent was removed under reduced pressure, the residue resolved in methanol and then concentrated. This procedure was repeated three times to afford the methylesters as white solids. The yields for the ester formation were excellent as observed before. (*S*)-**162** to (*S*)-**168** were obtained in quantitative yields except of (*S*)-**164** and (*S*)-**165**, both in 98% yield. The same is true for (*S*)-**168**, (*R*)-**162**, and (*R*)-**180** all obtained in quantitative yields. Ligand (*S*)-**178** and subsequent precursor were synthesised by the research intern OLIVER BORN.

Esters derived from amino acids with unfunctionalised side chains like (*R*)-**155**, (*S*)-**155**, (*S*)-**156**, (*S*)-**158**, (*S*)-**160**, and (*R*)-**179** could be processed straight forward. In contrast, functionalised amino acids (*S*)-**157**, (*S*)-**159**, and (*S*)-**161** had to be protected at different stages of the ligand synthesis to become compatible to the complexation conditions, see Scheme 25, Scheme 26, and Scheme 27. A reductive amination as described for (*R*)-**104** and (*S*)-**104**, see Chapter 3.3.2, was preferred over a nucleophilic substitution as described for (*R*)-**123** and (*S*)-**123**, see Chapter 3.3.5, to avoid side product formation. In general, palladium on carbon (3%) was suspended in methanol and picolinaldehyde (**103**) (1.2 eq.) was added at 0 °C. Sodium acetate (2 eq.) was added to the reaction mixture. Then, the methylester of the appropriate amino acid (1 eq.) was dissolved in methanol and added to the reaction mixture. The reaction mixture was stirred for 1 h and the nitrogen atmosphere was completely substituted by hydrogen in three turns during this time. The reaction was continued for 15 h allowing the mixture to warm up to ambient temperature. The reaction mixture was filtrated over CELITE to separate the palladium



Scheme 24: Synthesis of tridentate chiral ligands based on D-amino acids.



Scheme 25: Introduction of protection groups to mask the imidazole moiety of L-histidine derived (S)-164.

on carbon and the crude material was subjected to column chromatography using methylene chloride : methanol. The reductive amination products were obtained as yellow oil in modest to good yields, see Scheme 23 and Scheme 24.

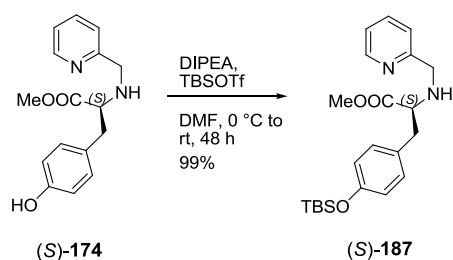
The L-histidine derived methylester (S)-164 afforded a special preparation due to the imidazole ring in the side chain. The side chain had to be protected to avoid interfering effects during complexation. For this purpose a sequential protection and selective deprotection procedure according to published methods was pursued.^[179,425]

Therefore, (S)-164 (15.4 g, 63.7 mmol) was dissolved in methanol (70.0 mL) and di-*tert*-butyl dicarbonate (27.8 g, 127 mmol) presolved in methanol (10.0 mL) was added drop wise. Then, triethylamine was added drop wise under extensive stirring at 0 °C for 1 h. The reaction was proceeded for 16 h and warmed up to ambient temperature. The entire reaction mixture was poured into water (100 mL) and then extracted with methylene chloride (3 x 100 mL). The combined organic layer was dried over sodium sulfate, filtrated and concentrated under reduced pressure. (S)-183 was purified by column chromatography using diethyl ether : ethyl acetate (3:1 → ethyl acetate) to obtain it as a white solid (16.6 g, 45.1 mmol, 70.7%). Due to protonation and deprotonation effects, determined by ¹H-NMR, a second fraction of the product was obtained as colourless oil (3.45 g, 8.50 mmol, 13.4%).

To cleave the *tert*-butyloxycarbonyl-protection group at the imidazole ring moiety (S)-183 (16.6 g, 44.7 mmol) was dissolved

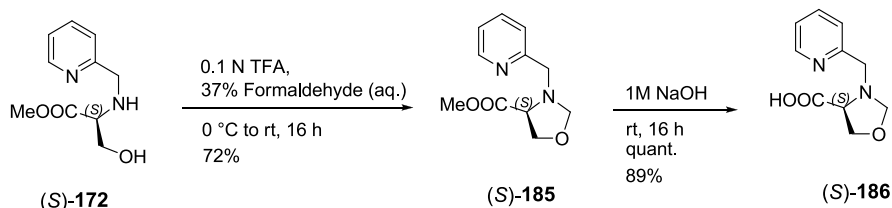
in methanol (65.0 mL) and potassium carbonate (617 mg, 4.47 mmol) was added. The reaction mixture was refluxed and the reaction was finished after 2 h. The entire mixture was cooled to ambient temperature and poured into water (80 mL) and extracted with ethyl acetate (3 x 80 mL). The combined organic layer was dried over sodium sulfate, filtrated and concentrated under reduced pressure. The product (S)-184 was obtained as a white solid (10.1 g, 37.5 mmol, 84.1%). Ligand (S)-184 and subsequent precursor were synthesised by the research intern KHANG NGO.

The hydroxyl group of the L-tyrosine derived intermediate (S)-174 can be protected in a late step of the ligand synthesis. Therefore, (S)-174 (2.00 g, 6.98 mmol) was dissolved in DMF (60 mL) and cooled to 0 °C. Then, DIPEA (6.0 mL, 34.90 mmol) was added drop wise over a period of 2 h followed by the dropwise addition of *tert*-butyldimethylsilyl trifluoromethanesulfonate (2.1 mL, 7.81 mmol) over a period of 1 h. The reaction was continued for 45 h and allowed to warm up to ambient temperature. Ammonium acetate (60 mL, 1 M *aq.*) was added and the reaction mixture was extracted with ethyl acetate (3 x 60 mL). The combined organic layer was washed with BRINE, dried over sodium sulfate, filtrated and concentrated under reduced pressure. After purification by column chromatography using methylene chloride : methanol (35:1) the product (S)-187 was obtained as yellow oil (2.77 g, 6.92 mmol, 99%). Ligand (S)-187 and subsequent precursor were synthesised by the research intern GEORG RENNAR.



Scheme 26: Protection of the hydroxyl group.

The protection of the hydroxyl function of the L-serine derived (S)-**172** intermediate was performed next to the reductive amination. Thus, to prevent a cross coordination of the hydroxyl group a cyclisation to an oxazolidine in analogy to Schölkopf *et al.*^[426] was performed. This published method was preferred over a more common protection with 2,2-dimethoxypropane due to concerns of the resulting dimethyl methylene group adjacent to the nitrogen atom potentially perturbing the ligand complexation to the metal centre. For this purpose, (S)-**172** (1.00 g, 4.75 mmol) was dissolved in methylene chloride (45 mL) at 0 °C and trifluoroacetic acid (366 μ L, 4.75 mmol, 0.1 N) was added drop wise followed by the dropwise addition of water (45 mL). Under extensive stirring formaldehyde (705 μ L, 7.12 mmol, 37% aq.) was added drop wise to the reaction mixture. The reaction was performed for a total period of 16 h at ambient temperature. The solvent was evaporated under reduced pressure and the crude material subjected to column chromatography using methylene chloride : methanol (35:1). After drying *in vacuo* (S)-**185** was obtained as yellow oil (760 mg, 3.72 mmol, 72%). The cleavage of the ester function was performed as established for the previous amino acids suspending (S)-**185** (760 mg, 3.42 mmol) in sodium hydroxide (4.50 mL, 1 M) at 0 °C for 16 h. The reaction



Scheme 27: Protection of the hydroxyl group of (S)-**173** via oxazolidine formation and subsequent ester cleavage.

mixture was washed with methylene chloride (3 x 20 mL) to separate organic side products. The combined aqueous layer was neutralised to pH 7 with hydrochloric acid (1 M) and solvent removed under reduced pressure. The residue was suspended in ethanol (5.00 mL) and filtrated via a syringe filter. After drying *in vacuo* (S)-**186** was obtained as a white solid (705 mg, 3.39 mmol, quant.).

Beside the chiral amino acids, additional achiral glycine derived tridentate ligands **188** and **189**, from the MEGGERS group intern compound library were applied for complex synthesis. These ligands were already applied in former studies and could therefore act as reference ligands for the complexation conditions.^[197]

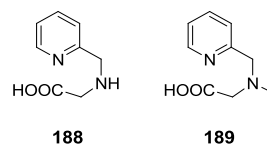
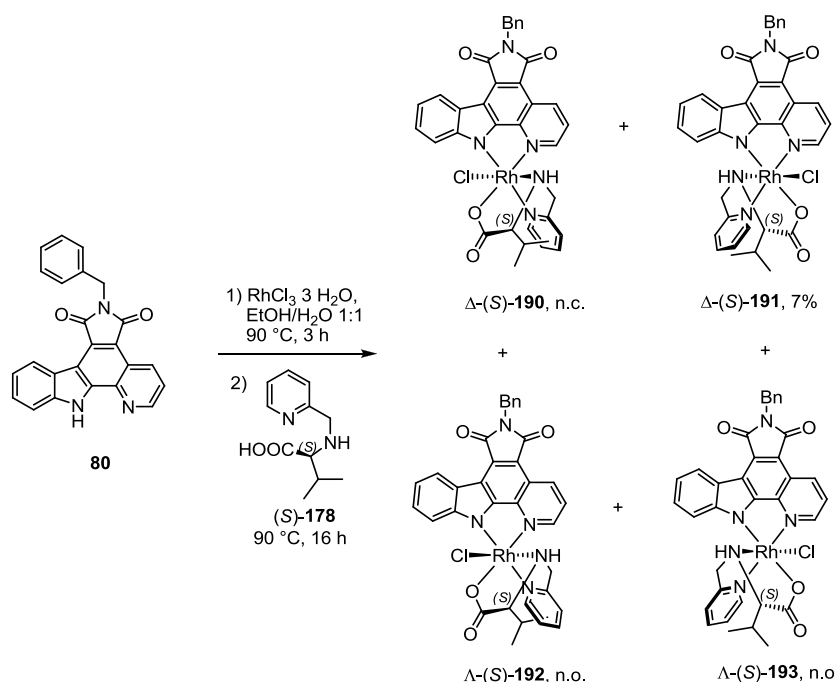


Figure 88: Glycine derived achiral tridentate ligands.



Scheme 28: Synthesis of rhodium(III) complexes Δ -(S)-**190**, Δ -(S)-**191**. The expected Λ -(S)-**192** and Λ -(S)-**193** were not observed (n.o.). Δ -(S)-**190** could not be characterised (n.c.).

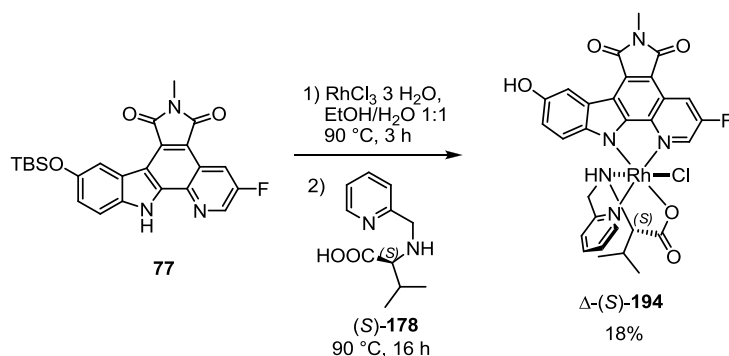
3.5.2 Complex Synthesis

The new amino acid derived ligands were processed to rhodium(III) complexes according to the same conditions applied for the synthesis of Λ -(R)-**106**, Δ -(S)-**106**, Λ -(R)-**107** and Δ -(S)-**107**, see Chapter 3.3.2, thus making the reactions comparable. However, using primary amino acid derived ligands, the formation of four diastereomers were expected, see Chapter 3.4.4.2.

Moreover, the diastereomers possessing the pyridine ring of the tridentate ligands in *cis*-coordination to the indole moiety of the pyridocarbazole ligand were expected to be identified via the ^1H -NMR spectra in analogy to the described procedure of Λ -(R)-**107**, see Figure 58. Nevertheless, the orientation of the coordinating amino group, either towards A3 or A4 of the hypothetical complex had to be identified. For this purpose, complexes of the L-valine derived ligand (S)-**178** were synthesised using the *N*-benzylated pyridocarbazole **80**, see Scheme 28. In former studies, organometallic complexes using the ligand **80** were

successfully applied as model systems to investigate their structural properties, as the resulting complexes had an increased crystallisation tendency.^[140,156,157,422] The subsequent studies, solving the chemical structure via X-ray experiments and correlating the retention times of each isomer of the *N*-benzyl pyridocarbazole complexes to the ones obtained using other pyridocarbazoles with distinct modification patterns, led to correct conclusions of their structural configuration.^[140,156,157,422]

However, after the complexation reaction and subsequent column chromatography using methylene chloride : methanol (15:1), only Δ -(S)-**191** (R_f value: 0.45) could be obtained as pure compound in 7% yield, synthesised by the research intern OLIVER BORN. The successful crystallisation of Δ -(S)-**191** allowed to solve its relative stereoconfiguration, see Figure 89. Moreover, only one additional spot via TLC analysis was observed (R_f = 0.19). Despite evaluating different solvent systems and preparative TLC conditions, to assign correct yields, the second compound could not be purified indicating the major disadvantage of the complex synthesis. On one hand, a sin-



Scheme 29: Synthesis of rhodium(III) based inhibitor Δ -(S)-194.

gle complexation reaction should have resulted in four different compounds to explore the chemical space; on the other, the complex purification seems to significantly limit the applicability of this concept.

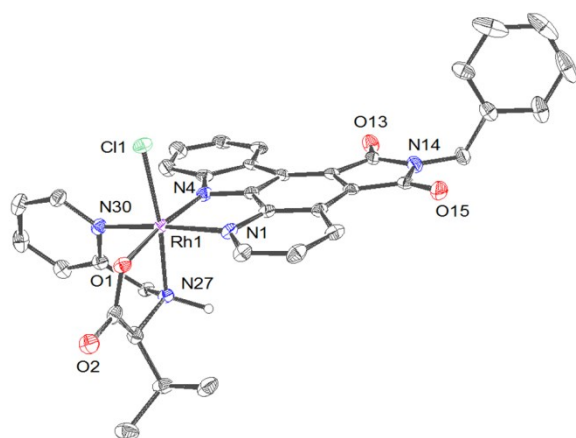


Figure 89: Crystal structures of Δ -(S)-191. Solvent Molecules were omitted for clarity. ORTEP drawing with 50% probability of thermal ellipsoids. Selected bond lengths [Å] for Δ -(S)-191: Rh1-N1 = 2.065(4), Rh1-N4 = 2.041(5), Rh1-N27 = 2.044(4), Rh1-N30 = 2.032(5), Rh1-O1 = 2.013(3), Rh1-Cl1 = 2.3575(13).

Despite the good crystallization tendency of pyridocarbazole **80** and resulting complexes, also adverse solubility characteristics and agglomeration effects were reported.^[140,156,157,422] These effects in combination with the increased number of possible isomers probably hindered the purification. These effects could be circumvented using pyridocarbazole ligands with distinct substitution patterns as intended for the development of PI3K γ selective inhibitors. Especially, pyridocarbazole **77** was identified as a pharmacophore ligand addressing metal based kinase inhibitors towards PI3K γ .^[188]

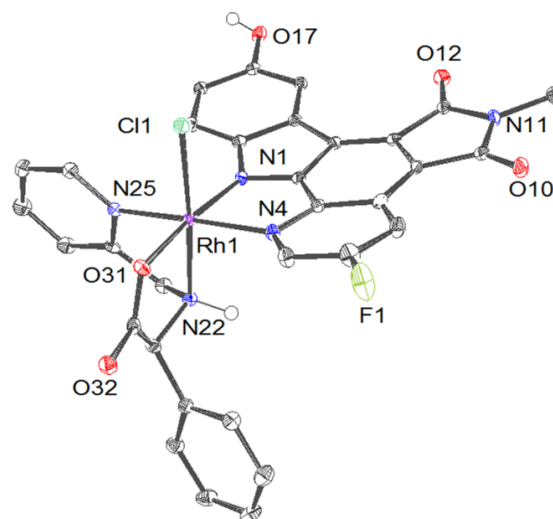
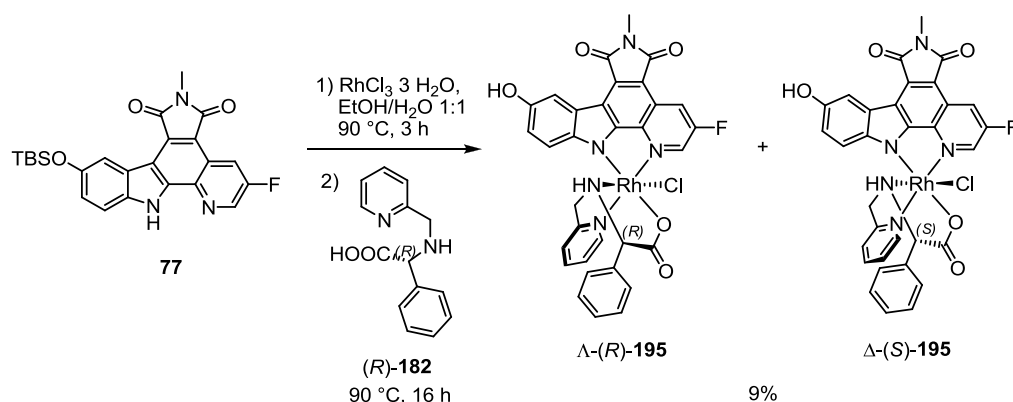


Figure 90: Crystal structure of Δ -(S)-195. Solvent Molecules were omitted for clarity. ORTEP drawing with 50% probability of thermal ellipsoids. Selected bond lengths [Å] for Δ -(S)-195: Rh1-N1 = 2.0284(17), Rh1-N4 = 2.0580(17), Rh1-N22 = 2.0436(17), Rh1-N25 = 2.0200(17), Rh1-O31 = 2.0320(14), Rh1-Cl1 = 2.3429(5).

Further, to synthesise biologically active PI3K γ inhibitors, the pyridocarbazole **77** was applied in the complexation reaction instead of **80**, see Scheme 29. Interestingly, the complexation reaction resulted in a single product formation observed by TLC control prohibiting comparisons between the retention times as intended by the model system using **80**. Thus, the relative stereoconfiguration of the purified complex Δ -(S)-194 (18%) could not be assigned or concluded by the comparison to the former results. Nevertheless, the relative position of the pyridine ring of the tridentate ligand could be determined due to the upfield shift of the pyridocarbazole H-11 proton in the ^1H -NMR spectra of Δ -(S)-194 in analogy to Δ -(R)-107.



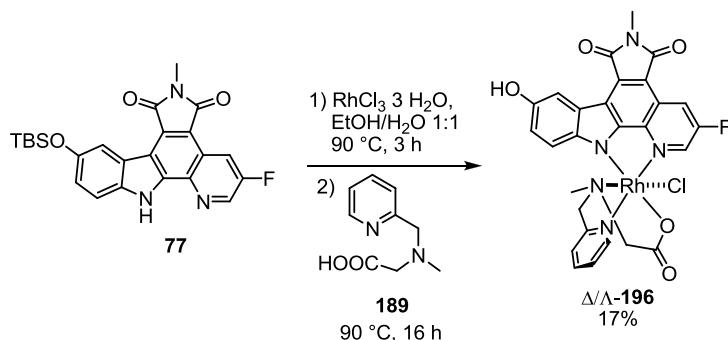
Scheme 30: Synthesis of rhodium(III) based inhibitors $\Delta\text{-(R)-195}$ and $\Delta\text{-(S)-195}$ obtained as racemic mixture.

A similar effect was observed using $(R)\text{-182}$ as chiral tridentate ligand, see Scheme 30. Again, only one spot during the complexation reaction was detected via TLC control during the synthesis performed by the research intern KHANG NGO. Moreover, the pyridine ring of the $(R)\text{-182}$ was again coordinated *cis* to the indole moiety of the pyridocarbazole **77** in the resulting complex, as observed for $\Delta\text{-(S)-194}$, verified by the $^1\text{H-NMR}$ spectra. Attempts to determine the relative stereoconfiguration of the $(R)\text{-182}$ derived complex via crystallisation were successful. However, beside the expected $\Delta\text{-(R)-195}$ the corresponding enantiomer $\Delta\text{-(S)-195}$ was formed as a racemic mixture in 9% yield, see Figure 90. As the optical rotation of $(R)\text{-182}$ was $[\alpha]_D^{20} = -16.3$, the racemisation must have been occurred during the complexation reaction itself, whereas the exact mechanism of this observation remains unclear. Perhaps, due to protonation and deprotonation effects at the carboxylate group, during the complexation reac-

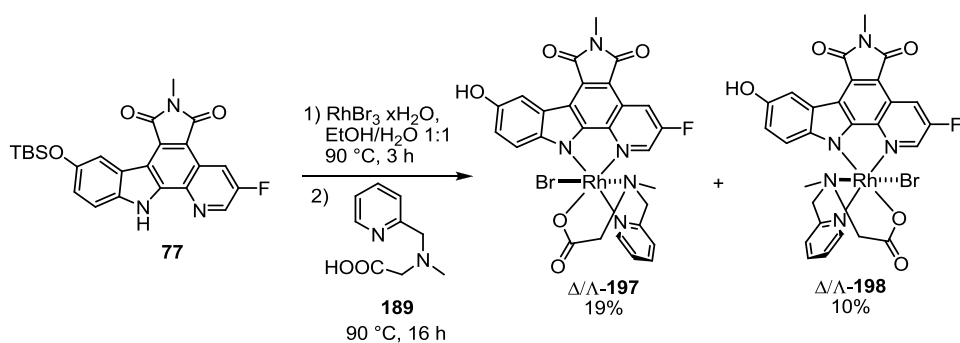
tion, a conjugated vinylogue double bond is formed, which subsequently eliminates the chiral information at the C_α atom of the D-phenylglycine derived ligand $(R)\text{-182}$.

Due to the unexpected difficulties during complexation and purification, a further application of the primary chiral amino acid derived ligands had to be discarded and several ligands were not finished as initially intended. The unreproducible reaction outcome excluded an adequate investigation of the possible isomers, because neither the intended directed formation or the proper purification could be handled.

Nevertheless, to generate as much different structural scaffolds as possible, the achiral ligand **189**, as well as the chiral proline derived ligands $(R)\text{-105}$ and $(S)\text{-105}$, due to their former successful application, were processed to the complexation reaction, Scheme 33. Moreover, chlorine was substituted by bromine to validate the influence of the monodentate ligand size, keep-



Scheme 31: Synthesis of rhodium(III) based inhibitor $\Delta/\Delta\text{-196}$ as racemic mixture.



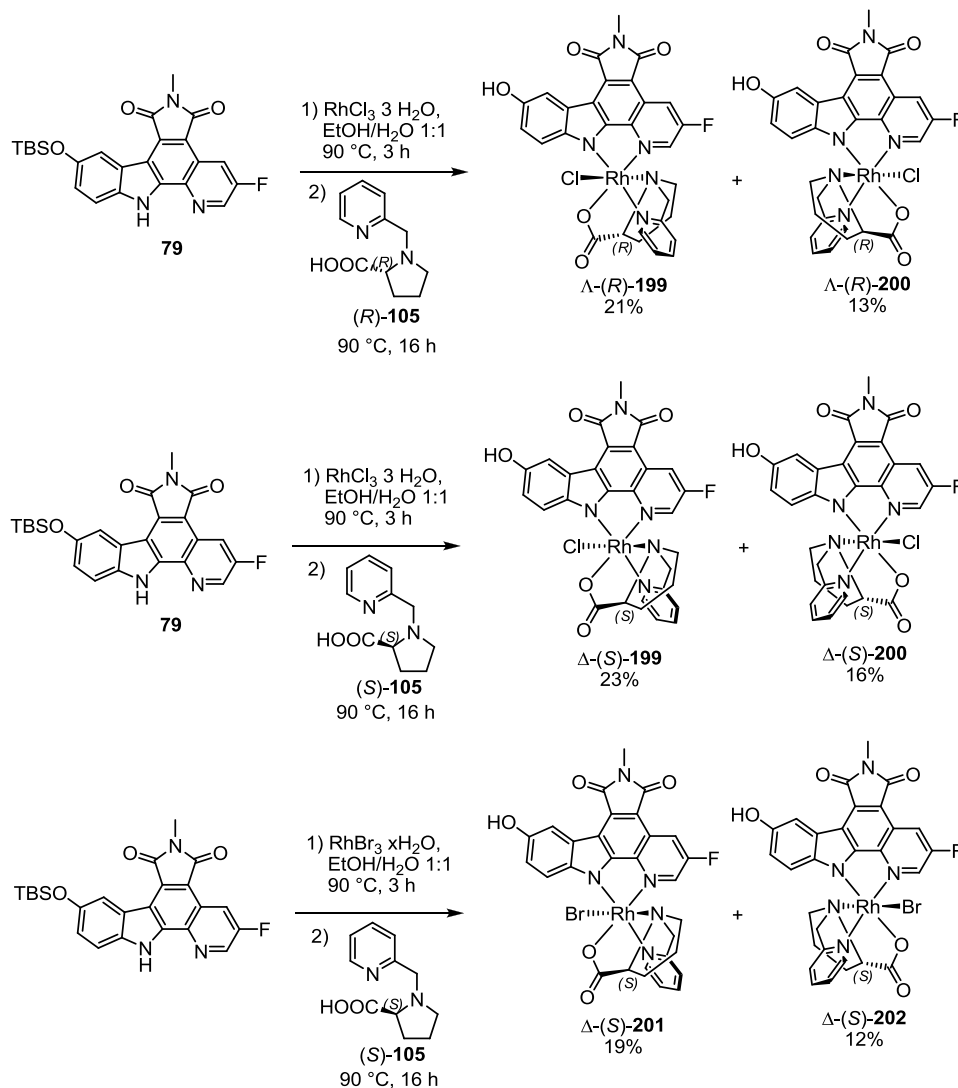
Scheme 32: Synthesis of rhodium(III) based inhibitors Δ/Λ -197 and Δ/Λ -198, both as racemic mixtures.

ing the established reaction conditions untouched but using RhBr_3 instead of RhCl_3 .

Interestingly, using the achiral ligand **189**, only the racemic mixture of Δ/Λ -196, where the pyridine ring of the tridentate ligand is coordinated *cis* to the pyridocarbazole moiety, could be obtained in 17% yield. In opposite, using RhBr_3 both ex-

pected diastereomers were obtained as racemic mixtures Δ/Λ -197 and Δ/Λ -198 in 19% and 10% yield, respectively.

The use of (*R*)-**105** and (*S*)-**105** resulted in enantiopure complexes with defined relative stereoconfiguration using pyridocarbazole ligand **79**, see Chapter 3.3.2. Moreover, due to the cumulated results, a



Scheme 33: Synthesis of rhodium(III) based inhibitors Δ -(*R*)-199, Δ -(*R*)-200, Δ -(*S*)-199, Δ -(*S*)-200, Δ -(*S*)-201, and Δ -(*S*)-202 as enantiopure compounds.

correct assignment of the stereoconfiguration is possible. The complexes Δ -(R)-**199** (21%), Δ -(S)-**199** (23%), Δ -(R)-**200** (13%), and Δ -(S)-**200** (16%) were obtained in expected yields. The same is true for Δ -(S)-**201** (19%) and Δ -(S)-**202** (12%), both with a substituted monodentate ligand from chlorine to bromine compared to Δ -(S)-**199** and Δ -(S)-**200**, see Scheme 33.

3.5.3 Biological Investigations and Target Selectivity

All synthesised PI3K γ inhibitors were tested in Kinase Glo-Assays performed by JASNA MAKSIMOSKA. Moreover, to achieve a first insight into the compounds selectivity among the PI3K isoforms, PI3K α was tested in parallel as target molecule, see Figure 91.

Table 3: Determined IC₅₀ values against PI3K α and PI3K γ . The single values for Δ / Δ -(R/S)-**195** were out of specification (OOS), as an intra- and interassay reproducibility at low inhibitor concentrations were not given, and thus an accurate calculation of the IC₅₀ value was not possible. Experiments were performed by JASNA MAKSIMOSKA. The data points for curve fitting were determined in triplicates and the experiments were repeated independently, the shown data points represent mean values.

Complex	IC ₅₀ PI3K α [μ M]	IC ₅₀ PI3K γ [μ M]
Δ -(S)- 194	21.5	14.2
Δ / Δ -(R/S)- 195	OOS	23.2
Δ / Δ - 196	130.8	67.6
Δ / Δ - 197	30.0	4.8
Δ / Δ - 198	26.3	3.2
Δ -(S)- 199	6.5	13.5
Δ -(R)- 199	14.5	1.4
Δ -(S)- 200	2.6	3.2
Δ -(R)- 200	7.7	2.7
Δ -(S)- 201	3.6	19.6
Δ -(S)- 202	4.4	4.1

Regarding PI3K α (Figure 91 c) and d)) the tested compounds possess following IC₅₀ values: Δ -(S)-**194** (21.5 μ M), Δ / Δ -**196** (130.8 μ M), Δ / Δ -**197** (30.0 μ M), Δ / Δ -**198** (26.3 μ M), Δ -(S)-**199** (6.5 μ M), Δ -(R)-**199** (14.5 μ M), Δ -(S)-**200** (2.6 μ M), Δ -(R)-**200** (7.7 μ M), Δ -(S)-**201** (3.6 μ M), Δ -(S)-**202**

(4.4 μ M). The obtained data for Δ / Δ -(R/S)-**195** in case of PI3K α were out of specification as the data points at low concentrations scattered irregularly. Thus, an accurate fit was not possible, see Table 3.

Regarding PI3K γ (Figure 91 a) and b)) the tested compounds possess following IC₅₀ values: Δ -(S)-**194** (14.2 μ M), Δ / Δ -(R/S)-**195** (23.2 μ M), Δ / Δ -**196** (67.6 μ M), Δ / Δ -**197** (4.8 μ M), Δ / Δ -**198** (3.2 μ M), Δ -(S)-**199** (13.5 μ M), Δ -(R)-**199** (1.4 μ M), Δ -(S)-**200** (3.2 μ M), Δ -(R)-**200** (2.7 μ M), Δ -(S)-**201** (19.6 μ M), Δ -(S)-**202** (4.1 μ M), see Table 3.

3.5.4 Interpretation

The biological investigations determining the IC₅₀ of each compound against the primary target PI3K γ , as well as the selectivity check against PI3K α , revealed mostly compounds inhibiting both with almost similar IC₅₀. However, some preferred either PI3K γ or PI3K α . Aligning the protein sequences of PI3K γ (UniProt Code: P48736.3) and PI3K α (UniProt Code: P42336.2) via BLAST identified 358 identical amino acids of 997 compared ones reflecting 36% sequence homology, and 536 chemically similar amino acids of 997 compared ones reflecting 53% sequence similarity. Moreover, an E-value of $1e^{-177}$ reflects a high relationship of both sequences.^[427,428]

A comparison of the three dimensional structure of PI3K γ (3CST) with the entire deposited entries in the PDB was performed using the program VAST. VAST is the acronym for Vector Alignment Search Tool, and is a open source computer algorithm developed at NCBI. This algorithm can be used to identify similar protein three dimensional structures by purely geometric criteria to identify distant homologues that cannot be recognized by sequence comparison.^[429]

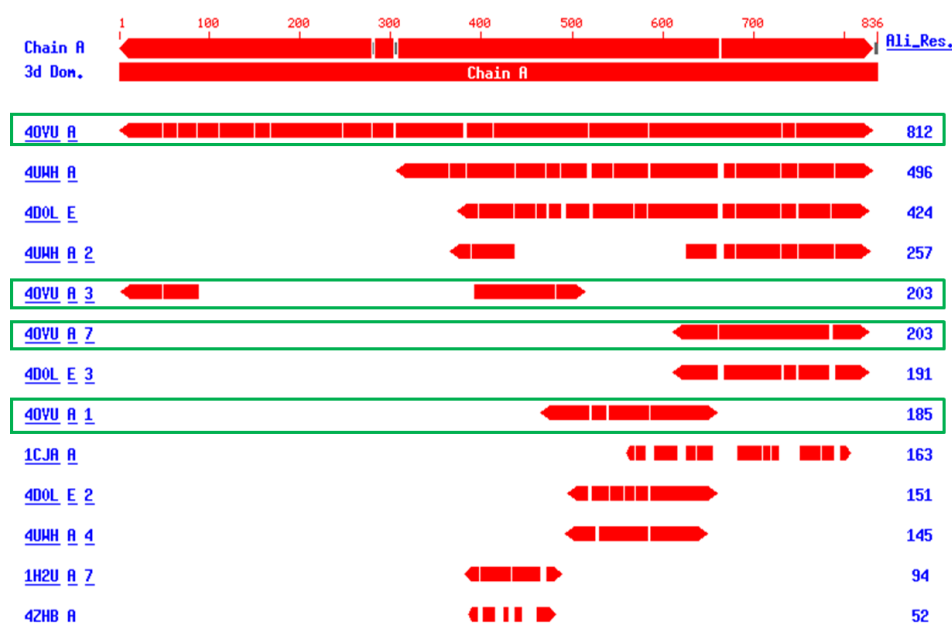


Figure 91: Results of the VAST search over the entire primary sequence. 13 neighbours were found for the three-dimensional structure of PI3K γ (pdb: 3CST) as starting point. 13 representatives from the medium redundancy subset are displayed, meaning that they possess a BLAST p value of $10e^{-40}$ to each other. The red regions are aligned segments, where a corresponding comparison of three-dimensional structures can be visualised on primary sequence level. Especially the structure deposited under the pdb code 4OVU reveals several three-dimensional motifs similar to the query 3CST. Indeed, the structure 4OVU belongs to the crystal structure of PI3K α .^[430]

The VAST search resulted in 13 neighbours applying the three-dimensional structure of PI3K γ (pdb: 3CST) as query starting point. These are representatives from the medium redundancy subset, meaning that they possess a BLAST p value of $10e^{-40}$ to each other. In Figure 91 the red regions are aligned segments forming three-dimensional structures compared and displayed on primary sequence level. The structure deposited under the pdb code 4OVU reveals several three-dimensional motifs related to the query starting structure 3CST. Indeed, the structure 4OVU belongs to the crystal structure of PI3K α .^[430]

Moreover, comparing the ATP binding site of both PI3K γ (pdb: 3CST) and PI3K α (pdb: 4OVU) reveals many identical amino acids on important motifs for ligand binding like the hinge region, the hydrophobic region I, or the catalytic region, see Figure 92.

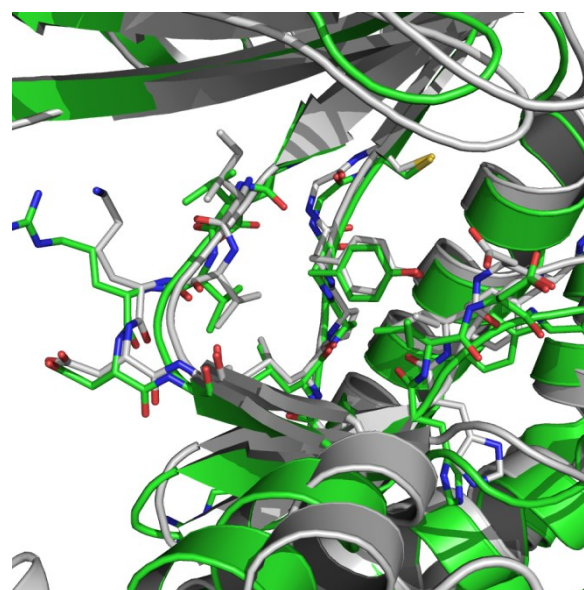


Figure 92: Alignment of the crystal structures of PI3K γ (pdb: 3CST) and PI3K α (pdb: 4OVU). The comparison of the ATP-binding site of both isoforms reveals highly conserved amino acids among these two isoforms. The amino acids of the hinge region, the hydrophobic region I, and the catalytic region, all depicted as sticks, indicate a related primary sequence. All structural motifs except the ATP binding site were omitted for clarity. PI3K γ is shown as cartoon in white. PI3K α is shown as cartoon in green. Nitrogen atoms are shown in blue, oxygen in red, and sulfur in yellow.



Figure 93: Comparison of the primary sequence of PI3K γ (VS82, an VAST query annotation) and PI3K α (pdb: 4OVU). Identical amino acids in aligned sequences are highlighted in red. The hinge region (residues 877 to 882 on 4OVU) possesses 3 identical amino acids between both isoforms. The catalytic loop from 957 to 964 on the primary sequence of PI3K α consists of 8 identical amino acids.

In addition, the sequence alignment and comparison of especially the ATP binding site reveals several identical amino acids, see Figure 93. For example, the hinge region represented by the residues 877 to 882 on the primary sequence of PI3K α (pdb 4OVU) possesses 3 identical amino acids to the primary sequence compared to PI3K γ . Moreover, both isoforms have the identical gatekeeper residue isoleucine. The similarities in the catalytic loop starting from 957 to 964 on the primary sequence of PI3K α compared to PI3K γ are much more impressive, as every amino acid residue of the 8 considered ones is identical.

Much more structural motifs could be investigated in detail as described above. However, the focus is set on the hinge region, hydrophobic region I, and the catalytic loop already highlights the similarities between the two isoforms at the ATP binding site. Therefore, selectively binding compounds are valuable tools not only for target inhibition for pharmacologic purpose, but also for systemic biological investigations.

However, a clear selectivity tendency for one of the two investigated PI3K isoforms by any of the tested complexes could not be identified. Moreover, it is noteworthy, that the complexes Δ/Δ -**196**, Δ/Δ -**197**, Δ/Δ -**198** were tested as racemic mixtures. Thus, a correct assignment which

enantiomer mediates the inhibition remains unclear. Using a racemic mixture, the affinities of the eutomer to the non-binding enantiomer may differ significantly. Therefore, the apparent IC₅₀ value of the racemic mixture is not representative for the true conditions.

The compounds Δ/Δ -**196** (1.93-fold), Δ/Δ -**197** (6.25-fold), Δ/Δ -**198** (8.21-fold), Δ -(*R*)-**199** (10.35-fold), and Δ -(*R*)-**200** (2.85-fold) showed a modest tendency of increased PI3K γ inhibition compared to PI3K α . In opposite, the compounds Δ -(*S*)-**199** (2.07-fold) and Δ -(*S*)-**201** (5.44-fold) offered an increased tendency towards PI3K α compared to PI3K γ . The compounds Δ -(*S*)-**200** (1.2-fold) and Δ -(*S*)-**202** (1.07-fold) showed no preferences and can be considered as unselective among the investigated kinases. Nevertheless, none of the compounds showed an IC₅₀ in the nanomolar range indicating structural potential to increase affinity. In contrast, former investigated half sandwich complexes targeting PI3K γ showed IC₅₀ values in the nanomolar range. This might be a hint of adverse steric effects for the octahedron itself.^[188]

A closer look on the obtained IC₅₀ values targeting PI3K γ could help to understand a potential correlation between the structure of the compounds and their corresponding activity. Potential hints could help to synthesise a second generation of PI3K γ

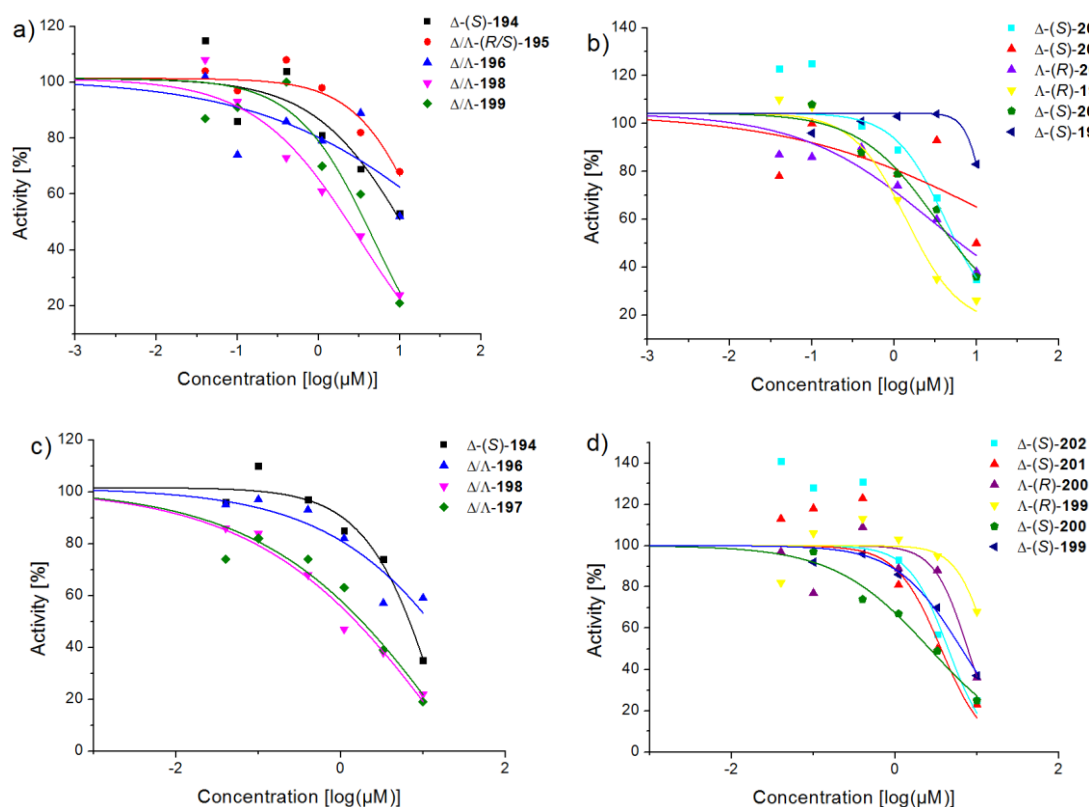


Figure 94: IC₅₀ values of metal based compounds against PI3K γ (a) and b)) and PI3K α (c) and d)). The IC₅₀ values of the synthesised inhibitors were determined using a Kinase-Glo Assay (Promega®) at 10 μ M ATP. Samples with 2% DMSO in absence of kinase served as 100% control and the corresponding signals were related to them. Each measuring point was determined in triplicates and the experiments were repeated independently, the shown data points represent mean values. Experiments were performed by JASNA MAKSIMOSKA. The sigmoidal dose response curve fitting was processed using Origin8.

inhibitors with enhanced selectivity profiles and affinities. However, the interpretation can only represent a conservative evaluation as for true structure-activity relationships the compounds must to be ultrapure to avoid misinterpretation. However, Figure 95 highlights the stereoconfigurations of Δ -(R)-200 and Δ -(R)-199 and correlates them to the binding areas, which could be hypothetically occupied as introduced in Figure 86.

Δ -(R)-200 possesses the tridentate ligand in *fac*-coordination with the pyridine ring *cis* to the indole moiety of the pyridocarbazole. This leads to an hypothetical occupation of the binding sphere Z1. Subsequently, the chlorine is oriented towards A4. In the PI3K γ binding site, it is the area next to the C-terminal domain of PI3K γ . Closing, the nitrogen of the amino group is oriented towards A3 converging to the N-terminal domain of PI3K γ . Δ -(R)-200 possesses an IC₅₀

of 2.7 μ M against PI3K γ and is one of the best inhibitors investigated during these studies.

However, the best investigated PI3K γ inhibitor is Δ -(R)-199 (1.4 μ M). This complex possesses the pyridine ring of the *fac*-coordinated tridentate ligand *cis* to the pyridine moiety of the pyridocarbazole. Thus, this moiety should occupy the binding sphere of Z2. Subsequently, the monodentate chlorine ligand is oriented towards A3. The proline moiety of complex Δ -(R)-199 is coordinated towards A4.

Thus, in case of PI3K γ the structural arrangement of the tridentate proline ligand, has little influence on the selectivity. The same is true for PI3K α . Moreover, as the other two proline based complexes, Δ -(S)-199 and Δ -(S)-200 are also single isomers with defined stereoconfigurations, their structural properties were analogously

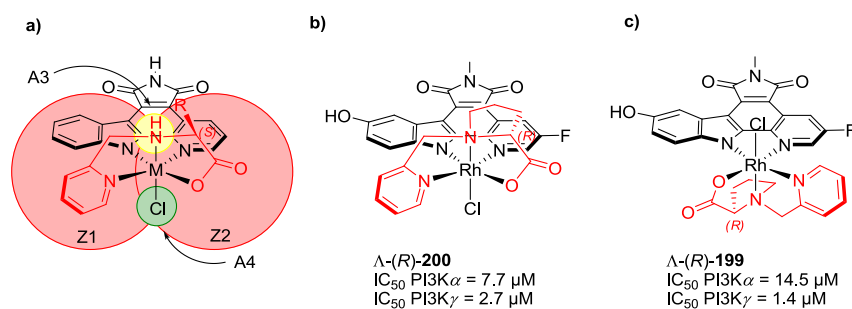


Figure 95: Comparison of the stereoconfiguration of Λ -(R)-199 and Λ -(R)-200 and the resulting affinities towards PI3K α and PI3K γ . **a)** In *fac* coordination the pyridine ring of the tridentate ligand could be either coordinated *cis* (shown in **a**)) or *trans* to the indole moiety of the pyridocarbazole occupying either zone Z1 (as shown in **a**)) or Z2 (red shaded circles). The amino acid moiety is then subsequently *fac*-coordinated in *cis* position to the pyridine moiety of the pyridocarbazole occupying the binding sphere of Z2 (red shaded circle). The nitrogen of the amino acid building block could be coordinated to the metal centre occupying A3 (yellow shaded circle). Thus, it would be oriented towards the N-terminal domain of the kinase. **b)** Λ -(R)-200 reflect the situation described in **a**). **c)** Λ -(R)-199 orientates the pyridine moiety towards binding sphere Z2, the carboxyl moiety towards binding sphere Z1, the coordinating amino acid towards A4, and the monodentate chlorido ligand towards the A3.

investigated as described for Λ -(R)-199 to Λ -(R)-200. However, again a clear correlation can not be elaborated. For instance, the conclusion that an orientation of the pyridine moiety of the tridentate ligand in the binding sphere of Z1 of PI3K γ is superior to an orientation towards the binding sphere of Z2 or vice versa is not legitimate. These observations again confirm, that the octahedral shape itself could be adverse for the inhibition of PI3K γ as former investigated half sandwich complexes showed IC_{50} values in the nanomolar range.^[188]

Closing, to investigate the influence of the monodentate ligand the demand of space from chlorine to bromine was compared. Interestingly, the obtained complexes Δ -(S)-201 (19.6 μ M) and Δ -(S)-202 (4.1 μ M) resulted in the same inhibition tendencies against PI3K γ as their chlorine counterparts Δ -(S)-199 (13.5 μ M) und Δ -(S)-200 (3.2 μ M). Thus, in this case the enlarged monodentate ligand seems to have little influence and had not resulted into significant alterations.

Unfortunately, the difficulties during the synthesis of rhodium(III) complexes derived from chiral primary amino acids resulted only into the complexes Δ -(S)-194 and Δ / Λ -(R/S)-195. Moreover, as the stereo-

configuration of Δ -(S)-194 was not entirely solved and Δ / Λ -(R/S)-195 was tested as racemic mixture, their value for structural interpretations compared to their affinities are limited. Nevertheless, both complexes inhibit PI3K γ and L-valine incorporated in Δ -(S)-194 was identified as a suitable building block. In case of Δ / Λ -(R/S)-195 a final statement which one, either Δ -(S)-195 or Λ -(R)-195, is the eutomer could not be verified with the investigations performed during this work.

Closing, a detailed interpretation reflecting the difficulties during the synthesis of primary chiral amino acid derived rhodium(III) complexes is mandatory to elucidate the basic principles. During the synthetic procedure, despite the expectation of four possible diastereomers, not all possible structural isomers were obtained.

The most likely reason could be steric effects, which have been overlooked during the conceptual planning of this project, see Figure 96. Introducing residues in the backbone of the tridentate ligand results in steric conflicts as highlighted by the methyl group of L-alanine in this example. The most important fact is that the tridentate ligand loses degrees of rotational freedom of at least four bonds during the coordination step. Moreover, the coordination to the metal forces the

tridentate ligand into sterically disfavoured conformations, as depicted in case of Figure 96 b) and c). In this coordination pattern, the methylene hydrogens adjacent to the pyridine ring of the tridentate ligand and the hydrogen atoms of the methyl residue of the amino acid experience a high steric repulsion. Moreover, the rigid structure of the complex offers no possibility for these residues to circumvent these repulsions by a conformational change. This is also true for any other amino acid as they possess larger residues than alanine. Moreover, the obtained crystal structures of Δ -(S)-**191** and Δ -(S)-**195** support the described hypothesis of steric hindrance.

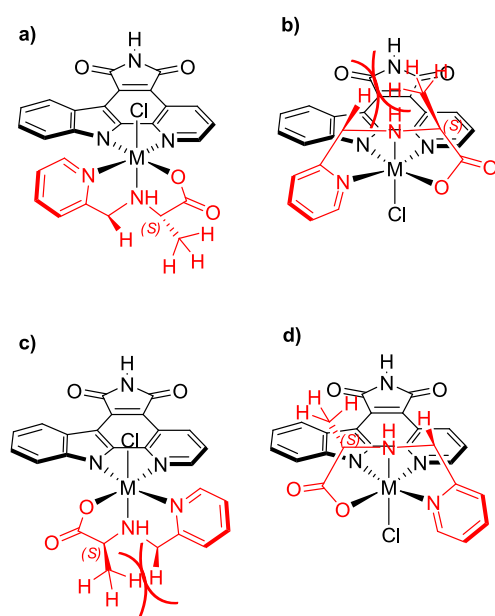


Figure 96: The incorporation of chiral primary amino acids into the design of tridentate ligands may cause adverse steric effects in at least two of the four possible diastereomers, **b)** and **c)** assuming a *fac*-coordination.

4 Conclusion and Outlook

We here reported our progress in developing structurally complicated and at the same time stereochemically defined organometallic protein kinase inhibitors. Multidentate prochiral ligands, tridentate chiral proline-based ligands and the attempts to introduce amino acids as building blocks for the ligand design represented the line-up.

In the first study, the development of an organometallic ruthenium compound and the structural comparison to other modified complexes inhibiting S6K1 were elucidated. The Millipore Kinase Profiler and radioactive kinase assays identified **85** as lead compound. The potent and selective inhibitor **85** using 100 nM inhibited 93% of S6K1 activity and only 16% of 283 kinases by less than 90%. The compound **86** possessing an isocyanate group instead of an isothiocyanate is about 1000-fold less potent. This indicated the importance of already slight differences in the coordination sphere and highlighted the potential for further potency and specificity optimisation.

Valuable insights for the complex design were gathered by the crystal structure of **85** bound to S6K1 lead to the development of **87**. The novel ligand scaffold of **87** resulted in an IC_{50} in the single digit nanomolar range targeting S6K1. Moreover, the crystal structure of **87** bound to S6K1 revealed the molecular basis for the compounds potency and selectivity. The subsequent *in vivo* testing of the compounds also lead to valuable insights. The cell permeability and effects on signaling pathways could be elaborated.

Taking all gathered data together also lead to the suggestion, that targeting S6K2 either alone or in combination with S6K1 inhibition could be a better option for direct S6 inhibition in melanoma and potentially other cancer cells. However, to date there are no commercially available S6K2 selective inhibitors. Thus, S6K2 could be target

for the next series of organometallic inhibitors.

However, the development of S6K1 selective metal based inhibitors also highlighted the issues arising with complicated coordinating ligands resulting in increased numbers of potential structural isomers. Thus, the enantiopure rhodium(III) complexes presented in this work highlight the importance to access defined structural isomers. They have unique properties regarding molecular recognition with chiral interaction partners like proteins. The remarkable differences in target specificity and affinity are an additional example for the potential of octahedral metal based compounds as kinase inhibitors. Moreover, we paired these benefits with the possibility to investigate single enantiomers, as it is standard for chiral organic compounds in the biological context. These possibilities turn organometallic compounds more and more adequate to the requirements of drug-like molecules and suitable for appropriate investigations.

Moreover, different structural isomers may not only possess different kinase inhibition effects, but also different toxicity profiles. They may be based on changes in the overall physico-chemical properties of each isomer. Finally, the scaffold offers plenty of possibilities to introduce additional functional groups in order to improve target specificity and affinity or to enhance pharmacological properties, as it is the subject of current investigations.

5 Experimental

5.1 General Information

All reactions were carried out under nitrogen atmosphere with magnetic stirring. The glass vessels were heated up and chilled down to ambient temperature for at least three times. HPLC-Grade solvents were used for reactions and distilled under nitrogen and dried using calcium hydride (CH_3CN , CH_2Cl_2 , CHCl_3 , DMF), sodium/benzophenone (THF, EtO_2), or magnesium shavings (MeOH) prior usage. All reagents, if not declared otherwise, were purchased from commercial suppliers and used without further purification.

Flash column chromatography was performed with distilled solvents using silica gel 60 M from Macherey–Nagel (irregular shape, 230–400 mesh, pH 6.8, pore volume: 0.81 mL/g, mean pore size: 66 Å, specific surface: 492 m²/g, particle size distribution: 0.5% < 25 µm and 1.7% > 71 µm, water content: 1.6 %).

¹H-NMR and proton decoupled ¹³C-NMR spectra were measured using either Avance 300 A (¹H-NMR: 300 MHz, ¹³C-NMR: 75 MHz), Avance 300 B (¹H-NMR 300 MHz, ¹³C-NMR: 75 MHz), DRX 400 (¹H-NMR: 400 MHz, ¹³C-NMR: 100 MHz), or a DRX 500 (¹H-NMR: 500 MHz, ¹³C-NMR: 125 MHz) spectrometer from Bruker at ambient temperature. The NMR data were evaluated using MestReNova 6.0.2-5475 (Mestrelab Research S.L.). NMR standards were used as follows: ¹H-NMR spectroscopy: δ = 7.26 ppm (residual CDCl_3), δ = 2.50 ppm (residual $(\text{CH}_3)_2\text{SO}$), δ = 2.05 ppm (residual $(\text{CH}_3)_2\text{CO}$), δ = 1.94 ppm (residual CD_3CN). ¹³C{¹H}-NMR spectroscopy: δ = 77.16 ppm (residual CDCl_3), δ = 39.52 ppm (residual $(\text{CH}_3)_2\text{SO}$), δ = 29.84 ppm (residual $(\text{CH}_3)_2\text{CO}$), δ = 1.32 ppm (residual CD_3CN).

IR spectra were measured using a Bruker Alpha FT-IR spectrophotometer. IR spectra were evaluated using OPUS 6.5 (Bruker Optik GmbH).

High-resolution mass spectra were measured using a LTQ-FT Ultra mass spectrometer (Thermo Fischer Scientific) using ESI technique.

Crystals were measured on a 'STOE IPDS2 Image Plate' or on a 'Bruker D8 QUEST area detector' diffractometer. The temperature was kept at 100.15 K during data collection. Using Olex2, the structure was solved with the SIR2011 structure solution program using Direct Methods and refined with the XLMP refinement package using Least Squares minimisation. The cell refinement software SAINT V8.27B (Bruker AXS Inc., 2012) and the data reduction software SAINT V8.27B (Bruker AXS Inc., 2012) as well as SAINT V8.30C (Bruker AXS Inc., 2013) and SAINT V8.30C (Bruker AXS Inc., 2013) were used. The programs applied for solution and refinement were SHELXS-97 (Sheldrick, 2008), SHELXL-2013 (Sheldrick, 2013), and DIAMOND (Crystal Impact) as well as XS (Sheldrick, 2008), SHELXL-2013 (Sheldrick, 2013) and DIAMOND (Crystal Impact). The programs used for visualization are either Pymol Molecular Graphics System, v0.99 (DeLano Scientific LLC) or ORTEP-III v1.0.3 (C.K. Johnson and M.N. Burnett).

CD spectra were recorded on a JASCO J-810 CD spectropolarimeter with cuvettes of 1 mm diameter.

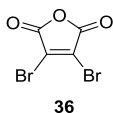
The counts per minute (CPM) performing radioactive kinase assays were measured using a Beckmann Coulter LS6500 multipurpose scintillation counter and corrected by the background CPM.

PyMOL Molecular Graphics System DeLano Scientific LLC, Version 1.1, was used to visualize the protein crystal-structures.^[431]

5.2 Synthetic Procedures

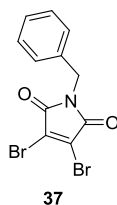
5.2.1 Synthesis of pyridocarbazoles and related intermediates

5.2.1.1 3,4-dibromofuran-2,5-dione (**36**)



1*H*-pyrrole-2,5-dione (40.0 g, 408 mmol), and aluminium trichloride (832 mg, 6.3 mmol) were suspended in bromine (42.0 mL, 810 mmol) and refluxed at 130 °C for 18 h. The resulting solid crude material was recrystallised from a mixture of toluene : ethylacetate (70 mL, 6:1). The precipitate was washed with hexane and dried *in vacuo*. The product **36** was obtained as beige solid (27.74 g, 108 mmol, 27%). After concentration of the filtrate and a second recrystallisation procedure under same conditions, additional product was obtained (20.72 g, 81 mmol, 20%). ¹³C-NMR (75 MHz, CDCl₃): δ(ppm) 157.9 (2xCO), 131.1 (2xCBr). IR (film): ν (cm⁻¹) 3081, 3000, 2649, 2520, 1699, 1584, 1417, 1389, 1268, 1224, 1181, 1136, 1056, 944, 906, 809, 761, 688.

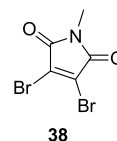
5.2.1.2 1-benzyl-3,4-dibromo-1*H*-pyrrole-2,5-dione (**37**)



36 (17.0 g, 66.3 mmol) and benzyl amine (10.7 g, 99.5 mmol) were dissolved in acetic acid (150 mL) and heated to 130 °C for 16 h. The solvent was removed under reduced pressure and residual acetic acid

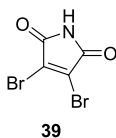
was coevaporated using toluene (3 x 40 mL). The dark crude material was subjected to column chromatography using hexane : ethylacetate (10:1) and dried *in vacuo*. The product **37** was obtained as beige solid (17.84 g, 51.7 mmol, 78%). *R*_f = 0.33 (hexane : ethylacetate 10:1). ¹H-NMR (300 MHz, CDCl₃): δ(ppm) 7.40–7.29 (m, 5H, *H*_{ar}), 4.75 (s, 2H, *H*_{benzyl}). ¹³C-NMR (75 MHz, CDCl₃): δ(ppm) 163.76 (2xCO), 135.37 (*C*_{ar}), 129.66 (2xCBr), 129.02 (2x*C*_{ar}), 128.93 (2x*C*_{ar}), 128.48 (*C*_{ar}), 43.41 (*C*_{benzyl}). IR (film): ν (cm⁻¹) 1781, 1709, 1592, 1519, 1491, 1432, 1388, 1336, 1233, 1158, 1100, 1060, 906, 851, 812, 752, 722, 695, 626, 583.

5.2.1.3 3,4-dibromo-1-methyl-1*H*-pyrrole-2,5-dione (**38**)



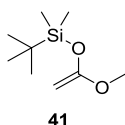
36 (5.0 g, 19.5 mmol) and methyl ammonium chloride (2.02 g, 29.9 mmol) were dissolved in acetic acid (50 mL) and heated to 130 °C for 16 h. The solvent was removed under reduced pressure and residual acetic acid was coevaporated using toluene (3 x 30 mL). The dark crude material was subjected to column chromatography using hexane : ethylacetate (3:1) and dried *in vacuo*. The product **38** was obtained as beige solid (2.85 g, 10.6 mmol, 55%). *R*_f = 0.46 (CHCl₃). ¹H-NMR (300 MHz, CDCl₃): δ(ppm) 3.13 (t, *J* = 2.1 Hz, 3H, CH₃). ¹³C-NMR (75 MHz, CDCl₃): δ(ppm) 164.1 (2xCO), 129.5 (2xCBr), 25.6 (CH₃). IR (film): ν (cm⁻¹) 2951, 2853, 1772, 1705, 1599, 1465, 1304, 1258, 1164, 1066, 1026, 848, 819, 790, 744, 706, 678.

5.2.1.4 3,4-dibromo-1H-pyrrole-2,5-dione (39)



36 (20.0 g, 78.2 mmol) and ammonium acetate (9.04 g, 117.2 mmol) were dissolved in acetic acid (250 mL) and heated to 130 °C for 16 h. The solvent was removed under reduced pressure and residual acetic acid was coevaporated using toluene (3 x 50 mL). The dark crude material was subjected to column chromatography using hexane : ethylacetate (5:1 → 2:1) and dried *in vacuo*. The product **39** was obtained as beige solid (10.81 g, 42.4 mmol, 54%). $R_f = 0.16$ (hexane : ethylacetate 8:1). $^1\text{H-NMR}$ (300 MHz, $(\text{CD}_3)_2\text{SO}$): $\delta(\text{ppm})$ 11.7 (bs, 1H, NH). $^{13}\text{C-NMR}$ (75 MHz, $(\text{CD}_3)_2\text{SO}$): $\delta(\text{ppm})$ 165.15 (2xCO), 129.72 (2xCBr). IR (film): ν (cm^{-1}) 3231, 3071, 1776, 1704, 1576, 1408, 1323, 1271, 1197, 1170, 1129, 1026, 994, 910, 872, 826, 788, 725.

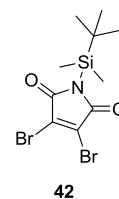
5.2.1.5 *tert*-butyl(1-methoxyvinyl)oxy dimethylsilane (41)



Diisopropylamine (22.4 mL, 159.6 mmol) were dissolved in THF (134 mL) and cooled to 0 °C. *n*-butyl lithium (58.5 mL, 146 mmol, 2.5 M in hexane) was added over a period of 30 min at -78 °C followed by the drop wise sequential addition of methylacetate (10.58 mL, 133 mmol), DMPU (24.1 mL, 199 mmol) over a period of 40 min. *Tert*-butyldimethylsilylchloride (20 g, 133 mmol) was dissolved in THF (32 mL) and added to the reaction mixture. The reac-

tion was continued for 1 h at -78 °C. The solvent was evaporated under reduced pressure and the crude material was solved in pentane (400 mL). The organic layer was washed with water (3 x 50 mL), saturated copper sulfate solution (3 x 50 mL) and saturated sodium carbonate solution (3 x 50 mL). The combined aqueous layer was extracted with pentane (4 x 50 mL). The combined organic layer was dried over sodium sulfate. The solvent was removed under reduced pressure and the crude material was subjected to bulb to bulb distillation (50 °C, 8 mbar). The product **41** was obtained as colourless oil (15 g, 68.7 mmol, 51%). $R_f = 0.48$ (hexane : ethylacetate 8:1). $^1\text{H-NMR}$ (300 MHz, CDCl_3): $\delta(\text{ppm})$ 3.53 (s, 3H, OCH_3), 3.23 (d, $J = 2.6$ Hz, 1H, $\text{C}_{\text{vinyl}}\text{HH}$), 3.10 (d, $J = 2.6$ Hz, 1H, $\text{C}_{\text{vinyl}}\text{HH}$), 0.93 (s, 9H, $\text{C}_q(\text{CH}_3)_3$), 0.17 (s, 6H, $\text{Si}(\text{CH}_3)_2$). $^{13}\text{C-NMR}$ (75 MHz, CDCl_3): $\delta(\text{ppm})$ 162.49 ($\text{C}_{\text{carbonyl}}$), 60.26 ($\text{C}_{\text{vinyl}}\text{H}_2$), 55.15 (OCH_3), 25.75 ($3 \times \text{C}_q(\text{CH}_3)_3$), 18.26 ($\text{C}_q(\text{CH}_3)_3$), -4.57 ($\text{Si}(\text{CH}_3)_2$).

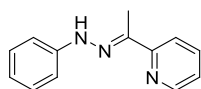
5.2.1.6 3,4-dibromo-1-(*tert*-butyldimethylsilyl)-1H-pyrrole-2,5-dione (42)



39 (10.7 g, 42 mmol) were dissolved in acetonitrile (100 mL) and stirred at ambient temperature. **41** (10 mL, 46 mmol) were added dropwise and the reaction was then refluxed for 5 h. The reaction mixture was cooled down to ambient temperature over a period of 8 h. The solvent was evaporated under reduced pressure and the crude material was subjected to column chromatography using hexane : ethyl acetate (9:1 → 3:1). The product was **42** was obtained as white solid (8.38 g, 22.65 mmol, 54%). $R_f = 0.67$ (hexane : ethylacetate 8:1).

$^1\text{H-NMR}$ (300 MHz, CDCl_3): $\delta(\text{ppm})$ 0.94 (s, 9H, $\text{C}_q(\text{CH}_3)_3$), 0.46 (s, 6H, $\text{Si}(\text{CH}_3)_2$). $^{13}\text{C-NMR}$ (75 MHz, CDCl_3): $\delta(\text{ppm})$ 168.87 (2xCO), 131.72 (2xCBr), 26.24 (3xC $_q(\text{CH}_3)_3$), 19.02 ($\text{C}_q(\text{CH}_3)_3$), -4.44 ($\text{Si}(\text{CH}_3)_2$).

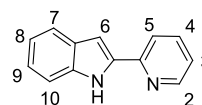
5.2.1.7 (E)-2-(1-(2-phenylhydrazono)ethyl)pyridine (**45**)



45

2-Methyl-pyridylketone (3.70 mL, 33.0 mmol) and phenylhydrazine (3.35 mL, 34.1 mmol) were dissolved in ethanol (10 mL, abs.) under nitrogen atmosphere. The reaction mixture was heated up slowly to 80 °C over a period of 15 min and refluxed for another 45 min until a yellow precipitate was formed. The reaction mixture was cooled down to 0 °C and filtrated. The yellow precipitate was washed with cooled ethanol (150 mL, abs.) and dried *in vacuo*. The residual filtrate was concentrated and cooled to 0 °C to precipitate additional crude material which was filtrated and washed with cooled ethanol (100 mL, abs.) and dried *in vacuo* as the first product fraction. The combined product fractions led to the product **45** as a yellow solid (6.84 g, 32.4 mmol, 98%). $R_f = 0.55$ (methylene chloride : methanol 15:1). $^1\text{H-NMR}$ (300 MHz, CDCl_3): $\delta(\text{ppm})$ 8.58 (d, $J = 4.7$ Hz, 1H, H_{ar}), 8.19-8.15 (m, 1H, H_{ar}), 7.73-7.68 (m, 1H, H_{ar}), 7.33-7.18 (m, 5H, H_{ar}), 6.93-6.88 (m, 1H, H_{ar}), 2.41 (s, 3H, CH_3). $^{13}\text{C-NMR}$ (75 MHz, CDCl_3): $\delta(\text{ppm})$ 148.0, 144.7, 136.5, 129.4, 122.4, 120.9, 120.2, 113.6, 10.1 (CH_3). IR (film): $\nu(\text{cm}^{-1})$ 3204, 3171, 3019, 2939, 1596, 1564, 1470, 1427, 1289, 1246, 1149, 1110, 1077, 1048, 993, 967, 892, 781, 748, 695, 652, 636, 549, 508, 411. HRMS calculated for $\text{C}_{13}\text{H}_{13}\text{N}_3\text{H}$ ($M + \text{H}^+$) 212.1188 found ($M + \text{H}^+$) 212.1183.

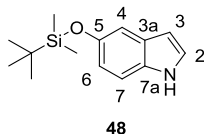
5.2.1.8 2-(pyridin-2-yl)-1H-indole (**46**)



46

Polyphosphoric acid (34.0 g, 1.1 g per mmol of educt) were heated to 95 °C and firm stirring. **45** (6.50 g, 30.8 mmol) was added sequentially in small portions to the clear viscose reaction mixture. After 4 h the reaction mixture was cooled down to ambient temperature and sodium hydroxide solution (20%) was added until pH 9 was set. A crude material precipitated as yellow solid. The reaction mixture was extracted with methylene chloride (3 x 150 mL). The combined organic layer was washed with BRINE (4 x 25 mL) dried over sodium sulfate, filtrated and dried *in vacuo*. The product **46** was obtained as yellow solid (5.63 g, 29.0 mmol, 94%). $R_f = 0.71$ (hexane : ethylacetate 10:1). $^1\text{H-NMR}$ (300 MHz, CDCl_3): $\delta(\text{ppm})$ 9.76 (s, 1H, NH), 8.57(dt, $J = 5.0$ Hz, $J = 1.1$ Hz, 1H, CH_{ar}), 7.83 (dt, $J = 8.0$ Hz, $J = 1.0$ Hz, 1H, CH_{ar}), 7.75 (td, $J = 7.7$ Hz, $J = 1.4$ Hz, 1H, CH_{ar}), 7.66 (d, $J = 7.9$ Hz, 1H, CH_{ar-10}), 7.44 (dd, $J = 8.1$ Hz, $J = 0.7$ Hz, 1H, CH_{ar}), 7.24-7.17 (m, 2H, CH_{ar}), 7.14-7.09 (m, 1H, CH_{ar}), 7.05 (dd, $J = 2.1$ Hz, $J = 0.7$ Hz, 1H, CH_{ar}). IR (film): $\nu(\text{cm}^{-1})$ 3114, 2968, 1591, 1557, 1439, 1408, 1337, 1299, 1255, 1143, 994, 776, 741, 616, 602, 563, 520, 493, 427, 400. HRMS calculated for $\text{C}_{13}\text{H}_{10}\text{N}_2\text{Na}$ ($M + \text{Na}^+$) 217.0742 found ($M + \text{Na}^+$) 217.0740.

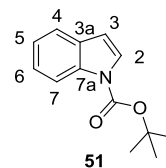
5.2.1.9 5-(*tert*-butyldimethylsilyloxy)-1*H*-indole (**48**)



5-(benzyloxy)-1*H*-indole (5.00 g, 22.39 mmol) were dissolved in 200 mL ethylacetate in a 1 L reaction flask. Pd/C (3.95 g, 3.81 mmol, 10% v/w) were suspended and the nitrogen atmosphere was completely substituted by hydrogen in three turns. The mixture was reacted at ambient temperature for 16 h under intensive stirring. The suspension was filtrated over CELITE and the filtrate was dried *in vacuo*. The residue was dissolved in 80 mL DMF and cooled to 4 °C. Over a period of 10 min diisopropylethylamine (19.4 mL, 111.95 mmol) were added drop wise. Then, *tert*-butyldimethylsilyltriflate (6.1 mL, 22.39 mmol) was added drop wise over 16 h and the reaction mixture was warmed up to ambient temperature simultaneously. The orange coloured reaction mixture was quenched with ammonium acetate (200 mL, 1 M) and then diluted with of water (100 mL). The mixture was then extracted with ethylacetate (4 x 200 mL), the organic layer was separated, washed with BRINE (3 x 50 mL), and dried over sodium sulfate. The crude material was dried *in vacuo* and subjected to silica gel chromatography hexane : ethylacetate (9:1). The product **48** was obtained as pale oil (3.78 g, 15.28 mmol, 68% over two steps). R_f = 0.57 (hexane : ethylacetate 3:1). $^1\text{H-NMR}$ (300 MHz, CDCl_3): δ (ppm) 8.03 (s, 1H, NH), 7.23 (d, J = 8.7 Hz, 1H, $\text{CH}_{\text{ar}}\text{-7}$), 7.18-7.15 (m, 1H, $\text{CH}_{\text{ar}}\text{-2}$), 7.07 (d, J = 2.3 Hz, 1H, $\text{CH}_{\text{ar}}\text{-4}$), 6.76 (dd, J = 8.7, 2.3, 1H, $\text{CH}_{\text{ar}}\text{-6}$), 6.44 (m, 1H, $\text{CH}_{\text{ar}}\text{-3}$), 1.01 (s, 9H, $\text{C}_q(\text{CH}_3)_3$), 0.20 (s, 6H, $\text{Si}(\text{CH}_3)_2$). $^{13}\text{C-NMR}$ (75 MHz, CDCl_3): δ (ppm) 149.53 ($\text{C}_{\text{ar}}\text{-5}$), 131.59 ($\text{C}_{\text{ar}}\text{-7a}$), 128.71 ($\text{C}_{\text{ar}}\text{-3a}$), 124.95 ($\text{C}_{\text{ar}}\text{-2}$), 116.48 ($\text{C}_{\text{ar}}\text{-6}$), 111.33 ($\text{C}_{\text{ar}}\text{-$

7), 110.23 ($\text{C}_{\text{ar}}\text{-4}$), 102.42 ($\text{C}_{\text{ar}}\text{-3}$), 25.97 ($3\times\text{C}_q(\text{CH}_3)_3$), 18.39 ($\text{C}_q(\text{CH}_3)_3$), -4.26 ($\text{Si}(\text{CH}_3)_2$), -4.45 ($\text{Si}(\text{CH}_3)_2$). HRMS calculated for $\text{C}_{14}\text{H}_{21}\text{NOSiNa}$ ($\text{M} + \text{Na}^+$) 270.1285, found ($\text{M} + \text{Na}^+$) 270.1285.

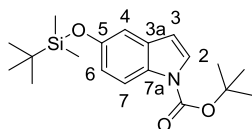
5.2.1.10 *tert*-butyl 1*H*-indole-1-carboxylate (**51**)



Indole (10.0 g, 85.4 mmol) was dissolved in THF (25 mL) and cooled to 4 °C. Di-*tert*-butyl-dicarbonate (18.6 g, 85.4 mmol) was presolved in THF (25 mL) and added to the reaction mixture. Dimethylaminopyridine (DMAP, 15.7 g, 128 mmol) was added slowly. The reaction mixture was stirred for 16 h and warmed up to ambient temperature. The reaction mixture was cooled to 4 °C and hydrochloric acid (60 mL, 1 M) was added followed by 15 min of stirring. The organic layer was separated. The aqueous layer was extracted with ethylacetate (5 x 50 mL). The combined organic layer was washed with BRINE (3 x 50 mL), and dried over sodium sulfate. The solvent was evaporated under reduced pressure and the crude material was subjected to column chromatography using hexane : ethylacetate (8:1). The product **51** was obtained as colourless oil (18.34 g, 84.5 mmol, quant.). R_f = 0.37 (hexane : ethylacetate 8:1). $^1\text{H-NMR}$ (300 MHz, CDCl_3): δ (ppm) 8.11 (d, J = 8.1 Hz, 1H, $\text{CH}_{\text{ar}}\text{-7}$), 7.55 (d, J = 3.7 Hz, 1H, $\text{CH}_{\text{ar}}\text{-2}$), 7.51 (ddd, J = 7.6, 1.3, 0.8 Hz, 1H, $\text{CH}_{\text{ar}}\text{-4}$), 7.26 (ddd, J = 8.4, 7.3, 1.4 Hz, 1H, $\text{CH}_{\text{ar}}\text{-6}$), 7.21-7.14 (m, 1H, $\text{CH}_{\text{ar}}\text{-5}$), 6.51 (dd, J = 3.7, 0.7 Hz, 1H, $\text{CH}_{\text{ar}}\text{-3}$), 1.62 (s, 9H, $\text{OC}_q(\text{CH}_3)_3$). $^{13}\text{C-NMR}$ (75 MHz, CDCl_3): δ (ppm) 149.92 ($\text{C}_{\text{carbonyl}}$), 135.35 ($\text{C}_{\text{ar}}\text{-7a}$), 130.71 ($\text{C}_{\text{ar}}\text{-3a}$), 125.98, 124.29, 122.74, 121.03, 115.28, 107.38, 83.70 ($\text{C}_q(\text{CH}_3)_3$), 28.31 ($\text{C}_q(\text{CH}_3)_3$). IR (film): ν (cm^{-1}) 2978,

2933, 1728, 1604, 1535, 1450, 1375, 1333, 1248, 1208, 1152, 1114, 1076, 1018, 935, 881, 850.

5.2.1.11 *tert*-butyl 5-(*tert*-butyldimethylsilyloxy)-1*H*-indole-1-carboxylate (**52**)

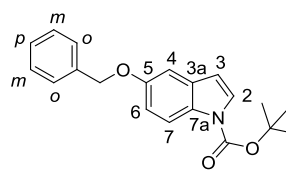


52

48 (3.78 g, 15.28 mmol) was dissolved in THF (12 mL) and cooled to 4 °C. Di-*tert*-butyl-dicarbonate (4.20 g, 19.32 mmol) was presolved in THF (3 mL) and added to the reaction mixture. Dimethylaminopyridine (DMAP, 2.35 g, 19.22 mmol) was added slowly. The reaction mixture was stirred for 16 h and turned from orange to green while warming to ambient temperature. The reaction mixture was cooled to 4 °C and hydrochloric acid (11 mL, 1 M) was added followed by 5 min of stirring. The organic layer was separated. The aqueous layer was extracted with ethylacetate (4 x 50 mL). The combined organic layer was washed with BRINE (3 x 50 mL), and dried over sodium sulfate. The solvent was removed *in vacuo* and the crude material subjected to column chromatography hexane : ethylacetate (20:1). The product **52** was obtained as colourless oil (4.95 g, 14.24 mmol, 93%). R_f = 0.63 (hexane : ethylacetate 10:1). $^1\text{H-NMR}$ (300 MHz, CDCl_3): δ (ppm) 7.96 (d, J = 8.6 Hz, 1H, $\text{CH}_{\text{ar-7}}$), 7.55 (d, J = 3.6, 1H, $\text{CH}_{\text{ar-2}}$), 6.99 (d, J = 2.4 Hz, 1H, $\text{CH}_{\text{ar-4}}$), 6.84 (dd, J = 8.9, 2.4, 1H, $\text{CH}_{\text{ar-6}}$), 6.46 (d, J = 3.7, 1H, $\text{CH}_{\text{ar-3}}$), 1.66 (s, 9H, $\text{OC}_q(\text{CH}_3)_3$), 1.00 (s, 9H, $\text{SiC}_q(\text{CH}_3)_3$), 0.20 (s, 6H, $\text{Si}(\text{CH}_3)_2$). $^{13}\text{C-NMR}$ (75 MHz, CDCl_3): δ (ppm) 151.53 ($\text{C}_{\text{carbonyl}}$), 131.66 ($\text{C}_{\text{ar-7a}}$), 130.54 ($\text{C}_{\text{ar-3a}}$), 126.61, 117.74, 115.70, 111.12, 107.16, 83.55 ($\text{OC}_q(\text{CH}_3)_3$), 28.39 ($\text{OC}_q(\text{CH}_3)_3$), 25.92 ($\text{SiC}_q(\text{CH}_3)_3$), 18.40 ($\text{SiC}_q(\text{CH}_3)_3$), -4.27

($\text{Si}(\text{CH}_3)_2$). IR (film): ν (cm^{-1}) 2956, 2932, 2892, 2858, 1731, 1614, 1580, 1462, 1372, 1274, 1218, 1149, 1118, 1081, 1022, 966, 878, 840, 811, 770. HRMS calculated for $\text{C}_{19}\text{H}_{29}\text{NO}_3\text{SiNa}$ ($\text{M} + \text{Na}^+$) 370.1809, found ($\text{M} + \text{Na}^+$) 370.1811.

5.2.1.12 *tert*-butyl 5-(benzyloxy)-1*H*-indole-1-carboxylate (**53**)

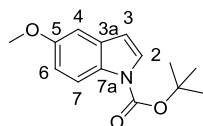


53

5-(benzyloxy)-1*H*-indole (**49**) (3.8 g, 17.1 mmol) was dissolved in THF (12.5 mL) and cooled to 4 °C. Di-*tert*-butyl-dicarbonate (3.9 g, 17.9 mmol) was presolved in THF (3 mL) and added to the reaction mixture. Dimethylaminopyridine (DMAP, 3.2 g, 25.6 mmol) was added slowly. The reaction mixture became solid and was fluidised by heating to 50 °C for 5 min. The reaction mixture was then stirred for 16 h at ambient temperature. The reaction mixture was cooled to 4 °C and hydrochloric acid (12 mL, 1 M) was added followed by 10 min of stirring. The organic layer was separated. The aqueous layer was extracted with ethylacetate (3 x 20 mL). The combined organic layer was washed with BRINE (3 x 50 mL), and dried over sodium sulfate. The solvent was evaporated under reduced pressure and the crude material was subjected to column chromatography using hexane : ethylacetate (15:1). The product **53** was obtained as colourless oil (5.08 g, 145.71 mmol, 92%). R_f = 0.59 (hexane : ethylacetate 8:1). $^1\text{H-NMR}$ (300 MHz, $(\text{CD}_3)_2\text{SO}$): δ (ppm) 7.93 (d, J = 9.1 Hz, 1H, $\text{CH}_{\text{ar-7}}$), 7.63 (d, J = 3.7 Hz, 1H, $\text{CH}_{\text{ar-2}}$), 7.48 (d, J = 1.7 Hz, 1H, $\text{CH}_{\text{ar-o}}$), 7.45 (d, J = 1.2 Hz, 1H, $\text{CH}_{\text{ar-o}}$), 7.43–7.29 (m, 3H, $\text{CH}_{\text{ar-p}}$, $\text{CH}_{\text{ar-m}}$), 7.23 (d, J = 2.5 Hz, 1H, $\text{CH}_{\text{ar-4}}$), 7.01 (dd, J = 9.0, 2.5 Hz, 1H,

CH_{ar-6}), 6.62 (d, $J = 4.3$ Hz, 1H, CH_{ar-3}), 5.13 (s, 2H, $CH_{2benzyl}$), 1.61 (s, 9H, $OC_q(CH_3)_3$).

5.2.1.13 *tert*-butyl 5-methoxy-1*H*-indole-1-carboxylate (**54**)

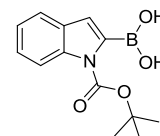


54

5-methoxy-1*H*-indole (**50**) (5.0 g, 33.9 mmol) was dissolved in THF (15 mL) and cooled to 4 °C. Di-*tert*-butyl-dicarbonate (7.5 g, 34 mmol) was presolved in THF (3 mL) and added to the reaction mixture. Dimethylaminopyridine (DMAP, 6.11 g, 50 mmol) was added slowly. The reaction mixture became solid and was fluidised by heating to 50 °C for 5 min. The reaction mixture was then stirred for 16 h at ambient temperature. The reaction mixture was cooled to 4 °C and hydrochloric acid (30 mL, 1 M) was added followed by 15 min of stirring. The organic layer was separated. The aqueous layer was extracted with ethylacetate (4 x 50 mL). The combined organic layer was washed with BRINE (3 x 50 mL), and dried over sodium sulfate. The solvent was evaporated under reduced pressure and the crude material was subjected to column chromatography using hexane : ethylacetate (10:1). The product **54** was obtained as white solid (8.2 g, 33.2 mmol, 98%). $R_f = 0.54$ (hexane : ethylacetate 8:1). 1H -NMR (300 MHz, $CDCl_3$): δ (ppm) 8.01 (d, $J = 8.0$ Hz, 1H, CH_{ar-7}), 7.56 (d, $J = 3.5$ Hz, 1H, CH_{ar-2}), 7.03 (d, $J = 2.5$ Hz, 1H, CH_{ar-4}), 6.92 (dd, $J = 9.0, 2.5$ Hz, 1H, CH_{ar-6}), 6.50 (d, $J = 3.7$ Hz, 1H, CH_{ar-3}), 3.85 (s, 3H, OCH_3), 1.66 (s, 9H, $OC_q(CH_3)_3$). ^{13}C -NMR (75 MHz, $CDCl_3$): δ (ppm) 155.98 (C_{ar-5}), 149.83 ($C_{carbonyl}$), 131.49 (C_{ar-7a}), 130.08 (C_{ar-3a}), 126.58, 115.91, 113.07, 107.21, 103.66, 83.53

($OC_q(CH_3)_3$), 55.74 (OCH_3), 28.28 ($OC_q(CH_3)_3$). IR (film): ν (cm^{-1}) 2978, 2937, 1726, 1614, 1585, 1471, 1443, 1373, 1342, 1260, 1152, 1117, 1081, 1019, 937, 842, 805, 761, 720, 627.

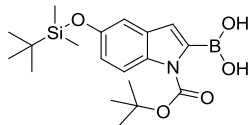
5.2.1.14 1-(*tert*-butoxycarbonyl)-1*H*-indol-2-ylboronic acid (**55**)



55

Diisopropylamine (19 mL, 135 mmol) was dissolved in THF (50 mL) and cooled to -78 °C. *n*-Butyllithium (54 mL, 135 mmol, 2.5 M in hexane) was added drop wise. The reaction mixture was warmed up to 0 °C and stirred for 30 min. **51** (19.7 g, 90 mmol) was predried *in vacuo*, and dissolved in a second flask with THF (100 mL). Triisopropyl borate (32 mL, 139 mmol) was added drop wise while cooling the reaction mixture to 0 °C. The lithium diisopropylamide solution was added over a period of 1.5 h. After 16 h of stirring hydrochloric acid (150 mL, 2 M) was added to quench the reaction over 15 min at ambient temperature. The organic layer was separated and the aqueous layer was extracted with ethylacetate (4 x 50 mL). The combined organic layer was washed with BRINE (3 x 50 mL), dried over sodium sulfate and concentrated *in vacuo* to dryness. The dark orange oil (23.5 g, 90 mmol, quant.) was processed directly to the coupling reaction without further characterisation due to the instability of the boronic acid intermediate.

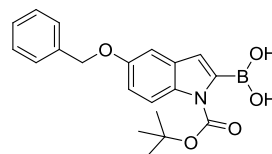
5.2.1.15 1-(*tert*-butoxycarbonyl)-5-(*tert*-butyldimethylsilyloxy)-1*H*-indol-2-ylboronic acid (**56**)



56

Diisopropylamine (1.21 mL, 8.64 mmol) was dissolved in THF (0.865 mL) and cooled to -78°C . *n*-Butyllithium (3.46 mL, 8.64 mmol, 2 M in hexane) was added drop wise. The reaction mixture was warmed up to 0°C and stirred for 30 min. **52** (1.95 g, 5.61 mmol) was predried *in vacuo*, and dissolved in a second flask with THF (15 mL). Triisopropyl borate (2.0 mL, 8.64 mmol) was added drop wise while cooling the reaction mixture to 0°C . The lithium diisopropylamide solution was added over a period of 1.5 h. The colour of the reaction mixture turned from pallid to yellow. After 2 h of stirring hydrochloric acid (15 mL, 2 M) was added to quench the reaction over 15 min at ambient temperature. The organic layer was separated and the aqueous layer was extracted with ethylacetate (4 x 25 mL). The combined organic layer was washed with BRINE (3 x 50 mL), dried over sodium sulfate and concentrated *in vacuo* to dryness. The dark brown oil (2.1 g, 5.5 mmol, 98%) was processed directly to the coupling reaction without further characterisation due to the instability of the boronic acid intermediate.

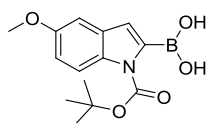
5.2.1.16 5-(benzyloxy)-1-(*tert*-butoxycarbonyl)-1*H*-indol-2-ylboronic acid (**57**)



57

53 (2.98 g, 9.2 mmol) was predried *in vacuo*, and dissolved in a second flask with THF (15 mL). Triisopropyl borate (3.2 mL, 14.2 mmol) was added drop wise while cooling the reaction mixture to 0°C . Lithium diisopropylamide solution (6.96 mL, 13.8 mmol, 2 M in hexane) was added over a period of 1 h. The colour of the reaction mixture turned from pallid to yellow. After 2 h of stirring hydrochloric acid (22 mL, 2 M) was added to quench the reaction over 15 min at ambient temperature. The organic layer was separated and the aqueous layer was extracted with ethylacetate (5 x 25 mL). The combined organic layer was washed with BRINE (3 x 50 mL), dried over sodium sulfate and concentrated *in vacuo* to dryness. The dark brown oil (3.3 g, 9 mmol, 98%) was processed directly to the coupling reaction without further characterisation due to the instability of the boronic acid intermediate.

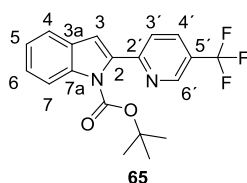
5.2.1.17 1-(*tert*-butoxycarbonyl)-5-methoxy-1*H*-indol-2-ylboronic acid (**58**)



58

54 (4 g, 16.2 mmol) was predried *in vacuo*, and dissolved in THF (18.8 mL). Triisopropyl borate (5.7 mL, 24.9 mmol) was added drop wise while cooling the reaction mixture to 0 °C. Lithium diisopropylamide solution (13.5 mL, 24.3 mmol, 1.8 M in hexane) was added over a period of 1 h. After 2 h of stirring hydrochloric acid (40 mL, 2 M) was added to quench the reaction over 15 min at 0 °C. The organic layer was separated and the aqueous layer was extracted with ethylacetate (5 x 25 mL). The combined organic layer was washed with BRINE (3 x 50 mL), dried over sodium sulfate and concentrated *in vacuo* to dryness. The dark orange oil (4.6 g, 15.8 mmol, 98%) was processed directly to the coupling reaction without further characterisation due to the instability of the boronic acid intermediate.

5.2.1.18 *tert*-butyl 2-(5-(trifluoromethyl) pyridin-2-yl)-1*H*-indole-1-carboxylate (**65**)

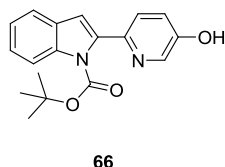


65

Sodium carbonate (4.7 g, 45.0 mmol), and tetrakis(triphenylphosphine)palladium (1.04 g, 0.90 mmol) were reacted with the boronic acid **55** (4.7 g, 18 mmol) dissolved in dimethoxyethane : water (95 mL, 4:1). 2-bromo-5-(trifluoromethyl)pyridine (3.7 g, 16.4 mmol) was

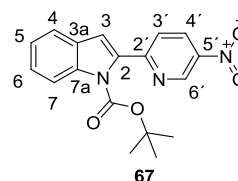
added and the entire reaction mixture refluxed for 16 h. The dark red suspension was cooled to ambient temperature and diluted with water (65 mL). The organic layer was separated. The aqueous layer was extracted with ethylacetate (3 x 50 mL), the combined organic layer was washed with BRINE (3 x 50 mL), dried over sodium sulfate. The crude material was concentrated *in vacuo* and subjected to column chromatography using hexane : ethylacetate (20:1 → 5:1). The product **65** was obtained as a white solid (3.71 g, 10.2 mmol, 61.6%). $R_f = 0.54$ (hexane : ethylacetate 8:1). $^1\text{H-NMR}$ (300 MHz, CDCl_3): δ (ppm) 8.80 (dd, $J = 1.4, 0.9$ Hz, 1H, $\text{CH}_{\text{ar}}\text{-6}'$), 8.05 (dd, $J = 8.4, 0.8$ Hz, 1H, $\text{CH}_{\text{ar}}\text{-7}$), 7.83 (ddd, $J = 8.2, 2.3, 0.6$ Hz, 1H, CH_{ar}), 7.52 – 7.43 (m, 2H, $\text{CH}_{\text{ar}}\text{-4}$, CH_{ar}), 7.26 (ddd, $J = 8.6, 7.2, 1.3$ Hz, 1H, $\text{CH}_{\text{ar}}\text{-6}$), 7.18 – 7.10 (m, 1H, $\text{CH}_{\text{ar}}\text{-5}$), 6.73 (d, $J = 0.6$ Hz, 1H, $\text{CH}_{\text{ar}}\text{-3}$), 1.25 (s, 9H, $\text{OC}_q(\text{CH}_3)_3$). $^{13}\text{C-NMR}$ (75 MHz, CDCl_3): δ (ppm) 156.62 ($\text{C}_{\text{ar}}\text{-2}'$), 149.93 ($\text{C}_{\text{carbonyl}}$), 145.98 (q, $J = 4.0$ Hz), 138.18, 138.08, 133.25 (q, $J = 3.4$ Hz), 128.80, 125.76, 125.22, 124.78, 123.31, 122.85, 121.45, 115.25, 112.67, 84.08 ($\text{OC}_q(\text{CH}_3)_3$), 27.74 ($\text{OC}_q(\text{CH}_3)_3$). IR (film): ν (cm^{-1}) 2983, 1726, 1601, 1557, 1479, 1449, 1398, 1367, 1316, 1227, 1153, 1114, 1076, 1036, 1008, 938, 852, 822, 770, 743.

5.2.1.19 *tert*-butyl 2-(5-hydroxypyridin-2-yl)-1*H*-indole-1-carboxylate (**66**)



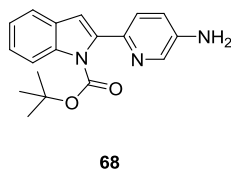
Sodium carbonate (4.7 g, 45 mmol), and tetrakis(triphenylphosphine)palladium (1.04 g, 0.9 mmol) were reacted with the boronic acid **55** (4.7 g, 18 mmol) dissolved in dimethoxyethane : water (95 mL, 4:1). 6-bromopyridin-3-ol (2.85 g, 16.4 mmol) was added and the entire reaction mixture refluxed for 16 h. The dark brown suspension was cooled to ambient temperature and diluted with water (65 mL). The organic layer was separated. The aqueous layer was extracted with ethylacetate (3 x 50 mL), the combined organic layer was washed with BRINE (3 x 50 mL), dried over sodium sulfate. The crude material was concentrated *in vacuo* and subjected to column chromatography using methylene chloride : methanol (35:1 → 10:1). The product **66** was obtained as brown oil (2.40 g, 7.7 mmol, 47%). R_f = 0.51 (hexane : ethylacetate 8:1). The product could only be obtained as mixture of *tert*-butoxycarbonyl protected and unprotected form and was therefore processed without further characterisation.

5.2.1.20 *tert*-butyl 2-(5-nitropyridin-2-yl)-1*H*-indole-1-carboxylate (**67**)



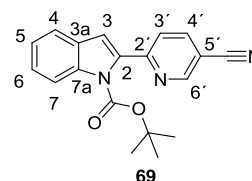
Sodium carbonate (4.7 g, 45.0 mmol), and tetrakis(triphenylphosphine)palladium (1.04 g, 0.90 mmol) were reacted with the boronic acid **55** (4.7 g, 18 mmol) dissolved in dimethoxyethane : water (95 mL, 4:1). 2-bromo-5-nitropyridine (3.3 g, 16.4 mmol) was added and the entire reaction mixture refluxed for 16 h. The dark red suspension was cooled to ambient temperature and diluted with water (65 mL). The organic layer was separated. The aqueous layer was extracted with ethylacetate (3 x 50 mL), the combined organic layer was washed with BRINE (3 x 50 mL), dried over sodium sulfate. The crude material was concentrated *in vacuo* and subjected to column chromatography using hexane : ethylacetate (20:1 → 5:1). The product **67** was obtained as a yellow solid (3.58 g, 10.5 mmol, 64%). R_f = 0.27 (hexane : ethylacetate 8:1). $^1\text{H-NMR}$ (300 MHz, CDCl_3): δ (ppm) 9.48 (dd, J = 2.6, 0.5 Hz, 1H, $\text{CH}_{\text{ar-6'}}$), 8.55 (dd, J = 8.7, 2.6 Hz, 1H, $\text{CH}_{\text{ar-4'}}$), 8.14 (d, J = 9.2 Hz, 1H, $\text{CH}_{\text{ar-7}}$), 7.72 (dd, J = 8.7, 0.6 Hz, 1H, $\text{CH}_{\text{ar-3'}}$), 7.64 (d, J = 7.8 Hz, 1H, $\text{CH}_{\text{ar-4}}$), 7.43 (ddd, J = 8.5, 7.2, 1.3 Hz, 1H, $\text{CH}_{\text{ar-6}}$), 7.35–7.28 (m, 1H, $\text{CH}_{\text{ar-5}}$), 7.02 (d, J = 0.6 Hz, 1H, $\text{CH}_{\text{ar-3}}$), 1.46 (s, 9H, $\text{OC}_q(\text{CH}_3)_3$). IR (film): ν (cm^{-1}) 3048, 2974, 2929, 1731, 1595, 1566, 1513, 1474, 1445, 1399, 1342, 1314, 1266, 1223, 1189, 1142, 1110, 944, 848, 830, 768.

5.2.1.21 *tert*-butyl 2-(5-aminopyridin-2-yl)-
1*H*-indole-1-carboxylate (**68**)



Sodium carbonate (4.7 g, 45 mmol), and tetrakis(triphenylphosphine)palladium (1.04 g, 0.9 mmol) were reacted with the boronic acid **55** (4.7 g, 18 mmol) dissolved in dimethoxyethane : water (95 mL, 4:1). 6-bromopyridin-3-amine (2.8 g, 16.4 mmol) was added and the entire reaction mixture refluxed for 16 h. The dark brown suspension was cooled to ambient temperature and diluted with water (65 mL). The organic layer was separated. The aqueous layer was extracted with ethylacetate (3 x 50 mL), the combined organic layer was washed with BRINE (3 x 50 mL), dried over sodium sulfate. The crude material was concentrated *in vacuo* and subjected to column chromatography using methylene chloride : methanol (35:1 → 10:1). The product **68** was obtained as a brown oil (2.40 g, 14 mmol, 77%). R_f = 0.56 (hexane : ethylacetate 8:1). The product could only be obtained as mixture of *tert*-butyloxycarbonyl protected and unprotected form and was therefore processed without further characterisation.

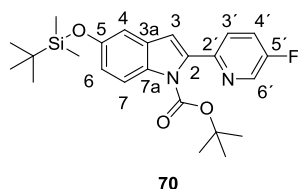
5.2.1.22 *tert*-butyl 2-(5-cyanopyridin-2-yl)-
1*H*-indole-1-carboxylate (**69**)



Sodium carbonate (4.7 g, 45.0 mmol), and tetrakis(triphenylphosphine)palladium (1.04 g, 0.90 mmol) were reacted with the boronic acid **55** (4.7 g, 18 mmol) dissolved in dimethoxyethane : water (95 mL, 4:1). 6-bromonicotinonitrile (2.9 g, 16.4 mmol) was added and the entire reaction mixture refluxed for 16 h. The dark red suspension was cooled to ambient temperature and diluted with water (65 mL). The organic layer was separated. The aqueous layer was extracted with ethylacetate (3 x 50 mL), the combined organic layer was washed with BRINE (3 x 50 mL), dried over sodium sulfate. The crude material was concentrated *in vacuo* and subjected to column chromatography using hexane : ethylacetate (15:1 → 3:1). The product **69** was obtained as a brown oil (3.9 g, 12.2 mmol, 68%). R_f = 0.62 (methylene chloride : methanol 35:1). $^1\text{H-NMR}$ (300 MHz, CDCl_3): δ (ppm) 8.76 (dd, J = 2.1, 0.8 Hz, 1H, $\text{CH}_{\text{ar-6'}}$), 8.00 (dd, J = 8.4, 0.8 Hz, 1H, $\text{CH}_{\text{ar-7}}$), 7.82 (dd, J = 8.2, 2.2 Hz, 1H, $\text{CH}_{\text{ar-4'}}$), 7.49–7.42 (m, 2H, $\text{CH}_{\text{ar-4}}$, $\text{CH}_{\text{ar-3'}}$), 7.26 (ddd, J = 8.3, 7.3, 1.3 Hz, 1H, $\text{CH}_{\text{ar-6}}$), 7.18–7.09 (m, 1H, $\text{CH}_{\text{ar-5}}$), 6.77 (d, J = 0.4 Hz, 1H, $\text{CH}_{\text{ar-3}}$), 1.28 (s, 9H, $\text{OC}_q(\text{CH}_3)_3$). $^{13}\text{C-NMR}$ (75 MHz, CDCl_3): δ (ppm) 156.26 ($\text{C}_{\text{ar-2'}}$), 151.74 ($\text{C}_{\text{carbonyl}}$), 139.09, 128.65, 126.10, 124.78, 123.40, 122.79, 121.87, 121.62, 120.87, 119.28, 116.89, 115.18, 113.52, 84.35 ($\text{OC}_q(\text{CH}_3)_3$), 27.81 ($\text{OC}_q(\text{CH}_3)_3$). IR (film): ν (cm^{-1}) 2227, 1731, 1587, 1552, 1470, 1445, 1391, 1363, 1316, 1227, 1139, 1023, 945, 849, 824, 794, 772, 743, 686, 660. HRMS calculated for

$C_{19}H_{18}N_3O_2$ ($M + H^+$) 320.1394 found
($M + H^+$) 320.1395.

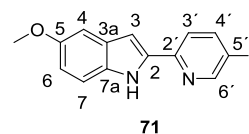
5.2.1.23 *tert*-butyl 5-(*tert*-butyldimethylsilyloxy)-2-(5-fluoropyridin-2-yl)-1*H*-indole-1-carboxylate (**70**)



Sodium carbonate (1.53 g, 14.44 mmol), and tetrakis(triphenylphosphine)palladium (350 mg, 0.303 mmol) were reacted with the boronic acid **56** (2.25 g, 5.76 mmol) dissolved in dimethoxyethane : water (30 mL, 4:1). 5-Fluoro-2-bromopyridine (0.95 g, 5.40 mmol) was added and the entire reaction mixture refluxed for 16 h. The dark red suspension was cooled to ambient temperature and diluted with water (25 mL). The organic layer was separated. The aqueous layer was extracted with ethylacetate (4 x 25 mL), the combined organic layer was washed with BRINE (3 x 50 mL), dried over sodium sulfate. The crude material was concentrated *in vacuo* and subjected to column chromatography with hexane : ethylacetate (15:1). The product **70** was obtained as a colourless oil (1.52 g, 3.43 mmol, 60%). $R_f = 0.53$ (hexane : ethylacetate 15:1). 1H -NMR (300 MHz, $CDCl_3$): δ (ppm) 8.52 (dd, $J = 2.0, 1.0$, 1H, $CH_{ar-6'}$), 8.01 (d, $J = 8.9$ Hz, 1H, CH_{ar-7}), 7.53 - 7.42 (m, 2H, $CH_{ar-3'}, CH_{ar-4'}$), 7.00 (d, $J = 2.3$ Hz, 1H, CH_{ar-4}), 6.89 (dd, $J = 8.9, 2.4$, 1H, CH_{ar-6}), 6.64 (s, 1H, CH_{ar-3}), 1.37 (s, 9H, $OC_q(CH_3)_3$), 1.00 (s, 9H, $SiC_q(CH_3)_3$), 0.20 (s, 6H, $Si(CH_3)_2$). ^{13}C -NMR (75 MHz, $CDCl_3$): δ (ppm) 158.72 (d, $J = 256$ Hz, $C_{ar-5'}$), 151.78 ($C_{carbonyl}$), 150.06 (C_{ar-5}), 149.71 (d, $J = 3.9$ Hz, $C_{ar-2'}$), 138.78 (C_{ar-2}), 137.23 (d, $J = 23.7$ Hz, $C_{ar-6'}$), 132.98 (C_{ar-7a}), 129.79 (C_{ar-3a}), 124.47 (d, $J = 4.4$ Hz, $C_{ar-3'}$), 122.99 (d, $J = 18.79$ Hz,

$C_{ar-4'}$), 118.77 (C_{ar-6}), 115.91 (C_{ar-7}), 111.28 (C_{ar-4}), 110.99 (C_{ar-3}), 83.59 ($OC_q(CH_3)_3$), 27.86 ($OC_q(CH_3)_3$), 25.91 ($SiC_q(CH_3)_3$), 18.40 ($SiC_q(CH_3)_3$), -4.28 ($Si(CH_3)_2$). HRMS calculated for $C_{24}H_{31}FN_2O_3SiNa$ ($M + Na^+$) 465.1980 found ($M + Na^+$) 465.1981.

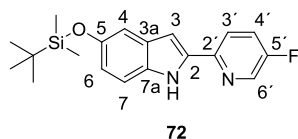
5.2.1.24 2-(5-fluoropyridin-2-yl)-5-methoxy-1*H*-indole (**71**)



Sodium carbonate (4.5 g, 42.5 mmol), and tetrakis(triphenylphosphine)palladium (1.9 g, 1.7 mmol) were reacted with the boronic acid **58** (4.95 g, 17 mmol) dissolved in dimethoxyethane : water (72 mL, 4:1). 2-Bromo-5-fluoropyridine (2.69 g, 15.4 mmol) was added and the entire reaction mixture refluxed for 16 h. The dark yellow suspension was cooled to ambient temperature and diluted with water (50 mL). The organic layer was separated. The aqueous layer was extracted with ethylacetate (5 x 30 mL), the combined organic layer was washed with BRINE (3 x 50 mL), dried over sodium sulfate. The crude material was concentrated *in vacuo* and subjected to column chromatography using hexane : ethylacetate (10:1). The *tert*-butyloxycarbonyl protected intermediate was obtained as a brown oil (4.43 g, 12.9 mmol). The intermediate was dissolved in methylene chloride and subjected to silica gel (40 g). After complete removal of the solvent under reduced pressure, the soaked compound was heated to 80 °C *in vacuo* for 16 h. The silica gel was suspended in ethylacetate and filtrated over CELITE. The product was dried *in vacuo* to obtained **71** as a beige solid (3.24 g, 13.4 mmol, 79% over 2 steps). $R_f = 0.26$ (hexane : ethylacetate 8:1). 1H -NMR (300 MHz, $CDCl_3$): δ (ppm) 9.38 (bs, 1H, NH), 8.41 (d, $J = 2.9$ Hz, 1H, CH_{ar-}

6'), 7.75 (dd, $J = 8.8, 4.3$ Hz, 1H, $CH_{ar-3'}$), 7.47–7.40 (m, 1H, $CH_{ar-4'}$), 7.30 (d, $J = 8.8$ Hz, 1H, CH_{ar-7}), 7.09 (d, $J = 2.4$ Hz, 1H, CH_{ar-4}), 6.90 (dd, $J = 8.9, 2.5$ Hz, 1H, CH_{ar-6}), 6.88–6.86 (m, 1H, CH_{ar-3}), 3.87 (s, 3H, OCH_3). ^{13}C -NMR (75 MHz, $CDCl_3$): δ (ppm) 158.63 (d, $J = 255.7$ Hz, $C_{ar-5'}$), 154.72 (C_{ar-5}), 147.01 (d, $J = 3.9$ Hz, $C_{ar-2'}$), 137.17 (d, $J = 24.4$ Hz, $C_{ar-6'}$), 136.48 (C_{ar-2}), 132.11 (C_{ar-7a}), 129.68 (C_{ar-3a}), 124.01 (d, $J = 19.1$ Hz, $C_{ar-4'}$), 120.73 (d, $J = 4.3$ Hz, $C_{ar-3'}$), 114.13 (C_{ar-6}), 112.26 (C_{ar-7}), 102.66 (C_{ar-4}), 100.34 (C_{ar-3}), 55.98 (OCH_3). IR (film): ν (cm^{-1}) 3446, 1545, 1455, 1354, 1297, 1216, 1148, 1111, 1027, 942, 888, 825, 787, 738, 652, 616, 577, 516.

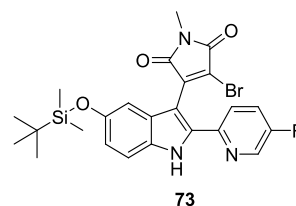
5.2.1.25 5-(*tert*-butyldimethylsilyloxy)-2-(5-fluoropyridin-2-yl)-1*H*-indole (**72**)



Pyridylindole **70** (1.44 g, 3.26 mmol) was dissolved in methylene chloride and subjected to silica gel (15 g). After complete removal of the solvent under reduced pressure, the soaked compound was heated to 80 °C *in vacuo* for 16 h. The silica gel was suspended in ethylacetate and filtrated over CELITE. The crude material was concentrated *in vacuo* and subjected to column chromatography with hexane : ethylacetate (6:1). The product **72** was dried *in vacuo* and obtained as a white solid (1.04 g, 3.04 mmol, 93%). $R_f = 0.40$ (hexane : ethylacetate 6:1). 1H -NMR (300 MHz, $CDCl_3$): δ (ppm) 9.35 (s, 1H, NH), 8.41 (d, $J = 2.8$ Hz, 1H, $CH_{ar-6'}$), 7.76 (dd, $J = 8.5, 4.3$ Hz, 1H, $CH_{ar-3'}$), 7.45 (ddd, $J = 8.7, 8.2, 2.9$ Hz, 1H, $CH_{ar-4'}$), 7.25 (d, $J = 8.7$ Hz, 1H, CH_{ar-7}), 7.06 (d, $J = 2.3$ Hz, 1H, CH_{ar-4}), 6.84 (d, $J = 1.4$ Hz, 1H, CH_{ar-3}), 6.80 (dd, $J = 8.7, 2.3$ Hz, CH_{ar-6}), 1.01 (s, 9H, $SiC_q(CH_3)_3$), 0.21 (s, 6H, $Si(CH_3)_2$). ^{13}C -NMR (75 MHz,

$CDCl_3$): δ (ppm) 158.59 (d, $J = 255.7$ Hz, $C_{ar-5'}$), 155.18 ($C_{ar-2'}$), 149.86 (C_{ar-5}), 136.99 (d, $J = 24.55$ Hz, $C_{ar-6'}$), 132.54 (C_{ar-2}), 132.53 (C_{ar-7a}), 129.85 (C_{ar-3a}), 124.18 (d, $J = 18.98$ Hz, $C_{ar-4'}$), 120.81 (d, $J = 4.46$, $C_{ar-3'}$), 118.12 (C_{ar-4}), 111.86 (C_{ar-6}), 110.40 (C_{ar-7}), 100.30 (C_{ar-3}), 25.96 ($SiC_q(CH_3)_3$), 18.40 ($SiC_q(CH_3)_3$), -4.25 ($Si(CH_3)_2$). IR (film): ν (cm^{-1}) 3457, 2957, 2858, 2251, 1625, 1549, 1459, 1385, 1288, 1229, 1152, 1118, 1010, 965, 903, 835, 784, 724, 650, 585, 527, 488, 440, 395. HRMS calculated for $C_{19}H_{23}FN_2OSiH$ ($M + H^+$) 343.1642 found ($M + H^+$) 343.1636.

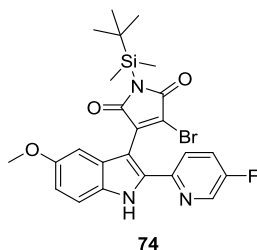
5.2.1.26 3-bromo-4-(5-(*tert*-butyldimethylsilyloxy)-2-(5-fluoropyridin-2-yl)-1*H*-indol-3-yl)-1-methyl-1*H*-pyrrole-2,5-dione (**73**)



72 (921 mg, 2.69 mmol) was dissolved in THF (8 mL) and cooled to -15 °C. Lithium bis(trimethylsilyl)amide (8.1 mL, 8.07 mmol, 1 M in hexane) was added drop wise over a period of 90 min and the solution turned from colourless to yellow. **38** (796 mg, 2.96 mmol) was dissolved in THF (5 mL) and added drop wise to the reaction mixture over a period of 20 min. An immediate colour change from yellow to dark purple was observed. The reaction mixture was protected from light and stirred for 1 h at -15 °C followed by 16 h at ambient temperature. The reaction was finished by pouring the entire reaction mixture into ice cooled hydrochloric acid (63 mL). The organic layer was separated and the aqueous layer was extracted with ethylacetate (4 x 50 mL). The combined organic layer was washed with BRINE (3 x 50 mL), and

dried over sodium sulfate. The crude material was concentrated in vacuo and subjected to column chromatography hexane : ethylacetate (6:1 \rightarrow 1:1). The product **73** was dried in vacuo and obtained as a red solid (923 mg, 1.74 mmol, 65%). R_f = 0.26 (hexane : ethylacetate 3:1). Due to its light sensitivity the mono bromide intermediate was directly processed to the cyclisation reaction without further characterisation.

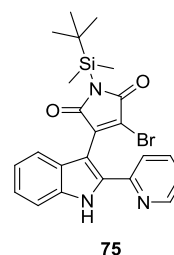
5.2.1.27 3-bromo-1-(*tert*-butyldimethylsilyl)-4-(2-(5-fluoropyridin-2-yl)-5-methoxy-1*H*-indol-3-yl)-1*H*-pyrrole-2,5-dione (**74**)



71 (3.25 g, 13.4 mmol) was dissolved in THF (40 mL) and cooled to -15°C . Lithium bis(trimethylsilyl)amide (40 mL, 40 mmol, 1 M in hexane) was added drop wise over a period of 90 min and the solution turned from colourless to yellow. **42** (5.43 g, 14.74 mmol) was dissolved in THF (30 mL) and added drop wise to the reaction mixture over a period of 30 min. An immediate colour change from yellow to dark purple was observed. The reaction mixture was protected from light and stirred for 1 h at -15°C followed by 16 h at ambient temperature. The reaction was finished by pouring the entire reaction mixture into ice cooled hydrochloric acid (400 mL). The organic layer was separated and the aqueous layer was extracted with ethylacetate (5 x 75 mL). The combined organic layer was washed with BRINE (3 x 50 mL), and dried over sodium sulfate. The crude material was concentrated in vacuo and subjected to column chromatography using hex-

ane : ethylacetate (8:1 \rightarrow 1:1). The product **74** was dried *in vacuo* and obtained as a red solid (5.03 g, 9.46 mmol, 71%). R_f = 0.78 (hexane : ethylacetate 1:1). Due to its light sensitivity the mono bromide intermediate was directly proceeded to the cyclisation reaction without further characterisation.

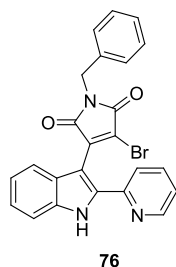
5.2.1.28 3-bromo-1-(*tert*-butyldimethylsilyl)-4-(2-(pyridin-2-yl)-1*H*-indol-3-yl)-1*H*-pyrrole-2,5-dione (**75**)



46 (875 g, 4.5 mmol) was dissolved in THF (15 mL) and cooled to -15°C . Lithium bis(trimethylsilyl)amide (13.5 mL, 1 M in hexane) was added drop wise over a period of 45 min and the solution turned from colourless to yellow. **42** (1.85 g, 5.0 mmol) was dissolved in THF (20 mL) and added drop wise to the reaction mixture over a period of 20 min. An immediate colour change from yellow to dark purple was observed. The reaction mixture was protected from light and stirred for 1 h at -15°C followed by 16 h at ambient temperature. The reaction mixture turned into a dark purple colour. The reaction was finished by pouring the entire reaction mixture into ice cooled hydrochloric acid (135 mL). The organic layer was separated and the aqueous layer was extracted with ethylacetate (5 x 50 mL). The combined organic layer was washed with BRINE (3 x 50 mL), and dried over sodium sulfate. The crude material was concentrated *in vacuo* and subjected to column chromatography using hexane : ethylacetate (6:1 \rightarrow 1:1). The product was dried *in vacuo* and obtained as a red solid (1.47 g, 3.1 mmol, 68%). Due to its light sensitivity the mono

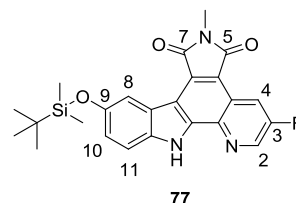
bromide intermediate was directly proceeded to the cyclisation reaction without further characterisation.

5.2.1.29 1-benzyl-3-bromo-4-(2-(pyridin-2-yl)-1H-indol-3-yl)-1H-pyrrole-2,5-dione (**76**)



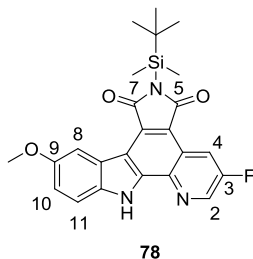
46 (1.1 g, 5.68 mmol) was dissolved in THF (14.5 mL) and cooled to -15°C . Lithium bis(trimethylsilyl)amide (25 mL, 1 M in hexane) was added drop wise over a period of 90 min and the solution turned from colourless to yellow. **37** (2.05 g, 5.95 mmol) was dissolved in THF (18 mL) and added drop wise to the reaction mixture over a period of 20 min. An immediate colour change from yellow to dark red was observed. The reaction mixture was protected from light and stirred for 1 h at -15°C followed by 16 h at ambient temperature. The reaction mixture turned into a dark purple colour. The reaction was finished by pouring the entire reaction mixture into ice cooled hydrochloric acid (125 mL). The organic layer was separated and the aqueous layer was extracted with ethylacetate (4 x 50 mL). The combined organic layer was washed with BRINE (3 x 50 mL), and dried over sodium sulfate. The crude material was concentrated *in vacuo* and subjected to column chromatography using hexane : ethylacetate (3:1 \rightarrow 1:1). The product **76** was dried *in vacuo* and obtained as a orange solid (1.4 mg, 3.7 mmol, 54%). $R_f = 0.51$ (hexane : ethylacetate 3:1). Due to its light sensitivity the mono bromide intermediate was directly proceeded to the cyclisation reaction without further characterisation.

5.2.1.30 9-(tert-butyldimethylsilyloxy)-3-fluoro-6-methylpyrido[2,3-a]pyrrolo[3,4-c]carbazole-5,7(6H,12H)-dione (**77**)



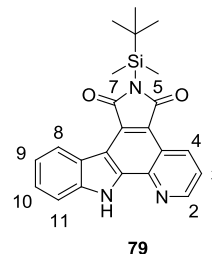
Mono bromide **73** (860 mg, 1.62 mmol) was suspended in toluene (900 mL), continuously purged with nitrogen and subjected 2 h to an iron iodide endowed mercury UV lamp (700 W, $\lambda_{\text{max}} = 350 \text{ nm}$) under intensive stirring and water cooling in a UV reactor. The crude material was concentrated under reduced pressure and subjected to column chromatography using methylene chloride : methanol (100:0 \rightarrow 20:1). The product **77** was dried *in vacuo* and obtained as an orange solid (388 mg, 0.86 mmol, 53%). $R_f = 0.39$ (methylene chloride 100%). $^1\text{H-NMR}$ (300 MHz, $\text{CDCl}_3/(\text{CD}_3)_2\text{SO}$ (4:1)): δ (ppm) 8.65 (dd, $J = 6.3, 2.7 \text{ Hz}$, 2H, $\text{CH}_{\text{ar-2}}, \text{CH}_{\text{ar-4}}$), 8.24 (d, $J = 2.3 \text{ Hz}$, 1H, $\text{CH}_{\text{ar-8}}$), 7.48 (d, $J = 8.6 \text{ Hz}$, 1H, $\text{CH}_{\text{ar-11}}$), 6.99 (dd, $J = 8.7, 2.4 \text{ Hz}$, 1H, $\text{CH}_{\text{ar-10}}$), 3.10 (s, 3H, NCH_3), 0.97 (s, 9H, $\text{SiC}_q(\text{CH}_3)_3$), 0.23 (s, 6H, $\text{Si}(\text{CH}_3)_2$). $^{13}\text{C-NMR}$ (75 MHz, $\text{CDCl}_3/(\text{CD}_3)_2\text{SO}$ (4:1)): δ (ppm) 168.90 ($\text{C}_{\text{ar-7}}$), 168.04 ($\text{C}_{\text{ar-5}}$), 156.80 (d, $J = 257.7 \text{ Hz}$, $\text{C}_{\text{ar-3}}$), 149.83 ($\text{C}_{\text{ar-9}}$), 140.20 (C_{ar}), 139.79 (d, $J = 27.6 \text{ Hz}$, $\text{C}_{\text{ar-2}}$), 135.05 (C_{ar}), 134.11 (C_{ar}), 128.67 (C_{ar}), 121.46 (C_{ar}), 121.29 (C_{ar}), 121.20 (C_{ar}), 120.51 (C_{ar}), 116.02 (d, $J = 19.0 \text{ Hz}$, $\text{C}_{\text{ar-4}}$), 113.22 (C_{ar}), 112.20 (C_{ar}), 25.29 ($\text{SiC}_q(\text{CH}_3)_3$), 23.13 (NCH_3), 17.70 ($\text{SiC}_q(\text{CH}_3)_3$), -4.88 ($\text{Si}(\text{CH}_3)_2$). IR (film): ν (cm^{-1}) 3322, 2931, 2892, 2857, 1753, 1689, 1620, 1566, 1527, 1468, 1442, 1415, 1373, 1331, 1279, 1250, 1219, 1167, 1125, 959, 891. HRMS calculated for $\text{C}_{24}\text{H}_{25}\text{FN}_3\text{O}_3\text{Si}$ ($\text{M} + \text{H}^+$) 450.1644 found ($\text{M} + \text{H}^+$) 450.1664.

5.2.1.31 6-(*tert*-butyldimethylsilyl)-3-fluoro-9-methoxypyrido[2,3-*a*]pyrrolo[3,4-*c*]carbazole-5,7(6*H*,12*H*)-dione (**78**)



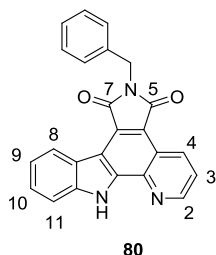
74 (2.2 g, 4.15 mmol) were dissolved in toluene (900 mL), continuously purged with nitrogen and subjected 5 h to an iron iodide endowed mercury UV lamp (700 W, $\lambda_{\text{max}} = 350$ nm) under intensive stirring and water cooling in a UV reactor. The orange coloured crude material was concentrated under reduced pressure and subjected to column chromatography using methylene chloride : methanol (100:1 \rightarrow 10:1). The product **78** was dried *in vacuo* and obtained as an orange solid (1.25 g, 2.7 mmol, 67%). $R_f = 0.42$ (hexane : ethylacetate 3:1). $^1\text{H-NMR}$ (300 MHz, CDCl_3): δ (ppm) 10.12 (bs, NH), 9.27 (dd, $J = 9.1, 2.6$ Hz, 1H, $\text{CH}_{\text{ar-4}}$), 8.89 (d, $J = 2.7$ Hz, 1H, $\text{CH}_{\text{ar-2}}$), 8.61 (d, $J = 2.2$ Hz, 1H, $\text{CH}_{\text{ar-8}}$), 7.63 (d, $J = 8.9$ Hz, 1H, $\text{CH}_{\text{ar-11}}$), 7.29 (m, 1H, $\text{CH}_{\text{ar-10}}$), 4.04 (s, 3H, OCH_3), 1.06 (s, 9H, $\text{SiC}_q(\text{CH}_3)_3$), 0.63 (s, 6H, $\text{Si}(\text{CH}_3)_2$). IR (film): ν (cm^{-1}) 3443, 2929, 2855, 1744, 1687, 1627, 1557, 1528, 1473, 1412, 1363, 1337, 1305, 1252, 1213, 1179, 1153, 1035, 938, 904, 823, 804. HRMS calculated for $\text{C}_{24}\text{H}_{25}\text{FN}_3\text{O}_3\text{Si}$ ($\text{M} + \text{H}^+$) 450.1644 found ($\text{M} + \text{H}^+$) 450.1644.

5.2.1.32 6-(*tert*-butyldimethylsilyl)pyrido[2,3-*a*]pyrrolo[3,4-*c*]carbazole-5,7(6*H*,12*H*)-dione (**79**)



Mono bromide **75** (1.00 g, 2.08 mmol) was suspended in toluene (900 mL), continuously purged with nitrogen and subjected 3 h to an iron iodide endowed mercury UV lamp (700 W, $\lambda_{\text{max}} = 350$ nm) under intensive stirring and water cooling in a UV reactor. The crude material was concentrated under reduced pressure and subjected to column chromatography using methylene chloride : methanol (100:0 \rightarrow 20:1). The product **79** was dried *in vacuo* and obtained as an orange solid (526 mg, 1.31 mmol, 63%). $R_f = 0.71$ (methylene chloride : methanol 15:1). $^1\text{H-NMR}$ (300 MHz, CDCl_3): δ (ppm) 10.27 (bs, 1H, NH), 9.41 (dd, $J = 8.6$ Hz, $J = 1.6$ Hz, 1H, CH_{ar}), 9.09 (d, $J = 7.9$ Hz, 1H, CH_{ar}), 9.02 (dd, $J = 4.2$ Hz, $J = 1.7$ Hz, 1H, CH_{ar}), 7.65 (dd, $J = 8.4$ Hz, $J = 4.3$ Hz, 1H, CH_{ar}), 7.65–7.54 (m, 2H, CH_{ar}), 7.45–7.40 (m, 1H, CH_{ar}), 1.07 (s, 9H, $\text{SiC}_q(\text{CH}_3)_3$), 0.64 (s, 6H, $\text{Si}(\text{CH}_3)_2$). $^{13}\text{C-NMR}$ (75 MHz, CDCl_3): δ (ppm) 175.5 ($\text{C}_{\text{ar-7}}$), 173.9 ($\text{C}_{\text{ar-5}}$), 150.4, 140.1, 139.7, 138.5, 134.5, 130.8, 127.3, 125.7, 122.8, 122.3, 121.7, 121.9, 120.9, 115.3, 111.6, 26.6 ($\text{SiC}_q(\text{CH}_3)_3$), 19.1 ($\text{SiC}_q(\text{CH}_3)_3$), -4.0 ($\text{Si}(\text{CH}_3)_2$). HRMS calculated for $\text{C}_{23}\text{H}_{24}\text{N}_3\text{O}_2\text{Si}$ ($\text{M} + \text{H}^+$) 402.1632 found ($\text{M} + \text{H}^+$) 402.1632.

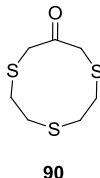
5.2.1.33 6-benzylpyrido[2,3-a]pyrrolo[3,4-c]carbazole-5,7(6H,12H)-dione (**80**)



76 (334 mg, 729 μmol) were dissolved in toluene (900 mL), continuously purged with nitrogen and subjected 2.5 h to an iron iodide endowed mercury UV lamp (700 W, $\lambda_{\text{max}} = 350 \text{ nm}$) under intensive stirring and water cooling in a UV reactor. The orange coloured crude material was concentrated under reduced pressure and subjected to column chromatography using methylene chloride : methanol (100:1 \rightarrow 10:1). The product **80** was dried *in vacuo* and obtained as an orange solid (220 mg, 583 μmol , 80%). $R_f = 0.28$ (hexane : ethylacetate 1:1). $^1\text{H-NMR}$ (300 MHz, CDCl_3): $\delta(\text{ppm})$ 10.40 (s, 1H, NH), 9.28 (dd, $J = 8.5, 1.6$, Hz, 1H, CH_{ar}), 8.93 (d, $J = 8.0$ Hz, 1H, CH_{ar}), 8.89 (dd, $J = 1.6, 4.3$ Hz, 1H, CH_{ar}), 7.58-7.50 (m, 5H, CH_{ar}), 7.41-7.28 (m, 4H, CH_{ar}), 4.94 (s, 2H, $\text{CH}_{\text{benzyl}}$). IR (film): $\nu(\text{cm}^{-1})$ 3334, 2924, 2853, 2078, 1754, 1695, 1640, 1529, 1499, 1461, 1430, 1385, 1334, 1295, 1234, 1145, 1104, 1070, 976, 934, 796, 737, 694, 624, 498. HRMS calculated for $\text{C}_{24}\text{H}_{15}\text{N}_3\text{O}_2\text{Na}$ ($\text{M} + \text{Na}^+$) 400.1062 found ($\text{M} + \text{Na}^+$) 400.1056.

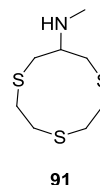
5.2.2 Synthesis of ligands and related intermediates

5.2.2.1 1,4,7-trithiacyclodecan-9-one (**90**)



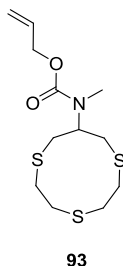
Caesium Carbonate (860 mg, 2.64 mmol) were suspended in 150 mL freshly distilled DMF and heated to 60 °C under a nitrogen atmosphere. The reaction mixture was stirred continuously while 2,2'-thiodiethanthiol (311 μ L, 2.39 mmol) and 1,3-dichloroacetone (304.5 mg, 2.39 mmol) were added dropwise via a dropping funnel diluted in a total amount of 150 mL DMF. The drop wise addition of the reactants was performed over a time period of 8 h followed by an additional 8 h of stirring at 60 °C. The white suspension turned into a pale red solution. The reaction mixture was concentrated to dryness *in vacuo*. The crude product was adsorbed onto silica gel and purified by column chromatography using hexane : ethylacetate (3:1). The combined product eluents were dried *in vacuo* to provide **90** as a white solid (229 mg, 1.09 mmol, 46%). R_f = 0.47 (hexane : ethylacetate 3:1). $^1\text{H-NMR}$ (300 MHz, CDCl_3): δ (ppm) 3.53 (s, 4H, $2 \times \text{SCH}_2\text{CO}$), 2.72 (s, 8H, $4 \times \text{CH}_2$). $^{13}\text{C-NMR}$ (75.5 MHz, CDCl_3): δ (ppm) 199.84 ($\text{C}_{\text{carbonyl}}$), 37.68, 32.03, 31.35. IR (film): ν (cm^{-1}) 2961, 1695, 1417, 1394, 1365, 1252, 1193, 1144, 1070, 680, 565, 485. HRMS calculated for $\text{C}_8\text{H}_{12}\text{OS}_3\text{Na}$ ($\text{M} + \text{Na}$) $^+$ 230.9948, found ($\text{M} + \text{Na}$) $^+$ 230.9975.

5.2.2.2 N-methyl-1,4,7-trithiacyclodecan-9-amine (**91**)



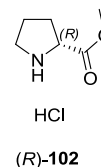
Potassium carbonate (548 mg, 3.97 mmol) was added to a solution of $\text{MeNH}_2 \cdot \text{HCl}$ (268 mg, 3.97 mmol) stirring in methanol (5 mL) at 0 °C under a nitrogen atmosphere. The resulting mixture was stirred at 0 °C for an additional 1 hour, followed by the addition of **90** (694.8 mg, 3.33 mmol) in methanol (45 mL). The suspension was then stirred at 34 °C for 1 hour. After the addition of NaBH_3CN (419 mg, 6.66 mmol) the reaction mixture was stirred over night at 34 °C. After the addition of saturated NaHCO_3 (25 mL) the crude product was extracted using methylene chloride (3 x 50 mL). The combined organic layers were dried using Na_2SO_4 , filtered and concentrated to dryness *in vacuo*. The crude material was adsorbed onto silica gel and subjected to silica gel chromatography with methylene chloride : methanol (35:1 \rightarrow 20:1). The combined product eluents were dried *in vacuo* to provide **91** (271 mg, 1.21 mmol, 36%) as a pale oil. R_f = 0.21 (methylene chloride : methanol 15:1). $^1\text{H-NMR}$ (300 MHz, CDCl_3): δ (ppm) 3.34-2.86 (m, 13H), 2.82 (br, 1H, NHCH_3), 2.51 (s, 3H, NHCH_3). $^{13}\text{C-NMR}$ (75.5 MHz, CDCl_3): δ (ppm) 59.85 (CNHCH_3), 34.33, 34.22, 34.09, 34.05. IR (film): ν (cm^{-1}) 3381, 3321, 2919, 1697, 1415, 1264, 1188, 1129, 1066, 1025, 951, 812, 685, 507, 429. HRMS calculated for $\text{C}_8\text{H}_{18}\text{NS}_3$ ($\text{M} + \text{H}$) $^+$ 224.0596, found ($\text{M} + \text{H}$) $^+$ 224.0596.

5.2.2.3 Allyl-N-methyl-(1,4,7-trithiacyclo-decan-9-y)carbamate (**93**)



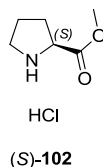
To a solution of **91** (271 mg, 1.21 mmol) in methylene chloride (9 mL) at 0 °C were added allyl chloroformate (**92**) (194 μ L, 1.82 mmol), pyridine (98 μ L, 1.21 mmol), and 4-dimethylaminopyridine (7 mg, 57 μ mol) under a nitrogen atmosphere. The resulting mixture solution was then allowed to warm up to ambient temperature slowly and stirred overnight. The solution was diluted with methylene chloride and washed with water (3 x 20 mL) and brine (3 x 20 mL). The organic layer was separated and dried using Na₂SO₄, filtered and concentrated to dryness *in vacuo*. The crude material was subjected to silica gel chromatography using hexane : ethyl acetate (10:1 \rightarrow 8:1). The product **93** (259 mg, 844 μ mol, 70%) was obtained as a pale oil. R_f = 0.47 (hexane : ethylacetate 3:1). ¹H-NMR (300 MHz, CDCl₃): δ (ppm) 6.01–5.88 (m, 1H, CCH₂), 5.34–5.19 (m, 2H, CCH₂), 4.60 (d, J = 5.5 Hz, 2H, CH₂_{allyl}), 3.29–3.00 (m, 13H), 2.88 (s, 3H, NCH₃). ¹³C-NMR (75.5 MHz, CDCl₃): δ (ppm) 71.0, 70.5, 70.4, 38.4, 36.7, 34.1, 33.8, 33.1, 32.4. IR (film): ν (cm⁻¹) 2910, 1692, 1448, 1399, 1321, 1266, 1231, 1198, 1145, 992, 928, 768. HRMS calculated for C₁₂H₂₁NO₂S₃Na (M + Na)⁺ 330.0627, found (M + Na)⁺ 330.0626.

5.2.2.4 (*R*)-methyl pyrrolidine-2-carboxylate hydrochloride ((*R*)-**102**)



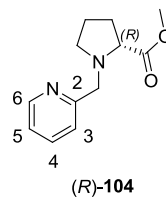
(*R*)-pyrrolidine-2-carboxylic acid (2.00 g, 17.4 mmol) was suspended in methanol (25.0 mL) and thionylchloride (1.52 mL, 20.8 mmol) was added drop wise at 0 °C. The reaction mixture was refluxed for 18 h. The solvent was removed under reduced pressure and the residue resolved in methanol (10.0 mL) then concentrated again under reduced pressure. This procedure was repeated three times. The product (*R*)-**102** was obtained as white solid (2.91 g, 17.6 mmol, quant.). R_f = 0.41 (methylene chloride : methanol 5:1). ¹H-NMR (300 MHz, CD₃OD): δ (ppm) 4.29 (s, 3H, OCH₃), 3.89 (m, 1H, CH_α), 2.90–2.78 (m, 2H), 1.98–1.80 (m, 1H), 1.68–1.46 (m, 3H). ¹³C-NMR (75 MHz, CD₃OD): δ (ppm) 170.47 (C_{carbonyl}), 60.67 (C_α), 53.94 (OCH₃), 47.16 (C_δ), 29.26 (C_β), 24.49 (C_γ). IR (film): ν (cm⁻¹) 3396, 2917, 2732, 2555, 1738, 1632, 1568, 1441, 1389, 1356, 1287, 1234, 1091, 1042, 1002, 918, 859, 658, 551, 459. HRMS calculated for C₆H₁₂NO₂ (M + H)⁺ 180.0863 found (M + H)⁺ 180.0863.

5.2.2.5 (S)-methyl pyrrolidine-2-carboxylate hydrochloride ((S)-**102**)



(S)-pyrrolidine-2-carboxylic acid (5.00 g, 43.5 mmol) was suspended in methanol (50.0 mL) and thionylchloride (3.17 mL, 43.5 mmol) was added drop wise at 0 °C. The reaction mixture was refluxed for 16 h. The solvent was removed under reduced pressure and the residue resolved in methanol (10.0 mL) then concentrated again under reduced pressure. This procedure was repeated three times. The product (S)-**102** was obtained as white solid (6.95 g, 42.0 mmol, 96%). R_f = 0.41 (methylene chloride : methanol 5:1). $^1\text{H-NMR}$ (300 MHz, CD_3OD): δ (ppm) 10.84 (s, 1H, NHH), 8.68 (s, 1H, NHH), 4.39–4.23 (m, 1H, CH_α), 3.68 (s, 3H, OCH_3), 3.48–3.33 (m, 2H), 2.34–2.20 (m, 1H), 2.07–1.81 (m, 3H). $^{13}\text{C-NMR}$ (75 MHz, CD_3OD): δ (ppm) 170.45 ($\text{C}_{\text{carbonyl}}$), 60.69 (C_α), 53.95 (OCH_3), 47.19 (C_δ), 29.27 (C_β), 24.51 (C_γ). IR (film): ν (cm^{-1}) 3403, 2952, 2731, 2551, 1739, 1632, 1569, 1443, 1389, 1355, 1234, 1091, 1046, 1003, 918, 862, 730. HRMS calculated for $\text{C}_6\text{H}_{12}\text{NO}_2$ ($\text{M} + \text{H}^+$) 130.0863 found ($\text{M} + \text{H}^+$) 130.0867.

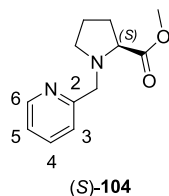
5.2.2.6 (R)-methyl 1-(pyridin-2-ylmethyl)pyrrolidine-2-carboxylate ((R)-**104**)



Palladium on carbon (460 mg, 0.4 mmol, 10 wt. %) was suspended in methanol (30.0 mL) and picolinaldehyde (**103**) (1.37 mL, 14.3 mmol) was added at 0 °C. Sodium acetate (2.34 g, 28.6 mmol) was added to the reaction mixture. Then, (R)-**102** (2.00 g, 14.3 mmol) was added. The reaction mixture was stirred for 1 h and the nitrogen atmosphere was completely substituted by hydrogen in three turns. The reaction was continued for 16 h allowing the mixture to warm up to ambient temperature. The reaction mixture was filtrated over CELITE and the crude material was subjected to column chromatography using methylene chloride : methanol (35:1 \rightarrow 10:1). The product (R)-**104** was obtained as a brown oil (1.92 g, 8.73 mmol, 61%). R_f = 0.45 (methylene chloride : methanol 15:1). $^1\text{H-NMR}$ (300 MHz, CDCl_3): δ (ppm) 8.53 (dd, J = 4.8, 0.7 Hz, 1H, $\text{CH}_{\text{ar-6}}$), 7.65 (td, J = 7.7, 1.8 Hz, 1H, $\text{CH}_{\text{ar-4}}$), 7.46 (d, J = 7.8 Hz, 1H, $\text{CH}_{\text{ar-3}}$), 7.20 – 7.12 (m, 1H, $\text{CH}_{\text{ar-5}}$), 4.05 (d, J = 13.5 Hz, 1H, NCHH), 3.79 (d, J = 13.5 Hz, 1H, NCHH), 3.66 (s, 3H, OCH_3), 3.49 – 3.33 (m, 1H, CH_α), 3.18 – 3.03 (m, 1H), 2.54 (dd, J = 16.7, 7.9 Hz, 1H), 2.26 – 2.09 (m, 1H), 2.05 – 1.72 (m, 3H). $^{13}\text{C-NMR}$ (75 MHz, CDCl_3): δ (ppm) 174.21 ($\text{C}_{\text{carbonyl}}$), 158.24 ($\text{C}_{\text{ar-2}}$), 148.65 ($\text{C}_{\text{ar-6}}$), 136.96 ($\text{C}_{\text{ar-4}}$), 123.83 ($\text{C}_{\text{ar-3}}$), 122.41 ($\text{C}_{\text{ar-5}}$), 65.33 (NCH_2), 59.76 (C_α), 53.56 (OCH_3), 51.87 (C_δ), 29.33 (C_β), 23.24 (C_γ). IR (film): ν (cm^{-1}) 3380, 3056, 2953, 1665, 1628, 1590, 1570, 1529, 1474, 1435, 1384, 1306, 1205, 1151, 1090, 1047, 995, 927, 888, 824, 752. HRMS calculated for

$C_{12}H_{17}N_2O_2$ ($M + H^+$) 221,1285 found
($M + H^+$) 221.1286.

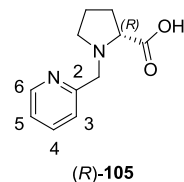
5.2.2.7 (*S*)-methyl 1-(pyridin-2-ylmethyl)
pyrrolidine-2-carboxylate ((*S*)-**104**)



Palladium on carbon (293 mg, 0.25 mmol, 10 wt. %) was suspended in methanol (20.0 mL) and picolinaldehyde (**103**) (870 μ L, 9.1 mmol) was added at 0 °C. Sodium acetate (1.5 g, 18.3 mmol) was added to the reaction mixture. Then, (*S*)-**102** (1.3 g, 9.1 mmol) was added. The reaction mixture was stirred for 1 h and the nitrogen atmosphere was completely substituted by hydrogen in three turns. The reaction was continued for 16 h allowing the mixture to warm up to ambient temperature. The reaction mixture was filtrated over CELITE and the crude material was subjected to column chromatography using methylene chloride : methanol (35:1 \rightarrow 10:1). The product (*S*)-**104** was obtained as a brown oil (1.83 g, 8.31 mmol, 58%). R_f = 0.45 (methylene chloride : methanol 15:1). 1H -NMR (300 MHz, $CDCl_3$): δ (ppm) 8.52 – 8.43 (m, 1H, CH_{ar-6}), 7.59 (td, J = 7.7, 1.8 Hz, 1H, CH_{ar-4}), 7.39 (d, J = 7.8 Hz, 1H, CH_{ar-3}), 7.09 (dd, J = 6.8, 5.5 Hz, 1H, CH_{ar-5}), 3.99 (d, J = 13.5 Hz, 1H, NCHH), 3.72 (d, J = 13.5 Hz, 1H, NCHH), 3.60 (s, 3H, OCH_3), 3.36 – 3.27 (m, 1H, CH_α), 3.11 – 2.99 (m, 1H), 2.47 (dd, J = 16.7, 7.9 Hz, 1H), 2.20 – 2.03 (m, 1H), 1.99 – 1.85 (m, 2H), 1.84 – 1.68 (m, 1H). ^{13}C -NMR (75 MHz, $CDCl_3$): δ (ppm) 174.49 ($C_{carbonyl}$), 158.96 (C_{ar-2}), 149.01 (C_{ar-6}), 136.39 (C_{ar-4}), 123.35 (C_{ar-3}), 122.01 (C_{ar-5}), 65.38 (NCH_2), 60.29 (C_α), 53.50 (OCH_3), 51.66 (C_δ), 29.38 (C_β), 23.31 (C_γ). IR (film): ν (cm^{-1}) 2952, 2877, 2814, 1735, 1591, 1470, 1434, 1362, 1276, 1197, 1169,

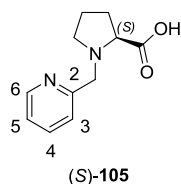
1089, 1041, 996, 929, 893, 836, 757, 698, 622, 469, 403.

5.2.2.8 (*R*)-1-(pyridin-2-ylmethyl)pyrrolidine-2-carboxylic acid ((*R*)-**105**)



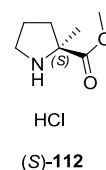
(*R*)-**104** (2.40 g, 11.0 mmol) was suspended in sodium hydroxide (15.0 mL, 1 M) at 0 °C and reacted for 18 h. The reaction mixture was washed with methylene chloride (5 x 20 mL). The combined aqueous layer was neutralised to pH 7 with hydrochloric acid (1 M). The aqueous layer was concentrated and the solvent removed under reduced pressure. The residue was suspended in ethanol (10.00 mL) and filtrated via a syringe filter. The residue was dried *in vacuo* to obtain the product (*R*)-**105** as a brown oil (2.06 g, 10.0 mmol, 91%). R_f = 0.05 (methylene chloride : methanol 10:1). 1H -NMR (300 MHz, CD_3OD): δ (ppm) 8.21 (d, J = 4.8 Hz, 1H, CH_{ar-6}), 7.45 (td, J = 7.7, 1.7 Hz, 1H, CH_{ar-4}), 7.13 (d, J = 7.8 Hz, 1H, CH_{ar-3}), 7.01 (dd, J = 7.6, 4.9 Hz, 1H, CH_{ar-5}), 4.22 (d, J = 13.9 Hz, 1H, NCHH), 4.09 (d, J = 13.9 Hz, 1H, NCHH), 3.37 – 3.26 (m, 1H, CH_α), 2.93–2.77 (m, 1H), 2.15–1.97 (m, 1H), 1.86–1.66 (m, 2H), 1.65–1.45 (m, 1H). ^{13}C -NMR (75 MHz, CD_3OD): δ (ppm) 173.29 ($C_{carbonyl}$), 152.36 (C_{ar-2}), 150.84 (C_{ar-6}), 138.88 (C_{ar-4}), 125.38 (C_{ar-3}), 125.32 (C_{ar-5}), 70.61 (NCH_2), 59.78 (C_α), 55.99 (C_δ), 29.98 (C_β), 24.40 (C_γ). IR (film): ν (cm^{-1}) 3374, 2982, 1620, 1440, 1390, 1316, 1209, 1157, 1098, 1052, 996, 928, 831, 76. HRMS calculated for $C_{11}H_{14}N_2O_2Na$ ($M + Na^+$) 229.0947 found ($M + Na^+$) 229.0946.

5.2.2.9 (S)-1-(pyridin-2-ylmethyl)pyrrolidine-2-carboxylic acid ((S)-**105**)



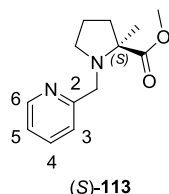
(S)-**104** (1.20 g, 5.5 mmol) were suspended in sodium hydroxide (7.08 mL, 1 M) at 0 °C and reacted for 16 h. The reaction mixture was washed with methylene chloride (3 x 20 mL). The combined aqueous layer was neutralised to pH 7 with hydrochloric acid (1 M). The aqueous layer was concentrated and the solvent removed under reduced pressure. The residue was suspended in ethanol (10.00 mL) and filtrated via a syringe filter. The residue was dried *in vacuo* to obtain the product (S)-**105** as brown oil (1.09 mg, 5.4 mmol, quant.). $R_f = 0.05$ (methylene chloride : methanol 10:1). $^1\text{H-NMR}$ (300 MHz, CD_3OD): δ (ppm) 8.63 (ddd, $J = 4.9, 1.5, 0.9$ Hz, 1H, $\text{CH}_{\text{ar-6}}$), 7.87 (td, $J = 7.7, 1.8$ Hz, 1H, $\text{CH}_{\text{ar-4}}$), 7.52 (d, $J = 7.8$ Hz, 1H, $\text{CH}_{\text{ar-3}}$), 7.42 (ddd, $J = 7.6, 4.9, 0.9$ Hz, 1H, $\text{CH}_{\text{ar-5}}$), 4.59 (d, $J = 13.9$ Hz, 1H, NCHH), 4.38 (d, $J = 13.9$ Hz, 1H, NCHH), 4.01 (dd, $J = 8.9, 6.2$ Hz, 1H), 3.72–3.62 (m, 1H), 3.22–3.11 (m, 1H), 2.53–2.36 (m, 1H), 2.24–1.91 (m, 3H). $^{13}\text{C-NMR}$ (75 MHz, CD_3OD): δ (ppm) 173.35 ($\text{C}_{\text{carbonyl}}$), 151.96 ($\text{C}_{\text{ar-2}}$), 151.04 ($\text{C}_{\text{ar-6}}$), 138.85 ($\text{C}_{\text{ar-4}}$), 125.38 ($\text{C}_{\text{ar-3}}$), 125.17 ($\text{C}_{\text{ar-5}}$), 70.57 (NCH_2), 59.78 (C_α), 55.99 (C_δ), 29.98 (C_β), 24.40 (C_γ). IR (film): ν (cm^{-1}) 3368, 2973, 1675, 1479, 1435, 1395, 1301, 1215, 1151, 997, 621, 571, 485, 401. HRMS calculated for $\text{C}_{11}\text{H}_{14}\text{N}_2\text{O}_2\text{Na}$ ($\text{M} + \text{Na}^+$) 229.0947 found ($\text{M} + \text{Na}^+$) 229.0946.

5.2.2.10 (S)-methyl 2-methylpyrrolidine-2-carboxylate hydrochloride ((S)-**112**)



(S)-2-methylpyrrolidine-2-carboxylic acid ((S)-**111**) (550 mg, 4.26 mmol) was suspended in methanol (5.0 mL) and thionylchloride (311 μL , 4.26 mmol) was added drop wise at 0 °C. The reaction mixture was refluxed for 16 h. The solvent was removed under reduced pressure and the residue resolved in methanol (15.0 mL) then concentrated again under reduced pressure. This procedure was repeated three times. The product (S)-**112** was obtained as white solid (757 mg, 4.21 mmol, quant.). $R_f = 0.27$ (methylene chloride : methanol 10:1). $^1\text{H-NMR}$ (300 MHz, CDCl_3): δ (ppm) 10.56 (s, 1H, NHH), 9.35 (s, 1H, NHH), 3.86 (s, 3H, OCH_3), 3.66–3.53 (m, 2H), 2.46–2.33 (m, 1H), 2.22–1.95 (m, 3H), 1.86 (s, 3H, CH_3). IR (film): ν (cm^{-1}) 2882, 2682, 2624, 2511, 2447, 1742, 1586, 1454, 1431, 1374, 1319, 1293, 1239, 1210, 1173, 1121, 1049, 978, 893, 863.

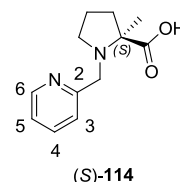
5.2.2.11 (*S*)-methyl 2-methyl-1-(pyridin-2-ylmethyl)pyrrolidine-2-carboxylate ((*S*)-**113**)



Palladium on carbon (142 mg, 0.13 mmol, 10 wt. %) was suspended in methanol (10.0 mL) and picolinaldehyde (**103**) (512 μ L, 5.37 mmol) was added at 0 °C. Sodium acetate (0.73 g, 8.96 mmol) was added to the reaction mixture. Then, (*S*)-**112** (802 mg, 4.48 mmol) was added. The reaction mixture was stirred for 1 h and the nitrogen atmosphere was completely substituted by hydrogen in three turns. The reaction was continued for 16 h allowing the mixture to warm up to ambient temperature. The reaction mixture was filtrated over CELITE and the crude material was subjected to column chromatography using methylene chloride : methanol (35:1 \rightarrow 15:1). The product (*S*)-**113** was obtained as a dark green oil (400 mg, 1.71 mmol, 38%). R_f = 0.65 (methylene chloride : methanol 10:1). $^1\text{H-NMR}$ (300 MHz, CDCl_3): δ (ppm) 8.48 (ddd, J = 4.9, 1.7, 0.9 Hz, 1H, $\text{CH}_{\text{ar-6}}$), 7.62 (td, J = 7.7, 1.8 Hz, 1H, $\text{CH}_{\text{ar-4}}$), 7.45 (d, J = 7.8 Hz, 1H, $\text{CH}_{\text{ar-3}}$), 7.11 (ddd, J = 7.3, 4.9, 1.0 Hz, 1H, $\text{CH}_{\text{ar-5}}$), 3.94 (d, J = 14.4 Hz, 1H, NCHH), 3.71 (d, J = 13.4 Hz, 1H, NCHH), 3.68 (s, 3H, OCH_3), 2.95–2.84 (m, 1H), 2.83–2.71 (m, 1H), 2.30–2.16 (m, 1H), 1.90–1.74 (m, 3H), 1.38 (s, 3H, CH_3). $^{13}\text{C-NMR}$ (75 MHz, CDCl_3): δ (ppm) 175.77 ($\text{C}_{\text{carbonyl}}$), 160.40 ($\text{C}_{\text{ar-2}}$), 148.92 ($\text{C}_{\text{ar-6}}$), 136.62 ($\text{C}_{\text{ar-4}}$), 122.65 ($\text{C}_{\text{ar-3}}$), 121.89 ($\text{C}_{\text{ar-5}}$), 67.98 (NCH_2), 55.76 (C_α), 51.81 (OCH_3), 51.49 (C_δ), 37.66 (CH_3), 21.77 (C_β), 21.59 (C_γ). IR (film): ν (cm^{-1}) 2973, 2950, 2878, 2835, 1722, 1588, 1569, 1459, 1431, 1372, 1361, 1307, 1256, 1189, 1169, 1120,

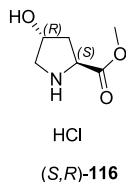
1045, 993, 976, 896, 839, 756. HRMS calculated for $\text{C}_{13}\text{H}_{19}\text{N}_2\text{O}_2$ ($\text{M} + \text{H}^+$) 235.1441 found ($\text{M} + \text{H}^+$) 235.1442.

5.2.2.12 (*S*)-2-methyl-1-(pyridin-2-ylmethyl)pyrrolidine-2-carboxylic acid ((*S*)-**114**)



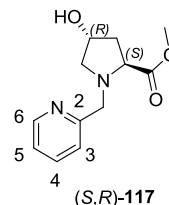
(*S*)-**113** (360 mg, 1.5 mmol) were suspended in sodium hydroxide (2 mL, 1 M) at 0 °C and reacted for 18 h. The reaction mixture was washed with methylene chloride (3 x 20 mL). The combined aqueous layer was neutralised to pH 7 with hydrochloric acid (1 M). The aqueous layer was concentrated and the solvent removed under reduced pressure. The residue was suspended in ethanol (5.00 mL) and filtrated via a syringe filter. The residue was dried *in vacuo* to obtain the product (*S*)-**114** as a brown oil (308 mg, 1.4 mmol, 93%). R_f = 0.05 (methylene chloride : methanol 10:1). $^1\text{H-NMR}$ (300 MHz, CD_3OD): δ (ppm) 8.66 (ddd, J = 4.9, 1.5, 0.9 Hz, 1H, $\text{CH}_{\text{ar-6}}$), 7.89 (td, J = 7.7, 1.8 Hz, 1H, $\text{CH}_{\text{ar-4}}$), 7.51 (d, J = 7.8 Hz, 1H, $\text{CH}_{\text{ar-3}}$), 7.43 (dd, J = 7.4, 5.0 Hz, 1H, $\text{CH}_{\text{ar-5}}$), 4.63 (d, J = 14.0 Hz, 1H, NCHH), 4.29 (d, J = 14.0 Hz, 1H, NCHH), 3.70–3.64 (m, 1H), 3.23–3.05 (m, 1H), 2.52–2.37 (m, 1H), 2.19–2.06 (m, 2H), 2.03–1.86 (m, 1H), 1.65 (s, 3H, CH_3). $^{13}\text{C-NMR}$ (75 MHz, CD_3OD): δ (ppm) 175.70 ($\text{C}_{\text{carbonyl}}$), 152.74 ($\text{C}_{\text{ar-2}}$), 150.77 ($\text{C}_{\text{ar-6}}$), 138.94 ($\text{C}_{\text{ar-4}}$), 125.21 ($\text{C}_{\text{ar-3}}$), 124.81 ($\text{C}_{\text{ar-5}}$), 76.82 (NCH_2), 55.58 (C_α), 54.80 (C_δ), 37.83 (CH_3), 22.69 (C_β), 18.91 (C_γ). IR (film): ν (cm^{-1}) 2959, 2926, 2756, 2128, 1735, 1443, 1365, 1285, 1243, 1216, 1172, 1074, 1031, 941, 829, 750. HRMS calculated for $\text{C}_{12}\text{H}_{17}\text{N}_2\text{O}_2$ ($\text{M} + \text{H}^+$) 221.1285 found ($\text{M} + \text{H}^+$) 221.1285.

5.2.2.13 (2*S*,4*R*)-methyl 4-hydroxypyrrolidine-2-carboxylate hydrochloride ((*S*,*R*)-**116**)



(2*S*,4*R*)-4-hydroxypyrrolidine-2-carboxylic acid ((*S*,*R*)-**115**) (10.00 g, 76.3 mmol) was suspended in methanol (88.0 mL) and thionylchloride (5.56 mL, 76.3 mmol) was added drop wise at 0 °C. The reaction mixture was refluxed for 16 h. The solvent was removed under reduced pressure and the residue resolved in methanol (15.0 mL) then concentrated again under reduced pressure. This procedure was repeated three times. The product (*S*,*R*)-**116** was obtained as white solid (13.85 g, 76.4 mmol, quant.). ¹H-NMR (300 MHz, (CD₃)₂SO): δ(ppm) 5.55 (d, *J* = 3.0 Hz, 1H *CH*_α), 4.49 (dd, *J* = 10.8, 7.6 Hz, 1H, *CH*_γ), 4.42 (bs, 1H, OH), 3.76 (s, 3H, OCH₃), 3.08 (dt, *J* = 12.1, 1.4 Hz, 1H), 2.24–2.02 (m, 3H). ¹³C-NMR (75 MHz, CD₃OD): δ(ppm) 161.06 (*C*_{carbonyl}), 61.09 (*C*_γ), 49.98 (*C*_α), 45.53 (*C*_δ), 44.49 (OCH₃), 29.05 (*C*_β). IR (film): ν (cm⁻¹) 3320, 2953, 2857, 2696, 2599, 2566, 2449, 2418, 1737, 1589, 1436, 1396, 1335, 1276, 1238, 1178, 1073, 1025, 955, 927, 900, 865, 781, 743. HRMS calculated for C₆H₁₂NO₃ (*M* + *H*⁺) 146.0812 found (*M* + *H*⁺) 146.0812.

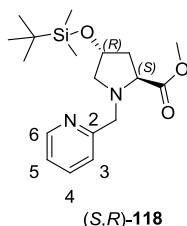
5.2.2.14 (2*S*,4*R*)-methyl 4-hydroxy-1-(pyridin-2-ylmethyl)pyrrolidine-2-carboxylate ((*S*,*R*)-**117**)



Palladium on carbon (2.43 g, 2.29 mmol, 10 wt. %) was suspended in methanol (150.0 mL) and picolinaldehyde (**103**) (9.45 mL, 99.14 mmol) was added at 0 °C. Sodium acetate (12.15 g, 152.5 mmol) was added to the reaction mixture. Then, (*S*,*R*)-**116** (13.85 g, 76.26 mmol) was dissolved in methanol (60 mL) and then added to the reaction mixture. The reaction mixture was stirred for 1 h and the nitrogen atmosphere was completely substituted by hydrogen in three turns. The reaction was continued for 72 h allowing the mixture to warm up to ambient temperature. The reaction mixture was filtrated over CELITE and the crude material was subjected to column chromatography using methylene chloride : methanol (35:1 → 25:1). The product (*S*,*R*)-**117** was obtained as a brown oil (7.17 g, 30.4 mmol, 40%). *R*_f = 0.41 (methylene chloride : methanol 10:1). ¹H-NMR (300 MHz, CD₃OD): δ(ppm) 8.11 (ddd, *J* = 5.0, 1.7, 0.8 Hz, 1H, *CH*_{ar-6}), 7.31 (td, *J* = 7.7, 1.8 Hz, 1H, *CH*_{ar-4}), 6.95 (d, *J* = 7.8 Hz, 1H, *CH*_{ar-3}), 6.83 (ddd, *J* = 7.4, 5.0, 1.0 Hz, 1H, *CH*_{ar-5}), 4.70 (bs, 1H, OH), 4.03 (dq, *J* = 7.2, 2.4 Hz, 1H, *CH*_γ), 3.81 (d, *J* = 15.7 Hz, 1H, NCHH), 3.69 (d, *J* = 15.7 Hz, 1H, NCHH), 3.60–3.50 (m, 1H, *CH*_α), 3.31 (s, 3H, OCH₃), 3.17–3.08 (m, 1H), 2.50 (ddd, *J* = 10.6, 2.2, 1.2 Hz, 1H), 1.86–1.75 (m, 2H). ¹³C-NMR (75 MHz, CDCl₃): δ(ppm) 174.57 (*C*_{carbonyl}), 158.43 (*C*_{ar-2}), 148.19 (*C*_{ar-6}), 137.17 (*C*_{ar-4}), 123.45 (*C*_{ar-3}), 122.29 (*C*_{ar-5}), 70.87 (NCH₂), 62.83 (*C*_γ), 61.28 (*C*_α), 56.88 (OCH₃), 51.82 (*C*_δ), 40.17 (*C*_β). IR (film): ν (cm⁻¹) 3359,

2948, 2837, 1733, 1642, 1593, 1472, 1434, 1355, 1270, 1199, 1086, 1047, 1002, 902, 838, 757, 624.

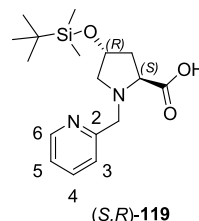
5.2.2.15 (2*S*,4*R*)-methyl 4-(*tert*-butyldimethylsilyloxy)-1-(pyridin-2-ylmethyl)pyrrolidine-2-carboxylate ((*S*,*R*)-**118**)



(*S*,*R*)-**117** (1.9 g, 8.04 mmol) was dissolved in dimethylformamide (30 mL) and diisopropylethylamine (7 mL, 40.20 mmol) was added over a period of 5 min. The reaction mixture was stirred for 10 min at 0 °C prior to the addition of *tert*-butyldimethylsilyl triflate (7.7 mL, 8.85 mmol) and stirred for 16 h. The reaction mixture was allowed to warm up to ambient temperature. The reaction mixture was then reacted with ammonium acetate solution (1 M, 40 mL) and the organic layer was separated. The aqueous layer was then extracted using methylene chloride (3 x 50 mL). The solvent was evaporated under reduced pressure and the crude material was subjected to column chromatography using methylene chloride : methanol (10:1). R_f = 0.70 (methylene chloride : methanol 10:1). The product (*S*,*R*)-**118** was obtained as brown oil (1.28 g, 3.7 mmol, 46%). $^1\text{H-NMR}$ (300 MHz, CDCl_3): δ (ppm) 8.51 (ddd, J = 4.9, 1.8, 0.9 Hz, 1H, $\text{CH}_{\text{ar-6}}$), 7.63 (td, J = 7.6, 1.8 Hz, 1H, $\text{CH}_{\text{ar-4}}$), 7.43 (d, J = 7.8 Hz, 1H, $\text{CH}_{\text{ar-3}}$), 7.13 (ddd, J = 7.4, 4.9, 1.1 Hz, 1H, $\text{CH}_{\text{ar-5}}$), 4.49 – 4.31 (m, 1H, CH_γ), 4.04 (d, J = 13.7 Hz, 1H, NCHH), 3.80 (d, J = 13.7 Hz, 1H, NCHH), 3.67 (dd, J = 6.5, 4.7 Hz, 1H, CH_α), 3.63 (s, 3H, OCH_3), 3.31 (dd, J = 9.8, 5.7 Hz, 1H, $\text{CH}_\delta\text{H}_\delta$), 2.47 (dd, J = 9.8, 4.9 Hz, 1H, $\text{CH}_\delta\text{H}_\delta$), 2.23 – 2.11 (m, 1H, $\text{CH}_\beta\text{H}_\beta$), 2.03 (ddd, J = 12.7, 8.3, 4.1 Hz, 1H,

$\text{CH}_\beta\text{H}_\beta$), 0.84 (s, 9H, $\text{SiC}_q(\text{CH}_3)_3$), -0.00 (d, J = 5.1 Hz, 6H, $\text{Si}(\text{CH}_3)_2$). $^{13}\text{C-NMR}$ (75 MHz, CD_3OD): δ (ppm) 174.25 ($\text{C}_{\text{carbonyl}}$), 158.77 ($\text{C}_{\text{ar-2}}$), 149.08 ($\text{C}_{\text{ar-6}}$), 136.56 ($\text{C}_{\text{ar-4}}$), 123.45 ($\text{C}_{\text{ar-3}}$), 122.16 ($\text{C}_{\text{ar-5}}$), 70.76 (NCH_2), 64.55 (C_γ), 62.11 (C_α), 60.93 (OCH_3), 51.91 (C_δ), 39.67 (C_β), 25.61 ($\text{SiC}_q(\text{CH}_3)_3$), 18.10 ($\text{SiC}_q(\text{CH}_3)_3$), -4.74 ($\text{Si}(\text{CH}_3)_2$). IR (film): ν (cm^{-1}) 2950, 2892, 2855, 1741, 1591, 1468, 1435, 1366, 1252, 1198, 1170, 1096, 1036, 905, 832, 771, 671.

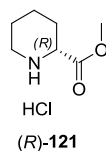
5.2.2.16 (2*S*,4*R*)-4-(*tert*-butyldimethylsilyloxy)-1-(pyridin-2-ylmethyl)pyrrolidine-2-carboxylic acid ((*S*,*R*)-**119**)



(*S*,*R*)-**118** (1.27 g, 3.6 mmol) were suspended in sodium hydroxide (4.8 mL, 1 M) at 0 °C and reacted for 18 h. The reaction mixture was washed with methylene chloride (3 x 30 mL). The combined aqueous layer was neutralised to pH 7 with hydrochloric acid (1 M). The aqueous layer was concentrated and the solvent removed under reduced pressure. The residue was suspended in ethanol (5.00 mL) and filtrated via a syringe filter. The residue was dried *in vacuo* to obtain the product (*S*,*R*)-**119** as orange highly viscous oil (985 mg, 2.92 mmol, 81%). R_f = 0.16 (methylene chloride : methanol 10:1). $^1\text{H-NMR}$ (300 MHz, CDCl_3): δ (ppm) 8.66 – 8.56 (m, 1H, $\text{CH}_{\text{ar-6}}$), 8.50 (bs, 1H, COOH), 7.72 (td, J = 7.7, 1.7 Hz, 1H, $\text{CH}_{\text{ar-4}}$), 7.37 (d, J = 7.7 Hz, 1H, $\text{CH}_{\text{ar-3}}$), 7.31 – 7.27 (m, 1H, $\text{CH}_{\text{ar-5}}$), 4.44 – 4.42 (m, 1H, CH_γ), 4.43 (d, J = 14.4 Hz, 1H, NCHH), 4.27 (d, J = 14.5 Hz, 1H, NCHH), 4.16 – 4.01 (m, 1H, CH_α), 3.60 (dd, J = 11.4, 4.4 Hz, 1H, $\text{CH}_\delta\text{H}_\delta$), 2.93 (dd, J = 11.3, 2.0 Hz, 1H, $\text{CH}_\delta\text{H}_\delta$), 2.32 (dt, J = 8.1, 4.1 Hz,

2H, $CH_\beta H_\beta$), 0.88 (s, 9H, $(SiC_q(CH_3)_3)$), 0.06 (d, $J = 4.5$ Hz, 6H, $(Si(CH_3)_2)$). ^{13}C -NMR (75 MHz, $CDCl_3$): δ (ppm) 173.72 (C_{carbonyl}), 155.22 (CH_{ar-2}), 149.24 (CH_{ar-6}), 137.68 (C_{ar-4}), 123.55 (C_{ar-3}), 123.49 (C_{ar-5}), 71.85 (NCH_2), 67.22 (C_γ), 62.46 (C_α), 61.43 (C_δ), 39.39 (C_β), 25.88 ($SiC_q(CH_3)_3$), 18.06 ($SiC_q(CH_3)_3$), -4.67 ($Si(CH_3)_2$). IR (film): ν (cm^{-1}) 2931, 2890, 2855, 1709, 1627, 1468, 1437, 1385, 1252, 1214, 1101, 1029, 1000, 886, 831, 769, 693, 668.

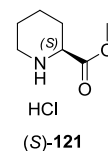
5.2.2.17 (*R*)-methyl piperidine-2-carboxylate hydrochloride ((*R*)-**121**)



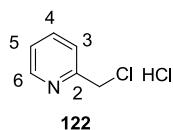
(*R*)-piperidine-2-carboxylic acid ((*R*)-**120**) (3.00 g, 23.2 mmol) was suspended in methanol (30.0 mL) and thionylchloride (1.69 mL, 23.2 mmol) was added drop wise at 0 °C. The reaction mixture was stirred for 16 h and warmed up to ambient temperature. The solvent was removed under reduced pressure and the residue resolved in methanol (10.0 mL) then concentrated again under reduced pressure. This procedure was repeated three times. The product (*R*)-**121** was obtained as white solid (4.16 g, 23.15 mmol, quant.). 1H -NMR (300 MHz, CD_3OD): δ (ppm) 4.31 (s, 3H, OCH_3), 3.53 (dd, $J = 11.3$, 3.5 Hz, 1H, CH_α), 2.95–2.83 (m, 1H, $CH_\epsilon H_\epsilon$), 2.53 (td, $J = 12.3$, 3.3 Hz, 1H, $CH_\epsilon H_\epsilon$), 1.74 (ddd, $J = 9.3$, 6.1, 3.8 Hz, 1H, $CH_\beta H_\beta$), 1.40–1.31 (m, 1H, $CH_\beta H_\beta$), 1.26–1.11 (m, 4H, $CH_\delta H_\delta$, $CH_\gamma H_\gamma$). ^{13}C -NMR (75 MHz, CD_3OD): δ (ppm) 170.30 (C_{carbonyl}), 57.85 (C_α), 53.71 (OCH_3), 45.20 (C_ϵ), 27.10 (C_δ), 22.82 (C_β), 22.71 (C_γ). IR (film): ν (cm^{-1}) 2919, 2802, 2680, 2564, 2499, 2411, 1742, 1581, 1448, 1422, 1366, 1340, 1275, 1211, 1131, 1052, 1038, 984, 948, 917, 889, 754, 687, 534. HRMS calcu-

lated for $C_7H_{14}NO_2$ ($M + H^+$) 144.1019 found ($M + H^+$) 144.1020.

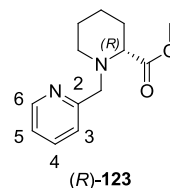
5.2.2.18 (*S*)-methyl piperidine-2-carboxylate hydrochloride ((*S*)-**121**)



(*S*)-piperidine-2-carboxylic acid ((*S*)-**120**) (2.00 g, 15.48 mmol) was suspended in methanol (20.0 mL) and thionylchloride (1.13 mL, 15.48 mmol) was added drop wise at 0 °C. The reaction mixture was stirred for 16 h and warmed up to ambient temperature. The solvent was removed under reduced pressure and the residue resolved in methanol (10.0 mL) then concentrated again under reduced pressure. This procedure was repeated three times. The product (*S*)-**121** was obtained as white solid (2.70 g, 15.07 mmol, 97%). 1H -NMR (300 MHz, CD_3OD): δ (ppm) 4.09 – 3.98 (m, 1H, CH_α), 3.85 (s, 3H, OCH_3), 3.42 (d, $J = 11.9$ Hz, 1H, $CH_\epsilon H_\epsilon$), 3.04 (t, $J = 11.2$ Hz, 1H, $CH_\epsilon H_\epsilon$), 2.28 (d, $J = 10.8$ Hz, 1H), 1.98–1.81 (m, 2H), 1.80–1.56 (m, 3H). ^{13}C -NMR (75 MHz, CD_3OD): δ (ppm) 170.24 (C_{carbonyl}), 57.83 (C_α), 53.72 (OCH_3), 45.23 (C_ϵ), 27.03 (C_δ), 22.75 (C_β), 22.68 (C_γ). IR (film): ν (cm^{-1}) 2919, 2802, 2681, 2564, 2499, 2412, 1743, 1581, 1449, 1422, 1366, 1340, 1275, 1211, 1132, 1052, 1038, 984, 949, 918. HRMS calculated for $C_7H_{14}NO_2$ ($M + H^+$) 144.1019 found ($M + H^+$) 144.1024.

5.2.2.19 2-(chloromethyl)pyridine (**122**)

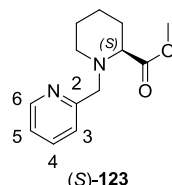
Pyridine-2-ylmethanol (11.3 g; 103.5 mmol) were dissolved in Et₂O (50 mL) and cooled to 0 °C under continuous stirring. Then, thionylchloride (8.26 mL, 13.5 g; 113.5 mmol) was added drop wise under formation of a pink precipitation. The reaction was continued for 16 h and the reaction mixture was allowed to warm up to ambient temperature. The solvent was evaporated unde reduced pressure and the residue was dried *in vacuo* to obtain the product as pink solid (14.79 g, 90 mmol, 87%). *R*_f = 0.67 (methylene chloride : methanol 10:1). ¹H-NMR (300 MHz, CDCl₃): δ(ppm) 8.74 (d, *J* = 5.2 Hz, 1H, CH_{ar}-6), 8.40 (t, *J* = 7.7 Hz, 1H, CH_{ar}-4), 8.05 (d, *J* = 8.0 Hz, 1H, CH_{ar}-3), 7.91 – 7.80 (m, 1H, CH_{ar}-5), 5.18 (s, 2H, CH₂Cl). ¹³C-NMR (75 MHz, CDCl₃): δ(ppm) 152.47 (C_{ar}-2), 145.83 (C_{ar}-6), 141.33 (C_{ar}-4), 127.01 (C_{ar}-3), 126.14 (C_{ar}-5), 39.85 (CH₂Cl). IR (film): ν (cm⁻¹) 3094, 3039, 2304, 2056, 1983, 1863, 1609, 1531, 1462, 1422, 1395, 1314, 1275, 1228, 1160, 1063, 1035, 995, 957, 904, 820, 772, 745, 685, 619. HRMS calculated for C₆H₇ClN (M + H⁺) 128.0262 found (M + H⁺) 128.0262.

5.2.2.20 (*R*)-methyl 1-(pyridin-2-ylmethyl)pyrrolidine-2-carboxylate ((*R*)-**123**)

122 (1.31 g, 8.02 mmol) was dissolved in DMF (30 mL) and stirred with sodium carbonate (0.935 g, 8.8 mmol) and sodium iodide (57 mg, 0.38 mmol) at 50 °C for 2 h. (*R*)-**121** (2.16 g, 12.02 mmol) was dissolved in DMF (15 mL) and added drop wise to the reaction mixture. The reaction was continued for 36 h. Water (50 mL) was added to the reaction mixture and the product was extracted with methylene chloride (3 x 50 mL). The combined organic layer was concentrated under reduced pressure and dried *in vacuo*. The crude material was subjected to column chromatography using methylene chloride : methanol (100:0 → 15:1). After evaporation of eluent solvent under reduced pressure, the residue was dried *in vacuo* to obtain the product as yellow oil (1.52 g, 6.49 mmol, 81%). *R*_f = 0.49 (methylene chloride : methanol 15:1). ¹H-NMR (300 MHz, CDCl₃): δ(ppm) 8.53 – 8.45 (m, 1H, CH_{ar}-6), 7.61 (td, *J* = 7.6, 1.8 Hz, 1H, CH_{ar}-4), 7.47 (d, *J* = 7.8 Hz, 1H, CH_{ar}-3), 7.11 (ddd, *J* = 7.4, 4.9, 1.0 Hz, 1H, CH_{ar}-5), 3.87 (d, *J* = 14.1 Hz, 1H, NCHH), 3.69 (s, 3H, OCH₃), 3.57 (d, *J* = 14.1 Hz, 1H, NCHH), 3.24 (dd, *J* = 7.6, 4.4 Hz, 1H, CH_α), 3.00 – 2.88 (m, 1H, CH_εH_ε), 2.31 – 2.18 (m, 1H, CH_εH_ε), 1.93 – 1.74 (m, 2H, CH_βH_β), 1.65 – 1.50 (m, 3H), 1.46 – 1.31 (m, 1H). ¹³C-NMR (75 MHz, CDCl₃): δ(ppm) 174.25 (C_{carbonyl}), 159.15 (C_{ar}-2), 149.07 (C_{ar}-6), 136.45 (C_{ar}-4), 123.24 (C_{ar}-3), 122.01 (C_{ar}-5), 64.44 (NCH₂), 62.41 (C_α), 51.56 (OCH₃), 50.60 (C_ε), 29.60 (C_δ), 25.35 (C_β), 22.37 (C_γ). IR (film): ν (cm⁻¹) 3008, 2936, 2855, 1733, 1646, 1589, 1569, 1471, 1432, 1368, 1340, 1281, 1265, 1191, 1164, 1146,

1127, 1106, 1060, 1048, 1009, 993, 969, 921, 888, 866, 830, 803, 755, 729, 634, 612, 590. HRMS calculated for $C_{13}H_{19}N_2O_2$ ($M + H^+$) 235.1441 found ($M + H^+$) 235.1448.

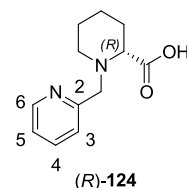
5.2.2.21 (*S*)-methyl 1-(pyridin-2-ylmethyl)piperidine-2-carboxylate ((*S*)-**123**)



122 (1.9 g, 12.06 mmol) was dissolved in DMF (25 mL) and stirred with sodium carbonate (2.6 g, 24.12 mmol) and sodium iodide (144 mg, 0.96 mmol) at 50 °C for 2 h. (*S*)-**121** (2.6 g, 14.47 mmol) was dissolved in DMF (25 mL) and added drop wise to the reaction mixture. The reaction was continued for 36 h. Water (50 mL) was added to the reaction mixture and the product was extracted with methylene chloride (3 x 50 mL). The combined organic layer was concentrated under reduced pressure and dried *in vacuo*. The crude material was subjected to column chromatography using methylene chloride : methanol (100:0 → 15:1). After evaporation of eluent solvent under reduced pressure, the residue was dried *in vacuo* to obtain the product as yellow oil (2.16 g, 9.25 mmol, 77%). R_f = 0.49 (methylene chloride : methanol 15:1). 1H -NMR (300 MHz, $CDCl_3$): δ (ppm) 8.45 (ddd, J = 4.9, 1.7, 0.9 Hz, 1H, CH_{ar-6}), 7.58 (td, J = 7.6, 1.8 Hz, 1H, CH_{ar-4}), 7.43 (d, J = 7.8 Hz, 1H, CH_{ar-3}), 7.08 (ddd, J = 7.4, 4.9, 1.1 Hz, 1H, CH_{ar-5}), 3.83 (d, J = 14.1 Hz, 1H, NCHH), 3.65 (s, 3H, OCH_3), 3.54 (d, J = 14.1 Hz, 1H, NCHH), 3.20 (dd, J = 7.5, 4.4 Hz, 1H, CH_α), 2.97 – 2.83 (m, 1H, $CH_\epsilon H_\epsilon$), 2.27 – 2.14 (m, 1H, $CH_\epsilon H_\epsilon$), 1.85 – 1.72 (m, 2H), 1.60 – 1.45 (m, 3H), 1.41 – 1.25 (m, 1H). ^{13}C -NMR (75 MHz, $CDCl_3$): δ (ppm) 174.17 ($C_{carbonyl}$), 159.02 (C_{ar-2}), 148.92 (C_{ar-6}), 136.41 (C_{ar-4}), 123.17 (C_{ar-3}),

121.94 (C_{ar-5}), 64.36 (NCH₂), 62.27 (C_α), 51.49 (OCH_3), 50.50 (C_ϵ), 29.51 (C_δ), 25.25 (C_β), 22.29 (C_γ). IR (film): ν (cm^{-1}) 3006, 2938, 2854, 1734, 1657, 1590, 1436, 1368, 1271, 1164, 1054, 1008, 925, 891, 830, 798, 756, 614. HRMS calculated for $C_{13}H_{19}N_2O_2$ ($M + H^+$) 235.1441 found ($M + H^+$) 235.1442.

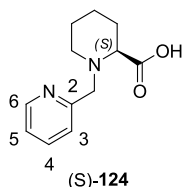
5.2.2.22 (*R*)-1-(pyridin-2-ylmethyl)piperidine-2-carboxylic acid ((*R*)-**124**)



(*R*)-**123** (300 g, 1.3 mmol) were suspended in sodium hydroxide (1.7 mL, 1 M) at 0 °C and reacted for 16 h. The reaction mixture was washed with methylene chloride (3 x 10 mL). The combined aqueous layer was neutralised to pH 7 with hydrochloric acid (1 M). The aqueous layer was concentrated and the solvent removed under reduced pressure. The residue was suspended in ethanol (5.00 mL) and filtrated via a syringe filter. The residue was dried *in vacuo* to obtain the product (*R*)-**124** as a yellow solid (283 mg, 1.28 mmol, quant.). R_f = 0.05 (methylene chloride : methanol 10:1). 1H -NMR (300 MHz, CD_3OD): δ (ppm) 8.62 (ddd, J = 4.9, 1.6, 0.8 Hz, 1H, CH_{ar-6}), 7.86 (td, J = 7.7, 1.8 Hz, 1H, CH_{ar-4}), 7.57 (d, J = 7.8 Hz, 1H, CH_{ar-3}), 7.41 (ddd, J = 7.6, 4.9, 0.9 Hz, 1H, CH_{ar-5}), 4.63 (d, J = 13.8 Hz, 1H, NCHH), 4.35 (d, J = 13.8 Hz, 1H, NCHH), 3.61 (dd, J = 10.1, 3.8 Hz, 1H, CH_α), 3.52 (dd, J = 12.4, 4.3 Hz, 1H, $CH_\epsilon H_\epsilon$), 3.13–2.98 (m, 1H, $CH_\epsilon H_\epsilon$), 2.31–2.15 (m, 1H, $CH_\beta H_\beta$), 2.07–1.90 (m, 1H, $CH_\beta H_\beta$), 1.88–1.71 (m, 3H), 1.65–1.48 (m, 1H). ^{13}C -NMR (75 MHz, CD_3OD): δ (ppm) 173.73 ($C_{carbonyl}$), 152.51 (C_{ar-2}), 150.65 (C_{ar-6}), 138.82 (C_{ar-4}), 126.14 (C_{ar-3}), 125.20 (C_{ar-5}), 68.24 (NCH₂), 60.11 (C_α), 52.74 (C_ϵ), 28.43 (C_δ), 23.37 (C_β), 22.62 (C_γ). HRMS

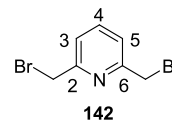
calculated for $C_{12}H_{17}N_2O_2$ ($M + H^+$) 221.1285
found ($M + H^+$) 221.1284.

5.2.2.23 (S)-1-(pyridin-2-ylmethyl)piperidine-2-carboxylic acid ((S)-**124**)



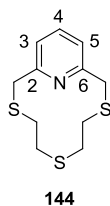
(S)-**123** (300 g, 1.3 mmol) were suspended in sodium hydroxide (1.7 mL, 1 M) at 0 °C and reacted for 16 h. The reaction mixture was washed with methylene chloride (3 x 10 mL). The combined aqueous layer was neutralised to pH 7 with hydrochloric acid (1 M). The aqueous layer was concentrated and the solvent removed under reduced pressure. The residue was suspended in ethanol (5.00 mL) and filtrated via a syringe filter. The residue was dried *in vacuo* to obtain the product (S)-**124** as a yellow solid (283 mg, 1.28 mmol, quant.). R_f = 0.05 (methylene chloride : methanol 10:1). 1H -NMR (300 MHz, CD_3OD): δ (ppm) 8.62 (ddd, J = 4.9, 1.6, 0.8 Hz, 1H, CH_{ar-6}), 7.86 (td, J = 7.7, 1.8 Hz, 1H, CH_{ar-4}), 7.57 (d, J = 7.8 Hz, 1H, CH_{ar-3}), 7.41 (ddd, J = 7.6, 4.9, 0.9 Hz, 1H, CH_{ar-5}), 4.63 (d, J = 13.8 Hz, 1H, NCHH), 4.35 (d, J = 13.8 Hz, 1H, NCHH), 3.61 (dd, J = 10.1, 3.8 Hz, 1H, CH_α), 3.52 (dd, J = 12.4, 4.3 Hz, 1H, $CH_\epsilon H_\epsilon$), 3.13–2.98 (m, 1H, $CH_\epsilon H_\epsilon$), 2.31–2.15 (m, 1H, $CH_\beta H_\beta$), 2.07–1.90 (m, 1H, $CH_\beta H_\beta$), 1.88–1.71 (m, 3H), 1.65–1.48 (m, 1H). ^{13}C -NMR (75 MHz, CD_3OD): δ (ppm) 173.73 ($C_{carbonyl}$), 152.51 (C_{ar-2}), 150.65 (C_{ar-6}), 138.82 (C_{ar-4}), 126.14 (C_{ar-3}), 125.20 (C_{ar-5}), 68.24 (NCH₂), 60.11 (C_α), 52.74 (C_ϵ), 28.43 (C_δ), 23.37 (C_β), 22.62 (C_γ). HRMS calculated for $C_{12}H_{17}N_2O_2$ ($M + H^+$) 221.1285 found ($M + H^+$) 221.1284.

5.2.2.24 2,6-bis(bromomethyl)pyridine (**142**)



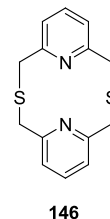
Phosphoryl bromide (3.6 g, 12.5 mmol) was melted at 60 °C turning the brown crystalline solid into a brown clear liquid. 2,6-Pyridinedimethanol (**141**) (100 mg, 0.72 mmol) was added drop wise at 70 °C and the reaction mixture turned into dark brown. The reaction was continued for 1.5 h at 70 °C. Distilled water (6 mL) was added carefully drop wise at 0 °C. The reaction mixture was poured into ice and neutralised using sodium hydroxide (2 M). The aqueous layer was extracted with methylene chloride (4 x 30 mL), dried over sodium sulfate, filtrated and concentrated *in vacuo*. The product **142** was obtained as white needles (188 mg, 0.71 mmol, 98%). R_f = 0.75 (methylene chloride : methanol 10:1). 1H -NMR (300 MHz, $CDCl_3$): δ (ppm) 7.71 (t, J = 7.8 Hz, 1H, CH_{ar-4}), 7.38 (d, J = 7.7 Hz, 2H, CH_{ar-3} & CH_{ar-5}), 4.54 (s, 4H, 2xCH₂Br). ^{13}C -NMR (75.5 MHz, $CDCl_3$): δ (ppm) 156.85 (2C, C_{ar-2} & C_{ar-6}), 138.34 (C_{ar-4}), 122.96 (2C, (C_{ar-3} & C_{ar-5}), 33.42 (2C, 2xCH₂Br). IR (film): ν (cm⁻¹) 2962, 1568, 1448, 1260, 1204, 1158, 1081, 1020, 954, 865, 809, 744, 585, 548. HRMS calculated for $C_7H_8Br_2N$ ($M + H^+$)⁺ 265.9003, found ($M + H^+$)⁺ 265.9008.

5.2.2.25 2,5,8-Trithia-{9}(2,6)pyridinophane
(**144**)



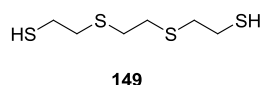
Caesium carbonate (430 mg, 1.32 mmol) was suspended in dimethylformamide (75 mL) at 60 °C. A homogeneous solution of **142** (316 mg, 1.20 mmol) and 2,2-Bis(2-mercaptoethyl) sulfide (**143**) (156 μ L, 1.20 mmol) dissolved in dimethylformamide (75 mL) were added drop wise via a syringe pump over a period of 18 h. The reaction was continued for 2 h. The solvent was evaporated under reduced pressure and the residual yellow oil was suspended in water (25 mL) and methylene chloride (40 mL). After sonification the crude product was extracted with methylene chloride (4 x 50 mL). The combined organic layer was washed with BRINE (2 x 30 mL), dried over sodium sulfate and concentrated under reduced pressure. The crude material was subjected to column chromatography using hexane : ethylacetate (10:1). The product **144** was obtained a white solid (88 mg, 0.34 mmol, 28 %). R_f = 0.50 (hexane : ethylacetate 10:1). $^1\text{H-NMR}$ (300 MHz, CDCl_3): δ (ppm) 7.77 (t, J = 7.5 Hz, 1H, $\text{CH}_{\text{ar-4}}$), 7.39 (d, J = 7.7 Hz, 2H, $\text{CH}_{\text{ar-3}}$ & $\text{CH}_{\text{ar-5}}$), 3.98 (s, 4H, $\text{C}_{\text{ar-2}}\text{CH}_2$ & $\text{C}_{\text{ar-6}}\text{CH}_2$), 2.56 (s, 8H, $4 \times \text{CH}_2$). $^{13}\text{C-NMR}$ (75 MHz, CDCl_3): δ (ppm) 157.65 (2C, $\text{C}_{\text{ar-2}}$ & $\text{C}_{\text{ar-6}}$), 138.59 ($\text{C}_{\text{ar-4}}$), 122.17 (2C, $\text{C}_{\text{ar-3}}$ & $\text{C}_{\text{ar-5}}$), 36.35 (2C, $\text{C}_{\text{ar-2}}\text{CH}_2$ & $\text{C}_{\text{ar-6}}\text{CH}_2$), 31.14 (2C, $\text{C}_{\text{ar-2}}\text{CH}_2\text{SCH}_2$ & $\text{C}_{\text{ar-6}}\text{CH}_2\text{SCH}_2$), 30.16 (2C, CH_2SCH_2). IR (film): ν (cm^{-1}) 2924, 2097, 2039, 1966, 1580, 1565, 1446, 1424, 1275, 1202, 1153, 1131, 1078, 1023, 991, 967, 911, 859, 813, 749. HRMS calculated for $\text{C}_{11}\text{H}_{15}\text{NS}_3\text{Na}$ ($\text{M} + \text{Na}^+$) 280.0264 found ($\text{M} + \text{Na}^+$) 280.0262.

5.2.2.26 2,11-dithia[3.3](2,6)pyridinophane
(**146**)



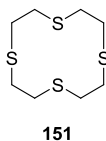
142 (495 mg, 1.86 mmol) and thioacetamide (140 mg, 1.86 mmol) were dissolved in dimethylformamide (9.5 mL) in separated syringes. Lithium carbonate (275 mg, 3.72 mmol) was suspended in dimethylformamide (30 mL) and stirred at 55 °C. Over a period of 30 min **142** as well as thioacetamide were added drop wise simultaneously. The reaction was continued for 2 h at 55 °C. The solvent was evaporated under reduced pressure and the residue was dissolved in water (50 mL). The turbid suspension was neutralised with hydrochloric acid (10% aq.). The aqueous layer was extracted using chloroform (4 x 50 mL). The combined organic layer was dried over sodium sulfate, filtrated and concentrated under reduced pressure. The crude material was subjected to column chromatography using methylene chloride : methanol (30:1 \rightarrow 8:1). The product **146** was obtained as yellow highly viscous oil (102 mg, 0.37 mmol, 20 %). R_f = 0.13 (hexane : ethylacetate 3:1). $^1\text{H-NMR}$ (300 MHz, $(\text{CD}_3)_2\text{SO}$): δ (ppm) 7.87–7.13 (m, 6H, $6 \times \text{CH}_{\text{ar}}$), 4.05–3.77 (m, 8H, $4 \times \text{CH}_2$). HRMS calculated for $\text{C}_{14}\text{H}_{15}\text{N}_2\text{S}_2$ ($\text{M} + \text{H}^+$) 275.0677, found ($\text{M} + \text{H}^+$) 275.0670.

5.2.2.27 2,2'-(ethane-1,2-diylbis(sulfane-diyl))diethanethiol (**149**)



2,2'-(ethane-1,2-diylbis(sulfanediyl))diethanol (**147**) (3.98 g, 21.8 mmol), thio-urea (**148**) (3.35 g, 4.40 mmol) were added in hydroboric acid (7.50 mL, 132 mmol, 47% aq.) and refluxed for 8.5 h. The yellow solution was cooled to ambient temperature and sodium hydroxide (5.28 g, 132 mmol) in water (30 mL) was added slowly. A white precipitate was observed and the reaction mixture was refluxed for 16 h. After cooling to ambient temperature, the reaction mixture was neutralised using hydrochloric acid. The aqueous layer was extracted with methylene chloride (3 x 100 mL). The combined organic layer was dried over sodium sulfate, filtrated and dried *in vacuo*. The product **149** was obtained as highly viscous pale oil (1.96 g, 9.17 mmol, 42 %). $^1\text{H-NMR}$ (300 MHz, CDCl_3): $\delta(\text{ppm})$ 2.89-2.68 (m, 12H, $6\times\text{CH}_2$), 1.76-1.70 (m, 2H, SH).

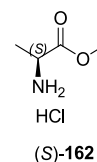
5.2.2.28 1,4,7,10-tetrathiacyclododecane (**151**)



Caesium carbonate (1.14 g, 3.50 mmol) suspended in DMF (100 mL) was heated to 50 °C. A homogeneous solution of **149** (519 mg, 2.42 mmol) and 1,2-dibromoethane (**150**) (208 μL , 2.24 mmol) dissolved in DMF (50 mL) was added drop wise over a period of 12 h at 50 °C via a syringe pump. The reaction was continued for an additional 2 h and then cooled to ambient temperature over a period of 16 h. The

solvent was evaporated under reduced pressure, water (50 mL) and methylene chloride (75 mL) was added to the residue and the mixture was stirred for 30 min at ambient temperature. Both layers were separated and the aqueous layer was extracted using methylene chloride (2 x 50 mL). The combined organic layer was washed with BRINE (3 x 50 mL), dried over sodium sulfate, filtrated and concentrated under reduced pressure. The crude material was recrystallised using chloroform. The product **151** was obtained as white crystals (58 mg, 0.24 mmol, 10%). $^1\text{H-NMR}$ (300 MHz, CDCl_3): $\delta(\text{ppm})$ 2.72 (s, 16H, $8\times\text{CH}_2$). $^{13}\text{C-NMR}$ (75 MHz, CDCl_3): $\delta(\text{ppm})$ 28.82 (8C). HRMS calculated for $\text{C}_8\text{H}_{16}\text{S}_4\text{Na}$ ($\text{M} + \text{Na}^+$) 263.0033 found ($\text{M} + \text{Na}^+$) 263.0027.

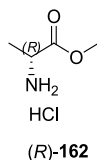
5.2.2.29 (S)-methyl 2-aminopropanoate hydrochloride ((S)-**162**)



(S)-2-aminopropanoic acid ((S)-**155**) (5.00 g, 56.1 mmol) was suspended in methanol (50.0 mL) and thionylchloride (4.09 mL, 56.1 mmol) was added drop wise at 0 °C. The reaction mixture was refluxed for 16 h. The solvent was removed under reduced pressure and the residue resolved in methanol (25.0 mL) then concentrated again under reduced pressure. This procedure was repeated three times. The product (S)-**162** was obtained as white solid (7.90 g, 56.6 mmol, quant.). $^1\text{H-NMR}$ (300 MHz, MeOD_3): $\delta(\text{ppm})$ 4.32 (s, 3H, OCH_3), 3.59 (q, $J = 7.2$ Hz, 1H, CH_α), 1.02 (d, $J = 7.2$ Hz, 3H, CH_3). $^{13}\text{C-NMR}$ (75 MHz, CD_3OD): $\delta(\text{ppm})$ 171.41 ($\text{C}_{\text{carbonyl}}$), 53.69 (OCH_3), 49.85 (C_α), 16.18 (C_β). IR (film): ν (cm^{-1}) 2957, 2895, 2736, 2698, 2605, 1739, 1599,

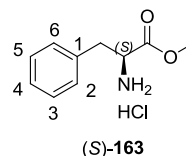
1474, 1383, 1336, 1232, 1212, 1113, 1009, 976, 902, 840.

5.2.2.30 (*R*)-methyl 2-aminopropanoate hydrochloride ((*R*)-**162**)



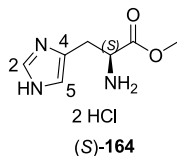
(*R*)-2-aminopropanoic acid ((*R*)-**155**) (1.79 g, 20.1 mmol) was suspended in methanol (20.0 mL) and thionylchloride (1.47 mL, 20.1 mmol) was added drop wise at 0 °C. The reaction mixture was refluxed for 16 h. The solvent was removed under reduced pressure and the residue resolved in methanol (15.0 mL) then concentrated again under reduced pressure. This procedure was repeated three times. The product (*R*)-**162** was obtained as white solid (2.83 g 20.2 mmol, quant.). ¹H-NMR (300 MHz, CDCl₃): δ(ppm) 4.37–4.15 (m, 1H, CH_α), 3.81 (s, 3H, OCH₃), 1.73 (d, J = 7.3 Hz, 3H, CH_{3β}). ¹³C-NMR (75 MHz, CD₃OD): δ(ppm) 171.40 (C_{carbonyl}), 53.70 (OCH₃), 49.87 (C_α), 16.18 (C_β). IR (film): ν (cm⁻¹) 2956, 2897, 2816, 2783, 2736, 2695, 2607, 2491, 2003, 1741, 1601, 1570, 1477, 1435, 1392, 1374, 1339, 1234, 1214, 1184, 1137, 1114, 1013, 976, 902.

5.2.2.31 (*S*)-methyl 2-amino-3-phenylpropanoate hydrochloride ((*S*)-**163**)



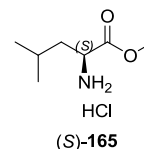
(*S*)-2-amino-3-phenylpropanoic acid ((*S*)-**156**) (10.00 g, 60.5 mmol) was suspended in methanol (70 mL). SOCl₂ (4.8 mL, 66.6 mmol) was added drop wise at 0 °C over a period of 30 min. The reaction mixture was stirred for an additional hour at 0 °C then refluxed for 28 h. The solvent was evaporated under reduced pressure and the residue was resolved in methanol (15.0 mL) then concentrated again under reduced pressure. This procedure was repeated three times. The product (*S*)-**163** was obtained as white solid (12.9 g, 59.8 mmol, quant.). R_f = 0.67 (methylene chloride : methanol 15:1). ¹H-NMR (300 MHz, CD₃OD): δ(ppm) 7.41–7.25 (m, 5H, 5xCH_{ar}), 4.33 (dd, 1H, J = 6.3, 7.3 Hz, CH_α), 3.80 (s, 3H, OCH₃), 3.27 (dd, 1H, J = 6.2, 14.4 Hz, CH_βH_β), 3.18 (dd, 1H, J = 7.3, 14.4 Hz, CH_βH_β). ¹³C-NMR (75 MHz, CD₃OD): δ(ppm) 170.39 (C_{carbonyl}), 135.36 (C_{ar-1}), 130.49 (2C, C_{ar-3} & C_{ar-5}), 130.13 (2C, C_{ar-2} & C_{ar-6}), 128.96 (C_{ar-4}), 55.25 (C_α), 53.58 (OCH₃), 37.34 (C_β). IR (film): ν (cm⁻¹) 3386, 2956, 2519, 2030, 1743, 1627, 1525, 1502, 1446, 1387, 1289, 1243, 1151, 1081, 1053, 994, 944, 910, 852, 811, 750, 699, 590, 475. HRMS calculated for C₁₀H₁₄NO₂ (M + H⁺) 180.1025 found (M + H⁺) 180.1019.

5.2.2.32 (*S*)-methyl 2-amino-3-(1*H*-imidazol-4-yl)propanoate dihydrochloride ((*S*)-**164**)



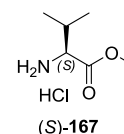
(*S*)-2-amino-3-(1*H*-imidazol-4-yl)propanoic acid ((*S*)-**157**) (10 g, 64.5 mmol) was dissolved in methanol (60.0 mL) and thionylchloride (5.14 mL, 70.9 mmol) was added dropwise at 0 °C. The reaction mixture was refluxed for 18 h. The solvent was removed under reduced pressure and the residue resolved in methanol (20.0 mL) then concentrated again under reduced pressure. This procedure was repeated three times. The product (*S*)-**164** was obtained as a beige solid (15.4 g, 63.7 mmol, 98.8 %). $R_f = 0.40$ (methylene chloride : methanol 7:3). $^1\text{H-NMR}$ (300 MHz, $(\text{CD}_3)_2\text{SO}$): δ (ppm) 9.08 (d, $J = 1.3$ Hz, 1H, $\text{CH}_{\text{ar-2}}$), 7.52 (d, $J = 1.1$ Hz, 1H, $\text{CH}_{\text{ar-5}}$), 4.48 (t, $J = 6.9$ Hz, 1H, CH_α), 3.73 (s, 3H, OCH_3) 3.31 (m, 2H, $\text{CH}_{2\beta}$). $^{13}\text{C-NMR}$ (75 MHz, $(\text{CD}_3)_2\text{SO}$): δ (ppm) 168.5 ($\text{C}_{\text{carbonyl}}$), 134.0 ($\text{C}_{\text{ar-2}}$), 126.6 ($\text{C}_{\text{ar-4}}$), 118.0 ($\text{C}_{\text{ar-5}}$), 53.0 (C_α), 51.0 (OCH_3), 25.0 (C_β). IR (film): ν (cm^{-1}) 3112, 2971, 2920, 2879, 2772, 2679, 2552, 1757, 1624, 1599, 1514, 1458, 1433, 1290, 1256, 1146, 1079, 1065, 987, 832, 817, 718, 621, 537, 408.

5.2.2.33 (*S*)-methyl 2-amino-4-methylpentanoate hydrochloride ((*S*)-**165**)



(*S*)-2-amino-4-methylpentanoic acid ((*S*)-**158**) (5.00 g, 38.11 mmol) was suspended in methanol (45.0 mL) and thionylchloride (2.78 mL, 38.11 mmol) was added drop wise at 0 °C. The reaction mixture was refluxed for 18 h. The solvent was removed under reduced pressure and the residue resolved in methanol (15.0 mL) then concentrated again under reduced pressure. This procedure was repeated three times. The product (*S*)-**165** was obtained as a white solid (6.78 g, 37.3 mmol, 98%). $R_f = 0.27$ (methylene chloride : methanol 10:1). $^1\text{H-NMR}$ (300 MHz, CD_3OD): δ (ppm) 4.07–4.00 (m, 1H, CH_α), 3.84 (s, 3H, OCH_3), 1.84–1.72 (m, 2H, $\text{CH}_{2\beta}$), 1.69–1.62 (m, 1H, CH_γ), 1.00 (dd, $J = 6.2, 3.4$ Hz, 6H, $\text{CH}_\gamma(\text{CH}_3)_2$). $^{13}\text{C-NMR}$ (75 MHz, CD_3OD): δ (ppm) 171.33 ($\text{C}_{\text{carbonyl}}$), 53.65 (C_α), 52.55 (OCH_3), 40.62 (C_β), 25.56 (C_γ), 22.51 (C_δ), 22.43 (C_δ').

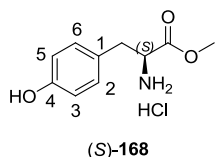
5.2.2.34 (*S*)-methyl 2-amino-3-methylbutanoate hydrochloride ((*S*)-**167**)



(*S*)-2-amino-3-methylbutanoic acid (*S*)-**160** (1.17 g, 10.0 mmol) was dissolved in methanol (15.0 mL) at 0 °C and thionylchloride (726 μL , 10.0 mmol) was added drop wise over a period of 15 min. The reaction mixture was stirred for 2 h at ambient temperature and then refluxed for 8 h. The

solvent was removed under reduced pressure and the residue resolved in methanol (50.0 mL) then concentrated again under reduced pressure. This procedure was repeated three times and then dried *in vacuo*. The product (S)-**167** was obtained as a white solid (1.68 g, 10.0 mmol, quant.). $R_f = 0.44$ (methylene chloride : methanol 15:1). $^1\text{H-NMR}$ (300 MHz, CD_3OD): $\delta(\text{ppm})$ 4.91 (m, 3H, NH_3Cl), 3.94 (d, $J = 4.4$ Hz, 1H, CH_α), 3.85 (s, 3H, OCH_3), 2.35–2.25 (m, 1H, CH_β), 1.07 (dd, $J = 6.8, 2.8$ Hz, 6H, $\text{CH}_\beta(\text{CH}_3)_2$). $^{13}\text{C-NMR}$ (75 MHz, CD_3OD): $\delta(\text{ppm})$ 170.4 ($\text{C}_{\text{carbonyl}}$), 59.4 (C_α), 53.4 (OCH_3), 31.0 (C_β), 18.4 (C_γ), 18.2 (C_γ').

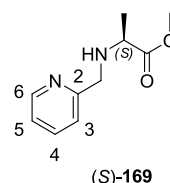
5.2.2.35 (S)-methyl 2-amino-3-(4-hydroxyphenyl)propanoate hydrochloride ((S)-**168**)



(S)-2-amino-3-(4-hydroxyphenyl)propanoate ((S)-**161**) (10.00 g, 55.2 mmol) was suspended in methanol (60 mL). SOCl_2 (4.4 mL, 60.7 mmol) was added drop wise at 0°C over a period of 30 min. The reaction mixture was stirred for an additional hour at 0°C then refluxed for 16 h. The solvent was evaporated under reduced pressure and the residue was resolved in methanol (15.0 mL) then concentrated again under reduced pressure. This procedure was repeated three times. The product (S)-**168** was obtained as white solid (12.6 g, 54.7 mmol, quant.). $R_f = 0.42$ (methylene chloride : methanol 15:1). $^1\text{H-NMR}$ (300 MHz, CD_3OD): $\delta(\text{ppm})$ 7.08 (d, 2H, $J = 8.6$ Hz, $\text{CH}_{\text{ar-2}}$ & $\text{CH}_{\text{ar-6}}$), 6.79 (d, 2H, $J = 8.5$ Hz, $\text{CH}_{\text{ar-3}}$ & $\text{CH}_{\text{ar-5}}$), 4.25 (dd, 1H, $J = 6.1, 7.1$ Hz, CH_α), 3.81 (s, 3H, OCH_3), 3.17 (dd, 1H, $J = 6.0, 14.5$ Hz, $\text{CH}_\beta\text{H}_\beta$), 3.09 (dd, 1H, $J = 7.2, 14.5$ Hz, $\text{CH}_\beta\text{H}_\beta$). $^{13}\text{C-NMR}$ (75 MHz, CD_3OD):

$\delta(\text{ppm})$ 170.51 ($\text{C}_{\text{carbonyl}}$), 158.36 ($\text{C}_{\text{ar-4}}$), 131.53 ($\text{C}_{\text{ar-1}}$), 125.60 (2C, $\text{C}_{\text{ar-2}}$ & $\text{C}_{\text{ar-6}}$), 116.89 (2C, $\text{C}_{\text{ar-3}}$ & $\text{C}_{\text{ar-5}}$), 55.42 (C_α), 53.54 (OCH_3), 36.59 (C_β). IR (film): ν (cm^{-1}) 3209, 3015, 2954, 1742, 1610, 1513, 1445, 1379, 1239, 1142, 1113, 1054, 988, 942, 897, 833, 729, 635, 553, 513. HRMS calculated for $\text{C}_{10}\text{H}_{14}\text{NO}_3$ ($\text{M} + \text{H}^+$) 196.0974 found ($\text{M} + \text{H}^+$) 196.0968.

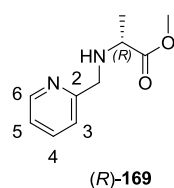
5.2.2.36 (S)-methyl 2-(pyridin-2-ylmethylamino)propanoate ((S)-**169**)



Palladium on carbon (1.70 g, 1.67 mmol, 10 wt. %) was suspended in methanol (120.0 mL) and picolinaldehyde (**103**) (6.39 mL, 67.0 mmol) was added at 0°C . Sodium acetate (9.15 g, 111.6 mmol) was added to the reaction mixture. Then, (S)-**162** (7.80 g, 55.8 mmol) was dissolved in methanol (45 mL) and then added to the reaction mixture. The reaction mixture was stirred for 1 h and the nitrogen atmosphere was completely substituted by hydrogen in three turns. The reaction was continued for 72 h allowing the mixture to warm up to ambient temperature. The reaction mixture was filtrated over CELITE and the crude material was subjected to column chromatography using methylene chloride : methanol (35:1 \rightarrow 20:1). The product (S)-**169** was obtained as a brown oil (7.08 g, 36.4 mmol, 65%). $R_f = 0.51$ (methylene chloride : methanol 10:1). $^1\text{H-NMR}$ (300 MHz, CDCl_3): $\delta(\text{ppm})$ 8.56 (ddd, $J = 4.8, 1.6, 0.9$ Hz, 1H, $\text{CH}_{\text{ar-6}}$), 7.67 (td, $J = 7.7, 1.8$ Hz, 1H, $\text{CH}_{\text{ar-4}}$), 7.35 (d, $J = 7.8$ Hz, 1H, $\text{CH}_{\text{ar-3}}$), 7.19 (dd, $J = 7.1, 5.3$ Hz, 1H, $\text{CH}_{\text{ar-5}}$), 4.03 (d, $J = 14.2$ Hz, 1H, NCHH), 3.96 (d, $J = 14.3$ Hz, 1H, NCHH), 3.74 (s, 3H, OCH_3), 3.63–3.54 (m, 1H, CH_α), 1.45 (d, $J = 7.0$ Hz, 3H, $\text{CH}_{3\beta}$).

^{13}C -NMR (75 MHz, CDCl_3): δ (ppm) 175.01 ($\text{C}_{\text{carbonyl}}$), 158.09 ($\text{C}_{\text{ar-2}}$), 149.30 ($\text{C}_{\text{ar-6}}$), 136.84 ($\text{C}_{\text{ar-4}}$), 122.54 ($\text{C}_{\text{ar-3}}$), 122.42 ($\text{C}_{\text{ar-5}}$), 56.19 (NCH_2), 52.62 (C_α), 52.14 (OCH_3), 18.49 (C_β). IR (film): ν (cm^{-1}) 2985, 2948, 1733, 1677, 1591, 1435, 1374, 1202, 1151, 1038, 992, 915, 729, 616, 530, 471, 404. HRMS calculated for $\text{C}_{10}\text{H}_{15}\text{N}_2\text{O}_2$ ($\text{M} + \text{H}^+$) 195.1128 found ($\text{M} + \text{H}^+$) 195.1128.

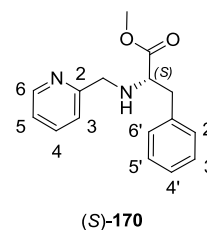
5.2.2.37 (*R*)-methyl 2-(pyridin-2-ylmethylamino)propanoate ((*R*)-**169**)



Palladium on carbon (637 mg, 0.6 mmol, 10 wt. %) was suspended in methanol (45.0 mL) and picolinaldehyde (**103**) (2.29 mL, 24.07 mmol) was added at 0 °C. Sodium acetate (3.29 g, 40.12 mmol) was added to the reaction mixture. Then, (*R*)-**162** (2.80 g, 20.06 mmol) was added. The reaction mixture was stirred for 1 h and the nitrogen atmosphere was completely substituted by hydrogen in three turns. The reaction was continued for 72 h allowing the mixture to warm up to ambient temperature. The reaction mixture was filtrated over CELITE and the crude material was subjected to column chromatography using methylene chloride : methanol (35:1 \rightarrow 20:1). The product (*R*)-**169** was obtained as a brown oil (2.21 g, 11.3 mmol, 57%). R_f = 0.51 (methylene chloride : methanol 10:1). ^1H -NMR (300 MHz, CDCl_3): δ (ppm) 8.56 (ddd, J = 4.9, 1.7, 0.9 Hz, 1H, $\text{CH}_{\text{ar-6}}$), 7.66 (td, J = 7.7, 1.8 Hz, 1H, $\text{CH}_{\text{ar-4}}$), 7.35 (d, J = 7.8 Hz, 1H, $\text{CH}_{\text{ar-3}}$), 7.22–7.16 (m, 1H, $\text{CH}_{\text{ar-5}}$), 4.02 (d, J = 14.1 Hz, 1H, NCHH), 3.95 (d, J = 14.1 Hz, 1H, NCHH), 3.74 (s, 3H, OCH_3), 3.57 (q, J = 7.0 Hz, 1H, CH_α), 1.45 (d, J = 7.0 Hz, 3H, $\text{CH}_{3\beta}$). ^{13}C -NMR (75 MHz, CDCl_3): δ (ppm) 175.79

($\text{C}_{\text{carbonyl}}$), 159.28 ($\text{C}_{\text{ar-2}}$), 149.41 ($\text{C}_{\text{ar-6}}$), 136.55 ($\text{C}_{\text{ar-4}}$), 122.26 ($\text{C}_{\text{ar-3}}$), 122.10 ($\text{C}_{\text{ar-5}}$), 56.37 (NCH_2), 53.27 (C_α), 51.92 (OCH_3), 19.03 (C_β). IR (film): ν (cm^{-1}) 2978, 2951, 1731, 1591, 1570, 1472, 1433, 1373, 1331, 1197, 1150, 1093, 1068, 1046, 994, 976, 851, 753, 656, 626, 529, 469, 403.

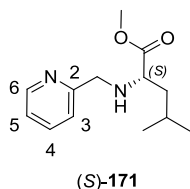
5.2.2.38 (*S*)-methyl 3-phenyl-2-(pyridin-2-ylmethylamino)propanoate ((*S*)-**170**)



Palladium on carbon (2.39 g, 2.26 mmol, 10 wt. %) was suspended in methanol (160.0 mL) and picolinaldehyde (7.2 mL, 75.28 mmol) was added at 0 °C. Sodium acetate (10.2 g, 125.46 mmol) was added to the reaction mixture. Then, (*S*)-**163** (13.53 g, 62.73 mmol) was added. The reaction mixture was stirred for 1 h and the nitrogen atmosphere was completely substituted by hydrogen in three turns. The reaction was continued for 22 h allowing the mixture to warm up to ambient temperature. The reaction mixture was filtrated over CELITE and the crude material was subjected to column chromatography using methylene chloride : methanol (35:1). The product (*S*)-**170** was obtained as a brown oil (14.58 g, 53.95 mmol, 86%). R_f = 0.39 (methylene chloride : methanol 15:1). ^1H -NMR (300 MHz, CD_3OD): δ (ppm) 8.42 (d, J = 4.8 Hz, 1H, $\text{CH}_{\text{ar-6}}$), 7.72 (ddd, J = 9.4, 7.8, 1.7 Hz, 1H, $\text{CH}_{\text{ar-4}}$), 7.33 (d, J = 8.0 Hz, 1H, $\text{CH}_{\text{ar-3}}$), 7.30–7.16 (m, 6H, $\text{CH}_{\text{ar-5}}$, $\text{CH}_{\text{ar-2'-5'}}$), 3.91 (d, J = 14.5 Hz, 1H, NCHH), 3.84 (d, 1H, J = 14.5 Hz, NCHH), 3.60 (s, 3H, OCH_3), 3.54 (t, 1H, J = 7.2 Hz, CH_α), 2.97 (d, 2H, J = 7.3 Hz, $\text{CH}_{2\beta}$), 1.97 (s, 1H, NH). ^{13}C -NMR (75 MHz, CD_3OD): δ (ppm) 175.66 ($\text{C}_{\text{carbonyl}}$), 160.18 ($\text{C}_{\text{ar-2}}$),

149.58 (C_{ar-6}), 138.61 (C_{ar-4}), 138.51 ($C_{ar-1'}$), 130.31 (2C, $C_{ar-3'}$ & $C_{ar-5'}$), 129.41 (2C, $C_{ar-2'}$ & $C_{ar-6'}$), 127.73 ($C_{ar-4'}$), 123.82 (C_{ar-3}), 123.62 (C_{ar-5}), 63.59 (NCH_2), 53.56 (C_α), 52.16 (OCH_3), 40.29 (C_β). IR (film): ν (cm^{-1}) 3322, 3060, 3026, 2948, 2848, 1732, 1593, 1435, 1362, 1264, 1200, 1170, 1076, 996, 753, 700, 621, 528, 490, 405. HRMS calculated for $C_{16}H_{19}N_2O_2$ ($M + H^+$) 271.1441 found ($M + H^+$) 271.1441.

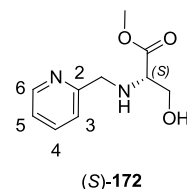
5.2.2.39 (*S*)-methyl 4-methyl-2-(pyridin-2-yl-methylamino)pentanoate ((*S*)-**171**)



Palladium on carbon (1.55 g, 1.46 mmol, 10 wt. %) was suspended in methanol (50.0 mL) and picolinaldehyde (**103**) (5.59 mL, 58.7 mmol) was added at 0 °C. Sodium acetate (8.02 g, 82.1 mmol) was added to the reaction mixture. Then, (*S*)-**165** (6.78 g, 37.8 mmol) was added. The reaction mixture was stirred for 1 h and the nitrogen atmosphere was completely substituted by hydrogen in three turns. The reaction was continued for 72 h allowing the mixture to warm up to ambient temperature. The reaction mixture was filtrated over CELITE and the crude material was subjected to column chromatography using methylene chloride : methanol (50:1 \rightarrow 25:1). The product (*S*)-**171** was obtained as a brown oil (4.88 g, 20.65 mmol, 55%). R_f = 0.62 (methylene chloride : methanol 10:1). 1H -NMR (300 MHz, $CDCl_3$): δ (ppm) 8.54 (ddd, J = 4.9, 1.7, 0.9 Hz, 1H, CH_{ar-6}), 7.65 (td, J = 7.7, 1.8 Hz, 1H, CH_{ar-4}), 7.35 (d, J = 7.8 Hz, 1H, CH_{ar-3}), 7.17 (dd, J = 7.0, 5.4 Hz, 1H, CH_{ar-5}), 3.98 (d, J = 14.2 Hz, 1H, $NCHH$), 3.85 (d, J = 14.2 Hz, 1H, $NCHH$), 3.72 (s, 3H, OCH_3), 3.42 (t, J = 7.2 Hz, 1H, CH_α), 1.83–1.71 (m, 1H, CH_γ), 1.58

(td, J = 7.1, 3.0 Hz, 2H, $CH_{2\beta}$), 0.95–0.84 (m, 6H, $CH_\gamma(CH_3)_2$). ^{13}C -NMR (75 MHz, $CDCl_3$): δ (ppm) 176.10 ($C_{carbonyl}$), 159.56 (C_{ar-2}), 149.31 (C_{ar-6}), 136.48 (C_{ar-4}), 122.24 (C_{ar-3}), 122.05 (C_{ar-5}), 59.76 (NCH_2), 53.60 (C_α), 51.74 (OCH_3), 42.82 (C_β), 25.00 (C_γ), 22.83 (C_δ), 22.37 ($C_{\delta'}$). IR (film): ν (cm^{-1}) 2953, 2869, 1732, 1590, 1570, 1468, 1433, 1385, 1367, 1330, 1308, 1269, 1230, 1194, 1149, 1046, 992, 826, 754.

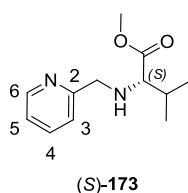
5.2.2.40 (*S*)-methyl 3-hydroxy-2-(pyridin-2-ylmethylamino)propanoate ((*S*)-**172**)



Palladium on carbon (258 mg, 0.23 mmol, 10 wt. %) was suspended in methanol (17.0 mL) and picolinaldehyde (**103**) (767 μ L, 8.17 mmol) was added at 0 °C. Sodium acetate (1.32 g, 16.02 mmol) was added to the reaction mixture. Then, (*S*)-methyl 2-amino-3-hydroxypropanoate hydrochloride ((*S*)-**166**) (1.25 g, 8.17 mmol) dissolved in methanol (8.5 mL) was added. The reaction mixture was stirred for 1 h and the nitrogen atmosphere was completely substituted by hydrogen in three turns. The reaction was continued for 16 h allowing the mixture to warm up to ambient temperature. The reaction mixture was filtrated over CELITE and the crude material was subjected to column chromatography using methylene chloride : methanol (50:1 \rightarrow 10:1). The product (*S*)-**172** was obtained as a yellow oil (1.03 g, 4.8 mmol, 58%). R_f = 0.41 (methylene chloride : methanol 10:1). 1H -NMR (300 MHz, $CDCl_3$): δ (ppm) 8.57 (ddd, J = 4.9, 1.6, 0.9 Hz, 1H, CH_{ar-6}), 7.68 (td, J = 7.7, 1.8 Hz, 1H, CH_{ar-4}), 7.31 (d, J = 7.8 Hz, 1H, CH_{ar-3}), 7.22 (dd, J = 7.0, 5.4 Hz, 1H, CH_{ar-5}), 4.13 (d, J = 14.7 Hz,

1H, NCHH), 4.01 (d, $J = 14.7$ Hz, 1H, NCHH), 3.89 (d, $J = 4.1$ Hz, 1H, CH_α), 3.80 (d, $J = 6.0$ Hz, 1H, $CH_\beta H_\beta$), 3.76 (s, 3H, OCH_3), 3.60 (dd, $J = 6.0, 4.0$ Hz, 1H, $CH_\beta H_\beta$). IR (film): ν (cm^{-1}) 3315, 2951, 2874, 1732, 1659, 1593, 1571, 1472, 1434, 1367, 1335, 1199, 1175, 1149, 1061, 1048, 995, 836, 756. HRMS calculated for $C_{10}H_{15}N_2O_3$ ($M + H^+$) 211.1083 found ($M + H^+$) 211.1078.

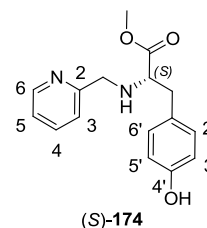
5.2.2.41 (*S*)-methyl 3-methyl-2-(pyridin-2-ylmethylamino)butanoate ((*S*)-**173**)



Palladium on carbon (200 mg, 0.19 mmol, 10 wt. %) was suspended in methanol (15.0 mL) and picolinaldehyde (**103**) (908 μ L, 9.5 mmol) was added at 0 °C. Sodium acetate (1.56 g, 19.0 mmol) was dissolved in methanol (15.0 mL) and added to the reaction mixture. Then, (*S*)-**167** (1.60 g, 9.5 mmol) presolved in methanol (10 mL) was added. The reaction mixture was stirred for 30 min and the nitrogen atmosphere was completely substituted by hydrogen in three turns. The reaction was continued for 5 h allowing the mixture to warm up to ambient temperature. The reaction mixture was filtrated over CELITE, dried over sodium sulfate, filtrated and concentrated under reduced pressure. The crude material was subjected to column chromatography using methylene chloride : methanol (35:1). The product (*S*)-**173** was obtained as a yellow oil (510 mg, 2.3 mmol, 24%). $R_f = 0.46$ (methylene chloride : methanol 35:1). 1H -NMR (300 MHz, $CDCl_3$): δ (ppm) 8.53 (d, $J = 4.9$ Hz, 1H, CH_{ar-6}), 7.64 (td, $J = 7.7$ Hz, 1.8 Hz, 1H, CH_{ar-4}), 7.38 (d, $J = 7.8$ Hz, 1H, CH_{ar-3}), 7.15 (dd, $J = 7.4$ Hz, 5.4 Hz, 1H, CH_{ar-5}), 3.97 (d, $J = 14.2$ Hz, 1H, NCHH), 3.78 (d, $J = 14.2$ Hz, 1H,

NCHH), 3.71 (s, 3H, OCH_3), 3.10 (dd, $J = 6.1$ Hz, 1.3 Hz, 1H, CH_α), 2.01-1.94 (m, 1H, CH_β), 0.97 (dd, $J = 10.4, 6.9$ Hz, 6H, $CH_\beta(CH_3)_2$). ^{13}C -NMR (75 MHz, $CDCl_3$): δ (ppm) 175.2 ($C_{carbonyl}$), 159.5 (C_{ar-2}), 149.2 (C_{ar-6}), 137.4 (C_{ar-4}), 126.6 (C_{ar-3}), 122.1 (C_{ar-5}), 67.1 (NCH₂), 54.0 (C_α), 51.6 (OCH_3), 31.7 (C_β), 19.3 (C_γ), 18.9 (C_γ). IR (film): ν (cm^{-1}) 2960, 2876, 1730, 1685, 1591, 1516, 1465, 1434, 1367, 1238, 1192, 1147, 1044, 994, 896, 757, 699, 619, 469, 409. HRMS calculated for $C_{12}H_{18}N_2O_2Na$ ($M + Na^+$) 245.1266 found ($M + Na^+$) 245.1270.

5.2.2.42 (*S*)-methyl 3-(4-hydroxyphenyl)-2-(pyridin-2-ylmethylamino)propanoate ((*S*)-**174**)

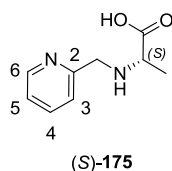


Palladium on carbon (2.15 g, 2.03 mmol, 10 wt. %) was suspended in methanol (100.0 mL) and picolinaldehyde (**103**) (6.4 mL, 67.6 mmol) was added at 0 °C. Sodium acetate (9.23 g, 112.52 mmol) was added to the reaction mixture. Then, (*S*)-**168** (13.05 g, 56.33 mmol) dissolved in methanol (70 mL) was added drop wise. The reaction mixture was stirred for 1 h and the nitrogen atmosphere was completely substituted by hydrogen in three turns. The reaction was continued for 16 h allowing the mixture to warm up to ambient temperature. The reaction mixture was filtrated over CELITE and the crude material was subjected to column chromatography using methylene chloride : methanol (35:1). The product (*S*)-**174** was obtained as a beige solid (10.66 g, 37.23 mmol, 66%). $R_f = 0.35$ (methylene chloride : methanol 15:1). 1H -NMR (300 MHz, CD_3OD): δ (ppm) 8.43 (d, $J = 4.2$ Hz, 1H, CH_{ar-6}), 7.74 (ddd, $J =$

9.2, 7.7, 1.5 Hz, 1H, CH_{ar-4}), 7.34 (d, $J = 7.9$ Hz, 1H, CH_{ar-3}), 7.27 (dd, $J = 5.4, 6.7$ Hz, 1H, CH_{ar-5}), 6.98 (d, $J = 8.5$ Hz, 2H, $CH_{ar-2'}$ & $CH_{ar-6'}$), 6.69 (d, $J = 8.5$ Hz, 2H, $CH_{ar-3'}$ & $CH_{ar-5'}$), 3.90 (d, $J = 14.3$ Hz, 1H, NCHH), 3.75 (d, $J = 14.5$ Hz, 1H, NCHH), 3.61 (s, 3H, (OCH₃)), 3.48 (t, $J = 6.9$ Hz, 1H, CH_{α}), 2.88 (d, $J = 7.9$ Hz, 2H, $CH_{2\beta}$). ¹³C-NMR (75 MHz, CD₃OD): δ (ppm) 175.94 ($C_{carbonyl}$), 160.27 (C_{ar-2}), 157.34 ($C_{ar-4'}$), 149.63 (C_{ar-6}), 138.58 (C_{ar-4}), 131.28 ($C_{ar-1'}$), 129.09 (2C, $C_{ar-2'}$ & $C_{ar-6'}$), 123.94 (C_{ar-3}), 123.67 (C_{ar-5}), 116.22 (2C, $C_{ar-3'}$ & $C_{ar-5'}$), 63.85 (NCH₂), 53.64 (C_{α}), 52.13 (OCH₃), 39.54 (C_{β}). IR (film): ν (cm⁻¹) 3319, 3014, 2947, 2852, 2680, 2597, 1731, 1595, 1513, 1438, 1368, 1236, 1203, 1170, 1049, 1001, 826, 759, 632, 551, 526, 491, 405. HRMS calculated for C₁₆H₁₉N₂O₃ ($M + H^+$) 287.1396 found ($M + H^+$) 287.1390.

5.2.2.43 (S)-2-(pyridin-2-ylmethylamino)

propanoic acid ((S)-175)

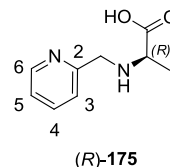


(S)-169 (1.63 g, 8.4 mmol) was suspended in sodium hydroxide solution (1 M, 16.8 mL) and stirred for 16 h at 0 °C. The reaction mixture was neutralised with hydrochloric acid (2 M) and extracted with methylene chloride (3 x 50 mL). The aqueous layer was concentrated and the solvent evaporated under reduced pressure. The residue was suspended in ethanol (25 mL) and filtrated over CELITE. The orange coloured filtrate was concentrated and dried in *vacuo* to provide the product (S)-175 as brown oil (605 mg, 3.36 mmol, 40%). $R_f = 0.85$ (methylene chloride : methanol 15:1). ¹H-NMR (300 MHz, CD₃OD): δ (ppm) 8.63–8.59 (m, 1H, CH_{ar-6}), 7.89–7.81 (m, 1H, CH_{ar-4}), 7.46 (d, $J = 7.9$ Hz, 1H, CH_{ar-3}), 7.39–7.28 (m, 1H, CH_{ar-5}) 4.29 (d, J

= 14.5 Hz, 1H, NCHH), 4.20 (d, $J = 14.6$ Hz, 1H, NCHH), 4.01 (d, $J = 7.7$ Hz, 1H, CH_{α}), 1.49 (d, $J = 7.2$ Hz, 3H, $CH_{3\beta}$). HRMS calculated for C₉H₁₃N₂O₂ ($M + H^+$) 181.0972 found ($M + H^+$) 181.0973.

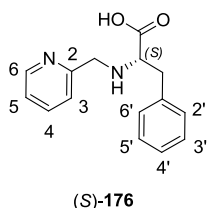
5.2.2.44 (R)-2-(pyridin-2-ylmethylamino)

propanoic acid ((R)-175)



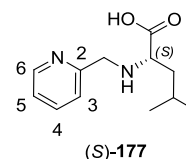
(R)-169 (530 g, 2.73 mmol) were suspended in sodium hydroxide (3.40 mL, 1 M) at 0 °C and reacted for 18 h. The reaction mixture was washed with methylene chloride (3 x 10 mL). The combined aqueous layer was neutralised to pH 7 with hydrochloric acid (1 M). The aqueous layer was concentrated and the solvent removed under reduced pressure. The residue was suspended in ethanol (5.00 mL) and filtrated via a syringe filter. The residue was dried *in vacuo* to obtain the product (R)-175 as a yellow oil (262 mg, 1.09 mmol, 40%). $R_f = 0.85$ (methylene chloride : methanol 15:1). ¹H-NMR (300 MHz, CD₃OD): δ (ppm) 8.52 (ddd, $J = 4.9, 1.6, 0.8$ Hz, 1H, CH_{ar-6}), 7.79 (td, $J = 7.7, 1.8$ Hz, 1H, CH_{ar-4}), 7.45 (d, $J = 7.8$ Hz, 1H, CH_{ar-3}), 7.30 (ddd, $J = 7.5, 5.0, 1.0$ Hz, 1H, CH_{ar-5}), 3.96 (d, $J = 13.8$ Hz, 1H, NCHH), 3.85 (d, $J = 13.9$ Hz, 1H, NCHH), 3.24 (q, $J = 6.9$ Hz, 1H, CH_{α}), 1.34 (d, $J = 7.0$ Hz, 3H, $CH_{3\beta}$). ¹³C-NMR (75 MHz, CD₃OD): δ (ppm) 181.78 ($C_{carbonyl}$), 159.80 (C_{ar-2}), 150.03 (C_{ar-6}), 138.51 (C_{ar-4}), 124.04 (C_{ar-3}), 123.69 (C_{ar-5}), 59.81 (C_{α}), 53.60 (OCH₃), 19.31 (C_{β}). IR (film): ν (cm⁻¹) 3307, 3056, 2975, 2931, 2844, 1572, 1470, 1430, 1397, 1358, 1281, 1147, 1093, 1053, 995, 826, 754, 675, 623, 540. HRMS calculated for C₉H₁₃N₂O₂ ($M + H^+$) 181.0972 found ($M + H^+$) 181.0972.

5.2.2.45 (S)-3-phenyl-2-(pyridin-2-ylmethyl-amino)propanoic acid ((S)-176)

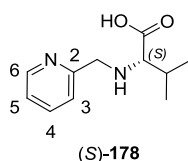


(S)-170 (3.05 g, 11.28 mmol) was suspended in sodium hydroxide (15 mL, 1 M *aq.*) and cooled to 0 °C. After 18 h the aqueous layer was extracted with methylene chloride (3 x 5 mL). The aqueous layer was then neutralised using hydrochloric acid (1 M *aq.*). The solvent was evaporated under reduced pressure. The residue was suspended in ethanol (10.00 mL) by sonification. The suspension was filtrated using a syringe filter and the filtrate was concentrated *in vacuo*. The product (S)-176 was obtained as brown solid (2.29 g, 8.93 mmol, 80%). $R_f = 0.10$ (methylene chloride : methanol 35:1). IR (film): ν (cm⁻¹) 3372, 3059, 2928, 2855, 1587, 1434, 1391, 1267, 1148, 1104, 1053, 1000, 896, 732, 698, 622, 547, 499, 404. HRMS calculated for C₁₅H₁₇N₂O₂ (M + H⁺) 257.1285 found (M + H⁺) 257.1285.

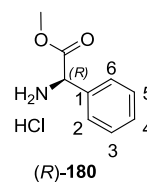
5.2.2.46 (S)-4-methyl-2-(pyridin-2-ylmethyl-amino)pentanoic acid ((S)-177)



(S)-171 (2.22 g, 9.40 mmol) were suspended in sodium hydroxide (12 mL, 1 M) at 0 °C and reacted for 18 h. The reaction mixture was washed with methylene chloride (3 x 20 mL). The combined aqueous layer was neutralised to pH 7 with hydrochloric acid (1 M). The aqueous layer was concentrated and the solvent removed under reduced pressure. The residue was suspended in ethanol (10.00 mL) and filtrated via a syringe filter. The residue was dried *in vacuo* to obtain the product (S)-177 as a yellow oil (1.94 g, 8.74 mmol, 93%). $R_f = 0.08$ (methylene chloride : methanol 10:1). ¹H-NMR (300 MHz, CD₃OD): δ (ppm) 8.57 – 8.53 (m, 1H, CH_{ar}-6), 7.82 (td, J = 7.7, 1.8 Hz, 1H, CH_{ar}-4), 7.47 (d, J = 7.8 Hz, 1H, CH_{ar}-3), 7.34 (dd, J = 7.1, 5.3 Hz, 1H, CH_{ar}-5), 4.20 (d, J = 14.5 Hz, 1H, NCHH), 4.07 (d, J = 14.5 Hz, 1H, NCHH), 3.39 (t, J = 7.1 Hz, 1H, CH_α), 1.94–1.79 (m, 1H, CH_γ), 1.75–1.51 (m, 2H, CH_{2β}), 0.97 (d, J = 6.5 Hz, 3H, CH_{3δ}), 0.93 (d, J = 6.6 Hz, 3H, CH_{3δ'}). ¹³C-NMR (75 MHz, CD₃OD): δ (ppm) 177.80 (C_{carbonyl}), 156.50 (C_{ar}-2), 150.11 (C_{ar}-6), 138.60 (C_{ar}-4), 124.26 (C_{ar}-3), 124.08 (C_{ar}-5), 63.13 (NCH₂), 52.48 (C_α), 42.60 (C_β), 26.15 (C_γ), 23.03 (C_δ), 22.99 (C_{δ'}). IR (film): ν (cm⁻¹) 2952, 2867, 1733, 1581, 1467, 1434, 1396, 1207, 1149, 1121, 1040, 997, 928, 815, 755, 679, 628, 546, 487.

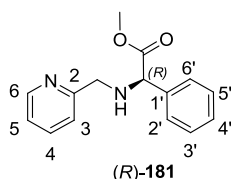
5.2.2.47 (*S*)-3-methyl-2-(pyridin-2-ylmethyl-amino)butanoic acid ((*S*)-**178**)

(*S*)-**173** (460 mg, 2.07 mmol) were suspended in sodium hydroxide solution (1 M, 4.14 mL, *aq.*) at 0 °C and stirred at ambient temperature for 16 h. The reaction mixture was neutralised with hydrochloric acid (2 M) and the solvent was evaporated under reduced pressure. The pale solid was suspended in ethanol (25 mL) and filtrated over CELITE. The filtrate was dried *in vacuo* to provide the product (*S*)-**178** as a yellow solid (420 mg, 2.02 mmol, 98%). R_f = 0.85 (methylene chloride : methanol 15:1). $^1\text{H-NMR}$ (300 MHz, CD_3OD): δ (ppm) 8.63 (d, J = 4.6 Hz, 1H, $\text{CH}_{\text{ar-6}}$), 7.85 (td, J = 7.7, 1.8 Hz, 1H, $\text{CH}_{\text{ar-4}}$), 7.47-7.38 (m, 2H, $\text{CH}_{\text{ar-3}}$ & $\text{CH}_{\text{ar-5}}$), 4.40 (d, J = 15.0 Hz, 1H, NCHH), 4.30 (d, J = 15.0 Hz, 1H, NCHH), 3.43 (d, J = 3.9 Hz, 1H, CH_α), 2.29 (m, 1H, CH_β), 1.10 (t, 6H, J = 6.9 Hz, $\text{CH}_\beta(\text{CH}_3)_2$). IR (film): ν (cm^{-1}) 3089, 2800, 2257, 1986, 1921, 1574, 1474, 1434, 1396, 1357, 1283, 1137, 1093, 1064, 1000, 880, 850, 817, 756, 679, 625, 545, 478, 437, 414. HRMS calculated for $\text{C}_{11}\text{H}_{17}\text{N}_2\text{O}_2$ ($\text{M} + \text{H}^+$) 209.1285 found ($\text{M} + \text{H}^+$) 209.1287.

5.2.2.48 (*R*)-methyl 2-amino-2-phenylacetate hydrochloride ((*R*)-**180**)

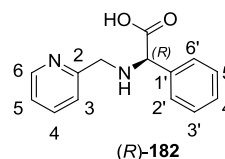
(*R*)-2-amino-2-phenylacetic acid ((*R*)-**179**) (5.00 g, 33.1 mmol) was suspended in methanol (30.0 mL) and thionylchloride (2.40 mL, 33.1 mmol) was added drop wise at 0 °C. The reaction mixture was refluxed for 18 h. The solvent was removed under reduced pressure and the residue resolved in methanol (10.0 mL) then concentrated again under reduced pressure. This procedure was repeated three times. The product (*R*)-**180** was obtained as white solid (6.05 g, 30 mmol, quant.). $^1\text{H-NMR}$ (300 MHz, CDCl_3): δ (ppm) 7.49 (m, 5H, $\text{CH}_{\text{ar-2-5}}$), 5.19 (s, 1H, CH_α), 3.81 (s, 3H, OCH_3). $^{13}\text{C-NMR}$ (75 MHz, CDCl_3): δ (ppm) 170.1 ($\text{C}_{\text{carbonyl}}$), 133.3 ($\text{C}_{\text{ar-1}}$), 131.2 (2C, $\text{C}_{\text{ar-2}}$ & $\text{C}_{\text{ar-6}}$), 130.6 (2C, $\text{C}_{\text{ar-3}}$ & $\text{C}_{\text{ar-5}}$), 129.1 ($\text{C}_{\text{ar-4}}$), 57.5 (C_α), 53.9 (OCH_3). IR (film): ν (cm^{-1}) 2959, 2839, 2697, 2625, 1736, 1568, 1501, 1456, 1432, 1361, 1384, 1239, 1179, 1142, 1054, 1027, 960, 920, 885, 726, 690, 588, 497. HRMS calculated for $\text{C}_9\text{H}_{12}\text{N}_1\text{O}_2$ ($\text{M} + \text{H}^+$) 166.0863 found ($\text{M} + \text{H}^+$) 166.0865.

5.2.2.49 (*R*)-methyl 2-phenyl-2-(pyridin-2-ylmethylamino)acetate ((*R*)-**181**)



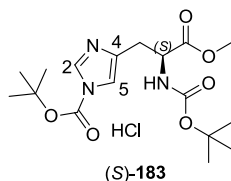
Palladium on carbon (1.06 g, 1.00 mmol, 10 wt. %) was suspended in methanol (70.0 mL) and picolinaldehyde (**103**) (2.62 mL, 40.2 mmol) was added at 0 °C. Sodium acetate (2.85 g, 67.0 mmol) was dissolved in methanol (30.0 mL) and added to the reaction mixture. Then, (*R*)-**180** (6.75 g, 33.5 mmol) was added. The reaction mixture was stirred for 30 min and the nitrogen atmosphere was completely substituted by hydrogen in three turns. The reaction was continued for 16 h allowing the mixture to warm up to ambient temperature. The reaction mixture was filtrated over CELITE and the crude material was subjected to column chromatography using methylene chloride : methanol (35:1). The product (*R*)-**181** was obtained as a brown oil (3.63 g, 14.2 mmol, 42.3%). R_f = 0.10 (methylene chloride : methanol 35:1). $^1\text{H-NMR}$ (300 MHz, CDCl_3): δ (ppm) 8.56 (d, J = 5.0 Hz, 1H, $\text{CH}_{\text{ar-6}}$), 7.68 (m, 1H, $\text{CH}_{\text{ar-4}}$), 7.44-7.34 (m, 7H, $\text{CH}_{\text{ar-3}}$, $\text{CH}_{\text{ar-5}}$, $\text{CH}_{\text{ar-2'-6'}}$), 4.63 (s, 1H, CH_α), 3.81-3.98 (m, 2H, NHCH_2), 3.72 (s, 3H, OCH_3), 2.08 (s, 1H, NH).

5.2.2.50 (*R*)-2-phenyl-2-(pyridin-2-ylmethylamino)acetic acid ((*R*)-**182**)



(*R*)-**181** (1.00 g, 3.90 mmol) were suspended in sodium hydroxide (4.90 mL, 1 M) at 0 °C and reacted for 18 h. The reaction mixture was washed with methylene chloride (3 x 20 mL). The combined aqueous layer was neutralised to pH 7 with hydrochloric acid (1 M). The aqueous layer was concentrated and the solvent removed under reduced pressure. The residue was suspended in ethanol (8.00 mL) and filtrated via a syringe filter. The residue was dried *in vacuo* to obtain the product (*R*)-**182** as a yellow solid (940 mg, 3.87 mmol, quant.). $^1\text{H-NMR}$ (300 MHz, CD_3OD): δ (ppm) 8.55 (d, J = 4.8 Hz, 1H, $\text{CH}_{\text{ar-6}}$), 7.83-7.77 (dt, J = 7.7, 1.8 Hz, 1H, $\text{CH}_{\text{ar-4}}$), 7.51-7.48 (m, 2H, $\text{CH}_{\text{ar-3}}$ & $\text{CH}_{\text{ar-5}}$), 7.42-7.32 (m, 5H, $5\times\text{CH}_{\text{ar}}$), 4.49 (s, 1H, CH_α), 4.35-4.01 (m, 2H, NCH_2). $^{13}\text{C-NMR}$ (75 MHz, CD_3OD): δ (ppm) 174.7 ($\text{C}_{\text{carbonyl}}$), 155.7 ($\text{C}_{\text{ar-2}}$), 150.2 ($\text{C}_{\text{ar-6}}$), 138.6 ($\text{C}_{\text{ar-3}}$), 137.6 ($\text{C}_{\text{ar-1'}}$), 129.8 (2C, $\text{C}_{\text{ar-2'}}$ & $\text{C}_{\text{ar-6'}}$), 129.6 (2C, $\text{C}_{\text{ar-3'}}$ & $\text{C}_{\text{ar-5'}}$), 124.3 ($\text{C}_{\text{ar-4'}}$), 124.1 ($\text{C}_{\text{ar-5}}$), 67.7 (NCH_2), 51.5 (C_α). IR (film): ν (cm^{-1}) 3377, 3058, 2836, 1589, 1569, 1473, 1454, 1434, 1382, 1361, 1262, 1191, 1150, 997, 746, 696, 611, 508. HRMS calculated for $\text{C}_{14}\text{H}_{15}\text{N}_2\text{O}_2$ ($\text{M} + \text{H}^+$) 243.1128 found ($\text{M} + \text{H}^+$) 243.1131.

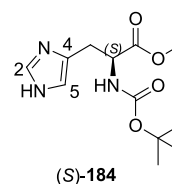
5.2.2.51 (*S*)-*tert*-butyl 4-(2-(*tert*-butoxycarbonylamino)-3-methoxy-3-oxopropyl)-1*H*-imidazole-1-carboxylate hydrochloride ((*S*)-**183**)



(*S*)-**164** (15.4 g, 63.7 mmol) was dissolved in methanol (70.0 mL) and di-*tert*-butyl dicarbonate (27.8 g, 127 mmol) pre-solved in methanol (10.0 mL) was added drop wise. Then, triethylamine was added drop wise under extensive stirring at 0 °C. The reaction was proceeded for 16 h and warmed up to ambient temperature. The entire reaction mixture was poured into water (100 mL) and then extracted with methylene chloride (3 x 100 mL). The combined organic layer was dried over sodium sulfate, filtrated and concentrated under reduced pressure. The crude material was subjected to column chromatography using diethyl ether : ethylacetate (3:1 → ethylacetate). The product (*S*)-**183** was obtained as white solid (16.6 g, 45.1 mmol, 70.7%). Due to protonation and deprotonation a second fraction of the product was obtained as colourless oil (3.45 g, 8.50 mmol, 13.4%). $R_f = 0.29$ (diethylether : hexane 3:1). $^1\text{H-NMR}$ (300 MHz, $(\text{CD}_3)_2\text{SO}$): $\delta(\text{ppm})$ 8.12 (d, $J = 1.1$ Hz, 1H, NH), 7.31-7.20 (m, 2H, $\text{CH}_{\text{ar-2}}$ & $\text{CH}_{\text{ar-5}}$), 4.24 (m, 1H, CH_α), 3.62 (s, 3H, OCH_3), 2.83 (m, 2H, $\text{CH}_{2\beta}$), 1.55 (s, 9H, $\text{OC}_q(\text{CH}_3)_3$), 1.34 (s, 9H, $\text{OC}_q(\text{CH}_3)_3$). $^{13}\text{C-NMR}$ (75 MHz, $(\text{CD}_3)_2\text{SO}$): $\delta(\text{ppm})$ 172.3 (COOMe), 155.2 ($\text{C}_\alpha\text{NHCOO}t\text{Bu}$), 146.6 ($\text{N}_{\text{ar}}\text{COO}t\text{Bu}$), 138.9 ($\text{C}_{\text{ar-2}}$), 136.7 ($\text{C}_{\text{ar-5}}$), 114.4 ($\text{C}_{\text{ar-4}}$), 85.1 ($\text{N}_{\text{ar}}\text{COOCq}(\text{CH}_3)_3$), 78.3 ($\text{NHCOOCq}(\text{CH}_3)_3$), 53.0 (C_α), 51.8 (OCH_3), 29.4 (C_β), 28.0 ($\text{NHCOOCq}(\text{CH}_3)_3$), 27.3 ($\text{N}_{\text{ar}}\text{COOCq}(\text{CH}_3)_3$). IR (film): ν (cm^{-1}) 3248, 3128, 2982, 1739, 1702, 1578, 1527, 1504,

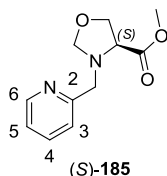
1484, 1388, 1366, 1334, 1300, 1274, 1255, 1227, 1155, 1130, 973, 839, 772, 755, 706, 603, 554. HRMS calculated for $\text{C}_{17}\text{H}_{27}\text{N}_3\text{O}_6\text{Na}$ ($\text{M} + \text{Na}^+$) 399.1792 found ($\text{M} + \text{H}^+$) 399.1800.

5.2.2.52 (*S*)-methyl 2-(*tert*-butoxycarbonylamino)-3-(1*H*-imidazol-4-yl)propanoate ((*S*)-**184**)



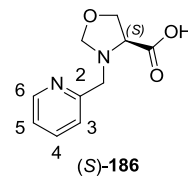
(*S*)-**183** (16.6 g, 44.7 mmol) was dissolved in methanol (65.0 mL) and potassium carbonate (617 mg, 4.47 mmol) was added. The reaction mixture was refluxed and the end of the reaction was monitored via TLC. The entire mixture was cooled to ambient temperature and poured into water (80 mL) and extracted with ethyl acetate (3 x 80 mL). The combined organic layer was dried over sodium sulfate, filtrated and concentrated under reduced pressure. The product (*S*)-**184** was obtained as a white solid (10.1 g, 37.5 mmol, 84.1%). $R_f = 0.81$ (methylene chloride : methanol 7:3). $^1\text{H-NMR}$ (300 MHz, $(\text{CD}_3)_2\text{SO}$): $\delta(\text{ppm})$ 11.8 (s, 1H, $\text{N}_{\text{ar}}\text{H}$), 7.54 (s, 1H, $\text{CH}_{\text{ar-2}}$), 7.17 (d, $J = 7.3$ Hz, 1H, $\text{CH}_{\text{ar-5}}$), 6.80 (s, 1H, $\text{NHCOO}t\text{Bu}$), 4.25-4.18 (m, 1H, CH_α), 3.58 (s, 3H, OCH_3), 2.84 (m, 2H, $\text{CH}_{2\beta}$), 1.35 (s, 9H, $\text{OC}_q(\text{CH}_3)_3$). IR (film): ν (cm^{-1}) 3384, 3153, 3131, 2985, 2956, 2935, 1736, 1696, 1561, 1517, 1451, 1420, 1367, 1308, 1255, 1218, 1155, 1113, 1071, 1057, 1041, 984, 850, 761, 619, 541, 463, 422. HRMS calculated for $\text{C}_{12}\text{H}_{20}\text{N}_3\text{O}_4$ ($\text{M} + \text{H}^+$) 270.1448 found ($\text{M} + \text{H}^+$) 270.1452.

5.2.2.53 (S)-methyl 3-(pyridin-2-ylmethyl)oxazolidine-4-carboxylate ((S)-**185**)



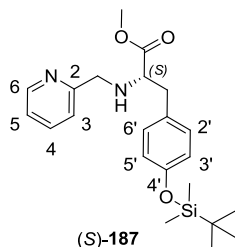
(S)-**172** (1.00 g, 4.75 mmol) was dissolved in methylene chloride (45 mL) at 0 °C. Trifluoroacetic acid (366 μ L, 4.75 mmol, 0.1 N) was added drop wise followed by water (45 mL). Under extensive stirring formaldehyde (705 μ L, 7.12 mmol, 37% aq.) was added drop wise to the reaction mixture. The reaction was continued for 16 h at ambient temperature. The solvent was evaporated under reduced pressure and the crude material subjected to column chromatography using methylene chloride : methanol (35:1). After drying *in vacuo* (S)-**185** was obtained as yellow oil (760 mg, 3.72 mmol, 72%). R_f = 0.65 (methylene chloride : methanol 10:1). $^1\text{H-NMR}$ (300 MHz, CDCl_3): δ (ppm) 8.54 (ddd, J = 4.9, 1.7, 0.9 Hz, 1H, $\text{CH}_{\text{ar-6}}$), 7.71 (td, J = 7.7, 1.8 Hz, 1H, $\text{CH}_{\text{ar-4}}$), 7.58 (d, J = 7.8 Hz, 1H, $\text{CH}_{\text{ar-3}}$), 7.21 (ddd, J = 7.4, 4.9, 1.2 Hz, 1H, $\text{CH}_{\text{ar-5}}$), 4.51 (s, 2H, NCH_2), 4.22–4.15 (m, 1H, CH_α), 4.05 (s, 2H, NCH_2O), 3.93–3.79 (m, 2H, $\text{CH}_{2\beta}$), 3.70 (s, 3H, OCH_3). $^{13}\text{C-NMR}$ (75 MHz, CDCl_3): δ (ppm) 172.44 ($\text{C}_{\text{carbonyl}}$), 149.06 ($\text{C}_{\text{ar-2}}$), 137.02 ($\text{C}_{\text{ar-6}}$), 123.25 ($\text{C}_{\text{ar-3}}$), 122.59 ($\text{C}_{\text{ar-5}}$), 87.50 (NCH_2O), 67.45 (NCH_2), 64.72 (C_α), 60.54 (C_β), 52.33 (OCH_3). IR (film): ν (cm^{-1}) 2951, 2883, 1734, 1670, 1593, 1470, 1435, 1360, 1277, 1201, 1166, 1119, 1047, 1007, 947, 869, 758, 701.

5.2.2.54 (S)-3-(pyridin-2-ylmethyl)oxazolidine-4-carboxylic acid ((S)-**186**)



(S)-**185** (760 mg, 3.42 mmol) were suspended in sodium hydroxide (4.50 mL, 1 M) at 0 °C and reacted for 16 h. The reaction mixture was washed with methylene chloride (3 x 20 mL). The combined aqueous layer was neutralised to pH 7 with hydrochloric acid (1 M). The aqueous layer was concentrated and the solvent removed under reduced pressure. The residue was suspended in ethanol (5.00 mL) and filtrated via a syringe filter. The residue was dried *in vacuo* to obtain the product (S)-**186** as a white solid (705 mg, 3.39 mmol, quant.). R_f = 0.05 (methylene chloride : methanol 10:1). $^1\text{H-NMR}$ (300 MHz, CD_3OD): δ (ppm) 8.44 (d, J = 5.0, 1H, $\text{CH}_{\text{ar-6}}$), 7.86 – 7.77 (m, 2H, $\text{CH}_{\text{ar-4}}$, $\text{CH}_{\text{ar-3}}$), 7.29 (dd, J = 8.8, 5.0 Hz, 1H, $\text{CH}_{\text{ar-5}}$), 4.40 (dd, J = 13.3, 5.2 Hz, 2H, NCH_2O), 4.17 (t, J = 8.0 Hz, 1H, CH_α), 4.03 (d, J = 14.7 Hz, 1H; NCHH), 3.91 (d, J = 14.5 Hz, 1H, NCHH), 3.78 (dd, J = 7.9, 5.7 Hz, 1H, $\text{CH}_\beta\text{H}_\beta$), 3.56–3.48 (m, 1H, $\text{CH}_\beta\text{H}_\beta$). IR (film): ν (cm^{-1}) 3380, 2481, 2077, 1639, 1590, 1441, 1212, 1116, 1087, 969, 528, 462. HRMS calculated for $\text{C}_{10}\text{H}_{13}\text{N}_2\text{O}_3$ ($M + \text{H}^+$) 209,0921 found ($M + \text{H}^+$) 209,0922.

5.2.2.55 (*S*)-methyl 3-(4-(*tert*-butyldimethylsilyloxy)phenyl)-2-(pyridin-2-ylmethylamino)propanoate ((*S*)-**187**)

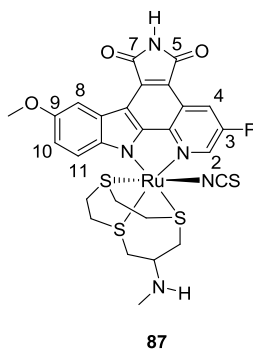


(*S*)-**174** (2.00 g, 6.98 mmol) was dissolved in dimethylformamide (60 mL) and cool to 0 °C. Diisopropylethylamine (6.0 mL, 34.90 mmol) was added drop wise over a period of 2 h. Then, *tert*-butyldimethylsilyl trifluoromethanesulfonate (2.1 mL, 7.81 mmol) was added drop wise over a period of 1 h. The reaction was continued for 24 h and the was allowed to warm up to ambient temperature. Ammonium acetate (60 mL, 1 M aq.) was added and the reaction mixture was extracted with ethylacetate (3 x 60 mL). The combined organic layer was washed with BRINE, dried over sodium sulfate, filtrated and concentrated under reduced pressure. The crude material was subjected to column chromatography using methylene chloride : methanol (35:1). R_f = 0.53 (methylene chloride : methanol 15:1). The product (*S*)-**187** was obtained as yellow oil (2.77 g, 6.92 mmol, 99%). $^1\text{H-NMR}$ (300 MHz, CD_3OD): δ (ppm) 7.08 (d, J = 4.9 Hz, 1H, $\text{CH}_{\text{ar-6}}$), 6.40-6.29 (m, 1H, $\text{CH}_{\text{ar-4}}$), 5.80 (d, J = 7.9 Hz, 1H, $\text{CH}_{\text{ar-3}}$), 5.93-5.89 (m, 1H, $\text{CH}_{\text{ar-5}}$), 5.69 (d, J = 8.4 Hz, 2H, $\text{CH}_{\text{ar-2'}}$ & $\text{CH}_{\text{ar-6'}}$), 5.40 (d, J = 8.4 Hz, 2H, $\text{CH}_{\text{ar-3'}}$ & $\text{CH}_{\text{ar-5'}}$), 2.56 (d, J = 14.5 Hz, 1H, NCHH), 2.40 (d, J = 14.5 Hz, 1H, NCHH), 2.25 (s, 3H, OCH_3), 2.15 (dd, J = 10.4, 7.1 Hz, 1H, CH_α), 1.96 (s, 1H, OH), 1.60 (d, J = 18.8 Hz, 1H, $\text{CH}_\beta\text{H}_\beta$), 1.52 (d, J = 12.6 Hz, 1H, $\text{CH}_\beta\text{H}_\beta$), -0.37 (s, 9H, $(\text{SiC}_q(\text{CH}_3)_3)$), -1.17 (s, 6H, $(\text{Si}(\text{CH}_3)_2)$). $^{13}\text{C-NMR}$ (75 MHz, CD_3OD): δ (ppm) 172.18 ($\text{C}_{\text{carbonyl}}$), 159.01 ($\text{C}_{\text{ar-2}}$), 154.39 ($\text{C}_{\text{ar-4'}}$), 148.45 ($\text{C}_{\text{ar-6}}$), 137.362

($\text{C}_{\text{ar-4}}$), 130.79 ($\text{C}_{\text{ar-1'}}$), 130.28 (2C, $\text{C}_{\text{ar-2'}}$ & $\text{C}_{\text{ar-6'}}$), 123.31 ($\text{C}_{\text{ar-3}}$), 122.42 ($\text{C}_{\text{ar-5}}$), 120.08 (2C, $\text{C}_{\text{ar-3'}}$ & $\text{C}_{\text{ar-5'}}$), 68.40 (NCH_2), 60.12 (C_α), 51.38 (OCH_3), 38.48 (C_β), 25.84 ($\text{SiC}_q(\text{CH}_3)_3$), 18.36 ($\text{SiC}_q(\text{CH}_3)_3$), -4.27 ($\text{Si}(\text{CH}_3)_2$). IR (film): ν (cm^{-1}) 3339, 2953, 2934, 2892, 2858, 1740, 1680, 1600, 1510, 1469, 1436, 1359, 1258, 1201, 1170, 1106, 1003, 915, 839, 781, 691, 634, 543, 475, 401. HRMS calculated for $\text{C}_{22}\text{H}_{33}\text{N}_2\text{O}_3\text{Si}$ ($\text{M} + \text{H}^+$) 401.2260 found ($\text{M} + \text{H}^+$) 437.2255.

5.21 (m, 2H, CHCH₂), 4.56-4.55 (m, 2H, CH₂_{allyl}) 3.93 (s, 3H, OCH₃), 3.69-2.92 (m, 13H, CHN & 6xCH₂), 2.78 (s, 3H, NCH₃). IR (film): $\nu(\text{cm}^{-1})$ 2923, 2098, 1699, 1558, 1468, 1403, 1327, 1285, 1206, 1141, 1024, 950, 810, 759, 694, 635, 516. HRMS calculated for C₃₁H₃₀FN₅O₅RuS₄Na⁺ (M + Na)⁺ 824.0050, found (M + Na)⁺ 824.0044. Measurable crystals of compound **96** were obtained after one week in (CD₃)₂CO at 4 °C.

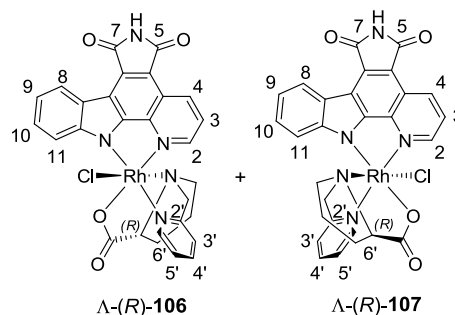
5.2.3.3 Synthesis of organoruthenium(II) complex **87**



To a solution of the solid product **96** (21 mg, 26 μmol) in methylene chloride (11 mL) was added 1,3-dimethylbarbituric acid (61 mg, 39 μmol) and Pd(PPh₃)₄ (4.5 mg, 4 μmol) under nitrogen. The resulting mixture was stirred at ambient temperature for 14 h, followed by the addition of saturated NaHCO₃ (1 x 0.5 mL) solution to quench the reaction. The resulting suspension was dried *in vacuo* and the crude material was adsorbed onto silica gel and subjected to silica gel chromatography with methylene chloride : methanol : 2% triethylamine (10:1 \rightarrow 5:1) as the eluting solvent to obtain the metal complex **87**. The purified complex **87** was then extracted with saturated NH₄Cl (2 x 20 mL), saturated NaHCO₃ (4 x 15 mL) and Brine (2 x 20 mL) to remove residual NEt₃. The metal complex **87** was obtained as a dark green solid (8.7 mg, 12 μmol , 47%). R_f = 0.38 (methylene chloride : methanol 2% triethylamine 15:1).

¹H-NMR (300 MHz, (CH₃)₂SO): $\delta(\text{ppm})$ 11.02 (s, 1H, NH), 8.98 (m, 1H, CH_{ar}-4), 8.80 (dd, J = 9.3, 2.4 Hz, 1H, CH_{ar}-2), 8.30 (d, J = 2.7 Hz, 1H, CH_{ar}-8), 8.04 (d, J = 9.0 Hz, 1H, CH_{ar}-11), 7.15 (dd, J = 9.0, 2.7 Hz, 1H, CH_{ar}-10), 3.89 (s, 3H, OCH₃), 3.58-3.39 (m, 13H, CHN & 6xCH₂), 2.40 (s, 3H, NHCH₃). ¹³C-NMR (125.8 MHz, (CH₃)₂SO): $\delta(\text{ppm})$ 170.7 (2C, C_{ar}-5 & C_{ar}-7), 170.52 (C_{ar}-3) 156.76 (C_{ar}-9), 153.7 (C_{ar}-12b), 147.7 (C_{ar}), 146.7 (C_{ar}), 141.1 (C_{ar}), 134.27 (NCS), 131.4 (C_{ar}), 131.1 (C_{ar}), 128.7 (C_{ar}), 124.1 (C_{ar}), 120.8 (C_{ar}), 115.7 (C_{ar}), 114.5 (C_{ar}), 110.5 (C_{ar}), 106.1 (C_{ar}-8), 69.7 (CHNHCH₃), 55.5 (OCH₃), 53.7 (SCH₂CHNHCH₃), 51.7 (SCH₂CHNHCH₃), 48.5 (CHNHCH₃), 35.9 (C_{aliph}), 34.2 (C_{aliph}), 33.3 (C_{aliph}), 31.8 (C_{aliph}). IR (film): $\nu(\text{cm}^{-1})$ 3452, 3058, 2924, 1747, 1677, 1615, 1561, 1492, 1439, 1408, 1369, 1328, 1287, 1225, 1022, 948, 883, 759, 610, 447. HRMS calculated for C₂₇H₂₆FN₅O₃RuS₄Na (M + Na)⁺ 739.8447, found (M + Na)⁺ 739.8443.

5.2.3.4 Synthesis of organorhodium(III) complexes Λ -(R)-**106** and Λ -(R)-**107**



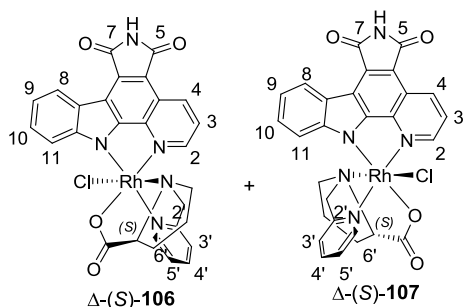
A suspension of **79** (17.6 mg, 44 μmol) and RhCl₃·3H₂O (11.5 mg, 44 μmol) in an ethanol : water mixture (1:1, 20 mL) under nitrogen atmosphere in a sealed vessel was heated to 90 °C for 3 h. During this time the suspension turned from pale brown into dark red. The reaction mixture was then cooled down slightly to add (R)-**105** (9.9 mg, 48 μmol). After addition of (R)-**105**, the reaction was further proceeded

at 90 °C for 16 h. The reaction mixture was then cooled down to ambient temperature and the solvent was removed *in vacuo*. The crude material was purified via column chromatography using methylene chloride : methanol (20:1 → 10:1). The separated diastereomers were further purified and concentrated via preparative TLC using methylene chloride : methanol (10:1). The products were obtained as red solids, Λ -(*R*)-**107** (4.2 mg, 6.6 μ mol, 15%) and Λ -(*R*)-**106** (6.1 mg, 9.7 μ mol, 22%).

Λ -(*R*)-**107**: R_f = 0.25 (methylene chloride : methanol 15:1). $^1\text{H-NMR}$ (500 MHz, $(\text{CD}_3)_2\text{SO}$): δ (ppm) 11.24 (s, 1H, NH), 9.68 (d, J = 5.7 Hz, 1H, $\text{CH}_{\text{ar}}-6'$), 9.30 (dd, J = 8.4, 1.1 Hz, 1H, $\text{CH}_{\text{ar}}-4$), 8.87 (d, J = 5.1 Hz, 1H, $\text{CH}_{\text{ar}}-2$), 8.68 (dd, J = 7.8, 0.5 Hz, 1H, $\text{CH}_{\text{ar}}-8$), 8.48 (td, J = 7.8, 1.5 Hz, 1H, $\text{CH}_{\text{ar}}-4'$), 8.08 (dd, J = 8.4, 5.2 Hz, 1H, $\text{CH}_{\text{ar}}-3$), 8.06 – 8.01 (m, 1H, $\text{CH}_{\text{ar}}-5'$), 7.99 (d, J = 7.8 Hz, 1H, $\text{CH}_{\text{ar}}-3'$), 7.28 – 7.24 (m, 1H, $\text{CH}_{\text{ar}}-10$), 7.21 (ddd, J = 8.4, 7.2, 1.4 Hz, 1H, $\text{CH}_{\text{ar}}-9$), 5.70 (d, J = 8.2 Hz, 1H, $\text{CH}_{\text{ar}}-11$), 4.60 (d, J = 15.6 Hz, 1H, NCHH), 4.34 (d, J = 15.7 Hz, 1H, NCHH), 3.81 (dd, J = 9.6, 4.3 Hz, 1H, CH_α), 2.50 (m, 1H, $\text{CH}_\delta\text{H}_\delta$), 2.28 – 2.15 (m, 2H, $\text{CH}_\delta\text{H}_\delta$ & $\text{CH}_\beta\text{H}_\beta$), 2.00 (dt, J = 11.3, 4.8 Hz, 1H, $\text{CH}_\beta\text{H}_\beta$), 1.58 (m, J = 11.7, 5.9 Hz, 1H, $\text{CH}_\gamma\text{H}_\gamma$), 1.11 – 1.01 (m, 1H, $\text{CH}_\gamma\text{H}_\gamma$). $^{13}\text{C-NMR}$ (126 MHz, $(\text{CD}_3)_2\text{SO}$): δ (ppm) 182.02 ($\text{C}_{\text{carbonyl}}$), 170.59 ($\text{C}_{\text{ar}}-7$), 170.23 ($\text{C}_{\text{ar}}-5$), 161.13 ($\text{C}_{\text{ar}}-2'$), 152.62 ($\text{C}_{\text{ar}}-6'$), 152.54 ($\text{C}_{\text{ar}}-12\text{b}$), 148.90 ($\text{C}_{\text{ar}}-12\text{a}$), 148.89 ($\text{C}_{\text{ar}}-11\text{a}$), 148.74 ($\text{C}_{\text{ar}}-2$), 142.09 ($\text{C}_{\text{ar}}-4'$), 141.17 ($\text{C}_{\text{ar}}-7\text{b}$), 135.24 ($\text{C}_{\text{ar}}-4$), 131.23 ($\text{C}_{\text{ar}}-7\text{a}$), 126.61 ($\text{C}_{\text{ar}}-9$), 126.27 ($\text{C}_{\text{ar}}-5'$), 124.75 ($\text{C}_{\text{ar}}-8$), 123.90 ($\text{C}_{\text{ar}}-3$), 123.47 ($\text{C}_{\text{ar}}-3'$), 121.34 ($\text{C}_{\text{ar}}-10$), 119.59 ($\text{C}_{\text{ar}}-4\text{a}$), 115.08 ($\text{C}_{\text{ar}}-7\text{c}$), 114.59 ($\text{C}_{\text{ar}}-4\text{b}$), 111.79 ($\text{C}_{\text{ar}}-11$), 72.91 (C_α), 70.02 (NCH₂), 61.27 (C_δ), 30.43 (C_β), 24.31 (C_γ). IR (film): ν (cm⁻¹) 3037, 2075, 1994, 1751, 1703, 1646, 1519, 1482, 1413, 1337, 1296, 1262, 1225, 1132, 1017, 930, 884, 856, 743, 704, 636, 493, 436. HRMS calculated for $\text{C}_{28}\text{H}_{21}\text{ClN}_5\text{O}_4\text{Rh}$ ($\text{M} + \text{Na}$)⁺ 652.0229, found ($\text{M} + \text{Na}$)⁺

652.0220. Λ -(*R*)-**106**: R_f = 0.08 (methylene chloride : methanol 15:1). $^1\text{H-NMR}$ (300 MHz, $(\text{CD}_3)_2\text{SO}$): δ (ppm) 11.24 (s, 1H, NH), 9.54 (d, J = 5.5 Hz, 1H, $\text{CH}_{\text{ar}}-6'$), 9.17 (d, J = 7.7 Hz, 1H, $\text{CH}_{\text{ar}}-4$), 8.71 (d, J = 7.8 Hz, 1H, $\text{CH}_{\text{ar}}-8$), 8.38 (m, 1H, $\text{CH}_{\text{ar}}-4'$), 7.99 – 7.89 (m, 3H, $\text{CH}_{\text{ar}}-2$, $\text{CH}_{\text{ar}}-5'$ & $\text{CH}_{\text{ar}}-11$), 7.82 (d, J = 8.3 Hz, 1H, $\text{CH}_{\text{ar}}-3'$), 7.74 (dd, J = 8.4, 5.3 Hz, 1H, $\text{CH}_{\text{ar}}-3$), 7.58 – 7.51 (m, 1H, $\text{CH}_{\text{ar}}-9$), 7.41 – 7.33 (m, 1H, $\text{CH}_{\text{ar}}-10$), 4.59 (s, 2H, NCH₂), 3.79 (dd, J = 9.4, 4.7 Hz, 1H, CH_α), 2.50 (m, 1H, $\text{CH}_\delta\text{H}_\delta$), 2.29 – 2.09 (m, 2H, $\text{CH}_\delta\text{H}_\delta$ & $\text{CH}_\beta\text{H}_\beta$), 1.86 (dt, J = 11.3, 5.9 Hz, 1H, $\text{CH}_\beta\text{H}_\beta$), 1.44 (dt, J = 11.7, 5.8 Hz, 1H, $\text{CH}_\gamma\text{H}_\gamma$), 1.10 (dt, J = 12.7, 7.0 Hz, 1H, $\text{CH}_\gamma\text{H}_\gamma$). $^{13}\text{C-NMR}$ (101 MHz, $(\text{CD}_3)_2\text{SO}$): δ (ppm) 181.89 ($\text{C}_{\text{carbonyl}}$), 159.96 ($\text{C}_{\text{ar}}-2'$), 151.72 ($\text{C}_{\text{ar}}-6'$), 151.25 ($\text{C}_{\text{ar}}-12\text{b}$), 150.17 ($\text{C}_{\text{ar}}-2$), 149.43 ($\text{C}_{\text{ar}}-12\text{a}$), 149.13 ($\text{C}_{\text{ar}}-11\text{a}$), 141.85 ($\text{C}_{\text{ar}}-7\text{b}$), 140.53 ($\text{C}_{\text{ar}}-4'$), 134.41 ($\text{C}_{\text{ar}}-4$), 130.75 ($\text{C}_{\text{ar}}-7\text{a}$), 125.67 ($\text{C}_{\text{ar}}-9$), 125.79 ($\text{C}_{\text{ar}}-5'$), 123.84 ($\text{C}_{\text{ar}}-3$), 123.57 ($\text{C}_{\text{ar}}-8$), 122.67 ($\text{C}_{\text{ar}}-11$), 120.87 ($\text{C}_{\text{ar}}-10$), 119.14 ($\text{C}_{\text{ar}}-4\text{a}$), 114.73 ($\text{C}_{\text{ar}}-3'$), 114.44 ($\text{C}_{\text{ar}}-7\text{c}$), 113.63 ($\text{C}_{\text{ar}}-4\text{b}$), 73.51 (C_α), 69.35 (NCH₂), 60.75 (C_δ), 30.74 (C_β), 24.01 (C_γ). The ^{13}C -signals of $\text{C}_{\text{ar}}-5$ and $\text{C}_{\text{ar}}-7$ are missing. IR (film): ν (cm⁻¹) 3045, 2724, 1819, 1750, 1704, 1644, 1519, 1481, 1413, 1336, 1297, 1225, 1134, 1014, 932, 824, 786, 743, 703, 635, 492, 436, 392. HRMS calculated for $\text{C}_{28}\text{H}_{21}\text{ClN}_5\text{O}_4\text{RhNa}$ ($\text{M} + \text{Na}$)⁺ 652.0229, found ($\text{M} + \text{Na}$)⁺ 652.0238.

5.2.3.5 Synthesis of organorhodium(III) complexes Δ -(S)-**106** and Δ -(S)-**107**

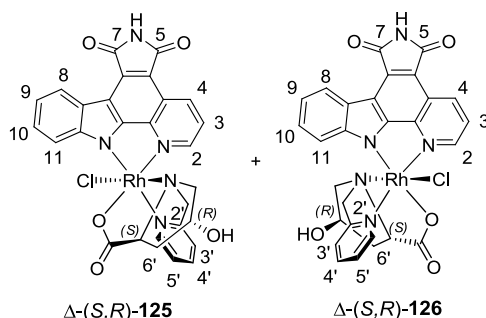


A suspension of **79** (17.6 mg, 44 μ mol) and $\text{RhCl}_3 \cdot 3\text{H}_2\text{O}$ (11.5 mg, 44 μ mol) in an ethanol : water mixture (1:1, 20 mL) under nitrogen atmosphere in a sealed vessel was heated to 90 °C for 3 h. During this time the suspension turned from pale brown into dark red. The reaction mixture was then cooled down slightly to add (S)-**105** (9.9 mg, 48 μ mol). After addition of (S)-**105**, the reaction was further proceeded at 90 °C for 16 h. The reaction mixture was then cooled down to ambient temperature and the solvent was removed *in vacuo*. The crude material was purified via column chromatography using methylene chloride : methanol (20:1 \rightarrow 10:1). The separated diastereomers were further purified and concentrated via preparative TLC using methylene chloride : methanol (10:1). The products were obtained as red solids, Δ -(S)-**107** (3.9 mg, 6.6 μ mol, 14%) and Δ -(S)-**106** (6.7 mg, 10.6 μ mol, 24%). Δ -(S)-**107**: R_f = 0.25 (methylene chloride : methanol 15:1). ^1H -NMR (500 MHz, $(\text{CD}_3)_2\text{SO}$): δ (ppm) 11.25 (s, 1H, NH), 9.68 (d, J = 5.4 Hz, 1H, $\text{CH}_{\text{ar}}-6'$), 9.30 (d, J = 8.3 Hz, 1H, $\text{CH}_{\text{ar}}-4$), 8.87 (d, J = 4.8 Hz, 1H, $\text{CH}_{\text{ar}}-2$), 8.68 (d, J = 7.7 Hz, 1H, $\text{CH}_{\text{ar}}-8$), 8.51 – 8.43 (m, 1H, $\text{CH}_{\text{ar}}-4'$), 8.08 (dd, J = 8.3, 5.2 Hz, 1H, $\text{CH}_{\text{ar}}-3$), 8.06 – 8.01 (m, 1H, $\text{CH}_{\text{ar}}-5'$), 7.99 (d, J = 7.7 Hz, 1H, $\text{CH}_{\text{ar}}-3'$), 7.26 (t, J = 7.4 Hz, 1H, $\text{CH}_{\text{ar}}-10$), 7.21 (t, J = 7.4 Hz, 1H, $\text{CH}_{\text{ar}}-9$), 5.70 (d, J = 8.2 Hz, 1H, $\text{CH}_{\text{ar}}-11$), 4.60 (d, J = 15.8 Hz, 1H, NCHH), 4.34 (d, J = 15.8 Hz, 1H, NCHH), 3.81 (dd, J

= 9.3, 4.0 Hz, 1H, CH_α), 2.50 (m, 1H, $\text{CH}_\delta\text{H}_\delta$), 2.21 (dd, J = 17.3, 10.9 Hz, 2H, $\text{CH}_\delta\text{H}_\delta$ & $\text{CH}_\beta\text{H}_\beta$), 2.04 – 1.97 (m, 1H, $\text{CH}_\beta\text{H}_\beta$), 1.61 – 1.54 (m, 1H, $\text{CH}_\gamma\text{H}_\gamma$), 1.11 – 1.01 (m, 1H, $\text{CH}_\gamma\text{H}_\gamma$). ^{13}C -NMR (126 MHz, $(\text{CD}_3)_2\text{SO}$): δ (ppm) 181.79 ($\text{C}_{\text{carbonyl}}$), 169.97 ($\text{C}_{\text{ar}}-7$), 169.89 ($\text{C}_{\text{ar}}-5$), 160.83 ($\text{C}_{\text{ar}}-2'$), 152.46 ($\text{C}_{\text{ar}}-6'$), 152.14 ($\text{C}_{\text{ar}}-12\text{b}$), 148.53 ($\text{C}_{\text{ar}}-12\text{a}$), 148.38 ($\text{C}_{\text{ar}}-11\text{a}$), 148.27 ($\text{C}_{\text{ar}}-2$), 141.77 ($\text{C}_{\text{ar}}-4'$), 140.87 ($\text{C}_{\text{ar}}-7\text{a}$), 134.93 ($\text{C}_{\text{ar}}-4$), 130.85 ($\text{C}_{\text{ar}}-7\text{a}$), 126.11 ($\text{C}_{\text{ar}}-9$), 125.92 ($\text{C}_{\text{ar}}-5'$), 124.34 ($\text{C}_{\text{ar}}-8$), 123.23 ($\text{C}_{\text{ar}}-3$), 123.01 ($\text{C}_{\text{ar}}-3'$), 121.07 ($\text{C}_{\text{ar}}-10$), 119.14 ($\text{C}_{\text{ar}}-4\text{a}$), 114.27 ($\text{C}_{\text{ar}}-7\text{c}$), 114.13 ($\text{C}_{\text{ar}}-4\text{b}$), 111.43 ($\text{C}_{\text{ar}}-11$), 72.27 (C_α), 69.75 (NCH_2), 61.02 (C_δ), 30.13 (C_β), 24.16 (C_γ). IR (film): ν (cm^{-1}) 3034, 2159, 2096, 1751, 1704, 1646, 1519, 1483, 1413, 1337, 1295, 1262, 1225, 1131, 1015, 930, 828, 784, 744, 705, 636, 527, 491. HRMS calculated for $\text{C}_{28}\text{H}_{21}\text{ClN}_5\text{O}_4\text{Rh}$ ($\text{M} + \text{Na}$) $^+$ 652.0229, found ($\text{M} + \text{Na}$) $^+$ 652.0208. Δ -(S)-**106**: R_f = 0.08 (methylene chloride : methanol 15:1). ^1H -NMR (300 MHz, $(\text{CD}_3)_2\text{SO}$): δ (ppm) 11.22 (s, 1H, NH), 9.54 (d, J = 5.1 Hz, 1H, $\text{CH}_{\text{ar}}-6'$), 9.18 (dd, J = 8.4, 1.0 Hz, 1H, $\text{CH}_{\text{ar}}-4$), 8.71 (d, J = 7.9 Hz, 1H, $\text{CH}_{\text{ar}}-8$), 8.38 (td, J = 7.7, 1.5 Hz, 1H, $\text{CH}_{\text{ar}}-4'$), 8.00 – 7.89 (m, 3H, $\text{CH}_{\text{ar}}-2$, $\text{CH}_{\text{ar}}-5'$ & $\text{CH}_{\text{ar}}-11$), 7.82 (d, J = 8.3 Hz, 1H, $\text{CH}_{\text{ar}}-3'$), 7.74 (dd, J = 8.4, 5.3 Hz, 1H, $\text{CH}_{\text{ar}}-3$), 7.59 – 7.50 (m, 1H, $\text{CH}_{\text{ar}}-9$), 7.41 – 7.33 (m, 1H, $\text{CH}_{\text{ar}}-10$), 4.58 (s, 2H, NCH_2), 3.79 (dd, J = 9.4, 4.8 Hz, 1H, CH_α), 2.51 – 2.48 (m, 1H, $\text{CH}_\delta\text{H}_\delta$), 2.25 – 2.12 (m, 2H, $\text{CH}_\delta\text{H}_\delta$ & $\text{CH}_\beta\text{H}_\beta$), 1.94 – 1.77 (m, 1H, $\text{CH}_\beta\text{H}_\beta$), 1.50 – 1.37 (m, 1H, $\text{CH}_\gamma\text{H}_\gamma$), 1.17 – 0.98 (m, 1H, $\text{CH}_\gamma\text{H}_\gamma$). ^{13}C -NMR (101 MHz, $(\text{CD}_3)_2\text{SO}$): δ (ppm) 182.29 ($\text{C}_{\text{carbonyl}}$), 160.16 ($\text{C}_{\text{ar}}-2'$), 152.22 ($\text{C}_{\text{ar}}-6'$), 151.65 ($\text{C}_{\text{ar}}-12\text{b}$), 150.37 ($\text{C}_{\text{ar}}-2$), 149.86 ($\text{C}_{\text{ar}}-12\text{a}$), 149.83 ($\text{C}_{\text{ar}}-11\text{a}$), 142.35 ($\text{C}_{\text{ar}}-7\text{a}$), 140.73 ($\text{C}_{\text{ar}}-4'$), 134.81 ($\text{C}_{\text{ar}}-4$), 131.25 ($\text{C}_{\text{ar}}-4\text{b}$), 126.57 ($\text{C}_{\text{ar}}-9$), 126.09 ($\text{C}_{\text{ar}}-5'$), 124.26 ($\text{C}_{\text{ar}}-3$), 123.90 ($\text{C}_{\text{ar}}-8$), 123.07 ($\text{C}_{\text{ar}}-11$), 121.10 ($\text{C}_{\text{ar}}-10$), 119.66 ($\text{C}_{\text{ar}}-4\text{a}$), 114.96 ($\text{C}_{\text{ar}}-3'$), 114.89 ($\text{C}_{\text{ar}}-7\text{c}$), 114.01 ($\text{C}_{\text{ar}}-7\text{b}$), 73.52 (C_α), 69.25 (NCH_2), 61.45 (C_δ), 30.38 (C_β), 23.83 (C_γ). The ^{13}C -signals of $\text{C}_{\text{ar}}-5$ and $\text{C}_{\text{ar}}-7$ are

missing. IR (film): ν (cm^{-1}) 3046, 2723, 1818, 1752, 1703, 1647, 1518, 1482, 1414, 1337, 1295, 1224, 1133, 1012, 932, 824, 786, 742, 701, 637, 492, 436. HRMS calculated for $\text{C}_{28}\text{H}_{21}\text{ClN}_5\text{O}_4\text{RhNa}$ ($M + \text{Na}$)⁺ 652.0229, found ($M + \text{Na}$)⁺ 652.0228.

5.2.3.6 Synthesis of organorhodium(III) complexes Δ -(*S,R*)-**125** and Δ -(*S,R*)-**126**

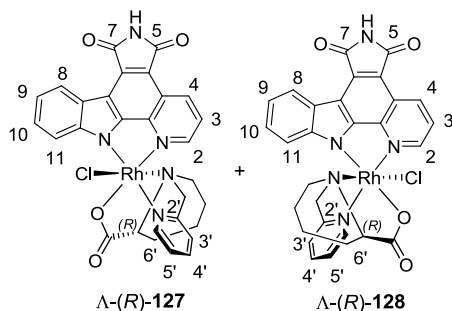


A suspension of **79** (30 mg, 75 μmol) and $\text{RhCl}_3 \cdot 3\text{H}_2\text{O}$ (19.6 mg, 75 μmol) in an ethanol : water mixture (1:1, 10 mL) under nitrogen atmosphere in a sealed vessel was heated to 90 °C for 3 h. During this time the suspension turned from pale brown into dark red. The reaction mixture was then cooled down slightly to add (*S,R*)-**119** (27.9 mg, 83 μmol). After addition of (*S,R*)-**119**, the reaction was further proceeded at 90 °C for 16 h. The reaction mixture was then cooled down to ambient temperature and the solvent was removed *in vacuo*. The crude material was purified via column chromatography using methylene chloride : methanol (20:1 \rightarrow 10:1). The separated diastereomers were further purified and concentrated via preparative TLC using methylene chloride : methanol (15:1). The products were obtained as red solids, Δ -(*S,R*)-**125** (11 mg, 17.3 μmol , 23%) and Δ -(*S,R*)-**126** (8.2 mg, 12.8 μmol , 17%). Δ -(*S,R*)-**125**: R_f = 0.14 (methylene chloride : methanol 15:1). $^1\text{H-NMR}$ (500 MHz, $(\text{CD}_3)_2\text{SO}$): δ (ppm) 9.55 (d, J = 5.8 Hz, 1H, $\text{CH}_{\text{ar}}\text{-6'}$), 9.18 (dd, J = 8.4, 1.0 Hz, 1H, $\text{CH}_{\text{ar}}\text{-4'}$), 8.71

(d, J = 8.0 Hz, 1H, $\text{CH}_{\text{ar}}\text{-8}$), 8.36 (td, J = 7.8, 1.5 Hz, 1H, $\text{CH}_{\text{ar}}\text{-4'}$), 8.10 – 7.87 (m, 3H, $\text{CH}_{\text{ar}}\text{-11}$, $\text{CH}_{\text{ar}}\text{-5'}$ & $\text{CH}_{\text{ar}}\text{-2}$), 7.77 (d, J = 8.3 Hz, 1H, $\text{CH}_{\text{ar}}\text{-3'}$), 7.76 – 7.73 (m, 1H, $\text{CH}_{\text{ar}}\text{-3}$), 7.54 (ddd, J = 8.3, 7.1, 1.3 Hz, 1H, $\text{CH}_{\text{ar}}\text{-9}$), 7.41 – 7.35 (m, 1H, $\text{CH}_{\text{ar}}\text{-10}$), 4.82 – 4.74 (m, 2H, NCH_2), 4.74 – 4.70 (m, 1H CH_γ) 4.01 (t, J = 8.8 Hz, 1H, CH_α), 3.72 – 3.62 (m, 1H, $\text{CH}_\delta\text{H}_\delta$), 3.51 (s, 1H, OH) 2.52 (d, J = 1.9 Hz, 1H, $\text{CH}_\delta\text{H}_\delta$), 2.26 – 2.11 (m, 1H, $\text{CH}_\beta\text{H}_\beta$), 1.91 – 1.78 (m, 1H, $\text{CH}_\beta\text{H}_\beta$). $^{13}\text{C-NMR}$ (126 MHz, $(\text{CD}_3)_2\text{SO}$): δ (ppm) 181.83 ($\text{C}_{\text{carbonyl}}$), 160.49 ($\text{C}_{\text{ar}}\text{-2'}$), 151.89 ($\text{C}_{\text{ar}}\text{-6'}$), 151.32 ($\text{C}_{\text{ar}}\text{-2}$), 151.31 ($\text{C}_{\text{ar}}\text{-12b}$), 150.81 ($\text{C}_{\text{ar}}\text{-12a}$), 146.75 ($\text{C}_{\text{ar}}\text{-11a}$), 142.44 ($\text{C}_{\text{ar}}\text{-7b}$) 140.95 ($\text{C}_{\text{ar}}\text{-4'}$), 135.27 ($\text{C}_{\text{ar}}\text{-4}$), 131.17 ($\text{C}_{\text{ar}}\text{-7a}$), 127.10 ($\text{C}_{\text{ar}}\text{-9}$), 126.21 ($\text{C}_{\text{ar}}\text{-5'}$), 124.81 ($\text{C}_{\text{ar}}\text{-3}$), 124.60 ($\text{C}_{\text{ar}}\text{-8}$), 124.09 ($\text{C}_{\text{ar}}\text{-11}$), 120.14 ($\text{C}_{\text{ar}}\text{-10}$), 119.70 ($\text{C}_{\text{ar}}\text{-4a}$), 115.09 ($\text{C}_{\text{ar}}\text{-3'}$), 114.66 ($\text{C}_{\text{ar}}\text{-7c}$), 114.22 ($\text{C}_{\text{ar}}\text{-4b}$), 73.71 (C_α), 72.66 (NCH_2), 72.64 (C_γ), 67.41 (C_δ), 39.82 (C_β). The ^{13}C -signals of $\text{C}_{\text{ar}}\text{-5}$ and $\text{C}_{\text{ar}}\text{-7}$ are missing. IR (film): ν (cm^{-1}) 2925, 2855, 2724, 2252, 2126, 1750, 1705, 1649, 1498, 1446, 1412, 1342, 1294, 1231, 1148, 1001, 878, 820, 755, 707, 635, 530, 490, 432. HRMS calculated for $\text{C}_{28}\text{H}_{21}\text{ClN}_5\text{NaO}_5\text{Rh}$ ($M + \text{Na}$)⁺ 668.0178, found ($M + \text{Na}$)⁺ 668.0178. Δ -(*S,R*)-**126**: R_f = 0.08 (methylene chloride : methanol 15:1). $^1\text{H-NMR}$ (300 MHz, $(\text{CD}_3)_2\text{SO}$): δ (ppm) 9.67 (d, J = 5.7 Hz, 1H, $\text{CH}_{\text{ar}}\text{-6'}$), 9.29 (dd, J = 8.4, 1.0 Hz, 1H, $\text{CH}_{\text{ar}}\text{-4'}$), 8.84 (d, J = 5.1 Hz, 1H, $\text{CH}_{\text{ar}}\text{-2}$), 8.71 – 8.65 (m, 1H, $\text{CH}_{\text{ar}}\text{-8}$), 8.47 (td, J = 7.8, 1.4 Hz, 1H, $\text{CH}_{\text{ar}}\text{-4'}$), 8.09 (d, J = 8.4 Hz, 1H, $\text{CH}_{\text{ar}}\text{-3}$), 8.07 (d, J = 8.4 Hz, 1H, $\text{CH}_{\text{ar}}\text{-5'}$), 8.01 (dd, J = 10.3, 4.2 Hz, 1H, $\text{CH}_{\text{ar}}\text{-3'}$), 7.32 – 7.11 (m, 2H, $\text{CH}_{\text{ar}}\text{-10}$ & $\text{CH}_{\text{ar}}\text{-9}$), 5.74 (d, J = 7.8 Hz, 1H, $\text{CH}_{\text{ar}}\text{-11}$), 5.23 (s, 1H, CH_δ), 4.84 (d, J = 15.8 Hz, 1H, NCHH), 4.44 (d, J = 15.8 Hz, 1H, NCHH), 4.01 (t, J = 8.5 Hz, 1H, CH_α), 3.77 (s, 1H, OH), 2.51 – 2.48 (m, 1H, $\text{CH}_\delta\text{H}_\delta$), 2.30 – 2.11 (m, 2H, $\text{CH}_\delta\text{H}_\delta$ & $\text{CH}_\beta\text{H}_\beta$), 2.08 – 1.87 (m, 1H, $\text{CH}_\beta\text{H}_\beta$). IR (film): ν (cm^{-1}) 2973, 2937, 2250, 1746, 1709, 1666, 1579, 1497, 1448, 1415, 1337, 1296, 1261, 1227, 1152,

1127, 1049, 1005, 878, 821, 763, 733, 707, 631, 532, 488. HRMS calculated for $C_{28}H_{21}ClN_5NaO_5Rh$ ($M + Na$)⁺ 668.0178, found ($M + Na$)⁺ 668.0178.

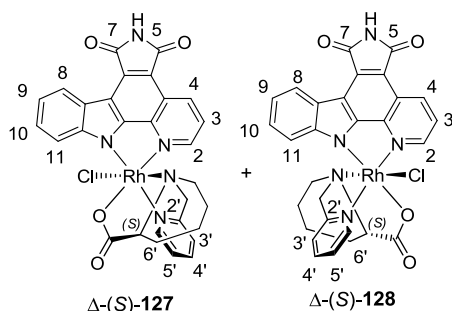
5.2.3.7 Synthesis of organorhodium(III) complexes Λ -(*R*)-**127** and Λ -(*R*)-**128**



A suspension of **79** (30 mg, 75 μ mol) and $RhCl_3 \cdot 3H_2O$ (19.6 mg, 75 μ mol) in an ethanol : water mixture (1:1, 10 mL) under nitrogen atmosphere in a sealed vessel was heated to 90 °C for 3 h. During this time the suspension turned from pale brown into dark red. The reaction mixture was then cooled down slightly to add (*R*)-**124** (18.3 mg, 83 μ mol). After addition of (*R*)-**124**, the reaction was further proceeded at 90 °C for 16 h. The reaction mixture was then cooled down to ambient temperature and the solvent was removed *in vacuo*. The crude material was purified via column chromatography using methylene chloride : methanol (20:1 \rightarrow 5:1). The separated diastereomers were further purified and concentrated via preparative TLC using methylene chloride : methanol (15:1). The products were obtained as red solids, Λ -(*R*)-**127** (11.5 mg, 18 μ mol, 24%) and Λ -(*R*)-**128** (7.7 mg, 12 μ mol, 16%). Λ -(*R*)-**127**: R_f = 0.11 (methylene chloride : methanol 15:1). 1H -NMR (300 MHz, $(CD_3)_2SO$): δ (ppm) 11.19 (s, 1H, NH), 9.55 (d, J = 5.6 Hz, 1H, $CH_{ar-6'}$), 9.16 (dd, J = 8.2, 1.2 Hz, 1H, CH_{ar-4}), 8.72 (d, J = 7.9 Hz, 1H, CH_{ar-8}), 8.39 (td, J = 7.8, 1.4 Hz, 1H, $CH_{ar-4'}$), 8.06 – 7.91 (m, 3H, CH_{ar-2} , $CH_{ar-5'}$

& CH_{ar-11}), 7.76 – 7.64 (m, 2H, $CH_{ar-3'}$ & CH_{ar-3}), 7.60 – 7.51 (m, 1H, CH_{ar-9}), 7.42 – 7.35 (m, 1H, CH_{ar-10}), 4.86 (d, J = 16.4 Hz, 1H, NCHH), 4.48 (d, J = 16.1 Hz, 1H, NCHH), 3.45 – 3.35 (m, 1H, CH_α), 2.45 – 2.35 (m, 1H, CH_{aliph}), 2.33 – 2.28 (m, 1H, CH_{aliph}), 1.99 – 1.82 (m, 1H, CH_{aliph}), 1.79 – 1.59 (m, 1H, CH_{aliph}), 1.56 – 1.39 (m, 1H, CH_{aliph}), 1.32 – 1.21 (m, 2H, CH_{aliph}), 1.07 – 0.92 (m, 1H, CH_{aliph}). A second set of signals for each proton was observed. IR (film): ν (cm^{-1}) 2956, 2920, 2853, 2268, 2209, 2169, 2133, 2058, 2008, 1754, 1708, 1648, 1444, 1339, 1229, 1012, 915, 748, 677, 637, 534, 488, 434. HRMS calculated for $C_{29}H_{23}ClN_5NaO_4Rh$ ($M + Na$)⁺ 666.0386, found ($M + Na$)⁺ 666.0387. Λ -(*R*)-**128**: R_f = 0.24 (methylene chloride : methanol 15:1). 1H -NMR (300 MHz, $(CD_3)_2SO$): δ (ppm) 11.25 (s, 1H, NH), 9.71 (d, J = 4.7 Hz, 1H, $CH_{ar-6'}$), 9.32 – 9.19 (m, 1H, CH_{ar-4}), 8.88 (d, J = 5.2 Hz, 1H, CH_{ar-2}), 8.67 (t, J = 7.2 Hz, 1H, CH_{ar-8}), 8.54 – 8.33 (m, 1H, $CH_{ar-4'}$), 8.20 – 8.07 (m, 1H, CH_{ar-3}), 8.05 (dd, J = 11.4, 6.2 Hz, 1H, $CH_{ar-5'}$), 7.96 – 7.84 (m, 1H, $CH_{ar-3'}$), 7.33 – 7.07 (m, 2H, CH_{ar-9} & CH_{ar-10}), 5.41 (d, J = 8.2 Hz, 1H, CH_{ar-11}), 4.92 (d, J = 15.5 Hz, 1H, NCHH), 4.20 (d, J = 15.7 Hz, 1H, NCHH), 3.43 (t, J = 5.5 Hz, 1H, CH_α), 2.38 – 2.19 (m, 2H, CH_{aliph}), 2.00 – 1.63 (m, 4H, CH_{aliph}), 1.58 – 1.40 (m, 2H, CH_{aliph}). A second set of signals for each proton was observed. IR (film): ν (cm^{-1}) 1751, 1705, 1653, 1521, 1491, 1415, 1339, 1296, 1261, 1225, 1080, 1016, 821, 792, 745, 707, 636, 527. HRMS calculated for $C_{29}H_{23}ClN_5NaO_4Rh$ ($M + Na$)⁺ 666.0386, found ($M + Na$)⁺ 666.0386.

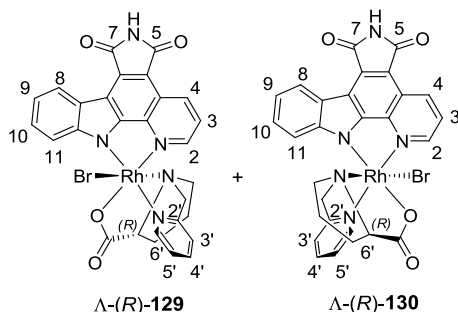
5.2.3.8 Synthesis of organorhodium(III) complexes Δ -(S)-**127** and Δ -(S)-**128**



A suspension of **79** (30 mg, 75 μ mol) and $\text{RhCl}_3 \cdot 3\text{H}_2\text{O}$ (19.6 mg, 75 μ mol) in an ethanol : water mixture (1:1, 10 mL) under nitrogen atmosphere in a sealed vessel was heated to 90 °C for 3 h. During this time the suspension turned from pale brown into dark red. The reaction mixture was then cooled down slightly to add (S)-**124** (18.3 mg, 83 μ mol). After addition of (S)-**124**, the reaction was further proceeded at 90 °C for 16 h. The reaction mixture was then cooled down to ambient temperature and the solvent was removed *in vacuo*. The crude material was purified via column chromatography using methylene chloride : methanol (35:1 \rightarrow 10:1). The separated diastereomers were further purified and concentrated via preparative TLC using methylene chloride : methanol (15:1). The products were obtained as red solids, Δ -(S)-**127** (10.5 mg, 15.8 μ mol, 21%) and Δ -(S)-**128** (7.5 mg, 11.3 μ mol, 15%). Δ -(S)-**127**: R_f = 0.11 (methylene chloride : methanol 15:1). ^1H -NMR (300 MHz, $(\text{CD}_3)_2\text{SO}$): δ (ppm) 9.54 (d, J = 5.7 Hz, 1H, $\text{CH}_{\text{ar}}\text{-6}'$), 9.16 (dd, J = 8.2, 1.2 Hz, 1H, $\text{CH}_{\text{ar}}\text{-4}$), 8.72 (d, J = 7.9 Hz, 1H, $\text{CH}_{\text{ar}}\text{-8}$), 8.39 (td, J = 7.7, 1.4 Hz, 1H, $\text{CH}_{\text{ar}}\text{-4}'$), 7.97 (d, J = 8.2 Hz, 3H, $\text{CH}_{\text{ar}}\text{-2}$, $\text{CH}_{\text{ar}}\text{-5}'$ & $\text{CH}_{\text{ar}}\text{-11}$), 7.70 (dt, J = 12.4, 4.8 Hz, 2H, $\text{CH}_{\text{ar}}\text{-3}'$ & $\text{CH}_{\text{ar}}\text{-3}$), 7.59 – 7.52 (m, 1H, $\text{CH}_{\text{ar}}\text{-9}$), 7.42 – 7.35 (m, 1H, $\text{CH}_{\text{ar}}\text{-10}$), 4.86 (d, J = 16.6 Hz, 1H, NCHH), 4.48 (d, J = 16.4 Hz, 1H, NCHH), 3.45 – 3.35 (m, 1H, CH_α), 2.44 – 2.32 (m, 1H, CH_{aliph}), 2.33 – 2.28 (m, 1H, CH_{aliph}), 1.94– 1.80 (m, 1H,

CH_{aliph}), 1.79 – 1.59 (m, 1H, CH_{aliph}), 1.56 – 1.39 (m, 1H, CH_{aliph}), 1.33 – 1.20 (m, 2H, CH_{aliph}), 1.06 – 0.90 (m, 1H, CH_{aliph}). A second set of signals for each proton was observed. IR (film): ν (cm^{-1}) 1750, 1705, 1650, 1524, 1497, 1413, 1339, 1268, 1228, 1017, 999, 822, 794, 753, 706, 635, 585, 527, 489, 438. HRMS calculated for $\text{C}_{29}\text{H}_{23}\text{ClN}_5\text{NaO}_4\text{Rh}$ ($\text{M} + \text{Na}$) $^+$ 666.0386, found ($\text{M} + \text{Na}$) $^+$ 666.0387. Δ -(S)-**128**: R_f = 0.24 (methylene chloride : methanol 15:1). ^1H -NMR (300 MHz, $(\text{CD}_3)_2\text{SO}$): δ (ppm) 11.22 (s, 1H, NH), 9.71 (d, J = 4.8 Hz, 1H, $\text{CH}_{\text{ar}}\text{-6}'$), 9.29 (ddd, J = 8.4, 4.5, 1.0 Hz, 1H, $\text{CH}_{\text{ar}}\text{-4}$), 8.88 (d, J = 5.1 Hz, 1H, $\text{CH}_{\text{ar}}\text{-2}$), 8.72 – 8.62 (m, 1H, $\text{CH}_{\text{ar}}\text{-8}$), 8.48 (td, J = 7.8, 1.4 Hz, 1H, $\text{CH}_{\text{ar}}\text{-4}'$), 8.13 (dd, J = 8.4, 5.2 Hz, 1H, $\text{CH}_{\text{ar}}\text{-3}$), 8.02 (d, J = 7.7 Hz, 1H, $\text{CH}_{\text{ar}}\text{-3}'$), 7.91 (dd, J = 13.5, 7.0 Hz, 1H, $\text{CH}_{\text{ar}}\text{-5}'$), 7.29 – 7.21 (m, 1H, $\text{CH}_{\text{ar}}\text{-9}$), 7.19 – 7.10 (m, 1H, $\text{CH}_{\text{ar}}\text{-10}$), 5.41 (d, J = 8.2 Hz, 1H, $\text{CH}_{\text{ar}}\text{-11}$), 4.91 (d, J = 15.7 Hz, 1H, NCHH), 4.20 (d, J = 15.5 Hz, 1H, NCHH), 3.42 (t, J = 5.6 Hz, 1H, CH_α), 2.38 – 2.19 (m, 1H, CH_{aliph}) 2.02 – 1.86 (m, 2H, CH_{aliph}), 1.86 – 1.63 (m, 1H, CH_{aliph}), 1.58 – 1.39 (m, 2H, CH_{aliph}), 1.38 – 1.25 (m, 1H, CH_{aliph}), 1.07 – 0.89 (m, 1H, CH_{aliph}). A second set of signals for each proton was observed. IR (film): ν (cm^{-1}) 1749, 1702, 1657, 1517, 1489, 1419, 1341, 1293, 1264, 1222, 1080, 1011, 818, 796, 745, 707, 636, 527.

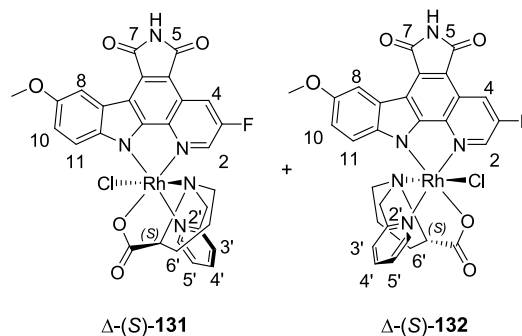
5.2.3.9 Synthesis of organorhodium(III) complexes Λ -(*R*)-**129** and Λ -(*R*)-**130**



A suspension of **79** (30 mg, 75 μ mol) and $\text{RhBr}_3 \cdot x\text{H}_2\text{O}$ (26 mg, 75 μ mol) in an ethanol : water mixture (1:1, 20 mL) under nitrogen atmosphere in a sealed vessel was heated to 90 °C for 3 h. During this time the suspension turned from pale brown into dark red. The reaction mixture was then cooled down slightly to add (*R*)-**105** (17 mg, 83 μ mol). After addition of (*R*)-**105**, the reaction was further proceeded at 90 °C for 16 h. The reaction mixture was then cooled down to ambient temperature and the solvent was removed *in vacuo*. The crude material was purified via column chromatography using methylene chloride : methanol (100:0 \rightarrow 10:1). The separated diastereomers were further purified and concentrated via preparative TLC using methylene chloride : methanol (15:1). The products were obtained as red solids, Λ -(*R*)-**129** (8.1 mg, 12 μ mol, 16%) and Λ -(*R*)-**130** (5.0 mg, 7.5 μ mol, 10%). Λ -(*R*)-**129**: R_f = 0.16 (methylene chloride : methanol 15:1). $^1\text{H-NMR}$ (300 MHz, $(\text{CD}_3)_2\text{SO}$): δ (ppm) 9.75 (d, J = 5.5 Hz, 1H, $\text{CH}_{\text{ar}}\text{-6}'$), 9.18 (dd, J = 8.4, 2.5 Hz, 1H, $\text{CH}_{\text{ar}}\text{-4}$), 8.71 (d, J = 7.9 Hz, 1H, $\text{CH}_{\text{ar}}\text{-8}$), 8.44 – 8.32 (m, 1H, $\text{CH}_{\text{ar}}\text{-4}'$), 7.98 – 7.91 (m, 3H, $\text{CH}_{\text{ar}}\text{-2}$, $\text{CH}_{\text{ar}}\text{-5}'$ & $\text{CH}_{\text{ar}}\text{-11}$), 7.82 (dd, J = 8.6, 4.2 Hz, 1H, $\text{CH}_{\text{ar}}\text{-3}'$), 7.74 (dd, J = 8.3, 5.3 Hz, 1H, $\text{CH}_{\text{ar}}\text{-3}$), 7.59 – 7.48 (m, 1H, $\text{CH}_{\text{ar}}\text{-9}$), 7.38 (t, J = 7.5 Hz, 1H, $\text{CH}_{\text{ar}}\text{-10}$), 4.59 (s, 2H, NCH_2), 3.83 – 3.68 (m, 1H, CH_α), 2.50 – 2.48 (m, 1H, $\text{CH}_\delta\text{H}_\delta$),

2.24 – 2.06 (m, 2H, $\text{CH}_\delta\text{H}_\delta$ & $\text{CH}_\beta\text{H}_\beta$), 1.90 – 1.78 (m, 1H, $\text{CH}_\beta\text{H}_\beta$), 1.51 – 1.35 (m, 1H, $\text{CH}_\gamma\text{H}_\gamma$), 1.12 – 0.98 (m, 1H, $\text{CH}_\gamma\text{H}_\gamma$). IR (film): ν (cm^{-1}) 2923, 2855, 2250, 2127, 1749, 1705, 1647, 1523, 1496, 1470, 1447, 1416, 1340, 1294, 1228, 1147, 1020, 1001, 820, 755, 707, 635, 573. HRMS calculated for $\text{C}_{28}\text{H}_{21}\text{BrN}_5\text{NaO}_4\text{Rh}$ ($\text{M} + \text{Na}$) $^+$ 695.9724, found ($\text{M} + \text{Na}$) $^+$ 695.9726. Λ -(*R*)-**130**: R_f = 0.37 (methylene chloride : methanol 15:1). $^1\text{H-NMR}$ (300 MHz, $(\text{CD}_3)_2\text{SO}$): δ (ppm) 9.68 (d, J = 5.6 Hz, 1H, $\text{CH}_{\text{ar}}\text{-6}'$), 9.29 (dd, J = 8.4, 1.1 Hz, 1H, $\text{CH}_{\text{ar}}\text{-4}$), 8.86 (d, J = 5.1 Hz, 1H, $\text{CH}_{\text{ar}}\text{-2}$), 8.68 (dd, J = 7.0, 1.0 Hz, 1H, $\text{CH}_{\text{ar}}\text{-8}$), 8.48 (td, J = 7.8, 1.5 Hz, 1H, $\text{CH}_{\text{ar}}\text{-4}'$), 8.08 (dd, J = 8.4, 5.2 Hz, 1H, $\text{CH}_{\text{ar}}\text{-3}$), 8.03 – 7.95 (m, 2H, $\text{CH}_{\text{ar}}\text{-5}'$ & $\text{CH}_{\text{ar}}\text{-3}'$), 7.30 – 7.16 (m, 2H, $\text{CH}_{\text{ar}}\text{-9}$ & $\text{CH}_{\text{ar}}\text{-10}$), 5.69 (d, J = 7.9 Hz, 1H, $\text{CH}_{\text{ar}}\text{-11}$), 4.60 (d, J = 16.0 Hz, 1H, NCHH), 4.33 (d, J = 15.4 Hz, 1H, NCHH), 3.81 (dd, J = 9.5, 4.3 Hz, 1H, CH_α), 2.50 – 2.48 (m, 1H, $\text{CH}_\delta\text{H}_\delta$) 2.25 – 2.14 (m, 2H, $\text{CH}_\delta\text{H}_\delta$ & $\text{CH}_\beta\text{H}_\beta$), 2.07 – 1.90 (m, 1H, $\text{CH}_\beta\text{H}_\beta$), 1.67 – 1.40 (m, 1H, $\text{CH}_\gamma\text{H}_\gamma$), 1.11 – 1.00 (m, 1H, $\text{CH}_\gamma\text{H}_\gamma$). IR (film): ν (cm^{-1}) 2921, 2852, 2246, 2182, 2129, 1750, 1703, 1645, 1569, 1520, 1482, 1446, 1409, 1336, 1288, 1222, 1157, 1129, 1020, 998, 931, 824, 742, 704, 635.

5.2.3.10 Synthesis of organorhodium(III) complexes Λ -(*S*)-**131** and Λ -(*S*)-**132**

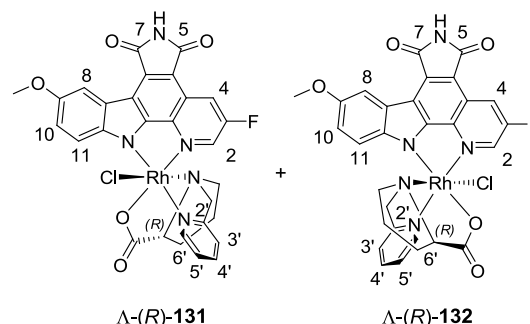


A suspension of **78** (34 mg, 75 μ mol) and $\text{RhCl}_3 \cdot 3\text{H}_2\text{O}$ (18.3 mg, 69 μ mol) in an ethanol : water mixture (1:1, 15 mL) under nitrogen atmosphere in a sealed vessel was

heated to 90 °C for 3 h. During this time the suspension turned from pale brown into dark red. The reaction mixture was then cooled down slightly to add (S)-**105** (15.5 mg, 75 µmol). After addition of (S)-**105**, the reaction was further proceeded at 90 °C for 16 h. The reaction mixture was then cooled down to ambient temperature and the solvent was removed *in vacuo*. The crude material was purified via column chromatography using methylene chloride : methanol (20:1 → 10:1). The separated diastereomers were further purified and concentrated via preparative TLC using methylene chloride : methanol (10:1). The products were obtained as dark purple solids, Δ-(S)-**131** (10.7 mg, 15.9 µmol, 23%) and Δ-(S)-**132** (5.6 mg, 8.3 µmol, 12%). Δ-(S)-**131**: $R_f = 0.14$ (methylene chloride : methanol 15:1). $^1\text{H-NMR}$ (300 MHz, $(\text{CD}_3)_2\text{SO}$): δ (ppm) 11.26 (s, 1H, NH), 9.51 (d, $J = 5.7$ Hz, 1H, $\text{CH}_{\text{ar}}-6'$), 8.85 (dd, $J = 9.2, 2.3$ Hz, 1H, $\text{CH}_{\text{ar}}-4$), 8.36 (td, $J = 7.8, 1.5$ Hz, 1H, $\text{CH}_{\text{ar}}-4'$), 8.23 (d, $J = 2.6$ Hz, 1H, $\text{CH}_{\text{ar}}-8$), 8.10 (td, $J = 2.5, 0.8$ Hz, 1H, $\text{CH}_{\text{ar}}-2$), 7.95 – 7.87 (m, 2H, $\text{CH}_{\text{ar}}-3'$ & $\text{CH}_{\text{ar}}-5'$), 7.71 (d, $J = 9.0$ Hz, 1H, $\text{CH}_{\text{ar}}-11$), 7.24 (dd, $J = 9.0, 2.7$ Hz, 1H, $\text{CH}_{\text{ar}}-10$), 4.75 (d, $J = 16.0$ Hz, 1H, NCHH), 4.55 (d, $J = 16.1$ Hz, 1H, NCHH), 3.92 (s, 3H, OCH_3), 3.77 (dd, $J = 9.4, 5.1$ Hz, 1H, CH_α), 2.50 – 2.48 (m, 1H, $\text{CH}_\delta\text{H}_\delta$), 2.28 – 2.10 (m, 2H, $\text{CH}_\delta\text{H}_\delta$ & $\text{CH}_\beta\text{H}_\beta$), 1.89 – 1.74 (m, 1H, $\text{CH}_\beta\text{H}_\beta$), 1.47 (tt, $J = 12.1, 6.1$ Hz, 1H, $\text{CH}_\gamma\text{H}_\gamma$), 1.17 – 0.95 (m, 1H, $\text{CH}_\gamma\text{H}_\gamma$). IR (film): ν (cm^{-1}) 2919, 1716, 1653, 1563, 1502, 1465, 1408, 1335, 1258, 1226, 1163, 1096, 1021, 924, 860, 814, 763, 725, 633, 582, 519, 478, 443. HRMS calculated for $\text{C}_{29}\text{H}_{22}\text{ClFN}_5\text{NaO}_5\text{Rh}$ ($\text{M} + \text{Na}$) $^+$ 700.0241, found ($\text{M} + \text{Na}$) $^+$ 700.0264. Δ-(S)-**132**: $R_f = 0.27$ (methylene chloride : methanol 15:1). $^1\text{H-NMR}$ (300 MHz, $(\text{CD}_3)_2\text{SO}$): δ (ppm) 11.31 (s, 1H, NH), 9.66 (d, $J = 5.8$ Hz, 1H, $\text{CH}_{\text{ar}}-6'$), 8.98 (dd, $J = 9.1, 2.4$ Hz, 1H, $\text{CH}_{\text{ar}}-4$), 8.70 (dt, $J = 2.3, 1.1$ Hz, 1H, $\text{CH}_{\text{ar}}-8$), 8.48 (td, $J = 7.8, 1.4$ Hz, 1H, $\text{CH}_{\text{ar}}-4'$), 8.21 (d, $J = 2.6$ Hz, 1H, $\text{CH}_{\text{ar}}-2$),

8.05 – 7.95 (m, 2H, $\text{CH}_{\text{ar}}-3'$ & $\text{CH}_{\text{ar}}-5'$), 6.92 (dd, $J = 9.0, 2.7$ Hz, 1H, $\text{CH}_{\text{ar}}-10$), 5.59 (d, $J = 9.0$ Hz, 1H, $\text{CH}_{\text{ar}}-11$), 4.61 (d, $J = 15.9$ Hz, 1H, NCHH), 4.32 (d, $J = 15.7$ Hz, 1H, NCHH), 3.83 (s, 3H, OCH_3), 3.82 – 3.74 (m, 1H, CH_α), 2.50 – 2.48 (m, 1H, $\text{CH}_\delta\text{H}_\delta$), 2.30 – 2.14 (m, 2H, $\text{CH}_\delta\text{H}_\delta$ & $\text{CH}_\beta\text{H}_\beta$), 2.10 – 1.94 (m, 1H, $\text{CH}_\beta\text{H}_\beta$), 1.69 – 1.58 (m, 1H, $\text{CH}_\gamma\text{H}_\gamma$), 1.46 (dd, $J = 15.5, 9.0$ Hz, 1H, $\text{CH}_\gamma\text{H}_\gamma$). IR (film): ν (cm^{-1}) 2919, 1718, 1650, 1563, 1500, 1468, 1408, 1337, 1277, 1259, 1228, 1167, 1098, 1023, 993, 923, 893, 857, 825, 793, 727, 701, 636, 523, 475, 442. HRMS calculated for $\text{C}_{29}\text{H}_{22}\text{ClFN}_5\text{NaO}_5\text{Rh}$ ($\text{M} + \text{Na}$) $^+$ 700.0241, found ($\text{M} + \text{Na}$) $^+$ 700.0263.

5.2.3.11 Synthesis of organorhodium(III) complexes Δ-(R)-**131** and Δ-(R)-**132**



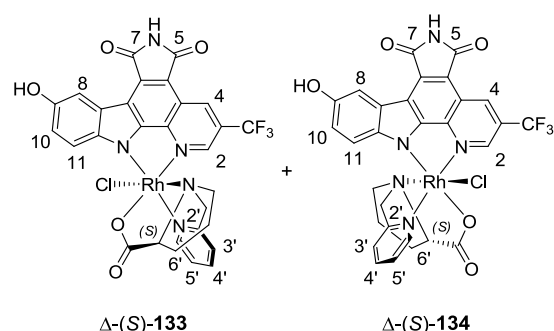
A suspension of **78** (34 mg, 75 µmol) and $\text{RhCl}_3 \cdot 3\text{H}_2\text{O}$ (18.3 mg, 69 µmol) in an ethanol : water mixture (1:1, 15 mL) under nitrogen atmosphere in a sealed vessel was heated to 90 °C for 3 h. During this time the suspension turned from pale brown into dark red. The reaction mixture was then cooled down slightly to add (R)-**105** (15.5 mg, 75 µmol). After addition of (R)-**105**, the reaction was further proceeded at 90 °C for 16 h. The reaction mixture was then cooled down to ambient temperature and the solvent was removed *in vacuo*. The crude material was purified via column chromatography using methylene chloride : methanol (15:1 → 10:1). The separated diastereomers were further purified and concentrated via prepar-

ative TLC using methylene chloride : methanol (15:1). The products were obtained as dark purple solids, Δ -(*R*)-**131** (10.3 mg, 15.2 μ mol, 22%) and Δ -(*R*)-**132** (6.0 mg, 8.9 μ mol, 13%). Δ -(*R*)-**131**: R_f = 0.14 (methylene chloride : methanol 15:1). $^1\text{H-NMR}$ (300 MHz, $(\text{CD}_3)_2\text{SO}$): δ (ppm) 11.17 (s, 1H, NH), 9.50 (d, J = 5.7 Hz, 1H, $\text{CH}_{\text{ar}}-6'$), 8.85 (dd, J = 9.2, 2.2 Hz, 1H, $\text{CH}_{\text{ar}}-4$), 8.35 (td, J = 7.7, 1.4 Hz, 1H, $\text{CH}_{\text{ar}}-4'$), 8.22 (d, J = 2.6 Hz, 1H, $\text{CH}_{\text{ar}}-8$), 8.09 (td, J = 2.5, 0.8 Hz, 1H, $\text{CH}_{\text{ar}}-2$), 7.99 – 7.84 (m, 2H, $\text{CH}_{\text{ar}}-3'$ & $\text{CH}_{\text{ar}}-5'$), 7.70 (d, J = 8.9 Hz, 1H, $\text{CH}_{\text{ar}}-11$), 7.23 (dd, J = 9.0, 2.7 Hz, 1H, $\text{CH}_{\text{ar}}-10$), 4.74 (d, J = 15.9 Hz, 1H, NCHH), 4.54 (d, J = 16.5 Hz, 1H, NCHH), 3.91 (s, 3H, OCH_3), 3.77 (dd, J = 9.2, 4.9 Hz, 1H, CH_α), 2.50 – 2.48 (m, 1H, $\text{CH}_\delta\text{H}_\delta$) 2.28 – 2.10 (m, 2H, $\text{CH}_\delta\text{H}_\delta$ & $\text{CH}_\beta\text{H}_\beta$), 1.89 – 1.74 (m, 1H, $\text{CH}_\beta\text{H}_\beta$), 1.47 (tt, J = 12.1, 6.1 Hz, 1H, $\text{CH}_\gamma\text{H}_\gamma$), 1.17 – 0.95 (m, 1H, $\text{CH}_\gamma\text{H}_\gamma$). $^{13}\text{C-NMR}$ (75 MHz, $(\text{CD}_3)_2\text{SO}$): δ (ppm) 182.54 ($\text{C}_{\text{carbonyl}}$), 170.54 ($\text{C}_{\text{ar}}-7$), 170.17 ($\text{C}_{\text{ar}}-5$), 160.25 ($\text{C}_{\text{ar}}-2'$), 156.93 (d, J = 249.7 Hz, $\text{C}_{\text{ar}}-3$), 154.05 ($\text{C}_{\text{ar}}-9$), 152.33 ($\text{C}_{\text{ar}}-6'$), 151.77 ($\text{C}_{\text{ar}}-12\text{b}$), 144.60 (C_{ar}), 141.20 (d, J = 33.9 Hz, $\text{C}_{\text{ar}}-2$), 140.85 (C_{ar}), 140.10 (C_{ar}), 132.23 (C_{ar}), 126.21 (C_{ar}), 124.05 (C_{ar}), 123.43 (C_{ar}), 120.77 (d, J = 8.8 Hz, $\text{C}_{\text{ar}}-4\text{a}$), 119.15 (d, J = 20.0 Hz, $\text{C}_{\text{ar}}-4$), 116.68 (C_{ar}), 115.65 (C_{ar}), 114.70 (C_{ar}), 112.77 (C_{ar}), 106.28 (C_{ar}), 73.53 (C_α), 69.48 (NCH₂), 61.53 (C_δ), 55.60 (OCH_3), 30.45 (C_β), 23.87 (C_γ). IR (film): ν (cm^{-1}) 1751, 1711, 1652, 1562, 1502, 1467, 1409, 1332, 1284, 1204, 1162, 1023, 997, 919, 856, 816, 760, 695, 632, 581, 520, 476, 445, 404. HRMS calculated for $\text{C}_{29}\text{H}_{23}\text{ClFN}_5\text{O}_5\text{Rh}$ ($\text{M} + \text{H}$)⁺ 678.0421, found ($\text{M} + \text{H}$)⁺ 678.0427. Δ -(*R*)-**132**: R_f = 0.27 (methylene chloride : methanol 15:1). $^1\text{H-NMR}$ (500 MHz, $(\text{CD}_3)_2\text{SO}$): δ (ppm) 9.65 (d, J = 5.7 Hz, 1H, $\text{CH}_{\text{ar}}-6'$), 8.98 (dd, J = 9.1, 2.4 Hz, 1H, $\text{CH}_{\text{ar}}-4$), 8.70 (dd, J = 2.2, 1.8 Hz, 1H, $\text{CH}_{\text{ar}}-8$), 8.47 (td, J = 7.8, 1.5 Hz, 1H, $\text{CH}_{\text{ar}}-4'$), 8.19 (d, J = 2.6 Hz, 1H, $\text{CH}_{\text{ar}}-2$), 8.02 (t, J = 6.8 Hz, 1H, $\text{CH}_{\text{ar}}-5'$), 7.98 (d, J = 7.9 Hz, 1H, $\text{CH}_{\text{ar}}-3'$), 6.91 (dd, J = 9.0, 2.7

Hz, 1H, $\text{CH}_{\text{ar}}-10$), 5.59 (d, J = 9.0 Hz, 1H, $\text{CH}_{\text{ar}}-11$), 4.62 (d, J = 15.7 Hz, 1H, NCHH), 4.32 (d, J = 15.6 Hz, 1H, NCHH), 3.82 (s, 3H, OCH_3), 3.82 – 3.77 (m, 1H, CH_α), 2.54 (dt, J = 11.2, 5.7 Hz, 1H, $\text{CH}_\delta\text{H}_\delta$), 2.29 – 2.18 (m, 2H, $\text{CH}_\delta\text{H}_\delta$ & $\text{CH}_\beta\text{H}_\beta$), 2.09 – 2.00 (m, 1H, $\text{CH}_\beta\text{H}_\beta$), 1.64 (dp, J = 12.5, 6.3 Hz, 1H, $\text{CH}_\gamma\text{H}_\gamma$), 1.27 – 1.15 (m, 1H, $\text{CH}_\gamma\text{H}_\gamma$). $^{13}\text{C-NMR}$ (126 MHz, $(\text{CD}_3)_2\text{SO}$): δ (ppm) 182.05 ($\text{C}_{\text{carbonyl}}$), 170.43 ($\text{C}_{\text{ar}}-7$), 170.07 ($\text{C}_{\text{ar}}-5$), 161.22 ($\text{C}_{\text{ar}}-2'$), 156.68 (d, J = 250.7 Hz, $\text{C}_{\text{ar}}-3$), 153.98 ($\text{C}_{\text{ar}}-6'$), 152.79 ($\text{C}_{\text{ar}}-12\text{b}$), 143.60 (C_{ar}), 141.41 (C_{ar}), 139.84 (C_{ar}), 138.31 (d, J = 35.1 Hz, $\text{CH}_{\text{ar}}-2$), 132.40 (C_{ar}), 126.45 (C_{ar}), 123.84 (C_{ar}), 123.71 (C_{ar}), 121.24 (d, J = 8.4 Hz, $\text{C}_{\text{ar}}-4\text{a}$), 119.80 (d, J = 20.2 Hz, $\text{C}_{\text{ar}}-4$), 116.43 (C_{ar}), 114.87 (C_{ar}), 113.36 (C_{ar}), 112.57 (C_{ar}), 107.09 (C_{ar}), 72.87 (C_α), 69.89 (NCH₂), 61.14 (OCH_3), 55.65 (C_δ), 30.25 (C_β), 24.33 (C_γ). IR (film): ν (cm^{-1}) 1752, 1714, 1652, 1562, 1499, 1470, 1408, 1336, 1285, 1207, 1167, 1055, 1025, 995, 920, 893, 856, 824, 793, 774, 699, 632, 614, 523. HRMS calculated for $\text{C}_{29}\text{H}_{22}\text{ClFN}_5\text{NaO}_5\text{Rh}$ ($\text{M} + \text{Na}$)⁺ 700.0241, found ($\text{M} + \text{Na}$)⁺ 700.0262.

5.2.3.12 Synthesis of organorhodium(III)

complexes Δ -(*S*)-**133** and Δ -(*S*)-**134**



A suspension of **81** (45 mg, 75 μ mol) and $\text{RhCl}_3 \cdot 3\text{H}_2\text{O}$ (18.3 mg, 69 μ mol) in an ethanol : water mixture (1:1, 15 mL) under nitrogen atmosphere in a sealed vessel was heated to 90 °C for 3 h. During this time the suspension turned from pale brown into dark red. The reaction mixture was then cooled

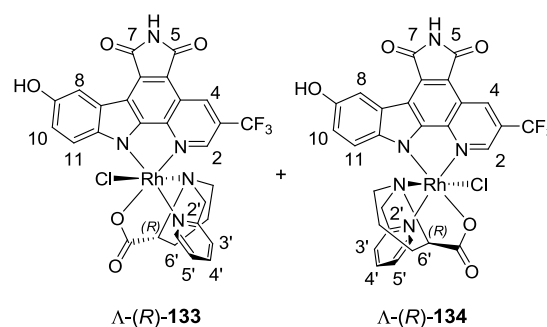
down slightly to add (S)-**105** (15.5 mg, 75 μmol). After addition of (S)-**105**, the reaction was further proceeded at 90 °C for 16 h. The reaction mixture was then cooled down to ambient temperature and the solvent was removed *in vacuo*. The crude material was purified via column chromatography using methylene chloride : methanol (35:1 \rightarrow 10:1). The separated diastereomers were further purified and concentrated via preparative TLC using methylene chloride : methanol (15:1). The products were obtained as dark purple solids, Δ -(S)-**133** (7.8 mg, 11.1 μmol , 16%) and Δ -(S)-**134** (4.4 mg, 6.2 μmol , 9%). Δ -(S)-**133**: R_f = 0.11 (methylene chloride : methanol 15:1). $^1\text{H-NMR}$ (300 MHz, $(\text{CD}_3)_2\text{SO}$): δ (ppm) 11.34 (s, 1H, NH), 9.53 (d, J = 5.3 Hz, 1H, $\text{CH}_{\text{ar-6'}}$), 9.43 (s, 1H, $\text{CH}_{\text{ar-4}}$), 9.33 (d, J = 0.8 Hz, 1H, $\text{CH}_{\text{ar-2}}$), 8.39 (td, J = 7.8, 1.4 Hz, 1H, $\text{CH}_{\text{ar-4'}}$), 8.17 (d, J = 2.4 Hz, 1H, $\text{CH}_{\text{ar-8}}$), 7.97 – 7.89 (m, 3H, OH, $\text{CH}_{\text{ar-3'}}$ & $\text{CH}_{\text{ar-5'}}$), 7.69 (d, J = 8.9 Hz, 1H, $\text{CH}_{\text{ar-11}}$), 7.14 (dd, J = 8.9, 2.5 Hz, 1H, $\text{CH}_{\text{ar-10}}$), 4.76 (d, J = 16.2 Hz, 1H, NCHH), 4.57 (d, J = 16.2 Hz, 1H, NCHH), 3.79 (dd, J = 9.4, 4.9 Hz, 1H, CH_a), 2.51 – 2.48 (m, 1H, $\text{CH}_\delta\text{H}_\delta$), 2.25 – 2.11 (m, 2H, $\text{CH}_\delta\text{H}_\delta$ & $\text{CH}_\beta\text{H}_\beta$), 1.84 (dt, J = 17.9, 5.9 Hz, 1H, $\text{CH}_\beta\text{H}_\beta$), 1.48 (ddd, J = 17.8, 11.7, 5.9 Hz, 1H, $\text{CH}_\gamma\text{H}_\gamma$), 1.16 – 1.00 (m, 1H, $\text{CH}_\gamma\text{H}_\gamma$). IR (film): ν (cm^{-1}) 3226, 2923, 1757, 1712, 1613, 1558, 1526, 1496, 1420, 1332, 1295, 1244, 1178, 1135, 1089, 1054, 1026, 924, 864, 767, 729, 699, 640, 531, 505, 446. HRMS calculated for $\text{C}_{29}\text{H}_{20}\text{ClF}_3\text{N}_5\text{NaO}_5\text{Rh}$ ($M + \text{Na}$) $^+$ 736.0052, found ($M + \text{Na}$) $^+$ 736.0074. Δ -(S)-**134**: R_f = 0.21 (methylene chloride : methanol 15:1). $^1\text{H-NMR}$ (300 MHz, $(\text{CD}_3)_2\text{SO}$): δ (ppm) 11.38 (s, 1H, NH), 9.65 (d, J = 5.8 Hz, 1H, $\text{CH}_{\text{ar-6'}}$), 9.46 (d, J = 0.9 Hz, 1H, $\text{CH}_{\text{ar-4}}$), 8.81 (d, J = 0.9 Hz, 1H, $\text{CH}_{\text{ar-4}}$), 8.48 (td, J = 7.8, 1.4 Hz, 1H, $\text{CH}_{\text{ar-4'}}$), 8.15 (d, J = 2.4 Hz, 1H, $\text{CH}_{\text{ar-8}}$), 8.06 – 7.87 (m, 3H, OH, $\text{CH}_{\text{ar-3'}}$ & $\text{CH}_{\text{ar-5'}}$), 6.80 (dd, J = 8.9, 2.5 Hz, 1H, $\text{CH}_{\text{ar-10}}$), 5.57 (d, J = 8.9 Hz, 1H, $\text{CH}_{\text{ar-11}}$), 4.63 (d, J = 15.7 Hz, 1H, NCHH), 4.33 (d, J = 15.7 Hz, 1H, NCHH),

3.83 (dd, J = 9.3, 4.5 Hz, 1H, CH_a), 2.51 – 2.48 (m, 1H, $\text{CH}_\delta\text{H}_\delta$), 2.31 – 2.14 (m, 2H, $\text{CH}_\delta\text{H}_\delta$ & $\text{CH}_\beta\text{H}_\beta$), 2.00 (td, J = 11.0, 5.5 Hz, 1H, $\text{CH}_\beta\text{H}_\beta$), 1.63 (ddd, J = 18.0, 11.9, 5.9 Hz, 1H, $\text{CH}_\gamma\text{H}_\gamma$), 1.14 – 0.97 (m, 1H, $\text{CH}_\gamma\text{H}_\gamma$). IR (film): ν (cm^{-1}) 3267, 2919, 1711, 1660, 1568, 1501, 1463, 1420, 1391, 1332, 1295, 1252, 1218, 1127, 1085, 1048, 1020, 933, 901, 860, 821, 781, 729, 697, 633, 530, 503, 481, 447, 409. HRMS calculated for $\text{C}_{29}\text{H}_{20}\text{ClF}_3\text{N}_5\text{NaO}_5\text{Rh}$ ($M + \text{Na}$) $^+$ 736.0052, found ($M + \text{Na}$) $^+$ 736.0076.

5.2.3.13 Synthesis of organorhodium(III)

complexes Δ -(R)-**133** and

Δ -(R)-**134**



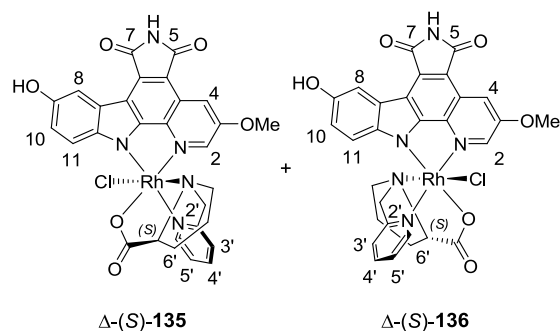
A suspension of **81** (45 mg, 75 μmol) and $\text{RhCl}_3 \cdot 3\text{H}_2\text{O}$ (18.3 mg, 69 μmol) in an ethanol : water mixture (1:1, 15 mL) under nitrogen atmosphere in a sealed vessel was heated to 90 °C for 3 h. During this time the suspension turned from pale brown into dark red. The reaction mixture was then cooled down slightly to add (R)-**105** (15.5 mg, 75 μmol). After addition of (R)-**105**, the reaction was further proceeded at 90 °C for 16 h. The reaction mixture was then cooled down to ambient temperature and the solvent was removed *in vacuo*. The crude material was purified via column chromatography using methylene chloride : methanol (20:1 \rightarrow 10:1). The separated diastereomers were further purified and concentrated via preparative TLC using methylene chloride : methanol (15:1). The products were obtained as dark purple solids, Δ -(R)-**133**

(8.6 mg, 12.4 μ mol, 18%) and Λ -(*R*)-**134** (4.9 mg, 6.9 μ mol, 10%). Λ -(*R*)-**133**: R_f = 0.11 (methylene chloride : methanol 15:1). $^1\text{H-NMR}$ (600 MHz, $(\text{CD}_3)_2\text{SO}$): δ (ppm) 11.33 (s, 1H, NH), 9.53 (d, J = 5.5 Hz, 1H, $\text{CH}_{\text{ar}}\text{-6}'$), 9.44 (s, 1H, $\text{CH}_{\text{ar}}\text{-4}$), 9.33 (d, J = 1.0 Hz, 1H, $\text{CH}_{\text{ar}}\text{-2}$), 8.38 (td, J = 7.8, 1.5 Hz, 1H, $\text{CH}_{\text{ar}}\text{-4}'$), 8.17 (d, J = 2.2 Hz, 1H, $\text{CH}_{\text{ar}}\text{-8}$), 7.99 – 7.92 (m, 3H, OH, $\text{CH}_{\text{ar}}\text{-3}'$ & $\text{CH}_{\text{ar}}\text{-5}'$), 7.91 (s, 1H, OH), 7.68 (d, J = 8.7 Hz, 1H, $\text{CH}_{\text{ar}}\text{-11}$), 7.14 (dd, J = 8.8, 2.5 Hz, 1H, $\text{CH}_{\text{ar}}\text{-10}$), 4.76 (d, J = 16.2 Hz, 1H, NCHH), 4.57 (d, J = 16.2 Hz, 1H, NCHH), 3.79 (dd, J = 9.5, 5.0 Hz, 1H, CH_α), 2.51 – 2.48 (m, 1H, $\text{CH}_\delta\text{H}_\delta$), 2.20 (td, J = 11.7, 5.9 Hz, 2H, $\text{CH}_\delta\text{H}_\delta$ & $\text{CH}_\beta\text{H}_\beta$), 1.84 (td, J = 11.8, 5.6 Hz, 1H, $\text{CH}_\beta\text{H}_\beta$), 1.55 – 1.40 (m, 1H, $\text{CH}_\gamma\text{H}_\gamma$), 1.16 – 1.00 (m, 1H, $\text{CH}_\gamma\text{H}_\gamma$). $^{13}\text{C-NMR}$ (151 MHz, $(\text{CD}_3)_2\text{SO}$): δ (ppm) 182.42 ($\text{C}_{\text{carbonyl}}$), 170.42 ($\text{C}_{\text{ar}}\text{-7}$), 170.00 ($\text{C}_{\text{ar}}\text{-5}$), 160.32 ($\text{C}_{\text{ar}}\text{-2}'$), 152.18 ($\text{C}_{\text{ar}}\text{-9}$), 151.86 ($\text{C}_{\text{ar}}\text{-6}'$), 151.07 ($\text{C}_{\text{ar}}\text{-12b}$), 144.20 (C_{ar}), 143.78 (C_{ar}), 140.93 (C_{ar}), 133.50 (C_{ar}), 132.55 (C_{ar}), 132.11 (C_{ar}), 126.25 (C_{ar}), 123.85 (C_{ar}), 121.75 (C_{ar}), 119.25 (C_{ar}), 118.11 (C_{ar}), 116.10 (C_{ar}), 115.77 (C_{ar}), 112.92 (C_{ar}), 111.33 (C_{ar}), 108.52 (C_{ar}), 73.41 (C_α), 69.36 (NCH₂), 61.52 (C_δ), 30.31 (C_β), 23.78 (C_γ). Due to the signal to noise ratio a unambiguous assignment of the CF_3 carbon signals was not possible. IR (film): ν (cm^{-1}) 1750, 1709, 1657, 1606, 1502, 1461, 1421, 1391, 1330, 1295, 1252, 1212, 1171, 1129, 1084, 1021, 934, 901, 858, 822, 777, 696, 631, 530, 500, 481. HRMS calculated for $\text{C}_{29}\text{H}_{20}\text{ClF}_3\text{N}_5\text{NaO}_5\text{Rh}$ ($\text{M} + \text{Na}$)⁺ 736.0052, found ($\text{M} + \text{Na}$)⁺ 736.0074. Λ -(*R*)-**134**: R_f = 0.21 (methylene chloride : methanol 15:1). $^1\text{H-NMR}$ (300 MHz, $(\text{CD}_3)_2\text{SO}$): δ (ppm) 9.65 (d, J = 5.4 Hz, 1H, $\text{CH}_{\text{ar}}\text{-6}'$), 9.47 – 9.45 (m, 1H, $\text{CH}_{\text{ar}}\text{-4}$), 8.81 (d, J = 0.8 Hz, 1H, $\text{CH}_{\text{ar}}\text{-2}$), 8.48 (td, J = 7.8, 1.3 Hz, 1H, $\text{CH}_{\text{ar}}\text{-4}'$), 8.15 (d, J = 2.4 Hz, 1H, $\text{CH}_{\text{ar}}\text{-8}$), 8.06 – 7.96 (m, 3H, OH, $\text{CH}_{\text{ar}}\text{-3}'$ & $\text{CH}_{\text{ar}}\text{-5}'$), 6.81 (dd, J = 8.9, 2.5 Hz, 1H, $\text{CH}_{\text{ar}}\text{-10}$), 5.57 (d, J = 8.9 Hz, 1H, $\text{CH}_{\text{ar}}\text{-9}$), 4.63 (d, J = 15.4 Hz, 1H, NCHH), 4.33 (d, J = 15.4 Hz, 1H, NCHH), 3.83 (dd, J = 9.2, 4.5

Hz, 1H, CH_α), 2.58 – 2.52 (m, 1H, $\text{CH}_\delta\text{H}_\delta$), 2.32 – 2.14 (m, 2H, $\text{CH}_\delta\text{H}_\delta$ & $\text{CH}_\beta\text{H}_\beta$), 2.00 (td, J = 11.6, 5.5 Hz, 1H, $\text{CH}_\beta\text{H}_\beta$), 1.64 (tt, J = 11.6, 5.8 Hz, 1H, $\text{CH}_\gamma\text{H}_\gamma$), 1.14 – 0.97 (m, 1H, $\text{CH}_\gamma\text{H}_\gamma$). $^{13}\text{C-NMR}$ (75 MHz, $(\text{CD}_3)_2\text{SO}$): δ (ppm) 182.05 ($\text{C}_{\text{carbonyl}}$), 170.38 ($\text{C}_{\text{ar}}\text{-7}$), 169.97 ($\text{C}_{\text{ar}}\text{-5}$), 161.19 ($\text{C}_{\text{ar}}\text{-2}'$), 152.65 ($\text{C}_{\text{ar}}\text{-9}$), 152.19 ($\text{C}_{\text{ar}}\text{-6}'$), 151.59 ($\text{C}_{\text{ar}}\text{-12b}$), 143.51 (C_{ar}), 143.31 (C_{ar}), 141.43 (C_{ar}), 139.65 (C_{ar}), 137.21 (C_{ar}), 132.71 (C_{ar}), 126.48 (C_{ar}), 124.12 (C_{ar}), 123.72 (C_{ar}), 121.18 (C_{ar}), 119.65 (C_{ar}), 118.06 (C_{ar}), 116.40 (C_{ar}), 113.61 (C_{ar}), 112.76 (C_{ar}), 109.09 (C_{ar}), 72.84 (C_α), 69.96 (NCH₂), 61.29 (C_δ), 30.25 (C_β), 24.50 (C_γ). Due to the signal to noise ratio a unambiguous assignment of the CF_3 carbon signals was not possible. IR (film): ν (cm^{-1}) 1757, 1715, 1663, 1611, 1565, 1497, 1419, 1337, 1293, 1246, 1134, 1083, 1049, 1022, 994, 914, 858, 822, 790, 762, 697, 629, 528, 499, 443. HRMS calculated for $\text{C}_{29}\text{H}_{20}\text{ClF}_3\text{N}_5\text{NaO}_5\text{Rh}$ ($\text{M} + \text{Na}$)⁺ 736.0052, found ($\text{M} + \text{Na}$)⁺ 736.0072.

5.2.3.14 Synthesis of organorhodium(III)

complexes Λ -(*S*)-**135** and Λ -(*S*)-**136**



A suspension of **82** (42.1 mg, 75 μ mol) and $\text{RhCl}_3 \cdot 3\text{H}_2\text{O}$ (18.3 mg, 69 μ mol) in an ethanol : water mixture (1:1, 15 mL) under nitrogen atmosphere in a sealed vessel was heated to 90 °C for 3 h. During this time the suspension turned from pale brown into dark red. The reaction mixture was then cooled down slightly to add (*S*)-**105** (15.5 mg, 75 μ mol). After addition of

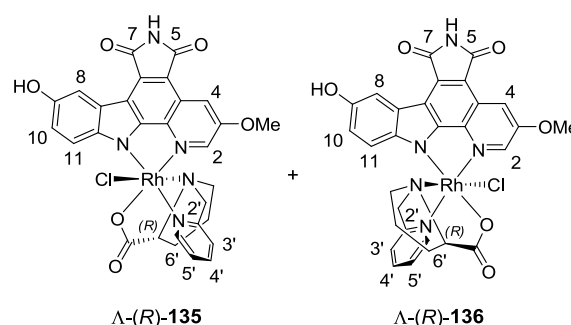
(*S*)-**105**, the reaction was further proceeded at 90 °C for 16 h. The reaction mixture was then cooled down to ambient temperature and the solvent was removed *in vacuo*. The crude material was purified via column chromatography using methylene chloride : methanol (25:1 → 10:1). The separated diastereomers were further purified and concentrated via preparative TLC using methylene chloride : methanol (15:1). The products were obtained as dark purple solids, Δ -(*S*)-**135** (7.9 mg, 11.7 μ mol, 17%) and Δ -(*S*)-**136** (5.1 mg, 7.6 μ mol, 11%). Δ -(*S*)-**135**: R_f = 0.11 (methylene chloride : methanol 15:1). ^1H -NMR (300 MHz, $(\text{CD}_3)_2\text{SO}$): δ (ppm) 11.12 (s, 1H, NH), 9.51 (dd, J = 5.8, 0.7 Hz, 1H, $\text{CH}_{\text{ar}}\text{-6'}$), 8.49 (d, J = 2.3 Hz, 1H, $\text{CH}_{\text{ar}}\text{-4}$), 8.36 (td, J = 7.8, 1.5 Hz, 1H, $\text{CH}_{\text{ar}}\text{-4'}$), 8.09 (d, J = 2.3 Hz, 1H, $\text{CH}_{\text{ar}}\text{-8}$), 7.96 – 7.85 (m, 2H, $\text{CH}_{\text{ar}}\text{-3'}$ & $\text{CH}_{\text{ar}}\text{-5'}$), 7.56 (d, J = 8.8 Hz, 1H, $\text{CH}_{\text{ar}}\text{-11}$), 7.45 (dd, J = 2.3, 0.9 Hz, 1H, $\text{CH}_{\text{ar}}\text{-2}$), 7.01 (dd, J = 8.8, 2.5 Hz, 1H, $\text{CH}_{\text{ar}}\text{-10}$), 4.70 (d, J = 16.3 Hz, 1H, NCHH), 4.55 (d, J = 16.3 Hz, 1H, NCHH), 3.97 (s, 3H, OCH_3), 3.77 (dd, J = 9.5, 4.8 Hz, 1H, CH_α), 2.58 – 2.52 (m, 1H, $\text{CH}_\delta\text{H}_\delta$), 2.30 – 2.21 (m, 2H, $\text{CH}_\delta\text{H}_\delta$ & $\text{CH}_\beta\text{H}_\beta$), 2.01 – 1.92 (m, 1H, $\text{CH}_\beta\text{H}_\beta$), 1.85 (dd, J = 12.5, 6.4 Hz, 1H, $\text{CH}_\gamma\text{H}_\gamma$), 1.67 – 1.59 (m, 1H, $\text{CH}_\gamma\text{H}_\gamma$). ^{13}C -NMR (126 MHz, $(\text{CD}_3)_2\text{SO}$): δ (ppm) 182.35 ($\text{C}_{\text{carbonyl}}$), 170.83 ($\text{C}_{\text{ar}}\text{-7}$), 170.33 ($\text{C}_{\text{ar}}\text{-5}$), 160.30 ($\text{C}_{\text{ar}}\text{-2'}$), 154.88 ($\text{C}_{\text{ar}}\text{-3}$), 152.96 ($\text{C}_{\text{ar}}\text{-9}$), 151.56 ($\text{C}_{\text{ar}}\text{-6'}$), 151.47 ($\text{C}_{\text{ar}}\text{-12b}$), 143.67 (C_{ar}), 142.17 (C_{ar}), 140.70 (C_{ar}), 137.46 (C_{ar}), 131.67 (C_{ar}), 129.59 (C_{ar}), 126.06 (C_{ar}), 123.81 (C_{ar}), 121.68 (C_{ar}), 73.50 (C_α), 69.78 (NCH₂), 61.45 (C_δ), 56.21 (OCH_3), 31.28 (C_β), 22.09 (C_γ). IR (film): ν (cm^{-1}) 2917, 2850, 1716, 1608, 1566, 1445, 1406, 1373, 1341, 1229, 1094, 1019, 931, 871, 800, 723. HRMS calculated for $\text{C}_{29}\text{H}_{23}\text{ClN}_5\text{NaO}_6\text{Rh}$ ($\text{M} + \text{Na}$)⁺ 698.0284, found ($\text{M} + \text{Na}$)⁺ 698.0286. Δ -(*S*)-**136**: R_f = 0.24 (methylene chloride : methanol 15:1). ^1H -NMR (300 MHz, $(\text{CD}_3)_2\text{SO}$): δ (ppm) 11.15 (s, 1H, NH), 9.65 (d, J = 5.2 Hz, 1H, $\text{CH}_{\text{ar}}\text{-6'}$), 9.18 (s, 1H, OH), 8.60 (d, J = 2.4 Hz, 1H, $\text{CH}_{\text{ar}}\text{-4}$),

8.46 (td, J = 7.8, 1.5 Hz, 1H, $\text{CH}_{\text{ar}}\text{-4'}$), 8.34 (dd, J = 2.4, 0.8 Hz, 1H, $\text{CH}_{\text{ar}}\text{-2}$), 8.08 (d, J = 2.4 Hz, 1H, $\text{CH}_{\text{ar}}\text{-8}$), 8.04 – 7.92 (m, 2H, $\text{CH}_{\text{ar}}\text{-3'}$ & $\text{CH}_{\text{ar}}\text{-5'}$), 6.67 (dd, J = 8.8, 2.5 Hz, 1H, $\text{CH}_{\text{ar}}\text{-10}$), 5.46 (d, J = 8.8 Hz, 1H, $\text{CH}_{\text{ar}}\text{-11}$), 4.70 – 4.52 (m, 2H, NCH₂), 4.12 (s, 3H, OCH_3), 3.80 (dd, J = 5.2, 4.1 Hz, 1H, CH_α), 2.51 – 2.48 (m, 1H, $\text{CH}_\delta\text{H}_\delta$), 2.07 – 1.88 (m, 2H, $\text{CH}_\delta\text{H}_\delta$ & $\text{CH}_\beta\text{H}_\beta$), 1.62 (dt, J = 11.5, 5.8 Hz, 1H, $\text{CH}_\beta\text{H}_\beta$), 1.56 – 1.38 (m, 1H, $\text{CH}_\gamma\text{H}_\gamma$), 1.17 – 0.98 (m, 1H, $\text{CH}_\gamma\text{H}_\gamma$). IR (film): ν (cm^{-1}) 2957, 2918, 2850, 1716, 1577, 1459, 1407, 1372, 1341, 1230, 1093, 1019, 931, 871, 800, 723, 468. HRMS calculated for $\text{C}_{29}\text{H}_{23}\text{ClN}_5\text{NaO}_6\text{Rh}$ ($\text{M} + \text{Na}$)⁺ 698.0284, found ($\text{M} + \text{Na}$)⁺ 698.0286.

5.2.3.15 Synthesis of organorhodium(III)

complexes Δ -(*R*)-**135** and

Δ -(*R*)-**136**



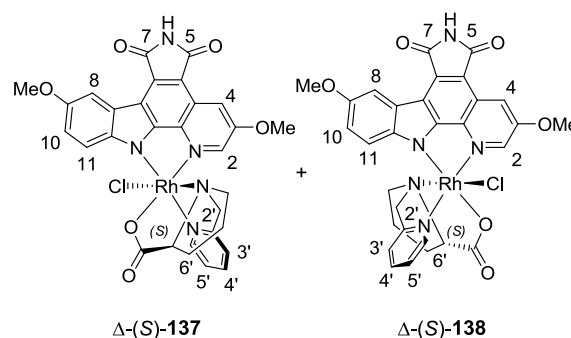
A suspension of **82** (42 mg, 75 μ mol) and $\text{RhCl}_3 \cdot 3\text{H}_2\text{O}$ (18.3 mg, 69 μ mol) in an ethanol : water mixture (1:1, 15 mL) under nitrogen atmosphere in a sealed vessel was heated to 90 °C for 3 h. During this time the suspension turned from pale brown into dark red. The reaction mixture was then cooled down slightly to add (*R*)-**105** (15.5 mg, 75 μ mol). After addition of (*R*)-**105**, the reaction was further proceeded at 90 °C for 16 h. The reaction mixture was then cooled down to ambient temperature and the solvent was removed *in vacuo*. The crude material was purified via column chromatography using methylene chloride : methanol (20:1 → 10:1). The separated diastereomers were

further purified and concentrated via preparative TLC using methylene chloride : methanol (15:1). The products were obtained as dark purple solids Δ -(R)-**135** (8.8 mg, 13.1 μ mol, 19%) and Δ -(R)-**136** (4.2 mg, 6.2 μ mol, 9%). Δ -(R)-**135**: R_f = 0.11 (methylene chloride : methanol 15:1). $^1\text{H-NMR}$ (600 MHz, $(\text{CD}_3)_2\text{SO}$): δ (ppm) 11.10 (s, 1H, NH), 9.51 (d, J = 5.5 Hz, 1H, $\text{CH}_{\text{ar}}-6'$), 9.22 (s, 1H, OH), 8.48 (d, J = 2.3 Hz, 1H, $\text{CH}_{\text{ar}}-4'$), 8.35 (td, J = 7.8, 1.4 Hz, 1H, $\text{CH}_{\text{ar}}-4'$), 8.09 (d, J = 2.5 Hz, 1H, $\text{CH}_{\text{ar}}-8$), 7.96 – 7.84 (m, 2H, $\text{CH}_{\text{ar}}-3'$ & $\text{CH}_{\text{ar}}-5'$), 7.55 (d, J = 8.8 Hz, 1H, $\text{CH}_{\text{ar}}-11$), 7.44 (d, J = 2.2 Hz, 1H, $\text{CH}_{\text{ar}}-2$), 7.01 (dd, J = 8.8, 2.5 Hz, 1H, $\text{CH}_{\text{ar}}-10$), 4.69 (d, J = 16.1 Hz, 1H, NCHH), 4.54 (d, J = 16.2 Hz, 1H, NCHH), 3.97 (s, 3H, OCH_3), 3.77 (dd, J = 9.6, 4.9 Hz, 1H, CH_a), 2.48 – 2.44 (m, 1H, $\text{CH}_\delta\text{H}_\delta$), 2.25 (dt, J = 11.7, 5.7 Hz, 1H, $\text{CH}_\delta\text{H}_\delta$), 2.21 – 2.13 (m, 1H, $\text{CH}_\beta\text{H}_\beta$), 1.85 (td, J = 11.6, 5.4 Hz, 1H, $\text{CH}_\beta\text{H}_\beta$), 1.51 – 1.41 (m, 1H, $\text{CH}_\gamma\text{H}_\gamma$), 1.16 – 1.08 (m, 1H, $\text{CH}_\gamma\text{H}_\gamma$). IR (film): ν (cm^{-1}) 1749, 1707, 1630, 1567, 1496, 1449, 1419, 1339, 1297, 1260, 1215, 1054, 1015, 927, 867, 819, 764, 732, 698, 635, 568, 510, 482, 448, 401. HRMS calculated for $\text{C}_{29}\text{H}_{23}\text{ClN}_5\text{NaO}_6\text{Rh}$ ($M + \text{Na}$) $^+$ 698.0284, found ($M + \text{Na}$) $^+$ 698.0286. Δ -(R)-**136**: R_f = 0.24 (methylene chloride : methanol 15:1). $^1\text{H-NMR}$ (500 MHz, $(\text{CD}_3)_2\text{SO}$): δ (ppm) 9.64 (d, J = 5.7 Hz, 1H, $\text{CH}_{\text{ar}}-6'$), 9.21 (bs, 1H, OH), 8.59 (d, J = 2.4 Hz, 1H, $\text{CH}_{\text{ar}}-4$), 8.45 (td, J = 7.8, 1.5 Hz, 1H, $\text{CH}_{\text{ar}}-4'$), 8.34 (d, J = 2.4 Hz, 1H, $\text{CH}_{\text{ar}}-2$), 8.07 (d, J = 2.5 Hz, 1H, $\text{CH}_{\text{ar}}-8$), 8.04 – 7.98 (m, 1H, $\text{CH}_{\text{ar}}-5'$), 7.96 (d, J = 8.0 Hz, 1H, $\text{CH}_{\text{ar}}-3'$), 6.67 (dd, J = 8.8, 2.5 Hz, 1H, $\text{CH}_{\text{ar}}-10$), 5.45 (d, J = 8.8 Hz, 1H, $\text{CH}_{\text{ar}}-11$), 4.59 (d, J = 15.5 Hz, 1H, NCHH), 4.30 (d, J = 15.6 Hz, 1H, NCHH), 4.12 (s, 3H, OCH_3), 3.79 (dd, J = 9.4, 4.5 Hz, 1H, CH_a), 2.54 – 2.51 (m, 1H, $\text{CH}_\delta\text{H}_\delta$), 2.27 – 2.16 (m, 2H, $\text{CH}_\delta\text{H}_\delta$ & $\text{CH}_\beta\text{H}_\beta$), 2.05 – 1.95 (m, 1H, $\text{CH}_\beta\text{H}_\beta$), 1.67 – 1.58 (m, 1H, $\text{CH}_\gamma\text{H}_\gamma$), 1.13 (tt, J = 13.5, 6.6 Hz, 1H, $\text{CH}_\gamma\text{H}_\gamma$). IR (film): ν (cm^{-1}) 1748, 1705, 1646, 1566, 1492, 1456, 1414, 1337, 1297, 1263, 1215, 1018, 925,

864, 818, 763, 701, 666, 634, 518, 484. HRMS calculated for $\text{C}_{29}\text{H}_{23}\text{ClN}_5\text{NaO}_6\text{Rh}$ ($M + \text{Na}$) $^+$ 698.0284, found ($M + \text{Na}$) $^+$ 698.0285.

5.2.3.16 Synthesis of organorhodium(III)

complexes Δ -(S)-**137** and Δ -(S)-**138**



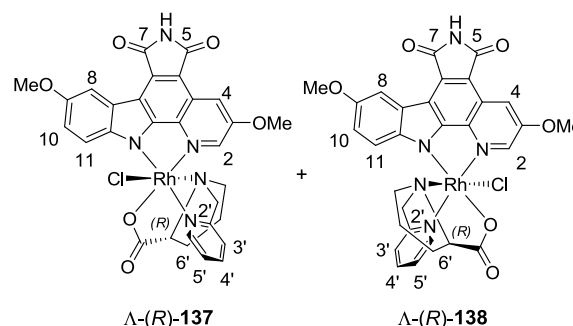
A suspension of **83** (34.6 mg, 75 μ mol) and $\text{RhCl}_3 \cdot 3\text{H}_2\text{O}$ (18.3 mg, 69 μ mol) in an ethanol : water mixture (1:1, 15 mL) under nitrogen atmosphere in a sealed vessel was heated to 90 $^\circ\text{C}$ for 3 h. During this time the suspension turned from pale brown into dark red. The reaction mixture was then cooled down slightly to add (S)-**105** (15.5 mg, 75 μ mol). After addition of (S)-**105**, the reaction was further proceeded at 90 $^\circ\text{C}$ for 16 h. The reaction mixture was then cooled down to ambient temperature and the solvent was removed *in vacuo*. The crude material was purified via column chromatography using methylene chloride : methanol (25:1 \rightarrow 10:1). The separated diastereomers were further purified and concentrated via preparative TLC using methylene chloride : methanol (15:1). The products were obtained as dark purple solids, Δ -(S)-**137** (11.9 mg, 17.3 μ mol, 25%) and Δ -(S)-**138** (6.6 mg, 9.7 μ mol, 14%). Δ -(S)-**137**: R_f = 0.16 (methylene chloride : methanol 15:1). $^1\text{H-NMR}$ (300 MHz, $(\text{CD}_3)_2\text{SO}$): δ (ppm) 11.17 (s, 1H, NH), 9.51 (d, J = 5.7 Hz, 1H, $\text{CH}_{\text{ar}}-6'$), 8.50 (d, J = 2.3 Hz, 1H, $\text{CH}_{\text{ar}}-4$), 8.36 (td, J = 7.8, 1.5 Hz, 1H, $\text{CH}_{\text{ar}}-4'$), 8.20 (d, J = 2.6 Hz, 1H, $\text{CH}_{\text{ar}}-8$), 7.97 – 7.84 (m, 2H, $\text{CH}_{\text{ar}}-3'$ &

$CH_{ar-5'}$), 7.66 (d, $J = 8.9$ Hz, 1H, CH_{ar-11}), 7.48 (dd, $J = 2.3, 0.8$ Hz, 1H, CH_{ar-2}), 7.19 (dd, $J = 8.9, 2.7$ Hz, 1H, CH_{ar-10}), 4.72 (d, $J = 16.2$ Hz, 1H, NCHH), 4.64 (d, $J = 15.7$ Hz, 1H, NCHH), 3.98 (s, 3H, OCH_3), 3.91 (s, 3H, OCH_3), 3.78 (dd, $J = 9.5, 4.8$ Hz, 1H, CH_α), 2.58 – 2.52 (m, 1H, $CH_\delta H_\delta$), 2.29 – 2.11 (m, 2H, $CH_\delta H_\delta$ & $CH_\beta H_\beta$), 1.70 – 1.57 (m, 1H, $CH_\beta H_\beta$), 1.46 (ddd, $J = 20.1, 13.3, 6.6$ Hz, 2H, $CH_\gamma H_\gamma$ & $CH_\gamma H_\gamma$). IR (film): ν (cm^{-1}) 3511, 3432, 3230, 2920, 2852, 1714, 1655, 1567, 1496, 1462, 1428, 1343, 1264, 1215, 1174, 1101, 1061, 1020, 925, 859, 820, 776, 728, 698, 658, 630, 575, 518, 476, 443, 400. HRMS calculated for $C_{30}H_{25}ClN_5NaO_6Rh$ ($M + Na$)⁺ 712.0441, found ($M + Na$)⁺ 712.0468. Δ -(S)-**138**: $R_f = 0.27$ (methylene chloride : methanol 15:1). 1H -NMR (300 MHz, $(CD_3)_2SO$): δ (ppm) 11.21 (s, 1H, NH), 9.66 (d, $J = 5.7$ Hz, 1H, $CH_{ar-6'}$), 8.61 (d, $J = 2.4$ Hz, 1H, CH_{ar-4}), 8.46 (td, $J = 7.8, 1.5$ Hz, 1H, $CH_{ar-4'}$), 8.36 (dd, $J = 2.4, 0.8$ Hz, 1H, CH_{ar-2}), 8.18 (d, $J = 2.6$ Hz, 1H, CH_{ar-8}), 8.04 – 7.93 (m, 2H, $CH_{ar-3'}$ & $CH_{ar-5'}$), 6.86 (dd, $J = 9.0, 2.7$ Hz, 1H, CH_{ar-10}), 5.55 (d, $J = 8.9$ Hz, 1H, CH_{ar-11}), 4.60 (d, $J = 15.9$ Hz, 1H, NCHH), 4.31 (d, $J = 15.7$ Hz, 1H, NCHH), 4.13 (s, 3H, OCH_3), 3.82 (s, 3H, OCH_3), 3.79 (d, $J = 4.8$ Hz, 1H, CH_α), 2.58 – 2.52 (m, 1H, $CH_\delta H_\delta$), 2.25 – 2.14 (m, 2H, $CH_\delta H_\delta$ & $CH_\beta H_\beta$), 2.01 (dt, $J = 18.9, 5.6$ Hz, 1H, $CH_\beta H_\beta$), 1.71 – 1.57 (m, 1H, $CH_\gamma H_\gamma$), 1.54 – 1.39 (m, 1H, $CH_\gamma H_\gamma$). IR (film): ν (cm^{-1}) 3350, 2971, 1599, 1451, 1388, 1297, 1270, 1235, 1179, 1155, 1099, 1011, 971, 911, 861, 831, 780, 739, 701, 655, 595. HRMS calculated for $C_{30}H_{25}ClN_5NaO_6Rh$ ($M + Na$)⁺ 712.0441, found ($M + Na$)⁺ 712.0466.

5.2.3.17 Synthesis of organorhodium(III)

complexes Δ -(R)-**137** and

Δ -(R)-**138**



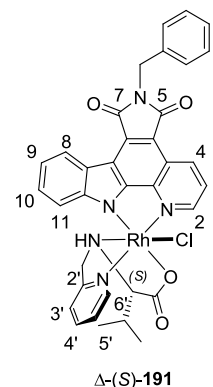
A suspension of **83** (34.6 mg, 75 μ mol) and $RhCl_3 \cdot 3H_2O$ (18.3 mg, 69 μ mol) in an ethanol : water mixture (1:1, 15 mL) under nitrogen atmosphere in a sealed vessel was heated to 90 °C for 3 h. During this time the suspension turned from pale brown into dark red. The reaction mixture was then cooled down slightly to add (R)-**105** (15.5 mg, 75 μ mol). After addition of (R)-**105**, the reaction was further proceeded at 90 °C for 16 h. The reaction mixture was then cooled down to ambient temperature and the solvent was removed *in vacuo*. The crude material was purified via column chromatography using methylene chloride : methanol (25:1 \rightarrow 10:1). The separated diastereomers were further purified and concentrated via preparative TLC using methylene chloride : methanol (15:1). The products were obtained as dark purple solids, Δ -(R)-**137** (11.4 mg, 16.6 μ mol, 24%) and Δ -(R)-**138** (6.6 mg, 9.7 μ mol, 14%). Δ -(R)-**137**: $R_f = 0.16$ (methylene chloride : methanol 15:1). 1H -NMR (300 MHz, $(CD_3)_2SO$): δ (ppm) 9.51 (d, $J = 5.7$ Hz, 1H, $CH_{ar-6'}$), 8.50 (d, $J = 2.3$ Hz, 1H, CH_{ar-4}), 8.36 (td, $J = 7.8, 1.5$ Hz, 1H, $CH_{ar-4'}$), 8.20 (d, $J = 2.6$ Hz, 1H, CH_{ar-8}), 7.98 – 7.87 (m, 2H, $CH_{ar-3'}$ & $CH_{ar-5'}$), 7.65 (d, $J = 8.9$ Hz, 1H, CH_{ar-11}), 7.48 (dd, $J = 2.3, 0.8$ Hz, 1H, CH_{ar-2}), 7.19 (dd, $J = 9.0, 2.7$ Hz, 1H, CH_{ar-10}), 4.72 (d, $J = 16.1$ Hz, 1H, NCHH), 4.55 (d, $J = 16.4$ Hz, 1H, NCHH), 3.97 (s,

3H, OCH₃), 3.90 (s, 3H, OCH₃), 3.78 (dd, J = 9.4, 4.8 Hz, 1H, CH_α), 2.47 – 2.41 (m, 1H, CH_δH_δ), 2.31 – 2.08 (m, 2H, CH_δH_δ & CH_βH_β), 1.92 – 1.78 (m, 1H, CH_βH_β), 1.53 – 1.38 (m, 1H, CH_γH_γ), 1.18 – 1.02 (m, 1H, CH_γH_γ). ¹³C-NMR (75 MHz, (CD₃)₂SO): δ(ppm) 182.43 (C_{carbonyl}), 170.88 (C_{ar}-7), 170.34 (C_{ar}-5), 160.32 (C_{ar}-2'), 155.01 (C_{ar}-3/C_{ar}-9), 153.72 (C_{ar}-9/C_{ar}-3), 153.08 (C_{ar}-6'), 151.63 (C_{ar}-12b), 144.57 (C_{ar}), 142.58 (C_{ar}), 140.76 (C_{ar}), 137.52 (C_{ar}), 132.97 (C_{ar}), 131.68 (C_{ar}), 126.12 (C_{ar}), 123.96 (C_{ar}), 123.50 (C_{ar}), 121.74 (C_{ar}), 115.95 (C_{ar}), 115.28 (C_{ar}), 113.84 (C_{ar}), 112.77 (C_{ar}), 112.10 (C_{ar}), 106.36 (C_{ar}), 73.53 (C_α), 65.07 (NCH₂), 61.53 (C_δ), 56.27 (OCH₃), 55.58 (OCH₃), 30.40 (C_β), 23.90 (C_γ). IR (film): ν (cm⁻¹) 1748, 1707, 1652, 1567, 1499, 1465, 1425, 1340, 1269, 1211, 1145, 1018, 929, 859, 815, 759, 696, 664, 631, 515, 474, 446, 400. HRMS calculated for C₃₀H₂₅ClN₅NaO₆Rh (M + Na)⁺ 712.0441, found (M + Na)⁺ 712.0461. Δ-(R)-**138**: R_f = 0.27 (methylene chloride : methanol 15:1). ¹H-NMR (500 MHz, (CD₃)₂SO): δ(ppm) 9.65 (d, J = 5.8 Hz, 1H, CH_{ar}-6'), 8.61 (d, J = 2.4 Hz, 1H, CH_{ar}-4), 8.46 (td, J = 7.8, 1.5 Hz, 1H, CH_{ar}-4'), 8.37 (dd, J = 2.4, 0.6 Hz, 1H, CH_{ar}-2), 8.18 (d, J = 2.6 Hz, 1H, CH_{ar}-8), 8.04 – 7.99 (m, 1H, CH_{ar}-5'), 7.97 (d, J = 7.7 Hz, 1H, CH_{ar}-3'), 6.86 (dd, J = 8.9, 2.7 Hz, 1H, CH_{ar}-10), 5.55 (d, J = 9.0 Hz, 1H, CH_{ar}-11), 4.60 (d, J = 15.7 Hz, 1H, NCHH), 4.31 (d, J = 15.7 Hz, 1H, NCHH), 4.13 (s, 3H, OCH₃), 3.81 (s, 3H, OCH₃), 3.79 (d, J = 4.7 Hz, 1H, CH_α), 2.55 – 2.51 (m, 1H, CH_δH_δ), 2.28 – 2.17 (m, 2H, CH_δH_δ & CH_βH_β), 2.00 (td, J = 12.1, 5.6 Hz, 1H, CH_βH_β), 1.68 – 1.58 (m, 1H, CH_γH_γ), 1.13 (tt, J = 14.7, 7.2 Hz, 1H, CH_γH_γ). ¹³C-NMR (126 MHz, (CD₃)₂SO): δ(ppm) 182.01 (C_{carbonyl}), 170.86 (C_{ar}-7), 170.31 (C_{ar}-5), 161.15 (C_{ar}-2'), 154.85 (C_{ar}-3/C_{ar}-9), 153.67 (C_{ar}-9/C_{ar}-3), 153.60 (C_{ar}-6'), 152.58 (C_{ar}-12b), 143.56 (C_{ar}), 141.25 (C_{ar}), 140.28 (C_{ar}), 137.24 (C_{ar}), 131.84 (C_{ar}), 126.32 (C_{ar}), 123.95 (C_{ar}), 123.58 (C_{ar}), 122.12 (C_{ar}), 115.71 (C_{ar}), 113.90 (C_{ar}), 113.36 (C_{ar}),

112.68 (C_{ar}), 112.17 (C_{ar}), 107.18 (C_{ar}), 72.75 (C_α), 69.89 (NCH₂), 61.09 (C_δ), 56.68 (OCH₃), 55.64 (OCH₃), 30.18 (C_β), 24.38 (C_γ). IR (film): ν(cm⁻¹) 1818, 1751, 1708, 1648, 1563, 1492, 1466, 1413, 1332, 1287, 1263, 1209, 1169, 1059, 1003, 880, 854, 821, 779, 760, 698, 670, 625, 521, 478. HRMS calculated for C₃₀H₂₅ClN₅NaO₆Rh (M + Na)⁺ 712.0441, found (M + Na)⁺ 712.0466.

5.2.3.18 Synthesis of organorhodium(III)

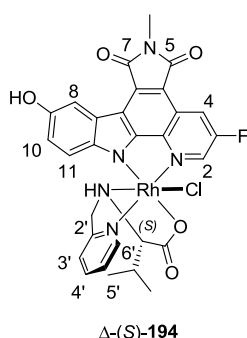
complex Δ-(S)-**191**



80 (50.0 mg, 0.13 mmol) was suspended in a mixture of ethanol/water (1:1, 15 mL) and rhodium(III)-chloride trihydrate (34.7 mg, 0.13 mmol) was added. The mixture was reacted at 90 °C for 3 h. Then, ligand (S)-**178** (30.2 mg, 0.13 mmol) was added and the reaction was continued at 90 °C for 16 h. The solvent was evaporated under reduced pressure and the crude material was subjected to column chromatography using methylene chloride : methanol (20:1) followed by preparative TLC using methylene chloride : methanol (15:1). The product Δ-(S)-**191** was obtained as red solid (6.5 mg, 9.1 μmol, 7%). R_f = 0.45 (methylene chloride : methanol 15:1). ¹H-NMR (300 MHz, (CD₃)₂SO): δ(ppm) 9.69 (d, J = 5.6 Hz, 1H, CH_{ar}-6'), 9.25 (dd, J = 8.4 Hz, 0.9 Hz, 1H, CH_{ar}-4), 8.78 (d, J = 5.2 Hz, 1H, CH_{ar}-2), 8.68 (d, J = 7.4 Hz, 1H, CH_{ar}-8), 8.45 (dd, J = 7.8 Hz, 1.3 Hz, 1H, CH_{ar}-4'), 8.06 – 7.96 (m, 3H, 3xCH_{ar}), 7.41 – 7.15 (m, 6H,

6xCH_{ar}), 7.10 – 6.99 (m, 1H, CH_{ar}-10), 5.54 (d, J = 8.1 Hz, 1H, CH_{ar}-11), 4.93 (s, 2H, CH_{2benzyl}), 4.23-4.07 (m, 3H, NCH₂ & CH_α), 2.21-2.12 (m, 1H, CH_β), 0.86 (d, J = 7.0 Hz, 6H, (CH_{3γ})₂). IR (film): ν (cm⁻¹) 3384, 1691, 1638, 1424, 1388, 1353, 1022, 995, 763, 698, 631, 552, 429. HRMS calculated for C₃₅H₂₉ClN₅O₄RhNa (M + Na)⁺ 744.0855, found (M + Na)⁺ 744.0857.

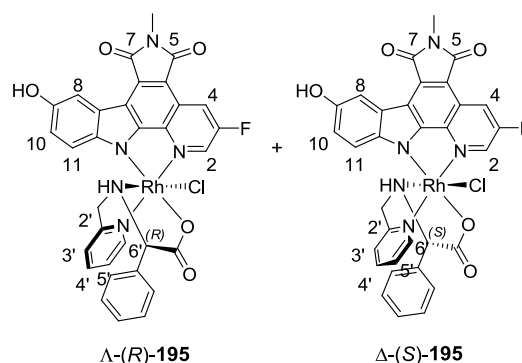
5.2.3.19 Synthesis of organorhodium(III) complex Δ-(S)-194



77 (58.4 mg, 0.13 mmol) was suspended in a mixture of ethanol/water (1:1, 15 mL) and rhodium(III)-chloride trihydrate (34.7 mg, 0.13 mmol) was added. The mixture was reacted at 90 °C for 3 h. Then, ligand (S)-**178** (30.2 mg, 0.13 mmol) was added and the reaction was continued at 90 °C for 16 h. The solvent was evaporated under reduced pressure and the crude material was subjected to column chromatography using methylene chloride : methanol (20:1 → 10:1) followed by preparative TLC using methylene chloride : methanol (15:1). The product Δ-(S)-**194** was obtained as purple solid (15.9 mg, 23.4 μmol, 18%,). R_f = 0.41 (methylene chloride : methanol 15:1). ¹H-NMR (300 MHz, (CD₃)₂SO): δ(ppm) 9.65 (d, J = 5.5 Hz, 1H, CH_{ar}-6'), 9.30 (s, 1H, OH), 8.95 (dd, J = 9.1 Hz, 2.3 Hz, 1H, CH_{ar}-4), 8.56 (s, 1H, CH_{ar}), 8.45 (ddd, J = 8.8 Hz, 7.7 Hz, 1.0 Hz, 1H, CH_{ar}-4'), 8.13 (d, J = 2.3 Hz, CH_{ar}-2), 8.03-7.96 (m, 2H, CH_{ar}-3' & CH_{ar}-5'), 7.12 (s, 1H, CH_{ar}), 6.69 (dd, J = 6.4 Hz, J = 2.3 Hz, 1H, CH_{ar}-10), 5.35 (d, J = 8.8

Hz, 1H, CH_{ar}-11), 4.25-4.09 (m, 3H, NCH₂ & CH_α), 3.18 (s, 3H, NCH₃), 2.24-2.11 (m, 1H, CH_β), 0.88 (d, J = 7.2 Hz, 3H, CH_{3γ}), 0.58 (d, J = 6.9 Hz, 3H, CH_{3γ}). IR (film): ν (cm⁻¹) 3393, 2960, 2874, 1746, 1695, 1653, 1566, 1464, 1416, 1374, 1331, 1300, 1158, 1029, 884, 803, 740, 610, 510, 456. HRMS calculated for C₂₉H₂₄ClFN₅O₅RhNa (M + Na)⁺ 702.0397, found (M + Na)⁺ 702.0392.

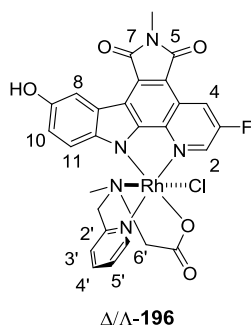
5.2.3.20 Synthesis of organorhodium(III) complexes Δ-(R)-195 and Δ-(S)-195



77 (60.0 mg, 139 μmol) was suspended in a mixture of ethanol/water (1:1, 15 mL) and rhodium(III)-chloride trihydrate (36.3 mg, 139 μmol) was added. The mixture was reacted at 90 °C for 3 h. Then, ligand (R)-**182** (37.1 mg, 153 μmol) was added and the reaction was continued at 90 °C for 16 h. The solvent was evaporated under reduced pressure and the crude material was subjected to column chromatography using methylene chloride : methanol (50:1 → 5:1) followed by preparative TLC using methylene chloride : methanol (20:1). The racemic products Δ-(R)-**195** and Δ-(S)-**195** were obtained as purple solid (8.9 mg, 12.5 μmol, 9%). R_f = 0.85 (methylene chloride : methanol 10:1). ¹H-NMR (300 MHz, (CD₃)₂SO): δ(ppm) 9.72 (d, J = 5.9 Hz, 1H, CH_{ar}-6'), 9.27 (s, 1H, OH), 8.98-8.49 (dd, J = 9.0, 2.4 Hz, 1H, CH_{ar}), 8.81 (s, 1H, CH_{ar}), 8.47 (m, 1H, CH_{ar}), 8.03 (m, 3H, 3xCH_{ar}), 7.78 (m, 1H, CH_{ar}), 7.13 (m, 5H, 5xCH_{ar}),

6.66 (m, 1H, CH_{ar-10}), 5.31 (m, 1H, CH_{ar-11}), 4.45 (m, 2H, NCH_2), 4.02–3.96 (m, 1H, CH_α), 3.16 (s, 3H, NCH_3).

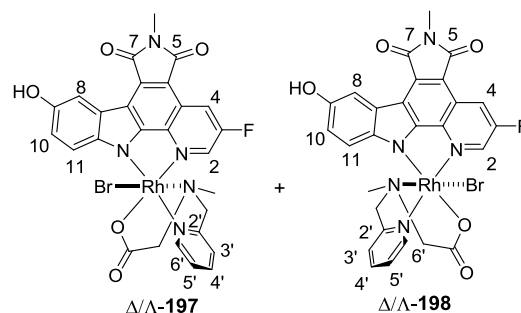
5.2.3.21 Synthesis of organorhodium(III) complexes Δ/Λ -**196**



77 (20.0 mg, 44 μ mol) was suspended in a mixture of ethanol/water (1:1, 15 mL) and rhodium(III)-chloride trihydrate (11.5 mg, 44 μ mol) was added. The mixture was reacted at 90 °C for 3 h. Then, ligand **189** (8.6 mg, 48 μ mol) was added and the reaction was continued at 90 °C for 16 h. The solvent was evaporated under reduced pressure and the crude material was subjected to column chromatography using methylene chloride : methanol (30:1 \rightarrow 5:1) followed by preparative TLC using methylene chloride : methanol (20:1). The racemic products Λ -(*R*)-**195** and Λ -(*S*)-**195** was obtained as dark green solid (4.9 mg, 7.5 μ mol, 17%). R_f = 0.45 (methylene chloride : methanol 10:1). 1H -NMR (300 MHz, $(CD_3)_2SO$): δ (ppm) 9.63 (d, J = 5.7 Hz, 1H, $CH_{ar-6'}$), 9.31 (s, 1H, OH), 8.94 (dd, J = 9.2, 2.3 Hz, 1H, $CH_{ar-4'}$), 8.73 (dd, J = 2.2, 1.6 Hz, 1H, CH_{ar-2}), 8.46 (td, J = 7.8, 1.4 Hz, 1H, $CH_{ar-4'}$), 8.11 (d, J = 2.4 Hz, 1H, CH_{ar-8}), 8.05 – 7.96 (m, 2H, $CH_{ar-3'}$ & $CH_{ar-5'}$), 6.74 (dd, J = 8.8, 2.5 Hz, 1H, CH_{ar-10}), 5.58 (d, J = 8.8 Hz, 1H, CH_{ar-11}), 4.55 (d, J = 16.0 Hz, 1H, $NCHH$), 4.25 (d, J = 15.9 Hz, 1H, $NCHH$), 3.97 (d, J = 17.5 Hz, 1H, $CH_\alpha H_\alpha$), 3.64 (d, J = 17.5 Hz, 1H, $CH_\alpha H_\alpha$), 3.16 (s, 3H, $N_{imid}CH_3$), 1.92 (s, 3H, NCH_3). HRMS calculated for

$C_{27}H_{20}ClFN_5NaO_5Rh$ ($M + Na$)⁺ 674.0084, found ($M + Na$)⁺ 674.0077.

5.2.3.22 Synthesis of organorhodium(III) complexes Δ/Λ -(*R*)-**197** and Δ/Λ -(*R*)-**198**



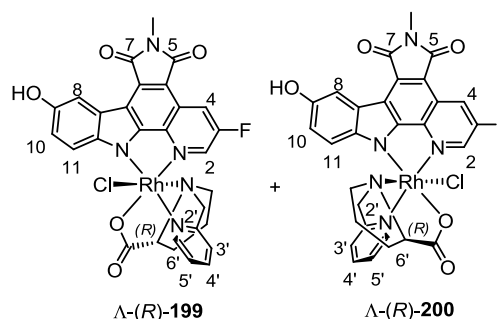
A suspension of KBr (94.5 mg, 792 μ mol) and $RhCl_3 \cdot 3H_2O$ (23 mg, 88 μ mol) in water (1:1, 8 mL) under nitrogen atmosphere in a sealed vessel was heated to 90 °C for 45 min. Then, **77** (40 mg, 88 μ mol) dissolved in ethanol (8 mL) was added and the reaction mixture was stirred for another 3 h at 90 °C. During this time the suspension turned from pale brown into dark green. The reaction mixture was then cooled down slightly to add **189** (17.2 mg, 96 μ mol). After addition of **189**, the reaction was further proceeded at 90 °C for 16 h. The reaction mixture was then cooled down to ambient temperature and the solvent was removed *in vacuo*. The crude material was purified via column chromatography using methylene chloride : methanol (20:1 \rightarrow 10:1). The separated diastereomers were further purified and concentrated via preparative TLC using methylene chloride : methanol (10:1). The products were obtained as dark green solids, Δ/Λ -**197** (11.6 mg, 16.7 μ mol, 19%) and Δ/Λ -**198** (6.1 mg, 8.8 μ mol, 10%). Δ/Λ -**197**: R_f = 0.30 (methylene chloride : methanol 10:1). 1H -NMR (300 MHz, $(CD_3)_2SO$): δ (ppm) 9.70 (dd, J = 5.0, 1.6 Hz, 1H, $CH_{ar-6'}$), 9.36 (s, 1H, OH), 8.82 (dt, J = 9.2, 2.4 Hz, 1H, $CH_{ar-4'}$), 8.39 – 8.29 (m, 1H,

CH_{ar-4}), 8.23 – 8.16 (m, 2H, CH_{ar-2} & CH_{ar-8}), 7.95 – 7.87 (m, 2H, $CH_{ar-3'}$ & $CH_{ar-5'}$), 7.56 (d, $J = 8.9$ Hz, 1H, CH_{ar-11}), 7.09 (dd, $J = 8.9, 2.6$ Hz, 1H, CH_{ar-10}), 4.75 (d, $J = 16.2$ Hz, 1H, NCHH), 4.52 (d, $J = 16.4$ Hz, 1H, NCHH), 3.68 (d, $J = 4.1$ Hz, 2H, $CH_{2\alpha}$), 3.16 (s, 3H, $N_{imid}CH_3$), 1.73 (s, 3H, NCH_3). IR (film): ν (cm^{-1}) 2922, 2852, 2243, 2181, 2126, 2001, 1749, 1696, 1650, 1564, 1502, 1443, 1411, 1368, 1330, 1296, 1221, 1153, 1021, 992, 882, 815, 758, 690, 608, 515, 451. HRMS calculated for $C_{27}H_{20}BrFN_5NaO_5Rh$ ($M + Na$)⁺ 719.2753, found ($M + Na$)⁺ 719.9553. Δ/Δ -**198**: $R_f = 0.48$ (methylene chloride : methanol 10:1). ¹H-NMR (300 MHz, $(CD_3)_2SO$): δ (ppm) 9.84 (d, $J = 5.8$ Hz, 1H, $CH_{ar-6'}$), 9.31 (s, 1H, CH_{ar}), 8.94 (dd, $J = 9.2, 2.4$ Hz, 1H, CH_{ar}), 8.75 – 8.70 (m, 1H, CH_{ar}), 8.45 (td, $J = 7.8, 1.4$ Hz, 1H, $CH_{ar-4'}$), 8.11 (d, $J = 2.4$ Hz, 1H, CH_{ar}), 8.04 – 7.95 (m, 2H, $CH_{ar-3'}$ & $CH_{ar-5'}$), 6.74 (dd, $J = 8.8, 2.5$ Hz, 1H, CH_{ar-10}), 5.57 (d, $J = 8.8$ Hz, 1H, CH_{ar-10}), 4.54 (d, $J = 16.1$ Hz, 1H, NCHH), 4.23 (d, $J = 15.9$ Hz, 1H, NCHH), 3.91 (d, $J = 17.4$ Hz, 1H, $CH_{\alpha}H_{\alpha}$), 3.59 (d, $J = 17.5$ Hz, 1H, $CH_{\alpha}H_{\alpha}$), 3.16 (s, 3H, $N_{imid}CH_3$), 1.86 (s, 3H, NCH_3). IR (film): ν (cm^{-1}) 1748, 1655, 1559, 1526, 1492, 1438, 1406, 1371, 1322, 1288, 1198, 1145, 1020, 984, 953, 924, 884, 842, 793, 753, 688, 610, 524, 447. HRMS calculated for $C_{27}H_{21}BrFN_5O_5Rh$ ($M + H$)⁺ 697.2935, found ($M + H$)⁺ 697.9729.

5.2.3.23 Synthesis of organorhodium(III)

complexes Λ -(*R*)-**199** and

Λ -(*R*)-**200**



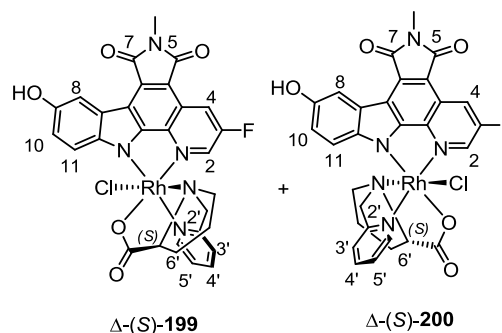
A suspension of **77** (20 mg, 44 μ mol) and $RhCl_3 \cdot 3H_2O$ (11.5 mg, 44 μ mol) in an ethanol : water mixture (1:1, 20 mL) under nitrogen atmosphere in a sealed vessel was heated to 90 °C for 3 h. During this time the suspension turned from pale brown into dark green. The reaction mixture was then cooled down slightly to add (*R*)-**105** (9.9 mg, 48 μ mol). After addition of (*R*)-**105**, the reaction was further proceeded at 90 °C for 16 h. The reaction mixture was then cooled down to ambient temperature and the solvent was removed *in vacuo*. The crude material was purified via column chromatography using methylene chloride : methanol (25:1 \rightarrow 10:1). The separated diastereomers were further purified and concentrated via preparative TLC using methylene chloride : methanol (15:1). The products were obtained as dark green solids, Λ -(*R*)-**199** (6.3 mg, 9.3 μ mol, 21%) and Λ -(*R*)-**200** (3.8 mg, 5.7 μ mol, 13%). Λ -(*R*)-**199**: $R_f = 0.13$ (methylene chloride : methanol 15:1). ¹H-NMR (300 MHz, $(CD_3)_2SO$): δ (ppm) 9.50 (d, $J = 5.6$ Hz, 1H, $CH_{ar-6'}$), 9.36 (s, 1H, OH), 8.81 (dd, $J = 9.2, 2.2$ Hz, 1H, CH_{ar-4}), 8.35 (td, $J = 7.8, 1.5$ Hz, 1H, $CH_{ar-4'}$), 8.14 (d, $J = 2.4$ Hz, 1H, CH_{ar-8}), 8.09 – 8.03 (m, 1H, CH_{ar-2}), 7.97 – 7.87 (m, 2H, $CH_{ar-3'}$ & $CH_{ar-5'}$), 7.62 (d, $J = 8.8$ Hz, 1H, CH_{ar-11}), 7.09 (dd, $J = 8.8, 2.5$ Hz, 1H, CH_{ar-10}), 4.75 (d, $J = 16.1$ Hz, 1H, NCHH), 4.57 (d, $J = 16.1$ Hz, 1H, NCHH), 3.77 (dd, J

= 9.4, 5.1 Hz, 1H, CH_α), 3.15 (s, 3H, NCH_3), 2.52 – 2.48 (m, 1H, $CH_\delta H_\delta$), 2.18 (dt, J = 13.4, 6.1 Hz, 2H, $CH_\delta H_\delta$ & $CH_\beta H_\beta$), 1.82 (td, J = 11.7, 5.6 Hz, 1H, $CH_\beta H_\beta$), 1.55 – 1.40 (m, 1H, $CH_\gamma H_\gamma$), 1.17 – 1.01 (m, 1H, $CH_\gamma H_\gamma$). ^{13}C -NMR (75 MHz, $(CD_3)_2SO$): δ (ppm) 182.28 (C_{carbonyl}), 169.02 ($C_{\text{ar-7}}$), 168.73 ($C_{\text{ar-5}}$), 160.17 ($C_{\text{ar-2'}}$), 156.77 (d, J = 252.4 Hz, $C_{\text{ar-3}}$), 152.15 ($C_{\text{ar-12b}}$), 151.87 ($C_{\text{ar-6'}}$), 151.62 ($C_{\text{ar-9}}$), 143.68 (C_{ar}), 140.87 (C_{ar}), 140.66 (C_{ar}), 140.41 (C_{ar}), 139.68 (C_{ar}), 131.37 (C_{ar}), 126.02 (C_{ar}), 123.90 (C_{ar}), 123.67 (C_{ar}), 120.57 (d, J = 8.1 Hz, $C_{\text{ar-4a}}$), 118.63 (d, J = 21.0 Hz, $C_{\text{ar-4}}$), 117.03 (C_{ar}), 115.32 (C_{ar}), 114.68 (C_{ar}), 111.04 (C_{ar}), 108.64 (C_{ar}), 73.42 (C_α), 69.36 (NCH_2), 61.33 (C_δ), 30.34 (C_β), 23.67 (C_γ), 23.63 (NCH_3). IR (film): ν (cm^{-1}) 2921, 2852, 1747, 1697, 1619, 1566, 1502, 1444, 1411, 1373, 1331, 1272, 1220, 1151, 1065, 987, 958, 882, 805, 766, 731, 690, 610, 579. HRMS calculated for $C_{29}H_{22}ClFN_5NaO_5Rh$ ($M + Na$)⁺ 700.0241, found ($M + Na$)⁺ 700.0257. Δ -(*R*)-**200**: 1H -NMR (300 MHz, R_f = 0.22 (methylene chloride : methanol 15:1). $(CD_3)_2SO$): δ (ppm) 9.65 (d, J = 5.6 Hz, 1H, $CH_{\text{ar-6'}}$), 9.32 (s, 1H, OH), 8.93 (dd, J = 9.1, 2.3 Hz, 1H, $CH_{\text{ar-4}}$), 8.72 – 8.60 (m, 1H, $CH_{\text{ar-2}}$), 8.47 (td, J = 7.7, 1.2 Hz, 1H, $CH_{\text{ar-4'}}$), 8.12 (d, J = 2.4 Hz, 1H, $CH_{\text{ar-8}}$), 8.06 – 7.93 (m, 2H, $CH_{\text{ar-3'}}$ & $CH_{\text{ar-5'}}$), 6.74 (dd, J = 8.8, 2.5 Hz, 1H, $CH_{\text{ar-10}}$), 5.51 (d, J = 8.8 Hz, 1H, $CH_{\text{ar-11}}$), 4.63 (d, J = 15.7 Hz, 1H, $NCHH$), 4.32 (d, J = 15.6 Hz, 1H, $NCHH$), 3.80 (dd, J = 9.3, 5.0 Hz, 1H, CH_α), 3.14 (s, 3H, NCH_3), 2.62 – 2.52 (m, 1H, $CH_\delta H_\delta$), 2.34 – 2.16 (m, 2H, $CH_\delta H_\delta$ & $CH_\beta H_\beta$), 2.12 – 1.98 (m, 1H, $CH_\beta H_\beta$), 1.65 (dt, J = 18.6, 6.0 Hz, 1H, $CH_\gamma H_\gamma$), 1.24 – 1.02 (m, 1H, $CH_\gamma H_\gamma$). ^{13}C -NMR (75 MHz, $(CD_3)_2SO$): δ (ppm) 181.83 (C_{carbonyl}), 168.94 ($C_{\text{ar-7}}$), 168.65 ($C_{\text{ar-5}}$), 161.12 ($C_{\text{ar-2'}}$), 156.54 (d, J = 252.9 Hz, $C_{\text{ar-3}}$), 152.72 ($C_{\text{ar-12b}}$), 152.58 ($C_{\text{ar-6'}}$), 151.87 ($C_{\text{ar-9}}$), 142.69 (C_{ar}), 142.67 (C_{ar}), 141.25 (C_{ar}), 139.46 (C_{ar}), 137.81 (d, J = 34.5 Hz, $C_{\text{ar-2}}$), 131.56 (C_{ar}), 126.29 (C_{ar}), 124.06 (C_{ar}), 123.56 (C_{ar}), 121.03 (d, J = 8.3 Hz, $C_{\text{ar-4a}}$),

119.31 (d, J = 20.2 Hz, $C_{\text{ar-4}}$), 116.92 (C_{ar}), 114.87 (C_{ar}), 112.28 (C_{ar}), 111.64 ($C_{\text{ar-10}}$), 109.19 ($C_{\text{ar-11}}$), 72.76 (C_α), 69.84 (NCH_2), 61.00 (C_δ), 30.17 (C_β), 24.20 (C_γ), 23.65 (NCH_3). IR (film): ν (cm^{-1}) 2921, 2850, 1744, 1694, 1615, 1563, 1502, 1441, 1411, 1370, 1329, 1270, 1217, 1151, 1062, 985, 958, 880, 801, 762, 731, 688, 607, 575. HRMS calculated for $C_{29}H_{22}ClFN_5NaO_5Rh$ ($M + Na$)⁺ 700.0241, found ($M + Na$)⁺ 700.0254.

5.2.3.24 Synthesis of organorhodium(III)

complexes Δ -(*S*)-**199** and Δ -(*S*)-**200**

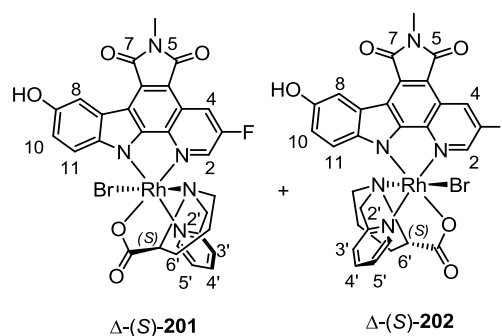


A suspension of **77** (20 mg, 44 μ mol) and $RhCl_3 \cdot 3H_2O$ (11.5 mg, 44 μ mol) in an ethanol : water mixture (1:1, 20 mL) under nitrogen atmosphere in a sealed vessel was heated to 90 °C for 3 h. During this time the suspension turned from pale brown into dark green. The reaction mixture was then cooled down slightly to add (*S*)-**105** (9.9 mg, 48 μ mol). After addition of (*S*)-**105**, the reaction was further proceeded at 90 °C for 16 h. The reaction mixture was then cooled down to ambient temperature and the solvent was removed *in vacuo*. The crude material was purified via column chromatography using methylene chloride : methanol (25:1 \rightarrow 10:1). The separated diastereomers were further purified and concentrated via preparative TLC using methylene chloride : methanol (15:1). The products were obtained as dark green solids, Δ -(*S*)-**199** (6.8 mg, 10.1 μ mol, 23%) and Δ -(*S*)-**200** (4.7 mg, 7.0 μ mol, 16%). Δ -(*S*)-**199**:

$R_f = 0.13$ (methylene chloride : methanol 15:1). $^1\text{H-NMR}$ (300 MHz, $(\text{CD}_3)_2\text{SO}$): $\delta(\text{ppm})$ 9.50 (d, $J = 5.6$ Hz, 1H, $\text{CH}_{\text{ar}}-6'$), 9.41 (s, 1H, OH), 8.82 (dd, $J = 9.2, 2.1$ Hz, 1H, $\text{CH}_{\text{ar}}-4$), 8.36 (td, $J = 7.8, 1.4$ Hz, 1H, $\text{CH}_{\text{ar}}-4'$), 8.14 (d, $J = 2.4$ Hz, 1H, $\text{CH}_{\text{ar}}-8$), 8.10 – 8.05 (m, 1H, $\text{CH}_{\text{ar}}-2$), 7.98 – 7.88 (m, 2H, $\text{CH}_{\text{ar}}-3'$ & $\text{CH}_{\text{ar}}-5'$), 7.61 (d, $J = 8.8$ Hz, 1H, $\text{CH}_{\text{ar}}-11$), 7.08 (dd, $J = 8.8, 2.5$ Hz, 1H, $\text{CH}_{\text{ar}}-10$), 4.74 (d, $J = 16.0$ Hz, 1H, NCHH), 4.54 (d, $J = 16.1$ Hz, 1H, NCHH), 3.77 (dd, $J = 9.5, 5.2$ Hz, 1H, CH_α), 3.16 (s, 3H, NCH_3), 2.45 – 2.38 (m, 1H, $\text{CH}_\delta\text{H}_\delta$), 2.24 – 2.10 (m, 2H, $\text{CH}_\delta\text{H}_\delta$ & $\text{CH}_\beta\text{H}_\beta$), 1.90 – 1.72 (m, 1H, $\text{CH}_\beta\text{H}_\beta$), 1.53 – 1.38 (m, 1H, $\text{CH}_\gamma\text{H}_\gamma$), 1.17 – 1.01 (m, 1H, $\text{CH}_\gamma\text{H}_\gamma$). $^{13}\text{C-NMR}$ (75 MHz, $(\text{CD}_3)_2\text{SO}$): $\delta(\text{ppm})$ 182.29 ($\text{C}_{\text{carbonyl}}$), 169.02 ($\text{C}_{\text{ar}}-7$), 168.73 ($\text{C}_{\text{ar}}-5$), 160.17 ($\text{C}_{\text{ar}}-2'$), 156.47 (d, $J = 245.5$ Hz, $\text{C}_{\text{ar}}-3$), 152.16 ($\text{C}_{\text{ar}}-12\text{b}$), 151.87 ($\text{C}_{\text{ar}}-6'$), 151.62 ($\text{C}_{\text{ar}}-9$), 147.32 (C_{ar}), 144.37 (C_{ar}), 143.68 (C_{ar}), 140.67 (C_{ar}), 139.81 (d, $J = 19.1$ Hz, $\text{C}_{\text{ar}}-2$), 132.52 (C_{ar}), 131.37 (C_{ar}), 126.02, 123.79 (d, $J = 18.0$ Hz, $\text{C}_{\text{ar}}-4$), 119.33 (C_{ar}), 118.49 (C_{ar}), 117.04 (C_{ar}), 115.32 (C_{ar}), 114.67 (C_{ar}), 110.98 (C_{ar}), 108.63 (C_{ar}), 73.42 (C_α), 69.35 (NCH_2), 61.33 (C_δ), 30.35 (C_β), 23.67 (C_γ), 23.64 (NCH_3). IR (film): $\nu(\text{cm}^{-1})$ 2920, 2852, 1747, 1698, 1619, 1567, 1502, 1444, 1412, 1374, 1332, 1272, 1221, 1152, 1089, 987, 960, 937, 882, 806, 770, 732, 691, 611, 581. HRMS calculated for $\text{C}_{29}\text{H}_{22}\text{ClFN}_5\text{NaO}_5\text{Rh}$ ($\text{M} + \text{Na}$) $^+$ 700.0241, found ($\text{M} + \text{Na}$) $^+$ 700.0225. Δ -(S)-**200**: $R_f = 0.22$ (methylene chloride : methanol 15:1). $^1\text{H-NMR}$ (300 MHz, CD_3CN): $\delta(\text{ppm})$ 9.82 – 9.73 (m, 1H, $\text{CH}_{\text{ar}}-6'$), 8.98 (dd, $J = 9.2, 2.4$ Hz, 1H, $\text{CH}_{\text{ar}}-4$), 8.69 (td, $J = 2.4, 0.9$ Hz, 1H, $\text{CH}_{\text{ar}}-4'$), 8.33 (td, $J = 7.8, 1.5$ Hz, 1H, $\text{CH}_{\text{ar}}-2$), 8.21 (d, $J = 2.6$ Hz, 1H, $\text{CH}_{\text{ar}}-8$), 7.94 – 7.79 (m, 2H, $\text{CH}_{\text{ar}}-3'$ & $\text{CH}_{\text{ar}}-5'$), 6.76 (dd, $J = 8.9, 2.6$ Hz, 1H, $\text{CH}_{\text{ar}}-10$), 5.66 – 5.57 (m, 1H, $\text{CH}_{\text{ar}}-11$), 4.44 (d, $J = 15.5$ Hz, 1H, NCHH), 4.36 (d, $J = 15.2$ Hz, 1H, NCHH), 3.67 (dd, $J = 9.4, 5.2$ Hz, 1H, CH_α), 3.19 (s, 3H, NCH_3), 2.52 – 2.41 (m, 1H, $\text{CH}_\delta\text{H}_\delta$), 2.40 – 2.31 (m, 2H, $\text{CH}_\delta\text{H}_\delta$ & $\text{CH}_\beta\text{H}_\beta$), 1.70 – 1.59 (m, 1H, $\text{CH}_\beta\text{H}_\beta$), 1.37 –

1.29 (m, 2H, $\text{CH}_\gamma\text{H}_\gamma$ & $\text{CH}_\gamma\text{H}_\gamma$). $^{13}\text{C-NMR}$ (75 MHz, $(\text{CD}_3)_2\text{SO}$): $\delta(\text{ppm})$ 181.84 ($\text{C}_{\text{carbonyl}}$), 168.94 ($\text{C}_{\text{ar}}-7$), 168.65 ($\text{C}_{\text{ar}}-5$), 161.12 ($\text{C}_{\text{ar}}-2'$), 156.56 (d, $J = 251.0$ Hz, $\text{C}_{\text{ar}}-3$), 152.72 ($\text{C}_{\text{ar}}-12\text{b}$), 152.58 ($\text{C}_{\text{ar}}-6'$), 151.88 ($\text{C}_{\text{ar}}-9$), 142.70 (C_{ar}), 141.26 (C_{ar}), 139.46 (C_{ar}), 137.82 (d, $J = 34.7$ Hz, $\text{C}_{\text{ar}}-2$), 131.57 (C_{ar}), 126.30 (C_{ar}), 124.06 (C_{ar}), 123.57 (C_{ar}), 121.03 (d, $J = 8.0$ Hz, $\text{C}_{\text{ar}}-4\text{a}$), 119.32 (d, $J = 20.3$ Hz, $\text{C}_{\text{ar}}-4$), 116.92 (C_{ar}), 114.87 (C_{ar}), 112.29 ($\text{C}_{\text{ar}}-10$), 111.58 (C_{ar}), 109.19 ($\text{C}_{\text{ar}}-11$), 72.76 (C_α), 69.85 (NCH_2), 61.00 (C_δ), 30.17 (C_β), 24.21 (C_γ), 23.66 (NCH_3). IR (film): $\nu(\text{cm}^{-1})$ 2923, 2851, 1747, 1678, 1622, 1562, 1492, 1439, 1408, 1369, 1328, 1291, 1225, 1201, 1154, 1058, 985, 957, 932, 883, 839, 794, 763, 688, 646, 611, 581, 520, 448, 397. HRMS calculated for $\text{C}_{29}\text{H}_{22}\text{ClFN}_5\text{NaO}_5\text{Rh}$ ($\text{M} + \text{Na}$) $^+$ 700.0241, found ($\text{M} + \text{Na}$) $^+$ 700.0254.

5.2.3.25 Synthesis of organorhodium(III) complexes Δ -(S)-**201** and Δ -(S)-**202**



A suspension of KBr (94.5 mg, 792 μmol) and $\text{RhCl}_3 \cdot 3\text{H}_2\text{O}$ (23 mg, 88 μmol) in water (1:1, 8 mL) under nitrogen atmosphere in a sealed vessel was heated to 90 $^\circ\text{C}$ for 45 min. Then, **77** (40 mg, 88 μmol) dissolved in ethanol (8 mL) was added and the reaction mixture was stirred for another 3 h at 90 $^\circ\text{C}$. During this time the suspension turned from pale brown into dark green. The reaction mixture was then cooled down slightly to add (S)-**105** (19.8 mg, 96 μmol). After addition of (S)-**105**, the reaction was further proceeded at 90 $^\circ\text{C}$ for 16 h.

The reaction mixture was then cooled down to ambient temperature and the solvent was removed *in vacuo*. The crude material was purified via column chromatography using methylene chloride : methanol (20:1 → 10:1). The separated diastereomers were further purified and concentrated via preparative TLC using methylene chloride : methanol (10:1). The products were obtained as dark green solids, Δ -(S)-**201** (12.1 mg, 16.7 μ mol, 19%) and Δ -(S)-**202** (7.6 mg, 10.6 μ mol, 12%). Δ -(S)-**201**: R_f = 0.11 (methylene chloride : methanol 15:1). $^1\text{H-NMR}$ (300 MHz, $(\text{CD}_3)_2\text{SO}$): δ (ppm) 9.70 (d, J = 6.3 Hz, 1H, $\text{CH}_{\text{ar}}\text{-6}'$), 9.35 (s, 1H, OH), 8.82 (dd, J = 9.2, 2.2 Hz, 1H, $\text{CH}_{\text{ar}}\text{-4}$), 8.35 (td, J = 7.8, 1.4 Hz, 1H, $\text{CH}_{\text{ar}}\text{-4}'$), 8.14 (d, J = 2.3 Hz, 1H, $\text{CH}_{\text{ar}}\text{-8}$), 8.11 – 8.04 (m, 1H, $\text{CH}_{\text{ar}}\text{-2}$), 7.98 – 7.86 (m, 2H, $\text{CH}_{\text{ar}}\text{-3}'$ & $\text{CH}_{\text{ar}}\text{-5}'$), 7.60 (d, J = 8.8 Hz, 1H, $\text{CH}_{\text{ar}}\text{-11}$), 7.07 (dd, J = 8.8, 2.5 Hz, 1H, $\text{CH}_{\text{ar}}\text{-10}$), 4.73 (d, J = 15.8 Hz, 1H, NCHH), 4.55 (d, J = 16.3 Hz, 1H, NCHH), 3.72 (dd, J = 9.4, 5.1 Hz, 1H, CH_α), 3.16 (s, 3H, NCH_3), 2.45 – 2.39 (m, 1H, $\text{CH}_\delta\text{H}_\delta$), 2.15 (ddd, J = 17.5, 12.3, 6.3 Hz, 2H, $\text{CH}_\delta\text{H}_\delta$ & $\text{CH}_\beta\text{H}_\beta$), 1.87 – 1.74 (m, 1H, $\text{CH}_\beta\text{H}_\beta$), 1.49 – 1.39 (m, 1H, $\text{CH}_\gamma\text{H}_\gamma$), 1.15 – 1.00 (m, 1H, $\text{CH}_\gamma\text{H}_\gamma$). IR (film): ν (cm^{-1}) 2928, 2872, 1748, 1695, 1651, 1564, 1502, 1442, 1411, 1371, 1330, 1290, 1203, 1150, 1102, 1053, 1026, 995, 962, 934, 882, 811, 766, 688, 649, 610, 522, 484, 453, 404. HRMS calculated for $\text{C}_{29}\text{H}_{22}\text{BrFN}_5\text{NaO}_5\text{Rh}$ ($\text{M} + \text{Na}$) $^+$ 743.9736, found ($\text{M} + \text{Na}$) $^+$ 743.9722. Δ -(S)-**202**: R_f = 0.30 (methylene chloride : methanol 15:1). $^1\text{H-NMR}$ (300 MHz, $(\text{CD}_3)_2\text{SO}$): δ (ppm) 9.86 (d, J = 6.5 Hz, 1H, $\text{CH}_{\text{ar}}\text{-6}'$), 9.33 (s, 1H, OH), 8.95 (dd, J = 9.2, 2.3 Hz, 1H, $\text{CH}_{\text{ar}}\text{-4}$), 8.66 (d, J = 2.5 Hz, 1H, $\text{CH}_{\text{ar}}\text{-2}$), 8.46 (td, J = 7.6, 1.4 Hz, 1H, $\text{CH}_{\text{ar}}\text{-4}'$), 8.13 (d, J = 2.5 Hz, 1H, $\text{CH}_{\text{ar}}\text{-8}$), 8.06 – 7.93 (m, 2H, $\text{CH}_{\text{ar}}\text{-3}'$ & $\text{CH}_{\text{ar}}\text{-5}'$), 6.73 (dd, J = 8.9, 2.5 Hz, 1H, $\text{CH}_{\text{ar}}\text{-10}$), 5.50 (d, J = 8.8 Hz, 1H, $\text{CH}_{\text{ar}}\text{-11}$), 4.61 (d, J = 15.4 Hz, 1H, NCHH), 4.29 (d, J = 14.8 Hz, 1H, NCHH), 3.75 (dd, J = 9.1, 4.4 Hz, 1H, CH_α), 3.17 (s, 3H, NCH_3), 2.60 – 2.56 (m, 1H, $\text{CH}_\delta\text{H}_\delta$), 2.24 – 2.12 (m,

2H, $\text{CH}_\delta\text{H}_\delta$ & $\text{CH}_\beta\text{H}_\beta$), 2.05 – 1.92 (m, 1H, $\text{CH}_\beta\text{H}_\beta$), 1.59 (ddd, J = 14.9, 11.0, 4.2 Hz, 1H, $\text{CH}_\gamma\text{H}_\gamma$), 1.37 – 1.27 (m, 1H, $\text{CH}_\gamma\text{H}_\gamma$). HRMS calculated for $\text{C}_{29}\text{H}_{22}\text{BrFN}_5\text{NaO}_5\text{Rh}$ ($\text{M} + \text{Na}$) $^+$ 743.9736, found ($\text{M} + \text{Na}$) $^+$ 743.9732.

5.3 Biological Experiments

5.3.1 PI3K Kinase-Glo Assay

The PI3K Kinase-Glo Assays for the IC_{50} determinations were performed in the MARMORSTEIN group by JIE QIN AND JULIE S. BARBER-ROTENBERG, the Wistar Institute, 3601 Spruce Street, Philadelphia, Pennsylvania 19104, United States. Recombinantly expressed human PI3K γ catalytic domain or PI3K α respectively, was preincubated with various concentrations of inhibitors with a final DMSO concentration of 2% in reaction buffer (20 mM Tris pH 7.5, 100 mM NaCl, 10 mM MgCl₂) for 1 h at RT. Then, this mixture was added to a solution of 0.1 mg/mL D-myo-phosphatidylinositol-4,5-bisphosphate (PtdIns(4,5)P₂, Echelon Bio-sciences) and 10 μ M ATP. 1.4 pmoles PI3K were used for each compound. The kinase reaction was carried out in a final volume of 50 μ L in a 96-well microtiter plate at 37 °C for 3 h. Then, 50 μ L of Kinase-Glo (Promega) developing solution was added into the mixture to generate a luminescence signal. The signal was recorded using the PerkinElmer Wallac 1420 luminometer using a luminescence filter. Data were processed and IC_{50} values were normalised to control samples using 2% DMSO and no kinase. The sigmoidal dose response curve fitting was processed using Origin8.

5.3.2 Cloning, Expression, and Purification of S6K1 Constructs

The cloning, expression and purification of S6K1 constructs were performed in the MARMORSTEIN group by JIE QIN, the Wistar Institute, 3601 Spruce Street, Philadelphia, Pennsylvania 19104, United States. Full length human S6K1 cDNA (1–525) was purchased from Epitope (catalogue number IHS1380-97652397). S6K1 constructs (84–384, 1–421, 1–421 T412E) were sub-

cloned into the pFASTbac HTB vector for protein expression. Sf9 cells were transfected with the recombinant bacmid DNA using Cellfectin (Invitrogen). Cells were harvested after being incubated for 48 h at 28 °C and stored at –80 °C. The 1–421 T412E construct was coexpressed with PDK1 to phosphorylate the T412E residue (cloned from cDNA purchased from OpenBioSystems). Frozen pellets of the S6K1 kinase domain, S6K1(84–384) used for crystallography were resuspended in sonication buffer (50 mM KPi, pH 7.0, 250 mM NaCl, 5% glycerol, 1:1000 PMSF) and sonicated at a power output of 5.5 for 120 s with 20 s intervals (Misonix Sonicator 3000). Lysates were cleared by highspeed centrifugation at 18 000 rpm for 35 min at 4 °C. Equilibrated Talon metal affinity resin (Clontech) was added to cleared lysates and incubated at 4 °C for 1 h with gentle shaking. The resin/lysate mixture was loaded into a gravityflow column, and the resin was extensively washed with wash buffer (50 mM KPi, pH 7.0, 250 mM NaCl, 5% glycerol). Protein was then eluted with elution buffer (50 mM KPi, pH 7.0, 250 mM NaCl, 500 mM imidazole, and 5% glycerol) in a single step. Pooled Talon eluent was diluted 3.5-fold in dilution buffer (50 mM KPi, pH 7.0, 5% glycerol) and loaded onto an SP anion exchange column pre-equilibrated with buffer A (50 mM KPi, pH 7.0, 50 mM NaCl, 5% glycerol). Protein was eluted with buffer B (50 mM KPi, pH 7.0, 500 mM NaCl, 5% glycerol) in a single step. Elution after the Q column was concentrated and loaded to a Superdex s200 column equilibrated with 50 mM Na citrate, pH 6.5, 300 mM NaCl, 1 mM DTT, 5% glycerol. The eluent was collected and concentrated to 3 mg/mL before protein was flash frozen in dry ice and stored at –80 °C. Purification of the 1–421 T412E construct was completed as above, with gel filtration on the Superdex s200 column using a buffer containing 25 mM Tris, pH 7.5, 200 mM NaCl, 1 mM EDTA, and 5% glycerol.

5.3.3 Cloning, Expression, and Purification of S6K2 Construct

The cloning, expression and purification of S6K2 constructs were performed in the MARMORSTEIN group by JULIE S. BARBER-ROTENBERG, the Wistar Institute, 3601 Spruce Street, Philadelphia, Pennsylvania 19104, United States. Full-length human S6K2 cDNA was purchased from GE Healthcare Dharmacon (RPS6KB2, clone identification number 2959036). The S6K2 1–423 construct, equivalent to S6K1 1–421, was subcloned into the pFASTbac HTB vector for protein expression. Sf9 cells were transfected and grown as described above. The construct was coexpressed with PDK1, similar to the S6K1 construct. Frozen pellets were purified identically to the S6K1 1–423 T412E pellets.

5.3.4 Radioactive Kinase Assay targeting S6K1 and S6K2 constructs

The radioactive kinase assay targeting S6K1 and S6K2 constructs were performed in the MARMORSTEIN group by JULIE S. BARBER-ROTENBERG, the Wistar Institute, 3601 Spruce Street, Philadelphia, Pennsylvania 19104, United States. Each reaction mixture contained 5 μ L of 5 \times reaction buffer (100 mM MOPS, pH 7.0, 150 mM MgCl_2), 2 μ L of inhibitor in 50% DMSO, 3.6 μ L of S6K1 substrate peptide (RRRLSSLRA), 1 μ L of BSA (20 mg/mL), 3.2 μ L of S6K1 (concentration as described in results), and 5 μ L of ATP/ATP* mix (concentration as described in results) in a total reaction volume of 25 μ L. Reaction mixtures were incubated for 1 h at ambient temperature before being transferred to Whatman paper and washed with 0.75% phosphoric acid. Data were collected using a scintillation counter. All experiments were performed in triplicate. IC_{50} values were determined using sigmoidal dose response with a variable curve in Origin 8.

5.3.5 Cell Culture and Western Blotting

Cell culture and Western blotting were performed in the MARMORSTEIN group by PATRICIA REYES-URIBE, the Wistar Institute, 3601 Spruce Street, Philadelphia, Pennsylvania 19104, United States. Human cell lines were cultured in RPMI (10-040-CM; Cellgro) supplemented with 5% fetal bovine serum and harvested at 70% confluence. For immunoblotting, cells were treated for the specified times with the indicated drugs, washed with cold phosphate buffered saline (PBS) containing 100 mM Na_3VO_4 , and lysed using TNE buffer (150 mM NaCl, 1% (v/v) NP-40, 2 mM EDTA, 50 mM Tris-HCl, pH 8.0) supplemented with protease inhibitors (11697498001; Roche). Proteins were separated by SDS-PAGE and transferred to nitrocellulose membranes (9004700; BioRad). After blocking for 1 h in 5% (wt/vol) dry milk/Tris-buffered saline (TBS)/0.1% (v/v) Tween-20, membranes were incubated overnight at 4 °C with primary antibodies followed by incubation with Alexa Fluor-labeled secondary antibodies (IRDye 680LT goat-antimouse or IRDye 800CW goat-anti-rabbit antibodies (LI-COR Biosciences) for 1 h. β -Actin (A5441) and vinculin (V9131) antibodies were obtained from Sigma. p-AKT (4056, 4060), S6 (2317), p-S6 (4858, 5364), S6K1 (2708), p-S6K1 (9234), p-eEF2k (3691), p-eIF4B (3591), and cleaved PARP (5625) were obtained from Cell Signaling Technologies. Fluorescent images were acquired and by LI-COR Odyssey Imaging System.

5.3.6 Yeast Cell Culture and Lysis

Yeast cell culture and lysis were performed in the DANG group by HAIYING LIU, Huffington Center on Aging, Baylor College of Medicine, Houston, Texas 77030, United States. Overnight cultures of wild-type yeast cells (BY4742) were diluted in synthetic complete (SC) medium and regrown at 30 °C to early log phase (OD600 of 0.2). **87** was added to an aliquot of culture to the final concentration of 1, 10, 100, and 1000 nM. The treated cultures were further grown at 30 °C for 4 h before harvesting. A culture of *sch9Δ* cells (KS68) was grown and harvested in parallel as a control. Yeast cell pellets were lysed by spinning down cultures at ~3000 rpm for 3 min at 4 °C, washing with ice-cold water, and broken in lysis buffer as previously described.^[432] Whole cell extracts were separated on a 4–12% Bolt gel with MOPS running buffer (Life Technologies), followed by transfer to a PVDF membrane in a Mini Trans-Blot cell (Bio-Rad) at 20 V overnight. The blot was blocked with 3% BSA at room temperature for 2 h and then at 4 °C for 4 h, followed by incubation with primary antibodies, Phospho-S6 (Cell Signaling, catalog no. 2211, 1:1000 dilution), and GAPDH (Thermo, catalog no. MA5-15738, 1:1000 dilution) at 4 °C overnight. Incubation with secondary antibodies (anti-rabbit-DyLight-680 and anti-mouse-DyLight-800, Pierce, 1:10000 dilution) was carried out at room temperature for 1 h before imaging with Li-Cor Odyssey.

5.3.7 Radioactive Kinase Assay targeting PIM-1, Aurora A, and FLT 3

Various concentrations of the rhodium(III) complexes were incubated at ambient temperature in 20 mM 3-(*N*-morpholino)propanesulfonic acid/ sodium hydroxide, 1 mM ethylenediaminetetraacetic acid (EDTA), 0.01% Brij 35, 5% 2-mercapto-

ethanol, 1 mg/mL bovine serum albumin (BSA), and 10% DMSO (resulting from the inhibitor stock solution) at pH 7.0 in the presence of a kinase substrate for an incubation time of T_1 . The reaction was then initiated by adding ATP in a final concentration of 10 μ M and approximately 0.1 μ Ci/ μ L of [γ -³³P]-ATP. Reactions were performed in a total volume of 25 μ L. After an incubation time of T_2 , the reaction was terminated by spotting 17.5 μ L of the reaction mixture on a circular P81 phosphocellulose paper (2.1 cm diameter, Whatman), followed by washing three times with 0.75% phosphoric acid and once with acetone. The dried P81 papers were transferred to scintillation vials and added with 5 mL of scintillation cocktail (purchased from Roth). The counts per minute (CPM) were measured using a Beckmann Coulter LS6500 multipurpose scintillation counter and corrected by the background CPM. The IC₅₀ values were determined in duplicate for each single concentration and compound. The experiments were repeated independently under the same conditions to verify the results. Non-linear regression and data evaluation were performed using OriginPro 8G (OriginLab). Modifications for the corresponding kinase targets: The amount of PIM-1 used was 0.1 ng/ μ L, the concentration of the kinase substrate S6 was 50 μ M (purchased from MoBiTec), and the incubation times were $T_1 = 30$ min and $T_2 = 30$ min. The amount of Aurora A used was 0.13 ng/ μ L, the concentration of the kinase substrate Kemptide was 250 μ M (purchased from Promega), and the incubation times were $T_1 = 45$ min and $T_2 = 45$ min. The amount of FLT-3 used was 1 ng/mL, the concentration of Abltide was 100 μ M (purchased from Merck Millipore), and incubation times were $T_1 = 90$ min and $T_2 = 90$ min. All kinases were purchased from Merck Millipore.

5.4 Kinase Profiling

5.4.1 Kinase Profiling of Complexes **85**, and **86**

The compounds **85** and **86** were profiled by the Millipore (KinaseProfiler™) against a panel of 263 kinases. Shown are the remaining kinase activities at a concentration of 100 nM of **85** or **86**. The presence of ATP is 10 μ M.

Table 4: Kinome Profiling **85** and **86**.

	85 (0.1 μ M)	86 (0.1 μ M)
Abl(h)	96	101
Abl(m)	96	103
Abl (H396P) (h)	96	99
Abl (M351T)(h)	95	106
Abl (Q252H) (h)	90	95
Abl(T315I)(h)	103	107
Abl(Y253F)(h)	118	120
ACK1(h)	53	96
ALK(h)	30	60
ALK4(h)	122	123
Arg(h)	93	93
AMPK(r)	49	93
Arg(m)	90	113
ARK5(h)	31	88
ASK1(h)	114	104
Aurora-A(h)	44	117
Axl(h)	63	100
Blk(m)	8	113
Bmx(h)	107	124
BRK(h)	110	114
BrSK1(h)	51	92
BrSK2(h)	32	80
BTK(h)	78	99
BTK(R28H)(h)	111	112

CaMKI(h)	79	108
CaMKII β (h)	28	63
CaMKII γ (h)	5	29
CaMKI δ (h)	21	49
CaMKII δ (h)	5	23
CaMKIV(h)	11	59
CDK1/cyclinB(h)	97	120
CDK2/cyclinA(h)	82	115
CDK2/cyclinE(h)	83	103
CDK3/cyclinE(h)	116	119
CDK5/p25(h)	69	106
CDK5/p35(h)	58	98
CDK7/cyclinH/MAT1(h)	25	114
CDK9/cyclin T1(h)	75	108
CHK1(h)	65	97
CHK2(h)	34	89
CHK2(I157T)(h)	37	87
CHK2(R145W)(h)	33	88
CK1 γ 1(h)	3	66
CK1 γ 2(h)	-3	44
CK1 γ 3(h)	-2	28
CK1 δ (h)	2	24
CK1(y)	3	14
CK2(h)	112	113
CK2 α 2(h)	113	107
CLK2(h)	1	2
CLK3(h)	90	105
cKit(h)	113	121
cKit(D816V)(h)	91	103
cKit(D816H)(h)	5	54
cKit(V560G)(h)	13	64
cKit(V654A)(h)	20	73
CSK(h)	108	102
c-RAF(h)	100	111
cSRC(h)	40	80

DAPK1(h)	2	21
DAPK2(h)	2	8
DCAMKL2(h)	72	97
DDR2(h)	92	92
DMPK(h)	112	110
DRAK1(h)	59	94
DYRK2(h)	110	114
eEF-2K(h)	105	107
EGFR(h)	114	121
EGFR(L858R)(h)	61	88
EGFR(L861Q)(h)	108	111
EGFR(T790M)(h)	83	111
EGFR(T790M,L858R)(h)	31	85
EphA1(h)	107	107
EphA2(h)	99	97
EphA3(h)	110	115
EphA4(h)	113	107
EphA5(h)	126	124
EphA7(h)	109	113
EphA8(h)	136	134
EphB2(h)	117	116
EphB1(h)	117	146
EphB3(h)	117	109
EphB4(h)	111	113
ErbB4(h)	109	111
FAK(h)	100	98
Fer(h)	56	101
Fes(h)	69	97
FGFR1(h)	74	132
FGFR1(V561M)(h)	16	83
FGFR2(h)	81	118
FGFR2(N549H)(h)	55	102
FGFR3(h)	95	100
FGFR4(h)	86	98
Fgr(h)	49	81

FLT1(h)	17	64
FLT3(D835Y)(h)	-3	5
FLT3(h)	5	32
FLT4(h)	42	55
Fms(h)	27	68
Fyn(h)	35	77
GCK(h)	108	109
GRK5(h)	55	65
GRK6(h)	42	53
GRK7(h)	39	46
GSK3 α (h)	20	58
GSK3 β (h)	56	90
Haspin(h)	71	79
Hck(h)	15	50
HIPK1(h)	35	85
HIPK2(h)	39	70
HIPK3(h)	63	91
IGF-1R(h)	82	92
IGF-1R(h), activated	43	54
IKK α (h)	111	119
IKK β (h)	83	97
IR(h)	96	104
IR(h), activated	27	60
IRR(h)	29	54
IRAK1(h)	40	97
IRAK4(h)	94	108
Itk(h)	66	96
JAK2(h)	71	108
JAK3(h)	61	103
JNK1 α 1(h)	103	106
JNK2 α 2(h)	93	98
JNK3(h)	95	86
KDR(h)	27	78
Lck(h)	35	105
LIMK1(h)	86	103

LKB1(h)	106	106
LOK(h)	86	93
Lyn(h)	7	86
Lyn(m)	7	72
MAPK1(h)	2	47
MAPK2(h)	7	89
MAPK2(m)	5	95
MAPKAP-K2(h)	112	115
MAPKAP-K3(h)	117	105
MEK1(h)	108	103
MARK1(h)	16	78
MELK(h)	1	4
Mer(h)	4	19
Met(h)	91	132
MINK(h)	51	77
MKK4(m)	55	103
MKK6(h)	100	115
MKK7 β (h)	38	63
MLCK(h)	0	2
MLK1(h)	74	86
Mnk2(h)	83	95
MRCK α (h)	110	108
MRCK β (h)	96	105
MSK1(h)	17	15
MSK2(h)	4	22
MSSK1(h)	68	57
MST1(h)	12	78
MST2(h)	6	50
MST3(h)	16	43
mTOR(h)	105	99
mTOR/FKBP12(h)	121	108
MuSK(h)	113	108
NEK2(h)	80	105
NEK3(h)	95	97
NEK6(h)	57	94

NEK7(h)	64	83
NEK11(h)	94	101
NLK(h)	85	104
p70S6K(h)	7	54
PAK2(h)	42	91
PAK3(h)	29	98
PAK4(h)	71	104
PAK5(h)	31	96
PAK6(h)	62	96
PAR-1B α (h)	7	54
PASK(h)	68	102
PDGFR α (h)	113	127
PDGFR α (D842V)(h)	7	63
PDGFR α (V561D)(h)	8	65
PDGFR β (h)	111	107
PDK1(h)	8	24
PhK γ 2(h)	93	95
PIM-1(h)	1	31
PIM-2(h)	3	24
PIM-3(h)	14	30
PKA(h)	13	72
PKB α (h)	10	76
PKB β (h)	57	90
PKB γ (h)	6	49
PKC α (h)	94	113
PKC β I(h)	56	99
PKC β II(h)	76	82
PKC γ (h)	90	99
PKC δ (h)	73	88
PKC ϵ (h)	62	90
PKC η (h)	84	106
PKC ι (h)	87	88
PKC μ (h)	76	100
PKC θ (h)	16	42
PKC ζ (h)	88	96

PKD2(h)	81	103
PKG1 α (h)	10	25
PKG1 β (h)	8	24
Plk1(h)	97	103
Plk3(h)	102	113
PRAK(h)	66	86
PRK2(h)	33	76
PrKX(h)	36	66
PTK5(h)	29	73
Pyk2(h)	40	62
Ret(h)	9	45
Ret (V804L)(h)	11	38
Ret(V804M)(h)	5	28
RIPK2(h)	87	87
ROCK-I(h)	98	113
ROCK-II(h)	91	99
ROCK-II(r)	80	107
Ron(h)	92	108
Ros(h)	112	102
Rse(h)	15	61
Rsk1(h)	5	26
Rsk1(r)	5	25
Rsk2(h)	6	21
Rsk3(h)	5	31
Rsk4(h)	3	22
SAPK2a(h)	111	111
SAPK2a(T106M)(h)	101	106
SAPK2b(h)	98	106
SAPK3(h)	102	109
SAPK4(h)	78	91
SGK(h)	51	82
SGK2(h)	27	53
SGK3(h)	74	92
SIK(h)	19	69
Snk(h)	93	96

Src(1-530)(h)	31	79
Src(T341M)(h)	35	94
SRPK1(h)	38	35
SRPK2(h)	39	30
STK33(h)	67	100
Syk(h)	120	114
TAK1(h)	104	107
TAO1(h)	96	105
TAO2(h)	93	103
TAO3(h)	89	100
TBK1(h)	40	90
Tec(h) activated	66	102
Tie2(h)	78	86
Tie2(R849W)(h)	93	98
Tie2(Y897S)(h)	100	108
TLK2(h)	110	108
TrkA(h)	17	104
TrkB(h)	68	75
TSSK1(h)	11	50
TSSK2(h)	61	100
Txk(h)	106	99
ULK2(h)	102	106
ULK3(h)	83	109
WNK2(h)	76	90
WNK3(h)	95	99
VRK2(h)	63	77
Yes(h)	26	81
ZAP-70(h)	134	123
ZIPK(h)	1	18

5.4.2 Kinase Profiling of Complexes **87**, Δ -(R)-**106**, Δ -(S)-**106**, Δ -(R)-**107**, and Δ -(S)-**107**

The compounds **87**, Δ -(R)-**106**, Δ -(S)-**106**, Δ -(R)-**107**, and Δ -(S)-**107** were

profiled by the KINOMEScan, DiscoverX profiling of Lead Hunter Discovery against a panel of 456. Shown are the remaining kinase activities at a concentration of 100 nM in case of **87** and 1 μ M in the cases of Δ -(R)-**106**, Δ -(S)-**106**, Δ -(R)-**107**, and Δ -(S)-**107** in the absence of ATP.

Table 5: Kinase Profiling of Complexes **87**, Δ -(R)-**106**, Δ -(S)-**106**, Δ -(R)-**107**, and Δ -(S)-**107**.

	87 (100 nM)	Δ -(S)- 106 (1 μ M)	Δ -(S)- 107 (1 μ M)	Δ -(R)- 106 (1 μ M)	Δ -(R)- 107 (1 μ M)
AAK1	100	71	89	100	82
ABL1(E255K)-phosphorylated	77	97	100	90	91
ABL1(F317I)-nonphosphorylated	92	89	91	87	66
ABL1(F317I)-phosphorylated	73	97	100	100	100
ABL1(F317L)-nonphosphorylated	100	92	97	87	78
ABL1(F317L)-phosphorylated	100	100	97	100	100
ABL1(H396P)-nonphosphorylated	88	92	100	94	70
ABL1(H396P)-phosphorylated	98	96	100	97	100
ABL1(M351T)-phosphorylated	100	98	100	94	99
ABL1(Q252H)-nonphosphorylated	90	100	99	82	70
ABL1(Q252H)-phosphorylated	94	96	99	100	93
ABL1(T315I)-nonphosphorylated	97	100	100	100	89
ABL1(T315I)-phosphorylated	100	100	81	100	95
ABL1(Y253F)-phosphorylated	93	100	100	100	100
ABL1-nonphosphorylated	97	85	88	91	71
ABL1-phosphorylated	100	89	97	94	91
ABL2	97	100	97	100	97
ACVR1	100	88	92	98	100
ACVR1B	92	85	86	97	99
ACVR2A	100	99	100	100	98
ACVR2B	100	100	100	96	94
ACVRL1	99	100	100	97	100
ADCK3	88	78	87	91	92
ADCK4	96	100	86	68	100
AKT1	99	98	82	99	96

AKT2	100	100	100	90	94
AKT3	100	87	73	96	98
ALK	95	100	90	100	85
ALK(C1156Y)	83	100	100	100	100
ALK(L1196M)	86	94	89	94	88
AMPK-alpha1	100	68	85	85	87
AMPK-alpha2	88	83	90	98	86
ANKK1	92	96	92	100	100
ARK5	85	69	72	76	92
ASK1	100	81	83	93	93
ASK2	88	86	95	93	90
AURKA	84	2.4	92	94	91
AURKB	87	29	82	91	80
AURKC	93	22	89	96	89
AXL	95	79	68	86	84
BIKE	100	86	85	90	91
BLK	90	73	69	94	95
BMPR1A	90	96	97	88	89
BMPR1B	100	75	82	90	85
BMPR2	100	100	100	100	98
BMX	84	95	97	100	96
BRAF	100	96	96	100	98
BRAF(V600E)	95	93	98	94	97
BRK	100	88	88	96	76
BRSK1	100	94	94	100	100
BRSK2	62	90	92	100	97
BTK	98	91	97	96	93
BUB1	88	87	96	100	93
CAMK1	93	93	71	89	89
CAMK1D	31	58	40	100	95
CAMK1G	96	68	92	100	98
CAMK2A	44	1.9	52	89	52
CAMK2B	71	3.2	72	77	68
CAMK2D	87	4.4	72	100	90
CAMK2G	84	5	72	100	79

CAMK4	15	100	81	100	89
CAMKK1	100	76	93	98	89
CAMKK2	99	79	94	100	85
CASK	94	88	97	100	84
CDC2L1	95	100	97	100	94
CDC2L2	96	98	91	97	94
CDC2L5	95	80	96	84	78
CDK11	74	100	100	100	88
CDK2	97	86	90	99	94
CDK3	95	83	100	100	91
CDK4-cyclinD1	95	86	96	100	98
CDK4-cyclinD3	100	100	100	100	100
CDK5	88	96	98	100	95
CDK7	96	51	80	100	95
CDK8	73	98	100	98	100
CDK9	90	90	87	100	98
CDKL1	100	78	98	98	81
CDKL2	92	82	100	100	100
CDKL3	82	100	100	98	90
CDKL5	98	100	100	100	100
CHEK1	71	85	100	100	99
CHEK2	91	71	100	100	95
CIT	92	100	90	100	91
CLK1	94	100	100	100	88
CLK2	1.8	23	54	76	18
CLK3	100	87	100	95	84
CLK4	50	74	82	95	68
CSF1R	55	90	78	100	94
CSF1R-autoinhibited	99	50	51	60	52
CSK	100	100	96	100	95
CSNK1A1	90	93	100	92	81
CSNK1A1L	89	100	85	96	100
CSNK1D	72	87	90	100	90
CSNK1E	100	97	100	95	93
CSNK1G1	100	82	82	99	94

CSNK1G2	95	98	77	100	100
CSNK1G3	100	100	100	97	80
CSNK2A1	97	87	83	79	47
CSNK2A2	78	82	48	69	27
CTK	91	87	73	95	98
DAPK1	3.1	76	16	93	68
DAPK2	5.8	65	33	76	54
DAPK3	5.7	73	25	74	61
DCAMKL1	52	74	76	60	60
DCAMKL2	100	100	93	99	97
DCAMKL3	48	60	80	100	88
DDR1	99	91	94	81	90
DDR2	100	97	100	68	58
DLK	92	71	75	86	93
DMPK	99	61	72	96	89
DMPK2	93	88	98	97	92
DRAK1	49	99	100	100	99
DRAK2	69	99	100	100	98
DYRK1A	85	73	94	100	33
DYRK1B	41	78	91	88	21
DYRK2	100	78	89	89	74
EGFR	100	100	100	95	100
EGFR(E746-A750del)	61	93	94	86	81
EGFR(G719C)	100	76	97	100	97
EGFR(G719S)	100	93	99	94	93
EGFR(L747-E749del, A750P)	92	86	91	100	87
EGFR(L747-S752del, P753S)	82	100	91	95	80
EGFR(L747-T751del,Sins)	97	97	75	89	88
EGFR(L858R)	98	89	90	98	92
EGFR(L858R,T790M)	100	77	86	97	96
EGFR(L861Q)	84	100	100	100	100
EGFR(S752-I759del)	98	77	100	86	93
EGFR(T790M)	100	66	85	96	88
EIF2AK1	82	66	80	100	90
EPHA1	100	83	100	96	80

EPHA2	92	86	93	100	89
EPHA3	58	81	86	87	89
EPHA4	96	87	100	100	94
EPHA5	86	97	97	100	91
EPHA6	94	83	86	96	90
EPHA7	99	89	96	98	88
EPHA8	100	100	99	100	92
EPHB1	100	84	100	100	89
EPHB2	100	95	100	100	100
EPHB3	90	82	94	100	89
EPHB4	90	88	99	97	96
EPHB6	93	92	94	99	93
ERBB2	100	98	100	86	89
ERBB3	100	100	100	97	100
ERBB4	100	96	98	100	98
ERK1	100	99	90	100	100
ERK2	91	98	100	100	92
ERK3	91	89	98	91	98
ERK4	86	85	96	82	93
ERK5	45	25	93	100	90
ERK8	100	26	69	88	27
ERN1	100	79	98	89	84
FAK	90	100	93	100	97
FER	100	90	86	88	89
FES	95	86	97	95	88
FGFR1	71	88	88	94	92
FGFR2	82	89	80	96	94
FGFR3	92	80	89	98	95
FGFR3(G697C)	100	81	81	95	67
FGFR4	100	82	94	100	88
FGR	90	85	91	100	83
FLT1	100	88	100	100	95
FLT3	31	71	4.9	67	50
FLT3(D835H)	30	44	41	95	49
FLT3(D835Y)	12	17	4.4	69	22

FLT3(ITD)	35	53	12	80	57
FLT3(K663Q)	34	81	7.8	71	53
FLT3(N841I)	23	20	2.8	43	28
FLT3(R834Q)	44	77	26	70	75
FLT3-autoinhibited	100	83	78	96	72
FLT4	100	91	58	97	82
FRK	100	91	94	100	87
FYN	100	78	79	90	86
GAK	14	97	95	93	100
GCN2(Kin.Dom.2,S808G)	91	100	88	90	100
GRK1	4.4	15	41	71	22
GRK4	100	84	100	100	98
GRK7	8.4	15	56	53	14
GSK3A	88	4.1	41	45	11
GSK3B	99	83	99	99	94
HASPIN	81	51	46	55	42
HCK	85	100	97	87	90
HIPK1	89	56	78	86	15
HIPK2	78	22	45	87	3.3
HIPK3	95	36	57	56	2.4
HIPK4	73	84	100	100	78
HPK1	94	83	81	100	85
HUNK	85	63	93	99	86
ICK	71	65	100	100	90
IGF1R	100	96	79	97	100
IKK-alpha	99	91	96	94	82
IKK-beta	80	100	100	100	96
IKK-epsilon	100	100	100	100	88
INSR	99	57	75	78	70
INSRR	100	88	95	100	90
IRAK1	87	83	100	100	91
IRAK3	71	17	73	93	81
IRAK4	85	62	69	69	73
ITK	100	100	100	100	100
JAK1(JH1domain-catalytic)	94	80	83	77	98

JAK1(JH2domain-pseudokinase)	98	91	80	91	82
JAK2(JH1domain-catalytic)	88	100	86	100	100
JAK3(JH1domain-catalytic)	70	45	37	53	63
JNK1	100	94	100	90	98
JNK2	96	79	78	95	97
JNK3	100	86	94	87	96
KIT	62	77	55	100	88
KIT(A829P)	30	81	35	78	93
KIT(D816H)	40	79	60	90	91
KIT(D816V)	14	68	22	100	78
KIT(L576P)	56	89	52	78	80
KIT(V559D)	53	77	41	89	81
KIT(V559D,T670I)	86	88	74	100	93
KIT(V559D,V654A)	75	100	96	100	94
KIT-autoinhibited	95	83	92	82	73
LATS1	89	82	72	90	88
LATS2	90	85	61	100	93
LCK	98	92	86	100	90
LIMK1	100	98	92	100	100
LIMK2	92	83	91	98	96
LKB1	100	92	82	88	72
LOK	100	94	100	90	90
LRRK2	85	91	96	94	99
LRRK2(G2019S)	80	70	60	94	78
LTK	100	100	100	98	95
LYN	96	97	93	100	100
LZK	98	80	81	87	81
MAK	51	93	79	72	96
MAP3K1	99	96	92	96	96
MAP3K15	98	60	81	100	91
MAP3K2	100	94	99	100	92
MAP3K3	96	100	100	100	94
MAP3K4	100	75	84	94	72
MAP4K2	89	93	86	95	80
MAP4K3	100	92	93	92	94

MAP4K4	97	100	100	100	93
MAP4K5	100	99	100	100	92
MAPKAPK2	90	92	100	100	98
MAPKAPK5	100	90	95	85	90
MARK1	62	56	68	86	77
MARK2	38	39	51	94	82
MARK3	61	12	62	92	99
MARK4	71	61	79	82	89
MAST1	77	20	100	96	96
MEK1	100	93	100	96	96
MEK2	100	80	82	85	84
MEK3	87	83	29	92	80
MEK4	100	100	64	95	100
MEK5	78	82	93	99	75
MEK6	100	83	53	100	98
MELK	29	59	53	95	77
MERTK	100	100	100	91	100
MET	100	89	88	100	82
MET(M1250T)	82	100	95	96	75
MET(Y1235D)	100	100	100	100	75
MINK	79	87	91	100	100
MKK7	100	98	98	90	99
MKNK1	77	82	80	94	96
MKNK2	89	94	100	99	100
MLCK	100	97	100	93	84
MLK1	99	100	90	96	100
MLK2	80	76	90	94	89
MLK3	98	99	100	100	96
MRCKA	99	100	100	94	98
MRCKB	100	94	95	100	92
MST1	100	96	80	70	85
MST1R	96	80	83	78	100
MST2	95	73	68	89	69
MST3	74	75	98	96	94
MST4	96	70	87	85	72

MTOR	98	72	90	77	100
MUSK	88	92	100	99	94
MYLK	0.8	34	33	52	30
MYLK2	85	92	99	99	94
MYLK4	97	94	89	100	81
MYO3A	92	69	86	89	87
MYO3B	70	84	93	86	90
NDR1	100	90	78	100	100
NDR2	100	74	93	100	76
NEK1	100	79	86	93	94
NEK10	100	71	71	64	73
NEK11	98	93	100	98	96
NEK2	100	97	95	89	97
NEK3	79	80	77	90	64
NEK4	100	93	100	100	93
NEK5	81	100	100	100	100
NEK6	88	87	100	100	92
NEK7	86	85	87	92	100
NEK9	87	86	87	96	97
NIK	100	80	100	90	90
NIM1	90	100	100	100	100
NLK	82	78	72	91	87
OSR1	56	94	88	99	100
p38-alpha	98	87	89	97	71
p38-beta	83	95	97	99	97
p38-delta	49	68	78	70	100
p38-gamma	94	84	94	96	55
PAK1	100	81	83	86	86
PAK2	100	61	58	71	48
PAK3	100	91	93	96	79
PAK4	100	90	87	98	86
PAK6	94	90	90	90	92
PAK7	80	81	98	88	86
PCTK1	100	75	89	96	100
PCTK2	100	85	80	98	97

PCTK3	93	76	90	98	94
PDGFRA	57	77	72	75	87
PDGFRB	15	85	5.4	100	76
PDPK1	58	52	57	85	77
PFCDPK1(P.falciparum)	100	96	100	95	100
PFPK5(P.falciparum)	99	100	97	96	100
PFTAIRE2	89	82	88	100	100
PFTK1	95	45	76	81	84
PHKG1	56	86	97	100	92
PHKG2	56	61	87	87	70
PIK3C2B	100	90	96	96	100
PIK3C2G	79	100	100	100	100
PIK3CA	100	100	92	100	97
PIK3CA(C420R)	89	100	100	92	91
PIK3CA(E542K)	97	87	100	100	79
PIK3CA(E545A)	82	79	83	84	77
PIK3CA(E545K)	100	96	100	98	84
PIK3CA(H1047L)	95	100	100	97	95
PIK3CA(H1047Y)	100	82	74	90	94
PIK3CA(I800L)	100	86	90	88	84
PIK3CA(M1043I)	77	100	100	94	100
PIK3CA(Q546K)	97	89	100	89	93
PIK3CB	77	92	95	94	82
PIK3CD	88	94	100	91	100
PIK3CG	100	94	93	100	98
PIK4CB	79	89	100	100	100
PIM-1	0.4	13	10	60	1.8
PIM-2	19	78	84	98	50
PIM-3	5.6	27	20	68	1.8
PIP5K1A	43	71	71	100	77
PIP5K1C	97	100	40	87	71
PIP5K2B	95	86	100	90	98
PIP5K2C	95	100	100	100	100
PKAC-alpha	98	78	61	91	75
PKAC-beta	86	64	80	84	68

PKMYT1	92	94	99	94	80
PKN1	88	32	57	100	89
PKN2	94	25	37	95	83
PKNB(M.tuberculosis)	99	93	100	99	95
PLK1	96	99	100	100	94
PLK2	67	84	86	99	89
PLK3	58	90	100	98	94
PLK4	53	71	82	92	87
PRKCD	53	2.2	11	84	39
PRKCE	68	6.6	38	88	25
PRKCH	82	25	58	100	73
PRKCI	100	45	48	82	73
PRKCQ	77	32	73	100	95
PRKD1	100	100	100	100	97
PRKD2	100	70	81	81	97
PRKD3	81	85	100	97	98
PRKG1	63	79	100	88	73
PRKG2	26	7.3	54	76	2.4
PRKR	68	100	99	100	100
PRKX	87	94	100	79	100
PRP4	100	94	72	95	65
PYK2	98	87	93	100	97
QSK	85	92	92	93	93
RAF1	100	100	100	97	76
RET	90	100	93	100	89
RET(M918T)	100	85	93	100	90
RET(V804L)	100	90	89	95	84
RET(V804M)	82	99	97	98	95
RIOK1	100	84	83	100	83
RIOK2	100	92	100	94	75
RIOK3	96	85	72	100	86
RIPK1	96	84	91	84	93
RIPK2	100	78	85	81	87
RIPK4	82	93	95	89	79
RIPK5	74	87	94	98	95

ROCK1	100	81	93	89	92
ROCK2	88	75	91	95	94
ROS1	100	86	95	98	92
RPS6KA4(Kin.Dom.1-N-terminal)	77	53	83	94	100
RPS6KA4(Kin.Dom.2-C-terminal)	7.2	89	88	89	94
RPS6KA5(Kin.Dom.1-N-terminal)	46	80	78	97	88
RPS6KA5(Kin.Dom.2-C-terminal)	35	92	100	88	93
RSK1(Kin.Dom.1-N-terminal)	80	49	88	94	84
RSK1(Kin.Dom.2-C-terminal)	77	76	85	90	83
RSK2(Kin.Dom.1-N-terminal)	33	4	76	84	75
RSK2(Kin.Dom.2-C-terminal)	100	72	94	87	85
RSK3(Kin.Dom.1-N-terminal)	84	41	93	100	100
RSK3(Kin.Dom.2-C-terminal)	69	93	100	100	94
RSK4(Kin.Dom.1-N-terminal)	20	47	96	100	89
RSK4(Kin.Dom.2-C-terminal)	58	65	91	80	90
S6K1	71	15	51	100	84
SBK1	92	67	88	70	71
SGK	77	66	100	100	94
SgK110	94	87	97	96	90
SGK2	86	88	100	99	95
SGK3	80	95	100	100	100
SIK	83	91	98	100	93
SIK2	100	94	89	97	94
SLK	97	100	90	100	86
SNARK	80	33	43	100	98
SNRK	96	77	93	86	95
SRC	98	98	82	92	100
SRMS	94	100	100	100	85
SRPK1	100	90	86	100	97
SRPK2	82	100	95	93	100
SRPK3	93	71	77	100	90
STK16	84	86	49	87	61
STK33	74	66	90	97	76
STK35	100	98	100	97	94
STK36	100	95	100	98	94

STK39	98	87	97	100	98
SYK	94	98	91	100	100
TAK1	99	98	99	100	89
TAOK1	84	99	100	92	73
TAOK2	100	81	76	91	61
TAOK3	88	100	100	100	99
TBK1	96	91	100	100	96
TEC	93	100	100	100	90
TESK1	100	83	87	95	78
TGFBR1	100	100	97	87	80
TGFBR2	99	96	100	100	89
TIE1	100	79	100	98	93
TIE2	88	85	100	98	92
TLK1	88	88	98	93	95
TLK2	95	84	94	90	93
TNIK	47	82	77	100	96
TNK1	100	86	77	100	100
TNK2	100	92	89	99	98
TNNI3K	100	88	98	92	81
TRKA	100	73	77	82	52
TRKB	100	80	87	97	65
TRKC	99	77	81	89	62
TRPM6	100	82	92	83	96
TSSK1B	100	68	56	88	70
TTK	49	90	43	97	82
TXK	100	82	85	92	88
TYK2(JH1domain-catalytic)	100	100	100	100	97
TYK2(JH2domain-pseudokinase)	87	100	100	100	79
TYRO3	94	88	79	100	98
ULK1	71	87	82	96	93
ULK2	96	98	100	100	100
ULK3	88	83	98	100	95
VEGFR2	96	92	62	100	84
VRK2	97	72	100	98	92
WEE1	100	99	100	96	91

WEE2	91	100	97	100	100
WNK1	100	92	100	98	87
WNK3	100	85	99	95	92
YANK1	88	70	91	72	89
YANK2	89	100	100	100	84
YANK3	100	100	100	100	92
YES	100	98	94	100	96
YSK1	98	82	93	91	94
YSK4	41	91	96	90	75
ZAK	100	89	94	97	87
ZAP70	100	80	80	86	90

5.5 Computational Procedures

5.5.1 The Hot Spot Analysis

The hot spot analysis to disclose favourable interactions of PI3K γ , using HOTSPOTSX developed in the KLEBE group by GERD NEUDERT, was applied analogously to published procedures, as in the case study of endothiapepsin.^[407] Beside HOTSPOTSX, GERD NEUDERT kindly provided the program FCONV for the calculation procedures to prepare protein and ligand molecule data.^[402]

5.5.1.1 FCONV

As main application, FCONV can be used to handle molecule data and data parsing problems. The working principle is to define internal atom types to source data, i.e.: protein crystal structure data in .pdb format or molecule data in .mol2 format.^[402] These internal annotation principle considers the chemical interactions, the hybridisation state, and the bonding type for each atom in a molecule. In total, 157 atom types were defined and classified into five different generic physico-chemical properties: H-bond donor, H-bond acceptor, doneptor (groups acting both as H-bond donor and H-bond acceptor), aromatic, and hydrophobic. Atoms which can not be assigned to any one of the five groups were assigned to the group X, see Figure 97. 12 atoms were assigned to the donor group, 29 atoms to the acceptor group, 15 atoms to the doneptor group, 9 atoms to the aromatic group, 18 atoms to the hydrophobic group, and 75 atoms to the X group.

Every atom in the crystal structure of PI3K γ (pdb: 3CST) was assigned according to the internal annotation; the coor-

dinates of the metal based kinase inhibitor were removed from the data set, and saved in a separate file, to provide the space in the binding site open for the hot spot calculation.

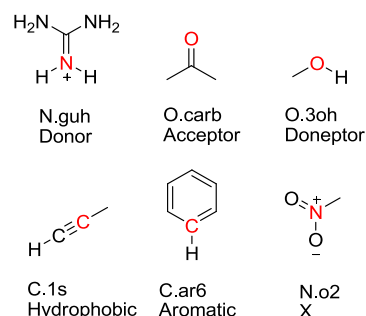


Figure 97: Representative atoms (highlighted in red) assigned according to the internal annotation of FCONV. The annotation includes element symbol, chemical environment, hybridisation state, bonding state and interaction group.

5.5.1.2 HOTSPOTSX

HOTSPOTSX developed in the KLEBE group by GERD NEUDERT is based on different knowledge based potentials to predict interaction fields for different predefined atom types in the binding pocket. The structural data, covering distances, angles, charge, hybridisation state, bonding state and corresponding interaction partner were evaluated of entries in the Cambridge Structural Database (CSD), as first potential set, and of entries in the Protein Data Bank (PDB), as second potential set.^[433,434] The atoms of these entries were assigned corresponding to the FCONV internal atom types. Then a inverse determination of coordinates for the structure of PI3K γ (pdb:3CST) of interaction partners were calculated by HOTSPOTSX resulting in specified contour maps. Areas with highly favorable interaction values were defined as hotspots (threshold $\geq 75\%$ above the minimal contour map level).

5.6 Crystallographic Data

5.6.1 Crystallographic Data of 96

Single crystals of compound **96**, $C_{40}D_{18}FH_{30}N_5O_8RuS_4$, were crystallised from acetone- d_6 after 1 week at 4 °C. A suitable crystal was selected and mounted on a cryo-loop using inert oil on a 'STOE

IPDS2 Image Plate' diffractometer. The crystal was kept at 100.15 K during data collection. Using Olex2,^[435] the structure was solved with the SIR2011^[436] structure solution program using Direct Methods and refined with the XLMP^[437] refinement package using Least Squares minimisation. The structure was solved by DR. KLAUS HARMS.

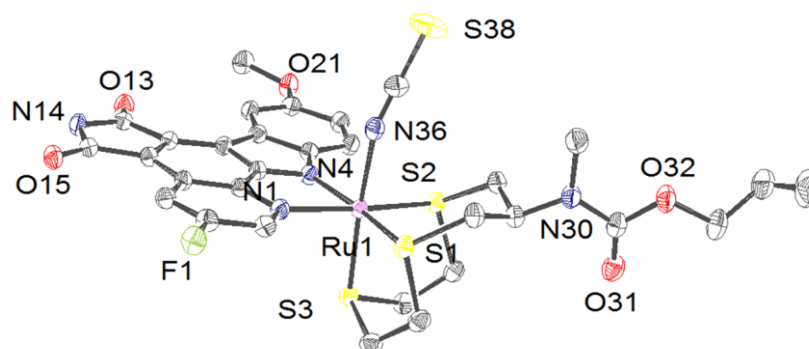


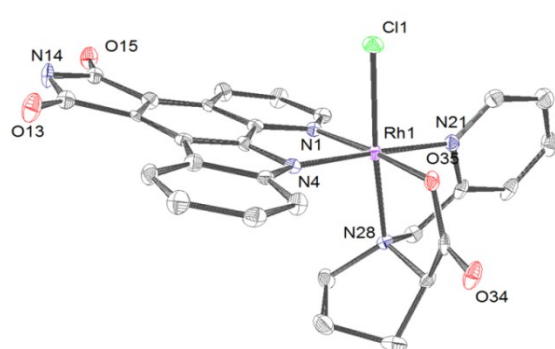
Table 6: Crystal data and structure refinement for **96**.

Identification code	96
Empirical formula	$C_{40}D_{18}FH_{30}N_5O_8RuS_4$
Formula weight	993.25
Temperature/K	100.15
Crystal system	triclinic
Space group	P-1
a/Å	9.2703(4)
b/Å	15.9175(6)
c/Å	17.0090(7)
$\alpha/^\circ$	116.428(3)
$\beta/^\circ$	90.389(3)
$\gamma/^\circ$	102.792(3)
Volume/Å ³	2175.77(16)
Z	2
$\rho_{\text{calc}}/\text{mg}/\text{mm}^3$	1.516
μ/mm^{-1}	0.613
F(000)	1008
Crystal size/mm ³	0.14 × 0.11 × 0.1
2 θ range for data collection	2.946 to 50.996°
Index ranges	-11 ≤ h ≤ 10, -16 ≤ k ≤ 19, -20 ≤ l ≤ 20
Reflections collected	15490
Independent reflections	8010 [R(int) = 0.0306]
Data/restraints/parameters	8010/6/565
Goodness-of-fit on F ²	0.938
Final R indexes [I > 2σ(I)]	R ₁ = 0.0304, wR ₂ = 0.0698
Final R indexes [all data]	R ₁ = 0.0430, wR ₂ = 0.0729
Largest diff. peak/hole / e Å ⁻³	0.65/-0.81

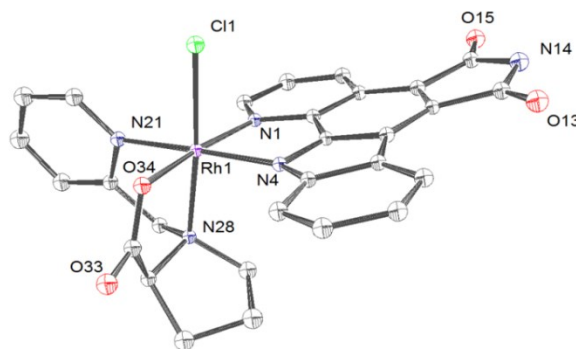
5.6.2 Crystallographic Data of Λ -(*R*)-106 and Δ -(*S*)-106

The crystal structures were depicted using ORTEP drawing with 50% probability of thermal ellipsoid and determined of single crystals of Λ -(*R*)-106 and Δ -(*S*)-106.^[438] The crystals were obtained after dissolution in methylene chloride/methanol mixture of (15:1) and slow evaporation of the solvent at 4 °C for several days. Both compounds crystallised as orthorhombic red plates with an additional methylene chloride molecule. Crystals were measured on a 'Bruker D8 QUEST area detector' diffractometer. The temperature was kept at 100.15 K during

data collection using a wavelength of 0.71073 Å. In both cases the data collection software BRUKER APEX II was applied and the cell refinement and data reduction software SAINT (Bruker AXS Inc.) was used.^[439] Data were corrected for absorption using the program SADABS (Bruker AXS Inc.).^[439] Non hydrogen atoms have been refined anisotropically. Hydrogen atoms were placed on idealised positions and refined using the 'riding model'. The programs applied for solution and refinement were SHELXS-97 (Sheldrick, 2008) and SHELXL-2013 (Sheldrick, 2013).^[439,440] The absolute structure of Λ -(*R*)-106 and Δ -(*S*)-106 were determined. The structures were solved by DR. KLAUS HARMS.



Λ -(*R*)-106



Δ -(*S*)-106

Table 7: Crystal data and structure refinement for Λ -(*R*)-106.

Crystal data

Identification code	Λ -(<i>R</i>)-106
Habitus, colour	plate, red
Crystal size	0.51 x 0.22 x 0.01 mm ³
Crystal system	Orthorhombic
Space group	P 2 ₁ 2 ₁ 2 ₁
Unit cell dimensions	<div> $a = 8.6511(6) \text{ \AA}$ $b = 13.3092(9) \text{ \AA}$ $c = 23.6366(14) \text{ \AA}$ </div> <div> $Z = 4$ $\alpha = 90^\circ$ $\beta = 90^\circ$ $\gamma = 90^\circ$ </div>
Volume	2721.5(3) Å ³
Cell determination	3995 peaks with Theta 2.3 to 27.2°.
Empirical formula	C ₂₉ H ₂₃ Cl ₃ N ₅ O ₄ Rh
Formula weight	714.78
Density (calculated)	1.745 Mg/m ³
Absorption coefficient	0.970 mm ⁻¹
F(000)	1440

Data collection:

Diffractometer type	Bruker D8 QUEST area detector
Wavelength	0.71073 Å
Temperature	100(2) K
Theta range for data collection	2.918 to 25.498°
Index ranges	-10 ≤ h ≤ 10, -14 ≤ k ≤ 16, -28 ≤ l ≤ 28
Data collection software	BRUKER APEX II
Cell refinement software	SAINT V8.30C (Bruker AXS Inc., 2013)
Data reduction software	SAINT V8.30C (Bruker AXS Inc., 2013)

Solution and refinement:

Reflections collected	11484
Independent reflections	5061 [R(int) = 0.0543]
Completeness to theta = 25.242°	99.8 %
Observed reflections	4306 [I > 2(I)]
Reflections used for refinement	5061
Absorption correction	Semi-empirical from equivalents
Max. and min. transmission	0.99 and 0.81
Flack parameter (absolute struct.)	-0.07(2)
Largest diff. peak and hole	0.514 and -0.488 e.Å ⁻³
Solution	Direct methods
Refinement	Full-matrix least-squares on F ²
Treatment of hydrogen atoms	Calculated positions, constr. ref.
Programs used	SHELXS-97 (Sheldrick, 2008) SHELXL-2013 (Sheldrick, 2013) DIAMOND (Crystal Impact)
Data / restraints / parameters	5061 / 0 / 369
Goodness-of-fit on F ²	1.010
R index (all data)	wR2 = 0.0689
R index conventional [I > 2σ(I)]	R1 = 0.0359

Table 8 Crystal data and structure refinement for Δ-(S)-**106**.

Crystal data

Identification code	Δ-(S)- 106
Habitus, colour	plate, red
Crystal size	0.26 x 0.12 x 0.02 mm ³
Crystal system	Orthorhombic
Space group	P 2 ₁ 2 ₁ 2 ₁ Z = 4
Unit cell dimensions	a = 8.6398(10) Å α = 90° b = 13.3545(14) Å β = 90° c = 23.619(3) Å γ = 90°
Volume	2725.2(5) Å ³
Cell determination	9855 peaks with Theta 2.5 to 27.5°
Empirical formula	C ₂₉ H ₂₃ Cl ₃ N ₅ O ₄ Rh
Formula weight	714.78
Density (calculated)	1.742 Mg/m ³
Absorption coefficient	0.969 mm ⁻¹
F(000)	1440

Data collection:

Diffractometer type	Bruker D8 QUEST area detector
Wavelength	0.71073 Å
Temperature	100(2) K
Theta range for data collection	2.302 to 27.574°
Index ranges	-11 ≤ h ≤ 10, -17 ≤ k ≤ 16, -29 ≤ l ≤ 30
Data collection software	BRUKER APEX II
Cell refinement software	SAINT V8.27B (Bruker AXS Inc., 2012)
Data reduction software	SAINT V8.27B (Bruker AXS Inc., 2012)

Solution and refinement:

Reflections collected	26345
Independent reflections	6038 [R(int) = 0.0419]
Completeness to theta = 25.242°	98.6 %
Observed reflections	5497[$I > 2(I)$]
Reflections used for refinement	6038
Absorption correction	Semi-empirical from equivalents
Max. and min. transmission	0.98 and 0.89
Flack parameter (absolute struct.)	-0.01(3)
Largest diff. peak and hole	0.467 and -0.731 e.Å ⁻³
Solution	Direct methods
Refinement	Full-matrix least-squares on F ²
Treatment of hydrogen atoms	Calculated positions, constr. Ref.
Programs used	XS (Sheldrick, 2008) SHELXL-2013 (Sheldrick, 2013) DIAMOND
Data / restraints / parameters	6038 / 0 / 379
Goodness-of-fit on F ²	1.035
R index (all data)	wR2 = 0.0579
R index conventional [$I > 2\sigma(I)$]	R1 = 0.0286

5.6.3 Crystallographic Data of Δ -(S,R)-125

The crystal structure was depicted using ORTEP drawing with 50% probability of thermal ellipsoid and determined of single crystals of Δ -(S,R)-125.^[438] The crystals were obtained after dissolution in methylene chloride/methanol mixture of (15:1) and slow evaporation of the solvent at 4 °C for several days. The compound crystallised as orthorhombic orange plates. Crystals were measured on a 'Bruker D8 QUEST area detector' diffractometer. The temperature was kept at 100 K during data collection

using a wavelength of 0.71073 Å. The data collection software BRUKER APEX II was applied and the cell refinement and data reduction software SAINT (Bruker AXS Inc.) was used.^[439] Data were corrected for absorption using the program SADABS (Bruker AXS Inc.).^[439] Non hydrogen atoms have been refined anisotropically. Hydrogen atoms were placed on idealised positions and refined using the 'riding model'. The programs applied for solution and refinement were SHELXS-97 (Sheldrick, 2008) and SHELXL-2014 (Sheldrick, 2014).^[439,440] The absolute structure of Δ -(S,R)-125 was determined. The structure was solved by DR. KLAUS HARMS.

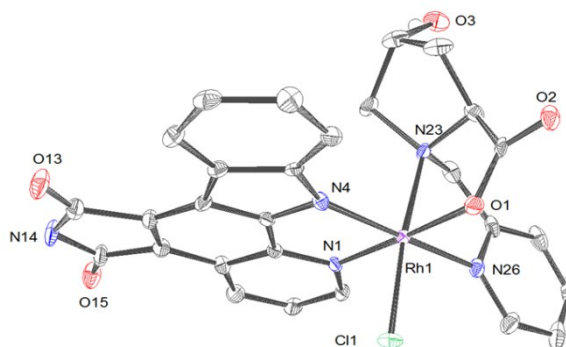


Table 9: Crystal data and structure refinement for Δ -(S,R)-125.

Crystal data

Identification code	Δ -(S,R)-125
Habitus, colour	plate, orange
Crystal size	0.30 x 0.23 x 0.05 mm ³
Crystal system	Orthorhombic
Space group	P 21 21 21
Unit cell dimensions	Z = 4 a = 9.0050(4) Å b = 12.9421(5) Å c = 24.3372(11) Å $\alpha = 90^\circ$ $\beta = 90^\circ$ $\gamma = 90^\circ$
Volume	2836.3(2) Å ³
Cell determination	9982 peaks with Theta 2.3 to 27.4°.
Empirical formula	C ₂₉ H ₂₃ Cl ₃ N ₅ O ₅ Rh
Formula weight	730.78
Density (calculated)	1.711 Mg/m ³
Absorption coefficient	0.935 mm ⁻¹
F(000)	1472

Data collection:

Diffractometer type	Bruker D8 QUEST area detector
Wavelength	0.71073 Å
Temperature	100(2) K

Theta range for data collection	2.297 to 27.508°.
Index ranges	-9<=h<=11, -16<=k<=16, -31<=l<=31
Data collection software	BRUKER APEX2
Cell refinement software	SAINT V8.34A (Bruker AXS Inc., 2013)
Data reduction software	SAINT V8.34A (Bruker AXS Inc., 2013)
Solution and refinement:	
Reflections collected	35650
Independent reflections	6529 [R(int) = 0.0763]
Completeness to theta = 25.242°	99.9 %
Observed reflections	5781[$I > 2(I)$]
Reflections used for refinement	6529
Absorption correction	Semi-empirical from equivalents
Max. and min. transmission	0.95 and 0.88
Flack parameter (absolute struct.)	-0.030(15)
Largest diff. peak and hole	0.560 and -0.443 e.Å ⁻³
Solution	Direct methods
Refinement	Full-matrix least-squares on F ²
Treatment of hydrogen atoms	CH calc, restr., NH, OH located, ref.
Programs used	SHELXS-97 (Sheldrick, 2008) SHELXL-2014 (Sheldrick, 2014) DIAMOND (Crystal Impact)
Data / restraints / parameters	6529 / 0 / 396
Goodness-of-fit on F ²	1.044
R index (all data)	wR2 = 0.0643
R index conventional [$I > 2\sigma(I)$]	R1 = 0.0320

5.6.4 Crystallographic Data of Λ -(R)-127

The crystal structure was depicted using ORTEP drawing with 50% probability of thermal ellipsoid and determined of single crystals of Λ -(R)-127.^[438] The crystals were obtained after dissolution in methylene chloride/methanol mixture of (15:1) and slow evaporation of the solvent at 4 °C for several days. The compound crystallised as orthorhombic red plates. Crystals were measured on a 'Bruker D8 QUEST area detector' diffractometer. The temperature was kept at 100 K during

data collection using a wavelength of 0.71073 Å. The data collection software BRUKER APEX II was applied and the cell refinement and data reduction software SAINT (Bruker AXS Inc.) was used.^[439] Data were corrected for absorption using the program SADABS (Bruker AXS Inc.).^[439] Non hydrogen atoms have been refined anisotropically. Hydrogen atoms were placed on idealised positions and refined using the 'riding model'. The programs applied for solution and refinement were SHELXS-97 (Sheldrick, 2008) and SHELXL-2013 (Sheldrick, 2013).^[439,440] The absolute structure of Λ -(R)-127 was determined. The structure was solved by DR. KLAUS HARMS.

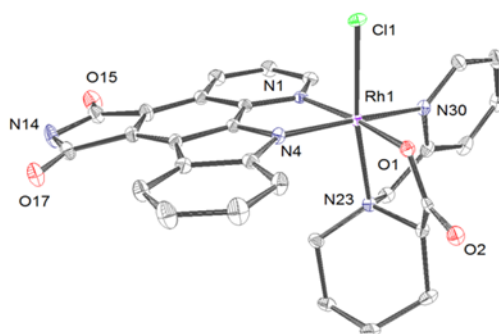


Table 10: Crystal data and structure refinement for Λ -(R)-127.

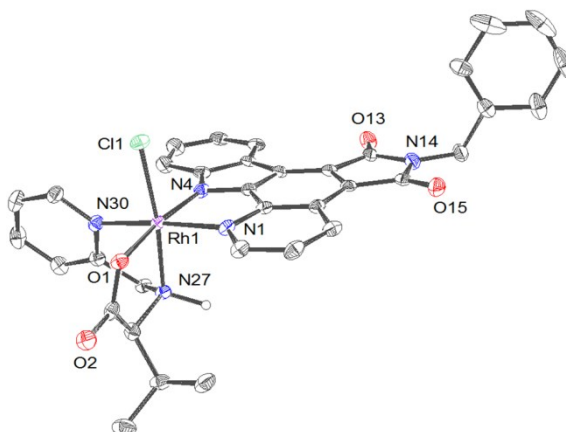
Crystal data

Identification code	Λ -(R)-127
Habitus, colour	plate, red
Crystal size	0.610 x 0.220 x 0.080 mm ³
Crystal system	Orthorhombic
Space group	P 2 ₁ 2 ₁ 2 ₁
Unit cell dimensions	$a = 9.3547(5)$ Å $b = 13.4551(7)$ Å $c = 22.6839(12)$ Å
	$Z = 4$ $\alpha = 90^\circ$ $\beta = 90^\circ$ $\gamma = 90^\circ$
Volume	2855.2(3) Å ³
Cell determination	9156 peaks with Theta 2.3 to 27.5°.
Empirical formula	C ₃₀ H ₂₅ Cl ₃ N ₅ O ₄ Rh
Formula weight	728.81
Density (calculated)	1.695 Mg/m ³
Absorption coefficient	0.926 mm ⁻¹
F(000)	1472
Data collection:	
Diffractometer type	Bruker D8 QUEST area detector
Wavelength	0.71073 Å
Temperature	100(2) K

Theta range for data collection	2.349 to 27.550°.
Index ranges	-12<= <i>h</i> <=12, -16<= <i>k</i> <=17, -29<= <i>l</i> <=29
Data collection software	BRUKER APEX2
Cell refinement software	SAINT V8.34A (Bruker AXS Inc., 2013)
Data reduction software	SAINT V8.34A (Bruker AXS Inc., 2013)
Solution and refinement:	
Reflections collected	38460
Independent reflections	6573 [R(int) = 0.0481]
Completeness to theta = 25.242°	99.9 %
Observed reflections	6163[<i>I</i> > 2(<i>I</i>)]
Reflections used for refinement	6573
Absorption correction	Numerical
Max. and min. transmission	0.93 and 0.69
Flack parameter (absolute struct.)	-0.039(10)
Largest diff. peak and hole	0.429 and -0.343 e.Å ⁻³
Solution	Direct methods
Refinement	Full-matrix least-squares on F ²
Treatment of hydrogen atoms	CH calc., constr., NH located, isotr. Ref.
Programs used	SHELXS-97 (Sheldrick, 2008) SHELXL-2013 (Sheldrick, 2013) DIAMOND (Crystal Impact)
Data / restraints / parameters	6573 / 4 / 410
Goodness-of-fit on F ²	1.052
R index (all data)	wR2 = 0.0514
R index conventional [<i>I</i> >2sigma(<i>I</i>)]	R1 = 0.0238

The crystal structure was depicted using ORTEP drawing with 50% probability of thermal ellipsoid and determined of a single crystal of Δ -(S)-**191**.^[438] The crystals were obtained after dissolution in methylene chloride and slow evaporation of the solvent at 4 °C for several days. The compound crystallised as trigonal red blocks. Crystals were measured on a 'Bruker D8 QUEST area detector ' diffractometer. The temperature was kept at 100 K during data collection

using a wavelength of 0.71073 Å. The data collection software BRUKER APEX II was applied and the cell refinement and data reduction software SAINT (Bruker AXS Inc.) was used.^[439] Data were corrected for absorption using the program SADABS (Bruker AXS Inc.).^[439] Non hydrogen atoms have been refined anisotropically. Hydrogen atoms were placed on idealised positions and refined using the 'riding model'. The programs applied for solution and refinement were SHELXS-97 (Sheldrick, 2008) and SHELXL-2013 (Sheldrick, 2013).^[439,440] The absolute structure of Δ -(S)-**191** was determined. The structure was solved by DR. KLAUS HARMS.



Crystal data

Identification code	Δ -(S)- 191	
Habitus, colour	block, red	
Crystal size	0.19 x 0.14 x 0.11 mm ³	
Crystal system	Trigonal	
Space group	R 3 :H	Z = 3
Unit cell dimensions	a = 24.8187(7) Å	α = 90°.
	b = 24.8187(7) Å	β = 90°.
	c = 16.1592(5) Å	γ = 120°.
Volume	8620.0(6) Å ³	
Cell determination	9835 peaks with Theta 2.7 to 27.5°.	
Empirical formula	C ₁₁₂ H ₁₀₀ Cl ₁₈ N ₁₅ O ₁₂ Rh ₃	
Formula weight	2794.89	
Density (calculated)	1.615 Mg/m ³	
Absorption coefficient	0.912 mm ⁻¹	
F(000)	4242	

Data collection:

Diffractometer type	Bruker D8 QUEST area detector
Wavelength	0.71073 Å
Temperature	100(2) K
Theta range for data collection	2.693 to 25.500°
Index ranges	-30 ≤ h ≤ 30, -30 ≤ k ≤ 30, -19 ≤ l ≤ 19
Data collection software	BRUKER APEX II
Cell refinement software	SAINT V8.32B (Bruker AXS Inc., 2013)
Data reduction software	SAINT V8.32B (Bruker AXS Inc., 2013)

Solution and refinement:

Reflections collected	54939
Independent reflections	7150 [R(int) = 0.0409]
Completeness to theta = 25.242°	99.9 %
Observed reflections	6897 [I > 2(I)]
Reflections used for refinement	7150
Absorption correction	Semi-empirical from equivalents
Max. and min. transmission	0.91 and 0.74
Flack parameter (absolute struct.)	-0.014(7)
Largest diff. peak and hole	0.610 and -0.993 e.Å ⁻³
Solution	Direct methods
Refinement	Full-matrix least-squares on F ²
Treatment of hydrogen atoms	CH riding, NH located, isotr. ref.
Programs used	SHELXS-97 (Sheldrick, 2008) SHELXL-2013 (Sheldrick, 2013) DIAMOND (Crystal Impact)
Data / restraints / parameters	7150 / 1 / 495
Goodness-of-fit on F ²	1.084
R index (all data)	wR2 = 0.0817
R index conventional [I > 2σ(I)]	R1 = 0.0303

5.6.6 Crystallographic Data of Δ -(S)-195

The crystal structure was depicted using ORTEP drawing with 50% probability of thermal ellipsoid and determined of a single crystal of Δ -(S)-**195**.^[438] The crystals were obtained after dissolution in methylene chloride/methanol (15:1) and slow evaporation of the solvent at 4 °C for several days. The compound crystallised as triclinic dark red plates. Crystals were measured on a 'Bruker D8 QUEST area detector' diffractometer. The temperature was kept at 100 K during data collection using a wavelength of

0.71073 Å. The data collection software BRUKER APEX II was applied and the cell refinement and data reduction software SAINT (Bruker AXS Inc.) was used.^[439] Data were corrected for absorption using the program SADABS (Bruker AXS Inc.).^[439] Non hydrogen atoms have been refined anisotropically. Hydrogen atoms were placed on idealised positions and refined using the 'riding model'. The programs applied for solution and refinement were SHELXS-97 (Sheldrick, 2008) and SHELXL-2013 (Sheldrick, 2013).^[439,440] The absolute structure of Δ -(S)-**195** was determined. The structure was solved by DR. KLAUS HARMS.

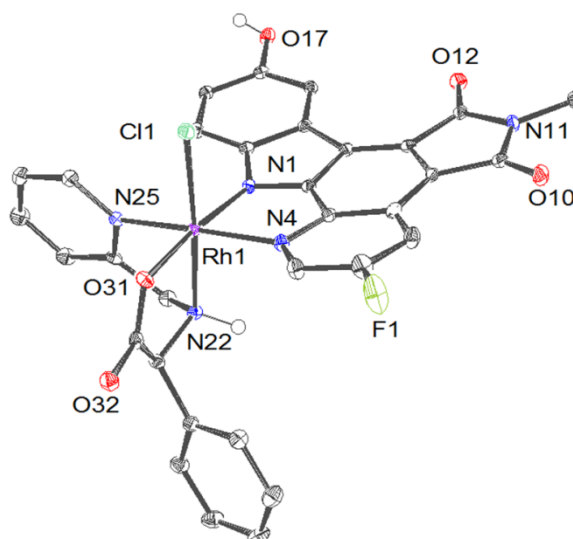


Table 12: Crystal data and structure refinement for Δ -(S)-**195**.

Crystal data

Identification code	Δ -(S)- 195
Habitus, colour	plate, dark red
Crystal size	0.14 x 0.08 x 0.05 mm ³
Crystal system	Triclinic
Space group	P -1
Unit cell dimensions	$a = 8.9766(4)$ Å $b = 13.1877(5)$ Å $c = 13.4671(5)$ Å
	$Z = 2$
	$\alpha = 82.9579(15)^\circ$
	$\beta = 72.1925(14)^\circ$
	$\gamma = 81.2475(14)^\circ$
Volume	1495.28(10) Å ³
Cell determination	120 peaks with Theta 3.7 to 24.1°.
Empirical formula	C ₃₂ H ₂₉ ClFN ₅ O _{8.5} Rh
Formula weight	776.96
Density (calculated)	1.726 Mg/m ³
Absorption coefficient	0.733 mm ⁻¹
F(000)	790

Data collection:

Diffractometer type	Bruker D8 QUEST area detector
Wavelength	0.71073 Å
Temperature	100(2) K
Theta range for data collection	2.462 to 27.165°
Index ranges	-11 ≤ h ≤ 11, -16 ≤ k ≤ 16, -17 ≤ l ≤ 17
Data collection software	Bruker Instrument Service v3.0.31
Cell refinement software	APEX2 v2013.10-0 (Bruker AXS)
Data reduction software	SAINT V8.34A (Bruker AXS Inc., 2013)

Solution and refinement:

Reflections collected	41431
Independent reflections	6635 [R(int) = 0.0515]
Completeness to theta = 25.242°	99.8 %
Observed reflections	5809 [I > 2(I)]
Reflections used for refinement	6635
Absorption correction	Semi-empirical from equivalents
Max. and min. transmission	0.7455 and 0.7184
Largest diff. peak and hole	0.424 and -0.560 e.Å ⁻³
Solution	Direct methods
Refinement	Full-matrix least-squares on F ²
Treatment of hydrogen atoms	CH calc., constr. Ref., NH, OH located, isotr. ref.
Programs used	SHELXS-97 (Sheldrick, 2008) SHELXL-2013 (Sheldrick, 2013) DIAMOND (Crystal Impact)
Data / restraints / parameters	6635 / 0 / 472
Goodness-of-fit on F ²	1.053
R index (all data)	wR2 = 0.0596
R index conventional [I > 2σ(I)]	R1 = 0.0268

5.6.7 Crystallisation and Structure Determination of S6K1

The crystallisation and structure determination of S6K1 in complex with **85**/staurosporine and in complex with **87** were performed in the MARMORSTEIN group by JOHN DOSMIC, the Wistar Institute, 3601 Spruce Street, Philadelphia, Pennsylvania 19104, United States. The S6K1 kinase domain crystals were obtained using room temperature hanging drop vapor diffusion by mixing equal volumes of protein (15 mg/mL) preincubated with 1 mM staurosporine with 20–25% (w/v) PEG335, 0.1 M Bis-Tris (pH 5.5–5.7), and 0.2 M LiSO₄. Following the growth of crystals, crystal soaking was carried out by incubation with a final inhibitor concentration of 1 mM in cryoprotectant containing the well solution and 15% (w/v) glycerol for 4 h to overnight and flash frozen in liquid nitrogen. Diffraction images were collected at APS beamline 23ID with a 5 µm microbeam. The structures were determined by molecular replacement using thereported S6K1/staurosporine complex (PDB accession code 3A60) as a search model with the staurosporine removed from the coordinate file and refined with CNS and Coot. The inhibitors were modeled last into the refined structures. Simulated annealing omit maps were employed to unambiguously confirm the modeled inhibitors. For the **85**-soaked crystals, this revealed that one protein molecule in the asymmetric unit was bound to staurosporine while the other protein molecule was bound to **85**. For the **87**-soaked crystals, the asymmetric unit contained a single, domain-swapped monomer and only the **87** inhibitor was modelled in the binding site. The structures were refined to convergence with a final $R_{\text{work}} = 19.15\%$ and $R_{\text{free}} = 22.21\%$ for the S6K1/**85** structure and a final $R_{\text{work}} = 20.63\%$ and $R_{\text{free}} = 23.01\%$ for the S6K1/**87** structure with excellent geometry, see Table 13.

Table 13: Data and refinement statistics of S6K1 in complex with **85**/Staurosporine or **87**

	S6K1-85/Staurosporine	S6K1-87
Resolution range (Å)	49.03-2.527 (2.618-2.527)	29.91-2.794 (2.893-2.794)
Space group	<i>P</i> 1 2 ₁ 1	C 2 2 2 ₁
Unit cell (<i>a</i> , <i>b</i> , <i>c</i> , α , β , γ)	78.515, 62.882, 86.718, 90, 94.02, 90	62.13, 126.371, 110.571, 90, 90, 90
Total reflections	110916	47648
Unique reflections	28440 (2745)	10829 (1028)
Multiplicity	3.9 (3.3)	4.4 (4.2)
Completeness (%)	99.71 (97.10)	97.06 (90.33)
Mean <i>I</i> / σ (<i>I</i>)	21.3 (4.1)	15.0 (2.0)
Wilson <i>B</i> -factor	43.06	51.11
<i>R</i> _{meas} (%)	7.9 (40.7)	8.9 (67.8)
<i>R</i> _{work} (%)	19.15 (23.61)	20.63 (29.64)
<i>R</i> _{free} (%)	22.21 (26.70)	23.01 (32.07)
No. of non-H atoms	4240	2114
Protein	4048	2040
Ligands	110	47
Solvent	82	27
RMS (bonds/angles)	0.015/1.25	0.012/1.03
Ramachandran (%favoured/outliers)	95.0/0	95.0/0
Average <i>B</i> -factor	40.7	55.0
Protein	40.6	55.0
Ligands	43.8	65.0
Solvent	37.3	38.8

6 Appendix

6.1 Kinase Classification

6.1.1 AGC Kinases

This group of kinases is named after the protein Kinase A, G, and C families (PKA, PKG, PKC). The AGC group of kinases covers 60 members containing many core intracellular signalling kinases which are modulated by cyclic nucleotides, phospholipids and calcium.^[1,23] Moreover, the group consists of 16 families, whereas eight are likely to have been in early eukaryotes, and another two (RSK, PKC) in the fungal/metazoan lineage. Six of the families (PKG, PKN, DMPK, YANK, RSKR, RSKL) have only been found in metazoans. Detailed reviews on AGC structure and function are provided in literature.^[23,441,442]

6.1.2 CMGC Kinases

CMGC is an acronym based on the initials of key members like cyclin dependent kinase (CDK), mitogen activated protein kinase (MAPK), glycogen synthase kinase (GSK), and CDK-like kinases (CDKL). Most of the kinase families belonging to this group are related to growth and stress-response and cellular effects mediated by the corresponding factors and hormones. Detailed reviews on CMGC members are provided in literature.^[50,443–448]

6.1.3 CK1 group

The Casein Kinase 1 (CK1) is a small group of kinases with high sequence similarity between each other. Nevertheless, they are very distinct from other kinase groups. Several conserved motifs are modified in CK1s, i.e.: the APE motif is substitut-

ed by the SIN motif. Beside CK1 the other members of this group are Vaccinia Related Kinase (VRK), Tau-Tubulin Kinase (TTBK), and TTBK-like kinases (TTBKL), whereas the last ones were found only in nematodes. They play a role in membrane trafficking, circadian rhythm, cell cycle progression, chromosome segregation, spermatogenesis, apoptosis, cellular differentiation, and amyloidogenesis. Detailed reviews on CK1 group members are provided in literature.^[449–452]

6.1.4 STE group

Three families of this group are the main members activating each other and finally regulating the MAP kinase family. For instance, Ste20 members (MAPKKKK) act on Ste11 (MAPKKK), thus phosphorylating the Ste7 (MAPKK) which by themselves directly phosphorylate MAPKs. The abbreviations are deviated from the canonical pheromone-responsive MAPK cascade in yeast and were named subsequently according to the phosphorylated target. Distinct sets of Ste7 and Ste11 kinases are linked with specific classes of MAPK (Erk, Jnk, p38 and others) but some cross-talk is also observed. Detailed reviews on STE kinases are provided in literature.^[453–455]

6.1.5 CAM Kinases

CAM is an acronym for the Ca^{2+} /calmodulin-dependent protein kinase class of enzymes. They are activated by increased concentrations of intracellular calcium ions and phosphorylate serine or threonine residues in substrate proteins. The CAMK's are divided into four families (CAMK I-IV) and play a versatile role covering inflammatory effects, cell contraction, cell motility or cell plasticity. Detailed reviews on CAMK members are provided in literature.^[456–459]

6.1.6 TK group

Despite the other groups introduced so far, this group phosphorylates almost exclusively tyrosine residues. Moreover, this group of kinases appears to be the youngest group from the evolutionary point of view, regarding their absence in plants and unicellular organisms like dictyostelium and yeast. The most important function of tyrosine kinases is particularly the transduction of extracellular signals into the cell: more than 50% of the tyrosine kinases (TK) are cell surface receptor tyrosine kinases (RTKs). Moreover, many of the residual kinases act close to the cell membrane. Due to their importance, the TKs are the most studied group covering the largest number of distinct families of any group. Subsequently, each family is further divided into a receptor or cytoplasmic tyrosine kinase subfamily. Tyrosine Kinases are related to many physiological effects covering proliferation, differentiation, and cell survival. Detailed reviews on TKs are provided in literature.^[53,460–462]

6.1.7 TKL group

The tyrosine kinase like (TKL) group consists of 7 subfamilies with relatively small similarity to each other. The group members generally phosphorylate serine/threonine residues. Moreover, all of them are similar to members of the TK group, although, in general, they do not possess the tyrosine kinase specific motifs. The TKL group is present in almost all eukaryotes but is conspicuously absent from the yeast kinome. However, the high sequence similarity between TKLs and TKs suggests that the latter ones may have evolved from the more ancient TKL kinases. TKLs are among others involved in mediating necrosis signalling pathways, cell cycle progression, and metabolic stress signaling. Detailed reviews on members of TKLs are provided in literature.^[463–466]

6.1.8 RGC group

Receptor Guanylate Cyclases (RGC) have an unusual structure among other receptor kinases possessing a single-pass transmembrane chain with an active guanylate cyclase domain and a catalytically inactive kinase domain on the intracellular side. The guanylate cyclase domain is responsible for the formation of the second messenger cyclic guanosine triphosphate (cGMP), whereas the kinase domain may have an allosterically mediated regulatory role via ATP binding. Moreover, also soluble cellular isoforms (CGC) are expressed and both together are present in nearly all cell types. GCs play physiological roles in different processes like vascular smooth muscle motility, intestinal fluid and electrolyte homeostasis, and retinal phototransduction. Detailed reviews on RGC and CGCs are provided in literature.^[467–469]

6.1.9 PKL group

Several diverse kinase families belong to the protein kinases like (PKL) group having the PKL fold and catalytic mechanism, but do not possess all structural refinements of the PKs. Many of these were previously classified as pseudokinases. The main subfamilies are ABC1 domain containing kinases (ADCK), alpha kinases, phosphatidyl inositol 3 kinase-related kinases (PIKK), phosphatidyl inositol kinases (PIK), golgi associated kinases (GASK), aminoglycoside phosphotransferase domain containing 1 (AGPHD1), phosphatidyl inositol phosphate kinases (PIPK). The PKL members play important roles in ribosome biogenesis, cell cycle progression, metabolism, phagocytosis, and other effects. Detailed reviews on members of the PKL group are provided in literature.^[470–473]

6.1.10 Pseudokinases

48 Pseudokinases were identified in the human phylogenetic kinome and they are defined by the lack of conservation of at least one of the catalytic site residues in the kinase core.^[1,4] Their function has been obscure but recent findings recognise them as participating proteins in signal transduction and cell-matrix adhesion.^[5] The changed motifs in the pseudokinases include the glycine-rich loop, the VAIK motif (β 3 lysine), HRD motif (catalytic aspartate), and DFG motif or combinations of them.^[4,474] For example, the giant protein titin contains a kinase domain with an EFG motif instead of DFG.^[475] Nevertheless, the altered structure and the increased space allow glutamate to perform the catalytic reaction. Detailed reviews on Pseudokinases are provided in literature.^[4,5,476]

6.2 Structural Overview of Synthesised Compounds

6.2.1 Compounds of Chapter 3.1

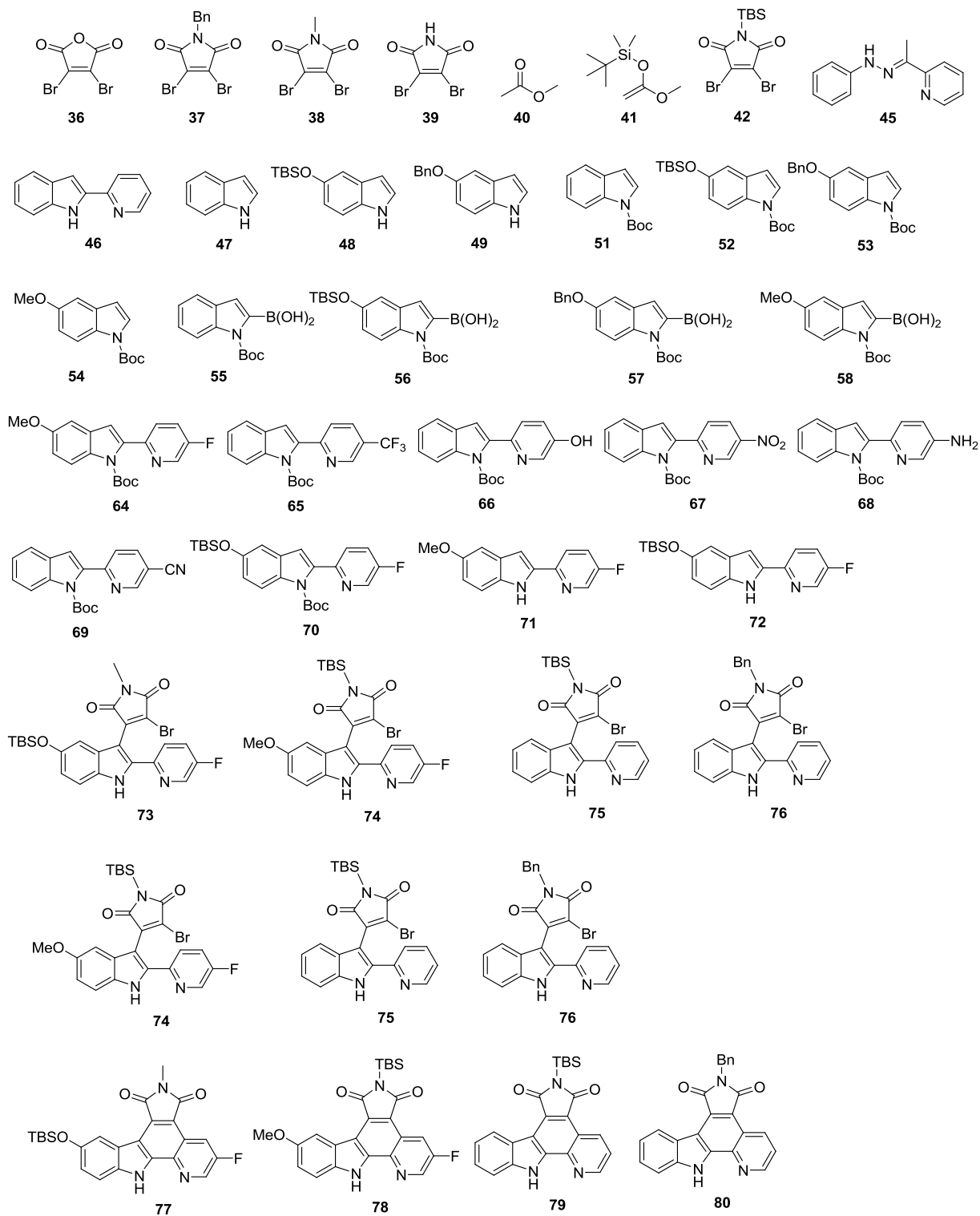


Figure 98: Synthesised compounds presented in Chapter 3.1.

6.2.2 Compounds of Chapter 3.2

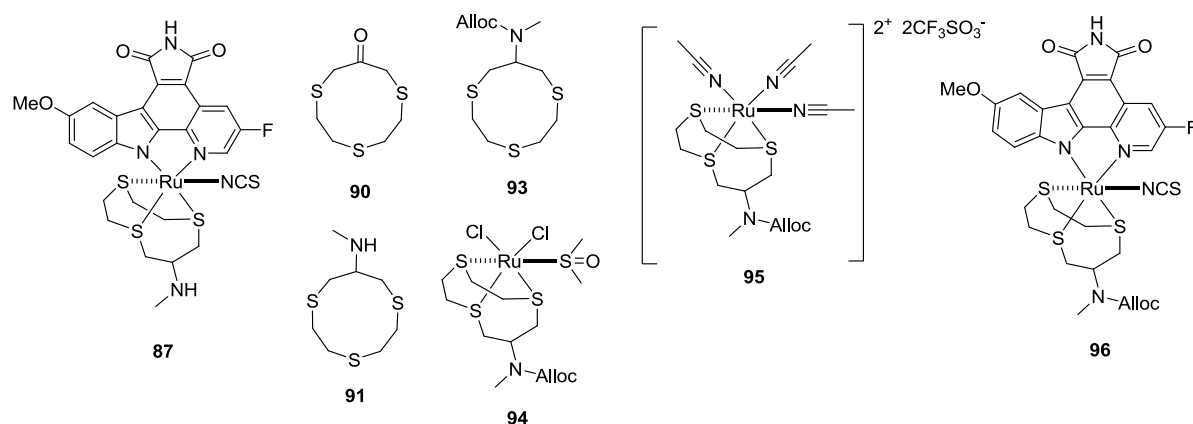


Figure 99: Synthesised compounds presented in Chapter 3.2.

6.2.3 Compounds of Chapter 3.3

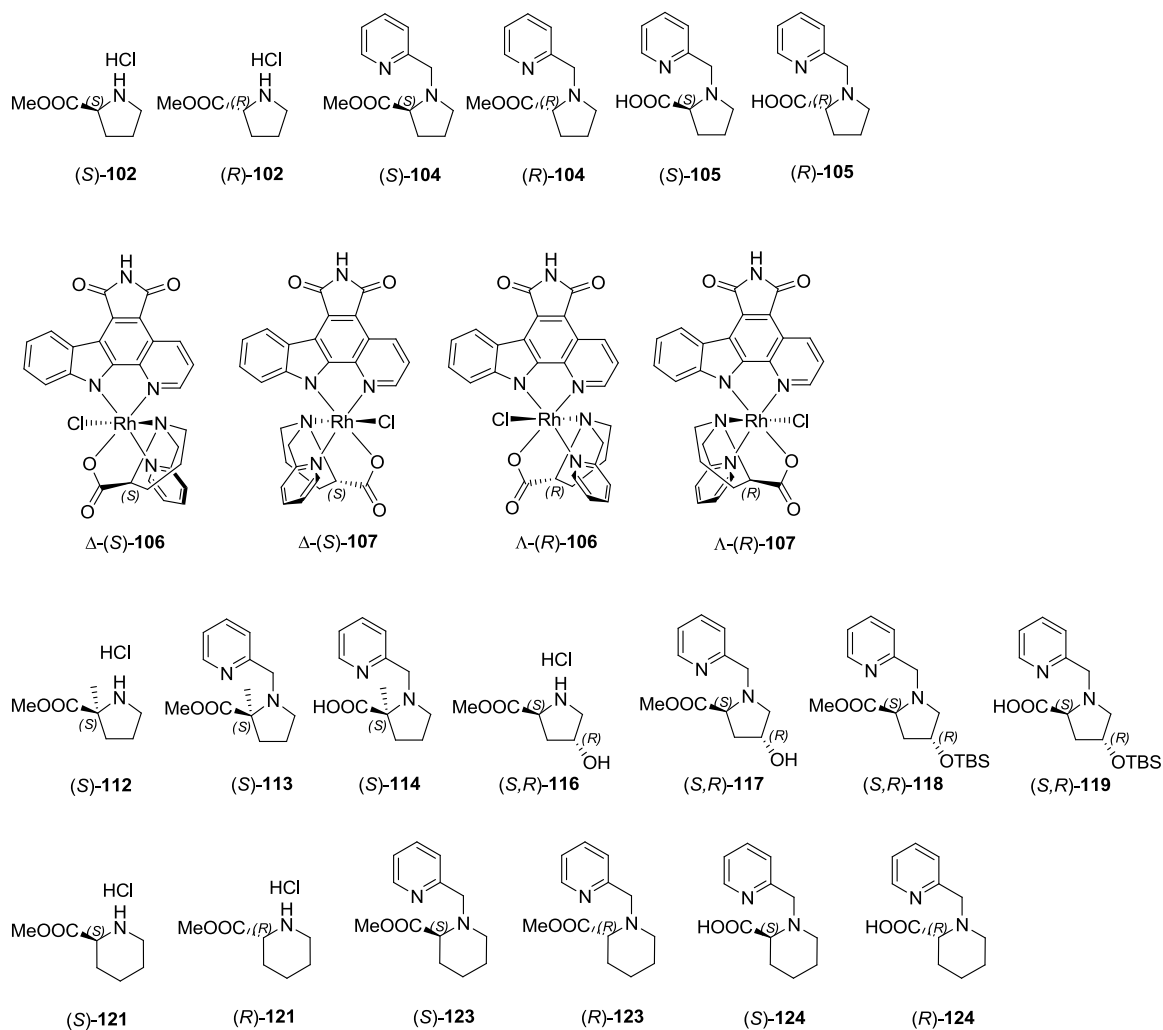


Figure 100: Synthesised compounds presented in Chapter 3.3 (I).

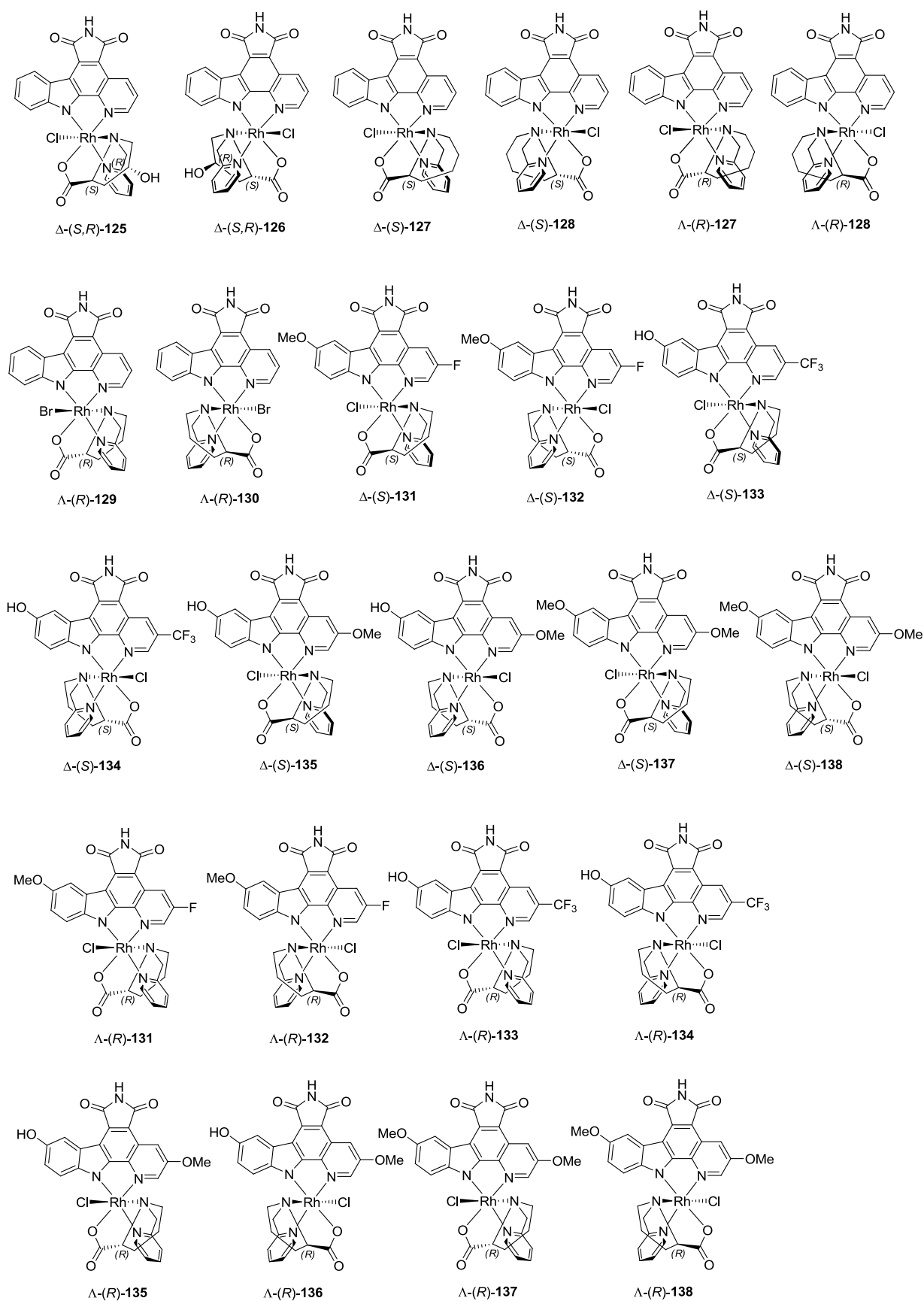


Figure 101: Synthesised compounds presented in Chapter 3.3 (II).

6.2.4 Compounds of Chapter 3.4

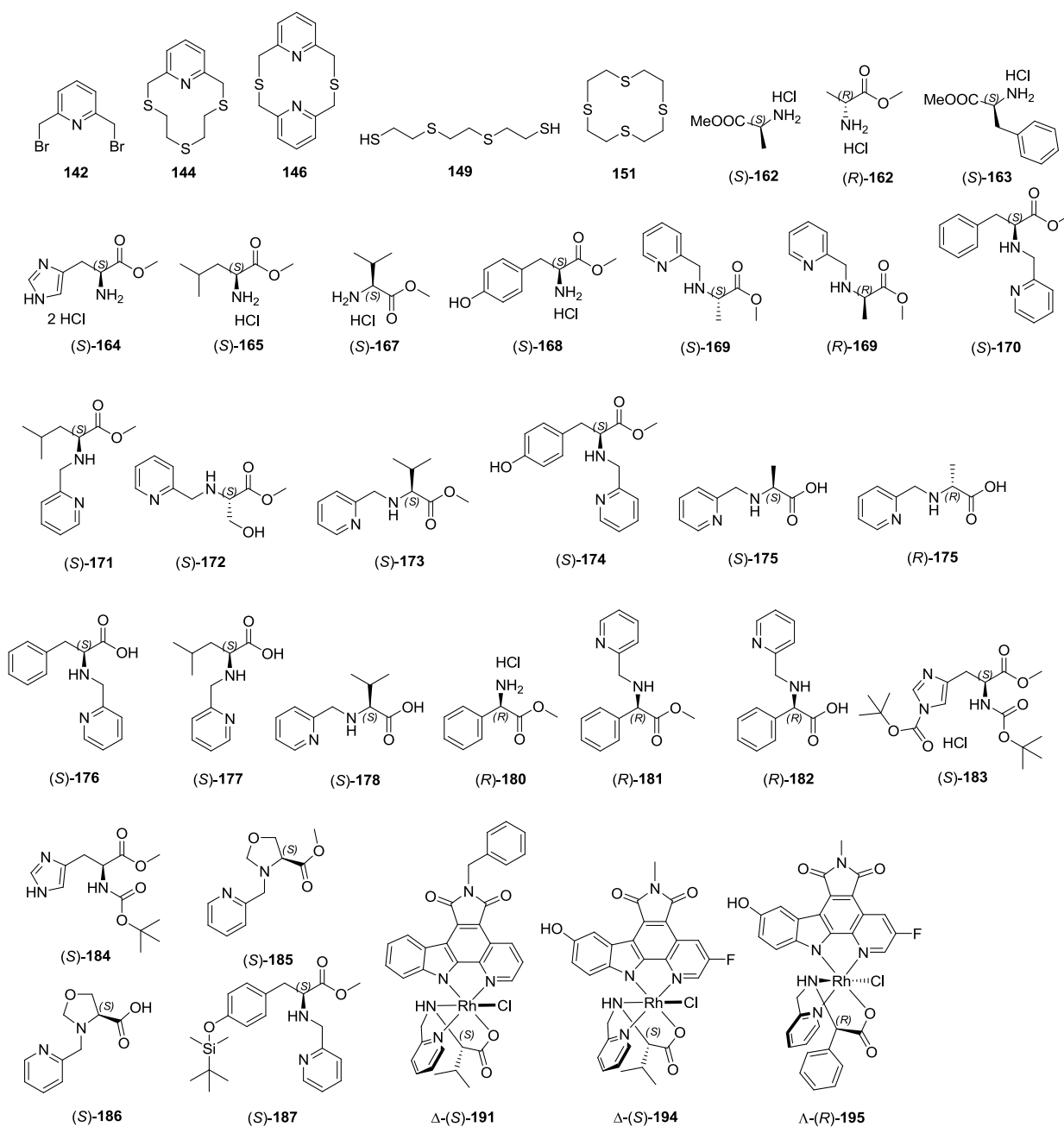


Figure 102: Synthesised compounds presented in Chapter 3.4 (I).

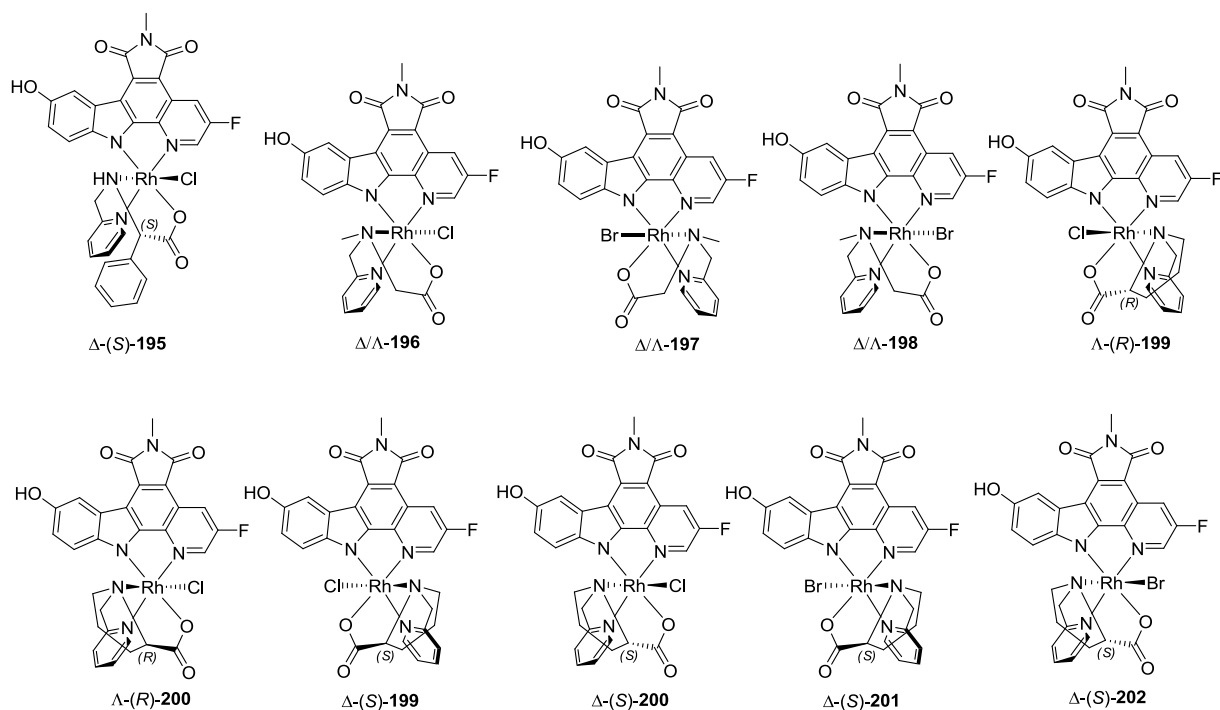


Figure 103: Synthesised compounds presented in Chapter 3.4 (II).

6.3 List of abbreviations

Å	ångström
ABL	abelson murine leukemia viral oncogene
AcOH	acetic acid
ADME	absorption, distribution, metabolism and excretion
ADP	adenosine diphosphate
AGC kinases	named after protein kinase A, G, and C
AKT	protein kinase B
AML	acute myeloic leukemia
APE-motif	conserved Ala Pro Glu motif
ATP	adenosine triphosphate
aq.	aqueous
BAD	BCL-2-associated death promoter
BCL-2	b-cell lymphoma 2
BCR-ABL	breakpoint cluster region - abelson murine leukemia viral oncogene homologue 1 fusion protein
BRAF = B-Raf	rapidly accelerated fibrosarcoma protein isoform B
BTK	Bruton's tyrosine kinase
CAMK kinases	acronym for Ca ²⁺ /Calmodulin-dependent protein kinases
cAMP	cyclic adenosine monophosphate
CCDC	cambridge crystallographic data center
CD	circular dichroism
CDCl ₃	deuterised chloroform
CDC25A	cell division cycle 25 homologue A
CDC25C	cell division cycle 25 homologue C
CDK2	cyclin-dependent protein kinase 2
CDK5	cyclin dependent kinase 5
CDKN1B	cyclin-dependent kinase inhibitor 1B
CHARMM	chemistry at harvard molecular mechanics
CIP	Cahn-Ingold-Prelog
CK1	casein kinase 1 group
CLL	chronic lymphocytic leukemia
CMGC kinases	acronym based on key members CDK, MAPK, GSK, CDK
CML	chronic myeloid leukemia
H,H-COSY	proton-proton correlation spectroscopy
CPM	counts per minute
d	doublet
δ	chemical shift
DAIM	decomposition and identification of molecules
DFG-motif	conserved Asp-Phe-Gly motif
DIPA	diisopropylamine
DIPEA	diisopropylethylamine
DMAP	4-dimethylaminopyridine
DME	dimethoxyethane
DMF	dimethylformamide
DMPU	1,3-Dimethyl-3,4,5,6-tetrahydro-2(1 <i>H</i>)-pyrimidinone

DMSO	dimethylsulfoxide
DMSO- d_6	deuterised dimethylsulfoxide
EGFR	epidermal growth factor receptor
eIF4B	eucaryotic translation initiation factor 4B
eIF4EBP1	eucaryotic translation initiation factor 4E-binding protein 1
ERK	extracellular-signaling-regulated kinase
EtOH	ethanol
eq.	equivalent
FDA	Food and Drug Administration
FLT-3	FMS-like tyrosine kinase 3
GAPDH	glyceraldehyde 3-phosphate dehydrogenase
GCK	glucokinase
GHI-domain	α G, α H and, α I helices
GIST	gastrointestinal stomal tumor
GSK-3 β	glycogen synthase kinase 3 beta
HCl	hydrochloric acid
HER	human epidermal growth factor receptor
HMBC	heteronuclear multiple bond correlation
HPLC	high performance liquid chromatography
HRD-motif	conserved His-Arg-Asp motif
HR-MS	high resolution mass spectrometry
HSQC	heteronuclear single quantum coherence
HTS	high-throughput screening
Hz	hertz
IC ₅₀	half maximal inhibitory constant
IL	interleukin
JAK	janus kinase
K	Kelvin
k	kilo
KD	dissocioation constant
L	liter
λ	wavelength
μ	mikro
m	milli
M	molarity
m	multiplatt
MAP3K5	mitogen-activated protein kinase kinase kinase 5
MAPKs	mitogen-activated protein kinases
MeCN	acetonitrile
MEK1	mitogen-activated protein kinase kinase
MEK2	mitogen-activated protein kinase kinase 2
MeOH	methanol
min	minute
mL	milli liter
MPEOE	modified partial equalization of orbital electronegativity
mTOR	mammalian target of rapamycin
mTORC1	mammalian target of rapamycin complex 1
mTORC2	mammalian target of rapamycin complex 2
NH	number of hits

NMR	nuclear magnetic resonance
ORTEP	oak ridge thermal ellipsoid plot program
pAKT	phosphorylated protein kinase B
PARP	poly (ADP-ribose) polymerase
PDB	protein data bank
PDGFR	platelet-derived growth factor receptors
PDK1	pyruvate dehydrogenase lipoamide kinase isozyme 1
PH	pleckstrin homology
PhK	phosphorylase kinase
PHLPP	PH domain and leucine rich repeat protein phosphatases
PI3K	phosphatidylinositide-3-kinase
PIM-1	proviral insertion in murine, proto-oncogene serine/threonine-protein kinase isoform 1
PIP3	phosphatidylinositol-3,4,5-trisphosphate
PKA	protein kinase A
POC	percent of control
ppm	part per million
PTEN	phosphate and tensine homologue
q	quartett
Quant.	quantitative
RCC	renal cell carcinoma
RGC kinases	receptor guanylate cyclase group
r.m.s.d.	root mean square deviation
RSK	ribosomal S6 kinases
RTK	receptor tyrosine kinases
RUNX1	runt-related transcription factor 1
RUNX3	runt-related transcription factor 3
s	singulett
S6K	S6 kinases
SAR	structure-activity relationship
SS	selectivity score
SST	selectivity score types
STE	homologues of yeast Sterile 7, Sterile 11, and Sterile 20
t	triplett
TBAF	tetra- <i>n</i> -butylammoniumfluoride
TBSOTf	<i>tert</i> -butyldimethylsilyl trifluoromethanesulfonate
TEC	terminal edge convention
TFA	trifluoroacetic acid
THF	tetrahydrofuran
TK	tyrosine kinases
TKL	tyrosine-like kinases
TLC	thin layer chromatography
TPX2	targeting protein for Xklp2
UV	ultra violet
VdW	VAN-DER-WAALS

7 Literature

- [1] G. Manning, D. B. Whyte, R. Martinez, T. Hunter, S. Sudarsanam, *Science (80-.)*. **2002**, 298, 1912–1934.
- [2] D. M. A. Martin, D. Miranda-Saavedra, G. J. Barton, *Nucleic Acids Res.* **2009**, 37, D244–D250.
- [3] G. Manning, G. D. Plowman, T. Hunter, S. Sudarsanam, *Trends Biochem. Sci.* **2002**, 27, 514–520.
- [4] J. Boudeau, D. Miranda-Saavedra, G. J. Barton, D. R. Alessi, *Trends Cell Biol.* **2006**, 16, 443–452.
- [5] E. Zehiraj, D. M. F. van Aalten, *Curr. Opin. Struct. Biol.* **2010**, 20, 772–781.
- [6] S. S. Taylor, E. Radzio-Andzelm, T. Hunter, *FASEB J.* **1995**, 9, 1255–1266.
- [7] J. A. Endicott, M. E. M. Noble, L. N. Johnson, *Annu. Rev. Biochem.* **2012**, 81, 587–613.
- [8] N. Kannan, A. F. Neuwald, *J. Mol. Biol.* **2005**, 351, 956–972.
- [9] N. Kannan, S. S. Taylor, Y. Zhai, J. C. Venter, G. Manning, *PLoS Biol* **2007**, 5, e17.
- [10] J. Brognard, T. Hunter, *Curr. Opin. Genet. Dev.* **2011**, 21, 4–11.
- [11] P. Cohen, *Nat. Cell Biol.* **2002**, 4, E127–E130.
- [12] L. N. Johnson, R. J. Lewis, *Chem. Rev.* **2001**, 101, 2209–2242.
- [13] J. Zheng, E. A. Trafny, D. R. Knighton, N.-H. Xuong, S. S. Taylor, L. F. Ten Eyck, J. M. Sowadski, *Acta Crystallogr. Sect. D Biol. Crystallogr.* **1993**, 49, 362–365.
- [14] J. A. Adams, *Biochemistry* **2003**, 42, 601–607.
- [15] L. N. Johnson, M. E. M. Noble, D. J. Owen, *Cell* **1996**, 85, 149–158.
- [16] D. R. Knighton, J. H. Zheng, L. F. Ten Eyck, V. A. Ashford, N.-H. Xuong, S. S. Taylor, J. M. Sowadski, *Science (80-.)*. **1991**, 253, 407–414.
- [17] H. L. De Bondt, J. Rosenblatt, J. Jancarik, H. D. Jones, D. O. Morgant, S.-H. Kim, **1993**.
- [18] D. A. Walsh, J. P. Perkins, E. G. Krebs, *J. Biol. Chem.* **1968**, 243, 3763–3765.
- [19] E. G. Krebs, *Annu. Rev. Biochem.* **1998**, 67, xiii–xxxii.
- [20] S. S. Taylor, J. Yang, J. Wu, N. M. Haste, E. Radzio-Andzelm, G. Anand, *Biochim. Biophys. Acta (BBA)-Proteins Proteomics* **2004**, 1697, 259–269.
- [21] D. R. Knighton, J. H. Zheng, L. F. Ten Eyck, N.-H. Xuong, S. S. Taylor, J. M. Sowadski, *Science (80-.)*. **1991**, 253, 414–420.
- [22] D. A. Johnson, P. Akamine, E. Radzio-Andzelm, and Madhusudan, S. S. Taylor, *Chem. Rev.* **2001**, 101, 2243–2270.
- [23] L. R. Pearce, D. Komander, D. R. Alessi, *Nat. Rev. Mol. cell Biol.* **2010**, 11, 9–22.
- [24] S. K. Hanks, T. Hunter, *FASEB J.* **1995**, 9, 576–596.
- [25] E. E. Thompson, A. P. Kornev, N. Kannan, C. Kim, L. F. Ten Eyck, S. S. Taylor, *Protein Sci.* **2009**, 18, 2016–2026.
- [26] M. Huse, J. Kuriyan, *Cell* **2002**, 109, 275–282.
- [27] M. Shudler, M. Y. Niv, *J. Phys. Chem. A* **2009**, 113, 7528–7534.
- [28] I. Tsigelny, J. P. Greenberg, S. Cox, W. L. Nichols, S. S. Taylor, L. F. Ten Eyck, *Biopolymers* **1999**, 50, 513–524.
- [29] P. Akamine, N.-H. Xuong, S. S. Taylor, *Nat. Struct. Mol. Biol.* **2002**, 9, 273–277.
- [30] C. Ramakrishnan, V. S. Dani, T. Ramasarma, *Protein Eng.* **2002**, 15, 783–798.
- [31] N. Narayana, S. Cox, S. Shaltiel, S. S. Taylor, N. Xuong, *Biochemistry* **1997**, 36, 4438–4448.

- [32] J. M. Steichen, G. H. Iyer, S. Li, S. A. Saldanha, M. S. Deal, V. L. Woods, S. S. Taylor, *J. Biol. Chem.* **2010**, *285*, 3825–3832.
- [33] J. Yang, S. M. Garrod, M. S. Deal, G. S. Anand, V. L. Woods, S. Taylor, *J. Mol. Biol.* **2005**, *346*, 191–201.
- [34] A. P. Kornev, S. S. Taylor, L. F. Ten Eyck, *Proc. Natl. Acad. Sci.* **2008**, *105*, 14377–14382.
- [35] L. F. Ten Eyck, S. S. Taylor, A. P. Kornev, *Biochim. Biophys. Acta (BBA)-Proteins Proteomics* **2008**, *1784*, 238–243.
- [36] L. R. Masterson, C. Cheng, T. Yu, M. Tonelli, A. Kornev, S. S. Taylor, G. Veglia, *Nat. Chem. Biol.* **2010**, *6*, 821–828.
- [37] S. J. Deminoff, V. Ramachandran, P. K. Herman, *Genetics* **2009**, *182*, 529–539.
- [38] A. Vulpetti, R. Bosotti, *Farm.* **2004**, *59*, 759–765.
- [39] Y. Liu, N. S. Gray, *Nat. Chem. Biol.* **2006**, *2*, 358–364.
- [40] B. Nolen, S. Taylor, G. Ghosh, *Mol. Cell* **2004**, *15*, 661–675.
- [41] J. Yang, P. Cron, V. Thompson, V. M. Good, D. Hess, B. A. Hemmings, D. Barford, *Mol. Cell* **2002**, *9*, 1227–1240.
- [42] E. D. Scheeff, P. E. Bourne, *PLoS Comput Biol* **2005**, *1*, e49.
- [43] J. A. Adams, *Chem. Rev.* **2001**, *101*, 2271–2290.
- [44] M. Valiev, J. Yang, J. A. Adams, S. S. Taylor, J. H. Weare, *J. Phys. Chem. B* **2007**, *111*, 13455–13464.
- [45] Y. Liu, K. Shah, F. Yang, L. Witucki, K. M. Shokat, *Bioorg. Med. Chem.* **1998**, *6*, 1219–1226.
- [46] F. Zuccotto, E. Ardini, E. Casale, M. Angiolini, *J. Med. Chem.* **2009**, *53*, 2681–2694.
- [47] R. J. Brushia, D. A. Walsh, *Front Biosci* **1999**, *4*, D618–D641.
- [48] N. Jura, X. Zhang, N. F. Endres, M. A. Seeliger, T. Schindler, J. Kuriyan, *Mol. Cell* **2011**, *42*, 9–22.
- [49] K. M. Ferguson, *Annu. Rev. Biophys.* **2008**, *37*, 353.
- [50] D. O. Morgan, *Annu. Rev. Cell Dev. Biol.* **1997**, *13*, 261–291.
- [51] J. Eswaran, A. Bernad, J. M. Ligos, B. Guinea, J. É. Debreczeni, F. Sobott, S. A. Parker, R. Najmanovich, B. E. Turk, S. Knapp, *Structure* **2008**, *16*, 115–124.
- [52] J. Eswaran, D. Patnaik, P. Filippakopoulos, F. Wang, R. L. Stein, J. W. Murray, J. M. G. Higgins, S. Knapp, *Proc. Natl. Acad. Sci.* **2009**, *106*, 20198–20203.
- [53] S. R. Hubbard, J. H. Till, *Annu. Rev. Biochem.* **2000**, *69*, 373–398.
- [54] A. P. Kornev, N. M. Haste, S. S. Taylor, L. F. Ten Eyck, *Proc. Natl. Acad. Sci.* **2006**, *103*, 17783–17788.
- [55] S. S. Taylor, A. P. Kornev, *Trends Biochem. Sci.* **2011**, *36*, 65–77.
- [56] L. M. Iakoucheva, P. Radivojac, C. J. Brown, T. R. O'Connor, J. G. Sikes, Z. Obradovic, A. K. Dunker, *Nucleic Acids Res.* **2004**, *32*, 1037–1049.
- [57] E. D. Lowe, M. E. M. Noble, V. T. Skamnaki, N. G. Oikonomakos, D. J. Owen, L. N. Johnson, *EMBO J.* **1997**, *16*, 6646–6658.
- [58] E. J. Goldsmith, R. Akella, X. Min, T. Zhou, J. M. Humphreys, *Chem. Rev.* **2007**, *107*, 5065–5081.
- [59] K.-Y. Cheng, M. E. M. Noble, V. Skamnaki, N. R. Brown, E. D. Lowe, L. Kontogiannis, K. Shen, P. A. Cole, G. Siligardi, L. N. Johnson, *J. Biol. Chem.* **2006**, *281*, 23167–23179.
- [60] A. Y. Kovalevsky, H. Johnson, B. L. Hanson, M. J. Waltman, S. Z. Fisher, S. Taylor, P. Langan, *Acta Crystallogr. Sect. D Biol. Crystallogr.* **2012**, *68*, 854–860.
- [61] O. Gerlits, M. J. Waltman, S. Taylor, P. Langan, A. Kovalevsky, *Biochemistry* **2013**, *52*, 3721–3727.

- [62] B. D. Grant, J. A. Adams, *Biochemistry* **1996**, 35, 2022–2029.
- [63] J. K. Lassila, J. G. Zalatan, D. Herschlag, *Annu. Rev. Biochem.* **2011**, 80, 669.
- [64] V. T. Skamnaki, D. J. Owen, M. E. M. Noble, E. D. Lowe, G. Lowe, N. G. Oikonomakos, L. N. Johnson, *Biochemistry* **1999**, 38, 14718–14730.
- [65] P. A. Cole, M. R. Grace, R. S. Phillips, P. Burn, C. T. Walsh, *J. Biol. Chem.* **1995**, 270, 22105–22108.
- [66] J. A. Adams, S. S. Taylor, *Biochemistry* **1992**, 31, 8516–8522.
- [67] K. Callaway, W. F. Waas, M. A. Rainey, P. Ren, K. N. Dalby, *Biochemistry* **2010**, 49, 3619–3630.
- [68] P. D. Jeffrey, A. A. Russo, K. Polyak, E. Gibbs, J. Hurwitz, J. Massague, N. P. Pavletich, *Nature* **1995**, 376, 313–320.
- [69] F. Sicheri, I. Moarefi, J. Kuriyan, *Nature* **1997**, 385, 602–609.
- [70] X. Wenqing, S. C. Harrison, M. J. Eck, *Nature* **1997**, 385, 595–602.
- [71] J. Yang, P. Cron, V. M. Good, V. Thompson, B. A. Hemmings, D. Barford, *Nat. Struct. Mol. Biol.* **2002**, 9, 940–944.
- [72] L. Hicke, R. Dunn, *Annu. Rev. Cell Dev. Biol.* **2003**, 19, 141–172.
- [73] K. Honda, H. Mihara, Y. Kato, A. Yamaguchi, H. Tanaka, H. Yasuda, K. Furukawa, T. Urano, *Oncogene* **2000**, 19, 2812–2819.
- [74] A. Castro, Y. Arlot-Bonnemains, S. Vigneron, J.-C. Labbé, C. Prigent, T. Lorca, *EMBO Rep.* **2002**, 3, 457–462.
- [75] E. K. Greuber, P. Smith-Pearson, J. Wang, A. M. Pendergast, *Nat. Rev. Cancer* **2013**, 13, 559–571.
- [76] B. Vogelstein, N. Papadopoulos, V. E. Velculescu, S. Zhou, L. A. Diaz, K. W. Kinzler, *Science (80-.)* **2013**, 339, 1546–1558.
- [77] C. Ballatore, V. M.-Y. Lee, J. Q. Trojanowski, *Nat. Rev. Neurosci.* **2007**, 8, 663–672.
- [78] S. Leclerc, M. Garnier, R. Hoessel, D. Marko, J. A. Bibb, G. L. Snyder, P. Greengard, J. Biernat, Y.-Z. Wu, E.-M. Mandelkow, *J. Biol. Chem.* **2001**, 276, 251–260.
- [79] B. K. Mueller, H. Mack, N. Teusch, *Nat. Rev. Drug Discov.* **2005**, 4, 387–398.
- [80] H. Shimokawa, A. Takeshita, *Arterioscler. Thromb. Vasc. Biol.* **2005**, 25, 1767–1775.
- [81] P. Wu, T. E. Nielsen, M. H. Clausen, *Trends Pharmacol. Sci.* **2015**.
- [82] F. Solca, G. Dahl, A. Zoephel, G. Bader, M. Sanderson, C. Klein, O. Kraemer, F. Himmelsbach, E. Haaksma, G. R. Adolf, *J. Pharmacol. Exp. Ther.* **2012**, 343, 342–350.
- [83] J. S. Tokarski, J. A. Newitt, C. Y. J. Chang, J. D. Cheng, M. Wittekind, S. E. Kiefer, K. Kish, F. Y. F. Lee, R. Borzilleri, L. J. Lombardo, *Cancer Res.* **2006**, 66, 5790–5797.
- [84] B. Nagar, W. G. Bornmann, P. Pellicena, T. Schindler, D. R. Veach, W. T. Miller, B. Clarkson, J. Kuriyan, *Cancer Res.* **2002**, 62, 4236–4243.
- [85] Q. Dong, D. R. Dougan, X. Gong, P. Halkowycz, B. Jin, T. Kanouni, S. M. O’Connell, N. Scorah, L. Shi, M. B. Wallace, *Bioorg. Med. Chem. Lett.* **2011**, 21, 1315–1319.
- [86] J. Zhang, F. J. Adrián, W. Jahnke, S. W. Cowan-Jacob, A. G. Li, R. E. Iacob, T. Sim, J. Powers, C. Dierks, F. Sun, *Nature* **2010**, 463, 501–506.
- [87] P. Yaish, A. Gazit, C. Gilon, A. Levitzki, *Sci.* **1988**, 242, 933–935.
- [88] A. Gazit, P. Yaish, C. Gilon, A. Levitzki, *J. Med. Chem.* **1989**, 32, 2344–2352.
- [89] L. K. Gavrin, E. Saiah, *Medchemcomm* **2013**, 4, 41–51.
- [90] Q. Wang, J. A. Zorn, J. Kuriyan, *Methods Enzymol.* **2013**, 548, 23–67.
- [91] M. Tong, M. A. Seeliger, *ACS Chem. Biol.* **2014**, 10, 190–200.

- [92] M. E. M. Noble, J. A. Endicott, L. N. Johnson, *Science (80-.)*. **2004**, 303, 1800–1805.
- [93] R. A. Norman, D. Toader, A. D. Ferguson, *Trends Pharmacol. Sci.* **2012**, 33, 273–278.
- [94] V. Lamba, I. Ghosh, *Curr. Pharm. Des.* **2012**, 18, 2936–2945.
- [95] A. Levitzki, *Annu. Rev. Pharmacol. Toxicol.* **2013**, 53, 161–185.
- [96] J. A. Burger, K. Okkenhaug, *Nat. Rev. Clin. Oncol.* **2014**, 11, 184–186.
- [97] R. W. Hendriks, S. Yuvaraj, L. P. Kil, *Nat. Rev. Cancer* **2014**, 14, 219–232.
- [98] J. C. Byrd, R. R. Furman, S. E. Coutre, I. W. Flinn, J. A. Burger, K. A. Blum, B. Grant, J. P. Sharman, M. Coleman, W. G. Wierda, *N. Engl. J. Med.* **2013**, 369, 32–42.
- [99] D. S. Johnson, E. Weerapana, B. F. Cravatt, *Future Med. Chem.* **2010**, 2, 949–964.
- [100] K. Garber, *Nat. Rev. Drug Discov.* **2014**, 13, 162–164.
- [101] D. L. Gibbons, S. Pricl, H. Kantarjian, J. Cortes, A. Quintás-Cardama, *Cancer* **2012**, 118, 293–299.
- [102] B. J. Druker, M. Talpaz, D. J. Resta, B. Peng, E. Buchdunger, J. M. Ford, N. B. Lydon, H. Kantarjian, R. Capdeville, S. Ohno-Jones, *N. Engl. J. Med.* **2001**, 344, 1031–1037.
- [103] L. S. Steelman, S. C. Pohnert, J. G. Shelton, R. A. Franklin, F. E. Bertrand, J. A. McCubrey, *Leukemia* **2004**, 18, 189–218.
- [104] S. Panjarian, R. E. Iacob, S. Chen, J. R. Engen, T. E. Smithgall, *J. Biol. Chem.* **2013**, 288, 5443–5450.
- [105] G. E. Winter, U. Rix, S. M. Carlson, K. V. Gleixner, F. Grebien, M. Gridling, A. C. Müller, F. P. Breitwieser, M. Bilban, J. Colinge, *Nat. Chem. Biol.* **2012**, 8, 905–912.
- [106] M. E. Gorre, M. Mohammed, K. Ellwood, N. Hsu, R. Paquette, P. N. Rao, C. L. Sawyers, *Science (80-.)*. **2001**, 293, 876–880.
- [107] A. J. Lamontanara, E. B. Gencer, O. Kuzyk, O. Hantschel, *Biochim. Biophys. Acta (BBA)-Proteins Proteomics* **2013**, 1834, 1449–1459.
- [108] L. Ma, Y. Shan, R. Bai, L. Xue, C. A. Eide, J. Ou, L. J. Zhu, L. Hutchinson, J. Cerny, H. J. Khoury, *Sci. Transl. Med.* **2014**, 6, 252ra121–252ra121.
- [109] M. Azam, M. A. Seeliger, N. S. Gray, J. Kuriyan, G. Q. Daley, *Nat. Struct. Mol. Biol.* **2008**, 15, 1109–1118.
- [110] H. Daub, K. Specht, A. Ullrich, *Nat. Rev. Drug Discov.* **2004**, 3, 1001–1010.
- [111] A. Quintás-Cardama, H. Kantarjian, J. Cortes, *Nat. Rev. Drug Discov.* **2007**, 6, 834–848.
- [112] E. Weisberg, P. W. Manley, W. Breitenstein, J. Brügger, S. W. Cowan-Jacob, A. Ray, B. Huntly, D. Fabbro, G. Fendrich, E. Hall-Meyers, *Cancer Cell* **2005**, 7, 129–141.
- [113] N. P. Shah, C. Tran, F. Y. Lee, P. Chen, D. Norris, C. L. Sawyers, *Science (80-.)*. **2004**, 305, 399–401.
- [114] T. Zhou, L. Commodore, W. Huang, Y. Wang, M. Thomas, J. Keats, Q. Xu, V. M. Rivera, W. C. Shakespeare, T. Clackson, *Chem. Biol. Drug Des.* **2011**, 77, 1–11.
- [115] H. A. Bradeen, C. A. Eide, T. O'Hare, K. J. Johnson, S. G. Willis, F. Y. Lee, B. J. Druker, M. W. Deininger, *Blood* **2006**, 108, 2332–2338.
- [116] H. Abe, S. Kikuchi, K. Hayakawa, T. Iida, N. Nagahashi, K. Maeda, J. Sakamoto, N. Matsumoto, T. Miura, K. Matsumura, *ACS Med. Chem. Lett.* **2011**, 2, 320–324.
- [117] Y. Zhao, A. A. Adjei, *Nat. Rev. Clin. Oncol.* **2014**, 11, 385–400.
- [118] K. T. Flaherty, J. R. Infante, A. Daud, R. Gonzalez, R. F. Kefford, J. Sosman, O. Hamid, L. Schuchter, J. Cebon, N. Ibrahim, *N. Engl. J. Med.* **2012**, 367, 1694–1703.
- [119] G. V Long, D. Stroyakovskiy, H. Gogas, E. Levchenko, F. de Braud, J. Larkin, C. Garbe, T. Jouary, A. Hauschild, J. J. Grob, *N. Engl. J. Med.* **2014**, 371, 1877–1888.
- [120] K. J. Cox, C. D. Shomin, I. Ghosh, *Future Med. Chem.* **2011**, 3, 29–43.

- [121] A. Wylie, J. Schoepfer, G. Berellini, H. Cai, G. Caravatti, S. Cotesta, S. Dodd, J. Donovan, B. Erb, P. Furet, *Blood* **2014**, *124*, 398.
- [122] T. G. Bivona, H. Hieronymus, J. Parker, K. Chang, M. Taron, R. Rosell, P. Moonsamy, K. Dahlman, V. A. Miller, C. Costa, *Nature* **2011**, *471*, 523–526.
- [123] M. Radi, S. Schenone, M. Botta, *Curr. Pharm. Biotechnol.* **2013**, *14*, 477–487.
- [124] J. Wu, F. Meng, Y. Ying, Z. Peng, L. Daniels, W. G. Bornmann, A. Quintas-Cardama, D. Roulston, M. Talpaz, L. F. Peterson, et al., *Leukemia* **2010**, *24*, 869–872.
- [125] F. J. Adrián, Q. Ding, T. Sim, A. Velentza, C. Sloan, Y. Liu, G. Zhang, W. Hur, S. Ding, P. Manley, *Nat. Chem. Biol.* **2006**, *2*, 95–102.
- [126] N. Vajpai, A. Strauss, G. Fendrich, S. W. Cowan-Jacob, P. W. Manley, S. Grzesiek, W. Jahnke, *J. Biol. Chem.* **2008**, *283*, 18292–18302.
- [127] B. Nagar, O. Hantschel, M. A. Young, K. Scheffzek, D. Veach, W. Bornmann, B. Clarkson, G. Superti-Furga, J. Kuriyan, *Cell* **2003**, *112*, 859–871.
- [128] O. Hantschel, B. Nagar, S. Guettler, J. Kretschmar, K. Dorey, J. Kuriyan, G. Superti-Furga, *Cell* **2003**, *112*, 845–857.
- [129] C. Wang, L.-A. Chen, H. Huo, X. Shen, K. Harms, L. Gong, E. Meggers, *Chem. Sci.* **2015**, *6*, 1094–1100.
- [130] H. Huo, X. Shen, C. Wang, L. Zhang, P. Röse, L.-A. Chen, K. Harms, M. Marsch, G. Hilt, E. Meggers, *Nature* **2014**, *515*, 100–103.
- [131] M. Helms, Z. Lin, L. Gong, K. Harms, E. Meggers, *Eur. J. Inorg. Chem.* **2013**, *2013*, 4164–4172.
- [132] L. Gong, Z. Lin, K. Harms, E. Meggers, *Angew. Chem. Int. Ed. Engl.* **2010**, *49*, 7955–7.
- [133] C. Fu, K. Harms, L. Zhang, E. Meggers, *Organometallics* **2014**, *33*, 3219–3222.
- [134] Y. Xiang, C. Fu, T. Breiding, P. K. Sasmal, H. Liu, Q. Shen, K. Harms, L. Zhang, E. Meggers, *Chem. Commun.* **2012**, *48*, 7131–7133.
- [135] A. T. Johnson, M. K. Schlegel, E. Meggers, L.-O. Essen, O. Wiest, *J. Org. Chem.* **2011**, *76*, 7964–74.
- [136] T. Völker, F. Dempwolff, P. L. Graumann, E. Meggers, *Angew. Chemie - Int. Ed.* **2014**, *53*, 10536–40.
- [137] P. K. Sasmal, C. N. Streu, E. Meggers, *Chem. Commun. (Camb.)* **2013**, *49*, 1581–7.
- [138] A. Kastl, S. Dieckmann, K. Wähler, T. Völker, L. Kastl, A. L. Merkel, A. Vultur, B. Shannan, K. Harms, M. Ocker, et al., *ChemMedChem* **2013**, *8*, 924–927.
- [139] K. Wähler, A. Ludewig, P. Szabo, K. Harms, E. Meggers, *Eur. J. Inorg. Chem.* **2014**, *2014*, 807–811.
- [140] E. Meggers, G. E. Atilla-Gokcumen, H. Bregman, J. Maksimoska, S. P. Mulcahy, N. Pagano, D. S. Williams, *Synlett* **2007**, *2007*, 1177–1189.
- [141] J. Qin, R. Rajaratnam, L. Feng, J. Salami, J. S. Barber-rotenberg, J. Domsic, P. Reyes-uribe, H. Liu, W. Dang, S. L. Berger, et al., **2014**.
- [142] E. K. Martin, N. Pagano, M. E. Sherlock, K. Harms, E. Meggers, *Inorganica Chim. Acta* **2014**, *423*, 530–539.
- [143] K. S. Smalley, R. Contractor, N. K. Haass, a N. Kulp, G. E. Atilla-Gokcumen, D. S. Williams, H. Bregman, K. T. Flaherty, M. S. Soengas, E. Meggers, et al., *Cancer Res* **2007**, *67*, 209–217.
- [144] A. D. Ostrowski, P. C. Ford, *Dalton Trans.* **2009**, 10660–9.
- [145] J. K. John, K. H. T. Paraiso, V. W. Rebecca, L. P. Cantini, E. V. Abel, N. Pagano, E. Meggers, R. Mathew, C. Krepler, V. Izumi, et al., *J. Invest. Dermatol.* **2012**, *132*, 2818–27.
- [146] H. Bregman, D. S. Williams, G. E. Atilla, P. J. Carroll, E. Meggers, **2004**, 13594–13595.
- [147] H. Bregman, E. Meggers, *Org. Lett.* **2006**, *8*, 5465–5468.

- [148] H. Bregman, D. S. Williams, E. Meggers, *Synthesis (Stuttg)*. **2005**, 1521–1527.
- [149] N. Pagano, J. Maksimoska, H. Bregman, D. S. Williams, R. D. Webster, F. Xue, E. Meggers, *Org. Biomol. Chem.* **2007**, 5, 1218–1227.
- [150] D. S. Williams, P. J. Carroll, E. Meggers, *Inorg. Chem.* **2007**, 46, 2944–2946.
- [151] S. Dieckmann, R. Riedel, K. Harms, E. Meggers, *Eur. J. Inorg. Chem.* **2012**, 2012, 813–821.
- [152] L. Feng, Y. Geisselbrecht, S. Blanck, A. Wilbuer, G. E. Atilla-Gokcumen, P. Filippakopoulos, K. Kräling, M. A. Celik, K. Harms, J. Maksimoska, et al., *J. Am. Chem. Soc.* **2011**, 133, 5976–5986.
- [153] J. Maksimoska, D. S. Williams, G. E. Atilla-Gokcumen, K. S. M. Smalley, P. J. Carroll, R. D. Webster, P. Filippakopoulos, S. Knapp, M. Herlyn, E. Meggers, *Chem. Eur. J* **2008**, 14, 4816–4822.
- [154] S. Blanck, Y. Geisselbrecht, K. Kraling, S. Middel, T. Mietke, K. Harms, L.-O. Essen, E. Meggers, *Dalt. Trans.* **2012**, 41, 9337–9348.
- [155] J. C. Bailar, *J. Chem. Educ.* **1957**, 34, 334–338.
- [156] H. Bregman, D. S. Williams, G. E. Atilla, P. J. Carroll, E. Meggers, *J. Am. Chem. Soc.* **2004**, 126, 13594–13595.
- [157] H. Bregman, P. J. Carroll, E. Meggers, *J. Am. Chem. Soc.* **2006**, 128, 877–884.
- [158] E. Meggers, *Angew. Chemie - Int. Ed.* **2011**, 50, 2442–2448.
- [159] J. Maksimoska, L. Feng, K. Harms, C. Yi, J. Kissil, R. Marmorstein, E. Meggers, *J. Am. Chem. Soc.* **2008**, 130, 15764–15765.
- [160] S. Mulcahy, E. Meggers, in *Med. Organomet. Chem. SE - 6* (Eds.: G. Jaouen, N. Metzler-Nolte), Springer Berlin Heidelberg, **2010**, pp. 141–153.
- [161] E. Meggers, *Chem. Commun. (Camb)*. **2009**, 1001–1010.
- [162] U. Knof, A. Von Zelewsky, *Angew. Chemie - Int. Ed.* **1999**, 38, 302–322.
- [163] V. I. Sokolov, *Russ. Chem. Rev.* **1973**, 6, 452–463.
- [164] E. J. Corey, J. C. J. Bailar, *J. Am. Chem. Soc.* **1959**, 81, 2620–2629.
- [165] R. A. D. Wentworth, **1972**, 9, 171–187.
- [166] R. Deeth, *Coord. Chem. Rev.* **2001**, 212, 11–34.
- [167] E. Meggers, *Eur. J. Inorg. Chem.* **2011**, 2011, 2911–2926.
- [168] P. Knight, *Coord. Chem. Rev.* **2003**, 242, 125–143.
- [169] J. Lacour, D. Linder, *Chem. Rec.* **2007**, 7, 275–85.
- [170] H. B. Jonassen, J. C. Bailar, E. H. Huffman, *J. Am. Chem. Soc.* **1948**, 70, 756–758.
- [171] F. Pezet, J.-C. Daran, I. Sasaki, H. Aït-Haddou, G. A. Balavoine, *Organometallics* **2000**, 19, 4008–4015.
- [172] D. Hesek, Y. Inoue, H. Ishida, S. R. L. Everitt, M. G. B. Drew, *Tetrahedron Lett.* **2000**, 41, 2617–2620.
- [173] D. Hesek, Y. Inoue, S. R. L. Everitt, H. Ishida, M. Kunieda, M. G. B. Drew, *Chem. Commun.* **1999**, 403–404.
- [174] S. D. Bergman, M. Kol, *Inorg. Chem.* **2005**, 44, 1647–1654.
- [175] A. M. Masdeu-Bultó, M. Diéguez, E. Martin, M. Gómez, *Coord. Chem. Rev.* **2003**, 242, 159–201.
- [176] D. Monchaud, J. J. Jodry, D. Pomeranc, V. Heitz, J.-C. Chambron, J.-P. Sauvage, J. Lacour, *Angew. Chemie Int. Ed.* **2002**, 41, 2317–2319.
- [177] J. Lacour, J. J. Jodry, C. Ginglinger, S. Torche-Haldimann, *Angew. Chemie Int. Ed.* **1998**, 37, 2379–2380.
- [178] D. Hesek, Y. Inoue, S. R. L. Everitt, H. Ishida, M. Kunieda, M. G. B. Drew, *Inorg. Chem.*

1999, 39, 317–324.

- [179] J. P. Abell, H. Yamamoto, *Chem. Soc. Rev.* **2010**, 39, 61–9.
- [180] N. Takenaka, G. Xia, H. Yamamoto, *J. Am. Chem. Soc.* **2004**, 126, 13198–9.
- [181] E. Sergeeva, J. Kopilov, I. Goldberg, M. Kol, *Chem. Commun. (Camb)*. **2009**, 3053–5.
- [182] P. Hayoz, A. Von Zelewsky, H. Stoeckli-Evans, *J. Am. Chem. Soc.* **1993**, 115, 5111–5114.
- [183] M. Seitz, A. Kaiser, D. R. Powell, A. S. Borovik, O. Reiser, *Adv. Synth. Catal.* **2004**, 346, 737–741.
- [184] J. Spencer, J. Amin, P. Coxhead, J. McGeehan, C. J. Richards, G. J. Tizzard, S. J. Coles, J. P. Bingham, J. A. Hartley, L. Feng, et al., *Organometallics* **2011**, 30, 3177–3181.
- [185] L. Gong, C. Müller, M. A. Celik, G. Frenking, E. Meggers, *New J. Chem.* **2011**, 35, 788.
- [186] L. Gong, M. Wenzel, E. Meggers, *Acc. Chem. Res.* **2013**, 46, 2635–2644.
- [187] J. Lacour, C. Goujon-Ginglinger, S. Torche-Haldimann, J. J. Jodry, *Angew. Chemie Int. Ed.* **2000**, 39, 3695–3697.
- [188] P. Xie, D. S. Williams, G. E. Atilla-Gokcumen, L. Milk, M. Xiao, K. S. M. Smalley, M. Herlyn, E. Meggers, R. Marmorstein, *ACS Chem. Biol.* **2008**, 3, 305–316.
- [189] M. Dörr, E. Meggers, *Curr. Opin. Chem. Biol.* **2014**, 19, 76–81.
- [190] S. Blanck, J. Maksimoska, J. Baumeister, K. Harms, R. Marmorstein, E. Meggers, *Angew. Chemie - Int. Ed.* **2012**, 51, 5244–5246.
- [191] L. Gong, S. P. Mulcahy, K. Harms, E. Meggers, *J. Am. Chem. Soc.* **2009**, 131, 9602–9603.
- [192] C. Fu, M. Wenzel, E. Treutlein, K. Harms, E. Meggers, *Inorg. Chem.* **2012**, 51, 10004–10011.
- [193] M. Wenzel, E. Meggers, *Eur. J. Inorg. Chem.* **2012**, 2012, 3168–3175.
- [194] M. Kraack, K. Harms, E. Meggers, *Organometallics* **2013**, 32, 5103–5113.
- [195] L. Gong, S. P. Mulcahy, D. Devarajan, K. Harms, G. Frenking, E. Meggers, *Inorg. Chem.* **2010**, 49, 7692–7699.
- [196] A. N. Bullock, S. Russo, A. Amos, N. Pagano, H. Bregman, J. É. Debreczeni, W. H. Lee, F. von Delft, E. Meggers, S. Knapp, *PLoS One* **2009**, 4, e7112.
- [197] S. Mollin, S. Blanck, K. Harms, E. Meggers, *Inorganica Chim. Acta* **2012**, 393, 261–268.
- [198] B. Robinson, *Chem. Rev.* **1963**, 63, 373–401.
- [199] K. Hara, Y. Maruki, X. Long, K. Yoshino, N. Oshiro, S. Hidayat, C. Tokunaga, J. Avruch, K. Yonezawa, *Cell* **2002**, 110, 177–189.
- [200] D.-H. Kim, D. D. Sarbassov, S. M. Ali, J. E. King, R. R. Latek, H. Erdjument-Bromage, P. Tempst, D. M. Sabatini, *Cell* **2002**, 110, 163–175.
- [201] E. J. Brown, P. A. Beai, C. T. Keith, J. Chen, T. B. Shin, S. L. Schreiber, *Nature* **1995**, 377, 441.
- [202] S. Frame, P. Cohen, *Biochem. J* **2001**, 359, 1–16.
- [203] H. H. Zhang, A. I. Lipovsky, C. C. Dibble, M. Sahin, B. D. Manning, *Mol. Cell* **2006**, 24, 185–197.
- [204] H. B. J. Jefferies, S. Fumagalli, P. B. Dennis, C. Reinhard, R. B. Pearson, G. Thomas, *EMBO J.* **1997**, 16, 3693–3704.
- [205] M. M. Chou, J. Blenis, *Curr. Opin. Cell Biol.* **1995**, 7, 806–814.
- [206] J. Montagne, M. J. Stewart, H. Stocker, E. Hafen, S. C. Kozma, G. Thomas, *Science (80-.)* **1999**, 285, 2126–2129.
- [207] H. Harada, J. S. Andersen, M. Mann, N. Terada, S. J. Korsmeyer, *Proc. Natl. Acad. Sci.* **2001**, 98, 9666–9670.
- [208] S. H. Um, F. Frigerio, M. Watanabe, F. Picard, M. Joaquin, M. Sticker, S. Fumagalli, P. R. Allegrini, S. C. Kozma, J. Auwerx, et al.,

- Nature* **2004**, 431, 200–205.
- [209] C. Selman, J. M. A. Tullet, D. Wieser, E. Irvine, S. J. Lingard, A. I. Choudhury, M. Claret, H. Al-Qassab, D. Carmignac, F. Ramadani, *Science* (80-.). **2009**, 326, 140–144.
- [210] M. Bärlund, F. Forozan, J. Kononen, L. Bubendorf, Y. Chen, M. L. Bittner, J. Torhorst, P. Haas, C. Bucher, G. Sauter, *J. Natl. Cancer Inst.* **2000**, 92, 1252–1259.
- [211] M. Karbowniczek, C. S. Spittle, T. Morrison, H. Wu, E. P. Henske, *J. Invest. Dermatol.* **2008**, 128, 980–987.
- [212] H.-K. Kwon, G.-U. Bae, J.-W. Yoon, Y. K. Kim, H.-Y. Lee, H.-W. Lee, J.-W. Han, *Arch. Pharm. Res.* **2002**, 25, 685–690.
- [213] V. S. Rodrik-Outmezguine, S. Chandarlapaty, N. C. Pagano, P. I. Poulikakos, M. Scaltriti, E. Moskatel, J. Baselga, S. Guichard, N. Rosen, *Cancer Discov.* **2011**, 1, 248–259.
- [214] J. Rodriguez-Pascual, E. Cheng, P. Maroto, I. Duran, *Anticancer. Drugs* **2010**, 21, 478–486.
- [215] M. J. Axelrod, V. Gordon, R. E. Mendez, S. S. Leimgruber, M. R. Conaway, E. R. Sharlow, M. J. Jameson, D. G. Gioeli, M. J. Weber, *Cell. Signal.* **2014**, 26, 1627–35.
- [216] J. Qin, R. Rajaratnam, L. Feng, J. Salami, J. S. Barber-Rotenberg, J. Domsic, P. Reyes-Urbe, H. Liu, W. Dang, S. L. Berger, et al., *J. Med. Chem.* **2014**, DOI 10.1021/jm5011868.
- [217] M. C. Etter, *Acc. Chem. Res.* **1990**, 23, 120–126.
- [218] M. C. Etter, *J. Phys. Chem.* **1991**, 95, 4601–4610.
- [219] J. Graton, M. Berthelot, C. Laurence, *J. Chem. Soc. Perkin Trans. 2* **2001**, 2130–2135.
- [220] M. Schadt, G. Haeusler, *J. Membr. Biol.* **1974**, 18, 277–294.
- [221] J. Gutknecht, A. Walter, *Biochim. Biophys. Acta - Biomembr.* **1981**, 649, 149–154.
- [222] A. C. Chakrabarti, D. W. Deamer, *Biochim. Biophys. Acta - Biomembr.* **1992**, 1111, 171–177.
- [223] P. J. Blower, S. R. Cooper, *Inorg. Chem.* **1987**, 26, 2009–2010.
- [224] S. R. Cooper, *Acc. Chem. Res.* **1988**, 21, 141–146.
- [225] L. Yet, *Chem. Rev.* **2000**, 100, 2963–3008.
- [226] M. Schelhaas, H. Waldmann, *Angew. Chemie Int. Ed. English* **1996**, 35, 2056–2083.
- [227] M. M. Keshwani, D. B. Ross, T. J. Ragan, T. K. Harris, *Protein Expr. Purif.* **2008**, 58, 32–41.
- [228] L. Pearce, G. Alton, D. Richter, J. Kath, L. Lingardo, J. Chapman, C. Hwang, D. Alessi, *Biochem. J* **2010**, 431, 245–255.
- [229] T. Sunami, N. Byrne, R. E. Diehl, K. Funabashi, D. L. Hall, M. Ikuta, S. B. Patel, J. M. Shipman, R. F. Smith, I. Takahashi, *J. Biol. Chem.* **2010**, 285, 4587–4594.
- [230] W. Jianchuan, Z. Chen, W. Fang, Q. Fangfang, D. Jianping, *Biochem. J.* **2013**, 454, 39–47.
- [231] R. Anand, J. Maksimoska, N. Pagano, E. Y. Wong, P. a. Gimotty, S. L. Diamond, E. Meggers, R. Marmorstein, *J. Med. Chem.* **2009**, 52, 1602–1611.
- [232] H. Zegzouti, M. Zdanovskaia, K. Hsiao, S. A. Goueli, *Assay Drug Dev. Technol.* **2009**, 7, 560–572.
- [233] I. Gout, T. Minami, K. Hara, Y. Tsujishita, V. Filonenko, M. D. Waterfield, K. Yonezawa, *J. Biol. Chem.* **1998**, 273, 30061–30064.
- [234] C. M. Chresta, B. R. Davies, I. Hickson, T. Harding, S. Cosulich, S. E. Critchlow, J. P. Vincent, R. Ellston, D. Jones, P. Sini, *Cancer Res.* **2010**, 70, 288–298.
- [235] P. Sini, D. James, C. Chresta, S. Guichard, *Autophagy* **2010**, 6, 553–554.
- [236] M. Pende, S. H. Um, V. Mieulet, M. Sticker, V. L. Goss, J. Mestan, M. Mueller, S. Fumagalli, S. C. Kozma, G. Thomas, *Mol. Cell. Biol.* **2004**, 24, 3112–3124.
- [237] M. Atefi, E. von Euw, N. Attar, C. Ng, C. Chu,

- D. Guo, R. Nazarian, B. Chmielowski, J. A. Glaspy, B. Comin-Anduix, *PLoS One* **2011**, 6, e28973.
- [238] O. E. Pardo, C. Wellbrock, U. K. Khanzada, M. Aubert, I. Arozarena, S. Davidson, F. Bowen, P. J. Parker, V. V. Filonenko, I. T. Gout, *EMBO J.* **2006**, 25, 3078–3088.
- [239] V. V. Filonenko, R. Tytarenko, S. K. Azatjan, L. O. Savinska, Y. A. Gaydar, I. T. Gout, V. S. Usenko, V. V. Lyzogubov, *Exp Oncol* **2004**, 26, 294–299.
- [240] V. V. Lyzogubov, D. I. Lytvyn, T. M. Dudchenko, N. V. Lubchenko, P. V. Pogrybnyi, S. V. Nespryadko, A. B. Vinnitska, V. S. Usenko, I. T. Gout, V. V. Filonenko, *Exp Oncol* **2004**, 26, 287–293.
- [241] G. Pérez-Tenorio, E. Karlsson, M. A. Waltersson, B. Olsson, B. Holmlund, B. Nordenskjöld, T. Fornander, L. Skoog, O. Stål, *Breast Cancer Res. Treat.* **2011**, 128, 713–723.
- [242] F. Catalanotti, D. B. Solit, M. P. Pulitzer, M. F. Berger, S. N. Scott, T. Iyriboz, M. E. Lacouture, K. S. Panageas, J. D. Wolchok, R. D. Carvajal, *Clin. Cancer Res.* **2013**, 19, 2257–2264.
- [243] T. R. Fenton, I. T. Gout, *Int. J. Biochem. Cell Biol.* **2011**, 43, 47–59.
- [244] H. T. Cuypers, G. Selten, W. Quint, M. Zijlstra, E. R. Maandag, W. Boelens, P. van Wezenbeek, C. Melief, A. Berns, *Cell* **1984**, 37, 141–150.
- [245] C. J. Fox, P. S. Hammerman, R. M. Cinalli, S. R. Master, L. A. Chodosh, C. B. Thompson, *Genes Dev.* **2003**, 17, 1841–1854.
- [246] K. C. Qian, L. Wang, E. R. Hickey, J. Studts, K. Barringer, C. Peng, A. Kronkaitis, J. Li, A. White, S. Mische, *J. Biol. Chem.* **2005**, 280, 6130–6137.
- [247] P. W. Larid, N. M. T. Van der Lugt, A. Clarke, J. Domen, K. Linders, J. McWhir, A. Berns, M. Hooper, *Nucleic Acids Res.* **1993**, 21, 4750–4755.
- [248] J. Domen, N. M. Van Der Lugt, P. W. Laird, C. J. Saris, A. R. Clarke, M. L. Hooper, A. Berns, *Blood* **1993**, 82, 1445–1452.
- [249] H. Mikkers, M. Nawijn, J. Allen, C. Brouwers, E. Verhoeven, J. Jonkers, A. Berns, *Mol. Cell. Biol.* **2004**, 24, 6104–6115.
- [250] J. D. Feldman, L. Vician, M. Crispino, G. Tocco, V. L. Marcheselli, N. G. Bazan, M. Baudry, H. R. Herschman, *J. Biol. Chem.* **1998**, 273, 16535–16543.
- [251] U. Konietzko, G. Kauselmann, J. Scafidi, U. Staubli, H. Mikkers, A. Berns, M. Schweizer, R. Waltereit, D. Kuhl, *EMBO J.* **1999**, 18, 3359–3369.
- [252] N. Katakami, H. Kaneto, H. Hao, Y. Umayahara, Y. Fujitani, K. Sakamoto, S. Gorogawa, T. Yasuda, D. Kawamori, Y. Kajimoto, *J. Biol. Chem.* **2004**, 279, 54742–54749.
- [253] J. A. Muraski, M. Rota, Y. Misao, J. Fransioli, C. Cottage, N. Gude, G. Esposito, F. Delucchi, M. Arcarese, R. Alvarez, *Nat. Med.* **2007**, 13, 1467–1475.
- [254] A. Zippo, A. De Robertis, M. Bardelli, F. Galvagni, S. Oliviero, *Blood* **2004**, 103, 4536–4544.
- [255] B. E. Stewart, R. H. Rice, *J. Invest. Dermatol.* **1995**, 105, 699–703.
- [256] L. A. Gapter, N. S. Magnuson, K. Ng, H. L. Hosick, *Biochem. Biophys. Res. Commun.* **2006**, 345, 989–997.
- [257] J. Domen, N. M. Van der Lugt, D. Acton, P. W. Laird, K. Linders, A. Berns, *J. Exp. Med.* **1993**, 178, 1665–1673.
- [258] C. T. Cottage, B. Bailey, K. M. Fischer, D. Avitable, B. Collins, S. Tuck, P. Quijada, N. Gude, R. Alvarez, J. Muraski, *Circ. Res.* **2010**, 106, 891–901.
- [259] I. Aksoy, C. Sakabedoyan, P. Bourillot, A. B. Malashicheva, J. Mancip, K. Knoblauch, M. Afanassieff, P. Savatier, *Stem Cells* **2007**, 25, 2996–3004.
- [260] C. J. Fox, P. S. Hammerman, C. B. Thompson, *J. Exp. Med.* **2005**, 201, 259–266.
- [261] G. Vlacich, M. C. Nawijn, G. C. Webb, D. F. Steiner, *Islets* **2010**, 2, 308–317.
- [262] Y. Zhang, Z. Wang, X. Li, N. S. Magnuson,

- Oncogene* **2008**, 27, 4809–4819.
- [263] L. M. Winn, W. Lei, S. A. Ness, *Cell Cycle* **2003**, 2, 257–261.
- [264] T. L. T. Aho, J. Sandholm, K. J. Peltola, Y. Ito, P. J. Koskinen, *BMC Cell Biol.* **2006**, 7, 21.
- [265] Z. Wang, N. Bhattacharya, P. F. Mixter, W. Wei, J. Sedivy, N. S. Magnuson, *Biochim. Biophys. Acta (BBA)-Molecular Cell Res.* **2002**, 1593, 45–55.
- [266] D. Morishita, R. Katayama, K. Sekimizu, T. Tsuruo, N. Fujita, *Cancer Res.* **2008**, 68, 5076–5085.
- [267] T. Mochizuki, C. Kitanaka, K. Noguchi, T. Muramatsu, A. Asai, Y. Kuchino, *J. Biol. Chem.* **1999**, 274, 18659–18666.
- [268] M. Bachmann, C. Kosan, P. X. Xing, M. Montenarh, I. Hoffmann, T. Mörröy, *Int. J. Biochem. Cell Biol.* **2006**, 38, 430–443.
- [269] X. P. Chen, J. A. Losman, S. Cowan, E. Donahue, S. Fay, B. Q. Vuong, M. C. Nawijn, D. Capece, V. L. Cohan, P. Rothman, *Proc. Natl. Acad. Sci.* **2002**, 99, 2175–2180.
- [270] K. J. Peltola, K. Paukku, T. L. T. Aho, M. Ruuska, O. Silvennoinen, P. J. Koskinen, *Blood* **2004**, 103, 3744–3750.
- [271] J. J. Gu, Z. Wang, R. Reeves, N. S. Magnuson, *Oncogene* **2009**, 28, 4261–4271.
- [272] C. Peng, A. Knebel, N. A. Morrice, X. Li, K. Barringer, J. Li, S. Jakes, B. Werneburg, L. Wang, *J. Biochem.* **2007**, 141, 353–362.
- [273] T. L. T. Aho, J. Sandholm, K. J. Peltola, H. P. Mankonen, M. Lilly, P. J. Koskinen, *FEBS Lett.* **2004**, 571, 43–49.
- [274] A. Macdonald, D. Campbell, R. Toth, H. McLauchlan, C. J. Hastie, J. S. Arthur, *BMC Cell Biol.* **2006**, 7, 1.
- [275] B. Yan, M. Zemskova, S. Holder, V. Chin, A. Kraft, P. J. Koskinen, M. Lilly, *J. Biol. Chem.* **2003**, 278, 45358–45367.
- [276] N. N. Danial, *Oncogene* **2008**, 27, S53–S70.
- [277] J. Zha, H. Harada, E. Yang, J. Jockel, S. J. Korsmeyer, *Cell* **1996**, 87, 619–628.
- [278] M. C. Nawijn, A. Alendar, A. Berns, *Nat. Rev. Cancer* **2011**, 11, 23–34.
- [279] C. V Dang, K. A. O'Donnell, T. Juopperi, *Cancer Cell* **2005**, 8, 177–178.
- [280] T. Shirogane, T. Fukada, J. M. M. Muller, D. T. Shima, M. Hibi, T. Hirano, *Immunity* **1999**, 11, 709–719.
- [281] D. Wingett, A. Long, D. Kelleher, N. S. Magnuson, *J. Immunol.* **1996**, 156, 549–557.
- [282] T. L. Cibull, T. D. Jones, L. Li, J. N. Eble, L. Ann Baldridge, S. R. Malott, Y. Luo, L. Cheng, *J. Clin. Pathol.* **2006**, 59, 285–288.
- [283] N. Shah, B. Pang, K.-G. Yeoh, S. Thorn, C. S. Chen, M. B. Lilly, M. Salto-Tellez, *Eur. J. Cancer* **2015**, 44, 2144–2151.
- [284] A. A. Alizadeh, M. B. Eisen, R. E. Davis, C. Ma, I. S. Lossos, A. Rosenwald, J. C. Boldrick, H. Sabet, T. Tran, X. Yu, *Nature* **2000**, 403, 503–511.
- [285] G. Wright, B. Tan, A. Rosenwald, E. H. Hurt, A. Wiestner, L. M. Staudt, *Proc. Natl. Acad. Sci.* **2003**, 100, 9991–9996.
- [286] C. B. Poulsen, R. Borup, F. C. Nielsen, N. Borregaard, M. Hansen, K. Grønbaek, M. B. Møller, E. Ralfkiaer, *Eur. J. Haematol.* **2005**, 74, 453–465.
- [287] E. D. Hsi, S.-H. Jung, R. Lai, J. L. Johnson, J. R. Cook, D. Jones, S. Devos, B. D. Cheson, L. E. Damon, J. Said, *Leuk. Lymphoma* **2008**, 49, 2081–2090.
- [288] C. Reiser-Erkan, M. Erkan, Z. Pan, S. Bekasi, N. A. Giese, S. Streit, C. W. Michalski, H. Friess, J. Kleeff, *Cancer Biol. Ther.* **2008**, 7, 1352–1359.
- [289] U. Warnecke-Eberz, E. Bollschweiler, U. Drebbler, A. Pohl, S. E. Baldus, A. H. Hoelscher, R. Metzger, *Oncol. Rep.* **2008**, 20, 619–624.
- [290] U. Warnecke-Eberz, E. Bollschweiler, U. Drebbler, R. Metzger, S. E. BALDUS, A. H. Hoelscher, S. Moenig, *Anticancer Res.* **2009**, 29, 4451–4455.

- [291] K. Peltola, M. Hollmen, S.-M. Maala, E. Rainio, R. Ristamäki, M. Luukkainen, J. Sandholm, M. Sundvall, K. Elenius, P. J. Koskinen, *Neoplasia* **2009**, *11*, 629–IN1.
- [292] A. L. Merkel, E. Meggers, M. Ocker, *Expert Opin. Investig. Drugs* **2012**, *21*, 425–436.
- [293] N. A. Warfel, A. S. Kraft, *Pharmacol. Ther.* **2015**.
- [294] F. Agnès, B. Shamoon, C. Dina, O. Rosnet, D. Birnbaum, F. Galibert, *Gene* **1994**, *145*, 283–288.
- [295] S. D. Lyman, L. James, J. Zappone, P. R. Sleath, M. P. Beckmann, T. Bird, *Oncogene* **1993**, *8*, 815–822.
- [296] C. E. Carow, M. Levenstein, S. H. Kaufmann, J. Chen, S. Amin, P. Rockwell, L. Witte, M. J. Borowitz, C. I. Civin, D. Small, *Blood* **1996**, *87*, 1089–1096.
- [297] S. Gonfloni, A. Weijland, J. Kretschmar, G. Superti-Furga, *Nat. Struct. Mol. Biol.* **2000**, *7*, 281–286.
- [298] A. M. Turner, N. L. Lin, S. Issarachai, S. D. Lyman, V. C. Broudy, *Blood* **1996**, *88*, 3383–3390.
- [299] A. Weiss, J. Schlessinger, *Cell* **1998**, *94*, 277–280.
- [300] D. L. Stirewalt, J. P. Radich, *Nat. Rev. Cancer* **2003**, *3*, 650–65.
- [301] M. Dosil, S. Wang, I. R. Lemischka, *Mol. Cell. Biol.* **1993**, *13*, 6572–6585.
- [302] R. Rottapel, C. W. Turck, N. Casteran, X. Liu, D. Birnbaum, T. Pawson, P. Dubreuil, *Oncogene* **1994**, *9*, 1755–1765.
- [303] S. Zhang, C. Mantel, H. E. Broxmeyer, *J. Leukoc. Biol.* **1999**, *65*, 372–380.
- [304] S. P. Srinivasa, P. D. Doshi, *Leukemia* **2002**, *16*, 244–253.
- [305] S. Zhang, H. E. Broxmeyer, *Biochem. Biophys. Res. Commun.* **2000**, *277*, 195–199.
- [306] S. Zhang, H. E. Broxmeyer, *Biochem. Biophys. Res. Commun.* **1999**, *254*, 440–445.
- [307] S. Marchetto, E. Fournier, N. Beslu, T. Aurran-Schleinitz, P. Dubreuil, J. P. Borg, D. Birnbaum, O. Rosnet, *Leukemia* **1999**, *13*, 1374–1382.
- [308] O. Rosnet, H. J. Bühring, S. Marchetto, I. Rappold, C. Lavagna, D. Sainty, C. Arnoulet, C. Chabannon, L. Kanz, C. Hannum, *Leukemia* **1996**, *10*, 238–248.
- [309] M. Gabbianelli, E. Pelosi, E. Montesoro, M. Valtieri, L. Luchetti, P. Samoggia, L. Vitelli, T. Barberi, U. Testa, S. Lyman, *Blood* **1995**, *86*, 1661–1670.
- [310] M. Z. Ratajczak, J. Ratajczak, J. Ford, R. Kregnow, W. Marlicz, A. M. Gewirtz, *Stem Cells* **1996**, *14*, 146–150.
- [311] M. Hjertson, C. Sundström, S. D. Lyman, K. Nilsson, G. Nilsson, *Exp. Hematol.* **1996**, *24*, 748–754.
- [312] O. Rosnet, D. Birnbaum, *Crit. Rev. Oncog.* **1992**, *4*, 595–613.
- [313] H. G. Drexler, *Leukemia* **1996**, *10*, 588–599.
- [314] F. M. Abu-Duhier, A. C. Goodeve, G. A. Wilson, R. S. Care, I. R. Peake, J. T. Reilly, *Br. J. Haematol.* **2001**, *113*, 983–988.
- [315] F. Ravandi, H. Kantarjian, S. Faderl, G. Garcia-Manero, S. O'Brien, C. Koller, S. Pierce, M. Brandt, D. Kennedy, J. Cortes, et al., *Leuk. Res.* **2010**, *34*, 752–756.
- [316] P. J. Martin, V. Najfeld, J. A. Hansen, G. K. Penfold, R. J. Jacobson, P. J. Fialkow, **1980**.
- [317] K. Mackarehtschian, J. D. Hardin, K. A. Moore, S. Boast, S. P. Goff, I. R. Lemischka, *Immunity* **1995**, *3*, 147–161.
- [318] M. R. Grunwald, M. J. Levis, *Int. J. Hematol.* **2013**, *97*, 683–694.
- [319] G. Vader, S. M. a Lens, *Biochim. Biophys. Acta* **2008**, *1786*, 60–72.
- [320] M. Carmena, W. C. Earnshaw, *Nat Rev Mol Cell Biol* **2003**, *4*, 842–854.
- [321] T. Sardon, I. Peset, B. Petrova, I. Vernos, *EMBO J.* **2008**, *27*, 2567–2579.

- [322] D. M. Glover, M. H. Leibowitz, D. A. McLean, H. Parry, *Cell* **1995**, *81*, 95–105.
- [323] J. M. Schumacher, N. Ashcroft, P. J. Donovan, A. Golden, *Development* **1998**, *125*, 4391–4402.
- [324] C. Roghi, R. Giet, R. Uzbekov, N. Morin, I. Chartrain, R. Le Guellec, A. Couturier, M. Dorée, M. Philippe, C. Prigent, *J. Cell Sci.* **1998**, *111*, 557–572.
- [325] K. Sugimoto, T. Urano, H. Zushi, K. Inoue, H. Tasaka, M. Tachibana, M. Dotsu, *Cell Struct. Funct.* **2002**, *27*, 457–467.
- [326] R. R. Adams, M. Carmena, W. C. Earnshaw, *Trends Cell Biol.* **2001**, *11*, 49–54.
- [327] E. A. Nigg, *Nat. Rev. Mol. cell Biol.* **2001**, *2*, 21–32.
- [328] J. R. Bischoff, L. Anderson, Y. Zhu, K. Mossie, L. Ng, B. Souza, B. Schryver, P. Flanagan, F. Clairvoyant, C. Ginther, *EMBO J.* **1998**, *17*, 3052–3065.
- [329] R. Giet, C. Prigent, *J. Cell Sci.* **1999**, *112*, 3591–3601.
- [330] R. Giet, C. Prigent, *J. Cell Sci.* **2001**, *114*, 2095–2104.
- [331] T. A. Kufer, H. H. W. Silljé, R. Körner, O. J. Gruss, P. Meraldi, E. A. Nigg, *J. Cell Biol.* **2002**, *158*, 617–623.
- [332] D. Berdnik, J. A. Knoblich, *Curr. Biol.* **2002**, *12*, 640–647.
- [333] E. Hannak, M. Kirkham, A. A. Hyman, K. Oegema, *J. Cell Biol.* **2001**, *155*, 1109–1116.
- [334] R. Giet, R. Uzbekov, F. Cubizolles, K. Le Guellec, C. Prigent, *J. Biol. Chem.* **1999**, *274*, 15005–15013.
- [335] T. Andrésson, J. V Ruderman, *EMBO J.* **1998**, *17*, 5627–5637.
- [336] L. E. Littlepage, H. Wu, T. Andresson, J. K. Deanehan, L. T. Amundadottir, J. V Ruderman, *Proc. Natl. Acad. Sci.* **2002**, *99*, 15440–15445.
- [337] Y. Terada, M. Tatsuka, F. Suzuki, Y. Yasuda, S. Fujita, M. Otsu, *EMBO J.* **1998**, *17*, 667–676.
- [338] M. Murata-Hori, M. Tatsuka, Y.-L. Wang, *Mol. Biol. Cell* **2002**, *13*, 1099–1108.
- [339] R. R. Adams, H. Maiato, W. C. Earnshaw, M. Carmena, *J. Cell Biol.* **2001**, *153*, 865–880.
- [340] M. J. Kallio, M. L. McClelland, P. T. Stukenberg, G. J. Gorbisky, *Curr. Biol.* **2002**, *12*, 900–905.
- [341] C. Ditchfield, V. L. Johnson, A. Tighe, R. Ellston, C. Haworth, T. Johnson, A. Mortlock, N. Keen, S. S. Taylor, *J. Cell Biol.* **2003**, *161*, 267–280.
- [342] S. Hauf, R. W. Cole, S. LaTerra, C. Zimmer, G. Schnapp, R. Walter, A. Heckel, J. Van Meel, C. L. Rieder, J.-M. Peters, *J. Cell Biol.* **2003**, *161*, 281–294.
- [343] L. R. GURLEY, J. A. D'ANNA, S. S. BARHAM, L. L. DEAVEN, R. A. TOBEY, *Eur. J. Biochem.* **1978**, *84*, 1–15.
- [344] H. Zhou, J. Kuang, L. Zhong, W. Kuo, J. Gray, A. Sahin, B. Brinkley, S. Sen, *Nat. Genet.* **1998**, *20*, 189–193.
- [345] M. M. Tanner, S. Grenman, A. Koul, O. Johannsson, P. Meltzer, T. Pejovic, Å. Borg, J. J. Isola, *Clin. Cancer Res.* **2000**, *6*, 1833–1839.
- [346] M. Tatsuka, H. Katayama, T. Ota, T. Tanaka, S. Odashima, F. Suzuki, Y. Terada, *Cancer Res.* **1998**, *58*, 4811–4816.
- [347] P. Meraldi, R. Honda, E. A. Nigg, *EMBO J.* **2002**, *21*, 483–492.
- [348] S. Doxsey, *Mol. Cell* **2002**, *10*, 439–440.
- [349] T. Ota, S. Suto, H. Katayama, Z.-B. Han, F. Suzuki, M. Maeda, M. Tanino, Y. Terada, M. Tatsuka, *Cancer Res.* **2002**, *62*, 5168–5177.
- [350] M. Malumbres, I. Pérez de Castro, *Expert Opin. Ther. Targets* **2014**, *18*, 1377–1393.
- [351] J. F. Hilton, G. I. Shapiro, W. Hospital, H. Medical, **2015**, *32*, 57–59.

- [352] A. Nikonova, I. Astsaturov, I. Serebriiskii, R. Dunbrack Jr., E. Golemis, *Cell. Mol. Life Sci.* **2013**, *70*, 661–687.
- [353] A. A. Dar, L. W. Goff, S. Majid, J. Berlin, W. El-Rifai, *Mol. Cancer Ther.* **2010**, *9*, 268–278.
- [354] N. Keen, S. Taylor, *Nat. Rev. Cancer* **2004**, *4*, 927–936.
- [355] B. Goldenson, J. D. Crispino, *Oncogene* **2015**, *34*, 537–545.
- [356] F. H. Jardine, in *Encycl. Inorg. Chem.*, John Wiley & Sons, Ltd, **2006**.
- [357] T. Damhus, R. M. Hartshorn, A. T. Hutton, *Nomenclature of Inorganic Chemistry: IUPAC Recommendations 2005*, Royal Society Of Chemistry, **2005**.
- [358] R. S. Cahn, C. Ingold, V. Prelog, *Angew. Chemie* **1966**, *78*, 413–447.
- [359] V. Prelog, G. Helmchen, *Angew. Chemie Int. Ed. English* **1982**, *21*, 567–583.
- [360] M. Brorson, T. Damhus, C. E. Schaffer, *Inorg. Chem.* **1983**, *22*, 1569–1573.
- [361] S. Mollin, R. Riedel, K. Harms, E. Meggers, *J. Inorg. Biochem.* **2015**.
- [362] M. A. Fabian, W. H. Biggs, D. K. Treiber, C. E. Atteridge, M. D. Azimioara, M. G. Benedetti, T. A. Carter, P. Ciceri, P. T. Edeen, M. Floyd, et al., *Nat Biotech* **2005**, *23*, 329–336.
- [363] M. W. Karaman, S. Herrgard, D. K. Treiber, P. Gallant, C. E. Atteridge, B. T. Campbell, K. W. Chan, P. Ciceri, M. I. Davis, P. T. Edeen, et al., *Nat Biotech* **2008**, *26*, 127–132.
- [364] C. L. Davies, E. L. Dux, A.-K. Duhme-Klair, *Dalt. Trans.* **2009**, 10141–10154.
- [365] C.-M. Che, F.-M. Siu, *Curr. Opin. Chem. Biol.* **2010**, *14*, 255–261.
- [366] K. J. Kilpin, P. J. Dyson, *Chem. Sci.* **2013**, *4*, 1410–1419.
- [367] C.-H. Leung, H.-Z. He, L.-J. Liu, M. Wang, D. S.-H. Chan, D.-L. Ma, *Coord. Chem. Rev.* **2013**, *257*, 3139–3151.
- [368] N. P. E. Barry, P. J. Sadler, *Chem. Commun.* **2013**, *49*, 5106–5131.
- [369] D. Mahadevan, C. Spier, K. Della Croce, S. Miller, B. George, C. Riley, S. Warner, T. M. Grogan, T. P. Miller, *Mol. Cancer Ther.* **2005**, *4*, 1867–1879.
- [370] L. A. Dakin, M. H. Block, H. Chen, E. Code, J. E. Dowling, X. Feng, A. D. Ferguson, I. Green, A. W. Hird, T. Howard, *Bioorg. Med. Chem. Lett.* **2012**, *22*, 4599–4604.
- [371] E. K. Keeton, K. McEachern, K. S. Dillman, S. Palakurthi, Y. Cao, M. R. Grondine, S. Kaur, S. Wang, Y. Chen, A. Wu, *Blood* **2014**, *123*, 905–913.
- [372] R. Amson, F. Sigaux, S. Przedborski, G. Flandrin, D. Givol, A. Telerman, *Proc. Natl. Acad. Sci.* **1989**, *86*, 8857–8861.
- [373] P. van der Geer, T. Hunter, R. A. Lindberg, *Annu. Rev. Cell Biol.* **1994**, *10*, 251–337.
- [374] A.-M. O'Farrell, T. J. Abrams, H. A. Yuen, T. J. Ngai, S. G. Louie, K. W. H. Yee, L. M. Wong, W. Hong, L. B. Lee, A. Town, *Blood* **2003**, *101*, 3597–3605.
- [375] M. Kollareddy, D. Zheleva, P. Dzubak, P. S. Brahmakshatriya, M. Lepsik, M. Hajdych, *Invest. New Drugs* **2012**, *30*, 2411–2432.
- [376] J. W. A. Ritchie, R. J. Williams, *Drug Discov. Today* **2015**.
- [377] S. Howard, V. Berdini, J. A. Boulstridge, M. G. Carr, D. M. Cross, J. Curry, L. A. Devine, T. R. Early, L. Fazal, A. L. Gill, *J. Med. Chem.* **2008**, *52*, 379–388.
- [378] J. Y. L. Chung, J. T. Wasicak, W. A. Arnold, C. S. May, A. M. Nadzan, M. W. Holladay, *J. Org. Chem.* **1990**, *55*, 270–275.
- [379] N. A. Sasaki, M. Dockner, A. Chiaroni, C. Riche, P. Potier, *J. Org. Chem.* **1997**, *62*, 765–770.
- [380] G. Priem, M. S. Anson, S. J. F. Macdonald, B. Pelotier, I. B. Campbell, *Tetrahedron Lett.* **2002**, *43*, 6001–6003.
- [381] R. Rios, I. Ibrahim, J. Vesely, H. Sundén, A. Córdova, *Tetrahedron Lett.* **2007**, *48*, 8695–

- 8699.
- [382] C. Nájera, J. M. Sansano, *Angew. Chemie Int. Ed.* **2005**, *44*, 6272–6276.
- [383] B. Vanhaesebroeck, S. J. Leeyers, G. Panayotou, M. D. Waterfield, *Trends Biochem. Sci.* **1997**, *22*, 267–272.
- [384] S. Jia, Z. Liu, S. Zhang, P. Liu, L. Zhang, S. H. Lee, J. Zhang, S. Signoretti, M. Loda, T. M. Roberts, *Nature* **2008**, *454*, 776–779.
- [385] K. Kok, B. Geering, B. Vanhaesebroeck, *Trends Biochem. Sci.* **2009**, *34*, 115–127.
- [386] R. C. Stein, *Endocr. Relat. Cancer* **2001**, *8*, 237–248.
- [387] L. C. Cantley, *Science (80-.)*. **2002**, *296*, 1655–1657.
- [388] P. T. Hawkins, L. R. Stephens, *Science (80-.)*. **2007**, *318*, 64–66.
- [389] M. P. Wymann, M. Zvelebil, M. Laffargue, *Trends Pharmacol. Sci.* **2003**, *24*, 366–376.
- [390] B. Vanhaesebroeck, J. Guillermet-Guibert, M. Graupera, B. Bilanges, *Nat. Rev. Mol. cell Biol.* **2010**, *11*, 329–341.
- [391] N. Chalhoub, S. J. Baker, *Annu. Rev. Pathol.* **2009**, *4*, 127.
- [392] M. A. Lemmon, *Nat. Rev. Mol. cell Biol.* **2008**, *9*, 99–111.
- [393] H. Kurosu, T. Maehama, T. Okada, T. Yamamoto, S. Hoshino, Y. Fukui, M. Ui, O. Hazeki, T. Katada, *J. Biol. Chem.* **1997**, *272*, 24252–24256.
- [394] U. Maier, A. Babich, B. Nürnberg, *J. Biol. Chem.* **1999**, *274*, 29311–29317.
- [395] X. Tang, C. P. Downes, *J. Biol. Chem.* **1997**, *272*, 14193–14199.
- [396] J. Guillermet-Guibert, K. Bjorklof, A. Salpekar, C. Gonella, F. Ramadani, A. Bilancio, S. Meek, A. J. H. Smith, K. Okkenhaug, B. Vanhaesebroeck, *Proc. Natl. Acad. Sci.* **2008**, *105*, 8292–8297.
- [397] M. Camps, T. Rückle, H. Ji, V. Ardissonne, F. Rintelen, J. Shaw, C. Ferrandi, C. Chabert, C. Gillieron, B. Françon, *Nat. Med.* **2005**, *11*, 936–943.
- [398] G. Servant, O. D. Weiner, P. Herzmark, T. Balla, J. W. Sedat, H. R. Bourne, *Science (80-.)*. **2000**, *287*, 1037–1040.
- [399] B. Heit, L. Liu, P. Colarusso, K. D. Puri, P. Kubes, *J. Cell Sci.* **2008**, *121*, 205–214.
- [400] M. A. Crackower, G. Y. Oudit, I. Kozieradzki, R. Sarao, H. Sun, T. Sasaki, E. Hirsch, A. Suzuki, T. Shioi, J. Irie-Sasaki, *Cell* **2002**, *110*, 737–749.
- [401] D. F. Barber, A. Bartolomé, C. Hernandez, J. M. Flores, C. Redondo, C. Fernandez-Arias, M. Camps, T. Rückle, M. K. Schwarz, S. Rodríguez, *Nat. Med.* **2005**, *11*, 933–935.
- [402] G. Neudert, G. Klebe, *Bioinformatics* **2011**, *27*, 1021–1022.
- [403] D. R. Hall, C. H. Ngan, B. S. Zerbe, D. Kozakov, S. Vajda, *J. Chem. Inf. Model.* **2012**, *52*, 199–209.
- [404] B. S. Zerbe, D. R. Hall, S. Vajda, A. Whitty, D. Kozakov, *J. Chem. Inf. Model.* **2012**, *52*, 2236–2244.
- [405] G. A. Jeffrey, G. A. Jeffrey, *An Introduction to Hydrogen Bonding*, Oxford University Press New York, **1997**.
- [406] M. A. Williams, J. E. Ladbury, *Protein Sci. Encycl.* **2005**.
- [407] T. F. Craan, **2011**.
- [408] N. Pagano, E. Y. Wong, T. Breiding, H. Liu, A. Wilbuer, H. Bregman, S. L. Diamond, E. Meggers, *J. Org. Chem.* **2009**, *74*, 8997–9009.
- [409] H. Gohlke, M. Hendlich, G. Klebe, *J. Mol. Biol.* **2000**, *295*, 337–356.
- [410] H. Gohlke, G. Klebe, *Angew. Chemie Int. Ed.* **2002**, *41*, 2644–2676.
- [411] A. Strecker, *Justus Liebigs Ann. Chem.* **1850**, *75*, 27–45.

- [412] G. Carturan, P. Ugaugliati, U. Belluco, *Inorg. Chem.* **1974**, 13, 542–546.
- [413] W. Hieber, H. Führling, *Zeitschrift für Anorg. und Allg. Chemie* **1971**, 381, 235–240.
- [414] K. Severin, R. Bergs, W. Beck, *Angew. Chemie Int. Ed.* **1998**, 37, 1634–1654.
- [415] B. Wagner, U. Taubald, W. Beck, *Chem. Ber.* **1989**, 122, 1031–1034.
- [416] Y. Shimazaki, M. Takani, O. Yamauchi, *Dalt. Trans.* **2009**, 7854–7869.
- [417] C. Tanford, *J. Am. Chem. Soc.* **1962**, 84, 4240–4247.
- [418] P. Y. Chou, G. D. Fasman, *Biochemistry* **1974**, 13, 211–222.
- [419] A. Nicholls, K. A. Sharp, B. Honig, *Proteins Struct. Funct. Bioinforma.* **1991**, 11, 281–296.
- [420] A. Horovitz, L. Serrano, B. Avron, M. Bycroft, A. R. Fersht, *J. Mol. Biol.* **1990**, 216, 1031–1044.
- [421] N. Shimokhina, A. Bronowska, S. W. Homans, *Angew. Chemie Int. Ed.* **2006**, 45, 6374–6376.
- [422] L. Zhang, P. Carroll, E. Meggers, *Org. Lett.* **2004**, 6, 521–523.
- [423] A. Tjernberg, N. Markova, W. J. Griffiths, D. Hallén, *J. Biomol. Screen.* **2006**, 11, 131–137.
- [424] O. Yamauchi, A. Odani, M. Takani, *J. Chem. Soc. Dalt. Trans.* **2002**, 3411–3421.
- [425] F. Turtaut, S. Ouahrani-Bettache, J.-L. Montero, S. Köhler, J.-Y. Winum, *Medchemcomm* **2011**, 2, 995–1000.
- [426] T. Beulshausen, U. Groth, U. Schöllkopf, *Liebigs Ann. der Chemie* **1992**, 1992, 523–526.
- [427] S. F. Altschul, T. L. Madden, A. A. Schäffer, J. Zhang, Z. Zhang, W. Miller, D. J. Lipman, *Nucleic Acids Res.* **1997**, 25, 3389–3402.
- [428] S. F. Altschul, J. C. Wootton, E. M. Gertz, R. Agarwala, A. Morgulis, A. A. Schäffer, Y.-K. Yu, *FEBS J.* **2005**, 272, 5101–5109.
- [429] J.-F. Gibrat, T. Madej, S. H. Bryant, *Curr. Opin. Struct. Biol.* **1996**, 6, 377–385.
- [430] M. S. Miller, O. Schmidt-Kittler, D. M. Bolduc, E. T. Brower, D. Chaves-Moreira, M. Allaire, K. W. Kinzler, I. G. Jennings, P. E. Thompson, P. A. Cole, *Oncotarget* **2014**, 5, 5198–5208.
- [431] W. L. DeLano, **2002**.
- [432] W. Dang, K. K. Steffen, R. Perry, J. A. Dorsey, F. B. Johnson, A. Shilatifard, M. Kaeberlein, B. K. Kennedy, S. L. Berger, *Nature* **2009**, 459, 802–807.
- [433] F. H. Allen, *Acta Crystallogr. Sect. B Struct. Sci.* **2002**, 58, 380–388.
- [434] A. Laederach, P. J. Reilly, *J. Comput. Chem.* **2003**, 24, 1748–1757.
- [435] O. V Dolomanov, L. J. Bourhis, R. J. Gildea, J. A. K. Howard, H. Puschmann, *J. Appl. Crystallogr.* **2009**, 42, 339–341.
- [436] T. Y. Tchesskaya, *J. Appl. Crystallogr.* **2007**, 40, s609–s613.
- [437] G. M. Sheldrick, *Acta Crystallogr. Sect. A Found. Crystallogr.* **2007**, 64, 112–122.
- [438] K. Brandenburg, H. Putz, *Cryst. Impact, Kreuzherrenstraße* **2012**, 102.
- [439] G. M. Sheldrick, *Acta Crystallogr. Sect. E Struct. Reports Online ISSN* **1997**, 1600–5368.
- [440] G. M. Sheldrick, *Acta Crystallogr. Sect. C Struct. Chem.* **2015**, 71, 3–8.
- [441] N. Kannan, N. Haste, S. S. Taylor, A. F. Neuwald, *Proc. Natl. Acad. Sci.* **2007**, 104, 1272–1277.
- [442] C. Breitenlechner, M. Gaßel, R. Engh, D. Bossemeyer, *Oncol. Res. Featur. Preclin. Clin. Cancer Ther.* **2003**, 14, 267–278.
- [443] T. M. Sielecki, J. F. Boylan, P. A. Benfield, G. L. Trainor, *J. Med. Chem.* **2000**, 43, 1–18.
- [444] G. Pearson, F. Robinson, T. Beers Gibson, B.

- Xu, M. Karandikar, K. Berman, M. H. Cobb, *Endocr. Rev.* **2001**, 22, 153–183.
- [445] R. L. Klemke, S. Cai, A. L. Giannini, P. J. Gallagher, P. De Lanerolle, D. A. Cheres, *J. Cell Biol.* **1997**, 137, 481–492.
- [446] A. Ali, K. P. Hoeflich, J. R. Woodgett, *Chem. Rev.* **2001**, 101, 2527–2540.
- [447] J. E. and Forde, T. C. Dale, *Cell. Mol. life Sci.* **2007**, 64, 1930–1944.
- [448] A. Martinez, A. Castro, I. Dorronsoro, M. Alonso, *Med. Res. Rev.* **2002**, 22, 373–384.
- [449] U. Knippschild, S. Wolff, G. Giamas, C. Brockschmidt, M. Wittau, P. U. WürL, T. Eismann, M. Stöter, *Oncol. Res. Treat.* **2005**, 28, 508–514.
- [450] Y. H. Choi, C.-H. Park, W. Kim, H. Ling, A. Kang, M. W. Chang, S.-K. Im, H.-W. Jeong, Y.-Y. Kong, K.-T. Kim, *PLoS One* **2010**, 5, e15254.
- [451] L. Buée, T. Bussiere, V. Buée-Scherrer, A. Delacourte, P. R. Hof, *Brain Res. Rev.* **2000**, 33, 95–130.
- [452] S. Sato, R. L. Cerny, J. L. Buescher, T. Ikezu, *J. Neurochem.* **2006**, 98, 1573–1584.
- [453] B. Errede, R. M. Cade, B. M. Yashar, Y. Kamada, D. E. Levin, K. Irie, K. Matsumoto, *Mol. Reprod. Dev.* **1995**, 42, 477–485.
- [454] E. Delpire, *Pflügers Arch. J. Physiol.* **2009**, 458, 953–967.
- [455] I. Herskowitz, *Cell* **1995**, 80, 187–197.
- [456] L. S. Maier, D. M. Bers, *Cardiovasc. Res.* **2007**, 73, 631–640.
- [457] P. Penzes, M. E. Cahill, K. A. Jones, D. P. Srivastava, *Trends Cell Biol.* **2015**, 18, 405–413.
- [458] X. Zhang, L. Guo, R. D. Collage, J. L. Stripay, A. Tsung, J. S. Lee, M. R. Rosengart, *J. Leukoc. Biol.* **2011**, 90, 249–261.
- [459] L. Racioppi, A. R. Means, *J. Biol. Chem.* **2012**, 287, 31658–31665.
- [460] W. J. Fantl, D. E. Johnson, L. T. Williams, *Annu. Rev. Biochem.* **1993**, 62, 453–481.
- [461] J. Schlessinger, *Cell* **2000**, 103, 211–225.
- [462] D. S. Krause, R. A. Van Etten, *N. Engl. J. Med.* **2005**, 353, 172–187.
- [463] L. H. Wang, C. G. Besirli, E. M. Johnson Jr, *Annu. Rev. Pharmacol. Toxicol.* **2004**, 44, 451–474.
- [464] L. Sun, H. Wang, Z. Wang, S. He, S. Chen, D. Liao, L. Wang, J. Yan, W. Liu, X. Lei, *Cell* **2012**, 148, 213–227.
- [465] A. Jaeschke, R. J. Davis, *Mol. Cell* **2007**, 27, 498–508.
- [466] F. Chang, L. S. Steelman, J. G. Shelton, J. T. Lee, P. M. Navolanic, W. L. Blalock, R. Franklin, J. A. McCubrey, *Int. J. Oncol.* **2003**, 22, 469–480.
- [467] M. Chinkers, D. L. Garbers, *Annu. Rev. Biochem.* **1991**, 60, 553–575.
- [468] K. A. Lucas, G. M. Pitari, S. Kazerounian, I. Ruiz-Stewart, J. Park, S. Schulz, K. P. Chepenik, S. A. Waldman, *Pharmacol. Rev.* **2000**, 52, 375–414.
- [469] M. Jaleel, S. Saha, A. R. Shenoy, S. S. Visweswariah, *Biochemistry* **2006**, 45, 1888–1898.
- [470] N. LaRonde-LeBlanc, A. Wlodawer, *Biochim. Biophys. Acta (BBA)-Proteins Proteomics* **2005**, 1754, 14–24.
- [471] G. Chimini, P. Chavrier, *Nat. Cell Biol.* **2000**, 2, E191–E196.
- [472] J. A. Engelman, J. Luo, L. C. Cantley, *Nat. Rev. Genet.* **2006**, 7, 606–619.
- [473] H. Wang, *Cell Biochem. Biophys.* **2014**, 70, 1963–1968.
- [474] X. Min, B.-H. Lee, M. H. Cobb, E. J. Goldsmith, *Structure* **2004**, 12, 1303–1311.
- [475] O. Mayans, P. F. M. van der Ven, M. Wilm, A. Mues, P. Young, D. O. Fürst, M. Wilmanns, M. Gautel, *Nature* **1998**, 395, 863–869.

- [476] H. Zhang, A. Photiou, A. Grothey, J. Stebbing, G. Giamas, *Cell. Signal.* **2012**, *24*, 1173–1184.

8 Declaration of Authorship

I hereby certify that the present PhD thesis

DESIGN AND SYNTHESIS OF ENANTIOPURE ORGANOMETALLIC KINASE INHIBITORS AS POTENTIAL
CHEMOTHERAPEUTICS

has been composed by me and is based on my own work, unless stated otherwise. No other person's work has been used without due acknowledgement in this thesis. All references and verbatim extracts have been quoted, and all sources of information, including graphs and data sets, have been declared and specifically acknowledged.

Moreover, this thesis was not previously presented to any other examination board and has not been published.

Place and Date

Signature

9 Scientific Career

- 01/2012-03/2015 Fast-Track PhD Student, PHILIPPS-UNIVERSITÄT MARBURG
Marburg, Division: Chemical Biology, Group: Prof. Dr. Eric Meggers;

DESIGN AND SYNTHESIS OF ENANTIOPURE ORGANOMETALLIC KINASE INHIBITORS AS POTENTIAL CHEMOTHERAPEUTICS
- 08/2010-01/2012 Master Student, PHILIPPS-UNIVERSITÄT MARBURG
Marburg, Program of Study: Medicinal Chemistry
- 09/2009-06/2010 Diploma Thesis at ABBOTT Laboratories GmbH & Co. KG
Ludwigshafen, Division: R & D Neuroscience, Group: Dr. Mario Mezler

PHARMACOLOGIC CHARACTERIZATION OF AMINO ACIDS INVOLVED IN THE BINDING OF HMGLU₂-SPECIFIC POSITIVE ALLOSTERIC MODULATORS
- 03/2005-06/2010 Diploma Student, University of Applied Sciences Mannheim
Mannheim, Program of Study: Biological Chemistry, Diploma (1.7)
- 06/2004 General Qualification for University Entrance, Gymnasium am Rotenbühl
Saarbrücken, Abitur (2.5)